

Dissertation zur Erlangung des Doktorgrades
der Fakultät für Chemie und Pharmazie
der Ludwig-Maximilians-Universität München



**Generation of Carbocations
by Laser Flash Photolysis:
Explorations, Limitations, Applications**

Johannes Ammer
aus
Vöcklabruck, Österreich

2012

~ ERKLÄRUNG ~

Diese Dissertation wurde im Sinne von §7 der Promotionsordnung vom 28. November 2011 von Herrn Prof. Dr. Herbert Mayr betreut.

~ EIDESSTATTLICHE VERSICHERUNG ~

Diese Dissertation wurde eigenständig und ohne unerlaubte Hilfe erarbeitet.

München, am 12. November 2012

Johannes Ammer

Dissertation eingereicht am 20. November 2012

- | | |
|--------------|---------------------------|
| 1. Gutachter | Prof. Dr. Herbert Mayr |
| 2. Gutachter | Prof. Dr. Eberhard Riedle |

Mündliche Prüfung am 18. Dezember 2012

Zuallererst möchte ich mich herzlich bei Professor Herbert Mayr für die Betreuung dieser Arbeit bedanken. Ohne die vielen Freiräume, die er mir gewährt hat, und ohne seine Freude am wissenschaftlichen Diskurs wäre diese Arbeit nicht möglich gewesen. Nicht zuletzt hat er für exzellente Arbeitsbedingungen in seiner Gruppe gesorgt, sowohl was die technische Ausstattung betrifft, als auch den Austausch mit anderen Wissenschaftlern (was mich sogar bis ins ferne Japan geführt hat).

Mein besonderer Dank gilt auch einigen Mitgliedern des Arbeitskreises, die durch umfangreiche gemeinsame Projekte einen wesentlichen Teil zum Gelingen dieser Arbeit beigetragen haben. Allen voran Christoph Nolte, sowie Tobias A. Nigst und Sami Lakhdar. Weiters zählen hierzu Thomas Singer, Mahiuddin Baidya und Professor Shinjiro Kobayashi.

Ich danke Armin R. Ofial für eine große Zahl an Verbesserungsvorschlägen sowie seine Unterstützung bei den Veröffentlichungen und Konstantin Troshin für Nachhilfe bei mathematischen Fragen. Beiden möchte ich außerdem für viele hilfreiche Diskussionen danken. Für ihre kritischen Anmerkungen danke ich allen, die Teile dieser Arbeit bzw. die Entwürfe zu den entsprechenden Publikationen gelesen haben.

Ein sehr schöner Aspekt dieser Arbeit waren die vielen gelungenen Kooperationen mit anderen Arbeitsgruppen aus der Physik und anderen Bereichen der Chemie.

- Christian F. Sailer gebührt als meinem „ständigen Ansprechpartner“ in der Physik besonderer Dank für den Spaß an der gemeinsamen Arbeit, seine Chemiker-freundlichen Erklärungen und den angenehm kurzen Draht per „Buschfunk“.
- Professor Eberhard Riedle danke ich für die gute Einbindung in seine Arbeitsgruppe, die unkomplizierte Zusammenarbeit und seine stete Diskussionsbereitschaft. Igor Pugliesi und Rupashree Balia Singh danke ich ebenfalls für die gute Zusammenarbeit, sowie allen Mitarbeitern des BMO für ihre Gastfreundschaft.
- Professor Regina de Vivie-Riedle, Benjamin Fingerhut und Sebastian Thallmair möchte ich für die gute Kooperation danken, insbesondere Sebastian für die quantenchemische Berechnung der Phosphoniumsalze und die hervorragende Zusammenarbeit auf informeller Ebene.
- Professor Konstantin Karaghiosoff danke ich dafür, dass er in seinem überaus vollen Terminplan Zeit für meine Phosphoniumsalz-Kristalle gefunden hat, und für das Ausmaß an Begeisterung, das er diesen entgegengebracht hat.
- Professor Kirsten Zeitler und ihren Mitarbeitern Matthias Neumann und Johannes Franz danke ich für die gelungene Zusammenarbeit mit Sami Lakhdar, zu der ich einen kleinen Beitrag beisteuern durfte.

Allen Beteiligten möchte ich für ihre Offenheit und Nachsicht gegenüber anderen Disziplinen danken, sowie für ihre Geduld und Ausdauer dabei, die verschiedenen Kulturen miteinander in Einklang zu bringen.

Professor Shinjiro Kobayashi gilt mein Dank für den Aufbau der Laserblitzphotolyse-Anlage, das äußerst gründliche Training zu deren Betrieb und Instandhaltung, und für seinen angenehm respektlosen Umgang mit der Welt der Wissenschaft.

Bernhard Kempf, Armin R. Ofial, Brigitte Janker und den Mitarbeitern der Forschungswerkstätten danke ich für ihre Unterstützung bei kleineren und größeren Reparaturen im Laserlabor.

Nathalie Hampel danke ich für die Herstellung von Tris(*p*-chlorphenyl)phosphin und anderen Ausgangsmaterialien unter Einsatz von Leib und Leben.

Meinem Vorgänger und überraschendem Nachfolger Jörg Bartl danke ich für seine umfangreichen Arbeiten in den Neunzigern, auf denen meine Arbeit aufbaut, sowie für die Weiterführung der von mir offen gelassenen Enden.

Meinen Kollegen und ehemaligen Kollegen Dominik Allgäuer, Anna Antipova, Roland Appel, Haruyasu Asahara, Jörg Bartl, Stefan T. A. Berger, Guillaume Berionni, Katharina Böck, Erik Breuer, Martin Breugst, Frank Brotzel, Saloua Chelli, Xi Chen, Francisco Corral Bautista, Julia Fleckenstein, Elsa Follet, Xingwei Guo, Nathalie Hampel, Markus Horn, Brigitte Janker, Tanja Kanzian, Oliver Kaumanns, Bernhard Kempf, Prof. Shinjiro Kobayashi, Konrad Koszinowski, Marie Kunze, Sami Lakhdar, Hans Laub, Hildegard Lipfert, Biplab Maji, Elizabeth Min, Varvara Morozova, Tobias Nigst, Christoph Nolte, Shyeni Paul, Thanh Binh Phan, Dorothea Richter, Nicolas Streidl, Heike Schaller, Florian Seeliger, Lei Shi, Thomas Singer, Konstantin Troshin, Alexander Wagner, Martin Westermaier, Elija Wiedemann und Ivo Zenz danke ich für die angenehme Arbeitsatmosphäre und so manchen hilfreichen Tip. Für den sportlichen Ausgleich nach getaner Arbeit bedanke ich mich bei Tobi und Konstantin.

David S. Stephenson und Claudia Dubler haben mich bei vielen NMR-Experimenten tatkräftig und beratend unterstützt. Robert Eicher und Susanne Sauerer haben große Geduld mit widerspenstigen Elementaranalysen bewiesen. Werner Spahl hat viele ESI-MS Spektren für mich gemessen und Peter Mayer hat eine entscheidende Kristallstruktur bestimmt. Ihnen allen möchte ich dafür danken.

Meiner Forschungspraktikantin Sandra Prell, meinem Teilzeit-Bacheloranden Henry Schurkus und vielen Studenten des Literaturpraktikums danke ich für ihre gute Arbeit.

Der Deutschen Forschungsgemeinschaft und ihrem Sonderforschungsbereich 749 danke ich für die finanzielle Unterstützung.

Zuletzt möchte ich mich noch bei all jenen bedanken, die dazu beigetragen haben, dass ich mich hier in München sehr wohlfühlt habe, und auch bei all jenen, die meine Verbindung zu Österreich aufrecht erhalten haben. Mein besonderer Dank gilt hier auch meiner Familie, die mich immer unterstützt hat.

Danke! Thank you!

Parts of this thesis have been published in the following articles:

CHAPTER 1

Ion-Pairing of Phosphonium Salts in Solution: C–H...Halogen and C–H... π Hydrogen Bonds

J. Ammer, C. Nolte, K. Karaghiosoff, S. Thallmair, P. Mayer, R. de Vivie-Riedle, H. Mayr, **2013**, submitted.

CHAPTER 2

Photolytic Generation of Benzhydryl Cations and Radicals from Quaternary Phosphonium Salts: How Highly Reactive Carbocations Survive Their First Nanoseconds

J. Ammer, C. F. Sailer, E. Riedle, H. Mayr, *J. Am. Chem. Soc.* **2012**, *134*, 11481-11494.

CHAPTER 3

Free Energy Relationships for Reactions of Substituted Benzhydrylium Ions: From Enthalpy over Entropy to Diffusion Control

J. Ammer, C. Nolte, H. Mayr, *J. Am. Chem. Soc.* **2012**, *134*, 13902-13911.

CHAPTER 4

Solvent Nucleophilicities of Hexafluoroisopropanol/Water Mixtures

J. Ammer, H. Mayr, *J. Phys. Org. Chem.* **2013**, *26*, 59-63.

CHAPTER 6

Electrophilic Reactivity of the α,α -Dimethylbenzyl (Cumyl) Cation

J. Ammer, H. Mayr, *Macromolecules* **2010**, *43*, 1719-1723.

CHAPTER 7

Generation of α,β -Unsaturated Iminium Ions by Laser Flash Photolysis

[Laserblitzphotolytische Erzeugung α,β -ungesättigter Iminium-Ionen]

S. Lakhdar, J. Ammer, H. Mayr, *Angew. Chem.* **2011**, *123*, 10127-10130; *Angew. Chem. Int. Ed.* **2011**, *50*, 9953-9956.

CHAPTER 9

Nucleophilic Reactivities of Tertiary Alkylamines

J. Ammer, M. Baidya, S. Kobayashi, H. Mayr, *J. Phys. Org. Chem.* **2010**, *23*, 1029-1035.

CHAPTER 10

Photogeneration of Benzhydryl Cations by Near-UV Laser Flash Photolysis of Pyridinium Salts

T. A. Nigst, J. Ammer, H. Mayr, *J. Phys. Chem. A* **2012**, *116*, 8494-8499.

CHAPTER 11

Photogeneration of Carbocations: Applications in Physical Organic Chemistry and the Design of Suitable Precursors

J. Ammer, H. Mayr, **2013**, submitted.

Related work has been published in the following articles:

Kinetic studies with photolytically generated carbocations:

Nucleophilic Reactivities and Lewis Basicities of 2-Imidazolines and Related N-Heterocyclic Compounds

B. Maji, M. Baidya, J. Ammer, S. Kobayashi, P. Mayer, A. R. Ofial, H. Mayr, **2013**, submitted.

Nucleofugality and Nucleophilicity of Fluoride in Protic Solvents

C. Nolte, J. Ammer, H. Mayr, *J. Org. Chem.* **2012**, *77*, 3325-3335.

Ambident Reactivities of Methylhydrazines

[Ambidente Reaktivität von Methylhydrazinen]

T. A. Nigst, J. Ammer, H. Mayr, *Angew. Chem.* **2012**, *124*, 1381-1385; *Angew. Chem. Int. Ed.* **2012**, *51*, 1353-1356.

Ultrafast spectroscopic investigations:

A Comprehensive Microscopic Picture of the Benzhydryl Radical and Cation Photo-Generation and Interconversion through Electron Transfer

C. F. Sailer, B. P. Fingerhut, S. Thallmair, C. Nolte, J. Ammer, H. Mayr, R. de Vivie-Riedle, I. Pugliesi, E. Riedle, *ChemPhysChem* **2013**, DOI: 10.1002/cphc.201201057.

Buildup and Decay of the Optical Absorption in the Ultrafast Photo-Generation and Reaction of Benzhydryl Cations in Solution

B. P. Fingerhut, C. F. Sailer, J. Ammer, E. Riedle, R. de Vivie-Riedle, *J. Phys. Chem. A*, **2012**, *116*, 11064-11074.

Encapsulation of Diphenylmethyl Phosphonium Salts in Reverse Micelles: Enhanced Bimolecular Reaction of the Photofragments

C. F. Sailer, R. B. Singh, J. Ammer, E. Riedle, I. Pugliesi, *Chem. Phys. Lett.* **2011**, *512*, 60-65.

The First Picoseconds in the Life of Benzhydryl Cations: Ultrafast Generation and Chemical Reactions

C. F. Sailer, B. P. Fingerhut, J. Ammer, C. Nolte, I. Pugliesi, H. Mayr, R. de Vivie-Riedle, E. Riedle, In: M. Chergui, D. Jonas, E. Riedle, R.W. Schoenlein, A. Taylor (Eds.), *Ultrafast Phenomena XVII*, Oxford University Press, New York **2011**, 427-429.

~ TABLE OF CONTENTS ~

A. Abstract	1
B. Introduction: Studying Carbocations by Laser Flash Photolysis	17
1. Ion-Pairing of Phosphonium Salts in Solution: C–H···Halogen and C–H···π Hydrogen Bonds	25
1.1 Introduction	25
1.2 Benzhydryl Triphenylphosphonium Salts	26
1.2.1 Syntheses	26
1.2.2 NMR Investigation of Benzhydryl Triphenylphosphonium Salts in Solution	27
1.2.3 Quantum Chemical Calculations and Crystal Structures of Benzhydryl Triphenylphosphonium Salts	37
1.2.4 Benzhydryl Triphenylphosphonium Salts: C–H···X ⁻ Hydrogen Bonds in Solution	44
1.3 Benzyl Triphenylphosphonium Salts	46
1.3.1 NMR Investigation of Benzyl Triphenylphosphonium Salts in Solution: A Moderate “BPh ₄ ⁻ Effect”	46
1.3.2 Crystal Structures of Benzyl Triphenylphosphonium Salts	51
1.3.3 What is the Nature of the “BPh ₄ ⁻ Effect” in Benzyl Triphenylphosphonium Salts?	55
1.4 Infrared Spectra	56
1.5 Conclusion	59
1.S Supplementary Data and Experimental Section	66
2. Photolytic Generation of Benzhydryl Cations and Radicals from Quaternary Phosphonium Salts: How Highly Reactive Carbocations Survive Their First Nanoseconds	95
2.1 Introduction	95
2.2 Results and Discussion	96
2.2.1 General	96
2.2.2 Effect of the Photo-electrofuge (i.e., Structure of the Benzhydrylium Ion)	97
2.2.3 Effect of the Photo-nucleofuge (i.e., Triarylphosphine)	103
2.2.4 Effect of Solvent on the Picosecond Dynamics	105
2.2.5 Effect of the Counterion in the Precursor Phosphonium Salt	105
2.2.6 Laser Flash Photolytic Generation of Highly Electrophilic Benzhydrylium Ions	112
2.2.7 Lifetimes of Benzhydrylium Ions in CH ₂ Cl ₂ , CH ₃ CN, and CF ₃ CH ₂ OH	114
2.2.8 Counterion Effects on Bimolecular Reactions	119
2.3 Conclusion	121
2.S Supplementary Data and Experimental Section	129

3.	Free Energy Relationships for Reactions of Substituted Benzhydrylium Ions: From Enthalpy over Entropy to Diffusion Control	147
3.1	Introduction	147
3.2	Results and Discussion	149
3.2.1	<i>Kinetics of the Reactions of Benzhydrylium Ions with π-Nucleophiles in CH_2Cl_2</i>	147
3.2.2	<i>New Electrophilicity Parameters</i>	156
3.2.3	<i>Free Energy Relationships</i>	161
3.2.4	<i>Kinetics of the Reactions of Benzhydrylium Ions with Other Classes of Nucleophiles</i>	163
3.3	Conclusion	166
3.S	Supplementary Data and Experimental Section	171
4.	Solvent Nucleophilicities of Hexafluoroisopropanol/Water Mixtures	225
4.1	Introduction	225
4.2	Results and Discussion	226
4.3	Conclusion	232
4.S	Supplementary Data and Experimental Section	235
5.	Substituent Effects on Intrinsic Barriers: A Closer Look at the Basic Principles Behind Linear Free Energy Relationships	241
5.1	Introduction	241
5.2	Results and Discussion	244
5.2.1	<i>Correlation of Electrophilicity Parameters E with Other Thermodynamic and Kinetic Data</i>	244
5.2.2	<i>Quantitative Free-energy Profiles for Combination Reactions of Benzhydrylium Ions with Nucleophiles</i>	249
5.2.3	<i>The Role of Intrinsic Barriers in Combination Reactions</i>	253
5.2.4	<i>Effect of Intrinsic Barriers on Electrophilicity and Electrophugality Parameters</i>	255
5.2.5	<i>Substituent Effects on Intrinsic Barriers</i>	257
5.2.6	<i>Solvent Effects</i>	259
5.2.7	<i>Why Do the Linear Free Energy Relationships Work?</i>	260
5.3	Conclusion	262
5.S	Supplementary Data and Experimental Section	266
6.	Electrophilic Reactivity of the α,α-Dimethylbenzyl (Cumyl) Cation	277
6.1	Introduction	277
6.2	Results and Discussion	278
6.2.1	<i>Laser-Flash-Photolytic Generation of the Cumyl Cation in CH_2Cl_2</i>	278
6.2.2	<i>Rates of the Reactions of Cumyl Cations with π-Systems</i>	281
6.2.3	<i>Comparison with Other Kinetic and Thermodynamic Data</i>	283
6.2.4	<i>Rate Constant for the Addition of the Cumyl Cation to α-Methylstyrene</i>	285
6.3	Note Added After Publication	286
6.S	Supplementary Data and Experimental Section	291

7.	Generation of α,β-Unsaturated Iminium Ions by Laser Flash Photolysis	297
7.1	Introduction	297
7.2	Results and Discussion	297
7.3	Conclusion	302
7.S	Supplementary Data and Experimental Section	307
8.	Electrophilic Reactivity of the 2-Phenyl-3,4-dihydroisoquinolinium Ion	315
8.1	Introduction	315
8.2	Kinetic Investigations	316
8.S	Supplementary Data and Experimental Section	325
9.	Nucleophilic Reactivities of Tertiary Alkylamines	327
9.1	Introduction	327
9.2	Results and Discussion	329
9.2.1	<i>Laser-flash-photolytic Generation of Benzhydryl Cations</i>	329
9.2.2	<i>Thermodynamics of the Combination Reactions</i>	331
9.2.3	<i>Kinetics of the Reactions of Tertiary Amines with Benzhydryl Cations</i>	331
9.S	Supplementary Data and Experimental Section	341
10.	Photogeneration of Benzhydryl Cations by Near-UV Laser Flash Photolysis of Pyridinium Salts	359
10.1	Introduction	359
10.2	Results and Discussion	362
10.2.1	<i>Photogeneration of Benzhydrylium Ions</i>	362
10.2.2	<i>Kinetic Investigations</i>	366
10.3	Conclusion	370
10.S	Supplementary Data and Experimental Section	374
11.	Photogeneration of Carbocations: Applications in Physical Organic Chemistry and the Design of Suitable Precursors	379
11.1	Introduction	379
11.2	When is the Use of Laser Flash Photolysis Advantageous?	380
11.3	Historic Perspective	384
11.4	Instrumentation	386
11.5	Requirements for Good Photo-leaving Groups	387
11.5.1	<i>Efficient Photogeneration of Diffusionally Separated Carbocations</i>	387
11.5.2	<i>Stability of the Precursor in the Sample Solution</i>	392
11.5.3	<i>Absorption of the Precursor at the Excitation Wavelength</i>	398
11.5.4	<i>Life-times of the Diffusionally Separated Photogenerated Carbocations</i>	399
11.6	Which Photo-leaving Group for Which Purpose?	401
11.7	Summary and Outlook	406
12.	Appendix	413
12.1	Abbreviations Used in Chapters 1-11	413
12.2	Numbering of the Reference Electrophiles in Chapters 1-11	417

Prior to this work, there was little systematic information about the suitability of different precursors for the photolytic generation of carbocations. The use of phosphonium salts and other onium salts for this purpose extends the scope of accessible carbocations, as well as the scope of tolerable reaction conditions for kinetic experiments.

CHAPTER 1. *Ion-Pairing of Phosphonium Salts in Solution: C–H···Halogen and C–H··· π Hydrogen Bonds.* The ^1H -NMR chemical shifts of the C(α)-H protons of benzhydryl triphenylphosphonium salts $\text{Ph}_2\text{CH}-\text{PPh}_3^+ \text{X}^-$ in CD_2Cl_2 solution strongly depend on the counter-anions X^- (e. g., $\delta_{\text{H}} = 8.25$ ppm for $\text{X}^- = \text{Cl}^-$, $\delta_{\text{H}} = 6.23$ ppm for $\text{X}^- = \text{BF}_4^-$, $\delta_{\text{H}} = 5.72$ ppm for $\text{X}^- = \text{BPh}_4^-$). Similar, albeit weaker, counterion-induced shifts are also observed for the *ortho*-protons of the benzhydryl and triphenylphosphonium groups. Concentration-dependent NMR studies show that the large shifts result from the deshielding of the protons by the anions, which decreases in the order $\text{Cl}^- > \text{Br}^- \gg \text{BF}_4^- > \text{SbF}_6^- \gg \text{BPh}_4^- \approx 0$ (Fig. A.1).

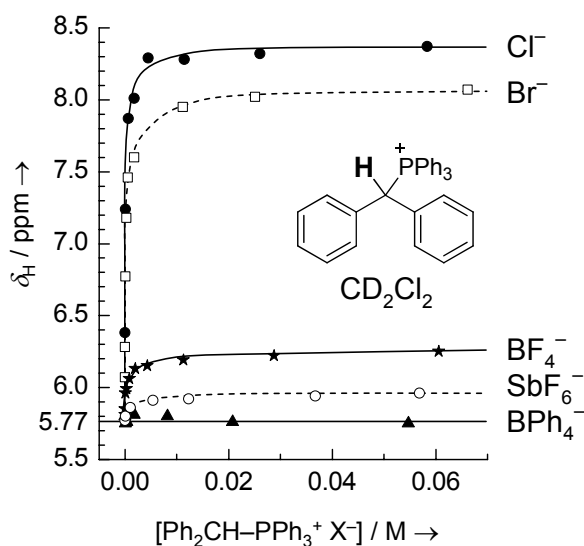


Figure A.1. Concentration-dependent ^1H -NMR (600 MHz, 27 °C) chemical shifts δ_{H} of the benzylic C(α)-H protons of $\text{Ph}_2\text{CH}-\text{PPh}_3^+ \text{X}^-$ with different counter-anions $\text{X}^- = \text{Cl}^-$ (●), Br^- (□), BF_4^- (★), SbF_6^- (○), or BPh_4^- (▲) in CD_2Cl_2 .

ABSTRACT

This observation contradicts literature reports that the shifts originate mainly from the ring current of the BPh_4^- anions. The concentration dependence of the ^1H -NMR chemical shifts allowed to determine the dissociation constants of the phosphonium salts in CD_2Cl_2 solution. The cation-anion interactions increase with the acidity of the $\text{C}(\alpha)\text{-H}$ protons and the basicity of the anion. In the case of the phosphonium tetrafluoroborate, the interaction can also be observed in the ^{19}F -NMR spectra of BF_4^- . The NMR data are explained by $\text{C-H}\cdots\text{X}^-$ hydrogen bonds between the cations and anions, which is confirmed by quantum chemical calculations of the ion pair structures, as well by the crystal structures.

Similar $\text{C-H}\cdots\text{X}^-$ hydrogen bonds are observed for benzyl triphenylphosphonium salts $\text{PhCH}_2\text{-PPh}_3^+ \text{X}^-$. For this phosphonium ion, we also find $\text{C-H}\cdots\text{Ph}$ interactions between the $\text{C}(\alpha)\text{-H}$ group and a phenyl group of the BPh_4^- anion, which result in upfield shifts of the $\text{C}(\alpha)\text{-H}$ protons in the NMR spectra. $\text{C-H}\cdots\text{Ph}$ interactions are also observed in solution as well as crystals of $(p\text{-CF}_3\text{-C}_6\text{H}_4)\text{CH}_2\text{-PPh}_3^+ \text{BPh}_4^-$ (Fig. A.2). However, the dominant effect causing the counterion-induced shifts in the NMR spectra are the $\text{C-H}\cdots\text{X}^-$ hydrogen bonds between the phosphonium ion and anions such as Cl^- or Br^- , which are good hydrogen bond acceptors. The IR spectra of the phosphonium chlorides and bromides in CD_2Cl_2 solution show strong red-shifts of the aliphatic C-H stretch vibrations. The C-H stretch bands of the tetrafluoroborate salt $\text{PhCH}_2\text{-PPh}_3^+ \text{BF}_4^-$ in CD_2Cl_2 , however, show a blue-shift compared to the corresponding tetraphenylborate salt.

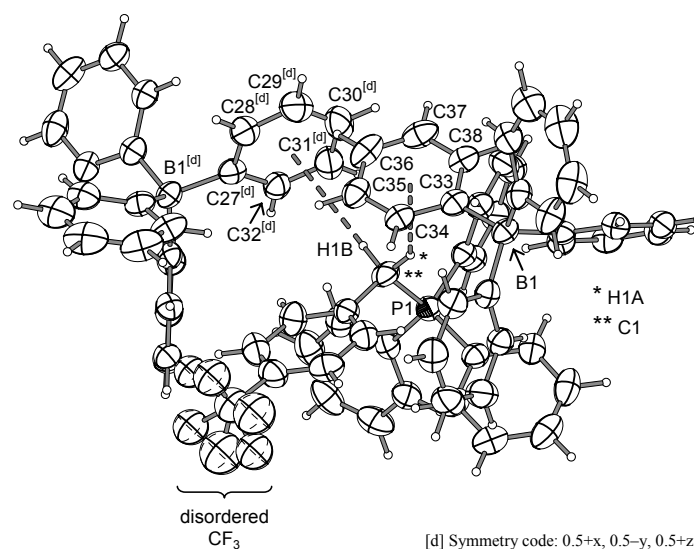
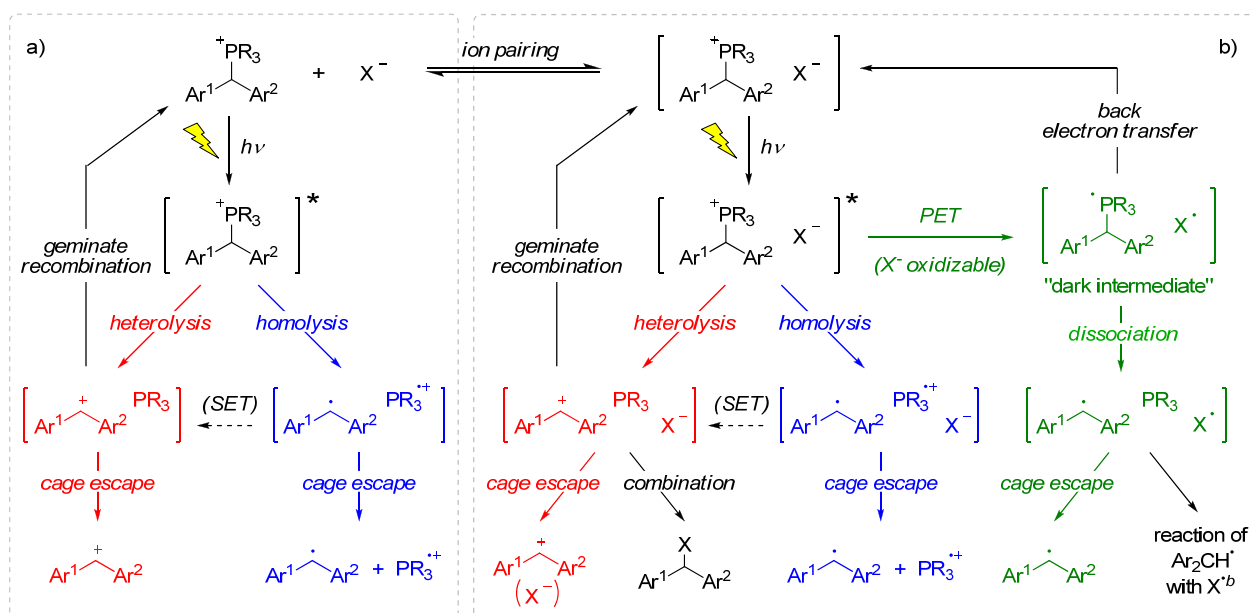


Figure A.2. Interactions between the $(p\text{-CF}_3\text{-C}_6\text{H}_5)\text{CH}_2\text{-PPh}_3^+$ cation (bottom) and two BPh_4^- anions (top) in crystals of **1b** BPh_4^- . The dashed lines indicate the distances between the α -protons (H1A and H1B) and the centers of the phenyl groups.

CHAPTER 2. *Photolytic Generation of Benzhydryl Cations and Radicals from Quaternary Phosphonium Salts: How Highly Reactive Carbocations Survive Their First Nanoseconds.* UV irradiation (266 or 280 nm) of benzhydryl triarylphosphonium salts $\text{Ar}_2\text{CH-PR}_3^+ \text{X}^-$ yields benzhydryl cations Ar_2CH^+ and/or benzhydryl radicals $\text{Ar}_2\text{CH}^\bullet$. The efficiency and mechanism (Scheme A.1) of the photo-cleavage were studied by nanosecond laser flash photolysis and by ultrafast spectroscopy with a state-of-the-art femtosecond transient spectrometer. The influences of the photoelectrofuge (Ar_2CH^+), the photo-nucleofuge (PPh_3 or $\text{P}(p\text{-Cl-C}_6\text{H}_4)_3$), the counterion ($\text{X}^- = \text{BF}_4^-, \text{SbF}_6^-, \text{Cl}^-, \text{or Br}^-$), and the solvent (CH_2Cl_2 or CH_3CN) were investigated. Photogeneration of carbocations from $\text{Ar}_2\text{CH-PR}_3^+ \text{BF}_4^-$ or SbF_6^- is considerably more efficient than from typical neutral precursors (e.g., benzhydryl chlorides or bromides).

Scheme A.1. Generation of Benzhydryl Cations E^+ and Benzhydryl Radicals E^\bullet by Photolysis of Phosphonium Salts $\text{E-PR}_3^+ \text{X}^-$ ($\text{R} = \text{Ph}$ or $p\text{-Cl-C}_6\text{H}_4$): (a) Reactions of Unpaired Phosphonium Ions (Predominant Mechanism in CH_3CN) and (b) Reactions of Paired Phosphonium Ions (Predominant Mechanism in CH_2Cl_2).^a



^a For the sake of simplicity, the geminate recombination reactions for the radical pairs are not shown. ^b Radical combination or electron transfer.

The photochemistry of the phosphonium salts is controlled by the degree of ion pairing, which depends on the solvent and the concentration of the phosphonium salts (Figure A.3). High yields of carbocations are obtained by photolyses of phosphonium salts with complex counterions ($\text{X}^- = \text{BF}_4^-$ or SbF_6^-), while photolyses of phosphonium halides $\text{Ar}_2\text{CH-PPh}_3^+ \text{X}^-$

($X^- = \text{Cl}^-$ or Br^-) in CH_2Cl_2 yield benzhydryl radicals $\text{Ar}_2\text{CH}^\bullet$ due to photo-electron transfer in the excited phosphonium halide ion pair (Scheme A.1, green pathway). At low concentrations in CH_3CN , the precursor salts are mostly unpaired, and the photo-cleavage mechanism is independent of the nature of the counter-anions.

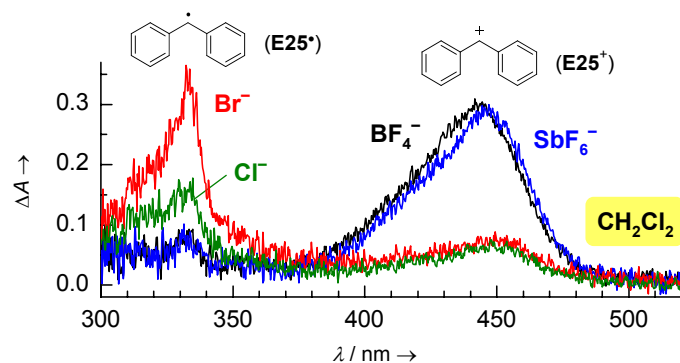


Figure A.3. Transient spectra obtained by irradiation of $\text{Ph}_2\text{CH}-\text{PPh}_3^+ X^-$ ($A_{266 \text{ nm}} = 0.5$, $(1.0-1.2) \times 10^{-4} \text{ M}$) with different counterions $X^- = \text{BF}_4^-$ (black), SbF_6^- (blue), Br^- (red) or Cl^- (green) in CH_2Cl_2 with a 7-ns laser pulse ($\lambda_{\text{exc}} = 266 \text{ nm}$, gate width: 10 ns).

Dichloromethane is better suited for generating the more reactive benzhydryl cations than the more polar and more nucleophilic solvents CH_3CN or $\text{CF}_3\text{CH}_2\text{OH}$. Efficient photo-generation of the most reactive benzhydryl cations $(3,5\text{-F}_2\text{-C}_6\text{H}_3)_2\text{CH}^+$ and $(4\text{-(CF}_3\text{)-C}_6\text{H}_4)_2\text{CH}^+$ was only achieved using the photo-leaving group $\text{P}(p\text{-Cl-C}_6\text{H}_4)_3$ and the counter-anion SbF_6^- in CH_2Cl_2 .

The lifetimes of the photogenerated benzhydryl cations depend greatly on the decay mechanisms, which can be reactions with the solvent, with the photo-leaving group PAR_3 , or with the counter-anion X^- of the precursor salt (Figure A.4).

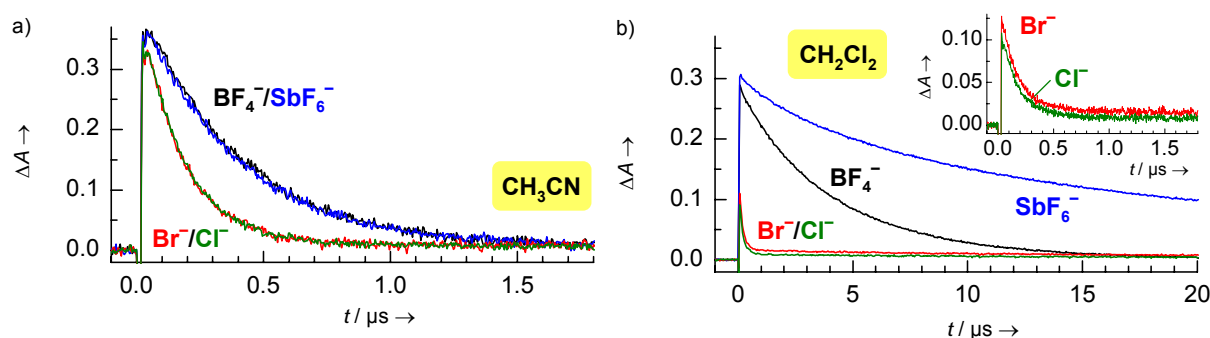


Figure A.4. Time-dependent absorbances of Ph_2CH^+ obtained after 7-ns irradiation of $\text{Ph}_2\text{CH}-\text{PPh}_3^+ X^-$ ($A_{266 \text{ nm}} = 0.5$, $(1.0-1.2) \times 10^{-4} \text{ M}$) with different counter-anions $X^- = \text{BF}_4^-$ (black), SbF_6^- (blue), Br^- (red) or Cl^- (green) with a 7-ns laser pulse: (a) in CH_3CN and (b) in CH_2Cl_2 (inset: enlarged decay curves for Ph_2CH^+ from precursors with halide counterions).

However, the nature of the photo-leaving group and the counterion of the precursor phosphonium salt do not affect the rates of the reactions of the obtained benzhydryl cations toward added nucleophiles (Figure A.5).

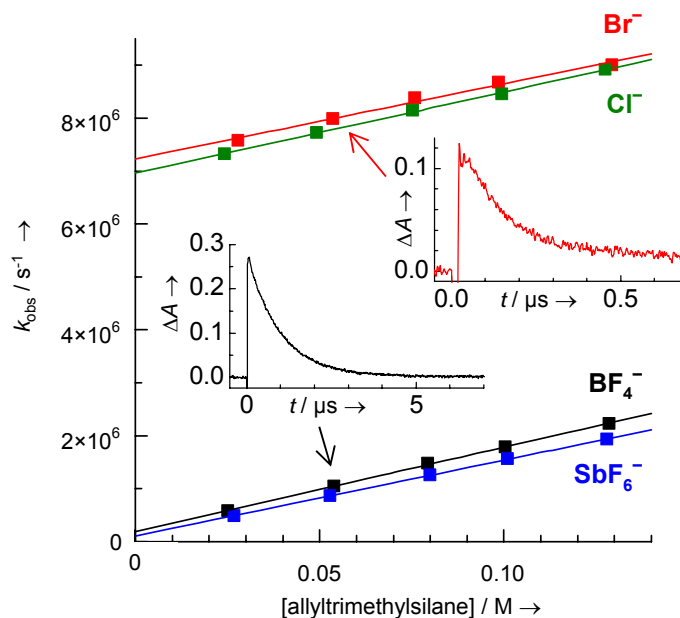


Figure A.5. Plots of the pseudo-first-order rate constants k_{obs} (s^{-1}) for the reactions of Ph_2CH^+ with allyltrimethylsilane in CH_2Cl_2 when Ph_2CH^+ was generated by irradiation of 1.0×10^{-4} M solutions of the precursors $\text{Ph}_2\text{CH}-\text{PPh}_3^+ \text{X}^-$ with different counter-anions $\text{X}^- = \text{BF}_4^-$ (black squares), SbF_6^- (blue squares), Br^- (red squares), or Cl^- (green squares) against the concentration of allyltrimethylsilane. The small graphs show the absorbance decays of Ph_2CH^+ in presence of 5.4×10^{-2} M allyltrimethylsilane (black curve, $\text{X}^- = \text{BF}_4^-$; red curve, $\text{X}^- = \text{Br}^-$).

The method presented in this work allows us to generate a wide range of donor- and acceptor-substituted benzhydryl cations Ar_2CH^+ for the purpose of studying their electrophilic reactivities.

CHAPTER 3. *Free Energy Relationships for Reactions of Substituted Benzhydrylium Ions: From Enthalpy- over Entropy- to Diffusion-Control.* Second-order rate constants k_2 for the reactions of various donor- and acceptor-substituted benzhydrylium ions Ar_2CH^+ with π -nucleophiles in CH_2Cl_2 were determined by laser flash irradiation of benzhydryl triarylphosphonium salts $\text{Ar}_2\text{CH}-\text{PAr}_3^+ \text{X}^-$ in the presence of a large excess of the nucleophiles. This method allowed us to investigate fast reactions up to the diffusional limit including reactions of highly reactive benzhydrylium ions with *m*-fluoro and

p-(trifluoromethyl) substituents. The rate constants determined in this work and relevant literature data were jointly subjected to a correlation analysis to derive the electrophilicity parameters E for acceptor-substituted benzhydrylium ions, as defined by the linear free energy relationship $\log k_2(20\text{ }^\circ\text{C}) = s_N(N + E)$. The new correlation analysis also leads to the N and s_N parameters of 18 π -nucleophiles, which have only vaguely been characterized previously. The correlations of $\log k_2$ versus E (Figure A.6) are linear well beyond the range where the activation enthalpies ΔH^\ddagger of the reactions are extrapolated to reach the value of $\Delta H^\ddagger = 0$, showing that the change from enthalpy control to entropy control does not cause a bend in the linear free energy relationship, a novel manifestation of the compensation effect. A flattening of the correlation lines only occurs for $k_2 > 10^8\text{ M}^{-1}\text{ s}^{-1}$ when the diffusion limit is approached.

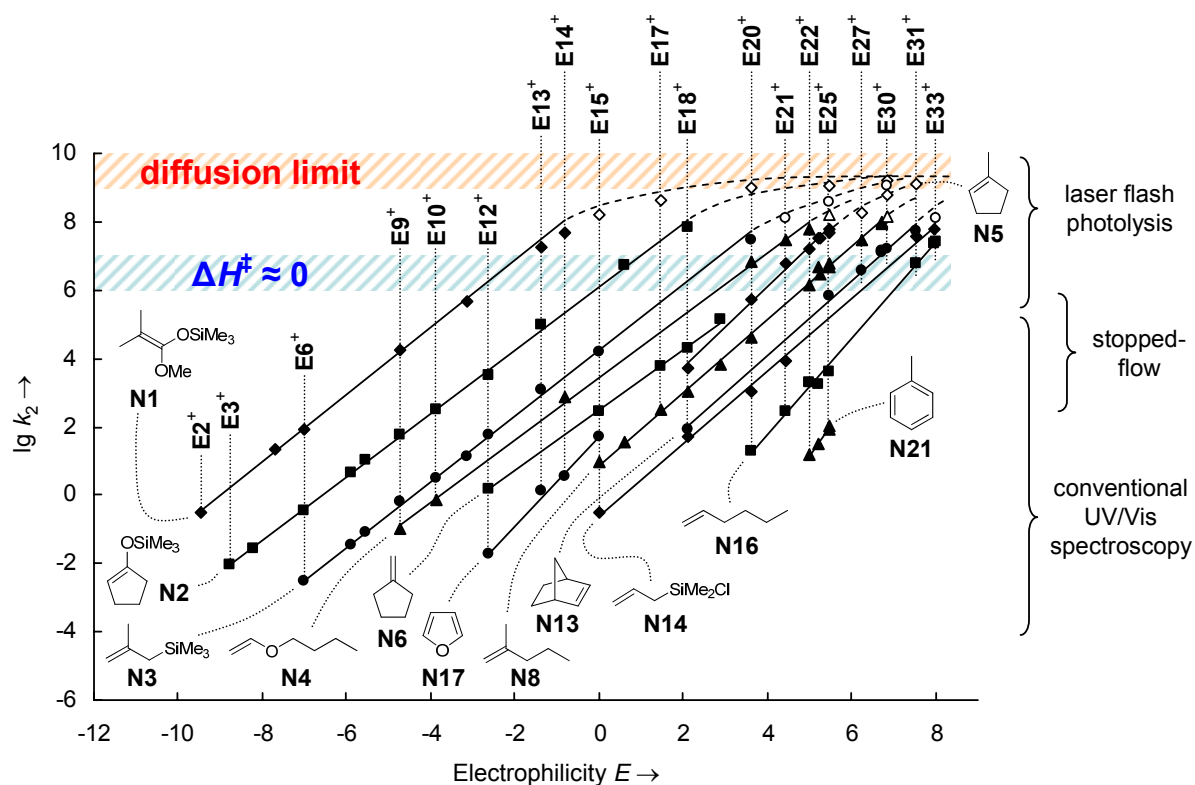


Figure A.6. Plot of $\log k_2$ versus E for the reactions of benzhydryl cations E^+ with π -nucleophiles N . Open symbols indicate rate constants $k_2 > 10^8\text{ M}^{-1}\text{ s}^{-1}$. The blue-shaded area indicates the region where the activation enthalpy reaches the value $\Delta H^\ddagger = 0$ (see text). For the substitution patterns of the benzhydrylium ions $E(1-33)^+$ in this and the following Figures, see Table 3.1 in CHAPTER 3.

The consistency of the newly determined E values was demonstrated by showing that the electrophilicity parameters derived from reactions with π -nucleophiles are also applicable to reactions of these carbenium ions with other types of nucleophiles, such as triethylsilane, acetonitrile, or trifluoroethanol.

CHAPTER 4. *Solvent Nucleophilicities of Hexafluoroisopropanol/Water Mixtures.* First-order rate constants k_1 for the trapping of various donor- and acceptor-substituted benzhydrylium ions in mixtures of 1,1,1,3,3,3-hexafluoro-2-propanol (HFIP) and water ranging from 50 to 99 % HFIP (w/w) were determined by laser flash photolytic generation of benzhydrylium ions from benzhydryl triarylphosphonium salts in these solvents. From these rate constants, we derived the solvent-specific reactivity parameters N_1 and s_N for HFIP/water mixtures as defined by the linear free energy relationship $\log k_1(20\text{ }^\circ\text{C}) = s_N(N_1 + E)$ (Figure A.7).

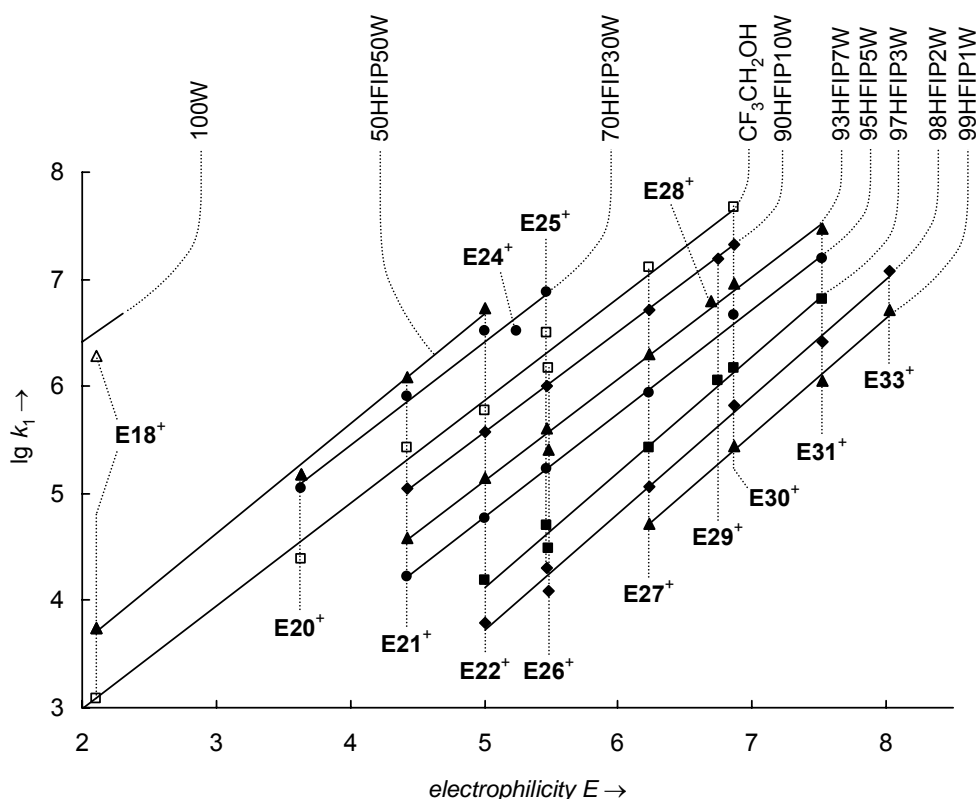


Figure A.7. Plot of $\lg k_1$ versus E for the reactions of benzhydryl cations E^+ with HFIP/water mixtures (filled symbols). For comparison, data for 100W and trifluoroethanol are also shown (open symbols; only a part of the correlation line is shown).

CHAPTER 5. *Substituent Effects on Intrinsic Barriers: A Closer Look on the Basic Principles Behind Linear Free Energy Relationships.* In our previous work, we have investigated reactions of benzhydrylium ions Ar_2CH^+ with different kinds of nucleophiles, including various π -systems, triethyl silane (hydride donor), trifluoroethanol, and different hexafluoroisopropanol/water mixtures. Despite the large structural variations of the nucleophiles, we always found linear correlations of $\lg k$ versus E in reaction series which included reactions of both donor- and acceptor-substituted systems (Fig. A.8).

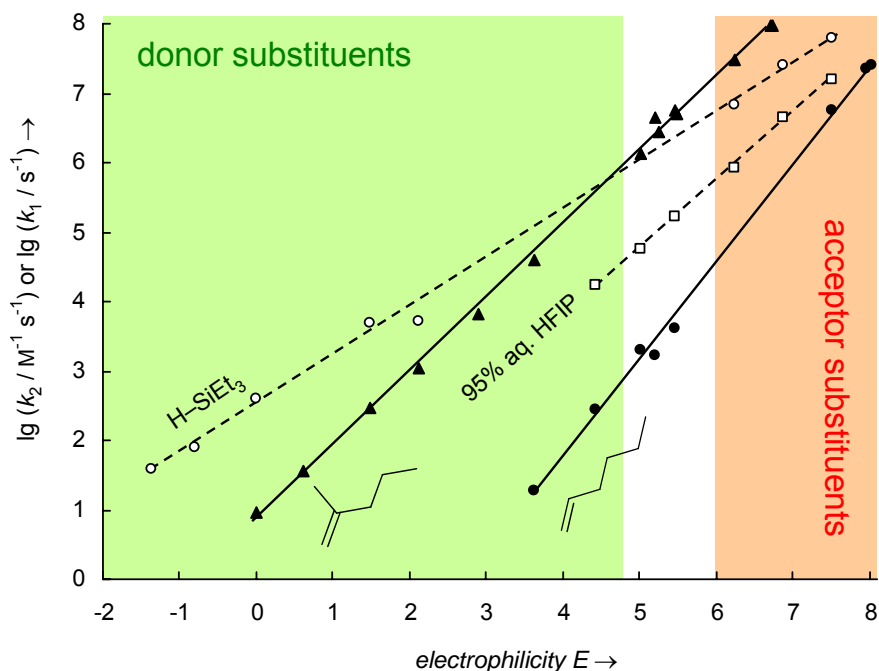


Figure A.8. Plots of $\lg k$ for the reactions of benzhydrylium ions with different nucleophiles against the electrophilicity parameters E of the benzhydrylium ions. Green: Benzhydrylium ions with donor substituents such as *p*-methyl or *p*-alkoxy. Red: Benzhydrylium ions with acceptor substituents such as *m*-fluoro or *p*-(trifluoromethyl). In between: Parent compound and benzhydrylium ions with substituents that combine electron-donating resonance effects with electron-withdrawing inductive effects (e.g., *p*-fluoro).

Gibbs free energy profiles for the reactions of benzhydrylium ions with π -nucleophiles illustrate that for the series of the donor-substituted benzhydrylium ions, the separations of the transition states are much smaller than the stability differences of the carbocations (shown in Fig. A.9 for reactions of 2-methylpent-1-ene with $\mathbf{E15}^+$ to $\mathbf{E20}^+$). In the series of the acceptor-substituted benzhydrylium ions, on the other hand, the separations of the transition states are comparably large and almost of the same magnitude as the stability differences of the carbocations (shown in Fig. A.9 for reactions of 2-methylpent-1-ene with $\mathbf{E25}^+$ to $\mathbf{E30}^+$). This behavior is due to the different dependence of the intrinsic barriers on the substitution of the benzhydrylium ions. While the intrinsic barriers ΔG_0^\ddagger for the reactions of $\mathbf{E(15-25)}^+$ with 2-methylpent-1-ene in CH_2Cl_2 increase linearly with the thermodynamic stabilities of $\mathbf{E(15-25)}^+$, the intrinsic barriers for the reactions of $\mathbf{N8}$ with $\mathbf{E(25-30)}^+$ are almost constant ($\Delta G_0^\ddagger \approx 45 \pm 2 \text{ kJ mol}^{-1}$). This behavior is rationalized by the principle of non-perfect synchronization, which states that the early loss of the resonance stabilization of the donor substituents in \mathbf{E}^+ causes an increase of the intrinsic barrier.

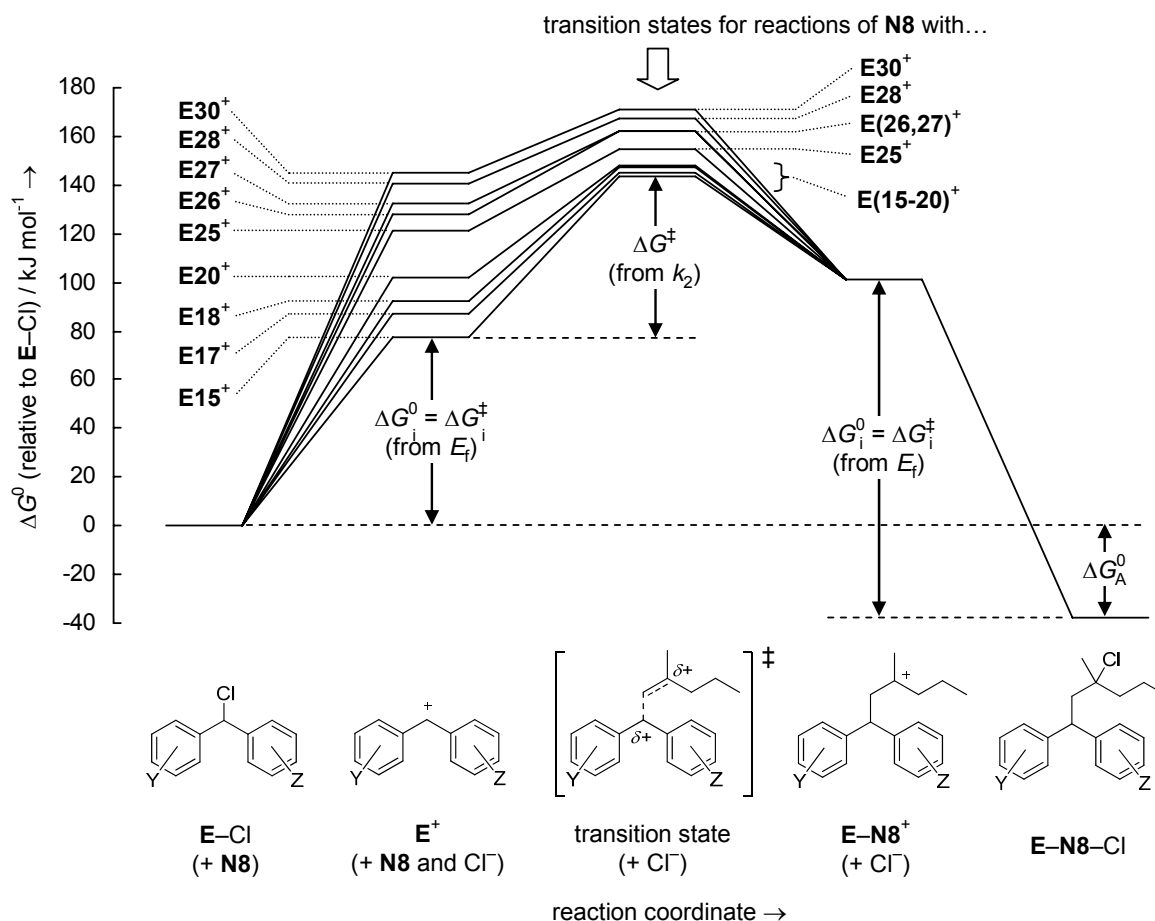


Figure A.9. Gibbs free energy profiles for the reactions of benzhydrylium ions \mathbf{E}^+ with 1 M 2-methylpent-1-ene (**N8**) in CH_2Cl_2 at 20 °C.

The increasing intrinsic barriers in the reactions of benzhydrylium ions with stronger donor substituents also explain the curvatures of plots of E or E_f versus the calculated gas phase methyl anion affinities ΔG_{MA} of the benzhydrylium ions.

From the linear correlations of $\lg k_2$ vs E for reactions of benzhydrylium ions with a variety of structurally different nucleophiles, we conclude that the transition state imbalances resulting from the resonance effects of the substituents in the benzhydryl moiety do not affect the reorganization energy of the nucleophile, but only that of the benzhydryl moiety.

CHAPTER 6. *Electrophilic Reactivity of the α,α -Dimethylbenzyl (Cumyl) Cation*. The cumyl cation was generated by laser flash photolysis of cumyl tris(4-chlorophenyl)phosphonium tetrafluoroborate in CH_2Cl_2 and identified by its UV spectrum (Figure A.10).

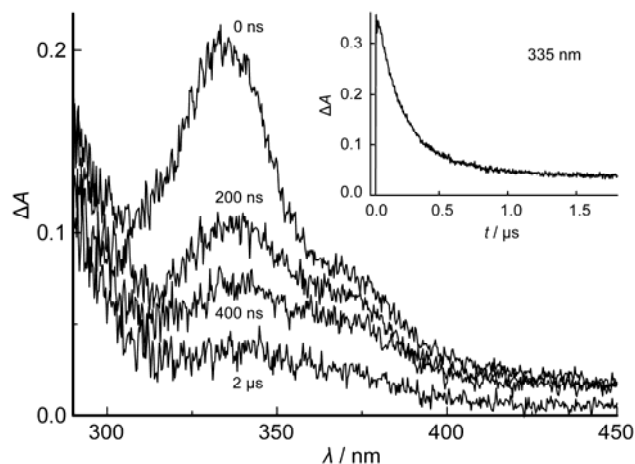
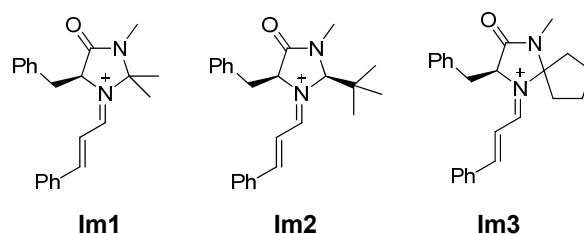


Figure A.10. Transient spectra obtained 0 ns, 200 ns, 400 ns, and 2 μs after 266 nm irradiation of cumyl tris(4-chlorophenyl)phosphonium tetrafluoroborate (8.9×10^{-5} M, $A_{266\text{nm}} = 0.9$) in CH_2Cl_2 . The inset shows the decay at 335 nm during the first 1.8 μs .

From the decay of its absorbance at $\lambda = 335$ nm in the presence of variable concentrations of several nucleophiles with CC double bonds, rate constants for the reactions of the cumyl cation with these nucleophiles were determined. The linear free energy relationship $\log k_2(20^\circ\text{C}) = s_{\text{N}}(N + E)$ was used to calculate the electrophilicity parameter $E = 5.74$ of the cumyl cation from the rate constants determined in this work and the previously reported N and s_{N} parameters of the nucleophilic reaction partners. Substitution of E of the cumyl cation and of the previously reported N and s_{N} parameters of α -methylstyrene into the linear free energy relationship predicts the temperature-independent rate constant of the addition of the cumyl cation to α -methylstyrene ($1.2 \times 10^8 \text{ M}^{-1} \text{ s}^{-1}$), which is relevant for the cationic polymerization of α -methylstyrene.

CHAPTER 7. *Generation of α,β -Unsaturated Iminium Ions by Laser Flash Photolysis.* Iminium ions **Im(1-3)** derived from cinnamaldehyde and imidazolidinones (Chart A.1) were generated by laser flash photolysis of their adducts with tributylphosphine (Figure A.11a).

Chart A.1. Iminium ions derived from cinnamaldehyde and imidazolidinones.



From the decay of the absorbances of the iminium ions in the presence of variable concentrations of added amines or phosphines (Figure A.11b), the rate constants for the reactions of the iminium ions with these nucleophiles were determined (Figure A.11c).

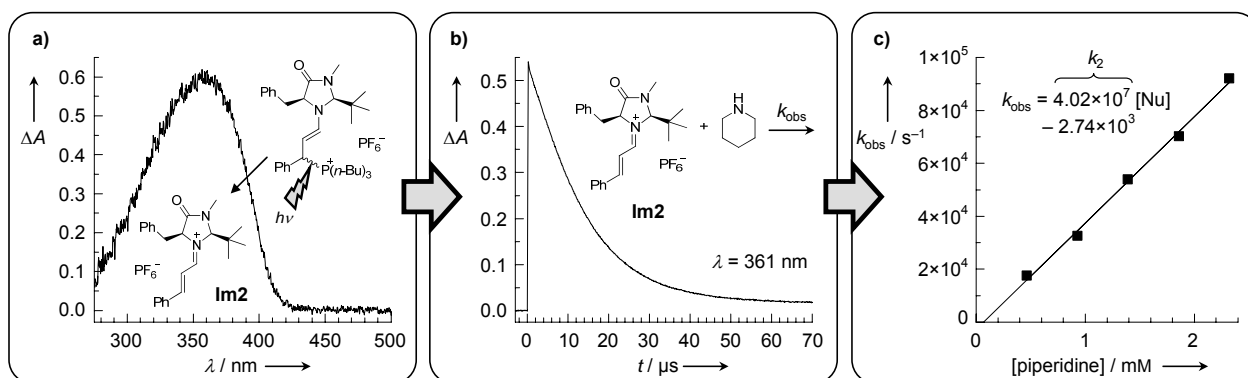


Figure A.11. (a) UV/vis spectrum of **Im2** immediately after the laser pulse in CH_3CN . (b) Decay of the absorbance of **Im2** obtained after irradiation of a 1.51×10^{-4} M solution of its tributylphosphine adduct in CH_3CN in the presence of piperidine (1.86×10^{-3} M). (c) Plot of the pseudo-first-order rate constants k_{obs} (s^{-1}) versus the concentration of piperidine.

The data from the laser flash photolysis measurements agree well with the rate constants for the reactions of the isolated (*E*)-isomers of the iminium salts with weaker nucleophiles, which were determined by conventional UV spectrophotometry and stopped-flow techniques. The rate constants obtained by the different methods and the previously reported N and s_N parameters of the nucleophiles were substituted into the linear free energy relationship $\log k_2(20^\circ\text{C}) = s_N(N + E)$ to calculate the electrophilicity parameters E of the iminium ions (Figure A.12). The iminium ion **Im2** derived from MacMillan's second-generation catalyst is about 10^2 times more reactive than the iminium ions **Im(1,3)**, which explains the greater scope of organocatalytic reactions accessible with MacMillan's second-generation catalyst.

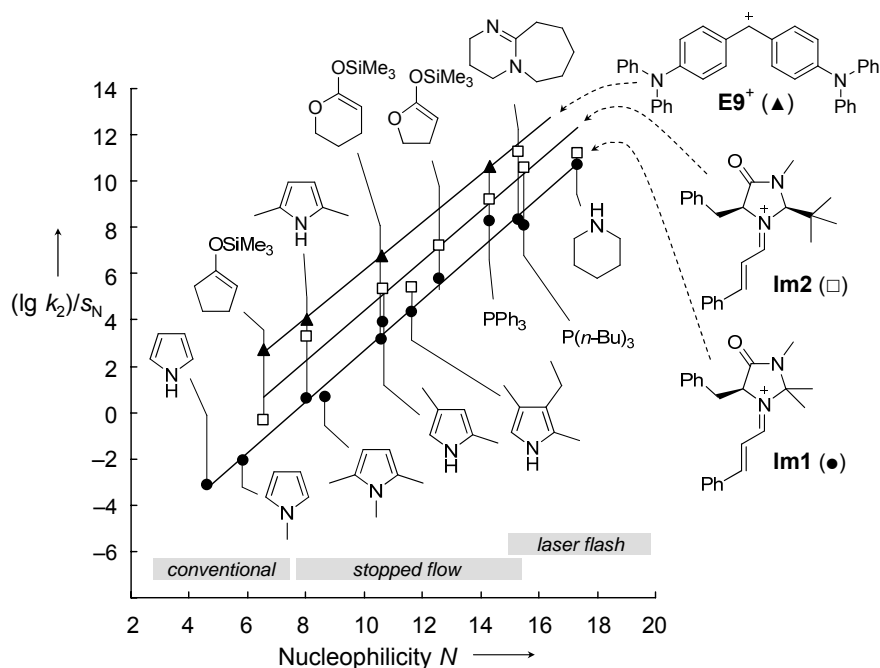
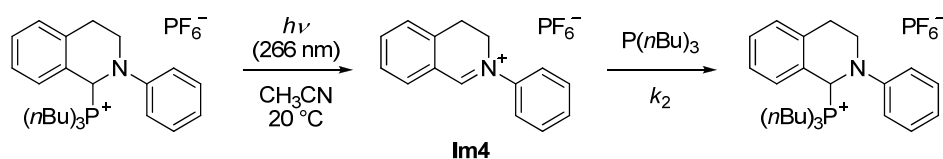


Figure A.12. Correlation of $(\lg k_2)/s_N$ against the nucleophilicity parameters N of the nucleophiles for their reactions with the iminium ions **Im1** and **Im2** and the benzhydrylium ion **E9⁺**.

CHAPTER 8. *Electrophilic Reactivity of the 2-Phenyl-3,4-dihydroisoquinolinium Ion.* The 2-phenyl-3,4-dihydroisoquinolinium ion (**Im4**) was generated by laser flash photolysis of its tributylphosphine adduct in CH_3CN . The second-order rate constant for the reaction of **Im4** with $\text{P}(n\text{Bu})_3$ was determined by generating **Im4** in presence of varying concentrations of PBu_3 and following the decay of its absorbance at 320 nm (Scheme A.2). The rate constants for the reactions of **Im4** with other nucleophiles could not be studied by the laser flash photolysis method, because the phosphonium salt precursor was not stable in the presence of added nucleophiles (irreversible trapping of the small equilibrium concentration of the iminium ion **Im4**).

Scheme A.2. Photogeneration of **Im4** by irradiation of its tributylphosphine adduct in CH_3CN and reaction of **Im4** with $\text{P}(n\text{Bu})_3$ to regenerate the phosphonium salt.



Together with further second-order rate constants for the reactions of **Im4** with nucleophiles, which were determined by stopped-flow UV/vis spectrophotometry, the rate constant for the reaction of **Im4** with $P(n\text{Bu})_3$ and the previously reported N and s_N parameters of the nucleophiles were substituted into the linear free energy relationship $\log k_2(20^\circ\text{C}) = s_N(N + E)$ to obtain the electrophilicity parameter $E = -6.79$ of **Im4** (Figure A.13). Rate constants for the reactions of **Im4** with chiral enamines were measured and compared with the values calculated by substituting the E parameter of **Im4** determined in this work into the linear free energy relationship.

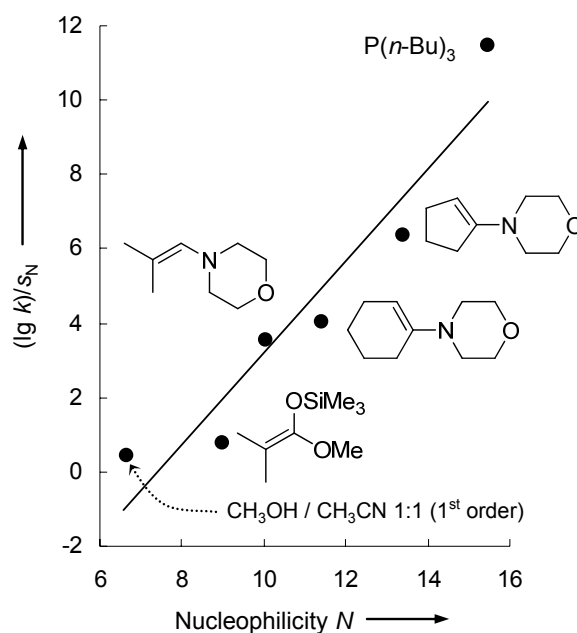


Figure A.13. Plot of $(\lg k_2)/s_N$ versus N for reactions of **Im4** with nucleophiles.

CHAPTER 9. *Nucleophilic Reactivities of Tertiary Alkylamines.* The kinetics of the reactions of triethylamine, *N*-methylpyrrolidine, *N*-methylpiperidine, and *N*-methylmorpholine with benzhydrylium ions have been studied in acetonitrile and dichloromethane. The benzhydryl cations were generated by laser flash photolysis of quaternary phosphonium and ammonium tetrafluoroborates. For most reactions, exponential decays of the absorbances of the benzhydryl cations were observed because the carbocations were generated in the presence of a high excess of the amines (pseudo-first-order conditions). From the linear plots of k_{obs} versus the amine concentrations, the second-order rate constants k_2 were obtained, which allowed us to calculate N and s_N for these amines in CH_3CN and CH_2Cl_2 . The linear free

energy relationship $\log k_2(20^\circ\text{C}) = s_N(N + E)$ was then used to integrate the tertiary amines into our comprehensive nucleophilicity scales (Figure A.14).

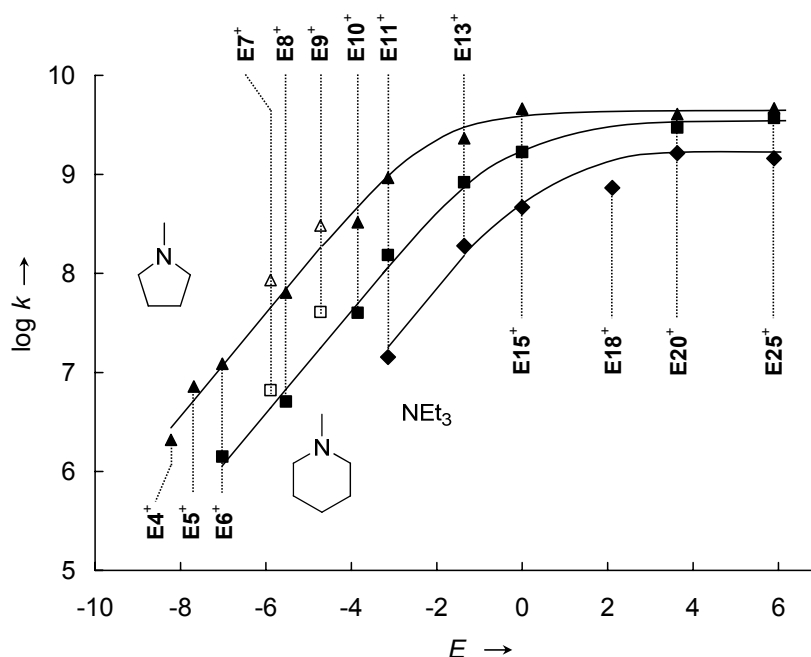
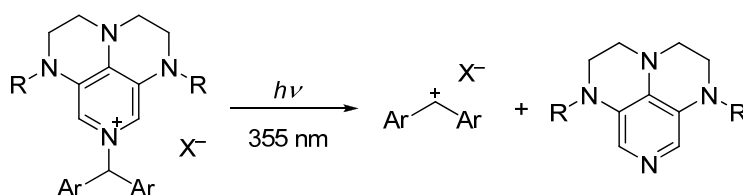


Figure A.14. Correlation of $\log k_2$ for the reactions of triethylamine (\blacklozenge), *N*-methylpyrrolidine (\blacktriangle), and *N*-methylpiperidine (\blacksquare) with benzhydrylium ions \mathbf{E}^+ in CH_3CN at 20°C with the electrophilicity parameters E of the benzhydrylium ions

CHAPTER 10. *Photogeneration of Benzhydryl Cations by Near-UV Laser Flash Photolysis of Pyridinium Salts.* Laser flash irradiation of substituted *N*-benzhydryl pyridinium salts yields benzhydryl cations and/or benzhydryl radicals. The use of 3,4,5-triamino-substituted pyridines as photoleaving groups allowed us to employ the third harmonic of a Nd/YAG laser (355 nm) for the photogeneration of benzhydryl cations (Scheme A.3). In this way, benzhydryl cations can also be photogenerated in the presence of aromatic compounds and in solvents which are opaque at the wavelength of the quadrupled Nd/YAG laser (266 nm).

Scheme A.3. Generation of Benzhydrylium Ions by 355 nm Laser Flash Photolysis of Pyridinium Ions.



To demonstrate scope and limitations of this method, we determined the rate constants for the bimolecular reactions of benzhydryl cations with several substituted pyridines in acetonitrile and with water in acetone. The obtained data agree with results obtained by stopped-flow UV/vis spectroscopic measurements. The rate constants for the reaction of the 4,4'-bis[methyl(2,2,2-trifluoroethyl)amino]benzhydrylium ion with 4-(dimethylamino)pyridine were also determined in dimethyl sulfoxide, *N,N*-dimethylformamide, and acetone. From the second-order rate constants, we derived the nucleophilicity parameters N and s_N for the substituted pyridines, as defined by the linear free energy relationship, $\log k_2(20^\circ\text{C}) = s_N(N + E)$ (Figure A.15).

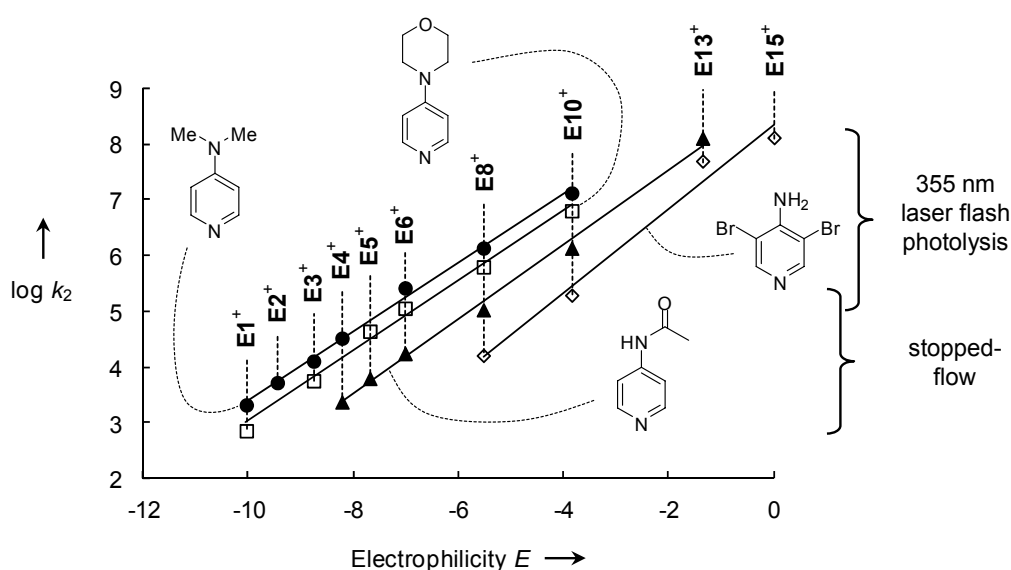


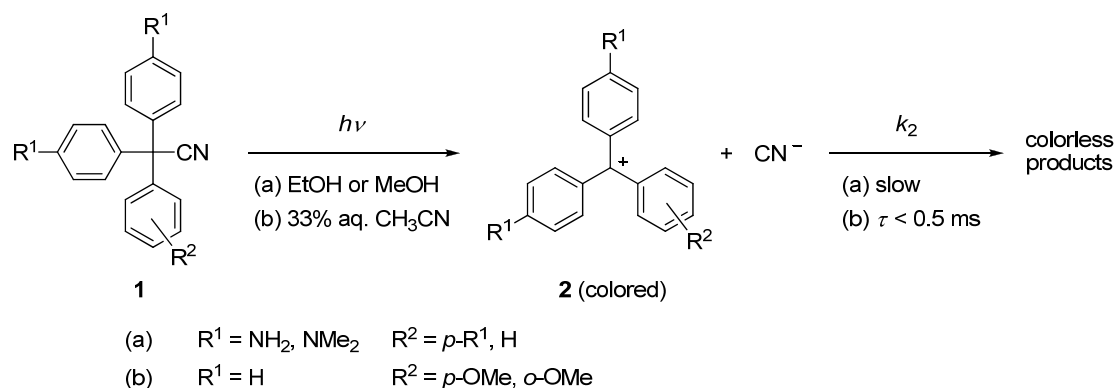
Figure A.15. Plot of $\log k_2$ for reactions of benzhydrylium ions E^+ with substituted pyridines vs the electrophilicity parameters E of the benzhydrylium ions.

CHAPTER 11. *Towards a Rational Design of Precursors for the Photogeneration of Carbocations.* While the previous chapters mostly focus on the chemistry of the photogenerated carbocations, this review chapter provides a summary of the aspects of this work which are relevant for the rational design of precursors for the photogeneration of carbocations, and offers some guidelines for the use of laser flash photolysis in kinetic experiments.

Studying Carbocations by Laser Flash Photolysis

The time-resolved spectroscopic observation of photo-generated transients has been of fundamental importance for the understanding of chemical reactivity. The development of this technique has been awarded with the Nobel Prize in Chemistry on two occasions: In 1967, for the early progress in flash photolysis,^[1,2] and in 1999, for the experimental observation of transition states of chemical reactions by femtosecond spectroscopy.^[3]

Almost a century ago, Lifschitz and Joffé reported the heterolytic photocleavage of amino-substituted 2,2,2-triphenylacetonitriles **1** to the corresponding tritylium ions **2** and cyanide, and observed the subsequent slow disappearance of the carbocations **2** (Scheme B.1a).^[4] However, it is easier to measure the rate constant for the reaction of **2** with cyanide by simply mixing a solution of **2** with a solution of CN^- .^[5]



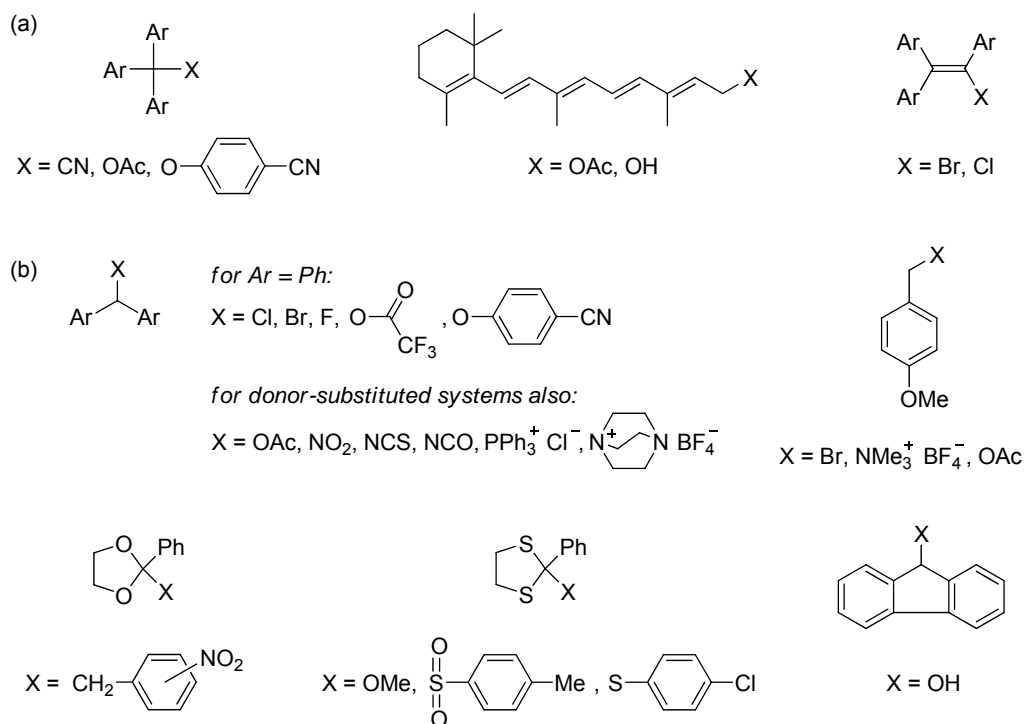
Scheme B.1. Photocleavage of triarylacetonitriles to tritylium ions and cyanide.

When shorter light pulses and faster measurement techniques became available, the photolytic generation of carbocations also became attractive from the viewpoint of a physical organic chemist who is interested in the kinetics of the subsequent reactions of the generated carbocations. The earliest example, where the flash photolysis technique was employed to study carbocations, was a reaction very similar to that described by Lifschitz and Joffé. In 1972, Ivanov *et al.* reported the flash-photolytic generation of methoxy-substituted tritylium ions (**2**) from the corresponding triarylacetonitriles **1** (Scheme B.1b).^[6] These carbocations could not have been investigated under the same reaction conditions by conventional

methods, since their lifetimes were considerably shorter (a few hundred μs) than the time required for the mixing of the reagents.

Other early flash photolysis studies of carbocations focused on triarylmethyl,^[6-8] retinyl,^[9] and triarylvinylyl^[10] cations, which were generated from the corresponding nitriles, acetates, halides, alcohols or *p*-cyanophenyl ethers (Chart B.1a).

Chart B.1. Substrates R–X which were reported to yield carbocations R⁺ upon irradiation.



Since the late 1980s, a large number of studies have employed nanosecond laser flash photolysis^[11] to study the generation and the decay kinetics of carbocations.^[12] Some of the substrates that were successfully employed for the photogeneration of carbocations are shown in Chart B.1b.^[13-19] Valuable information about the formation of carbocationic intermediates in photoreactions has also been derived indirectly from analyses of the products.^[20]

Many rate constants for bimolecular reactions of carbocations with added nucleophiles have been determined by McClelland's group^[8,18,21] and, more recently, by Mayr in collaboration with various other researchers.^[16] The preferred substrates used by these laboratories feature anionic photo-leaving groups such as acetates and *p*-cyanophenolates in alcoholic and aqueous media, as well as halides and pseudohalides in acetonitrile.

Systematic investigations dealing with the question which precursors R–X and reaction conditions are suitable for the generation of a particular carbocation R⁺ are rare. Steenken and

coworkers compared the efficiency of different anionic photo-leaving groups for the generation of Ph_2CH^+ in CH_3CN and achieved the highest yields of Ph_2CH^+ using $\text{Ph}_2\text{CH}-\text{Cl}$ or $\text{Ph}_2\text{CH}-\text{Br}$ as precursors.^[15] It is generally assumed that the photogeneration of carbocations requires solvents of high polarity such as acetonitrile or aqueous solvents.^[12c,20a] Highly reactive carbocations such as arylethyl, arylallyl, and donor-substituted benzyl cations could be observed in fluorinated alcohols like 2,2,2-trifluoroethanol or 1,1,1,3,3,3-hexafluoro-2-propanol.^[13,18,22]

As onium salts are common photoinitiators in cationic polymerizations,^[23] one may find it surprising that prior to this work there were only a handful of laser flash photolysis studies that employed onium salts as precursors for the generation of carbocations.^[13,14,16e] This can in part be explained by the fact that the typical photoinitiation mechanisms do *not* involve the formation of carbocations from the precursor salts.^[23] However, several examples are known where carbocations were thought to be one of the initial cleavage products of onium salt photoinitiators,^[24] and there is also clear evidence of carbocation-derived products from preparative photolyses of onium salts.^[20,25]

One objective of this work is to learn about the factors which control the efficiency of carbocation formation in laser flash photolysis experiments, and to use this knowledge to extend the scope of accessible carbocations, as well as the scope of tolerable reaction conditions for the kinetic experiments. It quickly became apparent that for this purpose, a detailed investigation of the photochemistry of onium salts would be worthwhile. Another objective of this work is to apply the technique to study the reactivities of the generated carbocations towards nucleophiles and acquire quantitative information about the electrophilic reactivities of such carbocations.

For the study of bimolecular reactions of carbocations in solution, a nanosecond laser flash photolysis setup is usually sufficient because the rates of such reactions are limited by diffusion (10^9 to $10^{10} \text{ M}^{-1} \text{ s}^{-1}$). Figure B.1 shows a schematic representation of the instrument employed in this work. A light pulse with a pulse width of a few nanoseconds is generated from a Nd/YAG laser. The fundamental emission is converted to the third or fourth harmonics to obtain laser pulses in the UV with a wavelength of 355 nm or 266 nm, respectively. In a typical experiment, the 266-nm pulses are employed to irradiate 10^{-5} to 10^{-4} M solutions of the precursor molecules, and the UV/vis absorbances of the photogenerated carbocations are monitored. The probe light originates from a xenon short-arc lamp and is collected by an ICCD camera or a photomultiplier. The setup is described in detail in CHAPTER 2.

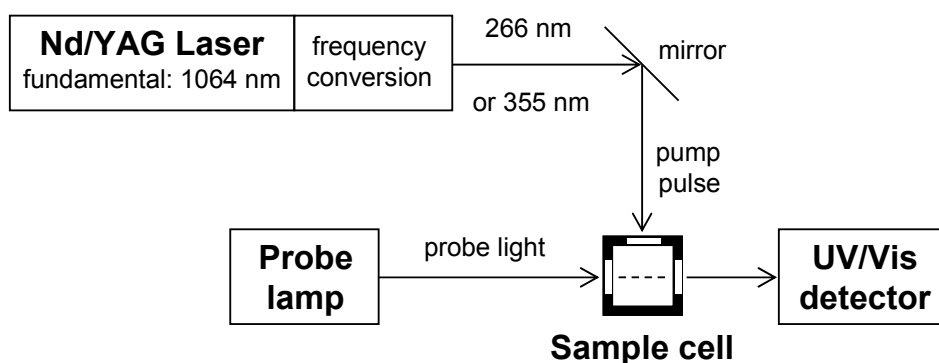


Figure B.1. Schematic setup of the nanosecond laser flash photolysis instrument.

It will be demonstrated that, in many cases, the use of charged precursors such as phosphonium ions is preferable over uncharged precursors which were employed in most of the previous investigations (see above).

Alkyl triarylphosphonium salts. CHAPTER 1 provides information about the structure of triarylphosphonium salts in solution, which forms the basis for an in-depth analysis of the photochemistry of benzhydryl triarylphosphonium salts in CHAPTER 2. This knowledge is used to generate acceptor-substituted benzhydrylium ions and to characterize their electrophilic reactivities towards π -nucleophiles in CHAPTER 3, which provides an extension of the linear free energy relationship $\lg k_2 = s_N(N + E)^{[26]}$ towards more electrophilic systems. By studying the rates of the reactions of photogenerated benzhydrylium ions in hexafluoroisopropanol/water mixtures, CHAPTER 4 demonstrates once more that the electrophilicity parameters E , which were derived from reactions of the benzhydrylium ions with π -nucleophiles in CH_2Cl_2 , are also applicable for reactions with other classes of nucleophiles. Taking advantage of the newly determined electrophilicities of the acceptor-substituted benzhydrylium ions, CHAPTER 5 makes a digression to look at substituent effects in linear free energy relationships. In CHAPTER 6, it is shown that the cumyl cation $\text{PhC}(\text{CH}_3)_2^+$ can only be generated photolytically when tris(*p*-chlorophenyl)phosphine is employed as photo-leaving group, and its electrophilic reactivity is investigated to provide an estimate of the propagation rate in the cationic polymerization of α -methylstyrene.

Other phosphonium, ammonium, and pyridinium salts. Stabilized α,β -unsaturated iminium ions, which are of relevance as intermediates in organocatalytic cycles, are generated by laser flash photolysis of their adducts with tributylphosphine in CHAPTER 7. The same method is employed in CHAPTER 8 to determine the electrophilic reactivity of the 2-phenyl-

3,4-dihydroisoquinolinium ion, which plays a role in oxidative coupling reactions, but the method reaches its limits due to the low Lewis acidity of the iminium ion. In CHAPTER 9, benzhydrylium ions are generated by photolysis of quaternary ammonium salts, and their reactivities towards tertiary amines are studied. Substituted pyridinium salts are employed as precursors for the generation of benzhydrylium ions by 355 nm irradiation in CHAPTER 10, and the usefulness of this approach is demonstrated by measuring the rates of the reactions of benzhydrylium ions with pyridines or acetone/water mixtures.

While the previous chapters focus on the practical applications, CHAPTER 11 provides a summary of the aspects which are relevant for the rational design of precursors for the photogeneration of carbocations, and offers some guidelines for the use of laser flash photolysis in kinetic experiments.

Many collaborators from my own and other research groups contributed to the success of this work, and their names are listed at the beginning of each chapter. To identify my own contributions to the investigations, the Experimental Sections report only those experiments which were performed by me.

References

- [1] (a) R. G. W. Norrish, in *Nobel Lectures, Chemistry 1963-1970*, Elsevier, Amsterdam, **1972**; (b) R. G. W. Norrish, *Angew. Chem.* **1968**, *80*, 868-881.
- [2] (a) G. Porter, in *Nobel Lectures, Chemistry 1963-1970*, Elsevier, Amsterdam, **1972**; (b) G. Porter, *Angew. Chem.* **1968**, *80*, 882-891.
- [3] (a) A. H. Zewail, in *Nobel Lectures, Chemistry 1996-2000* (Ed.: I. Grenthe), World Scientific Publishing, Singapore, **2003**; (b) A. H. Zewail, *Angew. Chem.* **2000**, *112*, 2688-2739; *Angew. Chem. Int. Ed.* **2000**, *39*, 2586-2631.
- [4] J. Lifschitz, *Ber. Dtsch. Chem. Ges.* **1919**, *52*, 1919-1926.
- [5] G. H. Brown, S. R. Adishes, J. E. Taylor, *J. Phys. Chem.* **1962**, *66*, 2426-2430.
- [6] V. B. Ivanov, V. L. Ivanov, M. G. Kuz'min, *Zh. Org. Khim.* **1971**, *8*, 621-623; *J. Org. Chem. USSR* **1971**, *8*, 626-628.
- [7] V. L. Ivanov, V. B. Ivanov, M. G. Kuz'min, *Zh. Org. Khim.* **1972**, *8*, 1248-1250; *J. Org. Chem. USSR* **1972**, *8*, 1263-1265.
- [8] R. A. McClelland, N. Banait, S. Steenken, *J. Am. Chem. Soc.* **1986**, *108*, 7023-7027.
- [9] (a) T. Rosenfeld, A. Alchalal, M. Ottolenghi, *Chem. Phys. Lett.* **1973**, *20*, 291-297; (b) S. K. Chattopadhyay, K. Bobrowski, P. K. Das, *Chem. Phys. Lett.* **1982**, *91*, 143-148; (c) K. K. N. Lo, E. J. Land, T. G. Truscott, *Photochem. Photobiol.* **1982**, *36*, 139-145.
- [10] (a) W. Schnabel, T. Kitamura, S. Kobayashi, H. Taniguchi, *Tetrahedron* **1980**, *36*, 3229-3231; (b) S. Kobayashi, T. Kitamura, H. Taniguchi, W. Schnabel, *Chem. Lett.*

- 1983**, 117-1120; (c) F. I. M. van Ginkel, R. J. Visser, C. A. G. O. Varma, G. Lodder, *J. Photochem.* **1985**, *30*, 453-473.
- [11] (a) J. C. Scaiano, in *Reactive Intermediate Chemistry* (Eds.: R. A. Moss, M. S. Platz, M. J. Jones), Wiley, Hoboken, NJ, **2004**, pp. 847-871; (b) N. P. Schepp, F. L. Cozens, in *Lasers in Chemistry, Vol. 2* (Ed.: M. Lackner), Wiley-VCH, Weinheim, **2008**, pp. 1073-1091.
- [12] Reviews: (a) P. K. Das, *Chem. Rev.* **1993**, *93*, 119-144; (b) R. A. McClelland, *Tetrahedron* **1996**, *52*, 6823-6858; (c) R. A. McClelland, in *Reactive Intermediate Chemistry* (Eds.: R. A. Moss, M. S. Platz, M. J. Jones), Wiley, Hoboken, NJ, **2004**, pp. 3-40.
- [13] R. A. McClelland, C. Chan, F. L. Cozens, A. Modro, S. Steenken, *Angew. Chem.* **1991**, *103*, 1389-1391; *Angew. Chem. Int. Ed.* **1991**, *30*, 1337-1339.
- [14] (a) E. O. Alonso, L. J. Johnston, J. C. Scaiano, V. G. Toscano, *J. Am. Chem. Soc.* **1990**, *112*, 1270-1271; (b) E. O. Alonso, L. J. Johnston, J. C. Scaiano, V. G. Toscano, *Can. J. Chem.* **1992**, *70*, 1784-1794.
- [15] J. Bartl, S. Steenken, H. Mayr, R. A. McClelland, *J. Am. Chem. Soc.* **1990**, *112*, 6918-6928.
- [16] (a) J. Bartl, S. Steenken, H. Mayr, *J. Am. Chem. Soc.* **1991**, *113*, 7710-7716 (b) R. Loos, S. Kobayashi, H. Mayr, *J. Am. Chem. Soc.* **2003**, *125*, 14126-14132; (c) S. Minegishi, R. Loos, S. Kobayashi, H. Mayr, *J. Am. Chem. Soc.* **2005**, *127*, 2641-2649; (d) A. A. Tishkov, U. Schmidhammer, S. Roth, E. Riedle, H. Mayr, *Angew. Chem.* **2005**, *117*, 4699-4703; *Angew. Chem. Int. Ed.* **2005**, *44*, 4623-4626; (e) M. Baidya, S. Kobayashi, F. Brotzel, U. Schmidhammer, E. Riedle, H. Mayr, *Angew. Chem.* **2007**, *119*, 6288-6292; *Angew. Chem. Int. Ed.* **2007**, *46*, 6176-6179; (f) H. F. Schaller, U. Schmidhammer, E. Riedle, H. Mayr, *Chem. Eur. J.* **2008**, *14*, 3866-3868.
- [17] (a) R. A. McClelland, V. M. Kanagasabapathy, S. Steenken, *J. Am. Chem. Soc.* **1988**, *110*, 6913-6914; (b) S. Steenken, R. A. McClelland, *J. Am. Chem. Soc.* **1989**, *111*, 4967-4973; (c) R. A. McClelland, N. Mathivanan, S. Steenken, *J. Am. Chem. Soc.* **1990**, *112*, 4857-4861.
- [18] F. L. Cozens, V. M. Kanagasabapathy, R. A. McClelland, S. Steenken, *Can. J. Chem.* **1999**, *77*, 2069-2082.
- [19] T. Okuyama, N. Haga, S.-y. Takane, K. Ueno, T. Fueno, *Bull. Chem. Soc. Jpn.* **1991**, *64*, 2751-2756.
- [20] Reviews: (a) S. J. Cristol, T. H. Bindel, *Organic Photochemistry* **1983**, *6*, 327-415; (b) P. Wan, K. Yates, *Rev. Chem. Intermed.* **1984**, *5*, 157-181.
- [21] (a) R. A. McClelland, V. M. Kanagasabapathy, N. S. Banait, S. Steenken, *J. Am. Chem. Soc.* **1991**, *113*, 1009-1014; (b) F. Cozens, J. Li, R. A. McClelland, S. Steenken, *Angew. Chem.* **1992**, *104*, 753-755; *Angew. Chem. Int. Ed.* **1992**, *31*, 743-745; (c) R. A. McClelland, V. M. Kanagasabapathy, N. Banait, S. Steenken, *J. Am. Chem. Soc.* **1992**, *114*, 1816-1823; (d) F. L. Cozens, R. A. McClelland, S. Steenken, *J. Am. Chem. Soc.* **1993**, *115*, 5050-5055; (e) S. Steenken, M. Ashokkumar, P. Maruthamuthu, R. A. McClelland, *J. Am. Chem. Soc.* **1998**, *120*, 11925-11931; (f) T. Van Pham, R. A. McClelland, *Can. J. Chem.* **2001**, *79*, 1887-1897.
- [22] G. Hallett-Tapley, F. L. Cozens, N. P. Schepp, *J. Phys. Org. Chem.* **2009**, *22*, 343-348.
- [23] Reviews: (a) J.-P. Fouassier, in *Photoinitiation, Photopolymerization, and Photocuring: Fundamentals and Applications*, Hanser, Munich, **1995**, pp. 102-144; (b) R. Lazauskaite, J. V. Grazulevicius, in *Handbook of Photochemistry and Photobiology, Vol. 2* (Ed.: H. S. Nalwa), American Scientific Publishers, Stevenson Ranch (CA),

- 2003**, pp. 335-392; (c) Y. Yagci, S. Jockusch, N. Turro, J., *Macromolecules* **2010**, *43*, 6245-6260.
- [24] (a) T. Takata, K. Takuma, T. Endo, *Makromol. Chem., Rapid Commun.* **1993**, *14*, 203-206; (b) K. Takuma, T. Takata, T. Endo, *J. Photopolym. Sci. Technol.* **1993**, *6*, 67-74; (c) A. Önen, N. Arsu, Y. Yagci, *Angew. Makromol. Chem.* **1999**, *264*, 56-59; (d) K. H. Jensen, J. E. Hanson, *Chem. Mater.* **2002**, *14*, 918-923; (e) F. Kasapoglu, M. Aydin, N. Arsu, Y. Yagci, *J. Photochem. Photobiol., A* **2003**, *159*, 151-159; (f) C. N. Sanrame, M. S. B. Brandao, C. Coenjarts, J. C. Scaiano, G. Pohlers, Y. Suzuki, J. F. Cameron, *Photochem. Photobiol. Sci.* **2004**, *3*, 1052-1057; (g) N. Yonet, N. Bicak, M. Yurtsever, Y. Yagci, *Polym. Int.* **2007**, *56*, 525-531.
- [25] (a) J. L. Dektar, N. P. Hacker, *J. Am. Chem. Soc.* **1990**, *112*, 6004-6015; (b) J. L. Dektar, N. P. Hacker, *J. Org. Chem.* **1991**, *56*, 1838-1844; (c) D. C. Appleton, D. C. Bull, R. S. Givens, V. Lillis, J. McKenna, J. M. McKenna, S. Thackeray, A. R. Walley, *J. Chem. Soc., Perkin Trans. 2* **1980**, 77-82; (d) C. Imrie, T. A. Modro, E. R. Rohwer, C. C. P. Wagener, *J. Org. Chem.* **1993**, *58*, 5643-5649; (e) C. Imrie, T. A. Modro, C. C. P. Wagener, *J. Chem. Soc., Perkin Trans. 2* **1994**, 1379-1382.
- [26] (a) H. Mayr, T. Bug, M. F. Gotta, N. Hering, B. Irrgang, B. Janker, B. Kempf, R. Loos, A. R. Ofial, G. Remennikov, H. Schimmel, *J. Am. Chem. Soc.* **2001**, *123*, 9500-9512; (b) H. Mayr, B. Kempf, A. R. Ofial, *Acc. Chem. Res.* **2003**, *36*, 66-77; (c) H. Mayr, A. R. Ofial, *J. Phys. Org. Chem.* **2008**, *21*, 584-595; (d) H. Mayr, *Angew. Chem.* **2011**, *123*, 3692-3698; *Angew. Chem. Int. Ed.* **2011**, *50*, 3612-3618.

Ion-Pairing of Phosponium Salts in Solution: C–H···Halogen and C–H··· π Hydrogen Bonds

Johannes Ammer, Christoph Nolte, Konstantin Karaghiosoff, Sebastian Thallmair,

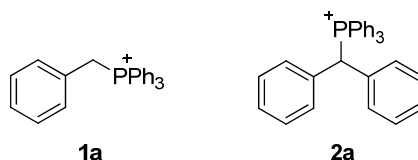
Peter Mayer, Regina de Vivie-Riedle, and Herbert Mayr, 2013, submitted

1.1 Introduction

Hydrogen bonds involving C–H donors have attracted considerable interest in the last two decades,^[1-3] and only recently it became generally recognized that, in many cases, these interactions have to be classified as moderate or even strong hydrogen bonds.^[4]

The C(α)–H protons of alkyl triphenylphosponium salts are particularly acidic^[5,6] so that C(α)–H···X[–] hydrogen bonds between the phosponium ion and its counter-ion X[–] should be quite favorable. The importance of such hydrogen bonds in crystals as well as in solutions of phosponium halides was already demonstrated in a 1964 report that received only little attention.^[7] For example, the CH₂ stretching vibrations of PhCH₂–PPh₃⁺ Cl[–] (**1a** Cl[–], Chart 1.1) in chloroform solution (2853 and 2780 cm^{–1}) are red-shifted ($\Delta\bar{\nu} \approx -80$ cm^{–1}) compared to those of the corresponding BPh₄[–] salt (2937 and 2857 cm^{–1}). Likewise, the CH₂ signals in the ¹H-NMR spectrum of the chloride salt **1a** Cl[–] were reported to be shifted downfield relative to those of the tetraphenylborate **1a** BPh₄[–] ($\Delta\delta_{\text{H}} \approx +0.4$ ppm in CH₃CN).^[7] Spectral shifts as those observed for **1a** Cl[–] are classical criteria for a hydrogen bond.^[8]

Chart 1.1. Structures of the phosponium ions **1a** and **2a**.



Schiemenz and coworkers have collected an enormous wealth of data on ¹H-NMR spectra of phosponium salts and found analogous trends, i. e., that the α -protons of phosponium ions

in chloroform or dichloromethane solution undergo upfield shifts of up to $\Delta\delta_{\text{H}} \approx -3$ ppm when the counter-ion is exchanged from halide to tetraphenylborate.^[9,10] Similar results were found for other onium salts.^[11-15] According to their view, the “ordinary” anion effect resulting from the interaction between the onium cations and “normal” inorganic anions such as halide ions plays only a minor role and is related to the phenomenon of solvation.^[9] Instead, the large upfield shifts for the BPh_4^- salts (e.g., $\Delta\delta_{\text{H}} = -1.41$ ppm for **1a** BPh_4^- compared to **1a** Br^- in CD_2Cl_2)^[9] are predominantly due to the ring current of the BPh_4^- anion’s phenyl rings, which reside above the $\text{C}(\alpha)\text{-H}$ protons of the phosphonium ion as the centers of charge approach each other as closely as possible due to Coulomb attraction.^[9,10,16,17] Based on this effect, many applications of the BPh_4^- anion as shift reagent in NMR spectroscopy have been described.^[9,11-15,18]

One of the examples used by Schiemenz to illustrate the usefulness of the “ BPh_4^- effect” was the possibility to determine $^2J_{\text{H,P}}$ for the α -proton of $\text{Ph}_2\text{CH-PPH}_3^+$ (**2a**).^[9] This could not be achieved in the absence of BPh_4^- due to the overlap of the $\text{C}(\alpha)\text{-H}$ signals with the aromatic protons in the NMR spectra of the corresponding halide salts. In the course of our studies of phosphonium salts as precursors for the photogeneration of carbocations,^[19,20] we required knowledge about the ion pairing of the phosphonium salt **2a** X^- in solution. Much to our surprise, our data clearly showed that the $\text{C}(\alpha)\text{-H}$ protons of **2a** BPh_4^- do not experience any significant ring current effect in CD_2Cl_2 solution. Considering the relevance of phosphonium ion – anion interactions in crystal engineering,^[21] anion recognition,^[22] salt-based solvent systems,^[23,24] photochemistry,^[19,20,25] structure determination,^[10,26] and organic synthesis,^[27,28] we decided to carry out a more detailed investigation of the ion pairing in **2a** X^- and related phosphonium salts.

1.2 Benzhydryl Triphenylphosponium Salts

1.2.1 Syntheses. The phosphonium salts $\text{Ar}_2\text{CH-PR}_3^+ \text{X}^-$ (**2**: $\text{R} = \text{Ph}$, **3**: $\text{R} = p\text{-Cl-C}_6\text{H}_4$), which we have previously used as substrates for the laser flash photolytic generation of benzhydrylium ions (Ar_2CH^+),^[19,20] were obtained by heating the benzhydrols $\text{Ar}_2\text{CH-OH}$ (**4**) with $\text{Ph}_3\text{PH}^+ \text{X}^-$ or by treating the benzhydryl bromides $\text{Ar}_2\text{CH-Br}$ (**5**) with PR_3 and subsequent anion exchange. The syntheses are straightforward but have not yet been described in detail. As the analytical data for these phosphonium salts are relevant for this

investigation, the synthetic procedures and product characterization are now reported in this work (see section 1.S.3).

1.2.2 NMR Investigation of Benzhydryl Triphenylphosphonium Salts (**2** X⁻) in Solution.

¹H-NMR signals for the C(α)-H protons of **2a** in CD₂Cl₂. Ion pairing of the salt Ph₂CH-PPh₃⁺ X⁻ (**2a** X⁻) in CD₂Cl₂ solution is evident from the fact that the NMR spectra of **2a** depend on the counterion X⁻ (Table 1.1).

Table 1.1. ³¹P-NMR (162 MHz), ¹H-NMR (400 MHz) and ¹³C-NMR (100 MHz) data for the phosphonium ion **2a** in CD₂Cl₂. Data for **2a** X⁻ were determined at concentrations where the phosphonium salts exist as ion pairs.

salt	P ⁺	CHP ⁺		<i>o</i> -CHPh ₂	<i>m</i> -CHPh ₂	<i>p</i> -CHPh ₂	<i>o</i> -PPh ₃	<i>m</i> -PPh ₃	<i>p</i> -PPh ₃
	δ _P / ppm	δ _H / ppm (² J _{HP} / Hz)	¹ J _{HC} ^[a] / Hz	δ _H / ppm					
2a Cl ⁻	22.1	8.25 (18.3)	131.3	7.55-7.60 ^[b]	7.20-7.30 ^[b]	7.20-7.30 ^[b]	7.79-7.84	7.55-7.60 ^[b]	7.72-7.77
2a Br ⁻	22.1	8.10 (18.0)	131.1	7.53-7.61 ^[b]	7.21-7.31 ^[b]	7.21-7.31 ^[b]	7.74-7.79 ^[b]	7.53-7.61 ^[b]	7.74-7.79 ^[b]
2a BF ₄ ⁻	21.8	6.23 (17.4)	130.2	7.19-7.22	7.28-7.33	7.35-7.40	7.43-7.49	7.59-7.65	7.81-7.85
2a SbF ₆ ⁻	21.7	5.98 (17.2)	129.3	7.15-7.17	7.30-7.34	7.38-7.44 ^[b]	7.38-7.44 ^[b]	7.61-7.66	7.82-7.87
2a BPh ₄ ⁻	21.6	5.72 (17.1)	128.7	7.05-7.10	7.27-7.36 ^[c]	7.39-7.47	7.27-7.36 ^[c]	7.55-7.62	7.79-7.86
“free” 2a ^[d]	– ^[e]	5.77 (17.0)	– ^[e]	7.09-7.11	7.33-7.37 ^[b]	7.42-7.45	7.33-7.37 ^[b]	7.62-7.65	7.85-7.89
Δ (Cl ⁻) ^[f]	+0.6	+2.53 (+1.2)	+2.6	~ +0.50	~ -0.07	~ -0.18	~ +0.50	~ ±0	~ -0.08
salt	CHP ⁺	<i>i</i> -CHPh ₂	<i>o</i> -CHPh ₂	<i>m</i> -CHPh ₂	<i>p</i> -CHPh ₂	<i>i</i> -PPh ₃	<i>o</i> -PPh ₃	<i>m</i> -PPh ₃	<i>p</i> -PPh ₃
	δ _C / ppm (¹ J _{CP} / Hz)	δ _C / ppm (² J _{CP} / Hz)	δ _C / ppm (³ J _{CP} / Hz)	δ _C / ppm (⁴ J _{CP} / Hz)	δ _C / ppm (⁵ J _{CP} / Hz)	δ _C / ppm (¹ J _{CP} / Hz)	δ _C / ppm (² J _{CP} / Hz)	δ _C / ppm (³ J _{CP} / Hz)	δ _C / ppm (⁴ J _{CP} / Hz)
2a Cl ⁻	45.3 (41.8)	134.3 (4.0)	131.7 (6.9)	129.4 (1.5)	129.0 (2.7)	119.2 (82.3)	135.7 (9.2)	130.3 (12.3)	135.2 (3.1)
2a Br ⁻	45.9 (42.3)	134.1 (4.0)	131.6 (6.8)	129.5 (1.7)	129.2 (2.5)	119.0 (82.4)	135.7 (9.3)	130.3 (12.4)	135.3 (3.1)
2a BF ₄ ⁻	49.6 (43.9)	132.9 (4.1)	131.1 (6.6)	130.0 (1.7)	129.9 (2.6)	118.3 (82.5)	135.3 (9.1)	130.8 (12.4)	135.9 (3.1)
2a SbF ₆ ⁻	50.5 (44.2)	132.6 (4.2)	130.9 (6.6)	130.1 (1.8)	130.0 (2.5)	118.1 (82.7)	135.2 (9.1)	130.8 (12.4)	136.0 (3.1)
2a BPh ₄ ⁻	51.3 (44.3)	132.3 (4.2)	130.8 (6.6)	130.25 (1.7)	130.32 (2.5)	117.9 (82.6)	135.2 (9.1)	131.0 (12.2)	136.3 (3.1)
Δ (Cl ⁻) ^[f]	-6.0 (-2.5)	+2.0 (-0.2)	+0.9 (+0.3)	-0.8 (-0.2)	-1.3 (+0.2)	+1.3 (-0.3)	+0.5 (+0.1)	-0.7 (+0.1)	-1.1 (±0)

[a] ¹J_{HC} determined from ¹³C-satellites in the ¹H-NMR (600 MHz) spectra. [b] Two signals superimposed. [c] Superimposed with *o*-protons of BPh₄⁻. [d] ¹H-NMR (600 MHz) spectrum of a 2.13 × 10⁻⁵ M solution of **2a** SbF₆⁻ in CD₂Cl₂. At this concentration, the phosphonium salt predominantly exists in the form of the free (unpaired) ions. [e] Not available. [f] Difference between **2a** Cl⁻ and **2a** BPh₄⁻ (the latter has virtually the same ¹H-NMR spectrum as “free” **2a**).

The most obvious effect is the large change of the ^1H -NMR chemical shifts ($\Delta\delta_{\text{H}} = +2.53$ ppm) for the $\text{C}(\alpha)\text{-H}$ protons (CHP^+) when X^- is varied from BPh_4^- via SbF_6^- , BF_4^- , and Br^- to Cl^- (Table 1.1). Figure 1.1 shows how this effect depends on the concentration of **2a** X^- .

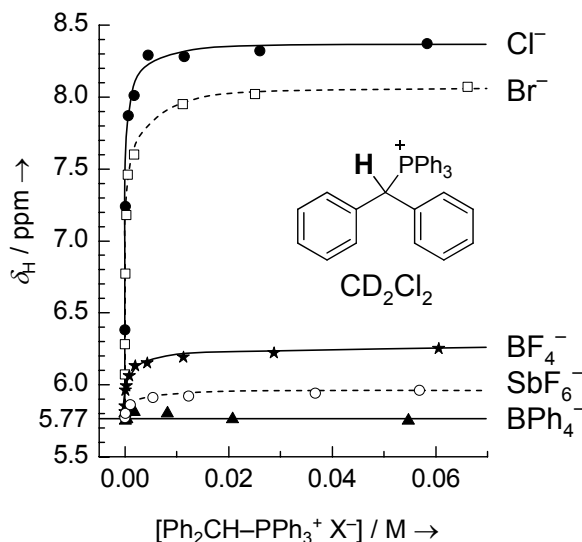


Figure 1.1. Concentration-dependent ^1H -NMR (600 MHz, 27 °C) chemical shifts δ_{H} of the benzylic $\text{C}(\alpha)\text{-H}$ protons of **2a** X^- with different counter-anions $\text{X}^- = \text{Cl}^-$ (●), Br^- (□), BF_4^- (★), SbF_6^- (○), or BPh_4^- (▲) in CD_2Cl_2 .

The δ_{H} values of the $\text{C}(\alpha)\text{-H}$ protons of **2a** BPh_4^- in CD_2Cl_2 are virtually independent of the salt concentration ($\delta_{\text{H}} \approx 5.78$ ppm, Table 1.2). Moreover, the values for **2a** BPh_4^- differ by only 0.2 ppm or less from those of **2a** SbF_6^- . These observations clearly rule out any significant influence of the ring current of the BPh_4^- anions' phenyl rings on the chemical shifts of the $\text{C}(\alpha)\text{-H}$ protons of **2a**, as suggested by Schiemenz.^[9]

Figure 1.1 shows that the δ_{H} values of the $\text{C}(\alpha)\text{-H}$ protons of **2a** X^- with $\text{X}^- = \text{Cl}^-$, Br^- , BF_4^- , or SbF_6^- reach plateaus at concentrations of $[\text{2a } \text{X}^-] > 0.02$ M and we can conclude that at these concentrations we observe ion pairs almost exclusively. Literature NMR spectra of phosphonium salts in CD_2Cl_2 or CDCl_3 solution, which were recorded under typical conditions of NMR measurements, can thus be expected to characterize the ion pairs.

At lower concentrations ($< 5 \times 10^{-3}$ M), the chemical shifts of the $\text{C}(\alpha)\text{-H}$ protons of **2a** X^- with all investigated anions except BPh_4^- decrease markedly and approach δ_{H} of the tetraphenylborate salt (Fig. 1.1). Finally, at a concentration of 2.13×10^{-5} M, the chemical shift of the $\text{C}(\alpha)\text{-H}$ proton of **2a** SbF_6^- reaches a value of $\delta_{\text{H}} = 5.77$ ppm (Table 1.2), which is

Table 1.2. Concentration-dependent $^1\text{H-NMR}$ chemical shifts δ_{H} (600 MHz, CD_2Cl_2) for the C(α)-H protons of $\text{Ph}_2\text{CH-PPH}_3^+$ ions (**2a**) and estimated dissociation constants K_{D} (M) for **2a** X^- salts with different counterions X^- in CD_2Cl_2 .

salt	$[\mathbf{2a} \text{X}^-]$ / M	δ_{H} / ppm	$x_{\text{paired, exp}}$	$K_{\text{D}}^{[\text{a}]}$ / M	$x_{\text{paired, calc}}^{[\text{b}]}$
2a BPh_4^-	1.75×10^{-5}	5.80	–	–	
	1.03×10^{-4}	5.75	–		
	4.07×10^{-4}	5.76	–		
	1.76×10^{-3}	5.81	–		
	8.25×10^{-3}	5.80	–		
	2.08×10^{-2}	5.76	–		
	5.47×10^{-2}	5.75	–		
average δ_{H}		5.78			
2a SbF_6^-	2.13×10^{-5}	5.77	0.00		0.03
	1.07×10^{-4}	5.80	0.16		0.13
	1.02×10^{-3}	5.86	0.47	6×10^{-4}	(0.47)
	5.44×10^{-3}	5.91	0.74		0.72
	1.23×10^{-2}	5.92	0.79		0.80
	3.68×10^{-2}	5.94	0.89		0.88
	5.68×10^{-2}	5.96	1.00		0.90
2a BF_4^-	2.12×10^{-5}	5.81	0.08		0.08
	4.22×10^{-5}	5.85	0.17		0.14
	1.03×10^{-4}	5.96	0.40		0.26
	3.36×10^{-4}	5.99	0.46	2.2×10^{-4}	(0.46)
	8.91×10^{-4}	6.06	0.60		0.61
	2.01×10^{-3}	6.13	0.75		0.72
	4.26×10^{-3}	6.15	0.79		0.80
	1.13×10^{-2}	6.19	0.88		0.87
	2.87×10^{-2}	6.22	0.94		0.92
6.06×10^{-2}	6.25	1.00		0.94	
2a Br^-	1.81×10^{-5}	6.07	0.13		0.17
	3.58×10^{-5}	6.28	0.22		0.26
	1.03×10^{-4}	6.77	0.43	7.6×10^{-5}	(0.43)
	3.04×10^{-4}	7.18	0.61		0.61
	6.09×10^{-4}	7.46	0.73		0.70
	1.83×10^{-3}	(7.6) ^[c]	0.80		0.82
	1.12×10^{-2}	7.95	0.95		0.92
	2.51×10^{-2}	8.02	0.98		0.95
	6.62×10^{-2}	8.07	1.00		0.97
2a Cl^-	2.31×10^{-5}	6.38	0.23		0.32
	1.00×10^{-4}	7.24	0.57	3.4×10^{-5}	(0.57)
	7.13×10^{-4}	7.87	0.81		0.81
	1.76×10^{-3}	8.01	0.86		0.87
	4.45×10^{-3}	8.29	0.97		0.92
	1.14×10^{-2}	8.28	0.97		0.95
	2.61×10^{-2}	8.32	0.98		0.96
	5.83×10^{-2}	8.37	1.00		0.98

[a] Estimate of K_{D} derived from the data for phosphonium salt concentrations where $x_{\text{paired, exp}} \approx 0.5$.[b] Calculated using K_{D} from this table. [c] Superimposed with signals of aryl protons.

practically identical to $\delta_{\text{H}} \approx 5.78$ ppm for **2a** BPh₄⁻. We can therefore assume that this δ_{H} value corresponds to the unpaired Ph₂CH–PPh₃⁺ ions (**2a**).

The assumption that the phosphonium salt **2a** SbF₆⁻ mostly exists in the form of the free ions at this concentration is corroborated by the excellent agreement between the ¹H-NMR spectrum obtained from 2.13×10^{-5} M **2a** SbF₆⁻ and the concentration-independent ¹H-NMR chemical shifts measured for **2a** BPh₄⁻ (Table 1.1). The determination of the K_{D} values listed in Table 1.2 will be discussed below.

Other NMR signals of 2a in CD₂Cl₂ solution. Besides the large change in δ_{H} for the C(α)-H protons, Table 1.1 also shows the effect of the counter-anion X⁻ on other ³¹P-NMR, ¹H-NMR, and ¹³C-NMR signals of **2a** in CD₂Cl₂.

In presence of the Cl⁻ anion, the bond between the α -C and α -H atoms becomes more polarized ($\Delta\delta_{\text{H}} = +2.53$ ppm, $\Delta\delta_{\text{C}} = -6.0$ ppm), while the effect on the positively charged phosphorus atom itself is rather small ($\Delta\delta_{\text{P}} = +0.6$ ppm). The coupling constant $^1J_{\text{H,C}} = 128.7$ Hz for the C(α)-H of **2a** BPh₄⁻ is typical for sp³ carbons,^[29] and increases slightly in the presence of the hydrogen-bond acceptor Cl⁻ ($\Delta^1J_{\text{H,C}} = +2.6$ Hz). A slight increase of $^1J_{\text{H,C}}$ by a few Hz was previously observed for other C–H⋯X hydrogen bonds and may result from the additional electric field component along the C–H bond in presence of the hydrogen bond acceptor.^[30] The 1J and 2J coupling constants between C(α)-H and P change by $\Delta^1J_{\text{C,P}} = -2.5$ Hz and $\Delta^2J_{\text{H,P}} = +1.2$ Hz, respectively.

The *ortho*-protons of the aromatic rings are also deshielded substantially ($\Delta\delta_{\text{H}} \approx +0.50$ ppm), especially if one considers that the effect of the Cl⁻ counter-anion is averaged over six *o*-PPh₃ protons or four *o*-CHPh₂ protons, respectively. Other effects are small: The *i*- and *o*-carbons are also deshielded slightly ($\Delta\delta_{\text{C}} \approx +0.5$ to $+2$ ppm) in the presence of Cl⁻, while the *m*- and *p*-positions of the aromatic rings, on the other hand, are slightly shielded ($\Delta\delta_{\text{H}} \approx 0$ to -0.18 ppm, $\Delta\delta_{\text{C}} \approx -0.7$ to -1.3 ppm). The effects of the Br⁻, BF₄⁻ and SbF₆⁻ anions on the NMR signals of **2a** are similar but less pronounced than those of Cl⁻.

NMR signals of the anions X⁻ in CD₂Cl₂ solution. In order to further characterize the interaction between the phosphonium ions and the anions, we also measured the NMR spectra of the anions. Figure 1.2a shows the ¹⁹F-NMR (376 MHz) spectrum of **2a** BF₄⁻ in CD₂Cl₂ at a concentration where the salt exists as ion pairs (6×10^{-2} M). We observed a 1:1:1:1 quartet

($^1J_{F,B} \approx 1.2$ Hz) at $\delta_F = -152.0$ ppm for the main isotopomer, $^{11}\text{BF}_4^-$ ($I = 3/2$ for the ^{11}B nucleus), together with the unresolved signal for the ^{10}B ($I = 3$) isotopomer ca. 0.05 ppm further downfield. The corresponding signal of the boron atom in the ^{11}B -NMR (128 MHz) spectrum is at $\delta_B = -2.0$ ppm.

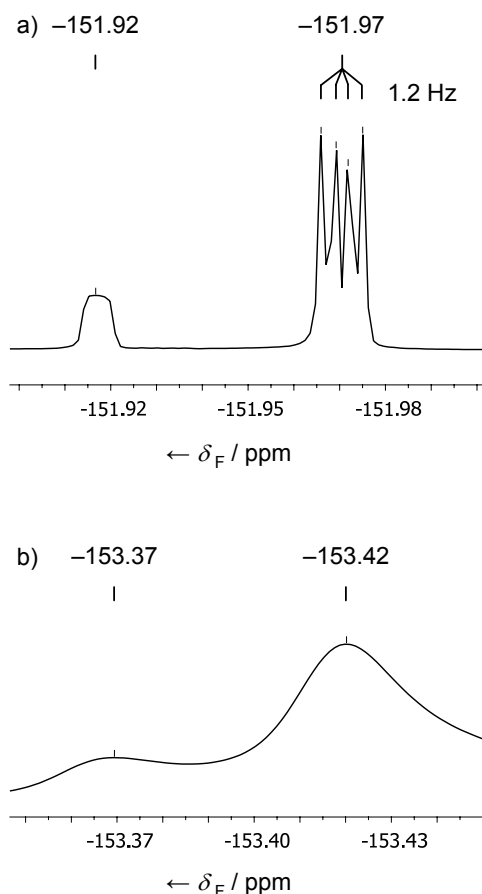


Figure 1.2. ^{19}F -NMR-spectrum (376 MHz) of **2a** BF_4^- in CD_2Cl_2 at concentrations of (a) 6×10^{-2} M, or (b) 2×10^{-5} M.

The ^{19}F -NMR is sensitive enough so that we could also determine the fluorine chemical shift of the BF_4^- anion at a concentration of 2×10^{-5} M, where **2a** BF_4^- exists as free ions in CD_2Cl_2 (Fig. 1.2b). Under these conditions, the signal for the main isotopomer is found at $\delta_F \approx -153.4$ ppm, which is shifted upfield by $\Delta\delta_F \approx -1.4$ ppm compared to the paired **2a** BF_4^- salt. Figure 1.3 shows the heteronuclear NMR spectra of a ca. 6×10^{-2} M solution of **2a** SbF_6^- in CD_2Cl_2 . The antimony isotopes ^{121}Sb ($I = 5/2$) and ^{123}Sb ($I = 7/2$) have similar natural abundances and comparable gyromagnetic ratios ($\gamma = 6.4435 \times 10^7$ rad T^{-1} s^{-1} and $\gamma = 3.4668 \times 10^7$ rad T^{-1} s^{-1} , respectively). The ^{19}F -NMR spectrum of **2a** SbF_6^- in CD_2Cl_2 (Fig. 1.3a) thus features two superimposed signals at $\delta_F = -123.6$ ppm: a sextet with

$^1J_{F,Sb} \approx 1950$ Hz for $^{121}\text{SbF}_6^-$ and an octet with $^1J_{F,Sb} \approx 1020$ Hz for $^{123}\text{SbF}_6^-$. The ratio of the $^1J_{F,Sb}$ coupling constants of the two isotopomers corresponds to the ratio of the gyromagnetic ratios of the antimony isotopes (i. e., the reduced coupling constants, $^1J_{F,Sb}/\gamma$, are the same for both isotopomers). The coupling constant of $^1J_{Sb,F} \approx 1960$ Hz is also found in the ^{121}Sb -NMR (65 MHz) spectrum, in which five peaks of the septet at $\delta_{Sb} \approx 86.2$ ppm are resolved (Fig. 1.3b). Due to the broadness of the signal, we could not detect the ^{19}F -NMR signal of **2a** SbF_6^- at lower concentrations, where the salt is mostly unpaired.

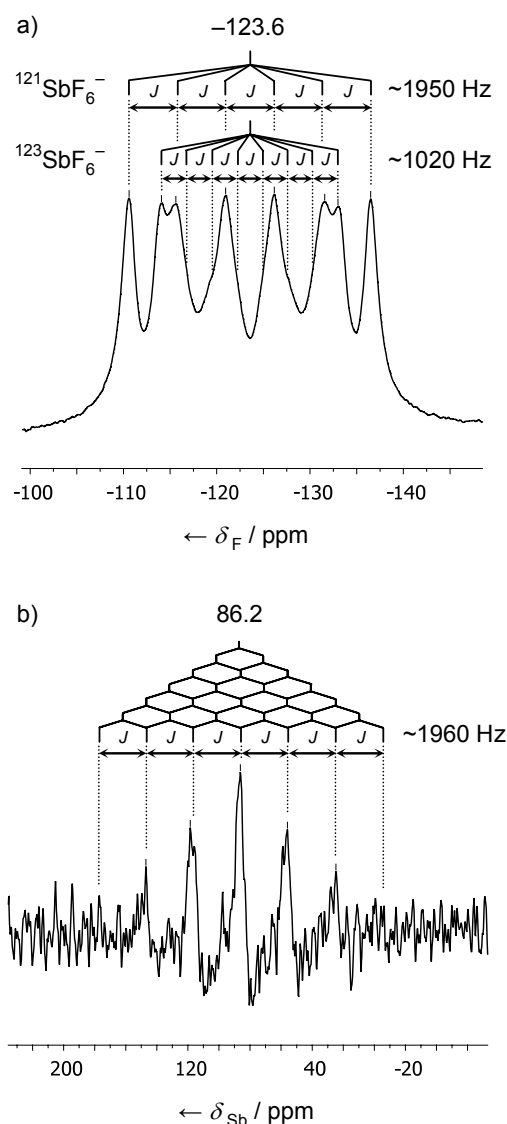


Figure 1.3. (a) ^{19}F -NMR-spectrum (376 MHz) and (b) ^{121}Sb -NMR-spectrum (65 MHz) of **2a** SbF_6^- in CD_2Cl_2 (ca. 0.06 M).

The NMR data for the BF_4^- and SbF_6^- anions shown in Figures 1.2a and 1.3 indicate a very high symmetry of the anions despite the fact that these spectra were recorded under conditions

where the phosphonium salts predominantly exist as ion pairs. This indicates that all fluorine atoms are equivalent on the NMR time scale. The interaction between the BF_4^- anion and the phosphonium ion **2a** can only be noticed by the slight downfield shift of the signal by $\Delta\delta_{\text{F}} \approx -1.4$ ppm, which indicates the averaged effect over four fluorine atoms.

Dissociation constants of 2a X⁻ in CD₂Cl₂. From the C(α)-H proton chemical shift of the unpaired phosphonium ions ($\delta_{\text{H, unpaired}} = 5.77$ ppm) and the chemical shifts of the fully paired phosphonium ions ($\delta_{\text{H, paired}} = \text{maximum } \delta_{\text{H}}$ for the α -proton measured at the highest concentration of **2a** X⁻, Table 1.2), we can derive the mole fraction of paired phosphonium ions, $x_{\text{paired, exp}}$ (Eq. 1).

$$x_{\text{paired, exp}} = \frac{\delta_{\text{H}} - \delta_{\text{H, unpaired}}}{\delta_{\text{H, paired}} - \delta_{\text{H, unpaired}}} \quad (1)$$

At phosphonium salt concentrations where $x_{\text{paired, exp}} \approx 0.5$, we estimated the association constants K_{D} (M) as defined by Eq. 2 in which $[\text{R}_4\text{P}^+ \text{X}^-]_0$ is the total salt concentration.

$$K_{\text{D}} = \frac{[\text{R}_4\text{P}^+]_{\text{unpaired}} \cdot [\text{X}^-]_{\text{unpaired}}}{[\text{R}_4\text{P}^+ \text{X}^-]_{\text{paired}}} = \frac{(1 - x_{\text{paired, exp}})^2}{x_{\text{paired, exp}}} \cdot [\text{R}_4\text{P}^+ \text{X}^-]_0 \quad (2)$$

The obtained dissociation constants K_{D} for **2a** X⁻ in CD₂Cl₂ are listed in Table 2; the mole fractions of unpaired ions $x_{\text{paired, calc}}$ calculated from these K_{D} values are in fair agreement with the experimental values $x_{\text{paired, exp}}$. The dissociation constants K_{D} determined in this manner decrease in the order $\text{SbF}_6^- > \text{BF}_4^- > \text{Br}^- > \text{Cl}^-$. Thus, the degree of association of the salts **2a** X⁻ increases with the deshielding of the C(α)-H protons in the respective ion pairs ($\text{SbF}_6^- < \text{BF}_4^- < \text{Br}^- < \text{Cl}^-$).

Effect of the solvent: ¹H-NMR signals for α -protons of 2a in CD₃CN solution. In CD₃CN, variation of the counter-anion X⁻ has a much lower effect on the ¹H-NMR chemical shifts of the C(α)-H protons of **2a** X⁻ than in CD₂Cl₂ (Fig. 1.4 and Table 1.S.1 in Section 1.S.1). As in CD₂Cl₂, the δ_{H} values for **2a** BPh₄⁻ do not vary with the concentration ($\delta_{\text{H}} = 6.27$ ppm, Fig. 1.4). The very similar δ_{H} values for **2a** BF₄⁻ and **2a** SbF₆⁻ suggest that these compounds are also mostly unpaired at concentrations of $\sim 1 \times 10^{-2}$ M in CD₃CN.

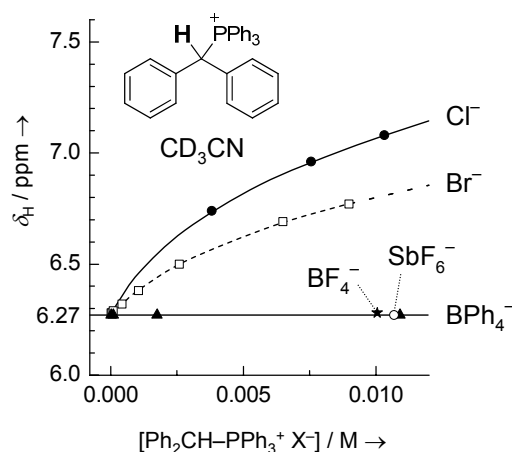


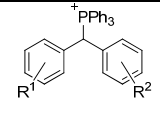
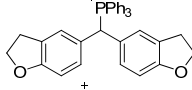
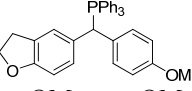
Figure 1.4. Concentration-dependent ^1H -NMR (600 MHz, 27 °C) chemical shifts δ_{H} of the benzylic C(α)-H protons of **2a** X $^-$ with different counter-anions X $^-$ = Cl $^-$ (●), Br $^-$ (□), BF $_4^-$ (★), SbF $_6^-$ (○), or BPh $_4^-$ (▲) in CD $_3$ CN.

The chemical shifts of $\delta_{\text{H}} \leq 6.29$ ppm determined for the C(α)-H protons of **2a** Br $^-$ in CD $_3$ CN at concentrations $\leq 1 \times 10^{-4}$ M indicate that ion pairing is negligible in this concentration range (Table 1.S.1 in Section 1.S.1). At larger concentrations, the phosphonium halides do form ion pairs to some extent. However, the δ_{H} values of the phosphonium halides in CD $_3$ CN do not reach a plateau in the concentration range where **2a** Br $^-$ is soluble in CD $_3$ CN ($< 1 \times 10^{-2}$ M). Therefore, we cannot estimate the degree of ion pairing or the dissociation constants K_{D} in CD $_3$ CN from the NMR data.

Effect of C(α)-H acidity: Substituent effects on the NMR spectra of phosphonium salts. In a series of benzhydryl triphenylphosphonium salts Ar $_2$ CH-PPh $_3^+$ X $^-$ (**2** X $^-$) with different Ar groups, the acidities of the C(α)-H groups increase with the electron-withdrawing character of the substituents on the benzhydryl moiety. The series of donor- and acceptor-substituted benzhydryl triphenylphosphonium tetrafluoroborates **2(a-t)** BF $_4^-$ (Table 1.3), which we required for our laser flash photolysis experiments,^[19,20] can thus be employed to study the interaction between C(α)-H and the BF $_4^-$ anion as a function of C(α)-H acidity. The NMR data for the **2(a-t)** BF $_4^-$ ion pairs in CD $_2$ Cl $_2$ solution are collected in Table 1.3, where the salts **2(a-t)** BF $_4^-$ are arranged according to the sums of their substituents' σ^- parameters.^[31] We use the σ^- parameters as a measure for the C(α)-H acidities of the phosphonium ions here, because the $\text{p}K_{\text{a}}$ values of **2(a-t)** BF $_4^-$ are not available and the $\text{p}K_{\text{a}}$ values of the closely related benzyl triphenylphosphonium salts in DMSO have been shown to correlate with the σ^- parameters of the benzyl substituents.^[6] The ^1H -NMR (400 MHz) chemical shifts of the

C(α)-H protons increase from $\delta_{\text{H}} \approx 6.04$ ppm to $\delta_{\text{H}} \approx 6.80$ ppm when the substituents of the benzhydryl group are varied from electron-donating (**2b**) to strongly electron-withdrawing (**2s** or **2t**). Figure 1.S.1 in Section 1.S.1 displays a moderate correlation of δ_{H} for the C(α)-H protons of **2** BF₄⁻ with the sums of the σ^- parameters.

Table 1.3. Selected NMR data for triphenylphosphonium tetrafluoroborates **2(a-t)** BF₄⁻ in CD₂Cl₂ solution. The spectra were recorded under conditions where the phosphonium salts exist as ion pairs unless otherwise indicated.

salt			P ⁺ -C(α)-H			¹¹ BF ₄ ⁻ [b]	
	R ¹	R ²	$\Sigma\sigma^-$ [a]	δ_{H} / ppm (² J _{H,P} / Hz)	δ_{C} / ppm (¹ J _{C,P} / Hz)	δ_{P} / ppm	δ_{F} / ppm (¹ J _{F,B} / Hz)
<i>Ion pairs:</i>							
2b BF ₄ ⁻			–[c]	6.04 (17.2)	49.1 (42.8)	20.5	–152.2 (–[d])
2c BF ₄ ⁻			–[c]	6.04 (17.2)	48.9 (43.1)	20.6	–152.3 (–[d])
2d BF ₄ ⁻	<i>p</i> -OMe	<i>p</i> -OMe	–0.52	6.15 (17.3)	48.2 (43.2)	20.8	–152.1 (–[d])
2e BF ₄ ⁻	<i>p</i> -OMe	<i>p</i> -Me	–0.43	6.08 (17.2)	48.9 (43.5)	21.0	–152.4 (1.0)
2f BF ₄ ⁻	<i>p</i> -OMe	<i>p</i> -OPh	–0.36	6.18 (17.4)	48.4 (43.5)	21.0	–152.1 (1.1)
2g BF ₄ ⁻	<i>p</i> -Me	<i>p</i> -Me	–0.34	6.04 (17.2)	49.4 (43.6)	21.1	–152.3 (1.1)
2h BF ₄ ⁻	<i>p</i> -OMe	H	–0.26	6.20 (17.2)	48.9 (43.5)	21.3	–152.1 (1.1)
2i BF ₄ ⁻	<i>p</i> -Me	H	–0.17	6.20 (17.4)	49.1 (43.8)	21.5	–152.2 (1.1)
2j BF ₄ ⁻	<i>p</i> -OPh	H	–0.10	6.31 (17.4)	48.6 (43.8)	21.5	–151.8 (1.1)
2k BF ₄ ⁻	<i>p</i> -F	<i>p</i> -F	–0.06	6.49 (17.7)	47.3 (44.7)	21.9	–151.3 (–[d])
2l BF ₄ ⁻	<i>p</i> -F	H	–0.03	6.40 (17.5)	48.1 (44.3)	21.9	–151.5 (1.2)
2a BF ₄ ⁻	H	H	0.00	6.23 (17.4)	49.6 (43.9)	21.8	–152.0 (1.2)
2m BF ₄ ⁻	<i>m</i> -F	H	0.34	6.39 (17.5)	48.5 (44.5)	22.0	–151.6 (1.1)
2n BF ₄ ⁻	<i>p</i> -Cl	<i>p</i> -Cl	0.38	6.48 (17.7)	47.4 (44.6)	21.8	–151.2 (1.2)
2o BF ₄ ⁻	<i>p</i> -CF ₃	H	0.65	6.53 (17.7)	48.4 (44.7)	22.1–22.2	–151.4 (1.2)
2p BF ₄ ⁻	<i>m,m'</i> -F ₂	H	0.68	6.51 (17.5)	47.9 (45.1)	22.2	–151.4 (1.2)
2q BF ₄ ⁻	<i>m</i> -F	<i>m</i> -F	0.68	6.52 (17.6)	47.7 (45.0)	22.3	–151.1 (1.2)
2r BF ₄ ⁻	<i>m,m'</i> -F ₂	<i>m</i> -F	1.02	6.61 (17.6)	47.1 (45.6)	22.5	–150.8 (1.3)
2s BF ₄ ⁻	<i>p</i> -CF ₃	<i>p</i> -CF ₃	1.30	6.80 (17.8)	47.5 (45.3)	22.4–22.5	–150.7 (–[d])
2t BF ₄ ⁻	<i>m,m'</i> -F ₂	<i>m,m'</i> -F ₂	1.36	6.68 (17.6)	46.6 (46.2)	22.6	–150.4 (1.3)
<i>“Free” ions:</i>							
2a ^[e,g]	H	H	0.00	5.77 (17.0)	–[c]	–[c]	–
BF ₄ ⁻ [f,g]	–	–	–	–	–	–	–153.4 (–[d])

[a] From ref.^[31] [b] Isotopomer signal for ¹⁰BF₄⁻ downfield by $\Delta\delta_{\text{F}} < +0.1$ ppm. [c] Not available. [d] Not resolved. [e] Determined from ¹H-NMR (600 MHz) spectrum of a 2.13×10^{-5} M solution of **2a** SbF₆⁻ in CD₂Cl₂. [f] Determined from ¹⁹F-NMR (376 MHz) spectrum of a $\sim 2 \times 10^{-5}$ M solution of **2a** BF₄⁻ in CD₂Cl₂. [g] At the employed concentrations, the salts predominantly exist in the form of the free (unpaired) ions.

If the observed increase of δ_{H} of the C(α)-H protons and the less pronounced concomitant variations in δ_{C} of the C(α) atom and δ_{P} of the phosphorus atom (Table 1.3) are linked with

stronger interactions with the BF_4^- anion, one should also observe the effect in the ^{19}F -NMR spectra of the BF_4^- ions. Indeed, the ^{19}F -NMR chemical shifts for $^{11}\text{BF}_4^-$ increase from $\delta_{\text{F}} \approx -152.2$ ppm to $\delta_{\text{F}} \approx -150.4$ ppm when going from **2b** BF_4^- to **2t** BF_4^- (Table 1.3 and Fig. 1.5). Thus, the greater the $\text{C}(\alpha)\text{-H}$ acidity of the phosphonium ion **2**, the larger the upfield shift $\Delta\delta_{\text{F}}$ for the BF_4^- anion due to the increasing strength of ion pairing with the phosphonium ion. The increasing $\text{C}(\alpha)\text{-H}$ acidity from **2a** BF_4^- ion pairs to **2t** BF_4^- ion pairs causes approximately the same shifts in the ^1H and ^{19}F signals ($\Delta\delta_{\text{H}} \approx +0.45$ ppm and $\Delta\delta_{\text{F}} \approx +1.6$ ppm) as going from the free ions **2a** and BF_4^- to the **2a** BF_4^- ion pairs ($\Delta\delta_{\text{H}} \approx +0.46$ ppm and $\Delta\delta_{\text{F}} \approx +1.4$ ppm). In analogous series of neutral benzhydryl derivatives such as benzhydryl halides, substituent variations induce considerably smaller changes of δ_{H} for the $\text{C}(\alpha)\text{-H}$ protons in the other direction (see Figure 1.S.1 in Section 1.S.1). Moreover, the α -protons of the *unpaired* benzyl triphenylphosphonium ions $\text{PhCH}_2\text{-PPh}_3^+$ (**1a**) and *p*-(CF_3)- $\text{C}_6\text{H}_4\text{-CH}_2\text{-PPh}_3^+$ (**1b**) have very similar δ_{H} values despite the differing substitution patterns (see below). All these observations suggest that the variations in δ_{H} of the benzhydryl methine protons observed for the ion pairs of the differently substituted benzhydryl triphenylphosphonium tetrafluoroborates **2** BF_4^- mainly result from the different interactions of the methine protons with the BF_4^- anions.

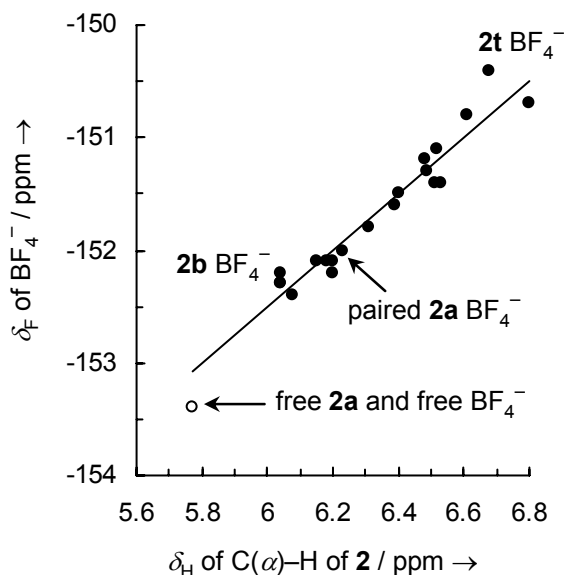


Figure 1.5. Correlation of ^{19}F -NMR (376 MHz) chemical shifts δ_{F} of the BF_4^- anions versus the ^1H -NMR (400 MHz) chemical shifts δ_{H} of the $\text{C}(\alpha)\text{-H}$ protons of the phosphonium ions **2** in the ion pairs **2a-t** BF_4^- in CD_2Cl_2 ($\delta_{\text{F}} = 2.5054\delta_{\text{H}} - 167.54$; $R^2 = 0.9299$). The open circle shows the chemical shifts of the free ions **2a** and BF_4^- (not used for the correlation).

The C(α)-H acidity of benzhydryltriarylphosphonium ions $\text{Ar}_2\text{CH}-\text{PAr}_3^+ \text{X}^-$ can also be increased by variation of the PAr_3 moiety. Table 1.S.2 in Section 1.S.1 illustrates that the δ_{H} values for the C(α)-H protons for the tris(4-chlorophenyl)phosphonium salts $\text{Ar}_2\text{CH}-\text{P}(p\text{-Cl-C}_6\text{H}_4)_3^+ \text{BF}_4^-$ (**3** BF_4^-) are 0.15 to 0.48 ppm higher and the δ_{F} values for the BF_4^- anion are 0.7 to 2.1 ppm higher than for the corresponding triphenylphosphonium salts $\text{Ar}_2\text{CH}-\text{PPh}_3^+ \text{BF}_4^-$ (**2** BF_4^-). Thus, electron-withdrawing substituents in the triphenylphosphonium group have analogous effects on δ_{H} and δ_{F} as substituents in the benzhydryl group.

1.2.3 Quantum Chemical Calculations and Crystal Structures of Benzhydryl Triphenylphosphonium Salts (2a** X^-).** To obtain further insights about the structure of the **2a** X^- ion pairs in solution, we will now compare the NMR data with the results of quantum chemical calculations as well as with the C-H \cdots X $^-$ interactions in the crystals. The structural features in solution and in the crystals resemble each other and will therefore be discussed together for each compound.

Strong hydrogen bonds are characterized by short H \cdots X $^-$ distances and C-H \cdots X $^-$ angles close to 180°, but there are no clear cut-off criteria to decide whether a C-H \cdots X $^-$ contact should be considered a hydrogen bond. According to the latest IUPAC definition of the hydrogen bond,^[8] weak hydrogen bonds may also be longer than the sum of the van der Waals radii, and the angle of a hydrogen bond “should preferably be above 110°”. In the calculated solution structures, as well as in the crystal structures, we have considered all H \cdots X $^-$ distances up to 2.90 Å, and also added some notable longer contacts, the most important of which are shown as dashed lines in the Figures. Particularly short (shorter than the sum of the van der Waals radii)^[32] or particularly linear (C-H \cdots X $^-$ angle $\geq 160^\circ$) contacts are indicated by bold type in the Tables listing the lengths and angles of the C-H \cdots X $^-$ contacts.

*Calculated structures of benzhydryl triphenylphosphonium salts (**2a** X^-) in CH_2Cl_2 solution.*

The solution phase structures of the salts **2a** X^- in dichloromethane were determined by DFT calculations on the M06-2X 6-31+G(d,p) level with a polarizable continuum model to describe the effect of the solvent (Figure 1.6). The solution structure of the BPh_4^- salt was not calculated due to the large size of the ions. Table 1.4 lists the distances and angles of the C-H \cdots X $^-$ contacts in the ion pairs.

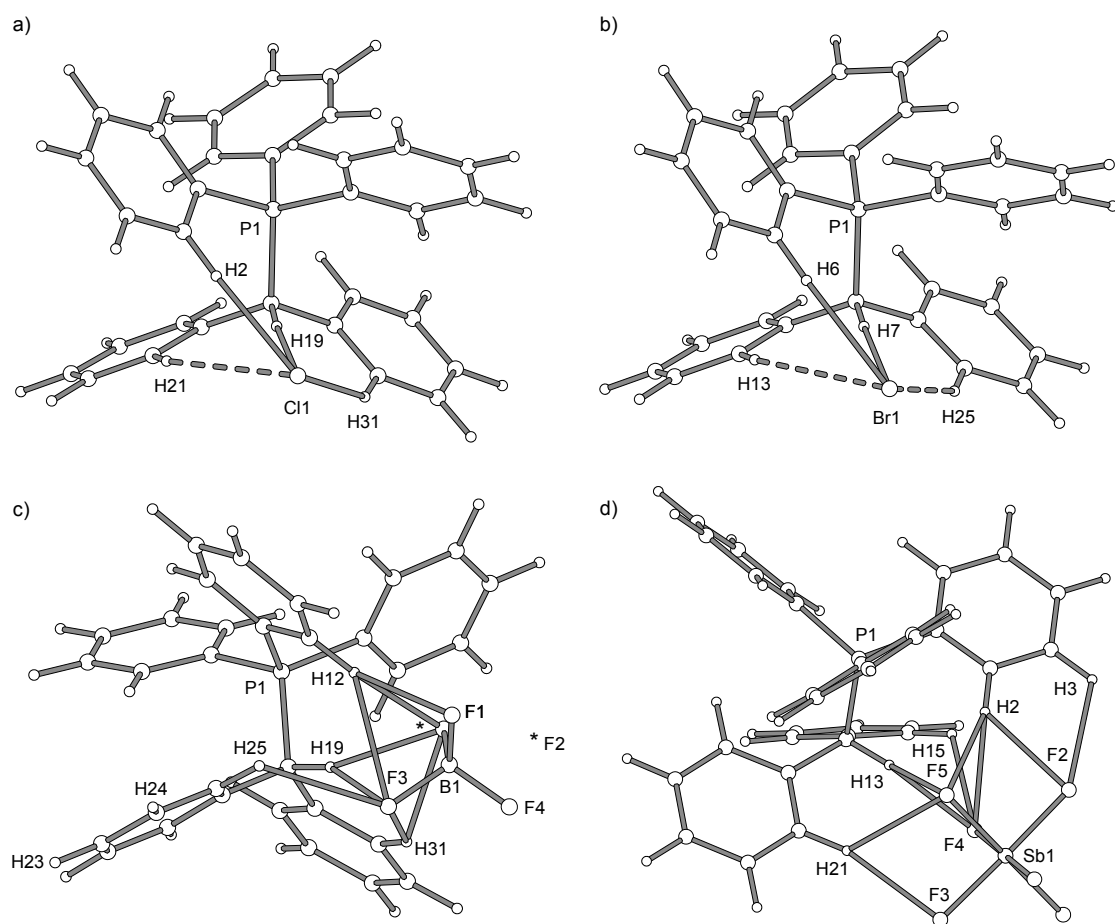


Figure 1.6. Calculated structures of **2a** X^- ion pairs in CH_2Cl_2 solution: (a) **2a** Cl^- , (b) **2a** Br^- , (c) **2a** BF_4^- , (d) **2a** SbF_6^- . The numbering corresponds to the atom numbers in the crystal structures (Fig. 1.7). All contacts with $d(\text{H}\cdots X^-) \leq 2.90 \text{ \AA}$ are shown as bonds, selected longer contacts are indicated by dashed lines. For C–H \cdots X $^-$ bond lengths and angles, see Table 1.4.

Table 1.4. Calculated distances and angles of C–H \cdots X $^-$ contacts in Ph $_2$ CH–PPh $_3^+$ X $^-$ (**2a** X $^-$) ion pairs in CH $_2$ Cl $_2$ solution.

salt	donor ^[a]	acceptor	$d(\text{H}\cdots\text{X}^-) / \text{\AA}$	$d(\text{C}\cdots\text{X}^-) / \text{\AA}$	$\angle(\text{C}-\text{H}\cdots\text{X}^-) / ^\circ$
2a Cl $^-$	H19 (α -H)	Cl1	2.44	3.54	176
	H2	Cl1	2.52	3.61	176
	H31	Cl1	2.81	3.77	147
	H25	Cl1	3.13	4.02	140
2a Br $^-$	H7 (α -H)	Br1	2.64	3.74	177
	H6	Br1	2.68	3.77	178
	H25	Br1	2.93	3.92	152
	H13	Br1	3.24	4.14	141
2a BF $_4^-$	H19 (α -H)	F2	2.30	3.24	142
	H19 (α -H)	F3	2.20	3.23	156
	H12	F2	2.25	3.29	158
	H12	F1	2.38	3.29	140
	H12	F3	2.66	3.56	140
	H31	F2	2.57	3.32	126
	H31	F3	2.71	3.63	142
	H25	F3	2.57	3.32	125
	2a SbF $_6^-$	H13 (α -H)	F4	2.28	3.28
H13 (α -H)		F5	2.44	3.37	141
H2		F4	2.74	3.45	122
H2		F5	2.30	3.36	165
H2		F2	2.42	3.19	126
H3		F2	2.66	3.30	117
H21		F5	2.59	3.34	126
H21		F3	2.44	3.50	165
H15	F4	2.54	3.22	120	

[a] See Figure 1.6 for numbering of atoms.

Crystal structures. Crystal structures of salts of the Ph $_2$ CH–PPh $_3^+$ cation (**2a**) have not been described previously. In this work, we have therefore determined the crystal structures of the salts **2a** X $^-$ with the same anions as we have investigated in solution, with the exception of the BPh $_4^-$ anion. Unfortunately, the tetraphenylborate **2a** BPh $_4^-$ crystallizes as very long thin needles and we could not obtain single crystals of sufficient size in all three dimensions to perform an X-ray structure determination of this salt.

In each of the crystal structures, the phosphonium ions have particularly many C–H \cdots X $^-$ interactions with one particular anion and fewer contacts with other anions (Figure 1.7). The solid state structures thus resemble the 1:1 ion pairs which are present in solution (Figure 1.6). Table 1.5 lists the distances and angles of the closest C–H \cdots X $^-$ contacts in the crystals.

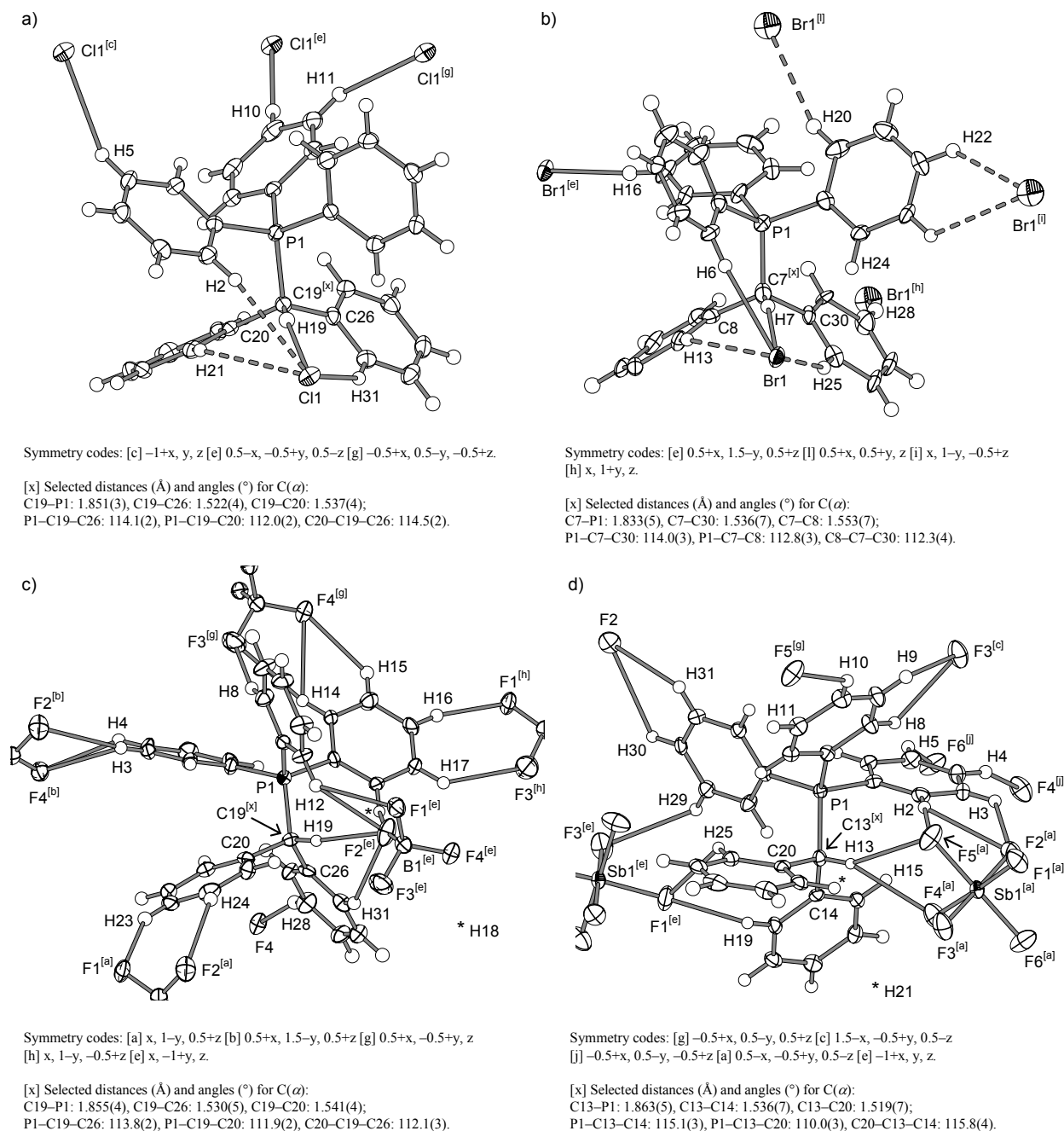


Figure 1.7. Interactions between **2a** and X^- in the crystals: (a) **2a** Cl^- , (b) **2a** Br^- , (c) **2a** BF_4^- , (d) **2a** SbF_6^- . All contacts with $d(H \cdots X^-) \leq 2.90$ Å are shown as bonds, selected longer contacts are indicated by dashed lines. For C-H \cdots X $^-$ bond lengths and angles, see Table 1.5.

Table 1.5. Distances and angles of C–H···X[−] contacts in crystals of Ph₂CH–PPh₃⁺ X[−] (**2a** X[−]).

salt	donor ^[a]	acceptor ^[a]	code ^[a]	$d(\text{H}\cdots\text{X}^-) / \text{\AA}$	$d(\text{C}\cdots\text{X}^-) / \text{\AA}$	$\angle(\text{C}-\text{H}\cdots\text{X}^-) / ^\circ$
2a Cl [−]	H19 (α -H)	Cl1	–	2.49(3)	3.444(3)	166(2)
	H31	Cl1	–	2.82	3.654(3)	147
	H2	Cl1	–	3.00	3.913 (3)	161
	H21	Cl1	–	3.20	3.900(3)	132
	H10	Cl1	e	2.58	3.526(3)	171
	H5	Cl1	c	2.76	3.573(3)	144
	H11	Cl1	g	2.81	3.526(3)	133
2a Br [−]	H7 (α -H)	Br1	–	2.90	3.894(5)	172
	H6	Br1	–	2.85	3.781(5)	167
	H13	Br1	–	3.19	4.000(5)	144
	H25	Br1	–	3.14	4.024(5)	156
	H24	Br1	–	3.68	4.491(5)	146
	H16	Br1	e	2.81	3.672(6)	151
	H20	Br1	l	3.02	3.915(6)	158
	H22	Br1	i	3.05	3.734(5)	131
	H23	Br1	i	3.22	3.828(5)	123
	H28	Br1	h	3.38	4.267(5)	156
2a BF ₄ [−]	H19 (α -H)	F2	e	2.23	3.218(4)	158
	H18	F2	e	2.59	3.340(4)	136
	H12	F2	e	2.53	3.329(4)	141
	H12	F1	e	2.80	3.450(4)	127
	H31	F2	e	2.73	3.423(4)	130
	H23	F1	a	2.44	3.259(4)	144
	H24	F2	a	2.84	3.643(5)	143
	H3	F2	b	2.54	3.467(3)	164
	H3	F4	b	2.67	3.236(4)	119
	H4	F4	b	2.70	3.247(4)	117
	H8	F3	g	2.56	3.482(5)	163
	H14	F3	g	2.59	3.527(4)	170
	H14	F4	g	2.62	3.192(4)	119
	H15	F4	g	2.60	3.179(5)	120
	H16	F1	h	2.29	3.221(3)	167
	H17	F3	h	2.62	3.357(4)	135
	H28	F4	–	2.48	3.407(4)	164
2a SbF ₆ [−]	H13 (α -H)	F4	a	2.67	3.505(5)	151
	H13 (α -H)	F5	a	2.84	3.683(5)	152
	H2	F5	a	2.42	3.372(6)	178
	H2	F2	a	2.72	3.293(5)	120
	H3	F2	a	2.60	3.234(5)	125
	H21	F3	a	3.16	4.096(5)	169
	H25	F1	e	2.85	3.561(6)	133
	H19	F1	e	2.58	3.074(5)	113
	H29	F3	e	2.74	3.208(5)	111
	H31	F2	–	2.59	3.265(5)	129
	H30	F2	–	2.80	3.365(6)	119
	H10	F5	g	2.66	3.373(6)	132
	H11	F5	g	2.95	3.511(6)	119
	H8	F3	c	2.50	3.097(6)	121
	H9	F3	c	2.53	3.114(6)	120
	H4	F4	j	2.54	3.374(6)	147
	H5	F6	j	2.76	3.571(6)	144

[a] See Figure 1.7 for numbering of atoms and symmetry codes.

Benzhydryl triphenylphosphonium chloride (2a Cl⁻). The calculated structure of **2a** Cl⁻ in CH₂Cl₂ (Fig. 1.6a) shows two strong hydrogen bonds between the Cl⁻ anion and the C(α)-H and one *o*-PPh₃ proton (H19...Cl distance 2.44 Å and C19-H19...Cl angle 176°; H2...Cl distance 2.52 Å and C2-H2...Cl angle 176°) (Table 1.4). The positioning of the chloride anion near the C(α)-H and *o*-PPh₃ protons is further stabilized by two weaker hydrogen bonds to *o*-CPh₂ protons of both phenyl rings of the benzhydryl group (H31...Cl distance 2.81 Å and C31-H31...Cl angle 147°; H25...Cl distance 3.13 Å and C25-H25...Cl angle 140°).

These interactions seem to be so favorable that they are also found in the crystal (Fig. 1.7a), which shows two short contacts between Cl⁻ and the C(α)-H as well as one *o*-CPh₂ proton (H19...Cl distance 2.49 Å and C19-H19...Cl⁻ angle 166°; H31...Cl distance 2.82 Å, C31-H31...Cl⁻ angle 147°), but a significantly longer distance between the Cl⁻ anion and the *o*-PPh₃ proton (H2...Cl distance 3.00 Å and C2-H2...Cl angle 161°) (Table 1.5). The packing of the molecules is controlled by additional C-H...Cl⁻ hydrogen bonds involving some of the *m*- and *p*-protons of the PPh₃ group, resulting in a different orientation of the phenyl groups compared to the solution structure. Particularly strong is the C-H...Cl⁻ interaction for one of the *p*-PPh₃ protons (H10...Cl distance 2.58 Å and C10-H10...Cl angle 171°). Thus, the distances and angles for the two shortest C-H...Cl⁻ interactions in crystals of **2a** Cl⁻ come very close to the typical values of O-H...Cl⁻ hydrogen bonds.^[3]

Benzhydryl triphenylphosphonium bromide (2a Br⁻). The calculated structure of the **2a** Br⁻ ion pair in CH₂Cl₂ (Fig. 1.6b) closely resembles that of the chloride (Fig. 1.6a); only the distances between the hydrogen (or carbon) atoms and the halide ion are longer by 0.1 to 0.2 Å (Table 1.4).

Again, a similar motif is found in the **2a** Br⁻ crystal (Fig. 1.7b and Table 1.5): The strongest interactions between cation and anion are the hydrogen bonds between the Br⁻ anion and the C(α)-H and *o*-PPh₃ protons (H7...Br distance 2.90 Å and C7-H7...Br⁻ angle 172°; H6...Br distance 2.85 Å, C6-H6...Br⁻ angle 167°), as well as the interaction of one *m*-PPh₃ proton with a second bromide anion (H16...Br⁻ distance 2.81 Å and C16-H16...Br⁻ angle 151°). Weaker interactions are observed between Br⁻ and the *o*-CHPh₂ protons as well as another *o*-PPh₃ proton, but these are already in the same range as the interactions between Br⁻ and various phenyl protons of further surrounding phosphonium ions (≥ 3.0 Å).

Benzhydryl triphenylphosphonium tetrafluoroborate (2a BF₄⁻). In the calculated structure of the tetrafluoroborate **2a** BF₄⁻ in dichloromethane solution (Fig. 1.6c), the C(α)-H (H19) as well as one *o*-PPh₃ (H12) and one *o*-CPh₂ proton (H31) show bifurcated hydrogen bonds with two of the fluorine atoms (F2 and F3) (Table 1.4). Additionally, the *o*-PPh₃ proton (H12) has a third C-H...F-BF₃⁻ interaction with a third fluorine atom (F1), and the second phenyl group of the benzhydryl moiety also shows one contact between *o*-CPh₂ (H25) and F-BF₃⁻ (F3).

In the **2a** BF₄⁻ crystal, all fluorine atoms of the BF₄⁻ anion exhibit multifurcated hydrogen bonds to several surrounding phosphonium ions. The usual pattern of close interactions between the the anion and the C(α)-H proton (H19), one *o*-PPh₃ (H12), and one *o*-CPh₂ proton (H31) is also found (Fig. 1.7c and Table 1.5), but it differs somewhat from the calculated structure in solution. Again, the shortest contact is the C(α)-H...F-BF₃⁻ interaction (H19...F2 distance 2.23 Å and C19-H19...F2 angle 158°), but in the crystal, only the *o*-PPh₃ proton (H12) shows bifurcated hydrogen bonds, while the other interactions are directed towards only one of the fluorine atoms. The fourth close C-H...F-BF₃⁻ contact is now a second *o*-PPh₃ proton (H18) instead of the second *o*-CPh₂ proton. This subtle variation between the solution and crystal structures is caused by the additional interactions between BF₄⁻ and the other surrounding phosphonium ions in the crystal (Table 1.5).

Benzhydryl triphenylphosphonium hexafluoroantimonate (2a SbF₆⁻). According to the calculations, the fluorine atoms of the SbF₆⁻ anions in the **2a** SbF₆⁻ ion pairs in CH₂Cl₂ solution also form multifurcated hydrogen bonds (Fig. 1.6d and Table 1.4). The C(α)-H proton forms a short bifurcated hydrogen bond with two of the fluorine atoms (H13...F4 distance 2.28 Å and C13-H13...F4 angle 151°; H13...F5 distance 2.44 Å and C13-H13...F5 angle 141°). The same two fluorine atoms are also involved in a bifurcated hydrogen bond with one of the *o*-PPh₃ protons (H2...F5 distance 2.30 Å and C2-H2...F5 angle 165°; H2...F4 distance 2.74 Å and C2-H2...F4 angle 122°), and each of them also has a weaker interaction with an *o*-CPh₂ proton (H15 or H21) (Table 1.4). A further strong hydrogen bond is found between one of the *o*-CPh₂ protons and a third fluorine atom (H21...F3 distance 2.44 Å and C21-H21...F3 angle 165°), and two weaker interactions between the *o*-PPh₃ (H2) and *m*-PPh₃ (H3) protons and a fourth fluorine atom (F2) (Table 1.4).

The fluorine atoms of the SbF₆⁻ anions in the **2a** SbF₆⁻ crystal also form multifurcated hydrogen bonds, but the C-H...F interactions differ somewhat from those in CH₂Cl₂ solution (Fig. 1.7d and Table 1.5). The closest C-H...F-SbF₅⁻ contact is between an *o*-PPh₃ proton and

one of the fluorine atoms (H2...F5 distance 2.42 Å and C2–H2...F5 angle 178°). This proton also has a second weaker interaction with another fluorine atom (F2), which also forms a hydrogen bond to the adjacent *m*-PPh₃ proton (H3). The bifurcated hydrogen bonds between the C(α)–H proton and the SbF₆[−] anion are significantly longer than in solution or in the crystals of the other salts (H13...F4 distance 2.67 Å and C13–H13...F4 angle 151°; H13...F5 distance 2.84 Å and C13–H13...F5 angle 153°), and the typical interaction with one or more *o*-CPh₂ protons is not found (Fig. 1.7d). Instead, the *o*-CPh₂ protons (H19 and H25) form hydrogen bonds to a second SbF₆[−] anion which is located on the far side of the C(α)–H proton. The packing of the ions is also influenced by several other contacts between the protons of the PPh₃ groups and neighboring SbF₆[−] anions (Fig. 1.7d and Table 1.5).

1.2.4 Benzhydryl Triphenylphosphonium Salts: C–H...X[−] Hydrogen Bonds in Solution.

The NMR data of the phosphonium salts **2a** X[−] in CD₂Cl₂ solution had shown that ion pairing with the counter-anion X[−] mainly affects the proton resonances of the C(α)–H, *o*-PPh₃, and *o*-CPh₂ protons of **2a** (Table 1.1). A comparison with the crystal structures of these salts (Fig. 1.7 and Table 1.5) reveals that these protons are also involved in the shortest and most linear C–H...X[−] contacts in the crystals. The formation of C–H...X[−] hydrogen bonds in solutions of **2** X[−] is consistent with the strong deshielding of the respective protons, as well as the observed increase of the deshielding with increasing C–H acidity and with increasing basicity of the anions X[−] (Cl[−] > Br[−] > BF₄[−] > SbF₆[−]).^[33]

An anion's ability to act as hydrogen bond acceptor is related to its single free ion energy of transfer ΔG_t^0 (H₂O → CH₃CN),^[34] since a large contribution to the transfer energy is the loss of the HO–H...X[−] hydrogen bonds with the good hydrogen bond donor H₂O. Figure 1.8 illustrates that the chemical shifts δ_H for the C(α)–H protons of **2a** X[−] and other arylmethyl phosphonium salts in CD₂Cl₂ or CDCl₃ correlate linearly with ΔG_t^0 (H₂O → CH₃CN) of the anions.

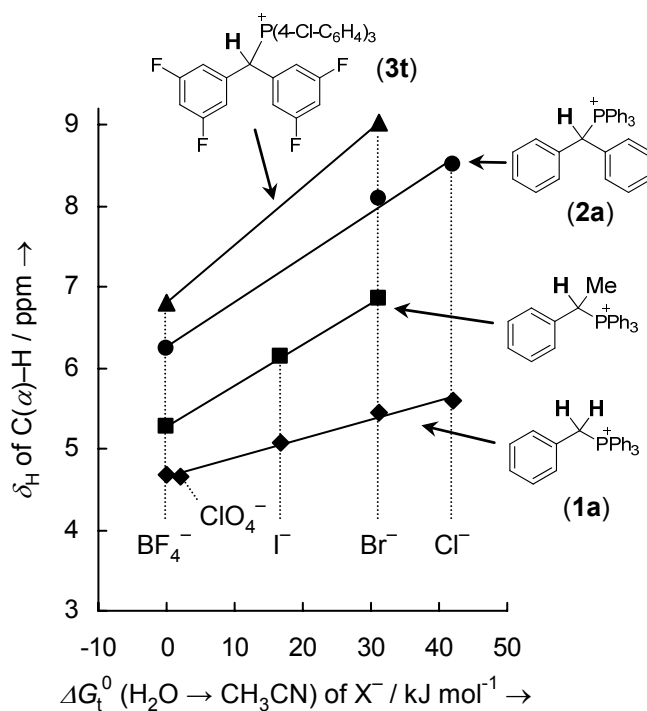


Figure 1.8. Plot of ^1H -NMR chemical shifts δ_{H} for the benzylic α -protons in arylmethyl triarylphosphonium salts (ion pairs) with different counter-anions X^- in CD_2Cl_2 (**2a**, **3t**) and CDCl_3 (other salts) against the single free ion energies of transfer $\Delta G_{\text{t}}^0 (\text{H}_2\text{O} \rightarrow \text{CH}_3\text{CN})$ of the anions X^- . The point for **2a** BPh_4^- deviates from the correlation (not shown). See Table 1.S.3 in Section 1.S.1 for numeric values and references.

The results of our quantum chemical calculations also confirm $\text{C-H}\cdots\text{X}^-$ hydrogen bonds for the $\text{C}(\alpha)\text{-H}$, $o\text{-PPh}_3$, and $o\text{-CPh}_2$ protons of **2a** X^- ion pairs in dichloromethane solution (Fig. 1.6 and Table 1.4). Moreover, we calculated the ^1H -NMR chemical shifts for the ion pairs in CD_2Cl_2 solution with the gauge-independent atomic orbital method (GIAO)^[35] and the functional WP04^[36] (Table 1.6). This method has been developed especially for the calculation of ^1H -NMR data.^[36] For the calculation of the ^1H -NMR data we additionally used pseudo potentials for all atoms from the third period on.^[37] For a comparison with the experimental data, the δ_{H} values were averaged for both α -protons of the benzyl systems, all $o\text{-CPh}$ protons, or all six $o\text{-PPh}_3$ protons, respectively. The experimentally observed trends are fairly well reproduced by the calculated ^1H -NMR shifts of the optimized solution structures. Slight deviations are caused by the fact that the calculations refer to the most stable configuration, while the experimental data reflect a statistical distribution of different configurations. The implicit solvent continuum used for the calculations is also a potential source of error.

Table 1.6. Comparison of calculated and experimental ^1H -NMR chemical shifts δ_{H} for **2a** X^- and **1a,b** X^- in CD_2Cl_2 solution under conditions where the salts exist as ion pairs.

salt	$\delta_{\text{H}}(\text{CHP}^+)^{[\text{a}]}$ / ppm		$\delta_{\text{H}}(o\text{-CPh})^{[\text{a}]}$ / ppm		$\delta_{\text{H}}(o\text{-PPh}_3)^{[\text{a}]}$ / ppm	
	calc. ^[b]	exp.	calc. ^[b]	exp.	calc. ^[b]	exp.
2a Cl^-	8.01	8.25	7.43	7.55-7.60	7.54	7.79-7.84
2a Br^-	7.71	8.10	7.61	7.53-7.61	7.34	7.74-7.79
2a BF_4^-	6.57	6.23	7.33	7.19-7.33	6.99	7.43-7.49
2a SbF_6^-	6.22	5.98	6.98	7.15-7.17	6.95	7.38-7.44
“free” 2a ^[c]	5.84	5.77	6.74	7.09-7.11	6.71	7.33-7.37
1a Cl^-	6.33	5.42	7.39	7.07-7.10	7.76	7.70-7.76
1a BF_4^-	5.04	4.56	6.58	6.91-6.94	7.16	7.48-7.54
“free” 1a ^[c]	4.09	~4.37	6.39	6.87-6.89	6.91	7.43-7.46
1b Br^-	5.07	5.78	7.19	7.36	7.33	7.76-7.82
1b BF_4^-	5.00	4.72	6.78	7.11	7.16	7.54-7.60
“free” 1b ^[c]	4.10	~4.44	6.39	7.04	6.95	7.47-7.51

[a] Averaged δ_{H} of both α -protons of the benzyl systems, all six $o\text{-PPh}_3$ protons, or all $o\text{-CPh}$ protons, respectively. [b] From quantum chemical calculations (see text). [c] Experimental values determined from ^1H -NMR (600 MHz) spectra of ca. 2×10^{-5} M solutions of the SbF_6^- , BF_4^- and/or BPh_4^- salts in CD_2Cl_2 . At these concentrations, the phosphonium salts predominantly exist in the form of the free (unpaired) ions.

In contrast to earlier statements by Schiemenz,^[9] we could not observe any effect of the BPh_4^- anion on the NMR spectrum of **2a** BPh_4^- . Instead, the large upfield shifts in the NMR signals of the benzhydryl triphenylphosphonium salts **2** X^- , which are observed upon variation of the counteranion from $\text{X}^- = \text{halide}$ to $\text{X}^- = \text{BPh}_4^-$, can exclusively be attributed to the loss of the strong $\text{C-H}\cdots\text{X}^-$ hydrogen bonds between the phosphonium ions **2** and the halide ions.

1.3 Benzyl Triphenylphosphonium Salts

1.3.1 NMR Investigation of Benzyl Triphenylphosphonium Salts (1 X^-) in Solution: A Moderate “ BPh_4^- Effect”. *NMR signals of 1a X^- in CD_2Cl_2 .* It was already noted by Schiemenz and coworkers, that the “ BPh_4^- effect” decreases with steric shielding,^[9,10] and this may be an explanation why we did not observe any effect of BPh_4^- on the δ_{H} values of the $\text{C}(\alpha)\text{-H}$ protons in **2a**, which are shielded by two phenyl groups in addition to the large triphenylphosphonium group. Since especially large “ BPh_4^- effects” were reported for relatively C-H -acidic phosphonium salts,^[9,10] and since red-shifts of the CH_2 stretching IR bands indicative of $\text{C-H}\cdots\text{X}^-$ hydrogen bonds were reported even for *alkyl* triphenylphosphonium halides,^[7] we wondered what role the $\text{C-H}\cdots\text{X}^-$ hydrogen bonds would play in these examples. For that reason, we also tested the “ BPh_4^- effect” in a sterically less

hindered system to see how its magnitude would compare to the enormous effect of the C–H···halide hydrogen bonds which we found in the benzhydryl derivatives.

We thus investigated the concentration-dependent effects of the counter-anions Cl^- , BF_4^- and BPh_4^- on the ^1H -NMR chemical shifts δ_{H} (600 MHz, CD_2Cl_2) of the $\text{C}(\alpha)$ –H protons of the benzyl triphenylphosphonium ions **1a** (Table 1.S.4 in Section 1.S.1). Figure 1.9a illustrates the data graphically.

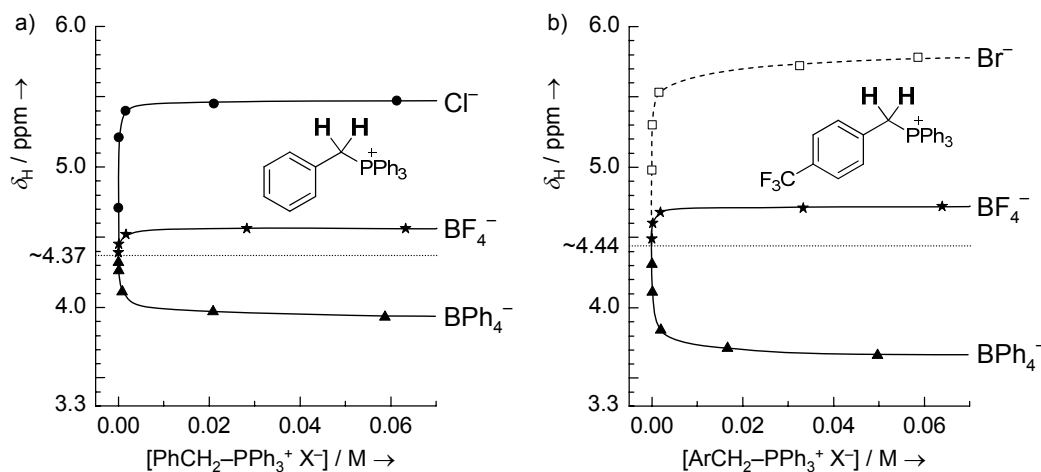


Figure 1.9. Concentration-dependent ^1H -NMR (600 MHz, 27 °C) chemical shifts δ_{H} of the benzylic $\text{C}(\alpha)$ –H protons of (a) **1a** X^- or (b) **1b** X^- with different counter-anions $\text{X}^- = \text{Cl}^-$ (●), Br^- (□), BF_4^- (★), or BPh_4^- (▲) in CD_2Cl_2 .

The phosphonium chloride **1a** Cl^- and tetrafluoroborate **1a** BF_4^- show similar behavior as the corresponding benzhydryl triphenylphosphonium salts. In the concentration range [**1a** X^-] ≥ 0.02 M, the δ_{H} values of the $\text{C}(\alpha)$ –H protons are virtually constant and we can conclude that **1a** Cl^- and **1a** BF_4^- predominantly exist as ion pairs under these conditions (Fig. 1.9a). At lower concentrations ($< 5 \times 10^{-3}$ M), the δ_{H} values decrease: For a 2.08×10^{-5} M solution of **1a** BF_4^- , we determined a chemical shift of $\delta_{\text{H}} = 4.39$ ppm for the $\text{C}(\alpha)$ –H protons (Table 1.S.4 in Section 1.S.1).

The $\text{C}(\alpha)$ –H protons of the tetraphenylborate salt **1a** BPh_4^- , however, show the opposite effect: Their chemical shifts are also virtually constant ($\delta_{\text{H}} \approx 3.95$ ppm) at concentrations ≥ 0.02 M, but *increase* with decreasing concentration until they reach the value of $\delta_{\text{H}} = 4.32$ ppm at [**1a** BPh_4^-] = 1.75×10^{-5} M (Fig. 1.9a).

Thus, the δ_{H} values of the $\text{C}(\alpha)$ –H protons of **1a** X^- with different counter-anions X^- approach a common value of $4.32 < \delta_{\text{H}} < 4.39$ ppm at low concentrations of **1a** X^- , and we can estimate

$\delta_{\text{H, unpaired}} \approx 4.37$ ppm for the C(α)-H protons of the free benzyl triphenylphosphonium ion **1a**. The knowledge of δ_{H} for the unpaired phosphonium ion **1a** allows us to directly compare the magnitude of the “BPh₄⁻ effect” to the influence of C(α)-H···halide hydrogen bonding. The large difference between the C(α)-H protons of the ion pairs **1a** Cl⁻ and **1a** BPh₄⁻ ($\Delta\delta_{\text{H}} = +1.54$ ppm) is mostly due to the deshielding effect of Cl⁻, whereas the shielding effect of BPh₄⁻ contributes less than 30 % to the observed $\Delta\delta_{\text{H}}$. The shielding of the C(α)-H protons by BPh₄⁻ ($\Delta\delta_{\text{H}} \approx -0.38$ ppm) is only about twice as large as the deshielding effect of the C(α)-H···F-BF₃⁻ interaction ($\Delta\delta_{\text{H}} \approx +0.17$ ppm). The smaller deshielding effects of the “normal” anions X⁻ = Cl⁻ and BF₄⁻ on the C(α)-H protons of **1a** (e.g., $\Delta\delta_{\text{H}} \approx +1.0$ ppm for **1a** Cl⁻ relative to unpaired **1a**) compared to those for the analogous benzhydryl derivatives **2a** X⁻ (e.g., $\Delta\delta_{\text{H}} \approx +2.5$ ppm for **2a** Cl⁻ relative to unpaired **2a**) are explained by the statistical factor of two C(α)-H protons in **1a** (vs. one in **2a**) and the lower C(α)-H acidity of **1a** ($\text{p}K_{\text{a}} = 17.4$ in DMSO)^[6] compared to that of **2a** ($\text{p}K_{\text{a}} \approx 9$ in DMSO estimated from the correlation equation published in ref.^[5] and $\text{p}K_{\text{a}} = 30.6$ for Ph₂CH₂^[38]).

Table 1.7 lists further ¹H-NMR, ¹³C-NMR, and ³¹P-NMR signals of phosphonium salts **1a** X⁻ with different counter-anions X⁻ in CD₂Cl₂. The table includes two sets of ¹H-NMR data for the free PhCH₂-PPh₃⁺ ion (**1a**), one determined from a 2.08×10^{-5} M solution of **1a** BF₄⁻, the other from a 1.75×10^{-5} M solution of **1a** BPh₄⁻. The good agreement between the two data sets confirms the assignment to the unpaired phosphonium ion **1a**.

Comparing the ¹H-NMR signals of **1a** Cl⁻ with those of the free phosphonium ions, one finds similar trends as for the corresponding benzhydryl triphenylphosphonium ions (**2a**): The C(α)-H protons experience the largest deshielding ($\Delta\delta_{\text{H}} \approx +1.03$ ppm, $\Delta^2J_{\text{H,P}} \approx +0.7$ ppm); a smaller but still significant deshielding effect is observed for the *ortho*-protons of the PPh₃ group ($\Delta\delta_{\text{H}} \approx +0.29$ ppm) and the *ortho*-protons of the benzyl group ($\Delta\delta_{\text{H}} \approx +0.20$ ppm). The *meta*- and *para*-protons of PPh₃ and benzyl are slightly shielded ($\Delta\delta_{\text{H}} \approx -0.07$ to -0.13 ppm).

The same protons which experience a deshielding by Cl⁻ are shielded in the tetraphenylborate **1a** BPh₄⁻ (Table 1.7): The C(α)-H protons are shielded by $\Delta\delta_{\text{H}} \approx -0.38$ ppm relative to the free phosphonium ion **1a**; the *ortho*-protons of the PPh₃ and benzyl groups are shielded by $\Delta\delta_{\text{H}} \approx -0.16$ ppm and $\Delta\delta_{\text{H}} \approx -0.12$ ppm, respectively. The changes in the chemical shifts of the other protons are in the same direction and of the same magnitude ($\Delta\delta_{\text{H}} \approx -0.08$ to -0.11 ppm) as in **1a** Cl⁻.

Table 1.7. ^{31}P -NMR (162 MHz), ^1H -NMR (400 MHz) and ^{13}C -NMR (100 MHz) data for the phosphonium ion **1a** in CD_2Cl_2 . Data for **1a** X^- were determined at concentrations where the phosphonium salts exist as ion pairs.

salt	P^+	CH_2P^+		<i>o</i> - CH_2Ph	<i>m</i> - CH_2Ph	<i>p</i> - CH_2Ph	<i>o</i> - PPh_3	<i>m</i> - PPh_3	<i>p</i> - PPh_3
	$\delta_{\text{P}} / \text{ppm}$	$\delta_{\text{H}} / \text{ppm}$ ($^2J_{\text{HP}} / \text{Hz}$)	$^1J_{\text{HC}}^{[\text{a}]}$ Hz	$\delta_{\text{H}} / \text{ppm}$					
1a Cl^-	23.1	5.42 (14.7)	134.6	7.07-7.10	7.14-7.18	7.24-7.29	7.70-7.76	7.60-7.66	7.77-7.82
1a BF_4^-	22.2	4.56 (14.1)	134.2	6.91-6.94	7.20-7.25	7.31-7.36	7.48-7.54	7.65-7.71	7.84-7.88
“free” 1a ^[b]	— ^[c]	4.39 (14.0)	— ^[c]	6.87-6.89	7.25-7.28	7.38-7.41	7.43-7.46	7.68-7.72	7.89-7.92
“free” 1a ^[d]	— ^[c]	4.32 (14.0)	— ^[c]	6.85-6.89 ^[e]	7.26-7.28	7.38-7.44 ^[f]	7.38-7.44 ^[f]	7.68-7.71	7.89-7.92
1a BPh_4^-	21.6	3.94 (13.8)	133.9	6.73-6.76	7.21-7.28 ^[f]	7.34-7.39	7.21-7.28 ^[f]	7.57-7.62	7.79-7.84
$\Delta\Box(\text{Cl}^-)^{[\text{g}]}$	— ^[c]	+1.03 (+0.7)	— ^[c]	\sim +0.20	\sim -0.10	\sim -0.13	\sim +0.29	\sim -0.07	\sim -0.10
$\Delta\Box(\text{BPh}_4^-)^{[\text{h}]}$	— ^[c]	-0.38 (-0.2)	— ^[c]	\sim -0.12	\leq -0.05	\sim -0.05	\sim -0.16	\sim -0.10	\sim -0.09
salt	CH_2P^+	<i>i</i> - CH_2Ph	<i>o</i> - CH_2Ph	<i>m</i> - CH_2Ph	<i>p</i> - CH_2Ph	<i>i</i> - PPh_3	<i>o</i> - PPh_3	<i>m</i> - PPh_3	<i>p</i> - PPh_3
	$\delta_{\text{C}} / \text{ppm}$ ($^1J_{\text{CP}} / \text{Hz}$)	$\delta_{\text{C}} / \text{ppm}$ ($^2J_{\text{CP}} / \text{Hz}$)	$\delta_{\text{C}} / \text{ppm}$ ($^3J_{\text{CP}} / \text{Hz}$)	$\delta_{\text{C}} / \text{ppm}$ ($^4J_{\text{CP}} / \text{Hz}$)	$\delta_{\text{C}} / \text{ppm}$ ($^5J_{\text{CP}} / \text{Hz}$)	$\delta_{\text{C}} / \text{ppm}$ ($^1J_{\text{CP}} / \text{Hz}$)	$\delta_{\text{C}} / \text{ppm}$ ($^2J_{\text{CP}} / \text{Hz}$)	$\delta_{\text{C}} / \text{ppm}$ ($^3J_{\text{CP}} / \text{Hz}$)	$\delta_{\text{C}} / \text{ppm}$ ($^4J_{\text{CP}} / \text{Hz}$)
1a Cl^-	31.2 (46.9)	128.1 (8.5)	131.9 (5.6)	129.4 (3.3)	129.0 (3.9)	118.5 (85.8)	135.0 (9.8)	130.6 (12.6)	135.5 (3.0)
1a BF_4^-	31.5 (49.0)	127.0 (8.5)	131.5 (5.5)	129.8 (3.2)	129.6 (3.8)	117.6 (86.1)	134.6 (9.7)	130.9 (12.6)	136.1 (3.1)
1a BPh_4^-	31.7 (49.0)	126.5 (8.4)	131.4 (5.4)	129.8 (3.2)	129.7 (3.8)	117.1 (86.4)	134.4 (9.7)	131.0 (12.6)	136.2 (3.0)
$\Delta\Box(\text{total})^{[\text{i}]}$	-0.5 (-2.1)	+1.6 (-0.1)	+0.5 (+0.2)	-0.4 (-0.1)	-0.7 (+0.1)	+1.4 (-0.6)	+0.6 (+0.1)	-0.4 (± 0)	-0.7 (± 0)

[a] $^1J_{\text{HC}}$ determined from ^{13}C -satellites in the ^1H -NMR (600 MHz) spectra. [b] Determined from ^1H -NMR (600 MHz) spectrum of a 2.08×10^{-5} M solution of **1a** BF_4^- in CD_2Cl_2 . [c] Not available. [d] Determined from ^1H -NMR (600 MHz) spectrum of a 1.75×10^{-5} M solution of **1a** BPh_4^- in CD_2Cl_2 . [e] Superimposed with *p*-protons of BPh_4^- . [f] Two signals superimposed. [g] “Ordinary anion effect”: Difference between **1a** Cl^- ion pairs and free ions (2.08×10^{-5} M **1a** BF_4^-). [h] “ BPh_4^- effect”: Difference between **1a** BPh_4^- ion pairs and free ions (1.75×10^{-5} M **1a** BPh_4^-). [i] Difference between **1a** Cl^- and **1a** BPh_4^- .

The ^{31}P -NMR signals for the phosphorus atom ($\Delta\delta_{\text{P}} \approx +1.5$ ppm when going from **1a** BPh_4^- to **1a** Cl^-) and the ^{13}C -NMR signals of **1a**, including that for C(α), vary only little with the counter-anion X^- (Table 1.7).

^1H -NMR signals for C(α)-H protons of **1b** X^- in CD_2Cl_2 . We also studied the concentration-dependent ^1H -NMR signals of the 4-(trifluoromethyl)benzyl triphenylphosphonium salts **1b** X^- with the counter-anions $\text{X}^- = \text{Br}^-$, BF_4^- , and BPh_4^- (Fig. 1.9b). The *p*- CF_3 -substituent decreases the $\text{p}K_{\text{a}}$ value of the phosphonium salt in DMSO to 14.6, compared to $\text{p}K_{\text{a}} = 17.6$ for the parent compound **1a**,^[6] which results in stronger $\text{C}-\text{H}\cdots\text{X}^-$ hydrogen bonds in the **1b**

X^- ion pairs. Accordingly, Fig. 1.9b shows comparably large downfield shifts for the C(α)-H protons in the **1b** Br $^-$ and **1b** BF $_4^-$ ion pairs (Table 1.S.5 in Section 1.S.1).

The “BPh $_4^-$ effect” also increases with the C(α)-H acidity: The upfield shift of $\Delta\delta_H \approx -0.78$ ppm for the C(α)-H protons of **1b** that results from ion pairing with the BPh $_4^-$ ion is almost twice as large as the upfield shift of $\Delta\delta_H \approx -0.44$ for **1a** BPh $_4^-$ (Fig. 1.9).

Dissociation constants of 1a X $^-$ and 1b X $^-$ in CD $_2$ Cl $_2$. Using equations (1) and (2), we can estimate the dissociation constants K_D for the salts **1a,b** X $^-$ in CD $_2$ Cl $_2$ which are compiled in Table 1.8. The K_D value for **1a** BF $_4^-$ is only a rough estimate, as the effect of ion pairing on the chemical shift is small for this salt ($\Delta\delta_H \approx 0.17$ ppm for C(α)-H protons) and we cannot determine $\delta_{H, \text{unpaired}}$ for the unpaired phosphonium **1a** very accurately (± 0.07 ppm). In agreement with the higher C(α)-H acidity of **1b** compared to **1a**,^[6] the dissociation constants K_D for all **1b** X $^-$ salts are smaller than those for the corresponding **1a** X $^-$ salts (e. g., K_D of **1b** Br $^-$ is already smaller than that of **1a** Cl $^-$ although Cl $^-$ is more basic than Br $^-$) (Table 1.8).

Table 1.8. Estimated dissociation constants K_D (M) for phosphonium salts **1a,b** X $^-$ and **2a** X $^-$ with different counterions X $^-$ in CD $_2$ Cl $_2$.

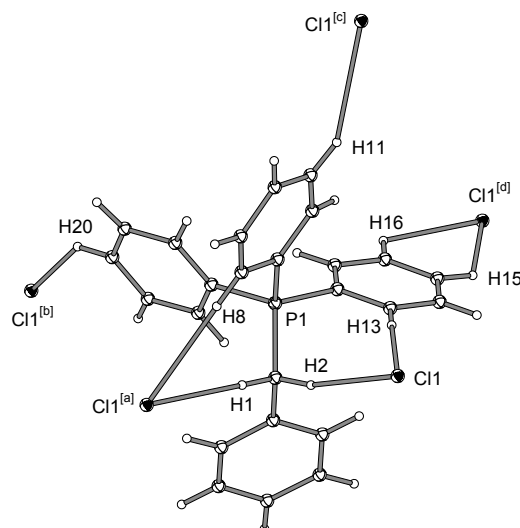
X $^-$	$\Delta G_{\text{acid}}^{[\text{a}]} / \Delta G_{\text{t}}^0 [\text{b}] /$		$K_D^{[\text{c}]} / \text{M}$		
	kcal mol $^{-1}$	kJ mol $^{-1}$	1a X $^-$	1b X $^-$	2a X $^-$
BPh $_4^-$	– ^[d]	–32.8	2.5×10^{-4}	1.1×10^{-4}	^[e]
SbF $_6^-$	256	– ^[d]	^[f]	^[f]	6×10^{-4}
BF $_4^-$	288	(~0) ^[g]	(1×10^{-4})	(5×10^{-5})	2.2×10^{-4}
Br $^-$	315	31.3	^[f]	2.9×10^{-5}	7.6×10^{-5}
Cl $^-$	324	42.1	6.8×10^{-5}	^[f]	3.4×10^{-5}
pK $_a$ for C(α)-H in DMSO:			17.6 ^[h]	14.6 ^[h]	(~9) ^[i]

[a] Calculated ΔG_{acid} (298 K) for deprotonation of the conjugate acids HX in the gas phase; from ref.^[33]
 [b] Single free ion energies of transfer ΔG_{t}^0 (H $_2$ O \rightarrow CH $_3$ CN, 25 °C) for the transfer of the anions X $^-$ from H $_2$ O to CH $_3$ CN; from ref.^[34]
 [c] Dissociation constants for the phosphonium salts in CD $_2$ Cl $_2$ based on the ^1H -NMR chemical shifts of the C(α)-H protons; this work. [d] Not available. [e] No effect of X $^-$ on δ_H of the C(α)-H protons. [f] Not determined. [g] For BF $_4^-$, $\Delta G_{\text{t}}^0 \approx 0$ was estimated.^[39] [h] From ref. ^[6] [i] Estimated from the correlation equation published in ref.^[5] and pK $_a = 30.6$ for Ph $_2$ CH $_2$.^[38]

Since **2a** has an even higher C(α)-H acidity than **1b**, one would also expect lower dissociation constants K_D for **2a** X $^-$ than for **1b** X $^-$. On the contrary, the K_D values for **2a** X $^-$ are higher than for **1b** X $^-$ (Table 1.8), i. e. the salts **2a** X $^-$ dissociate more readily. The reason for this may be a combination of steric hindrance and a statistical effect due to the fact that

there is only one C(α)–H proton in the benzhydryl derivatives **2a** X[−] but two in the benzyl derivatives **1b** X[−].

1.3.2 Crystal Structures of Benzyl Triphenylphosphonium Salts (1 X[−]). *Halide and tetrafluoroborate salts.* The calculated structures of **1a** Cl[−] and **1a** BF₄[−] in CH₂Cl₂ solution closely resemble those of the benzhydryl derivatives **2a** X[−] and are not shown here. In each case, the anions form hydrogen bonds with three donors: one of the C(α)–H, one *o*-PPh₃ and one *o*-CPh proton. The crystal structures of these salts are worth discussing briefly because there is the additional possibility of an interaction of the anion with the second C(α)–H proton of the benzyl group belonging to a second phosphonium ion.



Symmetry codes: [a] $-x, -y, 2-z$ [b] $-0.5-x, -0.5+y, z$ [c] $-0.5+x, 0.5-y, 2-z$ [d] $-0.5+x, y, 1.5-z$.

Figure 1.10. Interactions between **1a** and Cl[−] in the crystals of **1a** Cl[−].^[40b] All contacts with $d(\text{H}\cdots\text{X}^-) \leq 2.90 \text{ \AA}$ are shown as bonds. For C–H \cdots X[−] bond lengths and angles, see Table 1.9.

The crystal structure of **1a** Cl[−] has been reported previously (Fig. 1.10).^[40] The shortest contact between cation and anion is the interaction of one C(α)–H proton with the chloride anion (H1 \cdots Cl distance 2.52 Å and C1–H1 \cdots Cl angle 170°), which forms a second hydrogen bond to one of the *o*-PPh₃ protons (H8 \cdots Cl distance 2.83 Å and C9–H8 \cdots Cl angle 176°) (Table 1.9). The second C(α)–H proton shows a weaker hydrogen bond to a second chloride anion (H2 \cdots Cl distance 2.66 Å, C1–H2 \cdots Cl angle 163°), which also has a very short contact to another *o*-PPh₃ proton (H13 \cdots Cl[−] distance 2.57 Å, C15–H13 \cdots Cl[−] angle 176°). These strong bidirectional interactions result in the formation of one-dimensional chains of alternating

cations and anions in the crystal, which interact by weaker contacts between the chloride anions and some of the *p*- and *m*-PPh₃ protons.

Table 1.9. Distances and angles of C–H···X[−] contacts in crystals of ArCH₂–PPh₃⁺ X[−] (**1** X[−]).

salt	donor ^[a]	acceptor ^[a]	code ^[a]	<i>d</i> (H···X) / Å	<i>d</i> (C···X) / Å	∠ (C–H···X) / °
1a Cl [−] (ref. ^[40b])	H1 (α -H)	Cl1	a	2.52	3.490(6)	170
	H8	Cl1	a	2.83	3.803(5)	176
	H2 (α -H)	Cl1	–	2.66	3.602(5)	163
	H13	Cl1	–	2.57	3.550(6)	176
	H15	Cl1	d	2.76	3.424(6)	123
	H16	Cl1	d	2.84	3.472(7)	123
	H11	Cl1	c	2.87	3.771(7)	153
	H20	Cl1	b	2.81	3.532(7)	132
1a BF ₄ [−] · CH ₂ Cl ₂ (ref. ^[41])	H1 (α -H)	F3	–	2.52	3.437(3)	158
	H1 (α -H)	F4	–	2.81	3.643(3)	145
	H10	F1	–	2.49	3.298(2)	146
	H10	F4	–	2.76	3.594(3)	150
	H4 (CH ₂ Cl ₂)	F1	–	2.58	3.367(4)	139
	H4 (CH ₂ Cl ₂)	F4	–	2.52	3.478(5)	169
	H2 (α -H)	F1	b	2.51	3.422(3)	157
	H2 (α -H)	F3	b	2.54	3.403(3)	148
	H19	F1	b	2.57	3.448(2)	157
	H19	F3	b	2.64	3.490(3)	152
	H5	F1	b	2.68	3.391(3)	134
	H6	F1	a	2.56	3.435(3)	158
	H6	F2	a	2.88	3.552(3)	130
	H17	F2	c	2.52	3.283(3)	140
	H13	F3	d	2.65	3.350(3)	133
	H22	F2	e	2.75	3.376(3)	125
	H22	F4	e	2.78	3.398(4)	125
	H23	F2	e	2.80	3.396(3)	123
H20	Cl1	e	2.84	3.563(3)	135	
1a BF ₄ [−] · CHCl ₃	H19A (α -H)	F4	n	2.47	3.390(3)	159
	H19A (α -H)	F3	n	2.71	3.570(3)	149
	H18	F3	n	2.82	3.696(3)	154
	H18	F1	n	2.64	3.412(3)	139
	H26 (CHCl ₃)	F3	n	2.24(4)	3.192(3)	169(3)
	H26 (CHCl ₃)	F2	n	2.50(3)	3.250(4)	134(3)
	H19B (α -H)	F4	b	2.53	3.443(3)	157
	H8	F4	b	2.83	3.741(4)	162
	H8	F3	b	2.49	3.253(3)	138
	H21	F4	b	2.51	3.390(3)	154
	H24	F3	–	2.60	3.479(4)	153
	H23	F1	j	2.68	3.226(4)	117
	H4	F2	k	2.54	3.436(3)	157
	H10	F1	m	2.87	3.730(4)	151
	H17	F1	f	2.41	3.209(3)	141
H16	F2	f	2.87	3.738(3)	152	
1b BPh ₄ [−]	H1A (α -H)	phenyl ^[b]	–	2.80	3.633(2)	142
	H1B (α -H)	phenyl ^[c]	d	3.40	4.388(4)	180

[a] See Figures 1.10, 1.11, and 1.12 for numbering of atoms and symmetry codes. [b] Center of six atoms C33, C34, C35, C36, C37, C38. [c] Center of six atoms C27, C28, C29, C30, C31, C32.

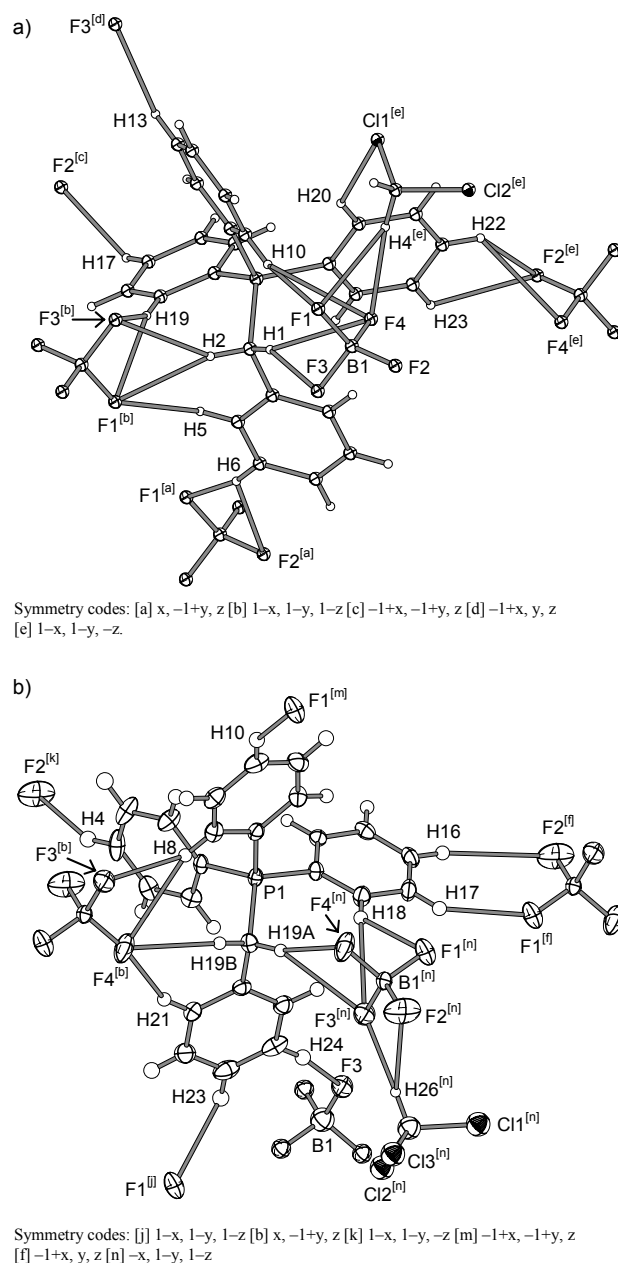


Figure 1.11. Interactions between **1a** and BF_4^- in the crystals of (a) **1a** $\text{BF}_4^- \cdot \text{CH}_2\text{Cl}_2$ (ref. ^[41]) and (b) **1a** $\text{BF}_4^- \cdot \text{CHCl}_3$ (this work). All contacts with $d(\text{H}\cdots\text{X}^-) \leq 2.90 \text{ \AA}$ are shown as bonds. For C–H \cdots X $^-$ bond lengths and angles, see Table 1.9.

The crystal structure of **1a** BF_4^- with cocrystallized CH_2Cl_2 has previously been reported.^[41] Figures 1.11a and b compare the structures of **1a** BF_4^- with cocrystallized CH_2Cl_2 ^[41] and cocrystallized CHCl_3 , respectively. Both structures resemble that of **1a** Cl^- (Fig. 1.10), except that some of the hydrogen bonds are bifurcated towards two of the BF_4^- anions' fluorine atoms (Fig. 1.11 and Table 1.9). On each side of the benzyl moiety, there are strong interactions between the anion and the C(α)–H (H1/H2 in Fig. 1.11a; H19A/H19B in Fig. 1.11b) and one *p*-PPh₃ proton (H10/H19 in Fig. 1.11a; H18/H8 in Fig. 1.11b). The larger

size of the BF_4^- anion and a slight rotation of the benzyl group's phenyl ring allow for an additional contact between one *o*-CPh proton and one of the BF_4^- anions, as shown on the left side in Figures 1.11a (H5) and 1.11b (H21). The second BF_4^- anion (shown on the right side) cannot undergo such an interaction, because the phenyl ring of the benzyl moiety is already twisted in the wrong direction. Instead, this anion forms strong hydrogen bonds to a solvent molecule. In the case of **1a** $\text{BF}_4^- \cdot \text{CH}_2\text{Cl}_2$ there is also a contact between an *o*-PPh₃ proton and a chlorine atom of CH_2Cl_2 (Fig. 1.11a), but this interaction is rather weak (H20...C11 distance 2.84 Å, C22–H20...C11 angle 135°).

The tetraphenylborate salts. Like **2a** BPh_4^- , **1a** BPh_4^- crystallizes as very long fine needles and we could not obtain suitable material for X-ray structure analyses. We could, however, crystallize (*p*-CF₃-C₆H₄)CH₂-PPh₃⁺ BPh_4^- (**1b** BPh_4^-) as platelets from $\text{CH}_2\text{Cl}_2/\text{Et}_2\text{O}$; its crystal structure is shown in Figure 1.12. The CF₃ group is disordered.

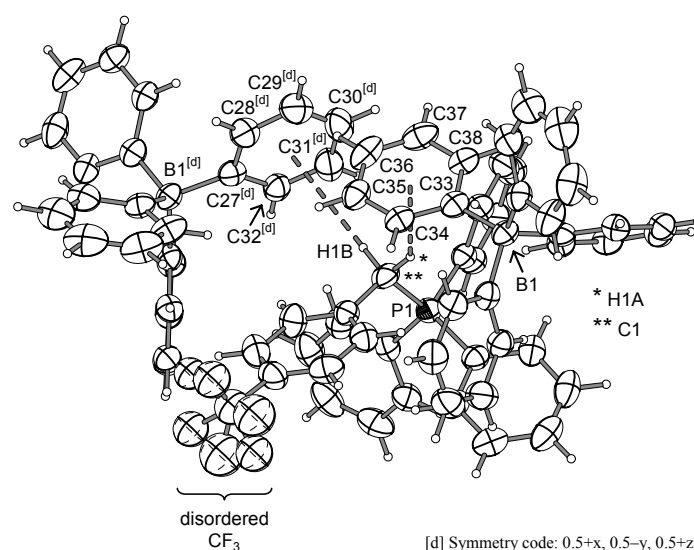


Figure 1.12. Interactions between **1b** and two BPh_4^- anions in crystals of **1b** BPh_4^- . The dashed lines indicate the distances between the α -protons and the centers of the phenyl groups. For C–H...X⁻ bond lengths and angles, see Table 1.9.

Both C(α)–H bonds (C1–H1A and C1–H1B) point towards phenyl rings of the BPh_4^- anions. The nature of these C–H... π contacts can be characterized by the distances between the H (or C) atoms and the centers of the phenyl rings, as well as the angles between the C–H bonds and the lines connecting the H atom and the center of the phenyl ring (Table 1.9). One of the C(α)–H bonds (C1–H1B) points exactly to the center of the phenyl ring of one BPh_4^- anion

(angle: 180°) (Fig. 1.12), but the distance to the center of the phenyl ring is relatively large (3.40 Å). The second C(α)–H proton (H1A) forms a much closer contact to a phenyl ring of another BPh₄[−] anion (distance: 2.80 Å, sum of C and H van der Waals radii: 2.79 Å), but in this case the projection of the C(α)–H bond does not point exactly at the phenyl ring (angle 142°).

1.3.3 What is the Nature of the “BPh₄[−] Effect” in Benzyl Triphenylphosphonium Salts?

NMR data (Table 1.7 and Fig. 1.9), quantum chemical calculations (Table 1.6), and crystal structures (Figures 1.10, 1.11 and Table 1.9) of the salts **1a,b** X[−] with X[−] = Cl[−], Br[−], or BF₄[−] show close similarities to the data for the benzhydryl derivatives and are consistent with the formation of C–H \cdots X[−] hydrogen bonds.

The crystallographic data of **1b** BPh₄[−] (Fig. 1.12) reveal C–H \cdots π interactions between **1b** and BPh₄[−], where the protons reside above the centers of the phenyl rings. Unlike the typical CH/ π interaction, which is mainly based on dispersion interactions,^[45] the interaction between **1b** and BPh₄[−] can be expected to have a strong electrostatic component due to the high acidity of the C–H bond and the negative charge on the phenyl rings of the BPh₄[−] anion. This notion is supported by the strong directionality of the C1–H1B \cdots Ph interaction, since the electrostatic interaction is the main source of directionality in CH/ π interactions.^[42] Hence, the C(α)–H \cdots Ph interactions in **1b** BPh₄[−] can be viewed as hydrogen bonds in which a phenyl ring of the tetraphenylborate anion acts as the hydrogen bond acceptor.^[2,43] Similar C(α)–H \cdots Ph hydrogen bonds have also been reported in the crystal structure of choline tetraphenylborate, Me₃N⁺–C(α)H₂–CH₂OH BPh₄[−] (H \cdots Ph distances 2.42 Å and 2.38 Å, C–H \cdots Ph angles 168° and 159°).^[43b]

A similar interaction between cation and anion in CD₂Cl₂ solution can explain the upfield shift of the C(α)–H resonances of **1a,b** BPh₄[−] in the ¹H-NMR spectra (Fig. 1.9): The resulting ring current effect^[44] over-compensates any small downfield shift in the ¹H-NMR spectrum that may be expected due to the formation of a weak hydrogen bond.

We also had a closer look at the NMR data of the BPh₄[−] anions in concentrated solutions of **1a,b** BPh₄[−] in CD₂Cl₂. However, the ¹¹B-, ¹H- and ¹³C-NMR signals of the BPh₄[−] anion in the phosphonium salts **1a,b** BPh₄[−] in CD₂Cl₂ do not differ significantly from those of the free BPh₄[−] ions or those of **2a** BPh₄[−] which does not show any “BPh₄[−] effect” (Table 1.S.6 in Section 1.S.1).

1.4. Infrared Spectra

An investigation of hydrogen bonding is incomplete without a look at the C–H stretching bands in the infrared spectra, which usually show a characteristic red-shift compared to the free C–H bonds. Figure 1.13 shows the appropriate regions of the IR spectra of different phosphonium salts in CD₂Cl₂ solution, which were acquired under conditions where the phosphonium salts are mostly paired (3×10^{-2} M solutions).

The red-shifted C(α)–H stretch vibrations ($\bar{\nu} \approx 2831$ and 2791 cm⁻¹) in the benzhydryl triphenylphosphonium halides **2a** Cl⁻ and **2a** Br⁻ are clearly visible (Fig. 1.13a), while the intensities of the aliphatic C–H stretching bands in the other benzhydryl triphenylphosphonium salts **2a** X⁻ with X⁻ = BF₄⁻, SbF₆⁻, and BPh₄⁻ are very low (Fig. 1.13a). These bands can be better discerned in the IR spectra of the benzyl triphenylphosphonium salts **1a** X⁻ (Fig. 1.13b) and **1b** X⁻ (Fig. 1.13c). For the halides, we again observe pronounced red-shifts of the C(α)–H stretching bands ($\bar{\nu} \approx 2852$ and 2778 cm⁻¹).

Interestingly, the C(α)–H bands of the tetrafluoroborates **1a,b** BF₄⁻ ($\bar{\nu} \approx 2963$ and 2921 cm⁻¹) in Figures 1.13b and 1.13c are located at *higher* wave numbers (i. e., blue-shifted) and have lower intensities than those of the corresponding tetraphenylborates **1a,b** BPh₄⁻ ($\bar{\nu} \approx 2936$ and 2900 cm⁻¹), although the dissociation constants K_D indicate stronger interactions of the phosphonium ions with the BF₄⁻ anions than with the BPh₄⁻ anions (Table 1.8). This may indicate the existence of so-called blue-shifting hydrogen bonds between the phosphonium ions and the tetrafluoroborate anions.

Blue-shifting hydrogen bonds show stretching vibrations at higher wave numbers, often accompanied by reduced intensities of the IR bands,^[45,46] which is the opposite behavior of normal hydrogen bonds.^[8] The nature of blue-shifting hydrogen bonds has been discussed controversially,^[45,46] but now there seems to be a general agreement that there is no fundamental difference between blue-shifting and normal red-shifting hydrogen bonds.^[47]

According to Joseph and Jemmis,^[46] there are two opposing effects, when the hydrogen bond acceptor X⁻ approaches the C–H proton. On the one hand, there is an attractive interaction between the positive H and the negative X⁻, which lengthens the C–H bond and reduces the force constant. On the other hand, the presence of X⁻ induces a greater polarization of the

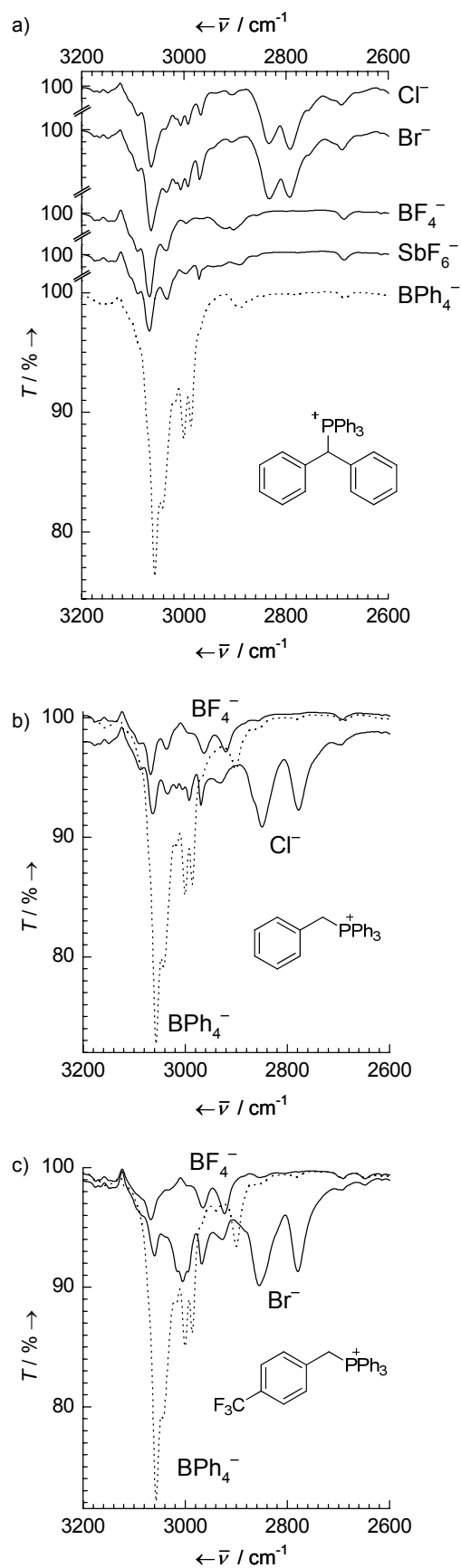


Figure 1.13. IR spectra of 3×10^{-2} M solutions of (a) **2a** X^- (vertical offset for visibility), (b) **1a** X^- , or (c) **1b** X^- with $\text{X}^- = \text{Cl}^-$, Br^- , BF_4^- , SbF_6^- , or BPh_4^- in CD_2Cl_2 .

C–H bond, because it compensates the resulting positive charge at H. As a result, the C–H bond is contracted and the force constant increases. If the former effect dominates, a classical red-shifting hydrogen bond is the result. If the latter dominates, a blue-shift of the frequency of the C–H stretch mode is observed.^[46]

Compared to classical hydrogen bond donors such as O–H or N–H, the C–H bond is longer and less polar. An approach of the hydrogen bond acceptor X^- will thus lead to a considerable polarization of the C–H bond, and the experimental ^1H - and ^{13}C -NMR chemical shifts for the respective atoms in **2a** X^- (Table 1.1) and **1a** X^- (Table 1.7) seem to support this interpretation (see above). Whether the increased polarization causes a contraction of the C–H bond and a blue shift of its IR stretching band, depends on the relative importance of the compensating attractive interaction between H and X^- . Increasing interaction energy between hydrogen bond donor and acceptor initially causes a blue shift (at relatively long equilibrium distances between H and X^-), which then decreases again and changes into a red shift as the equilibrium distance between H and X^- becomes shorter.^[46] For strong acceptors such as Cl^- or Br^- , the attraction between H and Cl^- clearly dominates and we observe the classical red-shifting hydrogen bonds (Fig. 1.13). The hydrogen bond acceptor BF_4^- seems to be of an intermediate strength, where we observe a blue shift with the C–H hydrogen bond donors **1a** and **1b** in CD_2Cl_2 solution (Fig. 1.13b and c).

An alternative explanation would be that the blue-shifting hydrogen bonds in the tetrafluoroborate ion pairs **1a,b** BF_4^- result from the fact that these are bifurcated hydrogen bonds. This interpretation is suggested by a theoretical study of linear and bifurcated hydrogen bonds between the proton donors H_2CZ ($Z = \text{O}, \text{S}, \text{Se}$) or H_2CZ_2 ($Z = \text{F}, \text{Cl}, \text{Br}$) and the halide ions Cl^- and Br^- , which found that all linear hydrogen bonds in the investigated systems were red-shifting, while all bifurcated hydrogen bonds were blue-shifting.^[48]

It would be interesting to compare the IR bands of **1a,b** BF_4^- ion pairs with those of the free ions **1a** and **1b** in CD_2Cl_2 solution. Unfortunately, the IR spectra cannot be determined at such low concentrations where **1a** and **1b** are mostly unpaired, and quantum chemical calculations of the IR bands of such large molecules are beyond the scope of this work, since reliable calculations require the explicit inclusion of at least two solvent shells.

As both the NMR and X-ray data indicated hydrogen bonding between the counter-anions and aryl protons (see above), it is also interesting to compare the aromatic C–H stretching vibrations. Indeed, the C(aryl)–H stretching bands of the BF_4^- salts are found above 3000 cm^{-1} , while those of the halides extend further into the red to well below 3000 cm^{-1}

(Figures 1.13 a-c). The IR spectra thus provide further evidence for C(aryl)–H \cdots X $^-$ hydrogen bonds in CD $_2$ Cl $_2$ solutions of the phosphonium halides.

1.5 Conclusion

The remarkably large counterion-induced shifts in the ^1H -NMR spectra of the phosphonium ion Ph $_2$ CH–PPh $_3^+$ (**2a**) (e. g., C(α)–H signals of **2a** Cl $^-$: 8.25 ppm; **2a** BPh $_4^-$: 5.72 ppm in CD $_2$ Cl $_2$) have previously been attributed mainly to the shielding by the ring current effect of the BPh $_4^-$ anions.^[9] In contrast, we have now demonstrated that the ^1H -NMR spectrum of the phosphonium ion **2a** is not affected by BPh $_4^-$ anions at all, and that the formation of ion pairs of **2a** with Cl $^-$ anions or other hydrogen bond acceptors is responsible for the large downfield shifts of the C(α)–H signals of **2a** in CD $_2$ Cl $_2$ relative to that of the unpaired cation (Fig. 1.1). Even weakly coordinating anions such as SbF $_6^-$ or BF $_4^-$ induce a noticeable downfield shift of +0.2 to +0.4 ppm. In sterically less congested systems such as PhCH $_2$ –PPh $_3^+$ (**1a**), the BPh $_4^-$ anion does induce a noticeable upfield shift, but the absolute magnitude of the effect remains second to the deshielding effect of Cl $^-$ or Br $^-$ anions (Fig. 1.9).

The counterion-induced NMR shifts in quaternary phosphonium salts are caused by the formation of charge-assisted C–H \cdots X $^-$ hydrogen bonds between the anion and the C(α)–H protons of the cation. The *o*-PPh $_3$ and *o*-CPh protons are likewise involved in such C–H \cdots X $^-$ hydrogen bonds. The strengths of the hydrogen bonds increase in the order BPh $_4^-$ < SbF $_6^-$ < BF $_4^-$ < Br $^-$ < Cl $^-$ and also increase with increasing C–H-acidities of the donor groups. A C–H $\cdots\pi$ hydrogen bond between the C(α)–H and the BPh $_4^-$ anion has also been observed in the crystal structure of **1b** BPh $_4^-$, and the NMR spectra indicate that a similar interaction is also relevant in dichloromethane solution. Ion pairing thus plays an important role in solutions of phosphonium salts even when weakly coordinating anions such as BF $_4^-$ and SbF $_6^-$ are employed in solvents such as CH $_2$ Cl $_2$ or CHCl $_3$. Stronger hydrogen bond acceptors such as Cl $^-$ or Br $^-$ also form ion pairs with the phosphonium ions in more polar solvents such as CH $_3$ CN.

Similar C–H \cdots X $^-$ hydrogen bonds probably also play a major role in solutions of other onium salts, as demonstrated by the large number of examples for the “BPh $_4^-$ effect” in phosphonium,^[9,10] ammonium,^[14] anilinium,^[11] pyridinium,^[13] sulfonium,^[15] arsonium,^[12] and stibonium^[12] salts, which were collected by Schiemenz and coworkers. Indeed, the crystal

structures reported for tetraarylborate salts of other onium ions^[43b,c] show similar cation – anion interactions as described for **1b** BPh₄[−] in this work (Fig. 1.12). However, if the conclusions drawn for the benzyl triphenylphosphonium salts **1a,b** X[−] in this work are also applicable to these other onium salts, the strongest anion effect has to be expected for the “ordinary” halide salts and not the BPh₄[−] salts. The fact that red-shifts of the C(α)–H IR stretching bands in CHCl₃ solution were reported even for *alkyl* triphenylphosphonium halides^[7] illustrates that hydrogen bonding also plays a role for substrates of lower C–H acidity.

In any case, the counter-anions and the structural features of the ion pairs play a decisive role for the spectroscopic characteristics and reactivities of onium salts in solution. For example, the photochemistry of quaternary phosphonium salts cannot be understood without considering the nature of the anion and the concentration of the salt.^[19] In the course of this work, we have encountered many of the concepts that were controversially debated in the field of hydrogen bonding during the last decades: hydrogen bonds involving C–H donors, bi- and multi-furcated hydrogen bonds, “aromatic” hydrogen bonds with phenyl groups as acceptors, and “improper” blue-shifting hydrogen bonds. It seems that these are widespread phenomena which should be considered when dealing with solutions of onium salts.

1.6 Acknowledgments

We thank Dr. David Stephenson and Claudia Dubler for assistance with the NMR experiments and the Deutsche Forschungsgemeinschaft for financial support.

1.7 References and Notes

- [1] (a) G. R. Desiraju, *Acc. Chem. Res.* **1991**, *24*, 290-296; (b) G. R. Desiraju, *Acc. Chem. Res.* **1996**, *29*, 441-449; (c) M. C. Wahl, M. Sundaralingam, *Trends Biochem. Sci.* **1997**, *22*, 97-102; (d) R. K. Castellano, *Curr. Org. Chem.* **2004**, *8*, 845-865; (e) H.-J. Steiner, *Angew. Chem.* **2009**, *121*, 3982-4036; *Angew. Chem. Int. Ed.* **2009**, *48*, 3924-3977; (f) Y. Hua, A. H. Flood, *Chem. Soc. Rev.* **2010**, *39*, 1262-1271; (g) J. J. Novoa, F. Mota, E. D’Oria, in *Hydrogen Bonding - New Insights* (Ed.: S. J. Grabowski),

- Springer, Dordrecht, **2006**, pp. 193-244; (h) S. Scheiner, in *Hydrogen Bonding - New Insights* (Ed.: S. J. Grabowski), Springer, Dordrecht, **2006**, pp. 263-292.
- [2] M. Nishio, *CrystEngComm* **2004**, *6*, 130-158.
- [3] T. Steiner, *Angew. Chem.* **2002**, *114*, 50-80; *Angew. Chem. Int. Ed.* **2002**, *41*, 48-76.
- [4] (a) B. P. Hay, V. S. Bryantsev, *Chem. Commun.* **2008**, 2417-2428; (b) L. Pedzisa, B. P. Hay, *J. Org. Chem.* **2009**, *74*, 2554-2560.
- [5] Y. Fu, H.-J. Wang, S.-S. Chong, Q.-X. Guo, L. Liu, *J. Org. Chem.* **2009**, *74*, 810-819.
- [6] J.-P. Cheng, B. Liu, Y. Zhao, Y. Sun, X.-M. Zhang, Y. Lu, *J. Org. Chem.* **1999**, *64*, 604-610.
- [7] L. B. Senyavina, V. I. Sheichenko, Y. N. Sheinker, A. V. Dombrovskii, M. I. Shevchuk, L. I. Barsukov, L. D. Bergel'son, *Zh. Obshch. Khim.* **1967**, *37*, 499-506; *J. Gen. Chem. USSR* **1967**, *37*, 469-474.
- [8] E. Arunan, G. R. Desiraju, R. A. Klein, J. Sadlej, S. Scheiner, I. Alkorta, D. C. Clary, R. H. Crabtree, J. J. Dannenberg, P. Hobza, H. G. Kjaergaard, A. C. Legon, B. Mennucci, D. J. Nesbitt, *Pure Appl. Chem.* **2011**, *83*, 1637-1641.
- [9] G. P. Schiemenz, *J. Magn. Reson.* **1972**, *6*, 291-297.
- [10] G. P. Schiemenz, E. Papageorgiou, *Phosphorus Sulfur* **1982**, *13*, 41-58.
- [11] G. P. Schiemenz, *Org. Magn. Reson.* **1973**, *5*, 257-261.
- [12] G. P. Schiemenz, *J. Organomet. Chem.* **1973**, *52*, 349-354.
- [13] G. P. Schiemenz, *J. Mol. Struct.* **1973**, *16*, 99-102.
- [14] G. P. Schiemenz, *Tetrahedron* **1973**, *29*, 741-745.
- [15] G. P. Schiemenz, H. P. Hansen, *Angew. Chem.* **1973**, *85*, 404; *Angew. Chem. Int. Ed.* **1973**, *12*, 400.
- [16] Recent examples where this view was expressed: (a) G. P. Schiemenz, C. Näther, S. Pörksen, *Z. Naturforsch., B: Chem. Sci.* **2003**, *58*, 59-73; (b) G. P. Schiemenz, *Magn. Reson. Chem.* **2010**, *48*, 261-269.
- [17] Also see: R. P. Taylor, I. D. Kuntz Jr., *J. Am. Chem. Soc.* **1970**, *92*, 4813-4823. In this study, an upfield shift of $\Delta\delta_{\text{H}} \approx -0.4$ ppm was observed for the methyl protons of $\text{CH}_3\text{PPh}_3^+ \text{X}^-$ in CDCl_3 solution, when the anion X^- was varied from chloride to picrate. The fact that the same anion variation caused much larger upfield shifts in aromatic solvents (e. g., $\Delta\delta_{\text{H}} \approx -1.6$ ppm in 1-bromonaphthalene) was explained by the ability of the smaller anions to form contact pairs with the onium ions, thus preventing the interaction of the aromatic solvent with the α -protons of the cation.

- [18] (a) G. P. Schiemenz, *Angew. Chem.* **1971**, *83*, 929-930; *Angew. Chem. Int. Ed.* **1971**, *10*, 855; (b) G. P. Schiemenz, H. Rast, *Tetrahedron Lett.* **1972**, *17*, 1697-1700; (c) G. P. Schiemenz, P. Klemm, *Org. Magn. Reson.* **1974**, *6*, 276-278.
- [19] J. Ammer, C. F. Sailer, E. Riedle, H. Mayr, *J. Am. Chem. Soc.* **2012**, *134*, 11481-11494.
- [20] J. Ammer, C. Nolte, H. Mayr, *J. Am. Chem. Soc.* **2012**, *134*, 13902-13911.
- [21] (a) C. K. Broder, M. G. Davidson, V. T. Forsyth, J. A. K. Howard, S. Lamb, S. A. Mason, *Cryst. Growth Des.* **2002**, *2*, 163-169; (b) I. Ling, Y. Alias, A. N. Sobolev, C. L. Raston, *CrystEngComm* **2011**, *12*, 4321-4327.
- [22] (a) A. Hamdi, K. C. Nam, B. J. Ryu, J. S. Kim, J. Vicens, *Tetrahedron Lett.* **2004**, *45*, 4689-4692; (b) H. M. Yeo, B. J. Ryu, K. C. Nam, *Org. Lett.* **2008**, *10*, 2931-2934; (c) H. M. Yeo, N. J. Jeon, K. C. Nam, *Bull. Korean Chem. Soc.* **2011**, *32*, 3171-3174; (d) W. Huang, H. Lin, H. Lin, *Sens. Actuators, B* **2011**, *153*, 404-408.
- [23] Ionic liquids: D. R. MacFarlane, M. Forsyth, E. I. Izgorodina, A. P. Abbott, G. Annat, K. Fraser, *Phys. Chem. Chem. Phys.* **2009**, *11*, 4962-4967.
- [24] Deep eutectic solvents: (a) M. A. Kareem, F. S. Mjalli, M. A. Hashim, I. M. AlNashef, *J. Chem. Eng. Data* **2010**, *55*, 4632-4637; (b) K. Shahbaz, F. S. Mjalli, M. A. Hashim, I. M. AlNashef, *Energy Fuels* **2011**, *25*, 2671-2678.
- [25] (a) E. O. Alonso, L. J. Johnston, J. C. Scaiano, V. G. Toscano, *Can. J. Chem.* **1992**, *70*, 1784-1794; (b) C. Imrie, T. A. Modro, E. R. Rohwer, C. C. P. Wagener, *J. Org. Chem.* **1993**, *58*, 5643-5649.
- [26] (a) G. P. Schiemenz, M. Sommerfeld, *Phosphorus Sulfur* **1979**, *6*, 273-274; (b) G. P. Schiemenz, R. Hinz, *Phosphorus Sulfur* **1983**, 237-240; (c) G. P. Schiemenz, R. Bukowski, L. Eckholtz, B. Varnskühler, *Z. Naturforsch., B: Chem. Sci.* **2000**, *55*, 12-20; (d) G. P. Schiemenz, C. Näther, S. Pörksen, *Z. Naturforsch., B: Chem. Sci.* **2003**, *58*, 663-671.
- [27] Counteranion effects in the Wittig reaction: (a) H. Bandmann, T. Bartik, S. Bauckloh, A. Behler, F. Brille, P. Heimbach, J.-W. Louven, P. Ndalut, H.-G. Preis, E. Zeppenfeld, *Z. Chem.* **1990**, *30*, 193-204; (b) H. Yung-Son, C.-F. Lee, *Tetrahedron* **2000**, *56*, 7893-7902.
- [28] Reviews about phosponium salts as organocatalysts: (a) T. Werner, *Adv. Synth. Catal.* **2009**, *351*, 1469 – 1481; (b) D. Enders, T. V. Nguyen, *Org. Biomol. Chem.*

- 2012**, *10*, 5327-5331; (c) D. Uraguchi, T. Ooi, *Yuki Gosei Kagaku Kyokaiishi* **2010**, *68*, 1185-1194.
- [29] H. Friebolin, *Basic One- and Two-Dimensional NMR Spectroscopy*, 3rd ed., Wiley-VCH, Weinheim, **1998**.
- [30] R. H. Contreras, J. E. Peralta, *Prog. Nucl. Magn. Reson. Spectrosc.* **2000**, *37*, 321-425.
- [31] C. Hansch, A. Leo, R. W. Taft, *Chem. Rev.* **1991**, *91*, 165-195.
- [32] (a) van der Waals radii of C (1.70 Å), F (1.47 Å), Cl (1.75 Å), Br (1.85 Å) taken from: A. Bondi, *J. Phys. Chem.* **1964**, *68*, 441-451; (b) radius of hydrogen (1.09 Å) taken from: R. S. Rowland, R. Taylor, *J. Phys. Chem.* **1996**, *100*, 7384-7391.
- [33] I. A. Koppel, P. Burk, I. Koppel, I. Leito, T. Sonoda, M. Mishima, *J. Am. Chem. Soc.* **2000**, *122*, 5114-5124.
- [34] Y. Marcus, *Pure Appl. Chem.* **1983**, *55*, 977-1021.
- [35] (a) R. Ditchfield, *Mol. Phys.* **1974**, *27*, 789-807; (b) F. London, *J. Phys. Radium* **1937**, *8*, 397-409; (c) K. Wolinski, J. F. Hinton, P. Pulay, *J. Am. Chem. Soc.* **1990**, *112*, 8251-8260.
- [36] K. W. Wiitala, T. R. Hoye, C. J. Cramer, *J. Chem. Theory Comput.* **2006**, *2*, 1085-1092.
- [37] (a) A. Bergner, M. Dolg, W. Küchle, H. Stoll, H. Preuß, *Mol. Phys.* **1993**, *80*, 1431-1441; (b) B. Metz, H. Stoll, M. Dolg, *J. Chem. Phys.* **2000**, *113*, 2563-2569.
- [38] F. G. Bordwell, *Acc. Chem. Res.* **1988**, *21*, 456-463.
- [39] H. Mayr, A. R. Ofial, E.-U. Würthwein, N. C. Aust, *J. Am. Chem. Soc.* **1997**, *119*, 12727-12733.
- [40] (a) A. C. Skapski, F. A. Stephens, *J. Cryst. Mol. Struct.* **1974**, *4*, 77-85; (b) A. Fischer, D. Wiebelhaus, *Z. Kristallogr. - New Cryst. Struct.* **1997**, *212*, 335-336.
- [41] M. C. Ramirez de Arellano, *Private Communication* **1997**, CCDC 100328.
- [42] S. Tsuzuki, A. Fujii, *Phys. Chem. Chem. Phys.* **2008**, *10*, 2584-2594.
- [43] (a) T. Steiner, A. M. M. Schreurs, J. A. Kanters, J. Kroon, J. van der Maas, B. Lutz, *J. Mol. Struct.* **1997**, *436-437*, 181-187; (b) T. Steiner, A. M. M. Schreurs, M. Lutz, J. Kroon, *New J. Chem.* **2001**, *25*, 174-178; (c) T. Alaviuhkola, J. Bobacka, M. Nissinen, K. Rissanen, A. Ivaska, J. Pursiainen, *Chem. Eur. J.* **2005**, *11*, 2071-2080.
- [44] (a) J. A. N. F. Gomes, R. B. Mallion, *Chem. Rev.* **2001**, *101*, 1349-1383; (b) G. Merino, T. Heine, G. Seifert, *Chem. Eur. J.* **2004**, *10*, 4367-4371.

- [45] (a) P. Hobza, Z. Havlas, *Chem. Rev.* **2000**, *100*, 4253-4264; (b) A. Masunov, J. J. Dannenberg, R. H. Contreras, *J. Phys. Chem. A* **2001**, *105*, 4737-4740; (c) K. Hermansson, *J. Phys. Chem. A* **2002**, *106*, 4695-4702; (d) I. V. Alabugin, M. Manoharan, S. Peabody, F. Weinhold, *J. Am. Chem. Soc.* **2003**, *125*, 5973-5987; (e) E. S. Kryachko, in *Hydrogen Bonding - New Insights* (Ed.: S. J. Grabowski), Springer, Dordrecht, **2006**, pp. 293-336; (f) A. D. Buckingham, J. E. Del Bene, S. A. C. McDowell, *Chem. Phys. Lett.* **2008**, *463*, 1-10.
- [46] J. Joseph, E. D. Jemmis, *J. Am. Chem. Soc.* **2007**, *129*, 4620-4632.
- [47] E. Arunan, G. R. Desiraju, R. A. Klein, J. Sadlej, S. Scheiner, I. Alkorta, D. C. Clary, R. H. Crabtree, J. J. Dannenberg, P. Hobza, H. G. Kjaergaard, A. C. Legon, B. Mennucci, D. J. Nesbitt, *Pure Appl. Chem.* **2011**, *83*, 1619-1636.
- [48] A. Y. Li, *J. Mol. Struct. (Theochem)* **2008**, *862*, 21-27.
- [S1] B. Denegri, A. Streiter, S. Jurić, A. R. Ofial, O. Kronja, H. Mayr, *Chem. Eur. J.* **2006**, *12*, 1648-1656, 5415.
- [S2] C. Nolte, H. Mayr, *Eur. J. Org. Chem.* **2010**, 1435-1439.
- [S3] J. Cvengros, S. Toma, S. Marque, A. Loupy, *Can. J. Chem.* **2004**, *82*, 1365-1371.
- [S4] H. Ohmori, S. Nakai, M. Sekuguchi, M. Masui, *Chem. Pharm. Bull.* **1980**, *28*, 910-915.
- [S5] R. Mazurkiewicz, T. Gorewoda, A. Kuźnik, M. Grymel, *Tetrahedron Lett.* **2006**, *47*, 4219-4220.
- [S6] Y. V. Belkin, N. A. Polezhaeva, B. A. Arbuzov, *Bull. Acad. Sci. USSR Div. Chem. Sci. (Engl. Transl.)* **1977**, *26*, 2423-2425.
- [S7] V. Hebbe, A. Londez, C. Goujon-Ginglinger, F. Meyer, J. Uziel, S. Jugé, J. Lacour, *Tetrahedron Lett.* **2003**, *44*, 2467-2471.
- [S8] E. Schaumann, F.-F. Grabley, *Liebigs Ann. Chem.* **1979**, 1702-1714.
- [S9] K. Okuma, T. Izaki, *Bull. Chem. Soc. Jpn.* **2005**, *78*, 1831-1833.
- [S10] S. Affandi, R. L. Green, B. T. Hsieh, M. S. Holt, J. H. Nelson, E. C. Alyea, *Synth. React. Inorg. Met.-Org. Chem.* **1987**, *17*, 307-318.
- [S11] D. A. Clark, P. L. Fuchs, *Synthesis* **1977**, 628-629.
- [S12] Z.-L. Zhou, J. F. W. Keana, *J. Org. Chem.* **1999**, *64*, 3763-3766.
- [S13] The ¹H- and ¹³C-NMR spectra of these compounds are shown in Section 1.S.3.4.4.

[S14] The small amounts of impurities are unproblematic for the photogeneration of benzhydryl cations from this precursor. Further purification of this compound was therefore considered unnecessary.

1.S Supplementary Data and Experimental Section

1.S.1 Supplementary Tables and Figures

Table 1.S.1. Concentration-dependent ^1H -NMR chemical shifts δ_{H} (600 MHz) for the C(α)-H protons of $\text{Ph}_2\text{CH-PPH}_3^+$ ions (**2a**) with different counterions X^- in CD_3CN .

salt	[2a X^-] / M	δ_{H} / ppm	salt	[2a X^-] / M	δ_{H} / ppm
2a BPh_4^-	1.74×10^{-5}	6.27	2a Br^-	2.57×10^{-5}	6.28
	1.03×10^{-4}	6.27		5.08×10^{-5}	6.28
	1.76×10^{-3}	6.27		9.97×10^{-5}	6.29
	1.09×10^{-2}	6.27		4.32×10^{-4}	6.32
	2.79×10^{-2}	6.27		1.05×10^{-3}	6.38
2a SbF_6^-	1.07×10^{-2}	6.27		2.59×10^{-3}	6.50
				6.50×10^{-3}	6.69
2a BF_4^-	1.01×10^{-2}	6.28		8.99×10^{-3}	6.77
				2.27×10^{-2}	not soluble
				2a Cl^-	3.81×10^{-3}
			7.55×10^{-3}		6.96
			1.03×10^{-2}		7.08

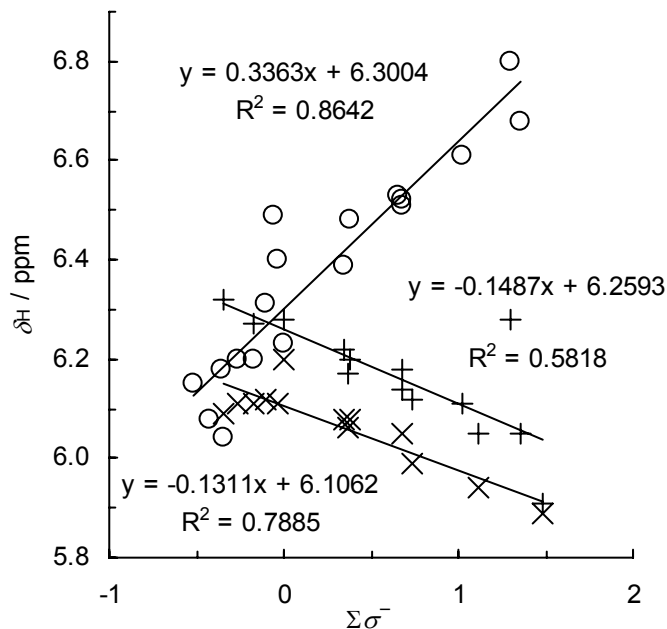
**Figure 1.S.1.** Hammett plot of ^1H -NMR chemical shifts δ_{H} for the C(α)-H protons of **2(a,d-t)** BF_4^- in CD_2Cl_2 (\circ), as well as substituted benzhydryl chlorides (\times) and benzhydryl bromides ($+$) in CDCl_3 (data from refs. ^[S1,S2] and this work) versus the sums of the σ^- parameters of their substituents.

Table 1.S.2. Selected NMR data for benzhydryl triarylphosphonium salts in CD₂Cl₂ solution. The spectra were recorded under conditions where the phosphonium salts exist as ion pairs.

salt	R ¹	R ²	PAr ₃	P ⁺ -C(α)-H			¹¹ BF ₄ ^{-a}	
				δ _H / ppm (² J _{H,P} / Hz)	δ _C / ppm (¹ J _{C,P} / Hz)	δ _p / ppm	δ _F / ppm (¹ J _{F,B} / Hz)	
2a	Br ⁻	H	H	PPh ₃	8.10 (18.0)	45.9 (42.3)	22.1	-
3a	Br ⁻	H	H	P(4-Cl-C ₆ H ₄) ₃	8.49 (18.3)	45.5 (41.2)	21.8	-
2a	BF ₄ ⁻	H	H	PPh ₃	6.23 (17.4)	49.6 (43.9)	21.8	-152.0 (1.2)
3a	BF ₄ ⁻	H	H	P(4-Cl-C ₆ H ₄) ₃	6.50 (17.6)	48.6 (42.8)	21.7	-151.0 (1.4)
2r	BF ₄ ⁻	<i>m,m'</i> -F ₂	<i>m</i> -F	PPh ₃	6.61 (17.6)	47.1 (45.6)	22.5	-150.8 (1.3)
3r	BF ₄ ⁻	<i>m,m'</i> -F ₂	<i>m</i> -F	P(4-Cl-C ₆ H ₄) ₃	6.76 (17.7)	46.6 (45.4)	22.4	-150.1 (1.3)
2t	BF ₄ ⁻	<i>m,m'</i> -F ₂	<i>m,m'</i> -F ₂	PPh ₃	6.68 (17.6)	46.6 (46.2)	22.6	-150.4 (1.3)
3t	BF ₄ ⁻	<i>m,m'</i> -F ₂	<i>m,m'</i> -F ₂	P(4-Cl-C ₆ H ₄) ₃	7.16 (18.4)	44.2 (45.9)	22.4	-148.3 (- ^b)

^a Isotopomer signal for ¹⁰BF₄⁻ downfield by Δδ_F < +0.1 ppm. ^b Not resolved.

Table 1.S.3. ¹H-NMR chemical shifts δ_H for the α-protons of selected phosphonium salts (ion pairs) with different counter-anions X⁻ in CD₂Cl₂ and CDCl₃ solution.

phosphonium salt	solvent	X ⁻	ΔG _t ^{0 a} / kJ mol ⁻¹	δ _H / ppm (² J _{H,P} / Hz)	ref.
PhCH ₂ -PPh ₃ ⁺ (1a)	CDCl ₃	Cl ⁻	42.1	5.59 (14.4) ^b	[S3]
		Br ⁻	31.3	5.44 (14.6) ^c	[S3]
		I ⁻	16.8	5.08 (13.5)	[7]
		ClO ₄ ⁻	2	4.65 (15)	[S4]
		BF ₄ ⁻	(~0) ^d	4.67 (14.2)	[S5]
		BPh ₄ ⁻	-32.8	3.91	[S6]
		CD ₂ Cl ₂	Cl ⁻	42.1	5.47 (14.7)
BF ₄ ⁻	(~0) ^d		4.56 (14.1)	^e	
BPh ₄ ⁻	-32.8		3.93 (13.8)	^e	
PhCH(CH ₃)-PPh ₃ ⁺	CDCl ₃	Br ⁻	31.3	~6.85 ^f	[S7]
		I ⁻	16.8	6.14	[S8]
		BF ₄ ⁻	(~0) ^d	5.27 (14.4)	[S9]
Ph ₂ CH-PPh ₃ ⁺ (2a)	CD ₂ Cl ₂	Cl ⁻	42.1	8.50 (18.3)	^e
		Br ⁻	31.3	8.10 (18.0)	^e
		BF ₄ ⁻	(~0) ^d	6.23 (17.4)	^e
		SbF ₆ ^{-g}	^g	5.98 (17.2)	^e
		BPh ₄ ⁻	-32.8	5.72 (17.1)	^e
dfp(mfp)CH-P(<i>p</i> -Cl-C ₆ H ₄) ₃ ⁺ (3r) dfp = 3,5-F ₂ -C ₆ H ₃ mfp = 3-F-C ₆ H ₄	CD ₂ Cl ₂	Br ⁻	31.3	8.91 (18.3)	^e
		BF ₄ ⁻	(~0) ^d	6.76 (17.7)	^e
		SbF ₆ ^{-g}	^g	6.22 (17.3)	^e

^a Single free ion energies of transfer ΔG_t⁰ (25 °C) for the transfer of the anions X⁻ from H₂O to CH₃CN; from ref.^[34] ^b Ref.^[7] lists δ_H = 5.29 and ²J_{H,P} = 14.25. ^c Ref.^[7] lists δ_H = 5.19 and ²J_{H,P} = 14.25. ^d For BF₄⁻, ΔG_t⁰ ≈ 0 was estimated.^[39] ^e This work. ^f Determined graphically from published spectrum. ^g Not available.

Table 1.S.4. Concentration-dependent ^1H -NMR chemical shifts δ_{H} (600 MHz, CD_2Cl_2) for the C(α)-H protons of $\text{PhCH}_2\text{-PPh}_3^+$ ions (**1a**) and estimated dissociation constants K_{D} (M) for **1a** X^- salts with different counterions X^- .

salt	[1a X^-] / M	δ_{H} / ppm	$x_{\text{paired, exp}}^a$	K_{D}^b / M	$x_{\text{paired, calc}}^c$
1a BPh_4^-	1.75×10^{-5}	4.32	0.11		0.06
	8.11×10^{-5}	4.26	0.25		0.20
	8.92×10^{-4}	4.11	0.59	2.5×10^{-4}	(0.59)
	2.09×10^{-2}	3.97	0.91		0.90
	5.88×10^{-2}	3.93	1.00		0.94
1a BF_4^-	2.08×10^{-5}	4.39	0.11		0.15
	1.53×10^{-4}	4.45	0.42	(1×10^{-4})	(0.42)
	1.68×10^{-3}	4.52	0.79		0.78
	2.83×10^{-2}	4.56	1.00		0.94
	6.33×10^{-2}	4.56	1.00		0.96
1a Cl^-	4.37×10^{-5}	4.71	0.31	6.8×10^{-5}	(0.31)
	1.50×10^{-4}	5.21	0.76		0.52
	1.65×10^{-3}	5.40	0.94		0.82
	2.10×10^{-2}	5.45	0.98		0.94
	6.14×10^{-2}	5.47	1.00		0.97

^a Assuming $\delta_{\text{H, unpaired}} = 4.37$ ppm. ^b Estimate of K_{D} derived from the data for phosphonium salt concentrations where $x_{\text{paired, exp}} \approx 0.5$. ^c Calculated using K_{D} from this table.

Table 1.S.5. Concentration-dependent ^1H -NMR chemical shifts δ_{H} (600 MHz, CD_2Cl_2) for the C(α)-H protons of $(p\text{-F}_3\text{C-C}_6\text{H}_4)\text{CH}_2\text{-PPh}_3^+$ ions (**1b**) and estimated dissociation constants K_{D} (M) for **1b** X^- salts with different counterions X^- .

salt	[1b X^-] / M	δ_{H} / ppm	$x_{\text{paired, exp}}^a$	K_{D}^b / M	$x_{\text{paired, calc}}^c$
1b BPh_4^-	1.97×10^{-5}	4.31	0.17		0.13
	1.44×10^{-4}	4.11	0.42	1.1×10^{-4}	(0.42)
	1.98×10^{-3}	3.84	0.77		0.79
	1.67×10^{-2}	3.71	0.94		0.92
	4.97×10^{-2}	3.66	1.00		0.95
1b BF_4^-	1.85×10^{-5}	4.49	0.18		0.21
	1.70×10^{-4}	4.60	0.57	(5×10^{-5})	(0.57)
	1.87×10^{-3}	4.68	0.86		0.84
	3.34×10^{-2}	4.71	0.96		0.96
	6.39×10^{-2}	4.72	1.00		0.97
1b Br^-	1.99×10^{-5}	4.98	0.40		0.32
	1.47×10^{-4}	5.3 ^d	0.64	2.9×10^{-5}	(0.64)
	1.62×10^{-3}	5.53	0.81		0.87
	3.26×10^{-2}	5.72	0.96		0.97
	5.87×10^{-2}	5.78	1.00		0.98

^a Assuming $\delta_{\text{H, unpaired}} = 4.44$ ppm. ^b Estimate of K_{D} derived from the data for phosphonium salt concentrations where $x_{\text{paired, exp}} \approx 0.5$. ^c Calculated using K_{D} from this table. ^d Superimposed with solvent signal.

Table 1.S.6. ^{11}B -NMR (128 MHz), ^1H -NMR (400 MHz) and ^{13}C -NMR (100 MHz) data for the BPh_4^- anion in the phosphonium salts **1a,b** BPh_4^- and **2a** BPh_4^- in CD_2Cl_2 . The data were determined at concentrations where the phosphonium salts exist as ion pairs.

	B^-	$o\text{-BPh}_4^-$	$m\text{-BPh}_4^-$	$p\text{-BPh}_4^-$
salt	$\delta_{\text{B}} / \text{ppm}$	$\delta_{\text{H}} / \text{ppm}$	$\delta_{\text{H}} / \text{ppm}$	$\delta_{\text{H}} / \text{ppm}$
1a BPh_4^-	-7.6	7.29-7.33	6.95-6.98	6.83-6.87
1b BPh_4^-	-7.6	7.28-7.32	6.92-6.96	6.82-6.86
2a BPh_4^-	-7.6	7.27-7.36 ^a	6.97-7.02	6.82-6.88
“free” BPh_4^- ^b	- ^c	7.29-7.32	7.01-7.04	6.86-6.89
	$i\text{-BPh}_4^-$	$o\text{-BPh}_4^-$	$m\text{-BPh}_4^-$	$p\text{-BPh}_4^-$
salt	$\delta_{\text{C}} / \text{ppm}$	$\delta_{\text{C}} / \text{ppm}$	$\delta_{\text{C}} / \text{ppm}$	$\delta_{\text{C}} / \text{ppm}$
	($^1J_{\text{C,B}} / \text{Hz}$)	($^2J_{\text{C,B}} / \text{Hz}$)	($^3J_{\text{C,B}} / \text{Hz}$)	
1a BPh_4^-	164.6	136.5	126.2	122.3
	(49.3)	(1.4)	(2.8)	(-) ^d
1b BPh_4^-	164.5	136.6	126.3	122.4
	(49.0)	(-) ^e	(-) ^e	(-) ^d
2a BPh_4^-	~165	136.5	126.2	122.3
	(49.4)	(1.4)	(2.8)	(-) ^d

^a Superimposed with other signals. ^b Identical values were determined from ^1H -NMR (600 MHz) spectra of ca. 2×10^{-5} M solutions of **1a,b** BPh_4^- or **2a** BPh_4^- in CD_2Cl_2 . At these concentrations, the salts predominantly exist in the form of the free (unpaired) ions. ^c Not determined. ^d Singlet. ^e Not resolved.

1.S.2 General

NMR measurements. The concentration-dependent ^1H -NMR studies were performed with a Varian 600 MHz NMR spectrometer equipped with a cryoprobe. The other NMR spectra were recorded with Varian 300 or 400 MHz NMR spectrometers and with a JEOL Eclipse 400 MHz NMR spectrometer.

The ^1H - and ^{13}C -NMR chemical shifts are given in ppm relative to the deuterated solvent CDCl_3 ($\delta_{\text{H}} = 7.240$ ppm, $\delta_{\text{C}} = 77.23$ ppm), CD_2Cl_2 ($\delta_{\text{H}} = 5.320$ ppm, $\delta_{\text{C}} = 54.00$ ppm), $(\text{CD}_3)_2\text{SO}$ ($\delta_{\text{H}} = 2.500$ ppm, $\delta_{\text{C}} = 39.51$ ppm), or CD_3CN ($\delta_{\text{H}} = 1.940$ ppm). Signal assignment was aided by HSQC and HMBC experiments. In order to assign the signals of the “free” ions, the signal shapes and positions for slightly more diluted samples were compared with the unambiguously assigned signals at high sample concentrations, and this procedure was repeated until the signals for the sample with the lowest concentration could be assigned. The $^1J_{\text{H,C}}$ coupling constants were determined from the ^{13}C -satellites in the ^1H -NMR (600 MHz) spectra.

IR measurements. IR spectra of $\sim 2 \times 10^{-2}$ M solutions of the phosphonium salts in CD_2Cl_2 solution were recorded in a cuvette with KBr windows using a Perkin Elmer Spectrum 1000 infrared spectrometer.

Syntheses and further product characterization. Yields of the syntheses are not optimized. Mass spectra were recorded with a Thermo Finnigan MAT 95 (EI) or a Thermo Finnigan LTQ FT (ESI) mass spectrometer. Elemental analyses were performed with an Elementar vario micro cube (C, H) or a Metrohm 888 Titrando (Br) apparatus; compounds containing Sb were not analyzed. Melting points were determined with a Büchi Melting Point B-540 apparatus and are uncorrected. The samples for the X-ray structure analyses were crystallized from $\text{CH}_2\text{Cl}_2/\text{EtOH}$ or $\text{CH}_2\text{Cl}_2/\text{Et}_2\text{O}$ allowing for very slow evaporation of the solvent.

1.S.3 Synthetic procedures

1.S.3.1 General procedures for benzhydryl triarylphosponium salts (2 X⁻ and 3 X⁻)

General procedure A – Triphenylphosponium tetrafluoroborates (Ar₂CH–PPh₃⁺ BF₄⁻; **2** BF₄⁻). Triphenylphosphine and 8.0 M aqueous HBF₄ (1.0 equiv.) were heated to 120 °C for 30 min or, alternatively, isolated HPPh₃⁺BF₄⁻ was employed. The substituted benzhydrol (**4**, 1.0 equiv.) was added and the mixture was heated to 120-160 °C for 10-120 min. The obtained solid was recrystallized from CH₂Cl₂/EtOH or CH₂Cl₂/Et₂O, yielding 42-90% of the phosponium tetrafluoroborates.

product	conditions	recrystallized from	yield ^a
2a BF ₄ ⁻	145 °C / 1 hr	CH ₂ Cl ₂ /EtOH	64%
2c BF ₄ ⁻	120 °C / 1 hr	CH ₂ Cl ₂ /Et ₂ O	83%
2d BF ₄ ⁻	140 °C / 1 hr	CH ₂ Cl ₂ /EtOH	74%
2e BF ₄ ⁻	145 °C / 2 hrs	CH ₂ Cl ₂ /EtOH	81% ^b
2f BF ₄ ⁻	120 °C / 30 min	CH ₂ Cl ₂ /EtOH	59% ^b
2g BF ₄ ⁻	145 °C / 1 hr	CH ₂ Cl ₂ /EtOH	73%
2h BF ₄ ⁻	145 °C / 1 hr	CH ₂ Cl ₂ /EtOH	73%
2i BF ₄ ⁻	145 °C / 1 hr	CH ₂ Cl ₂ /EtOH	77%
2j BF ₄ ⁻	145 °C / 1 hr	CH ₂ Cl ₂ /EtOH	90% ^b
2k BF ₄ ⁻	145 °C / 1 hr	CH ₂ Cl ₂ /EtOH	73%
2l BF ₄ ⁻	145 °C / 1 hr	CH ₂ Cl ₂ /EtOH	66%
2n BF ₄ ⁻	145 °C / 1 hr	CH ₂ Cl ₂ /EtOH	86%
2o BF ₄ ⁻	145 °C / 1 hr	CH ₂ Cl ₂ /EtOH	71%
2s BF ₄ ⁻	160 °C / 1 hr	CH ₂ Cl ₂ /EtOH	51%

^a Not optimized. ^b Containing small amounts of impurities.

General procedure B – Triarylphosponium bromides (Ar₂CH–PAr₃⁺ Br⁻; **2** Br⁻ and **3** Br⁻). The benzhydryl bromide (**5**) and the phosphine (1.0 equiv.) were heated to 150-180 °C for 0.25-5.5 hrs. The obtained solid was recrystallized from CH₂Cl₂/EtOH or CH₂Cl₂/Et₂O, yielding 49-77% of the phosponium bromides.

product	conditions	recrystallized from	yield ^a
3a Br ⁻	175 °C / 5.5 hrs	CH ₂ Cl ₂ /Et ₂ O	77%
3s Br ⁻	170 °C / 2 hrs	CH ₂ Cl ₂ /EtOH	51%

^a Not optimized.

General procedure C – Tris(4-chlorophenyl)phosphonium tetrafluoroborates ($\text{Ar}_2\text{CH-P}(\text{p-Cl-C}_6\text{H}_4)_3^+ \text{BF}_4^-$; **3** BF_4^-). The phosphonium bromide **3** Br^- was dissolved in CH_2Cl_2 and repeatedly treated with a 5% aqueous NaBF_4 solution. After drying and removal of the solvent, the obtained solid was typically recrystallized from $\text{CH}_2\text{Cl}_2/\text{EtOH}$, yielding 39-99% of the phosphonium tetrafluoroborates.

product	yield ^a
3a BF_4^-	99%

^a Not optimized.

General procedure D – Triarylphosphonium hexafluoroantimonates ($\text{Ar}_2\text{CH-PAr}_3^+ \text{SbF}_6^-$; **2** SbF_6^- and **3** SbF_6^-). The phosphonium bromide **2** Br^- or **3** Br^- was dissolved in CH_2Cl_2 and a solution of AgSbF_6 (1.0-1.1 equiv.) in CH_3CN was added. The silver bromide was filtered off and the solvent was removed in vacuo. The residue was dissolved in CH_2Cl_2 and EtOH was added. Slow evaporation of the CH_2Cl_2 yielded 57-69 % of the phosphonium hexafluoroantimonates.

product	yield ^a
3s SbF_6^-	60%
3t SbF_6^-	69%

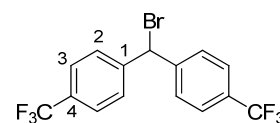
^a Not optimized.

Photochemistry of 2 X⁻ and 3 X⁻. We have previously tested many of the benzhydryl triarylphosphonium salts **2** X^- and **3** X^- as precursors for the photogeneration of benzhydrylium ions.^[19,20] The synthetic procedures in the following will be accompanied by additional information about the photochemistry of the phosphonium salts:

- 👉 Denotes those benzhydryl triarylphosphonium salts, which are well-suited for the photolytic generation of benzhydrylium ions.
- 🔗 Denotes cross references to articles, which describe the behavior of the respective phosphonium salt upon laser flash irradiation (refs. ^[19,20]).

As small impurities in the phosphonium salts **2b,e,f,j** BF_4^- are unproblematic for the photolytic generation of benzhydryl cations from these salts, further purification of these precursors was considered unnecessary.

1.S.3.2 Starting materials

4,4'-Bis(trifluoromethyl)benzhydryl bromide (**5s**)

Analogous to the literature procedure,^[S2] 4,4'-bis(trifluoromethyl)benzhydryl bromide (**5s**, 5.12 g, 16.0 mmol) was dissolved in CH₂Cl₂ (40 ml) at 0 °C in a flame-dried flask under nitrogen atmosphere. A solution of PBr₃ (1.80 ml, 5.18 g, 19.1 mmol) in CH₂Cl₂ (30 ml) was added dropwise and the solution was allowed to warm to room temperature and stirred overnight. Solvent and excess PBr₃ were removed under reduced pressure and the remainder was vacuum-distilled to obtain 4.39 g (11.5 mmol, 72%) of a colorless liquid, b.p. 108 °C / 4.2 × 10⁻² mbar.

¹H NMR (300 MHz, CDCl₃): δ 6.28 (s, 1 H, CHBr), 7.55 (d, *J* = 8.3 Hz, 4 H, 2-Ar), 7.62 (d, ³*J*_{H,H} = 8.7 Hz, 4 H, 3-Ar);

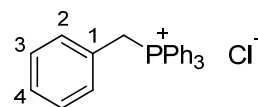
¹³C NMR (75 MHz, CDCl₃): δ 52.5 (s, CHBr), 124.0 (q, ¹*J*_{C,F} = 272.3 Hz, 4-CF₃), 126.0 (q, ³*J*_{C,F} = 3.7 Hz, 3-Ar), 129.0 (s, 2-Ar), 130.9 (q, ²*J*_{C,F} = 32.7 Hz, 4-Ar), 144.3 (q, ⁵*J*_{C,F} = 1.3 Hz, 1-Ar);

¹⁹F NMR (282 MHz, CDCl₃): δ -62.8 (s, 4-CF₃).

HR-MS (EI, positive): Calcd *m/z* for C₁₅H₁₀⁷⁹BrF₅⁺: 363.9883, Found: 363.9888.

Elemental analysis: Calcd for C₁₅H₉BrF₆: C, 47.02; H, 2.37; Br, 20.86, Found: C, 47.01; H, 2.31; Br, 20.65.

Other starting materials. Triphenylphosphine (Acros, 99%), aqueous HBF₄ (~50% in H₂O, purum, Fluka), HBF₄·Et₂O (BASF, 95-98%), NaBF₄ (Apollo, 97%), NaBPh₄ (Fluka, p.a.), AgSbF₆ (Aldrich, 98%) and AgBF₄ (Roth, purum, water-free) were obtained commercially. Tris(4-chlorophenyl)phosphine was purchased (ABCR, 98%) or prepared by a literature method.^[S10] Isolated HPPH₃⁺BF₄⁻ was obtained as described previously.^[S11]

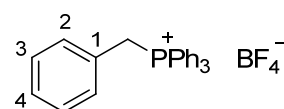
1.S.3.3 Benzyl triphenylphosphonium salts (**1 X⁻**)Benzyltriphenylphosphonium chloride (**1a Cl⁻**)

As purchased (Fluka, >99%).

¹H NMR (400 MHz, CD₂Cl₂): δ 5.42 (d, ²*J*_{H,P} = 14.7 Hz, 2 H, CH₂P⁺), 7.07-7.10 (m, 2 H, 2-Ar), 7.14-7.18 (m, 2 H, 3-Ar), 7.24-7.29 (m, 1 H, 4-Ar), 7.60-7.66 (m, 6 H, *m*-PPh₃), 7.70-7.76 (m, 6 H, *o*-PPh₃), 7.77-7.82 (m, 3 H, *p*-PPh₃);

¹³C NMR (100 MHz, CD₂Cl₂): δ 31.2 (d, ¹*J*_{C,P} = 46.9 Hz, CH₂P⁺), 118.5 (d, ¹*J*_{C,P} = 85.8 Hz, *i*-PPh₃), 128.1 (d, ²*J*_{C,P} = 8.5 Hz, 1-Ar), 129.0 (d, ⁵*J*_{C,P} = 3.9 Hz, 4-Ar), 129.4 (d, ⁴*J*_{C,P} = 3.3 Hz, 3-Ar), 130.6 (d, ³*J*_{C,P} = 12.6 Hz, *m*-PPh₃), 131.9 (d, ³*J*_{C,P} = 5.6 Hz, 2-Ar), 135.0 (d, ²*J*_{C,P} = 9.8 Hz, *o*-PPh₃), 135.5 (d, ⁴*J*_{C,P} = 3.0 Hz, *p*-PPh₃);

³¹P NMR (162 MHz, CD₂Cl₂): δ 23.1.

Benzyltriphenylphosphonium tetrafluoroborate (**1a** BF₄⁻)

As purchased (Acros, 97%).

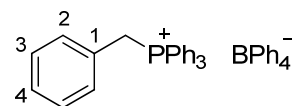
¹H NMR (400 MHz, CD₂Cl₂): δ 4.56 (d, ²J_{H,P} = 14.1 Hz, 2 H, CH₂P⁺), 6.91-6.94 (m, 2 H, 2-Ar), 7.20-7.25 (m, 2 H, 3-Ar), 7.31-7.36 (m, 1 H, 4-Ar), 7.48-7.54 (m, 6 H, *o*-PPh₃), 7.65-7.71 (m, 6 H, *m*-PPh₃), 7.84-7.88 (m, 3 H, *p*-PPh₃);

¹³C NMR (100 MHz, CD₂Cl₂): δ 31.5 (d, ¹J_{C,P} = 49.0 Hz, CH₂P⁺), 117.6 (d, ¹J_{C,P} = 86.1 Hz, *i*-PPh₃), 127.0 (d, ²J_{C,P} = 8.5 Hz, 1-Ar), 129.6 (d, ⁵J_{C,P} = 3.8 Hz, 4-Ar), 129.8 (d, ⁴J_{C,P} = 3.2 Hz, 3-Ar), 130.9 (d, ³J_{C,P} = 12.6 Hz, *m*-PPh₃), 131.5 (d, ³J_{C,P} = 5.5 Hz, 2-Ar), 134.6 (d, ²J_{C,P} = 9.7 Hz, *o*-PPh₃), 136.1 (d, ⁴J_{C,P} = 3.1 Hz, *p*-PPh₃);

¹¹B NMR (128 MHz, CD₂Cl₂): δ -2.1;

¹⁹F NMR (376 MHz, CD₂Cl₂): δ -152.2 (1:1:1:1 quartet, ¹J_{F,B} = 1.0 Hz, ¹¹BF₄⁻), -152.1 (br s, ¹⁰BF₄⁻);

³¹P NMR (162 MHz, CD₂Cl₂): δ 22.2.

Benzyltriphenylphosphonium tetraphenylborate (**1a** BPh₄⁻)

A solution of **1a** Cl⁻ (0.563 g, 1.45 mmol) in CH₂Cl₂ (20 ml) was repeatedly treated with 5% aqueous NaBPh₄ solution (3 × 20 ml) and washed with H₂O (3 × 20 ml). Removal of the solvent in vacuo and drying under high vacuum yielded 0.800 g (1.19 mmol, 82%) of the phosphonium salt as colorless solid, m.p. 224-225 °C.

¹H NMR (400 MHz, CD₂Cl₂): δ 3.94 (d, ²J_{H,P} = 13.8 Hz, 2 H, CH₂P⁺), 6.73-6.76 (m, 2 H, 2-Ar), 6.83-6.87 (m, 4 H, *p*-BPh₄), 6.95-6.98 (m, 8 H, *m*-BPh₄), 7.21-7.28 (m, 8 H, 3-Ar and *o*-PPh₃), 7.29-7.33 (m, 8 H, *o*-BPh₄), 7.34-7.39 (m, 1 H, 4-Ar), 7.57-7.62 (m, 6 H, *m*-PPh₃), 7.79-7.84 (m, 3 H, *p*-PPh₃);

¹³C NMR (100 MHz, CD₂Cl₂): δ 31.7 (d, ¹J_{C,P} = 49.0 Hz, CH₂P⁺), 117.1 (d, ¹J_{C,P} = 86.4 Hz, *i*-PPh₃), 122.3 (s, *p*-BPh₄), 126.2 (1:1:1:1 quartet, ³J_{C,B} = 2.8 Hz, *m*-BPh₄), 126.5 (d, ²J_{C,P} = 8.4 Hz, 1-Ar), 129.7 (d, ⁵J_{C,P} = 3.8 Hz, 4-Ar), 129.8 (d, ⁴J_{C,P} = 3.2 Hz, 3-Ar), 131.0 (d, ³J_{C,P} = 12.6 Hz, *m*-PPh₃), 131.4 (d, ³J_{C,P} = 5.4 Hz, 2-Ar), 134.4 (d, ²J_{C,P} = 9.7 Hz, *o*-PPh₃), 136.2 (d, ⁴J_{C,P} = 3.0 Hz, *p*-PPh₃), 136.5 (1:1:1:1 quartet, ²J_{C,B} = 1.4 Hz, *o*-BPh₄), 164.6 (1:1:1:1 quartet, ¹J_{C,B} = 49.3 Hz, *i*-BPh₄);

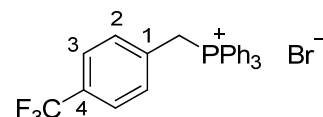
¹¹B NMR (128 MHz, CD₂Cl₂): δ -7.6;

³¹P NMR (162 MHz, CD₂Cl₂): δ 21.6.

HR-MS (ESI, positive): Calcd *m/z* for C₂₅H₂₂P⁺: 353.1454, Found: 353.1456.

HR-MS (ESI, negative): Calcd *m/z* for C₂₄H₂₀B⁻: 319.1664, Found: 319.1661.

Elemental analysis: Calcd for C₄₉H₄₂BP: C, 87.49; H, 6.29, Found: C, 87.23; H, 6.42.

4-(Trifluoromethyl)benzyltriphenylphosphonium bromide (**1b** Br⁻)

p-Trifluoromethylbenzyl bromide and triphenylphosphine were reacted according to a literature procedure.^[S12]

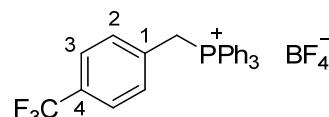
¹H NMR (400 MHz, CD₂Cl₂): δ 5.78 (d, ²*J*_{H,P} = 15.5 Hz, 2 H, CH₂P⁺), 7.36 (m, 4 H, 2-Ar, 3-Ar), 7.58-7.63 (m, 6 H, *m*-PPh₃), 7.76-7.82 (m, 9 H, *o*-PPh₃, *p*-PPh₃);

¹³C NMR (100 MHz, CD₂Cl₂): δ 30.6 (d, ¹*J*_{C,P} = 46.2 Hz, CH₂P⁺), 118.1 (d, ¹*J*_{C,P} = 86.1 Hz, *i*-PPh₃), 124.5 (qm, ¹*J*_{C,F} = 271.4 Hz, ⁷*J*_{C,P} not resolved, 4-CF₃), 125.9 (m, ³*J*_{C,F} and ⁴*J*_{C,P} not resolved, 3-Ar), 130.6 (d, ³*J*_{C,P} = 12.4 Hz, *m*-PPh₃), ~131 (m, superimposed with *m*-PPh₃ signals, 4-Ar), 132.6 (d, ³*J*_{C,P} = 5.2 Hz, 2-Ar), 133.0 (dm, ²*J*_{C,P} = 8.3 Hz, 1-Ar), 135.0 (d, ²*J*_{C,P} = 9.9 Hz, *o*-PPh₃), 135.6 (m, ⁴*J*_{C,P} not resolved, *p*-PPh₃);

¹⁹F NMR (376 MHz, CD₂Cl₂): δ -63.1 (br d, ⁷*J*_{F,P} = 2.7 Hz, 4-CF₃);

³¹P NMR (162 MHz, CD₂Cl₂): δ 23.7 (q, ⁷*J*_{P,F} = 2.7 Hz).

Elemental analysis: Calcd for C₂₆H₂₁BrF₃P: C, 62.29; H, 4.22, Found: C, 62.11; H, 4.24.

4-(Trifluoromethyl)benzyltriphenylphosphonium tetrafluoroborate (**1b** BF₄⁻)

A solution of **1b** Br⁻ (0.334 g, 0.666 mmol) in CH₂Cl₂ (10 ml) was repeatedly treated with 5% aqueous NaBF₄ solution (3 × 7 ml) and washed with H₂O (3 × 7 ml). Removal of the solvent in vacuo and drying under high vacuum yielded 0.291 g (0.573 mmol, 86%) of the phosphonium salt as colorless solid.

¹H NMR (400 MHz, CD₂Cl₂): δ 4.72 (d, ²*J*_{H,P} = 14.7 Hz, 2 H, CH₂P⁺), 7.11 (dd, ³*J*_{H,H} = 8.1 Hz, ⁴*J*_{H,H} = 1.9 Hz, 2-Ar), 7.46 (d, ³*J*_{H,H} = 8.1 Hz, 3-Ar), 7.54-7.60 (m, 6 H, *o*-PPh₃), 7.66-7.71 (m, 6 H, *m*-PPh₃), 7.83-7.88 (m, 3 H, *p*-PPh₃);

¹³C NMR (100 MHz, CD₂Cl₂): δ 30.8 (d, ¹*J*_{C,P} = 49.3 Hz, CH₂P⁺), 117.3 (d, ¹*J*_{C,P} = 86.4 Hz, *i*-PPh₃), 124.3 (qm, ¹*J*_{C,F} = 271.4 Hz, ⁷*J*_{C,P} not resolved, 4-CF₃), 126.5 (m, ³*J*_{C,F} and ⁴*J*_{C,P} not resolved, 3-Ar), 131.0 (d, ³*J*_{C,P} = 12.7 Hz, *m*-PPh₃), ~131 (m, superimposed with *m*-PPh₃ signals, 4-Ar), 131.9 (dm, ²*J*_{C,P} = 8.6 Hz, 1-Ar), 132.1 (d, ³*J*_{C,P} = 5.3 Hz, 2-Ar), 134.6 (d, ²*J*_{C,P} = 9.8 Hz, *o*-PPh₃), 136.1 (d, ⁴*J*_{C,P} = 3.0 Hz, *p*-PPh₃);

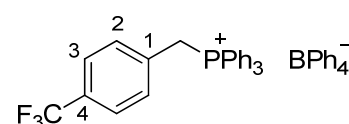
¹¹B NMR (128 MHz, CD₂Cl₂): δ -2.0;

¹⁹F NMR (376 MHz, CD₂Cl₂): δ -151.5 (m, ¹¹BF₄⁻), -151.5 (m, ¹⁰BF₄⁻), -63.2 (m);

³¹P NMR (162 MHz, CD₂Cl₂): δ 22.8 (m).

HR-MS (ESI, positive): Calcd *m/z* for C₂₆H₂₁F₃P⁺: 421.1327, Found: 421.1324.

Elemental analysis: Calcd for C₂₆H₂₁BF₇P: C, 61.45; H, 4.16, Found: C, 61.11; H, 4.21.

4-(Trifluoromethyl)benzyltriphenylphosphonium tetraphenylborate (**1b** BPh₄⁻)

A solution of **1b** Br⁻ (0.271 g, 0.541 mmol) in CH₂Cl₂ (15 ml) was repeatedly treated with 5% aqueous NaBPh₄ solution (3 × 10 ml) and washed with H₂O (3 × 10 ml). Removal of the solvent in vacuo and drying under high vacuum yielded 0.265 g (0.358 mmol, 66%) of the phosphonium salt as colorless solid, m.p. 200-203 °C.

¹H NMR (400 MHz, CD₂Cl₂): δ 3.66 (d, ²J_{H,P} = 14.2 Hz, 2 H, CH₂P⁺), 7.75 (dd, ³J_{H,H} = 8.0 Hz, ⁴J_{H,H} = 1.6 Hz, 2-Ar), 6.82-6.86 (m, 4 H, *p*-BPh₄), 6.92-6.96 (m, 8 H, *m*-BPh₄), 7.19-7.24 (m, 6 H, *o*-PPh₃), 7.28-7.32 (m, 8 H, *o*-BPh₄), 7.45 (d, ³J_{H,H} = 8.0 Hz, 3-Ar), 7.57-7.62 (m, 6 H, *m*-PPh₃), 7.80-7.85 (m, 3 H, *p*-PPh₃);

¹³C NMR (100 MHz, CD₂Cl₂): δ 30.9 (d, ¹J_{C,P} = 48.5 Hz, CH₂P⁺), 116.7 (d, ¹J_{C,P} = 85.3 Hz, *i*-PPh₃), 122.4 (s, *p*-BPh₄), 124.3 (qm, ¹J_{C,F} = 271.7 Hz, ⁷J_{C,P} not resolved, 4-CF₃), 126.3 (m, ³J_{C,B} not resolved, *m*-BPh₄), 126.5 (m, ³J_{C,F} and ⁴J_{C,P} not resolved, 3-Ar), 131.1 (d, ³J_{C,P} = 12.6 Hz, *m*-PPh₃), ~131 (m, superimposed with *m*-PPh₃, 1-Ar), ~131 (m, superimposed with other 131-132 ppm signals, 4-Ar), 132.0 (d, ³J_{C,P} = 5.2 Hz, 2-Ar), 134.3 (d, ²J_{C,P} = 9.8 Hz, *o*-PPh₃), 136.3 (m, ⁴J_{C,P} not resolved, *p*-PPh₃), 136.6 (br s, ²J_{C,B} not resolved, *o*-BPh₄), 164.5 (1:1:1:1 quartet, ¹J_{C,B} = 49.0 Hz, *i*-BPh₄);

¹¹B NMR (128 MHz, CD₂Cl₂): δ -7.6;

¹⁹F NMR (376 MHz, CD₂Cl₂): δ -63.2 (br d, ⁷J_{F,P} = 2.5 Hz, 4-CF₃);

³¹P NMR (162 MHz, CD₂Cl₂): δ 21.8 (q, ⁷J_{P,F} = 2.5 Hz).

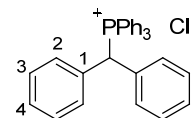
HR-MS (ESI, positive): Calcd *m/z* for C₂₆H₂₁F₃P⁺: 421.1327, Found: 421.1326.

HR-MS (ESI, negative): Calcd *m/z* for C₂₄H₂₀B⁻: 319.1664, Found: 319.1664.

Elemental analysis: Calcd for C₅₀H₄₁BF₃P: C, 81.08; H, 5.58, Found: C, 80.97; H, 5.46.

1.S.3.4 Benzhydryl triarylposphonium salts (2 X⁻ and 3 X⁻)1.S.3.4.1 Benzhydryl triphenylphosphonium salts (2a X⁻)Benzhydryltriphenylphosphonium chloride (2a Cl⁻)

E12-PPh₃⁺ Cl⁻ in ref.^[19]



Triphenylphosphine (2.10 g, 8.01 mmol) and 37% aqueous HCl (1.54 g, 15.2 mmol) were heated to 120 °C for 30 min. Benzhydrol (1.47 g, 7.98 mmol) was added and the mixture was heated to 145 °C for 1 hr. The obtained solid was recrystallized from 35 ml CH₂Cl₂/Et₂O (6:1 v/v), washed with Et₂O and dried, yielding 2.13 g (4.58 mmol, 57%) of a colorless solid with m.p. 255-256 °C (CH₂Cl₂/Et₂O).

¹H NMR (400 MHz, CD₂Cl₂): δ 7.20-7.30 (m, 6 H, 3-Ar and 4-Ar), 7.55-7.60 (m, 10 H, 2-Ar and *m*-PPh₃), 7.72-7.77 (m, 3 H, *p*-PPh₃), 7.79-7.84 (m, 6 H, *o*-PPh₃), 8.25 (d, ²J_{H,P} = 18.3 Hz, 1 H, CHP⁺);

^{13}C NMR (100 MHz, CD_2Cl_2): δ 45.3 (d, $^1J_{\text{C,P}} = 41.8$ Hz, CHP^+), 119.2 (d, $^1J_{\text{C,P}} = 82.3$ Hz, *i*-PPh₃), 129.0 (d, $^5J_{\text{C,P}} = 2.7$ Hz, 4-Ar), 129.4 (d, $^4J_{\text{C,P}} = 1.5$ Hz, 3-Ar), 130.3 (d, $^3J_{\text{C,P}} = 12.3$ Hz, *m*-PPh₃), 131.7 (d, $^3J_{\text{C,P}} = 6.9$ Hz, 2-Ar), 134.3 (d, $^2J_{\text{C,P}} = 4.0$ Hz, 1-Ar), 135.2 (d, $^4J_{\text{C,P}} = 3.1$ Hz, *p*-PPh₃), 135.7 (d, $^2J_{\text{C,P}} = 9.2$ Hz, *o*-PPh₃);

^{31}P NMR (162 MHz, CD_2Cl_2): δ 22.1.

HR-MS (ESI, positive): Calcd m/z for $\text{C}_{31}\text{H}_{26}\text{P}^+$: 429.1767, Found: 429.1765.

Elemental analysis: Calcd for $\text{C}_{31}\text{H}_{26}\text{ClP}$: C, 80.08; H, 5.64, Found: C, 79.85; H, 5.66.

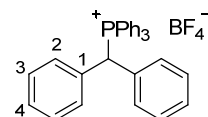
Benzhydryltriphenylphosphonium tetrafluoroborate (**2a** BF_4^-)



precursor for Ph_2CH^+



E12– $\text{PPh}_3^+ \text{BF}_4^-$ in ref. [19]
E25– $\text{PPh}_3^+ \text{BF}_4^-$ in ref. [20]



Benzhydryltriphenylphosphonium tetrafluoroborate (**2a** BF_4^-). Triphenylphosphine (2.10 g, 8.01 mmol) and 8.0 M aqueous HBF_4 (1.00 ml, 8.00 mmol) were heated to 120 °C for 30 min. Benzhydrol (1.47 g, 7.98 mmol) was added and the mixture was heated to 145 °C for 1 hr. The obtained solid was dissolved in hot CH_2Cl_2 (100 ml) and EtOH (150 ml) was added. Colorless crystals formed after slow evaporation of the CH_2Cl_2 and were filtered off, washed with EtOH and dried, yielding 2.62 g (5.07 mmol, 64%) of a colorless solid with m.p. 303–304 °C ($\text{CH}_2\text{Cl}_2/\text{EtOH}$).

^1H NMR (400 MHz, CD_2Cl_2): δ 6.23 (d, $^2J_{\text{H,P}} = 17.4$ Hz, 1 H, CHP^+), 7.19–7.22 (m, 4 H, 2-Ar), 7.28–7.33 (m, 4 H, 3-Ar), 7.35–7.40 (m, 2 H, 4-Ar), 7.43–7.49 (m, 6 H, *o*-PPh₃), 7.59–7.65 (m, 6 H, *m*-PPh₃), 7.81–7.85 (m, 3 H, *p*-PPh₃);

^{13}C NMR (100 MHz, CD_2Cl_2): δ 49.6 (d, $^1J_{\text{C,P}} = 43.9$ Hz, CHP^+), 118.3 (d, $^1J_{\text{C,P}} = 82.5$ Hz, *i*-PPh₃), 129.9 (d, $^5J_{\text{C,P}} = 2.6$ Hz, 4-Ar), 130.0 (d, $^4J_{\text{C,P}} = 1.7$ Hz, 3-Ar), 130.8 (d, $^3J_{\text{C,P}} = 12.4$ Hz, *m*-PPh₃), 131.1 (d, $^3J_{\text{C,P}} = 6.6$ Hz, 2-Ar), 132.9 (d, $^2J_{\text{C,P}} = 4.1$ Hz, 1-Ar), 135.3 (d, $^2J_{\text{C,P}} = 9.1$ Hz, *o*-PPh₃), 135.9 (d, $^4J_{\text{C,P}} = 3.1$ Hz, *p*-PPh₃);

^{11}B NMR (128 MHz, CD_2Cl_2): δ –2.0;

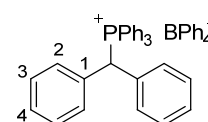
^{19}F NMR (376 MHz, CD_2Cl_2): δ –152.0 (1:1:1:1 quartet, $^1J_{\text{F,B}} = 1.2$ Hz, $^{11}\text{BF}_4^-$), –151.9 (br s, $^{10}\text{BF}_4^-$);

^{31}P NMR (162 MHz, CD_2Cl_2): δ 21.8.

HR-MS (ESI, positive): Calcd m/z for $\text{C}_{31}\text{H}_{26}\text{P}^+$: 429.1767, Found: 429.1769.

Elemental analysis: Calcd for $\text{C}_{31}\text{H}_{26}\text{BF}_4\text{P}$: C, 72.11; H, 5.08, Found: C, 72.29; H, 5.02.

Alternative synthesis of 2a BF_4^- by anion metathesis using AgBF_4 . A solution of AgBF_4 (0.20 g, 1.0 mmol) in anhydrous CH_3CN (7 ml) was added dropwise to a solution of **2a** Br^- (0.47 g, 0.92 mmol) in CH_2Cl_2 (7 ml). After stirring for 30 minutes, the solution was decanted from the precipitated AgBr and the solvent was removed under reduced pressure. The obtained solid was dissolved in hot CH_2Cl_2 (14 ml) and EtOH (10 ml) was added. Colorless crystals formed after slow evaporation of the CH_2Cl_2 and were filtered off, washed with EtOH and dried, yielding 0.43 g (0.83 mmol, 90%) of a colorless solid. Spectroscopic data: see above. Elemental analysis: Calcd for $\text{C}_{31}\text{H}_{26}\text{BF}_4\text{P}$: C, 72.11; H, 5.08, Found: C, 72.04; H, 5.05.

Benzhydryltriphenylphosphonium tetraphenylborate (**2a** BPh₄⁻)

A solution of **2a** Br⁻ (0.56 g, 1.1 mmol) in CH₂Cl₂ (20 ml) was repeatedly treated with 5% aqueous NaBPh₄ solution (6 × 20 ml) and washed with H₂O (3 × 20 ml). Removal of the solvent in vacuo and drying under high vacuum yielded 0.59 g (0.79 mmol, 71%) of the phosphonium salt as colorless needles with m.p. 190-191 °C.

¹H NMR (400 MHz, CD₂Cl₂): δ 5.72 (d, ²J_{H,P} = 17.1 Hz, 1 H, CHP⁺), 6.82-6.88 (m, 4 H, *p*-BPh₄), 6.97-7.02 (m, 8 H, *m*-BPh₄), 7.05-7.10 (m, 4 H, 2-Ar), 7.27-7.36 (m, 18 H, 3-Ar, *o*-PPh₃ and *o*-BPh₄), 7.39-7.47 (m, 2 H, 4-Ar), 7.55-7.62 (m, 6 H, *m*-PPh₃), 7.79-7.86 (m, 3 H, *p*-PPh₃);

¹³C NMR (100 MHz, CD₂Cl₂): δ 51.3 (d, ¹J_{C,P} = 44.3 Hz, CHP⁺), 117.9 (d, ¹J_{C,P} = 82.6 Hz, *i*-PPh₃), 122.3 (s, *p*-BPh₄), 126.2 (1:1:1:1 quartet, ³J_{C,B} = 2.8 Hz, *m*-BPh₄), 130.25 (d, ⁴J_{C,P} = 1.7 Hz, 3-Ar), 130.32 (d, ⁵J_{C,P} = 2.5 Hz, 4-Ar), 130.8 (d, ³J_{C,P} = 6.6 Hz, 2-Ar), 131.0 (d, ³J_{C,P} = 12.2 Hz, *m*-PPh₃), 132.3 (d, ²J_{C,P} = 4.2 Hz, 1-Ar), 135.2 (d, ²J_{C,P} = 9.1 Hz, *o*-PPh₃), 136.3 (d, ⁴J_{C,P} = 3.1 Hz, *p*-PPh₃), 136.5 (1:1:1:1 quartet, ²J_{C,B} = 1.4 Hz, *o*-BPh₄), ~165 (1:1:1:1 quartet, ¹J_{C,B} = 49.4 Hz, *i*-BPh₄);

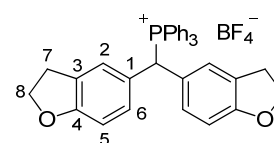
¹¹B NMR (128 MHz, CD₂Cl₂): δ -7.6;

³¹P NMR (162 MHz, CD₂Cl₂): δ 21.6.

HR-MS (ESI, positive): Calcd *m/z* for C₃₁H₂₆P⁺: 429.1767, Found: 429.1772.

HR-MS (ESI, negative): Calcd *m/z* for C₂₄H₂₀B⁻: 319.1664, Found: 319.1665.

Elemental analysis: Calcd for C₅₅H₄₆BP: C, 88.23; H, 6.19, Found: C, 87.91; H, 6.13.

1.S.3.4.2 Substituted benzhydryl triphenylphosphonium tetrafluoroborates (**2b-u** BF₄⁻)[Bis(2,3-dihydrobenzofuran-5-yl)methyl]triphenylphosphonium tetrafluoroborate (**2b** BF₄⁻)precursor for (fur)₂CH⁺
 E1-PPh₃⁺ BF₄⁻ in ref.^[19]
 E13-PPh₃⁺ BF₄⁻ in ref.^[20]


Bis(2,3-dihydrobenzofuran-5-yl)methanol (**4b**, 0.45 g, 1.7 mmol) and PPh₃ (0.44 g, 1.7 mmol) were dissolved in anhydrous CH₂Cl₂ (15 ml) in a nitrogen atmosphere at room temperature and HBF₄·Et₂O (0.23 ml, 0.27 g, 1.7 mmol) was added dropwise to the stirred solution. After addition of Et₂O (15 ml) and refrigeration, the crystallized product was filtered off, washed with Et₂O (20 ml), and dried, yielding a reddish-white solid (0.74 g, 1.2 mmol, 71%), m.p. 219-220 °C (decomp.) (CH₂Cl₂/Et₂O). Another 0.11 g (0.18 mmol, 11%) were obtained from the mother liquor. Both fractions still contained a small amount of impurities.^[S14]

¹H NMR (400 MHz, CD₂Cl₂): δ 3.02-3.15 (m, 4 H, 7-CH₂), 4.55 (t, 4 H, ³J_{H,H} = 8.8 Hz, 8-OCH₂), 6.04 (d, ²J_{H,P} = 17.2 Hz, 1 H, CHP⁺), 6.63 (d, ³J_{H,H} = 8.4 Hz, 2 H, 5-Ar), 6.84 (dt, ³J_{H,H} = 8.3 Hz, ⁴J_{H,H} = 1.9 Hz, 2 H, 6-Ar), 6.96-6.98 (m, 2 H, 2-Ar), 7.43-7.49 (m, 6 H, *o*-PPh₃), 7.60-7.65 (m, 6 H, *m*-PPh₃), 7.80-7.85 (m, 3 H, *p*-PPh₃);

^{13}C NMR (100 MHz, CD_2Cl_2): δ 30.0 (s, 7- CH_2), 49.1 (d, $^1J_{\text{C,P}} = 42.8$ Hz, CHP^+), 72.4 (s, 8- OCH_2), 110.1 (d, $^4J_{\text{C,P}} = 1.7$ Hz, 5-Ar), 118.7 (d, $^1J_{\text{C,P}} = 81.8$ Hz, *i*- PPh_3), 124.6 (d, $^2J_{\text{C,P}} = 3.7$ Hz, 1-Ar), 127.8 (d, $^3J_{\text{C,P}} = 7.1$ Hz, 2-Ar), 129.6 (d, $^4J_{\text{C,P}} = 1.3$ Hz, 3-Ar), 130.6 (d, $^3J_{\text{C,P}} = 12.1$ Hz, *m*- PPh_3), 130.7 (d, $^3J_{\text{C,P}} = 5.8$ Hz, 6-Ar), 135.4 (d, $^2J_{\text{C,P}} = 8.8$ Hz, *o*- PPh_3), 135.7 (d, $^4J_{\text{C,P}} = 3.1$ Hz, *p*- PPh_3), 161.4 (d, $^5J_{\text{C,P}} = 2.5$ Hz, 4-Ar);

^{19}F NMR (376 MHz, CD_2Cl_2): δ -152.2 (m, $^{11}\text{BF}_4^-$ and $^{10}\text{BF}_4^-$);

^{31}P NMR (162 MHz, CD_2Cl_2): δ 20.5.

HR-MS (ESI, positive): Calcd m/z for $\text{C}_{35}\text{H}_{30}\text{O}_2\text{P}^+$: 513.1976, Found: 513.1978.

Elemental analysis: Calcd for $\text{C}_{35}\text{H}_{30}\text{BF}_4\text{O}_2\text{P}$: C, 70.02; H, 5.04, Found: C 69.35, H, 5.00.^[S14]

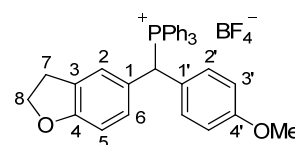
[(2,3-dihydrobenzofuran-5-yl)(4-methoxyphenyl)methyl]-
triphenylphosphonium tetrafluoroborate (2c BF₄⁻)



precursor for fur(ani)CH⁺



E2- $\text{PPh}_3^+ \text{BF}_4^-$ in ref. ^[19]
E14- $\text{PPh}_3^+ \text{BF}_4^-$ in ref. ^[20]



Triphenylphosphine (2.10 g, 8.01 mmol) and 8.0 M aqueous HBF_4 (1.00 ml, 8.00 mmol) were heated to 120 °C for 30 min. Then, (2,3-dihydrobenzofuran-5-yl)(4-methoxyphenyl)methanol (**4c**, 2.05 g, 8.00 mmol) was added and the temperature was kept at 120 °C for another 1 hr. Recrystallizing the obtained solid from $\text{CH}_2\text{Cl}_2/\text{Et}_2\text{O}$ yielded 3.93 g (6.68 mmol, 83%) of a colorless solid, m.p. 222-224 °C (decomp.) ($\text{CH}_2\text{Cl}_2/\text{Et}_2\text{O}$).

^1H NMR (400 MHz, CD_2Cl_2): δ 3.04-3.13 (m, 2 H, 7- CH_2), 3.77 (s, 3 H, 4'- OMe), 4.56 (t, 2 H $^3J_{\text{H,H}} = 8.8$ Hz, 8- OCH_2), 6.04 (d, $^2J_{\text{H,P}} = 17.2$ Hz, 1 H, CHP^+), 6.63 (d, $^3J_{\text{H,H}} = 8.3$ Hz, 1 H, 5-Ar), 6.80-6.84 (m, 3 H, 3'-Ar and 6-Ar), 6.96 (s, 1 H, 2-Ar), 7.05-7.08 (m, 2 H, 2'-Ar), 7.41-7.48 (m, 6 H, *o*- PPh_3), 7.60-7.65 (m, 6 H, *m*- PPh_3), 7.81-7.85 (m, 3 H, *p*- PPh_3);

^{13}C NMR (100 MHz, CD_2Cl_2): δ 30.0 (s, 7- CH_2), 48.9 (d, $^1J_{\text{C,P}} = 43.1$ Hz, CHP^+), 55.9 (s, 4'- OMe), 72.4 (s, 8- OCH_2), 110.1 (d, $^4J_{\text{C,P}} = 1.8$ Hz, 5-Ar), 115.2 (d, $^4J_{\text{C,P}} = 1.6$ Hz, 3'-Ar), 118.6 (d, $^1J_{\text{C,P}} = 81.8$ Hz, *i*- PPh_3), 124.3 (d, $^2J_{\text{C,P}} = 3.8$ Hz, 1-Ar), 124.8 (d, $^2J_{\text{C,P}} = 3.5$ Hz, 1'-Ar), 127.8 (d, $^3J_{\text{C,P}} = 6.9$ Hz, 2-Ar), 129.6 (d, $^4J_{\text{C,P}} = 1.5$ Hz, 3-Ar), 130.67 (d, $^3J_{\text{C,P}} = 12.2$ Hz, *m*- PPh_3), 130.73 (d, $^3J_{\text{C,P}} = 6.4$ Hz, 6-Ar), 132.1 (d, $^3J_{\text{C,P}} = 6.6$ Hz, 2'-Ar), 135.3 (d, $^2J_{\text{C,P}} = 9.0$ Hz, *o*- PPh_3), 135.7 (d, $^4J_{\text{C,P}} = 3.0$ Hz, *p*- PPh_3), 160.7 (d, $^5J_{\text{C,P}} = 2.3$ Hz, 4'-Ar), 161.5 (d, $^5J_{\text{C,P}} = 2.5$ Hz, 4-Ar);

^{19}F NMR (376 MHz, CD_2Cl_2): δ -152.1 (br s, $^{11}\text{BF}_4^-$), -152.1 (br s, $^{10}\text{BF}_4^-$);

^{31}P NMR (162 MHz, CD_2Cl_2): δ 20.6.

HR-MS (ESI, positive): Calcd m/z for $\text{C}_{34}\text{H}_{30}\text{O}_2\text{P}^+$: 501.1976, Found: 501.1979.

Elemental analysis: Calcd for $\text{C}_{34}\text{H}_{30}\text{BF}_4\text{O}_2\text{P}$: C, 69.40; H, 5.14, Found: C 69.37, H, 5.07.

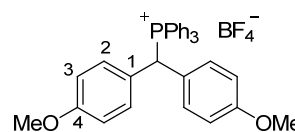
[Bis(4-methoxyphenyl)methyl]triphenylphosphonium
tetrafluoroborate (2d BF₄⁻)



precursor for (ani)₂CH⁺



E3- $\text{PPh}_3^+ \text{BF}_4^-$ in ref. ^[19]
E15- $\text{PPh}_3^+ \text{BF}_4^-$ in ref. ^[20]



Triphenylphosphine (2.10 g, 8.01 mmol) and 8.0 M aqueous HBF_4 (1.00 ml, 8.00 mmol) were heated to 120 °C for 30 min. Then, bis(4-methoxyphenyl)methanol (**4d**, 1.95 g, 7.99 mmol)

was added and the temperature was kept at 140 °C for another 1 hr. The obtained solid was dissolved in hot CH₂Cl₂ (16 ml) and EtOH (16 ml) was added. Colorless crystals formed after slow evaporation of the CH₂Cl₂ and were filtered off, washed with EtOH and dried, yielding 3.41 g (5.92 mmol, 74%) of a colorless solid with m.p. 217 °C (CH₂Cl₂/EtOH).

¹H NMR (400 MHz, CD₂Cl₂): δ 3.76 (s, 6 H, 4-OMe), 6.15 (d, ²J_{H,P} = 17.3 Hz, 1 H, CHP⁺), 6.78-6.82 (m, 4 H, 3-Ar), 7.07-7.11 (m, 4 H, 2-Ar), 7.43-7.49 (m, 6 H, *o*-PPh₃), 7.60-7.65 (m, 6 H, *m*-PPh₃), 7.80-7.85 (m, 3 H, *p*-PPh₃);

¹³C NMR (100 MHz, CD₂Cl₂): δ 48.2 (d, ¹J_{C,P} = 43.2 Hz, CHP⁺), 55.9 (s, 4-OMe), 115.2 (d, ⁴J_{C,P} = 1.7 Hz, 3-Ar), 118.5 (d, ¹J_{C,P} = 82.0 Hz, *i*-PPh₃), 124.7 (d, ²J_{C,P} = 3.8 Hz, 1-Ar), 130.6 (d, ³J_{C,P} = 12.1 Hz, *m*-PPh₃), 132.2 (d, ³J_{C,P} = 6.5 Hz, 2-Ar), 135.3 (d, ²J_{C,P} = 9.0 Hz, *o*-PPh₃), 135.7 (d, ⁴J_{C,P} = 3.1 Hz, *p*-PPh₃), 160.6 (d, ⁵J_{C,P} = 2.5 Hz, 4-Ar);

¹⁹F NMR (376 MHz, CD₂Cl₂): δ -152.1 (br s, ¹¹BF₄⁻), -152.1 (br s, ¹⁰BF₄⁻);

³¹P NMR (162 MHz, CD₂Cl₂): δ 20.8.

HR-MS (ESI, positive): Calcd *m/z* for C₃₃H₃₀O₂P⁺: 489.1976, Found: 489.1975.

Elemental analysis: Calcd for C₃₃H₃₀BF₄O₂P: C, 68.77; H, 5.25, Found: C, 68.49; H, 5.16.

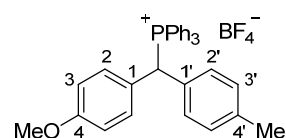
*[(4-Methoxyphenyl)-*p*-tolylmethyl]triphenylphosphonium tetrafluoroborate (2e BF₄⁻)*



precursor for ani(tol)CH⁺



E5-PPh₃⁺ BF₄⁻ in ref. [19]
E17-PPh₃⁺ BF₄⁻ in ref. [20]



Triphenylphosphine (2.10 g, 8.01 mmol) and 8.0 M aqueous HBF₄ (1.00 ml, 8.00 mmol) were heated to 120 °C for 30 min. (4-Methoxyphenyl)-*p*-tolylmethanol (**4e**, 1.80 g, 7.88 mmol) was added and the mixture was heated to 145 °C for 2 hrs. The obtained solid was dissolved in hot CH₂Cl₂ (12 ml) and EtOH (20 ml) was added. Colorless crystals formed after slow evaporation of the CH₂Cl₂ and were filtered off, washed with EtOH and dried, yielding 3.59 g (6.41 mmol, 81%) of a colorless solid, m.p. 203-206 °C (CH₂Cl₂/EtOH), with a small amount of impurities.^[S14]

¹H NMR (400 MHz, CD₂Cl₂): δ 2.32 (s, 3 H, 4'-Me), 3.77 (s, 3 H, 4-OMe), 6.08 (d, ²J_{H,P} = 17.2 Hz, 1 H, CHP⁺), 6.79-6.82 (m, 2 H, 3-Ar), 7.03-7.12 (m, 3 H, 2-Ar, 2'-Ar and 3'-Ar), 7.41-7.46 (m, 6 H, *o*-PPh₃), 7.60-7.65 (m, 6 H, *m*-PPh₃), 7.81-7.85 (m, 3 H, *p*-PPh₃);

¹³C NMR (100 MHz, CD₂Cl₂): δ 21.4 (d, ⁶J_{C,P} = 1.0 Hz, 4'-Me), 48.9 (d, ¹J_{C,P} = 43.5 Hz, CHP⁺), 55.9 (s, 4-OMe), 115.2 (d, ⁴J_{C,P} = 1.8 Hz, 3-Ar), 118.5 (d, ¹J_{C,P} = 82.1 Hz, *i*-PPh₃), 124.4 (d, ²J_{C,P} = 4.1 Hz, 1-Ar), 130.1 (d, ²J_{C,P} = 3.7 Hz, 1'-Ar), 130.6 (d, overlapped with *m*-PPh₃, 3'-Ar), 130.7 (d, ³J_{C,P} = 12.3 Hz, *m*-PPh₃), 130.8 (d, ³J_{C,P} = 6.7 Hz, 2'-Ar) 132.3 (d, ³J_{C,P} = 6.4 Hz, 2-Ar), 135.3 (d, ²J_{C,P} = 9.1 Hz, *o*-PPh₃), 135.8 (d, ⁴J_{C,P} = 3.1 Hz, *p*-PPh₃), 140.1 (d, ⁵J_{C,P} = 2.6 Hz, 4'-Ar), 160.8 (d, ⁵J_{C,P} = 2.4 Hz, 4-Ar);

¹⁹F NMR (376 MHz, CD₂Cl₂): δ -152.4 (1:1:1:1 quartet, ¹J_{F,B} = 1.0 Hz, ¹¹BF₄⁻), -152.3 (br s, ¹⁰BF₄⁻);

³¹P NMR (162 MHz, CD₂Cl₂): δ 21.0.

HR-MS (ESI, positive): Calcd *m/z* for C₃₃H₃₀OP⁺: 473.2027, Found: 473.2029.

Elemental analysis: Calcd for C₃₃H₃₀BF₄OP: C, 70.73; H, 5.40, Found: C, 70.08; H, 5.40.^[S14]

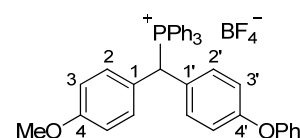
[(4-Methoxyphenyl)(4-phenoxyphenyl)methyl]-
triphenylphosphonium tetrafluoroborate (**2f** BF₄⁻)



precursor for ani(pop)CH⁺



E4-PPh₃⁺ BF₄⁻ in ref. [19]
E16-PPh₃⁺ BF₄⁻ in ref. [20]



Triphenylphosphine (0.71 g, 2.7 mmol) and 8.0 M aqueous HBF₄ (0.34 ml, 2.7 mmol) were heated to 120 °C for 30 min. (4-Methoxyphenyl)(4-phenoxyphenyl)methanol (**4f**, 0.83 g, 2.7 mmol) was added and the mixture was heated to 120 °C for 30 min. The obtained solid was dissolved in hot CH₂Cl₂ (4 ml) and EtOH (6 ml) was added. Colorless crystals formed after slow evaporation of the CH₂Cl₂ and were filtered off, washed with EtOH and dried, yielding 1.0 g (1.6 mmol, 59%) of a colorless solid, m.p. 211-212 °C (CH₂Cl₂/EtOH), with a small amount of impurities.^[S14]

¹H NMR (400 MHz, CD₂Cl₂): δ 3.78 (s, 3 H, 4-OMe), 6.18 (d, ²J_{H,P} = 17.4 Hz, 1 H, CHP⁺), 6.80-6.84 (m, 2 H, 3-Ar), 6.86-6.90 (m, 2 H, 3'-Ar), 6.98-7.02 (m, 2 H, *o*-OPh), 7.07-7.14 (m, 4

H, 2-Ar and 2'-Ar), 7.14-7.19 (m, 1 H, *p*-OPh), 7.34-7.39 (m, 2 H, *m*-OPh), 7.44-7.50 (m, 6 H, *o*-PPh₃), 7.61-7.66 (m, 6 H, *m*-PPh₃), 7.81-7.86 (m, 3 H, *p*-PPh₃);

¹³C NMR (100 MHz, CD₂Cl₂): δ 48.4 (d, ¹J_{C,P} = 43.5 Hz, CHP⁺), 56.0 (s, 4-OMe), 115.3 (d, ⁴J_{C,P} = 1.7 Hz, 3-Ar), 118.5 (d, ¹J_{C,P} = 82.0 Hz, *i*-PPh₃), 119.2 (d, ⁴J_{C,P} = 1.7 Hz, 3'-Ar), 120.2 (s,

o-OPh), 124.4 (d, ²J_{C,P} = 3.9 Hz, 1-Ar), 124.9 (s, *p*-OPh), 127.3 (d, ²J_{C,P} = 3.7 Hz, 1'-Ar), 130.6 (s, *m*-OPh), 130.8 (d, ³J_{C,P} = 12.2 Hz, *m*-PPh₃), 132.3 (d, ³J_{C,P} = 6.5 Hz, 2-Ar), 132.5 (d, ³J_{C,P} = 6.6 Hz, 2'-Ar), 135.4 (d, ²J_{C,P} = 9.1 Hz, *o*-PPh₃), 135.8 (d, ⁴J_{C,P} = 3.0 Hz, *p*-PPh₃), 156.5 (s,

i-OPh), 159.0 (d, ⁵J_{C,P} = 2.5 Hz, 4'-Ar), 160.9 (d, ⁵J_{C,P} = 2.3 Hz, 4-Ar);

¹⁹F NMR (376 MHz, CD₂Cl₂): δ -152.1 (1:1:1:1 quartet, ¹J_{F,B} = 1.1 Hz, ¹¹BF₄⁻), -152.1 (br s, ¹⁰BF₄⁻);

³¹P NMR (162 MHz, CD₂Cl₂): δ 21.0.

HR-MS (ESI, positive): Calcd *m/z* for C₃₈H₃₂O₂P⁺: 551.2132, Found: 551.2130.

Elemental analysis: Calcd for C₃₈H₃₂BF₄O₂P: C, 71.49; H, 5.05, Found: C, 71.01; H, 5.03.^[S14]

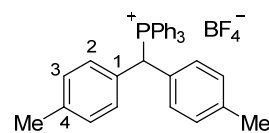
Di-*p*-tolylmethyltriphenylphosphonium tetrafluoroborate (**2g** BF₄⁻)



precursor for (tol)₂CH⁺



E8-PPh₃⁺ BF₄⁻ in ref. [19]
E20-PPh₃⁺ BF₄⁻ in ref. [20]



Triphenylphosphine (1.1 g, 4.2 mmol) and 8.0 M aqueous HBF₄ (0.50 ml, 4.0 mmol) were heated to 120 °C for 30 min. Di-*p*-tolylmethanol (**4g**, 0.85 g, 4.0 mmol) was added and the mixture was heated to 145 °C for 1 hr. The obtained solid was dissolved in hot CH₂Cl₂ (5 ml) and EtOH (10 ml) was added. Colorless crystals formed after slow evaporation of the CH₂Cl₂ and were filtered off, washed with EtOH and dried, yielding 1.6 g (2.9 mmol, 73%) of a colorless solid with m.p. 256 °C (CH₂Cl₂/EtOH).

¹H NMR (400 MHz, CD₂Cl₂): δ 2.32 (d, ⁷J_{H,P} = 1.7 Hz, 6 H, 4-Me), 6.04 (d, ²J_{H,P} = 17.2 Hz, 1 H, CHP⁺), 7.01-7.05 (m, 4 H, 2-Ar), 7.09-7.12 (m, 4 H, 3-Ar), 7.40-7.46 (m, 6 H, *o*-PPh₃), 7.59-7.65 (m, 6 H, *m*-PPh₃), 7.81-7.86 (m, 3 H, *p*-PPh₃);

^{13}C NMR (100 MHz, CD_2Cl_2): δ 21.4 (d, $^6J_{\text{C,P}} = 1.0$ Hz, 4-Me), 49.4 (d, $^1J_{\text{C,P}} = 43.6$ Hz, CHP^+), 118.5 (d, $^1J_{\text{C,P}} = 82.3$ Hz, *i*-PPh₃), 129.8 (d, $^2J_{\text{C,P}} = 4.1$ Hz, 1-Ar), 130.6 (d, $^4J_{\text{C,P}} = 1.8$ Hz, 3-Ar), 130.7 (d, $^3J_{\text{C,P}} = 12.3$ Hz, *m*-PPh₃), 130.8 (d, $^3J_{\text{C,P}} = 6.7$ Hz, 2-Ar), 135.3 (d, $^2J_{\text{C,P}} = 9.1$ Hz,

o-PPh₃), 135.9 (d, $^4J_{\text{C,P}} = 3.0$ Hz, *p*-PPh₃), 140.3 (d, $^5J_{\text{C,P}} = 2.6$ Hz, 4-Ar);

^{19}F NMR (376 MHz, CD_2Cl_2): δ -152.3 (1:1:1:1 quartet, $^1J_{\text{F,B}} = 1.1$ Hz, $^{11}\text{BF}_4^-$), -152.2 (br s, $^{10}\text{BF}_4^-$);

^{31}P NMR (162 MHz, CD_2Cl_2): δ 21.1.

HR-MS (ESI, positive): Calcd m/z for $\text{C}_{33}\text{H}_{30}\text{P}^+$: 457.2078, Found: 457.2079.

Elemental analysis: Calcd for $\text{C}_{33}\text{H}_{30}\text{BF}_4\text{P}$: C, 72.81; H, 5.55, Found: C, 72.59; H, 5.40.

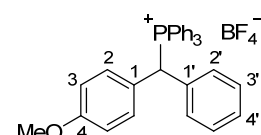
[(4-Methoxyphenyl)phenylmethyl]triphenylphosphonium tetrafluoroborate (**2h** BF_4^-)



precursor for $\text{ani}(\text{Ph})\text{CH}^+$



E5-PPh₃⁺ BF₄⁻ in ref. [19]
E18-PPh₃⁺ BF₄⁻ in ref. [20]



Triphenylphosphine (1.1 g, 4.2 mmol) and 8.0 M aqueous HBF_4 (0.50 ml, 4.0 mmol) were heated to 120 °C for 30 min. 4-Methoxybenzhydrol (**4h**, 0.86 g, 4.0 mmol) was added and the mixture was heated to 145 °C for 1 hr. The obtained solid was dissolved in hot CH_2Cl_2 (50 ml) and EtOH (100 ml) was added. Colorless crystals formed after slow evaporation of the CH_2Cl_2 and were filtered off, washed with EtOH and dried, yielding 1.6 g (2.9 mmol, 73%) of a colorless solid with m.p. 221-223 °C ($\text{CH}_2\text{Cl}_2/\text{EtOH}$).

^1H NMR (400 MHz, CD_2Cl_2): δ 3.76 (s, 3 H, 4-OMe), 6.20 (d, $^2J_{\text{H,P}} = 17.2$ Hz, 1 H, CHP^+), 6.79-6.81 (m, 2 H, 3-Ar), 7.09-7.12 (m, 2 H, 2-Ar), 7.19-7.21 (m, 2 H, 2'-Ar), 7.28-7.32 (m, 2 H,

3'-Ar), 7.35-7.39 (m, 1 H, 4'-Ar), 7.43-7.49 (m, 6 H, *o*-PPh₃), 7.60-7.65 (m, 6 H, *m*-PPh₃), 7.80-7.85 (m, 3 H, *p*-PPh₃);

^{13}C NMR (100 MHz, CD_2Cl_2): δ 48.9 (d, $^1J_{\text{C,P}} = 43.5$ Hz, CHP^+), 55.9 (s, 4-OMe), 115.2 (d, $^4J_{\text{C,P}} = 1.6$ Hz, 3-Ar), 118.4 (d, $^1J_{\text{C,P}} = 82.3$ Hz, *i*-PPh₃), 124.2 (d, $^2J_{\text{C,P}} = 4.4$ Hz, 1-Ar), 129.7 (d, $^5J_{\text{C,P}} = 2.3$ Hz, 4'-Ar), 129.9 (d, $^4J_{\text{C,P}} = 1.3$ Hz, 3'-Ar), 130.7 (d, $^3J_{\text{C,P}} = 12.2$ Hz, *m*-PPh₃), 131.0 (d, $^3J_{\text{C,P}} = 6.9$ Hz, 2'-Ar), 132.4 (d, $^3J_{\text{C,P}} = 6.4$ Hz, 2-Ar), 133.4 (d, $^2J_{\text{C,P}} = 3.5$ Hz, 1'-Ar), 135.3 (d, $^2J_{\text{C,P}} = 9.1$ Hz, *o*-PPh₃), 135.8 (d, $^4J_{\text{C,P}} = 3.0$ Hz, *p*-PPh₃), 160.8 (d, $^5J_{\text{C,P}} = 2.3$ Hz, 4-Ar);

^{19}F NMR (376 MHz, CD_2Cl_2): δ -152.1 (1:1:1:1 quartet, $^1J_{\text{F,B}} = 1.1$ Hz, $^{11}\text{BF}_4^-$), -152.1 (br s, $^{10}\text{BF}_4^-$);

^{31}P NMR (162 MHz, CD_2Cl_2): δ 21.3.

HR-MS (ESI, positive): Calcd m/z for $\text{C}_{32}\text{H}_{28}\text{OP}^+$: 459.1872, Found: 459.1864.

Elemental analysis: Calcd for $\text{C}_{32}\text{H}_{28}\text{BF}_4\text{OP}$: C, 70.35; H, 5.17, Found: C, 70.01; H, 4.94.

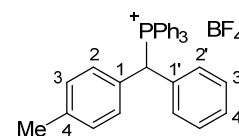
*Triphenyl(phenyl-*p*-tolylmethyl)phosphonium tetrafluoroborate*
(**2i** BF₄⁻)



precursor for **tol(Ph)CH⁺**



E9–PPh₃⁺ BF₄⁻ in ref. [19]
E21–PPh₃⁺ BF₄⁻ in ref. [20]



Triphenylphosphine (2.10 g, 8.01 mmol) and 8.0 M aqueous HBF₄ (1.00 ml, 8.00 mmol) were heated to 120 °C for 30 min. 4-Methylbenzhydrol (**4i**, 1.60 g, 8.07 mmol) was added and the mixture was heated to 145 °C for 1 hr. The obtained solid was dissolved in hot CH₂Cl₂ (20 ml) and EtOH (20 ml) was added. Colorless crystals formed after slow evaporation of the CH₂Cl₂ and were filtered off, washed with EtOH and dried, yielding 3.29 g (6.19 mmol, 77%) of a colorless solid with m.p. 268-269 °C (CH₂Cl₂/EtOH).

¹H NMR (400 MHz, CD₂Cl₂): δ 2.31 (d, ⁷J_{H,P} = 1.9 Hz, 3 H, 4-Me), 6.20 (d, ²J_{H,P} = 17.4 Hz, 1 H, CHP⁺), 7.06-7.11 (m, 4 H, 2-Ar and 3-Ar), 7.19-7.22 (m, 2 H, 2'-Ar), 7.27-7.32 (m, 2 H, 3'-Ar), 7.34-7.39 (m, 1 H, 4'-Ar), 7.43-7.49 (m, 6 H, *o*-PPh₃), 7.59-7.65 (m, 6 H, *m*-PPh₃), 7.80-7.85 (m, 3 H, *p*-PPh₃);

¹³C NMR (100 MHz, CD₂Cl₂): δ 21.3 (d, ⁶J_{C,P} = 1.0 Hz, 4-Me), 49.1 (d, ¹J_{C,P} = 43.8 Hz, CHP⁺), 118.3 (d, ¹J_{C,P} = 82.3 Hz, *i*-PPh₃), 129.6 (d, ²J_{C,P} = 4.4 Hz, 1-Ar), 129.7 (d, ⁵J_{C,P} = 2.5 Hz, 4'-Ar), 129.9 (d, ⁴J_{C,P} = 1.7 Hz, 3'-Ar), 130.5 (d, ⁴J_{C,P} = 1.9 Hz, 3-Ar), 130.7 (d, ³J_{C,P} = 12.3 Hz, *m*-PPh₃), 130.9 (d, ³J_{C,P} = 6.5 Hz, 2-Ar), 131.0 (d, ³J_{C,P} = 6.7 Hz, 2'-Ar), 133.2 (d, ²J_{C,P} = 3.8 Hz, 1'-Ar), 135.3 (d, ²J_{C,P} = 9.0 Hz, *o*-PPh₃), 135.8 (d, ⁴J_{C,P} = 3.1 Hz, *p*-PPh₃), 140.1 (d, ⁵J_{C,P} = 2.9 Hz, 4-Ar);

¹⁹F NMR (376 MHz, CD₂Cl₂): δ -152.2 (1:1:1:1 quartet, ¹J_{F,B} = 1.1 Hz, ¹¹BF₄⁻), -152.2 (br s, ¹⁰BF₄⁻);

³¹P NMR (162 MHz, CD₂Cl₂): δ 21.5.

HR-MS (ESI, positive): Calcd *m/z* for C₃₂H₂₈P⁺: 443.1923, Found: 443.1922.

Elemental analysis: Calcd for C₃₂H₂₈BF₄P: C, 72.47; H, 5.32, Found: C, 72.43; H, 5.27.

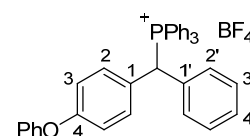
[(4-Phenoxyphenyl)phenylmethyl]triphenylphosphonium
tetrafluoroborate (**2j** BF₄⁻)



precursor for **pop(Ph)CH⁺**



E7–PPh₃⁺ BF₄⁻ in ref. [19]
E19–PPh₃⁺ BF₄⁻ in ref. [20]



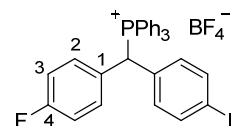
Triphenylphosphine (1.1 g, 4.2 mmol) and 8.0 M aqueous HBF₄ (0.50 ml, 4.0 mmol) were heated to 120 °C for 30 min. 4-Phenoxybenzhydrol (**4j**, 1.1 g, 4.0 mmol) was added and the mixture was heated to 145 °C for 1 hr. The obtained solid was dissolved in hot CH₂Cl₂ (6 ml) and EtOH (10 ml) was added. Colorless crystals formed after slow evaporation of the CH₂Cl₂ and were filtered off, washed with EtOH and dried, yielding 2.2 g (3.6 mmol, 90%) of a colorless solid, m.p. 194-195 °C (CH₂Cl₂/EtOH), containing small amounts of impurities.^[S14]

¹H NMR (400 MHz, CD₂Cl₂): δ 6.31 (d, ²J_{H,P} = 17.4 Hz, 1 H, CHP⁺), 6.85-6.89 (m, 2 H, 3-Ar), 6.98-7.01 (m, 2 H, *o*-OPh), 7.14-7.18 (m, 3 H, 2-Ar and *p*-OPh), 7.21-7.24 (m, 2 H, 2'-Ar), 7.28-7.32 (m, 2 H, 3'-Ar), 7.33-7.39 (m, 3 H, 4'-Ar and *m*-OPh), 7.48-7.52 (m, 6 H, *o*-PPh₃), 7.61-7.65 (m, 6 H, *m*-PPh₃), 7.80-7.85 (m, 3 H, *p*-PPh₃);

^{13}C NMR (100 MHz, CD_2Cl_2): δ 48.6 (d, $^1J_{\text{C,P}} = 43.8$ Hz, CHP^+), 118.3 (d, $^1J_{\text{C,P}} = 82.4$ Hz, *i*- PPh_3), 119.1 (d, $^4J_{\text{C,P}} = 1.8$ Hz, 3-Ar), 120.2 (s, *o*-OPh), 124.8 (s, *p*-OPh), 126.9 (d, $^2J_{\text{C,P}} = 4.2$ Hz, 1-Ar), 129.8 (d, $^5J_{\text{C,P}} = 2.4$ Hz, 4'-Ar), 130.0 (d, $^4J_{\text{C,P}} = 1.5$ Hz, 3'-Ar), 130.5 (s, *m*-OPh), 130.7 (d, $^3J_{\text{C,P}} = 12.4$ Hz, *m*- PPh_3), 131.0 (d, $^3J_{\text{C,P}} = 6.8$ Hz, 2'-Ar), 132.6 (d, $^3J_{\text{C,P}} = 6.5$ Hz, 2-Ar), 133.2 (d, $^2J_{\text{C,P}} = 3.7$ Hz, 1'-Ar), 135.3 (d, $^2J_{\text{C,P}} = 9.1$ Hz, *o*- PPh_3), 135.8 (d, $^4J_{\text{C,P}} = 3.1$ Hz, *p*- PPh_3), 156.4 (s, *i*-OPh), 159.0 (d, $^5J_{\text{C,P}} = 2.7$ Hz, 4-Ar);
 ^{19}F NMR (376 MHz, CD_2Cl_2): δ -151.8 (1:1:1:1 quartet, $^1J_{\text{F,B}} = 1.1$ Hz, $^{11}\text{BF}_4^-$), -151.7 (br s, $^{10}\text{BF}_4^-$);
 ^{31}P NMR (162 MHz, CD_2Cl_2): δ 21.5.
 HR-MS (ESI, positive): Calcd m/z for $\text{C}_{37}\text{H}_{30}\text{OP}^+$: 521.2027, Found: 521.2024.
 Elemental analysis: Calcd for $\text{C}_{37}\text{H}_{30}\text{BF}_4\text{OP}$: C, 73.04; H, 4.97, Found: C, 72.20; H, 4.91.^[S14]

[Bis(4-fluorophenyl)methyl]triphenylphosphonium tetrafluoroborate (**2k** BF_4^-)

 **precursor for (pfp) $_2\text{CH}^+$**
 **E10**- $\text{PPh}_3^+ \text{BF}_4^-$ in ref. ^[19]
E22- $\text{PPh}_3^+ \text{BF}_4^-$ in ref. ^[20]



Triphenylphosphine (1.1 g, 4.2 mmol) and 8.0 M aqueous HBF_4 (0.50 ml, 4.0 mmol) were heated to 120 °C for 30 min. Bis(4-fluorophenyl)methanol (**4k**, 0.88 g, 4.0 mmol) was added and the mixture was heated to 145 °C for 1 hr. The obtained solid was dissolved in hot CH_2Cl_2 (10 ml) and EtOH (20 ml) was added. Colorless crystals formed after slow evaporation of the CH_2Cl_2 and were filtered off, washed with EtOH and dried, yielding 1.6 g (2.9 mmol, 73%) of a colorless solid with m.p. 283-284 °C (decomp.) ($\text{CH}_2\text{Cl}_2/\text{EtOH}$).

^1H NMR (400 MHz, CD_2Cl_2): δ 6.49 (d, $^2J_{\text{H,P}} = 17.7$ Hz, 1 H, CHP^+), 6.96-7.02 (m, 4 H, 3-Ar), 7.20-7.25 (m, 4 H, 2-Ar), 7.49-7.54 (m, 6 H, *o*- PPh_3), 7.62-7.67 (m, 6 H, *m*- PPh_3), 7.81-7.85 (m, 3 H, *p*- PPh_3);

^{13}C NMR (100 MHz, CD_2Cl_2): δ 47.3 (d, $^1J_{\text{C,P}} = 44.7$ Hz, CHP^+), 117.0 (dd, $^2J_{\text{C,F}} = 21.9$ Hz, $^4J_{\text{C,P}} = 1.6$ Hz, 3-Ar), 118.0 (d, $^1J_{\text{C,P}} = 82.5$ Hz, *i*- PPh_3), 129.1 (dd, $^2J_{\text{C,P}} = 3.5$ Hz, $^4J_{\text{C,F}} = 3.5$ Hz,

1-Ar), 130.8 (d, $^3J_{\text{C,P}} = 12.4$ Hz, *m*- PPh_3), 133.0 (dd, $^3J_{\text{C,F}} = 8.3$ Hz, $^3J_{\text{C,P}} = 6.7$ Hz, 2-Ar), 135.3 (d, $^2J_{\text{C,P}} = 9.2$ Hz, *o*- PPh_3), 135.9 (d, $^4J_{\text{C,P}} = 3.1$ Hz, *p*- PPh_3), 163.5 (dd, $^1J_{\text{C,F}} = 250.1$ Hz, $^3J_{\text{C,P}} = 2.6$ Hz, 4-Ar);

^{19}F NMR (376 MHz, CD_2Cl_2): δ -151.3 (m, $^1J_{\text{F,B}}$ not resolved, $^{11}\text{BF}_4^-$), -151.2 (br s, $^{10}\text{BF}_4^-$), -112.1 - -112.0 (m, 2 F, 3-F);

^{31}P NMR (162 MHz, CD_2Cl_2): δ 21.9.

HR-MS (ESI, positive): Calcd m/z for $\text{C}_{31}\text{H}_{24}\text{F}_2\text{P}^+$: 465.1578, Found: 465.1568.

Elemental analysis: Calcd for $\text{C}_{31}\text{H}_{24}\text{BF}_6\text{P}$: C, 67.42; H, 4.38, Found: C, 67.20; H, 4.12.

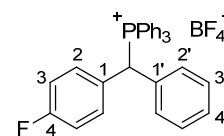
[(4-Fluorophenyl)phenylmethyl]triphenylphosphonium
tetrafluoroborate (**2l** BF₄⁻)



precursor for pfp(Ph)CH⁺



E11–PPh₃⁺ BF₄⁻ in ref. [19]
E23–PPh₃⁺ BF₄⁻ in ref. [20]



Triphenylphosphine (1.1 g, 4.2 mmol) and 8.0 M aqueous HBF₄ (0.50 ml, 4.0 mmol) were heated to 120 °C for 30 min. 4-fluorobenzhydrol (**4l**, 0.81 g, 4.0 mmol) was added and the mixture was heated to 145 °C for 1 hr. The obtained solid was dissolved in hot CH₂Cl₂ (15 ml) and EtOH (10 ml) was added. Colorless crystals formed after slow evaporation of the CH₂Cl₂ and were filtered off, washed with EtOH and dried, yielding 1.4 g (2.62 mmol, 66%) of a colorless solid with m.p. 258-260 °C (decomp.) (CH₂Cl₂/EtOH).

¹H NMR (400 MHz, CD₂Cl₂): δ 6.40 (d, ²J_{H,P} = 17.5 Hz, 1 H, CHP⁺), 6.95-7.00 (m, 2 H, 3-Ar), 7.21-7.25 (m, 4 H, 2-Ar and 2'-Ar), 7.28-7.32 (m, 2 H, 3'-Ar), 7.35-7.39 (m, 1 H, 4'-Ar), 7.47-7.53 (m, 6 H, *o*-PPh₃), 7.60-7.66 (m, 6 H, *m*-PPh₃), 7.80-7.85 (m, 3 H, *p*-PPh₃);

¹³C NMR (100 MHz, CD₂Cl₂): δ 48.1 (d, ¹J_{C,P} = 44.3 Hz, CHP⁺), 116.8 (dd, ²J_{C,F} = 21.8 Hz, ⁴J_{C,P} = 1.8 Hz, 3-Ar), 118.1 (d, ¹J_{C,P} = 82.7 Hz, *i*-PPh₃), 129.0 (dd, ²J_{C,P} = 3.7 Hz, ⁴J_{C,F} = 3.7 Hz,

1-Ar), 129.8 (d, ⁵J_{C,P} = 2.3 Hz, 4'-Ar), 130.0 (d, ⁴J_{C,P} = 1.5 Hz, 3'-Ar), 130.7 (d, ³J_{C,P} = 12.3 Hz, *m*-PPh₃), 131.0 (d, ³J_{C,P} = 6.9 Hz, 2'-Ar), 133.1 (dd, ³J_{C,F} = 8.5 Hz, ³J_{C,P} = 6.3 Hz, 2-Ar), ~133.1 (superimposed by 2-Ar, 1'-Ar), 135.3 (d, ²J_{C,P} = 9.0 Hz, *o*-PPh₃), 135.8 (d, ⁴J_{C,P} = 3.1 Hz,

p-PPh₃), 163.4 (dd, ¹J_{C,F} = 249.7 Hz, ³J_{C,P} = 2.9 Hz, 4-Ar);

¹⁹F NMR (376 MHz, CD₂Cl₂): δ -151.5 (1:1:1:1 quartet, ¹J_{F,B} = 1.2 Hz, ¹¹BF₄⁻), -151.5 (br s, ¹⁰BF₄⁻), -112.3 - -112.2 (m, 1 F, 3-F);

³¹P NMR (162 MHz, CD₂Cl₂): δ 21.9 (d, ⁶J_{P,F} = 4.7 Hz).

HR-MS (ESI, positive): Calcd *m/z* for C₃₁H₂₅FP⁺: 447.1672, Found: 447.1670.

Elemental analysis: Calcd for C₃₁H₂₅BF₅P: C, 69.69; H, 4.72, Found: C, 69.48; H, 4.66.

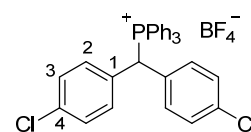
[Bis(4-chlorophenyl)methyl]triphenylphosphonium
tetrafluoroborate (**2n** BF₄⁻)



precursor for (pcp)₂CH⁺



E13–PPh₃⁺ BF₄⁻ in ref. [19]
E26–PPh₃⁺ BF₄⁻ in ref. [20]



Triphenylphosphine (2.10 g, 8.01 mmol) and 8.0 M aqueous HBF₄ (1.00 ml, 8.00 mmol) were heated to 120 °C for 30 min. 4,4'-Dichlorobenzhydrol (**4n**, 2.03 g, 8.02 mmol) was added and the mixture was heated to 145 °C for 1 hr. The obtained solid was dissolved in hot CH₂Cl₂ (15 ml) and EtOH (15 ml) was added. Colorless crystals formed after slow evaporation of the CH₂Cl₂ and were filtered off, washed with EtOH and dried, yielding 4.03 g (6.89 mmol, 86%) of a colorless solid with m.p. 251-252 °C (decomp.) (CH₂Cl₂/EtOH).

¹H NMR (400 MHz, CD₂Cl₂): δ 6.48 (d, ²J_{H,P} = 17.7 Hz, 1 H, CHP⁺), 7.15-7.19 (m, 4 H, 2-Ar), 7.25-7.29 (m, 4 H, 3-Ar), 7.51-7.56 (m, 6 H, *o*-PPh₃), 7.62-7.68 (m, 6 H, *m*-PPh₃), 7.81-7.86 (m, 3 H, *p*-PPh₃);

¹³C NMR (100 MHz, CD₂Cl₂): δ 47.4 (d, ¹J_{C,P} = 44.6 Hz, CHP⁺), 117.9 (d, ¹J_{C,P} = 82.7 Hz, *i*-PPh₃), 130.1 (d, ⁴J_{C,P} = 1.7 Hz, 3-Ar), 130.9 (d, ³J_{C,P} = 12.5 Hz, *m*-PPh₃), 131.6 (d, ²J_{C,P} =

4.1 Hz, 1-Ar), 132.5 (d, $^3J_{C,P} = 6.6$ Hz, 2-Ar), 135.3 (d, $^2J_{C,P} = 9.2$ Hz, *o*-PPh₃), 136.0 (two doublets, $J_{C,P} = 3.0$ Hz, second $J_{C,P}$ unresolved, 4-Ar and *p*-PPh₃);

^{19}F NMR (376 MHz, CD₂Cl₂): δ -151.2 (m, BF₄⁻);

^{19}F NMR (376 MHz, CD₂Cl₂): δ -151.2 (1:1:1:1 quartet, $^1J_{F,B} = 1.2$ Hz, $^{11}\text{BF}_4^-$), -151.2 (br s, $^{10}\text{BF}_4^-$);

^{31}P NMR (162 MHz, CD₂Cl₂): δ 21.8.

HR-MS (ESI, positive): Calcd m/z for C₃₁H₂₄³⁵Cl₂P⁺: 497.0988, Found: 497.0983.

Elemental analysis: Calcd for C₃₁H₂₄BCl₂F₄P: C, 63.62; H, 4.13, Found: C, 63.59; H, 4.00.

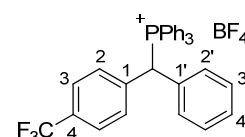
Triphenyl{phenyl[4-(trifluoromethyl)phenyl]methyl}phosphonium tetrafluoroborate (2o BF₄⁻)



precursor for tfm(Ph)CH⁺



E15-PPh₃⁺ BF₄⁻ in ref. [19]
E28-PPh₃⁺ BF₄⁻ in ref. [20]



Triphenylphosphine (2.10 g, 8.01 mmol) and 8.0 M aqueous HBF₄ (1.00 ml, 8.00 mmol) were heated to 120 °C for 30 min. [4-(Trifluoromethyl)phenyl]methanol (**4o**, 2.02 g, 8.00 mmol) was added and the mixture was heated to 145 °C for 1 hr. The obtained solid was dissolved in hot CH₂Cl₂ (36 ml) and EtOH (25 ml) was added. Colorless crystals formed after slow evaporation of the CH₂Cl₂ and were filtered off, washed with EtOH and dried, yielding 3.32 g (5.68 mmol, 71%) of a colorless solid with m.p. 236 °C (CH₂Cl₂/EtOH).

^1H NMR (400 MHz, CD₂Cl₂): δ 6.53 (d, $^2J_{H,P} = 17.7$ Hz, 1 H, CHP⁺), 7.21-7.24 (m, 2 H, 2'-Ar), 7.29-7.33 (m, 2 H, 3'-Ar), 7.36-7.40 (m, 1 H, 4'-Ar), 7.42 (d, $^3J_{H,H} = 7.7$ Hz, 2 H, 2-Ar), 7.50-7.55 (m, 8 H, 3-Ar and *o*-PPh₃), 7.61-7.67 (m, 6 H, *m*-PPh₃), 7.81-7.86 (m, 3 H, *p*-PPh₃);

^{13}C NMR (100 MHz, CD₂Cl₂): δ 48.4 (d, $^1J_{C,P} = 44.7$ Hz, CHP⁺), 118.0 (d, $^1J_{C,P} = 83.0$ Hz, *i*-PPh₃), 124.3 (qd, $^1J_{C,F} = 272.4$ Hz, $^7J_{C,P} = 1.1$ Hz, 4-CF₃), 126.7 (qd, $^3J_{C,F} = 3.9$ Hz, $^4J_{C,P} = 1.7$ Hz, 3-Ar), 130.05 (d, $^5J_{C,P} = 2.5$ Hz, 4'-Ar), 130.11 (d, $^4J_{C,P} = 1.6$ Hz, 3'-Ar), 130.9 (d, $^3J_{C,P} = 12.5$ Hz, *m*-PPh₃), ~131 (qd, $^2J_{C,F} = 33.0$ Hz, $^5J_{C,P} = 2.8$ Hz, superimposed with other 131 ppm signals, 4-Ar), 131.2 (d, $^3J_{C,P} = 6.7$ Hz, 2-Ar or 2'-Ar), 131.7 (d, $^3J_{C,P} = 6.5$ Hz, 2'-Ar or 2-Ar), 132.5 (d, $^2J_{C,P} = 4.4$ Hz, 1'-Ar), 135.3 (d, $^2J_{C,P} = 9.2$ Hz, *o*-PPh₃), 136.0 (d, $^4J_{C,P} = 3.1$ Hz, *p*-PPh₃), 137.6 (m, $^2J_{C,P}$ and $^5J_{C,F}$ not resolved, 1-Ar);

^{19}F NMR (376 MHz, CD₂Cl₂): δ -151.4 (1:1:1:1 quartet, $^1J_{F,B} = 1.2$ Hz, $^{11}\text{BF}_4^-$), -151.4 (br s, $^{10}\text{BF}_4^-$), -63.3 (m, 3 F, CF₃);

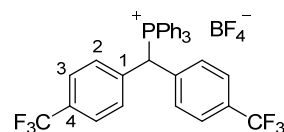
^{31}P NMR (162 MHz, CD₂Cl₂): δ 22.1-22.2 (m).

HR-MS (ESI, positive): Calcd m/z for C₃₂H₂₅F₃P⁺: 497.1640, Found: 497.1641.

Elemental analysis: Calcd for C₃₂H₂₅BF₇P: C, 65.78; H, 4.31, Found: C, 65.66; H, 4.32.

Bis[4-(trifluoromethyl)phenyl]methyl triphenylphosphonium tetrafluoroborate (2s BF₄⁻)

 E19–PPh₃⁺ BF₄⁻ in ref.^[19]



Triphenylphosphine (2.10 g, 8.01 mmol) and 8.0 M aqueous HBF₄ (1.00 ml, 8.00 mmol) were heated to 120 °C for 30 min. Bis[4-(trifluoromethyl)phenyl]methanol (**4s**, 2.56 g, 7.99 mmol) was added and the mixture was heated to 160 °C for 1 hr. The obtained solid was dissolved in hot CH₂Cl₂ (7.5 ml) and EtOH (5 ml) was added. Colorless crystals formed after slow evaporation of the CH₂Cl₂ and were filtered off, washed with EtOH and dried, yielding 2.68 g (4.11 mmol, 51%) of a colorless solid with m.p. 234 °C (CH₂Cl₂/EtOH).

¹H NMR (400 MHz, CDCl₃): δ 6.80 (d, ²J_{H,P} = 17.8 Hz, 1 H, CHP⁺), 7.43 (d, ³J_{H,H} = 7.6 Hz, 4 H, 2-Ar), 7.54-7.61 (m, 10 H, 3-Ar and *o*-PPh₃), 7.63-7.69 (m, 6 H, *m*-PPh₃), 7.82-7.87 (m, 3 H,

p-PPh₃);

¹³C NMR (100 MHz, CDCl₃): δ 47.5 (d, ¹J_{C,P} = 45.3 Hz, CHP⁺), 117.6 (d, ¹J_{C,P} = 83.2 Hz, *i*-PPh₃), 124.2 (qd, ¹J_{C,F} = 272.5 Hz, ⁷J_{C,P} = 0.9 Hz, 4-CF₃), 126.9 (qd, ³J_{C,F} = 3.8 Hz, ⁴J_{C,P} = 1.6 Hz, 3-Ar), 131.0 (d, ³J_{C,P} = 12.5 Hz, *m*-PPh₃), 131.7 (qd, ²J_{C,F} = 32.9 Hz, ⁵J_{C,P} = 2.6 Hz, 4-Ar), 131.8 (d, ³J_{C,P} = 6.6 Hz, 2-Ar), 135.3 (d, ²J_{C,P} = 9.3 Hz, *o*-PPh₃), 136.2 (d, ⁴J_{C,P} = 3.1 Hz, *p*-PPh₃), 137.1 (dq, ²J_{C,P} = 4.0 Hz, ⁵J_{C,F} = 1.1 Hz, 1-Ar);

¹⁹F NMR (376 MHz, CD₂Cl₂): δ -150.7 (m, ¹J_{F,B} not resolved, ¹¹BF₄⁻), -150.7 (br s, ¹⁰BF₄⁻), -63.3 (s, 6 F, CF₃);

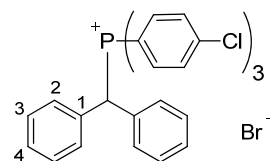
³¹P NMR (162 MHz, CD₂Cl₂): δ 22.4-22.5 (m).

HR-MS (ESI, positive): Calcd *m/z* for C₃₃H₂₄F₆P⁺: 565.1514, Found: 565.1515.

Elemental analysis: Calcd for C₃₃H₂₄BF₁₀P: C, 60.76; H, 3.71, Found: C, 60.55; H, 3.64.

1.S.3.4.3 Benzhydryl tris(4-chlorophenyl)phosphonium salts (3 X⁻)

Benzhydryl tris(4-chlorophenyl)phosphonium bromide (3a Br⁻)



Benzhydryl bromide (**5a**, 1.13 g, 4.59 mmol) and P(*p*-Cl-C₆H₄)₃ (1.67 g, 4.56 mmol) were heated to 175 °C for 5.5 hrs. The obtained solid was recrystallized from CH₂Cl₂/Et₂O, yielding 2.17 g (3.54 mmol, 77%) of a colorless solid with m.p. 206-207 °C (CH₂Cl₂/Et₂O).^[S13]

¹H NMR (400 MHz, CD₂Cl₂): δ 7.26-7.35 (m, 6 H, 3-Ar and 4-Ar), 7.56-7.62 (m, 10 H, 2-Ar and *m*-PAr₃), 7.72-7.78 (m, 6 H, *o*-PAr₃), 8.49 (d, ²J_{H,P} = 18.3 Hz, 1 H, CHP⁺);

¹³C NMR (100 MHz, CD₂Cl₂): δ 45.5 (d, ¹J_{C,P} = 41.2 Hz, CHP⁺), 117.0 (d, ¹J_{C,P} = 85.2 Hz, *i*-PAr₃), 129.5 (d, ⁵J_{C,P} = 2.5 Hz, 4-Ar), 129.8 (d, ⁴J_{C,P} = 1.5 Hz, 3-Ar), 131.0 (d, ³J_{C,P} = 13.1 Hz, *m*-PAr₃), 131.5 (d, ³J_{C,P} = 7.0 Hz, 2-Ar), 133.6 (d, ²J_{C,P} = 4.1 Hz, 1-Ar), 137.1 (d, ²J_{C,P} = 10.5 Hz, *o*-PAr₃), 142.9 (d, ⁴J_{C,P} = 3.7 Hz, *p*-PAr₃);

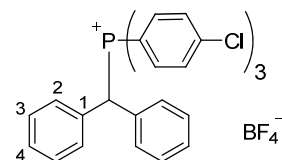
^{31}P NMR (162 MHz, CD_2Cl_2): δ 21.8.

HR-MS (ESI, positive): Calcd m/z for $\text{C}_{31}\text{H}_{23}^{35}\text{Cl}_3\text{P}^+$: 531.0599, Found: 531.0600.

*Benzhydryl*tris(4-chlorophenyl)phosphonium tetrafluoroborate
(**3a** BF_4^-)



E12-P(4-Cl-C₆H₄)₃⁺ BF_4^- in ref.^[19]



The phosphonium bromide **3a** Br^- (0.735 g, 1.20 mmol) was dissolved in CH_2Cl_2 (30 ml) and shaken vigorously with 5% aqueous NaBF_4 solution (3×20 ml). The organic phase was washed with H_2O (20 ml) and dried with MgSO_4 . Removal of the solvent in vacuo yielded 0.736 g (1.19 mmol, 99%) of a colorless solid with m.p. 249-251 °C (decomp.) (CH_2Cl_2).^[S13]

^1H NMR (400 MHz, CD_2Cl_2): δ 6.50 (d, $^2J_{\text{H,P}} = 17.6$ Hz, 1 H, CHP^+), 7.24-7.27 (m, 4 H, 2-Ar), 7.31-7.35 (m, 4 H, 3-Ar), 7.37-7.44 (m, 8 H, 4-Ar and *o*- PAR_3), 7.60-7.64 (m, 6 H, *m*- PAR_3);

^{13}C NMR (100 MHz, CD_2Cl_2): δ 48.6 (d, $^1J_{\text{C,P}} = 42.8$ Hz, CHP^+), 116.3 (d, $^1J_{\text{C,P}} = 85.4$ Hz, *i*- PAR_3), 130.1 (d, $^5J_{\text{C,P}} = 2.8$ Hz, 4-Ar), 130.2 (d, $^4J_{\text{C,P}} = 1.5$ Hz, 3-Ar), 131.2 (d, $^3J_{\text{C,P}} = 6.6$ Hz,

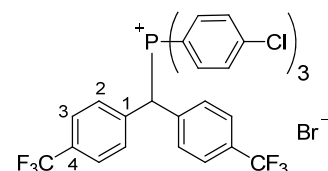
2-Ar), 131.4 (d, $^3J_{\text{C,P}} = 13.1$ Hz, *m*- PAR_3), 132.5 (d, $^2J_{\text{C,P}} = 4.3$ Hz, 1-Ar), 136.6 (d, $^2J_{\text{C,P}} = 10.2$ Hz, *o*- PAR_3), 143.4 (d, $^4J_{\text{C,P}} = 3.7$ Hz, *p*- PAR_3);

^{19}F NMR (376 MHz, CD_2Cl_2): δ -151.0 (1:1:1:1 quartet, $^1J_{\text{F,B}} = 1.4$ Hz, $^{11}\text{BF}_4^-$), -151.0 (br s, $^{10}\text{BF}_4^-$);

^{31}P NMR (162 MHz, CD_2Cl_2): δ 21.7.

HR-MS (ESI, positive): Calcd m/z for $\text{C}_{31}\text{H}_{23}^{35}\text{Cl}_3\text{P}^+$: 531.0599, Found: 531.0599.

{Bis[4-(trifluoromethyl)phenyl]methyl}tris(4-chlorophenyl)-
phosphonium bromide (3s Br^-)



Bis[4-(trifluoromethyl)phenyl]methyl bromide (**5s**, 3.33 g, 8.69 mmol) and $\text{P}(p\text{-Cl-C}_6\text{H}_4)_3$ (3.18 g, 8.70 mmol) were heated to 170 °C for 2 hrs. The obtained solid was dissolved in hot CH_2Cl_2 (45 ml) and EtOH (35 ml) was added. Slow evaporation of the CH_2Cl_2 yielded a colorless precipitate which was filtered off, washed with EtOH (2×5 ml) and dried, yielding 3.35 g (4.47 mmol, 51%) of a colorless solid with m.p. 246-247 °C ($\text{CH}_2\text{Cl}_2/\text{EtOH}$).^[S13]

^1H NMR (400 MHz, CDCl_3): δ 7.57 (d, $^3J_{\text{H,H}} = 8.3$ Hz, 4 H, 3-Ar), 7.63-7.67 (m, 6 H, *m*- PAR_3), 7.78 (d, $^3J_{\text{H,H}} = 8.2$ Hz, 4 H, 2-Ar), 7.79-7.86 (m, 6 H, *o*- PAR_3), 9.09 (d, $^2J_{\text{H,P}} = 18.6$ Hz, 1 H, CHP^+);

^{13}C NMR (100 MHz, CDCl_3): δ 44.0 (d, $^1J_{\text{C,P}} = 43.4$ Hz, CHP^+), 116.2 (d, $^1J_{\text{C,P}} = 86.0$ Hz, *i*- PAR_3), 124.2 (qd, $^1J_{\text{C,F}} = 272.5$ Hz, $^7J_{\text{C,P}} = 1.0$ Hz, 4- CF_3), 126.8 (qd, $^3J_{\text{C,F}} = 3.8$ Hz, $^4J_{\text{C,P}} = 1.6$ Hz, 3-Ar), 131.4 (d, $^3J_{\text{C,P}} = 13.3$ Hz, *m*- PAR_3), 131.6 (qd, $^2J_{\text{C,F}} = 32.8$ Hz, $^5J_{\text{C,P}} = 2.6$ Hz, 4-Ar), 132.0 (d, $^3J_{\text{C,P}} = 7.0$ Hz, 2-Ar), 136.9 (d, $^2J_{\text{C,P}} = 10.7$ Hz, *o*- PAR_3), 137.5 (dq, $^2J_{\text{C,P}} = 4.1$ Hz, $^5J_{\text{C,F}}$ not resolved, 1-Ar), 143.5 (d, $^4J_{\text{C,P}} = 3.7$ Hz, *p*- PAR_3);

^{19}F NMR (376 MHz, CDCl_3): δ -63.2 (m, 4- CF_3);

^{31}P NMR (162 MHz, CD_2Cl_2): δ 22.3-22.4 (m).

HR-MS (ESI, positive): Calcd m/z for $\text{C}_{33}\text{H}_{21}^{35}\text{Cl}_3\text{F}_6\text{P}^+$: 667.0347, Found: 667.0347.

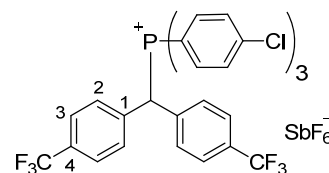
{Bis[4-(trifluoromethyl)phenyl]methyl}tris(4-chlorophenyl)-phosphonium hexafluoroantimonate(V) (3s SbF_6^-)



precursor for $(\text{tfm})_2\text{CH}^+$



E19- $\text{P}(4\text{-Cl-C}_6\text{H}_4)_3^+ \text{SbF}_6^-$ in ref. [19]
E32- $\text{P}(4\text{-Cl-C}_6\text{H}_4)_3^+ \text{SbF}_6^-$ in ref. [20]



A solution of AgSbF_6 (427 mg, 1.24 mmol) in CH_3CN (10 ml) was added to a solution of **3s** Br^- (862 mg, 1.15 mmol) in CH_2Cl_2 (20 ml). After stirring at room temperature for 1 hr, the AgBr was filtered off and the solvent was removed in vacuo. The residue was dissolved in hot CH_2Cl_2 (4 ml). Addition of EtOH (6 ml) yielded a colorless precipitate which was filtered off, washed with EtOH (10 ml) and dried, yielding 623 mg (0.689 mmol, 60%) of a colorless solid with m.p. 297-299 $^\circ\text{C}$ ($\text{CH}_2\text{Cl}_2/\text{EtOH}$). A test for Br^- with AgNO_3 was negative. [S13]

^1H NMR (400 MHz, CDCl_3): δ 6.43 (d, $^2J_{\text{H,P}} = 17.6$ Hz, 1 H, CHP^+), 7.35 (d, $^3J_{\text{H,H}} = 7.9$ Hz, 4 H, 2-Ar), 7.38-7.44 (m, 6 H, $o\text{-PAR}_3$), 7.63 (d, $^3J_{\text{H,H}} = 8.1$ Hz, 4 H, 3-Ar), 7.66-7.70 (m, 6 H, $m\text{-PAR}_3$);

^{13}C NMR (100 MHz, CDCl_3): δ 48.5 (d, $^1J_{\text{C,P}} = 45.3$ Hz, CHP^+), 115.0 (d, $^1J_{\text{C,P}} = 86.4$ Hz, $i\text{-PAR}_3$), 124.0 (qd, $^1J_{\text{C,F}} = 272.6$ Hz, $^7J_{\text{C,P}} = 1.0$ Hz, 4- CF_3), 127.4 (qd, $^3J_{\text{C,F}} = 3.7$ Hz, $^4J_{\text{C,P}} = 1.3$ Hz, 3-Ar), 131.5 (d, $^3J_{\text{C,P}} = 6.7$ Hz, 2-Ar), 131.9 (d, $^3J_{\text{C,P}} = 13.4$ Hz, $m\text{-PAR}_3$), 132.4 (qd, $^2J_{\text{C,F}} = 33.1$ Hz, $^5J_{\text{C,P}} = 2.5$ Hz, 4-Ar), 136.0 (dq, $^2J_{\text{C,P}} = 4.1$ Hz, $^5J_{\text{C,F}}$ not resolved, 1-Ar), 136.3 (d, $^2J_{\text{C,P}} = 10.5$ Hz, $o\text{-PAR}_3$), 144.2 (d, $^4J_{\text{C,P}} = 3.7$ Hz, $p\text{-PAR}_3$);

^{19}F NMR (376 MHz, CDCl_3): δ -63.4 (br s, 4- CF_3), SbF_6^- not resolved;

^{31}P NMR (162 MHz, CD_2Cl_2): δ 22.2 (m).

HR-MS (ESI, positive): Calcd m/z for $\text{C}_{33}\text{H}_{21}^{35}\text{Cl}_3\text{F}_6\text{P}^+$: 667.0347, Found: 667.0347.

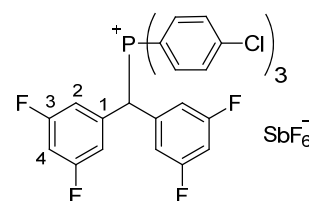
[Bis(3,5-difluorophenyl)methyl]tris(4-chlorophenyl)phosphonium hexafluoroantimonate(V) (3t SbF_6^-)



precursor for $(\text{dfp})_2\text{CH}^+$



E20- $\text{P}(4\text{-Cl-C}_6\text{H}_4)_3^+ \text{SbF}_6^-$ in ref. [13]
E33- $\text{P}(4\text{-Cl-C}_6\text{H}_4)_3^+ \text{SbF}_6^-$ in ref. [20]



A solution of AgSbF_6 (0.278 g, 0.810 mmol) in CH_3CN (4 ml) was added to a solution of **3t** Br^- (0.506 g, 0.739 mmol) in CH_2Cl_2 (10 ml). The AgBr was filtered off and the solvent removed in vacuo. The residue was dissolved in hot CH_2Cl_2 and EtOH was added. Slow evaporation of CH_2Cl_2 lead to the formation of colorless needles which were filtered off and dried under high vacuum, yielding 0.426 g of a colorless solid (0.507 mmol; 69%) with m.p. 278-280 $^\circ\text{C}$ ($\text{CH}_2\text{Cl}_2/\text{EtOH}$). [S13]

^1H NMR (400 MHz, CD_2Cl_2): δ 6.29 (d, $^2J_{\text{H,P}} = 17.3$ Hz, 1 H, CHP^+), 6.70-6.77 (m, 4 H, 2-Ar), 6.90-6.96 (m, 2 H, 4-Ar), 7.41-7.47 (m, 6 H, $o\text{-PAR}_3$), 7.69-7.73 (m, 6 H, $m\text{-PAR}_3$);

^{13}C NMR (100 MHz, CD_2Cl_2): δ 47.6 (dm, $^1J_{\text{C,P}} = 46.3$ Hz, CHP^+), 106.5 (td, $^2J_{\text{C,F}} = 25.0$ Hz, $^5J_{\text{C,P}} = 2.3$ Hz, 4-Ar), 114.2-114.5 (doublet of AXX' -systems, $^3J_{\text{C,P}} = 6.8$ Hz, 2-Ar), 114.8 (d, $^1J_{\text{C,P}} = 86.6$ Hz, $i\text{-PAR}_3$), 132.0 (d, $^3J_{\text{C,P}} = 13.4$ Hz, $m\text{-PAR}_3$), 135.0 (td, $^3J_{\text{C,F}} = 9.3$ Hz, $^2J_{\text{C,P}} =$

4.0 Hz, 1-Ar), 136.3 (d, $^2J_{C,P} = 10.5$ Hz, *o*-PAr₃), 144.4 (d, $^4J_{C,P} = 3.7$ Hz, *p*-PAr₃), 164.0 (ddd, $^1J_{C,F} = 252.9$ Hz, $^3J_{C,F} = 13.0$ Hz, $^4J_{C,P} = 1.7$ Hz, 3-Ar);

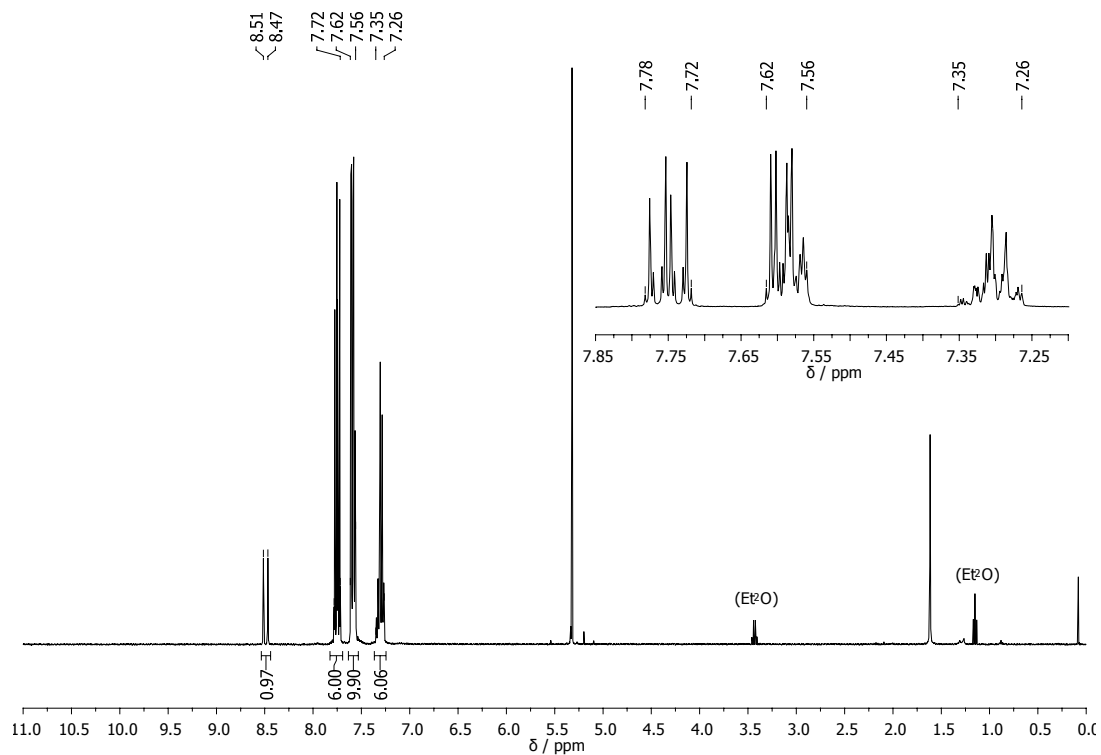
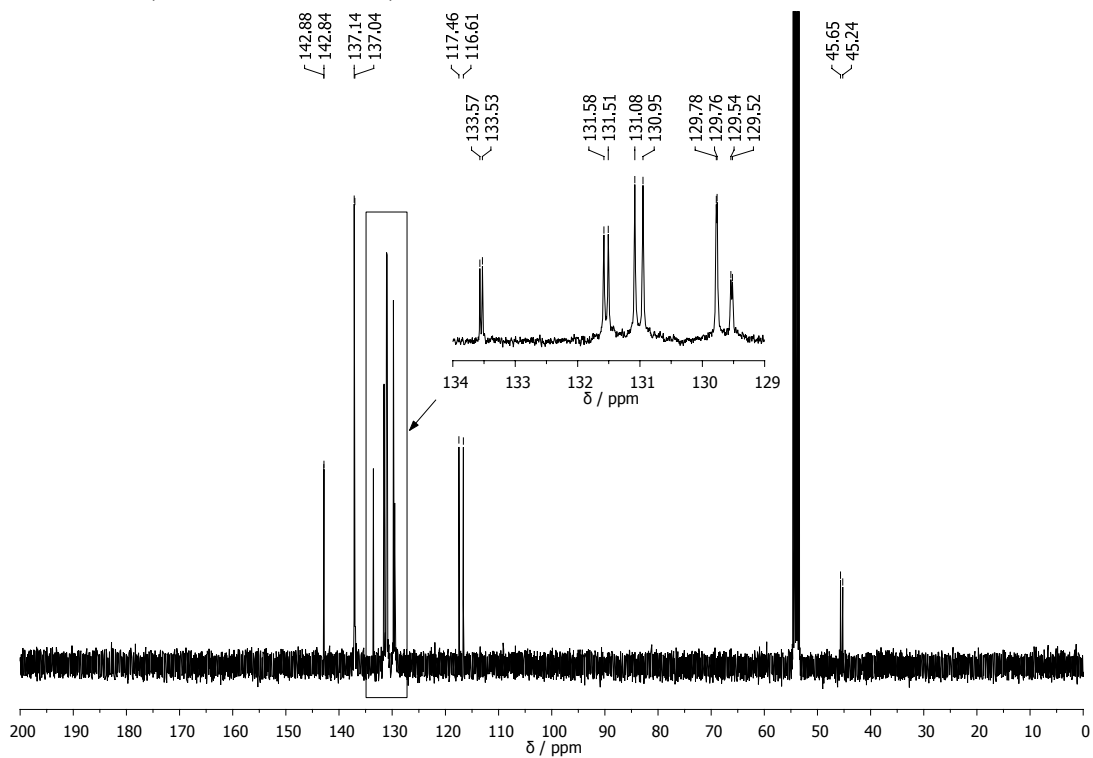
^{19}F NMR (376 MHz, CD₂Cl₂): δ -105.5 (m, 3-F), SbF₆⁻ not resolved;

^{31}P NMR (162 MHz, CD₂Cl₂): δ 22.4 (m).

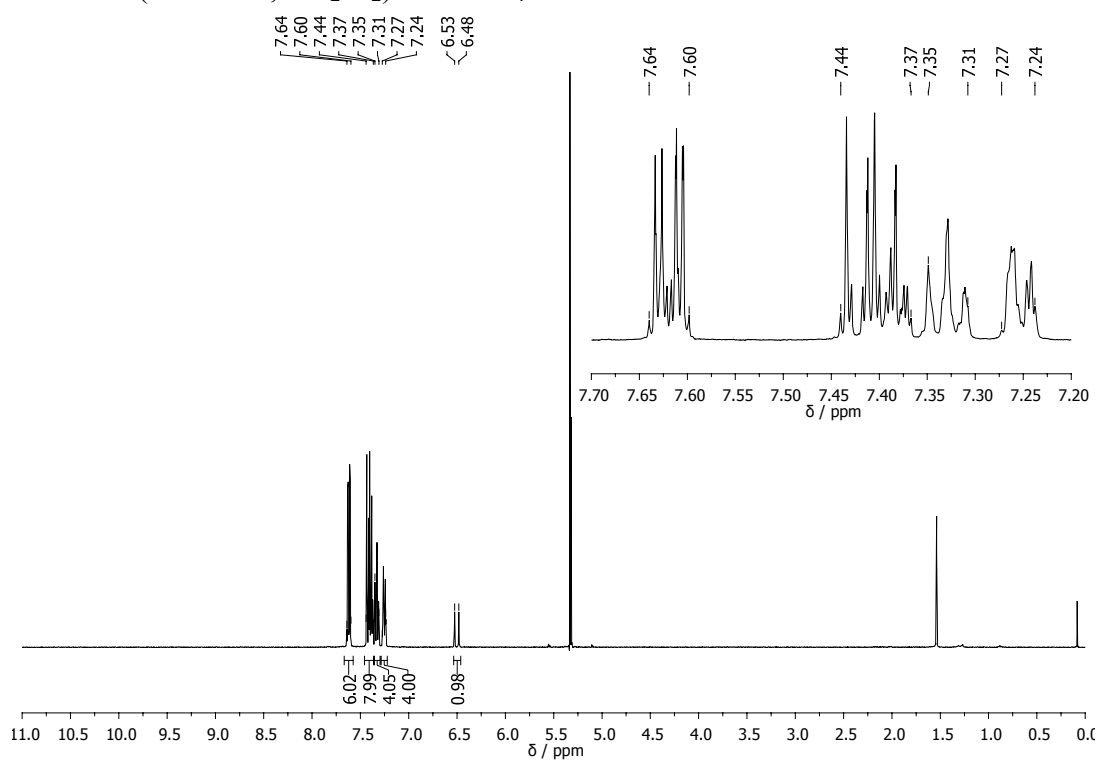
HR-MS (ESI, positive): Calcd *m/z* for C₃₁H₁₉³⁵Cl₃F₄P⁺: 603.0223, Found: 603.0215.

1.S.3.4.4 NMR spectra of selected benzhydryl triarylphosphonium salts

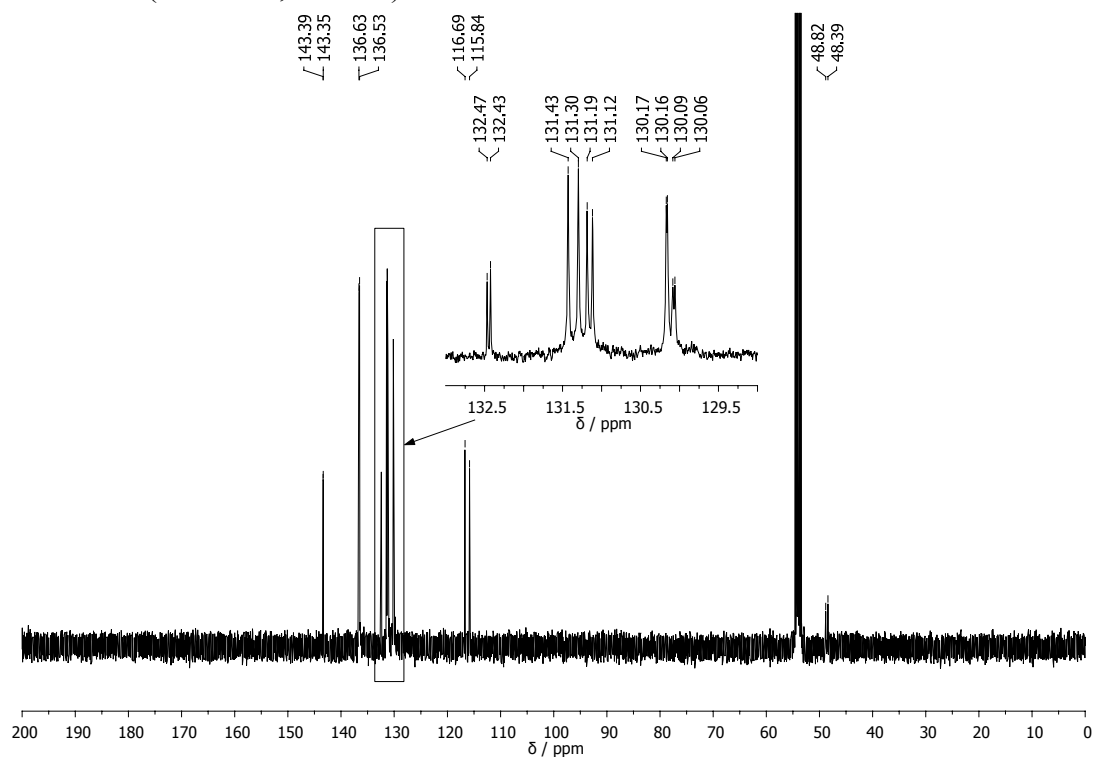
As we were unable to provide satisfactory elemental analyses for the hexafluoroantimonates (which were not analyzed because of the presence of Sb) and some of the highly halogenated phosphonium salts, we provide the ^1H - and ^{13}C -NMR spectra of these compounds in the following as evidence of their purity.

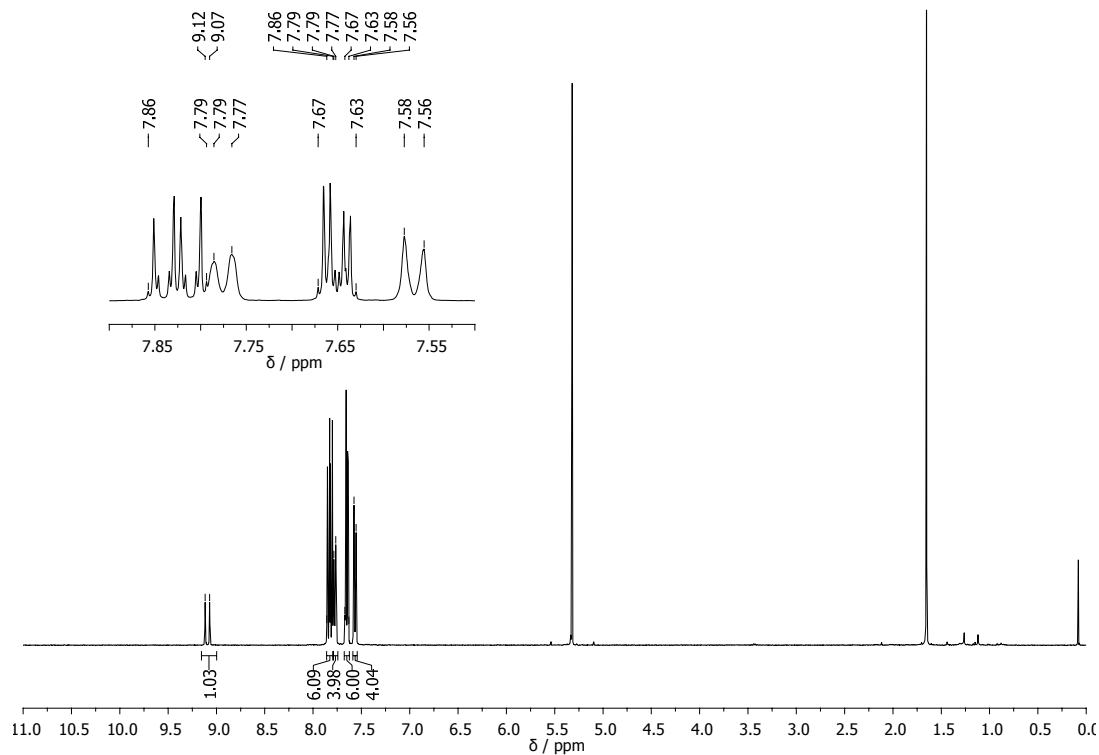
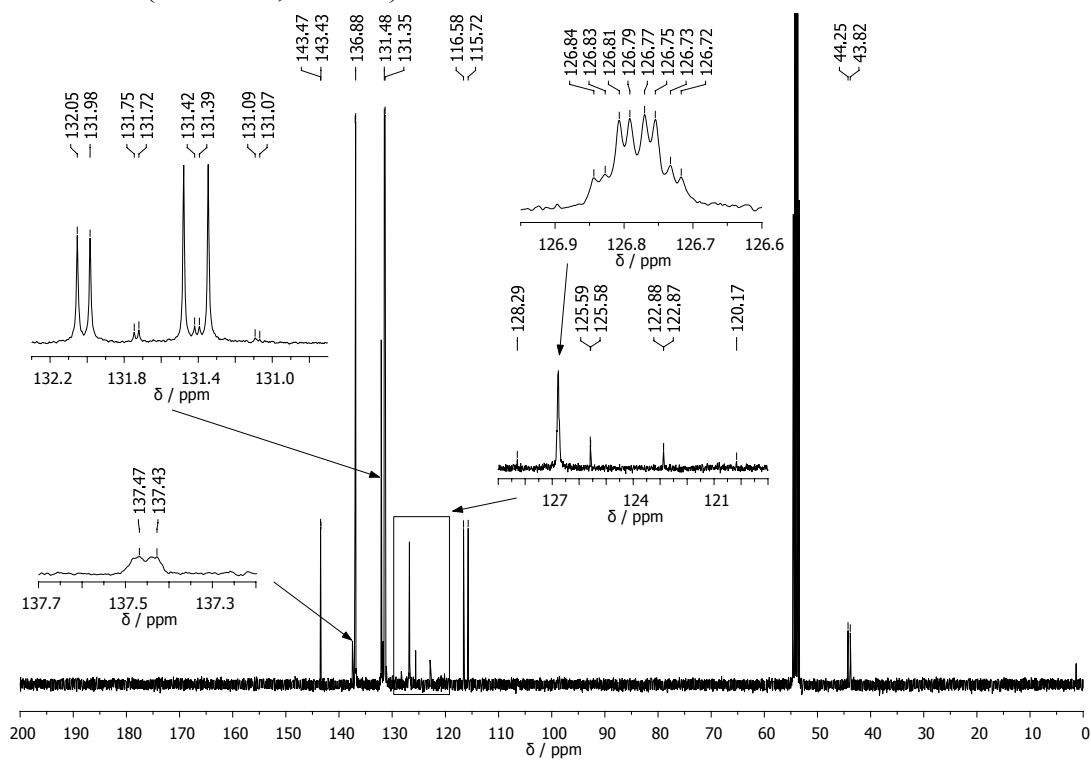
$^1\text{H-NMR}$ (400 MHz, CD_2Cl_2) of **3a** Br^-  $^{13}\text{C-NMR}$ (100 MHz, CD_2Cl_2) of **3a** Br^- 

$^1\text{H-NMR}$ (400 MHz, CD_2Cl_2) of **3a** BF_4^-

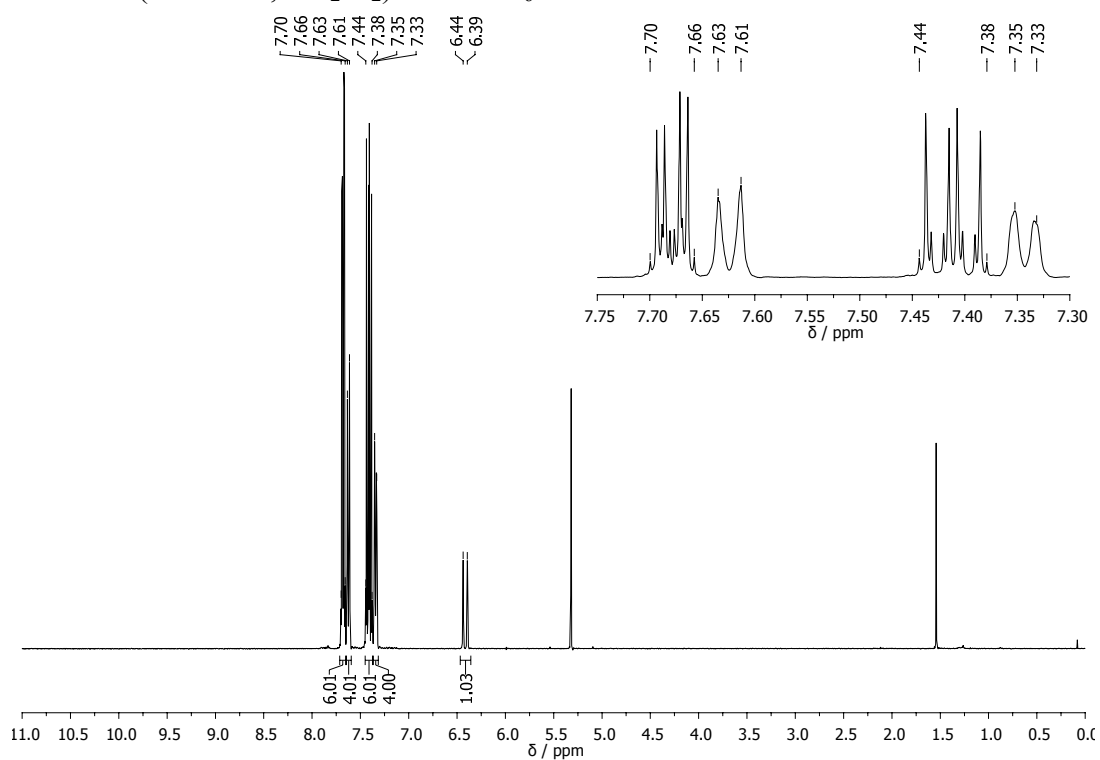


$^{13}\text{C-NMR}$ (100 MHz, CD_2Cl_2) of **3a** BF_4^-

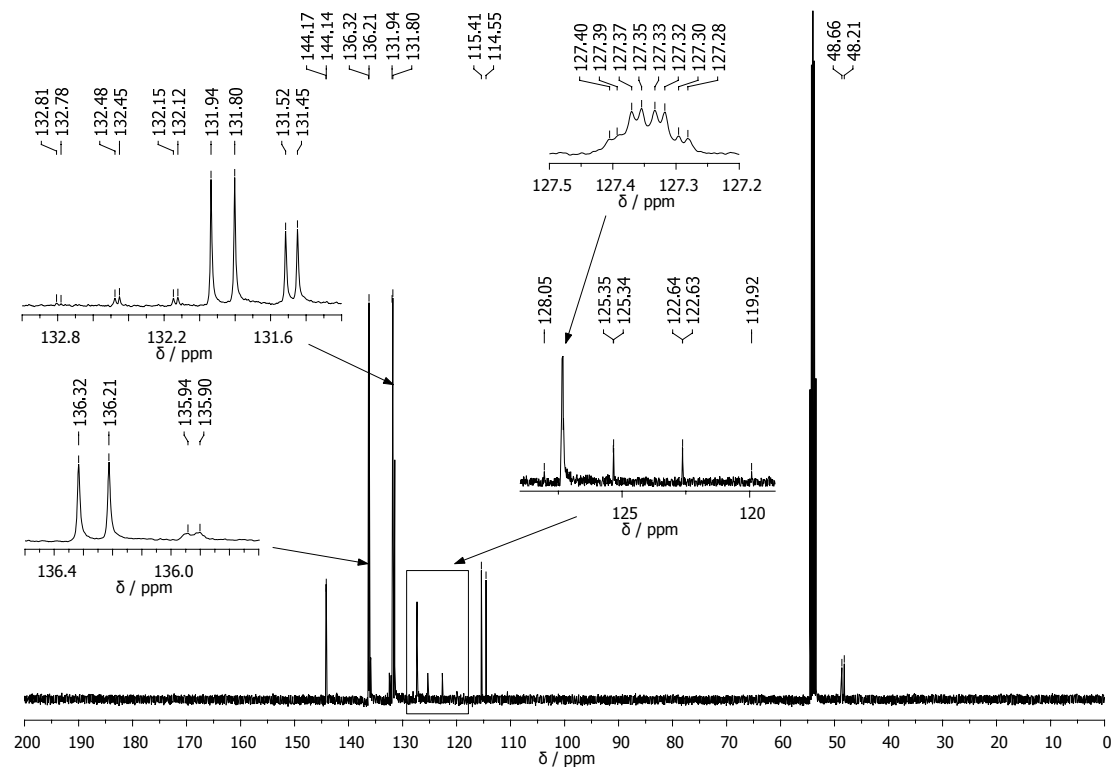


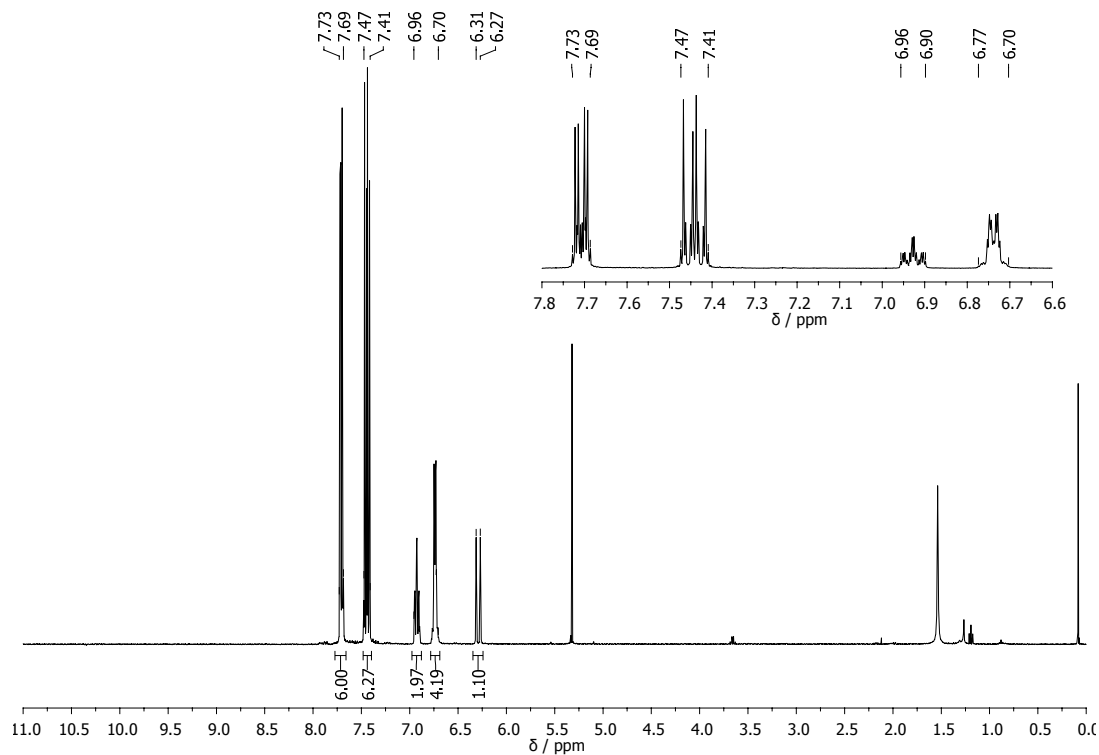
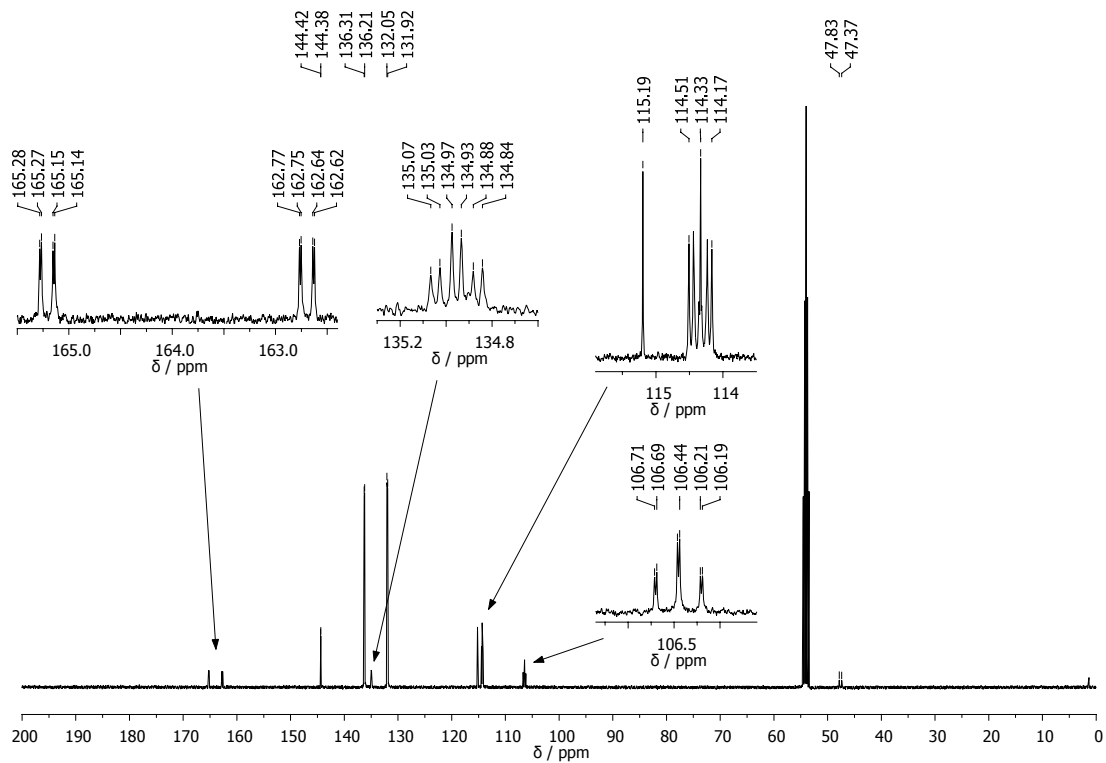
$^1\text{H-NMR}$ (400 MHz, CD_2Cl_2) of 3s Br^-  $^{13}\text{C-NMR}$ (100 MHz, CD_2Cl_2) of 3s Br^- 

$^1\text{H-NMR}$ (400 MHz, CD_2Cl_2) of $\mathbf{3s SbF}_6^-$



$^{13}\text{C-NMR}$ (100 MHz, CD_2Cl_2) of $\mathbf{3s SbF}_6^-$



$^1\text{H-NMR}$ (400 MHz, CD_2Cl_2) of 3t SbF_6^-  $^{13}\text{C-NMR}$ (100 MHz, CD_2Cl_2) of 3t SbF_6^- 

Photolytic Generation of Benzhydryl Cations and Radicals from Quaternary Phosphonium Salts: How Highly Reactive Carbocations Survive Their First Nanoseconds

Johannes Ammer, Christian F. Sailer, Eberhard Riedle, and Herbert Mayr

J. Am. Chem. Soc. **2012**, *134*, 11481-11494

2.1 Introduction

The photolytic generation of carbocations by heterolytic cleavage of neutral (R–X) and charged (R–X⁺) precursors has been employed not only for studying the rates of fast reactions of carbocations with nucleophiles¹⁻¹⁹ but also for the photoinitiation of carbocationic polymerizations.²⁰ Furthermore, photogenerated carbenium ions are the initial cleavage products of the photolysis of certain photoacid and photobase generators.²¹⁻²⁶ Common precursors for such applications are halides R–Hal,^{2-5,21a,27} acetates R–OAc,^{6-10,28} aryl ethers,⁶⁻⁹ and onium salts such as halonium,^{25,29} sulfonium,^{21b,25,30} ammonium,^{2,11,14,22,31} and phosphonium salts.^{14-20,23,32-34} Heterolytic bond cleavages are often accompanied by formation of radicals via homolytic processes, particularly when the resulting carbocations are not highly stabilized and less polar solvents are employed.³⁵

Among the many photo-leaving groups, phosphines turned out to be particularly advantageous, because they combine high stability,³⁶ even in alcoholic and aqueous solution, with a high preference for heterolytic cleavage and low tendency to produce radicals.^{14-20,32-34,38} While we have recently reported several examples for the photolytic generation of carbocations from quaternary phosphonium salts,¹⁴⁻¹⁹ there was no systematic investigation about the relationship between the structure of the precursor salt and the yield of the generated carbocations. The lack of information became obvious when we failed to generate benzhydrylium ions with empirical electrophilicity parameters $E > 7$ by laser flash photolysis of phosphonium salts Ar₂CH–PPh₃⁺ BF₄[–]. As the photolytic generation of highly electrophilic carbocations is of general importance, we have now examined how the

efficiency of carbocation formation can be influenced by the reactivity of the photo-electrofuge (carbocation-to-be), the photo-nucleofuge (photo-leaving group), and the counterion of the phosphonium salt. To gain insight into the ultrafast dynamics of these processes, the nanosecond laser flash photolysis experiments are supplemented by experiments on a state-of-the-art femtosecond transient spectrometer.³⁹

The use of benzhydryl derivatives is advantageous for these investigations because of the clearly assignable distinct spectra of the resulting cations and radicals.⁴⁰ Benzhydryl cations furthermore do not have β -protons and therefore cannot eliminate H^+ , which reduces the number of subsequent processes.¹⁵ Moreover, a systematic variation of the reactivity of the generated carbocations is achieved by using substituted benzhydryl cations Ar_2CH^+ (E^+) whose electrophilic reactivities are quantified accurately by the empirical electrophilicity parameters E .⁴¹

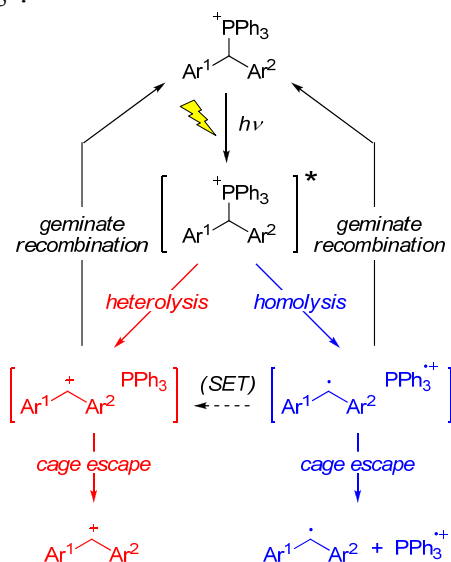
In the following, we will first investigate how the yields and dynamics of the photoproducts change with variations of the benzhydryl (section 2.2.2) and phosphine moieties (section 2.2.3) of the precursor molecules, of the solvent (section 2.2.4), and of the counter-anions of the phosphonium salts (section 2.2.5). We will then show how this information can be employed to generate highly reactive carbocations such as $E(31-33)^+$ (section 2.2.6). After discussing how the reaction conditions affect the lifetimes of the carbocations on the >10 ns time scale (section 2.2.7), we will finally demonstrate that the method presented in this work is well suitable for the study of bimolecular reactions of the generated benzhydryl cations (section 2.2.8).

2.2 Results and Discussion

2.2.1 General. Scheme 2.1 shows a mechanism for the photogeneration of benzhydryl cations E^+ and benzhydryl radicals E^\bullet from benzhydryl phosphonium ions $E-PPh_3^+$ in line with previously proposed mechanisms for similar systems.³⁵ The excited precursor molecules can either undergo heterolytic bond cleavage to the carbocation/triphenylphosphine pair [$E^+ PPh_3$] (red pathway) or homolytic bond cleavage to the radical pair [$E^\bullet PPh_3^{\bullet+}$] (blue pathway). Both pairs can then either undergo geminate recombination to the starting material or diffusional separation, which results in the free benzhydryl cations E^+ or radicals E^\bullet . Only the UV/vis-absorbing species which escape the geminate solvent cage (E^+ , E^\bullet , and $PR_3^{\bullet+}$; bottom line of

Scheme 2.1) have sufficient lifetimes (>10 ns) to be observed spectroscopically with a nanosecond laser flash setup.

Scheme 2.1. Generation of Benzhydryl Cations \mathbf{E}^+ and Benzhydryl Radicals \mathbf{E}^\bullet by Photolysis of Phosphonium Ions $\mathbf{E}-\text{PPh}_3^+$.



2.2.2 Effect of the Photo-electrofuge (i.e., Structure of the Benzhydrylium Ion).

Nanosecond Spectroscopy in CH_2Cl_2 . The transient spectra which we obtained by irradiation of 10^{-5} to 10^{-4} M solutions of $\mathbf{E}(\mathbf{13-33})-\text{PPh}_3^+ \text{BF}_4^-$ in CH_2Cl_2 with a 7-ns laser pulse (266 nm, 30-60 mJ/pulse) are compiled in section 2.S.3; four characteristic examples are shown in Figure 2.1. The transient spectra feature three types of absorption bands: (i) broad bands with $\lambda_{\text{max}} = 426\text{-}535$ nm, which can be assigned to the cations \mathbf{E}^+ by comparison with the previously reported spectra of benzhydrylium ions,⁴⁰ and the cation-like reactivities (see below); (ii) sharp bands with $\lambda_{\text{max}} = 328\text{-}344$ nm, which closely resemble the published spectra of benzhydryl radicals \mathbf{E}^\bullet in CH_3CN ;⁴⁰ and (iii) a shoulder at ca. 350-360 nm, which we assign to the triphenylphosphine radical cation PPh_3^{++} , in agreement with its reported spectrum in CH_2Cl_2 solution (with $\lambda_{\text{max}} \approx 330$ nm).⁴⁴

The photo-cleavage of the phosphonium ions $\mathbf{E}(\mathbf{13-21})-\text{PPh}_3^+$ in CH_2Cl_2 yields the stabilized benzhydrylium ions $\mathbf{E}(\mathbf{13-21})^+$ exclusively. When we irradiated solutions of $\mathbf{E}(\mathbf{22-33})-\text{PPh}_3^+ \text{BF}_4^-$ in CH_2Cl_2 , the ratios of the absorbances of the benzhydryl cations \mathbf{E}^+ and benzhydryl radicals \mathbf{E}^\bullet decreased with increasing electrophilicity E of the carbocations (Table 2.1). The least stable carbocations in the series, $\mathbf{E}(\mathbf{31-33})^+$ are hardly detectable after photolysis of

E(31-33)-PPh₃⁺ BF₄⁻, and the radicals **E(31-33)**[•] are obtained almost exclusively (Figure 2.1d and Figure 2.S.3 in section 2.S.3).

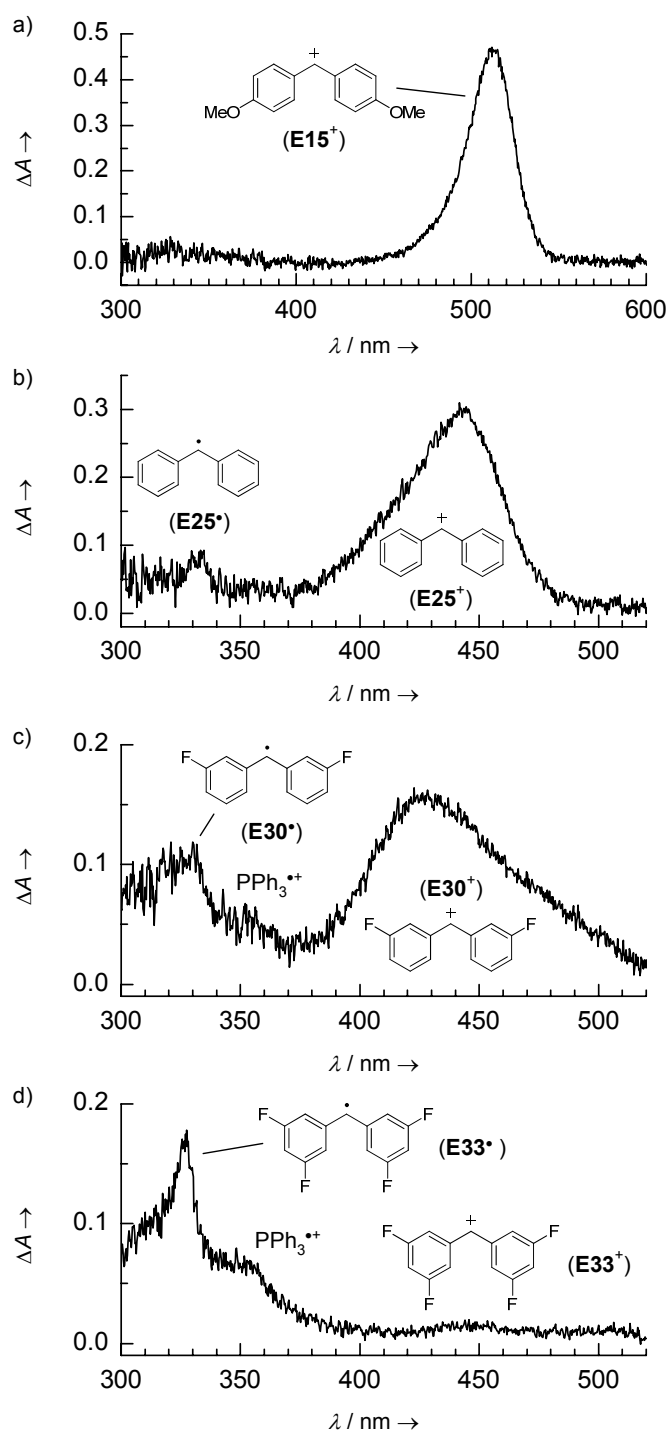
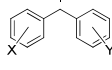
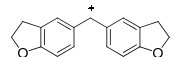
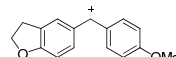


Figure 2.1. Transient spectra obtained after irradiation (7-ns pulse, $\lambda_{\text{exc}} = 266 \text{ nm}$, gate width = 10 ns) of CH_2Cl_2 solutions of benzhydryl triphenylphosphonium tetrafluoroborates: (a) **E15**-PPh₃⁺ BF₄⁻ ($A_{266 \text{ nm}} = 0.16$), (b) **E25**-PPh₃⁺ BF₄⁻ ($A_{266 \text{ nm}} = 0.49$), (c) **E30**-PPh₃⁺ BF₄⁻ ($A_{266 \text{ nm}} = 0.90$), (d) **E33**-PPh₃⁺ BF₄⁻ ($A_{266 \text{ nm}} = 0.64$).

Table 2.1. Electrophilicity Parameters E of the Benzhydryl Cations $\mathbf{E(13-33)}^+$ and Absorption Maxima λ_{\max} (nm) of Benzhydryl Radicals \mathbf{E}^\bullet and Benzhydryl Cations \mathbf{E}^+ in CH_2Cl_2 .

no.			$E(\mathbf{E}^+)^a$	$\lambda_{\max} / \text{nm}$		absorbance ratio ^b
	X	Y		\mathbf{E}^\bullet	\mathbf{E}^+	
E13 ⁺			-1.36	^c	535	^c
E14 ⁺			-0.81 ^d	^c	524	^c
E15 ⁺	4-MeO	4-MeO	0.00	^c	513	^c
E16 ⁺	4-MeO	4-PhO	0.61	^c	517	^c
E17 ⁺	4-MeO	4-Me	1.48	^c	484	^c
E18 ⁺	4-MeO	H	2.11	^c	466	^c
E19 ⁺	4-PhO	H	2.90	^c	473	^c
E20 ⁺	4-Me	4-Me	3.63	^c	473	^c
E21 ⁺	4-Me	H	4.43 ^d	^c	456	^c
E22 ⁺	4-F	4-F	5.01 ^d	~327	447	≥ 7
E23 ⁺	4-F	H	5.20 ^d	~333	451	≥ 5
E25 ⁺	H	H	5.47 ^d	~332	443	~4
E26 ⁺	4-Cl	4-Cl	5.48 ^d	~344	480	~4
E27 ⁺	3-F	H	6.23 ^d	~337	438	~3
E28 ⁺	4-(CF ₃)	H	6.70 ^d	~338	430	~2
E29 ⁺	3,5-F ₂	H	6.74 ^d	~332	434	~1.7
E30 ⁺	3-F	3-F	6.87 ^d	~331	426	~1.5
E31 ⁺	3,5-F ₂	3-F	7.52 ^d	~328	435	~0.25
E32 ⁺	4-(CF ₃)	4-(CF ₃)	(7.96) ^{d,e}	~337	439	<0.1
E33 ⁺	3,5-F ₂	3,5-F ₂	(8.02) ^{d,e}	~328	445	<0.1

^a Electrophilicity parameters E of the benzhydryl cations \mathbf{E}^+ ; from ref 41a unless noted otherwise. ^b Ratio of absorbances at $\lambda_{\max}(\mathbf{E}^+)$ and at $\lambda_{\max}(\mathbf{E}^\bullet)$ obtained by laser flash photolysis (7-ns pulse, $\lambda_{\text{exc}} = 266 \text{ nm}$) of $\mathbf{E(13-33)}\text{-PPh}_3^+\text{BF}_4^-$ in CH_2Cl_2 . Due to the overlap with the PPh_3^{++} band, absorbances at $\lambda_{\max}(\mathbf{E}^\bullet)$ overestimate the amount of radicals present. ^c No radicals detected. ^d New or revised E parameters, see CHAPTER 3 of this work. ^e Approximate values.

Picosecond Dynamics in CH₂Cl₂. The processes which lead to the formation of **E**⁺ and **E**[•] are too fast to be followed with the nanosecond laser flash photolysis instrument. A closer look at these processes is provided by transient absorption measurements with sub-100-fs time resolution which we performed for selected benzhydryl triarylphosphonium salts. Figure 2.2 shows a false color representation of the ps transient absorption data obtained by irradiating **E25**–PPh₃⁺ BF₄[−] in CH₂Cl₂ with a ~35-fs pulse (280 nm, 200 nJ/pulse): The wavelength is plotted on the horizontal axis and the time after the laser pulse on the vertical axis. Blue color indicates low absorbance and red color high absorbance.

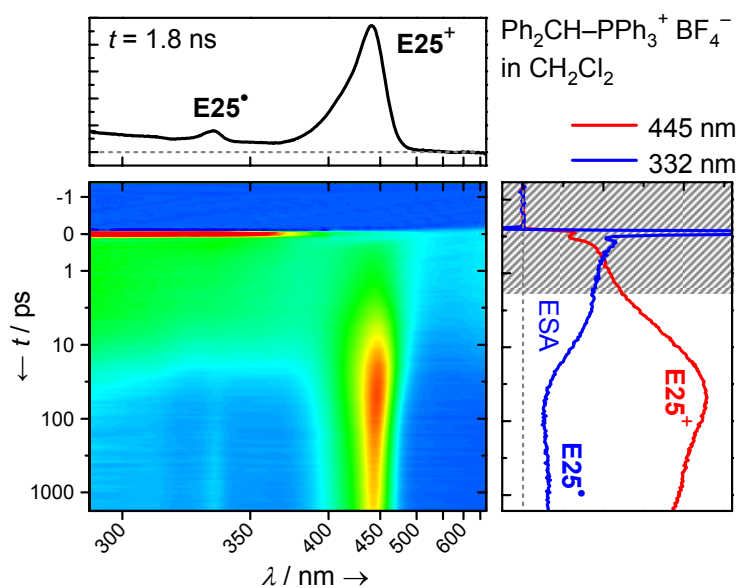


Figure 2.2. Transient absorptions observed after irradiating a 5.2×10^{-3} M solution of **E25**–PPh₃⁺ BF₄[−] in CH₂Cl₂ by a 35-fs pulse ($\lambda_{\text{exc}} = 280$ nm, $A_{280 \text{ nm}} = 0.2$, $d = 120$ μm). The graph above the color plot shows the spectrum after 1.8 ns (black). The graph on the right shows the dynamics of the absorbances at selected wavelengths: Absorbance of benzhydryl cation **E25**⁺ (445 nm, red); and absorbance of the excited state (ESA) of the phosphonium ion and the benzhydryl radical **E25**[•] (332 nm, blue). The time scale is linear between −1 and +1 ps and logarithmic above 1 ps.

The plot features three types of bands: (i) a broad absorption band below 400 nm, which disappears in the first 30 ps, is assigned to the excited state absorption (ESA) of the phosphonium salt precursor; (ii) the band of the benzhydryl cation **E25**⁺ ($\lambda_{\text{max}} \approx 443$ nm), which reaches a maximum within the first 25 ps; and (iii) a small band of the benzhydryl radical **E25**[•] ($\lambda_{\text{max}} \approx 332$ nm), which becomes visible after the decay of the excited state of the phosphonium ion. The graph to the right of the color plot shows the dynamics of the

absorbance at λ_{max} of the carbocation **E25⁺** (red) and at 332 nm (blue, λ_{max} of the radical **E25[•]** overlapping with the excited-state absorption in the first tens of picoseconds).

The intense short-lived (<0.1 ps) signal directly after the laser pulse is a coherent artifact that is also observed in the pure solvent and will be ignored in the following.³⁹ A discussion of the absorption changes during the first 2 ps (shaded area) which include relaxation, planarization, and solvation effects is beyond the scope of this paper and is treated in detail elsewhere.⁴⁵

The ESA disappears during the first 30 ps, accompanied by a simultaneous increase of the absorbance of **E25⁺** which suggests that **E25⁺** is formed by direct heterolysis of the excited precursor salt. It does not, however, exclude the generation of the benzhydryl cations **E25⁺** by homolytic bond cleavage and subsequent considerably faster single electron transfer (SET) in the geminate radical pair (Scheme 2.1, dashed arrow).

After the ESA has disappeared and the absorbance of **E25⁺** has reached its maximum, the population of **E25⁺** decreases as a result of the geminate recombination of **E25⁺** with the photoleaving group PPh₃; in part, the photo-fragments diffuse away from each other and these **E25⁺** persist on this time scale. Once the band of the radical **E25[•]** is clearly developed, it does not show noticeable dynamics. After 1.8 ns, we observe the spectrum shown in the graph above the color plot (Figure 2.2), which is essentially the same as the spectrum obtained by the 7-ns laser pulse (Figure 2.1b).

The heterolysis of the tetrafluoro-substituted benzhydryl phosphonium ion **E33–PPh₃⁺ BF₄[–]** in CH₂Cl₂ is much less effective and the radical **E33[•]** is formed predominantly. In addition, the small initial concentration of carbocations **E33⁺** decays rapidly so that only a very low concentration can be observed on the nanosecond time scale (Figure 2.1d; also see Table 2.2).⁴⁶

Picosecond Dynamics in CH₃CN. In CH₃CN essentially the same kind of photo-processes occur after irradiation of **E25–PPh₃⁺ BF₄[–]** as in CH₂Cl₂ (Figure 2.2). Figure 2.3 shows the time-dependent quantum yields of the substituted benzhydryl cations **E⁺** during the first 1.6 ns after the excitation pulse; the numeric values are listed in Table 2.2. It is evident that the quantum yields of the initial heterolytic photo-cleavage, Φ_{het} , decrease with increasing electrophilicity of the generated benzhydryl cations. At the same time, homolytic bond cleavage becomes more favorable although the overall efficiency of bond cleavage decreases (not shown). Due to the overlap of the bands of **E[•]** with the ESA and the PAR₃⁺⁺ band we could not evaluate the radical yields on the early picosecond time scale.

Table 2.2. Yields and Rate Constants Associated with the Dynamics of \mathbf{E}^+ after Irradiation of $\mathbf{E-PAr}_3^+ \text{BF}_4^-$ with Ar = Ph or *p*-Cl-C₆H₄ (Bold) in CH₃CN or CH₂Cl₂ with a 35-fs Laser Pulse ($\lambda_{\text{exc}} = 280 \text{ nm}$).^a

\mathbf{E}^+	$E(\mathbf{E}^+)^b$	PAr ₃	solvent	$\Phi_{\text{het}}^c / \%$	$Y_{\text{recomb}}^d / \%$	$\Phi_{\text{free}}^e / \%$	$k_{\text{recomb}}^f / \text{s}^{-1}$	$k_{\text{esc}}^g / \text{s}^{-1}$
E20⁺	3.63	PPh ₃	CH ₃ CN	34	21	27	1.9×10^9	7.2×10^9
E21⁺	4.43	PPh ₃	CH ₃ CN	30	25	23	2.5×10^9	7.5×10^9
E25⁺	5.47	PPh ₃	CH ₃ CN	24	25	18	2.7×10^9	8.3×10^9
			CH ₂ Cl ₂	11	19	9	1.1×10^9	4.9×10^9
		P(<i>p</i>-Cl-C₆H₄)₃	CH₃CN	25	21	20	7.9×10^8	3.0×10^9
			CH₂Cl₂	(~16)^h	(~10)^h	14	$(6 \times 10^8)^h$	$(5 \times 10^9)^h$
E27⁺	6.23	PPh ₃	CH ₃ CN	6-10 ⁱ	29	4-7 ⁱ	3.6×10^9	8.5×10^9
E30⁺	6.87	PPh ₃	CH ₃ CN	5-8 ⁱ	32	3-5 ⁱ	3.6×10^9	7.5×10^9
E31⁺	7.52	PPh ₃	CH ₃ CN	4-7 ⁱ	35	3-4 ⁱ	3.8×10^9	6.9×10^9
		P(<i>p</i>-Cl-C₆H₄)₃	CH₃CN	8-12ⁱ	36	5-7ⁱ	8.9×10^9	1.6×10^{10}
E33⁺	(8.02)	PPh ₃	CH ₃ CN	3-4 ⁱ	42	~2 ⁱ	6.6×10^9	9.3×10^9
			CH ₂ Cl ₂	(~1) ^{ij}	(29) ^j	(≤1) ^{ij}	$(2 \times 10^9)^j$	$(5 \times 10^9)^j$
		P(<i>p</i>-Cl-C₆H₄)₃	CH₃CN	8-12ⁱ	36	5-8i	8.8×10^9	1.6×10^{10}

^a See section S5 in the Supporting Information of *J. Am. Chem. Soc.* **2012**, *134*, 11481-11494 for details.

^b Electrophilicity parameters E of the benzhydryl cations \mathbf{E}^+ ; see Table 2.1 for references. ^c Quantum yield of heterolytic bond cleavage (including the possibility of initial homolytic bond cleavage and subsequent fast electron transfer). ^d Yield of geminate recombination of \mathbf{E}^+ with the phosphine PAr₃. ^e Overall quantum yield of free \mathbf{E}^+ (at ~2 ns) after diffusional separation of the photo-leaving group. ^f First-order rate constant for the geminate recombination of \mathbf{E}^+ with PAr₃. ^g First-order rate constant for the diffusional separation of \mathbf{E}^+ and PAr₃. ^h The different behavior of this photo-leaving group in the early photo-dissociation process in CH₂Cl₂ reduces the accuracy of our fit and we give only approximate values for this system. ⁱ To calculate the quantum yields, absorbance coefficients of $(5.0\text{-}7.5) \times 10^4 \text{ M}^{-1} \text{ cm}^{-1}$ were assumed for the benzhydryl cations **E(27,30,31,33)⁺** in analogy to reported values for similar benzhydrylium ions.⁴⁰ ^j The values have to be considered approximate because of the low absorbance of **E33⁺**.

As illustrated by Figure 2.3, the concentrations of the benzhydryl cations \mathbf{E}^+ decrease considerably during the first 300 ps after their formation which is rationalized by the geminate recombination with the photo-leaving group PPh₃. Immediately after C–P bond cleavage, the two photofragments are in close vicinity (ion pairs). They can either undergo geminate recombination or the fragments diffuse apart. After complete diffusional separation of \mathbf{E}^+ from the photo-leaving group, bond formation is no longer possible (more precisely: is too slow to be observable on this time scale) and the absorbances of \mathbf{E}^+ reach a plateau (Figure

2.3). The yields for the geminate recombination of the benzhydryl cations \mathbf{E}^+ with the phosphine PPh_3 , Y_{recomb} , increase with the electrophilicity E of the carbocations \mathbf{E}^+ , and diminish the final quantum yields of the diffusionally separated (free) benzhydryl cations, Φ_{free} (Table 2.2).

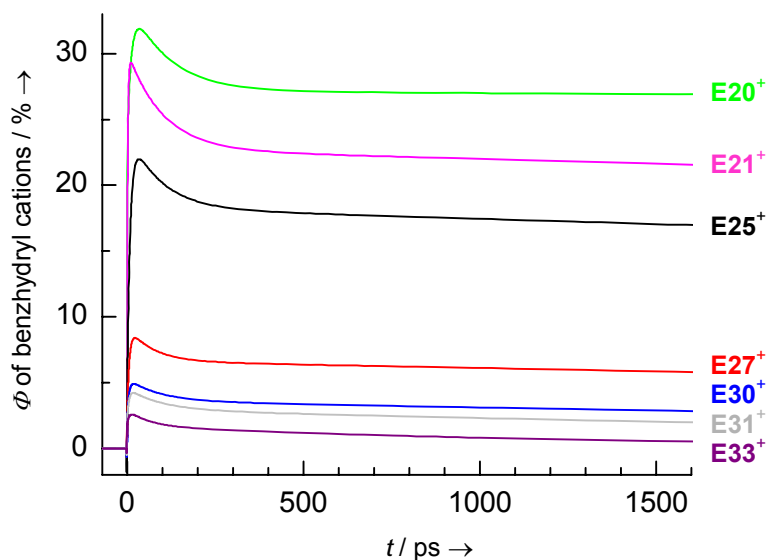


Figure 2.3. Time-dependent quantum yields Φ of \mathbf{E}^+ observed after irradiation of $\mathbf{E}-\text{PPh}_3^+ \text{BF}_4^-$ solutions in CH_3CN with a 35-fs laser pulse ($\lambda_{\text{exc}} = 280 \text{ nm}$).

The rate constants listed in Table 2.2 for the geminate recombination of \mathbf{E}^+ with PPh_3 , k_{recomb} (s^{-1}), and for the diffusional separation of \mathbf{E}^+ from PPh_3 , k_{esc} (s^{-1}), can be derived from $Y_{\text{recomb}} = k_{\text{recomb}}/(k_{\text{recomb}}+k_{\text{esc}})$ and the observed rate constants for the decrease of the benzhydrylium ions. With increasing electrophilicity E of the benzhydryl cations \mathbf{E}^+ , the recombination rate constant k_{recomb} increases steadily while k_{esc} remains almost constant at $(7\text{-}9) \times 10^9 \text{ s}^{-1}$.

2.2.3 Effect of the Photo-nucleofuge (i.e., Triarylphosphine). It was already observed by Modro and co-workers that the use of a more nucleophilic phosphine as photo-leaving group decreased the amount of cation-derived photo-products in photolyses of phosphonium salts.³² When we employed tris(4-chlorophenyl)phosphine $\text{P}(p\text{-Cl-C}_6\text{H}_4)_3$ as a photo-leaving group instead of PPh_3 , the formation of benzhydryl cations \mathbf{E}^+ was considerably more efficient and even allowed us to generate highly electrophilic benzhydrylium ions.

Figure 2.4 shows the transient spectra obtained after irradiation of the benzhydryl triarylphosphonium tetrafluoroborates $\mathbf{E31}-\text{PAR}_3^+ \text{BF}_4^-$ with $\text{PAR}_3 = \text{PPh}_3$ (black curves) and $\text{PAR}_3 = \text{P}(p\text{-Cl-C}_6\text{H}_4)_3$ (orange curves). Considerably higher concentrations of the carbocations $\mathbf{E31}^+$ and lower amounts of the radicals $\mathbf{E31}^\bullet$ were obtained when $\text{P}(p\text{-Cl-C}_6\text{H}_4)_3$

was employed as photoleaving group. Similarly, irradiation of **E33**– $P(p\text{-Cl-C}_6\text{H}_4)_3^+ \text{BF}_4^-$ gave higher yields of **E33**⁺ and lower yields of **E33**[•] than irradiation of **E33**– $\text{PPh}_3^+ \text{BF}_4^-$, but the absorbance of **E33**⁺ was still too low ($A < 0.04$) to study its reaction rates on the nanosecond time scale. The shoulders of the radical bands ($\text{PAR}_3^{\bullet+}$) are weaker and red-shifted to 350–380 nm when $\text{P}(p\text{-Cl-C}_6\text{H}_4)_3$ is used as photo-leaving group (Figure 2.4), in agreement with the fact that the absorbance maxima of the tris(4-chlorophenyl)phosphine radical cation $\text{P}(p\text{-Cl-C}_6\text{H}_4)_3^{\bullet+}$ are slightly red-shifted compared to $\text{PPh}_3^{\bullet+}$.⁴⁷

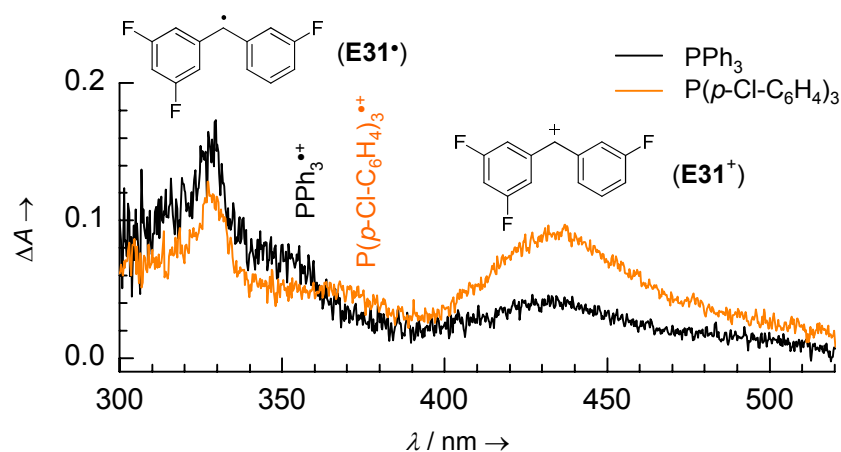


Figure 2.4. Transient spectra obtained after irradiation (7-ns pulse, $\lambda_{\text{exc}} = 266 \text{ nm}$, gate width: 10 ns) of CH_2Cl_2 solutions of benzhydryl triarylphosphonium tetrafluoroborates **E31**– $\text{PAR}_3^+ \text{BF}_4^-$ with different photoleaving groups $\text{PAR}_3 = \text{PPh}_3$ (black, $A_{266 \text{ nm}} = 1.0$) and $\text{PAR}_3 = \text{P}(p\text{-Cl-C}_6\text{H}_4)_3$ (orange, $A_{266 \text{ nm}} = 1.0$).

Two reasons might account for the increased carbocation yields with $\text{P}(p\text{-Cl-C}_6\text{H}_4)_3$ as photoleaving group: First, the oxidation potentials of the two phosphines ($E_{\text{ox}}^0 = 1.06 \text{ V}$ for PPh_3 and 1.28 V for $\text{P}(p\text{-Cl-C}_6\text{H}_4)_3$ in CH_3CN)⁴⁸ indicate a higher thermodynamic preference of **E**⁺/ PAR_3 pairs over **E**[•]/ $\text{PAR}_3^{\bullet+}$ pairs in the case of $\text{P}(p\text{-Cl-C}_6\text{H}_4)_3$ than in the case of PPh_3 . Thus, the preference for the heterolytic over the homolytic pathway should be larger for **E**– $\text{P}(p\text{-Cl-C}_6\text{H}_4)_3^+$ than for **E**– PPh_3^+ . Furthermore, $\text{P}(p\text{-Cl-C}_6\text{H}_4)_3$ is less nucleophilic than PPh_3 ($\Delta N = 1.75$)³⁷ and, therefore, allows more carbocations to undergo diffusional separation instead of geminate recombination.

The data from the ultrafast spectroscopic measurements illustrate that both effects contribute to the better overall quantum yields Φ_{free} when $\text{P}(p\text{-Cl-C}_6\text{H}_4)_3$ is used as photoleaving group instead of PPh_3 (Table 2.2, bold entries): For this leaving group, the observed initial quantum yields of the heterolytic bond cleavage, Φ_{het} , are higher and the yields of the geminate recombination, Y_{recomb} , are lower. While the differences are small for the photolysis of

E25– $\text{PAr}_3^+ \text{BF}_4^-$ in CH_3CN , the effects are more important in CH_2Cl_2 and crucial for the generation of the most reactive benzhydryl cations (Table 2.2).

2.2.4 Effect of Solvent on the Picosecond Dynamics. The overall quantum yields of the free carbocations, Φ_{free} , are considerably lower in CH_2Cl_2 than in CH_3CN (Table 2.2), which is a consequence of the decreased quantum yields for the heterolytic bond cleavage, Φ_{het} . The lower solvent nucleophilicity of CH_2Cl_2 compared to CH_3CN only becomes relevant at longer time scales (see below).

The rate constants for the cage escape, k_{esc} , are of comparable magnitude in CH_2Cl_2 and CH_3CN for both photo-nucleofuges PAr_3 (Table 2.2). In contrast, the diffusional separation of E^+ from Cl^- is very slow after the photolysis of $\text{E}-\text{Cl}$ in CH_2Cl_2 due to the Coulombic attraction between the charged photo-fragments,⁴ which explains why photolyses of $\text{E}-\text{PAr}_3^+$ give much higher yields of carbocations in CH_2Cl_2 than photolyses of $\text{E}-\text{Cl}$.

2.2.5 Effect of the Counterion in the Precursor Phosphonium Salt. *Transient Spectra in CH_3CN and CH_2Cl_2 .* At low phosphonium salt concentrations ($\sim 1 \times 10^{-4}$ M), the association equilibria of **E25**– $\text{PPh}_3^+ \text{X}^-$ in acetonitrile are entirely on the side of the free (unpaired) ions.⁴² Since the lifetime of the excited state is only a few ps, which is too short for the diffusive approach of external X^- , the photochemistry of **E25**– PPh_3^+ is not affected by the counter-anion X^- under these conditions.

Accordingly, $\sim 1.2 \times 10^{-4}$ M solutions of **E25**– $\text{PPh}_3^+ \text{X}^-$ with different counter-anions X^- in CH_3CN gave very similar transient spectra upon irradiation with a 7-ns laser pulse (Figure 2.5a): Irrespective of the counter-anion X^- , the predominant photoproduct was the benzhydrylium ion **E25**⁺ ($\lambda_{\text{max}} \approx 436$ nm) together with small amounts of the radical **E25**[•] ($\lambda_{\text{max}} \approx 329$ nm). Since the absorption coefficients of **E25**⁺ and **E25**[•] are similar,⁴⁰ the absorbance ratios in Figure 2.5 directly translate to concentration ratios. The slightly lower concentrations of **E25**⁺ obtained from precursors with $\text{X}^- = \text{Cl}^-$ or Br^- (Figure 2.5a) result from the diffusion-controlled trapping of **E25**⁺ by the halide ions (see below),⁷ which can already be noticed on this time scale (first 10 ns).

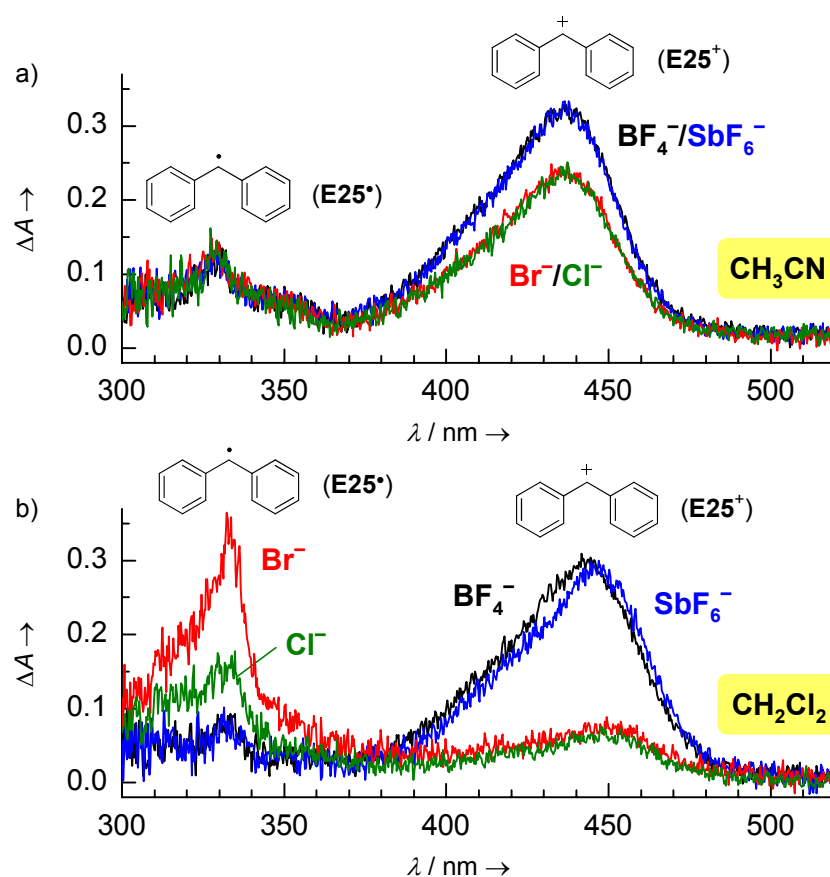


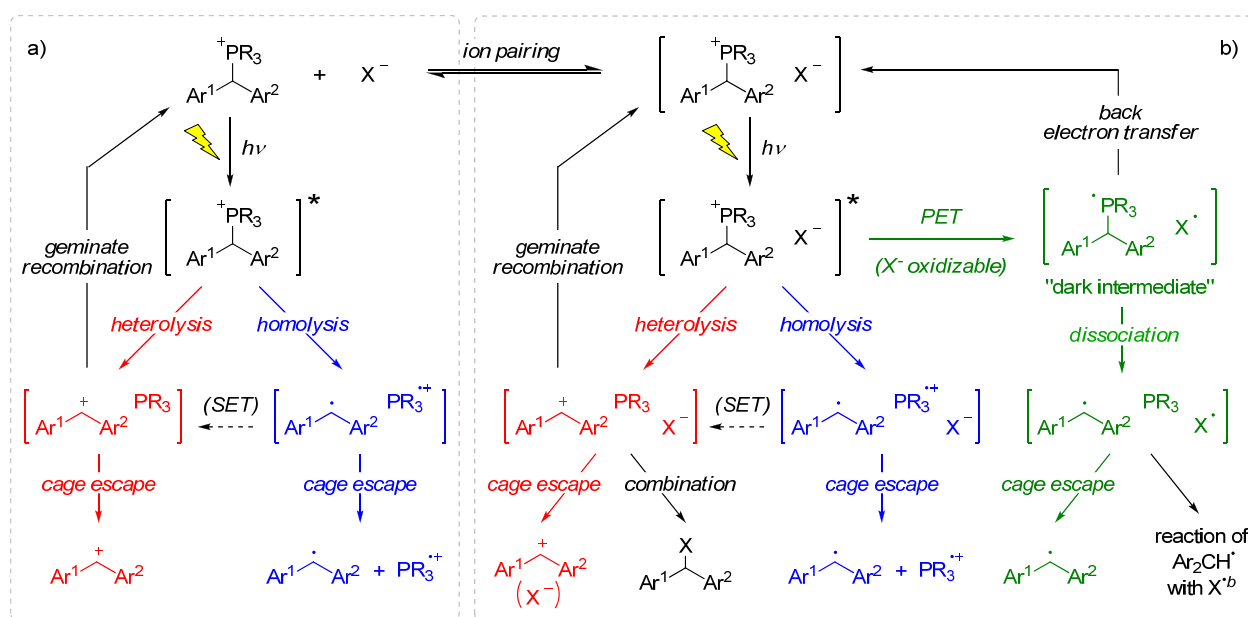
Figure 2.5. Transient spectra obtained by irradiation of **E25**– $\text{PPh}_3^+ \text{X}^-$ ($A_{266 \text{ nm}} = 0.5$, $(1.0\text{--}1.2) \times 10^{-4} \text{ M}$) with different counterions $\text{X}^- = \text{BF}_4^-$ (black), SbF_6^- (blue), Br^- (red) or Cl^- (green) in CH_3CN (a) and CH_2Cl_2 (b) with a 7-ns laser pulse ($\lambda_{\text{exc}} = 266 \text{ nm}$, gate width: 10 ns).

In CH_2Cl_2 , the phosphonium salts **E25**– $\text{PPh}_3^+ \text{X}^-$ have a considerably higher tendency to form ion pairs. At concentrations of $1 \times 10^{-4} \text{ M}$, which we typically used in the nanosecond laser flash photolysis experiments, $\sim 57\%$ of the Cl^- , $\sim 43\%$ of the Br^- , $\sim 40\%$ of the BF_4^- , and roughly (10–30)% of the SbF_6^- salts exist as ion pairs in CD_2Cl_2 .⁴² When we irradiated solutions of **E25**– $\text{PPh}_3^+ \text{BF}_4^-$ in CH_2Cl_2 , we obtained mostly the benzhydrylium ion **E25** $^+$ ($\lambda_{\text{max}} \approx 443 \text{ nm}$) together with small amounts of the radical **E25** $^\bullet$ ($\lambda_{\text{max}} \approx 332 \text{ nm}$) (Figure 2.5b, black curve). Irradiation of CH_2Cl_2 solutions of **E25**– $\text{PPh}_3^+ \text{SbF}_6^-$ gave almost the same concentrations of **E25** $^+$ and **E25** $^\bullet$ as the tetrafluoroborate precursor (Figure 2.5b, blue curve). In contrast, the concentration ratio of **E25** $^+$ and **E25** $^\bullet$ was reversed when we used the phosphonium bromide **E25**– $\text{PPh}_3^+ \text{Br}^-$ as precursor (Figure 2.5b, red curve). Irradiation of the phosphonium chloride **E25**– $\text{PPh}_3^+ \text{Cl}^-$ gave an intermediate amount of **E25** $^\bullet$ while the concentration of **E25** $^+$ was almost the same as with the phosphonium bromide precursor (Figure 2.5b, green curve). Transient spectra obtained by analogous experiments with

$\mathbf{E25-PPH_3^+ BPh_4^-}$ are difficult to interpret because of the overlap with the absorbances of photoproducts derived from BPh_4^- and are discussed in section 2.S.4.

Mechanism. The reduced yield of carbocations $\mathbf{E25^+}$ obtained from the phosphonium halides in CH_2Cl_2 (Figure 2.5b) can in part be explained by the immediate combination of $\mathbf{E25^+}$ with Br^- or Cl^- which are in close vicinity if they have been generated from the paired phosphonium halides. However, the increased yields of the radicals obtained from the phosphonium halides cannot be explained by the mechanism in Scheme 2.1 and subsequent reactions with the counterions, because Cl^- and Br^- do not reduce the benzhydrylium ions in the dark. Scheme 2.1, therefore, has to be extended as depicted in Scheme 2.2.

Scheme 2.2. Generation of Benzhydryl Cations $\mathbf{E^+}$ and Benzhydryl Radicals $\mathbf{E^\bullet}$ by Photolysis of Phosphonium Salts $\mathbf{E-PR_3^+ X^-}$ ($\text{R} = \text{Ph}$ or $p\text{-Cl-C}_6\text{H}_4$): (a) Reactions of Unpaired Phosphonium Ions (Predominant Mechanism in CH_3CN) and (b) Reactions of Paired Phosphonium Ions (Predominant Mechanism in CH_2Cl_2).^a



^a For the sake of simplicity, the geminate recombination reactions for the radical pairs are not shown. ^b Radical combination or electron transfer.⁴

The phosphonium precursors can exist as free phosphonium ions or paired with the counterions. Like the unpaired phosphonium ions (Scheme 2.2a), the ion pairs can undergo heterolytic bond cleavage to the benzhydryl cations $\mathbf{E^+}$ (Scheme 2.2b, red pathway) or homolytic bond cleavage to the benzhydryl radicals $\mathbf{E^\bullet}$ (Scheme 2.2b, blue pathway). If the counter-anion is oxidizable, there is the additional possibility of a photo-electron transfer

(PET) in the excited phosphonium ion pair (Scheme 2.2b, green pathway). Such a PET was already proposed by Griffin et al.⁴⁹ and further substantiated by Modro and co-workers who suggested a mechanism similar to Scheme 2.2 for the photolysis of arylmethyl phosphonium salts with oxidizable counterions.^{32,50} As expected for an electron transfer mechanism, the yields of the radicals **E25**[•] obtained from **E25**-PPh₃⁺ X⁻ increase with decreasing oxidation potentials of the counterions X⁻ (Br⁻ < Cl⁻ << BF₄⁻ and SbF₆⁻). Related to the degree of ion pairing of the precursor salts in these solvents,⁴² Scheme 2.2a is the predominant pathway in CH₃CN and Scheme 2.2b predominates in CH₂Cl₂.

Our results agree with those of Johnston, Scaiano, and coworkers, who studied the photolyses of arylmethyl triphenylphosphonium chlorides in CH₃CN and other solvents under conditions where ion-pairing is not negligible.³³ They had already noticed that the concentrations of transient arylmethyl cations increased and the concentrations of radicals decreased when inorganic salts of non-nucleophilic anions (e.g., LiClO₄, NaBF₄) were added to the phosphonium chloride solutions, because these anions replace the Cl⁻ in the initial phosphonium salt ion pairs. As expected, this effect is larger in less polar solvents.³³

Picosecond Dynamics in CH₃CN and CH₂Cl₂. The data from the ultrafast measurements corroborate this interpretation. Figure 2.6 shows the false color representations of the ps transient absorptions obtained after irradiation of **E25**-PPh₃⁺ X⁻ with different counter-anions (X⁻ = SbF₆⁻, Cl⁻, and Br⁻) in CH₃CN or CH₂Cl₂. The plots for **E25**-PPh₃⁺ SbF₆⁻ in CH₃CN (Figure 2.6a) and CH₂Cl₂ (Figure 2.6d) are very similar to that of the tetrafluoroborate precursor (Figure 2.2) and can be interpreted analogously (see above). Likewise, the color plot obtained with 4 × 10⁻⁴ M **E25**-PPh₃⁺ Br⁻ in CH₃CN (Figure 2.6b) closely resembles that of **E25**-PPh₃⁺ SbF₆⁻ (Figure 2.6a), because ion pairing is negligible at these concentrations⁴² and the PET mechanism depicted in Scheme 2.2b (green pathway) cannot occur. In all these cases, **E25**⁺ is the predominant photo-product, and only very small amounts of **E25**[•] are obtained.

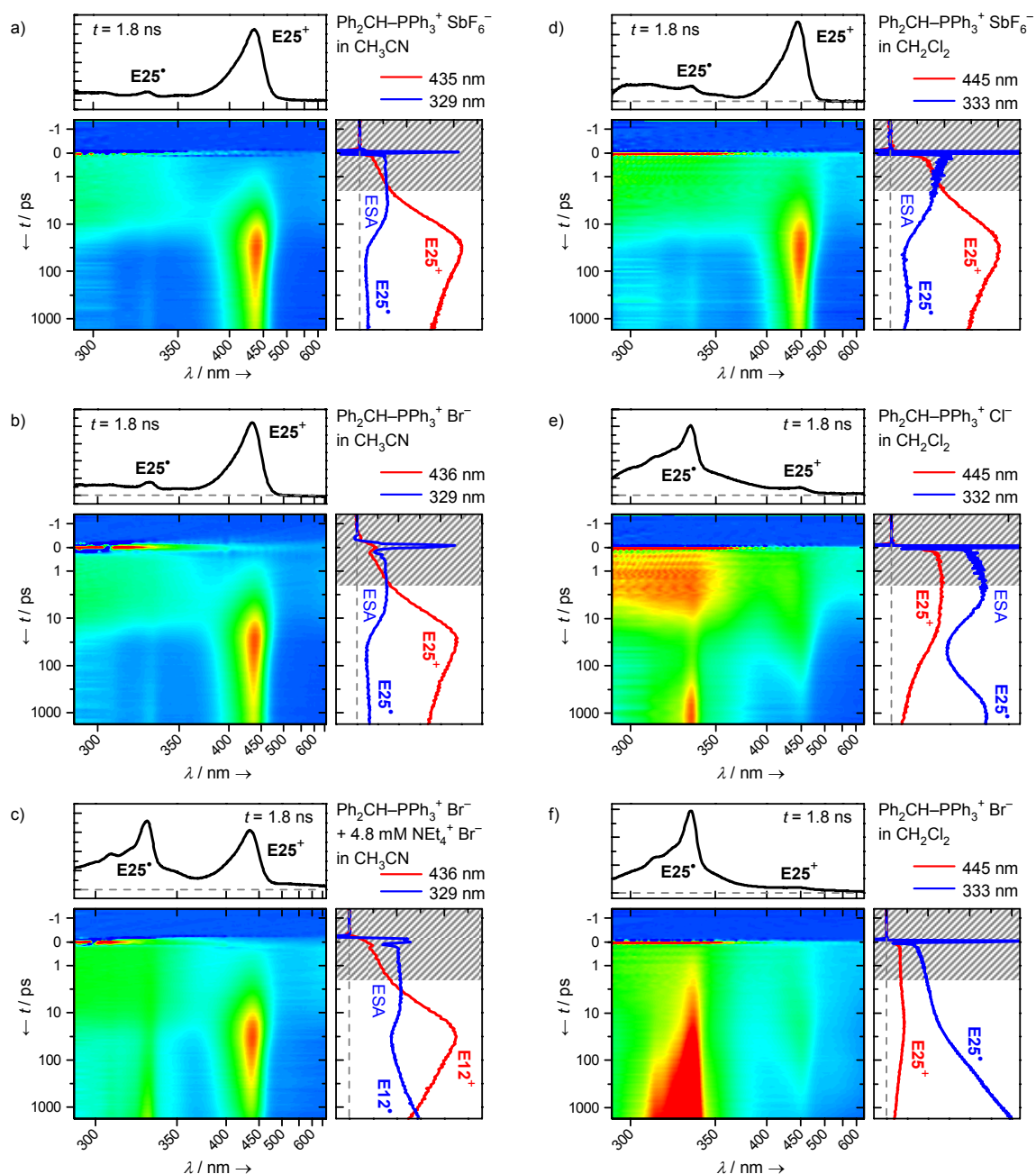


Figure 2.6. Transient absorptions obtained after irradiating solutions of $\mathbf{E25-PPH_3^+ X^-}$ with different counterions X^- in CH_3CN (a-c) and CH_2Cl_2 (d-f) by a 35-fs laser pulse ($\lambda_{\text{exc}} = 280 \text{ nm}$). The graphs above the color plots show the spectra after 1.8 ns (black). The graphs on the right show the dynamics of the absorbances at certain wavelengths: absorbance of benzhydryl cation $\mathbf{E25^+}$ (436 or 445 nm, red) and absorbance of the excited state (ESA) and the benzhydryl radical $\mathbf{E25^\bullet}$ (329 or 333 nm, blue). (a) $X^- = \text{SbF}_6^-$ in CH_3CN ; (b) $X^- = \text{Br}^-$ in CH_3CN ; (c) $X^- = \text{Br}^-$ in CH_3CN with $4.8 \times 10^{-3} \text{ M}$ added $\text{NEt}_4^+ \text{Br}^-$; (d) $X^- = \text{SbF}_6^-$ in CH_2Cl_2 ; (e) $X^- = \text{Cl}^-$ in CH_2Cl_2 ; (f) $X^- = \text{Br}^-$ in CH_2Cl_2 . The color scales in the false color plots are comparable in Figures (a-f), but the absorbances in the small graphs (spectra and dynamics) were scaled to the available space and cannot be compared directly. The time scale is linear between -1 and $+1 \text{ ps}$ and logarithmic above 1 ps . For the reasons discussed in context of Figure 2.2, the absorption changes during the first 2 ps (shaded area) are discussed elsewhere.⁴⁵ Experimental conditions: (a,d-f) $(5-7) \times 10^{-3} \text{ M}$ precursor ($A_{280 \text{ nm}} = 0.2$), $d = 120 \mu\text{m}$; (b,c) $4 \times 10^{-4} \text{ M}$ precursor ($A_{280 \text{ nm}} = 0.1$), $d = 1 \text{ mm}$.

At larger precursor concentrations or in the presence of added bromide, however, the association equilibrium of the precursor phosphonium salt is shifted toward the ion pairs, and the PET pathway becomes available also in CH₃CN. Figure 2.6c shows the false color plot obtained after irradiation of **E25**–PPh₃⁺ Br[–] in the presence of 4.8 × 10^{–3} M added NEt₄⁺ Br[–]. We now observed a significant amount of benzhydryl radicals **E25**[•] while the yield of the benzhydryl cations **E25**⁺ decreased.

The false color representations of the transient absorption data recorded after irradiation of **E25**–PPh₃⁺ X[–] with different counter-anions (X[–] = SbF₆[–], Cl[–], and Br[–]) in CH₂Cl₂ are shown in Figure 2.6d-f. As already discussed, the plot for **E25**–PPh₃⁺ SbF₆[–] (Figure 2.6d) is similar to that observed in CH₃CN. Irradiation of **E25**–PPh₃⁺ Cl[–] gave the color plot shown in Figure 2.6e, which is an intermediate case between the SbF₆[–] and the Br[–] salts. At any time, only a small amount of carbocations **E25**⁺ is present. In addition, most of the initially generated **E25**⁺ decay during the first 1.8 ns due to the combination reaction of **E25**⁺ with Cl[–]. The decay of the ESA is not associated with an increase of the carbocation absorbance, indicating that the excited state disappears predominantly by the PET mechanism and not by heterolytic bond cleavage. The dynamics at 332 nm is most interesting (Figure 2.6e, blue curve), because the ESA decreases within ~30 ps, while the benzhydryl radicals **E25**[•] appear with a marked delay ($k_{\text{obs}} = 3.8 \times 10^9 \text{ s}^{-1}$). The dent between the decrease of the ESA and the formation of **E25**[•] implies the accumulation of a “dark” intermediate with a relatively low absorption coefficient which cannot be detected within the large probe range from 290 to 700 nm. This intermediate might be the phosphoranyl/chlorine radical pair [**E25**–PPh₃[•] Cl[•]] (Scheme 2.2b, green pathway), which can either dissociate to **E25**[•] and PPh₃ or undergo a back electron transfer to regenerate the phosphonium chloride **E25**–PPh₃⁺ Cl[–]. After ~800 ps, the “dark” intermediate is completely consumed and the formation of **E25**[•] ceases.

Due to the lower oxidation potential of bromide, electron transfer reactions from Br[–], which generate Br[•], are more favorable than the corresponding reactions of Cl[–]. Thus, the PET pathway yielding the radical **E25**[•] from the excited state is extremely effective when X[–] = Br[–]. As a result, the ESA disappears almost instantaneously and the band of **E25**[•] appears within a few ps (Figure 2.6f). Accordingly, only a very small amount of carbocation **E25**⁺ is generated from **E25**–PPh₃⁺ Br[–] in CH₂Cl₂; again the decay of **E25**⁺ is very effective due to combination with Br[–]. In contrast to the observations with the chloride precursor, the radical band keeps rising with an observed rate constant of $k_{\text{obs}} = 6.3 \times 10^8 \text{ s}^{-1}$ throughout the whole time scale (Figure 2.6f, blue curve), i.e., the radical formation is slower but more effective in the case of

$X^- = Br^-$. This effect is also explained by the lower oxidation potential of Br^- : After formation of the not observable phosphoranyl radical, homolytic cleavage of $E25-PPh_3^*$ yields Ph_2CH^* (green pathway in Scheme 2.2b). On the other hand, the concurrent back electron transfer depends greatly on the reduction potential of X^* and is much less important with Br^* than with Cl^* . As the back electron transfer decay pathway for the “dark” state is suppressed, this state becomes longer-lived and benzhydryl radicals $E25^*$ keep forming over the whole time scale (Figure 2.6f) in a more effective and longer-ongoing⁵¹ process. Furthermore, many benzhydryl radicals $E25^*$ survive due to the less important electron transfer and radical combination reactions between $E25^*$ and Br^* .

Ion-Pairing and UV/vis Spectra of the Photo-generated Benzhydryl Cations. It should be noted that the carbocations E^+ which are obtained by the heterolytic cleavage from the paired precursor salts $[E-PR_3^+ X^-]$ (Scheme 2.2b, red pathway) may remain paired with the negatively charged counterions during escape of PR_3 from the solvent cage $[E^+ PR_3 X^-]$. Thus, if the association equilibrium of the benzhydrylium salt $E^+ X^-$ is favorable enough and X^- is a weakly nucleophilic counterion (e.g., SbF_6^-), photolysis of $[E-PR_3^+ X^-]$ yields long-lived ion pairs $[E^+ X^-]$.

Figure 2.5b shows that the absorption maxima of the carbocations in CH_2Cl_2 vary slightly with the counter-anions. The absorption maxima λ_{max} of the benzhydryl cations $E25^+$ which were generated from the phosphonium halide precursors are at slightly higher wavelengths ($\lambda_{max} \approx 450$ nm, Figure 2.5b, red and green curves) than those of the benzhydrylium ions generated from the phosphonium tetrafluoroborate or hexafluoroantimonate precursors ($\lambda_{max} \approx 443$ and 445 nm, Figure 2.5b, black and blue curves). It has previously been reported that the absorption maxima of the paired benzhydrylium tetrachloroborates $[E(15-20)^+ BCl_4^-]$ are at ~ 2 nm shorter wavelengths than those of the free ions.⁵² Thus, the lower λ_{max} of the benzhydrylium ions $E25^+$ which were generated from BF_4^- or SbF_6^- salts are in agreement with the presence of benzhydrylium ion pairs. The same λ_{max} as shown in Figure 2.5b (determined with 10 ns gate width) are also observed by the ultrafast measurements after ~ 1 ns and then remain constant during the whole lifetime (μs time scale) of $E25^+$ (see Figure 2.S.5 in section 2.S.5). As the diffusional approach of external anions is comparably slow, the paired benzhydrylium ions observed after ~ 1 ns must originate from paired phosphonium salts.

The higher λ_{max} for the benzhydryl cations $E25^+$ obtained from the halide precursors (Figure 2.5b, red and green curves) can be explained by the fact that carbocations which originate

from the paired fraction of the phosphonium halide precursors are immediately trapped by the halide anions. Thus, the carbocations which we can observe spectrophotometrically on the >10 ns time scale⁵³ are only the free (unpaired) benzhydrylium ions **E25**⁺ which are obtained from the unpaired fraction of the phosphonium halides. External halide ions subsequently consume the unpaired benzhydrylium ions in a diffusion-controlled reaction (see below) which does not affect λ_{max} of the remaining unpaired benzhydrylium ions but only reduces the signal intensity.

In CH₃CN, the precursor salts as well as the benzhydryl cations are mostly unpaired in the concentration range employed in our experiments, and we observe the unpaired carbocations **E25**⁺ predominantly. Thus, the absorption bands of **E25**⁺ feature identical absorption maxima ($\lambda_{\text{max}} \approx 436$ nm) irrespective of the counterions in this solvent (Figure 2.5a).

Counterion Effects in the Photochemistry of Other Onium Salts. The counterion effects discussed in the preceding paragraphs should also be relevant for the photochemistry of other onium salts. For example, we have previously shown that one can generate **E25**⁺ in CH₂Cl₂ by laser flash photolysis of the quaternary ammonium tetrafluoroborate **E25**–DABCO⁺ BF₄[−] (DABCO = 1,4-diazabicyclo[2.2.2]octane) but not from the corresponding quaternary ammonium bromide.¹⁴ Benzhydryl trimethylammonium iodide has also been used as photo-base-generator because irradiation of **E25**–NMe₃⁺ I[−] yields trimethylamine but not the benzhydryl cation **E25**⁺ which would trap the amine.²² To account for the formation of NMe₃ and the absence of **E25**⁺, Jensen and Hanson discarded the PET mechanism and favored a photo-S_N1 reaction in CH₃CN and CH₃OH which involves photoheterolysis of the precursor with subsequent trapping of the benzhydryl cations **E25**⁺ by the I[−] anions or the nucleophilic solvent.^{22b} Our results with the phosphonium analogues suggest that the PET mechanism may well be a relevant pathway for the generation of tertiary amines in less polar solvents.

2.2.6 Laser Flash Photolytic Generation of Highly Electrophilic Benzhydrylium Ions.

The information on the influence of photo-nucleofuges (PAR₃) and counterions X[−] on carbocation yields derived in the previous sections have subsequently been used to generate highly reactive carbocations in order to study their reactivities in bimolecular reactions on the >10 ns time scale. For these investigations, we were restricted to the solvent CH₂Cl₂, because CH₃CN reacts fast with highly electrophilic benzhydrylium ions such as **E(27-33)**⁺ (see below). In section 2.2.3 we have already demonstrated that the use of P(*p*-Cl-C₆H₄)₃ as photo-nucleofuge gives higher yields of carbocations than when PPh₃ is employed. Figure 2.7a

shows the transient spectra obtained by irradiating solutions of the phosphonium salts $\mathbf{E31}\text{-P}(p\text{-Cl-C}_6\text{H}_4)_3^+ \text{X}^-$ with different counter-anions X^- in CH_2Cl_2 with a 7-ns laser pulse ($\lambda_{\text{exc}} = 266 \text{ nm}$). As discussed in section 2.2.3, the phosphonium tetrafluoroborate $\mathbf{E31}\text{-P}(p\text{-Cl-C}_6\text{H}_4)_3^+ \text{BF}_4^-$ gave a moderate yield of $\mathbf{E31}^+$ along with significant amounts of $\mathbf{E31}^\bullet$ (Figure 2.7a, black curve). In view of the results presented in section 2.2.5 it is no surprise that we could not observe any carbocation $\mathbf{E31}^+$ but only the radical $\mathbf{E31}^\bullet$ when we irradiated the phosphonium bromide $\mathbf{E31}\text{-P}(p\text{-Cl-C}_6\text{H}_4)_3^+ \text{Br}^-$ (Figure 2.7a, red curve).

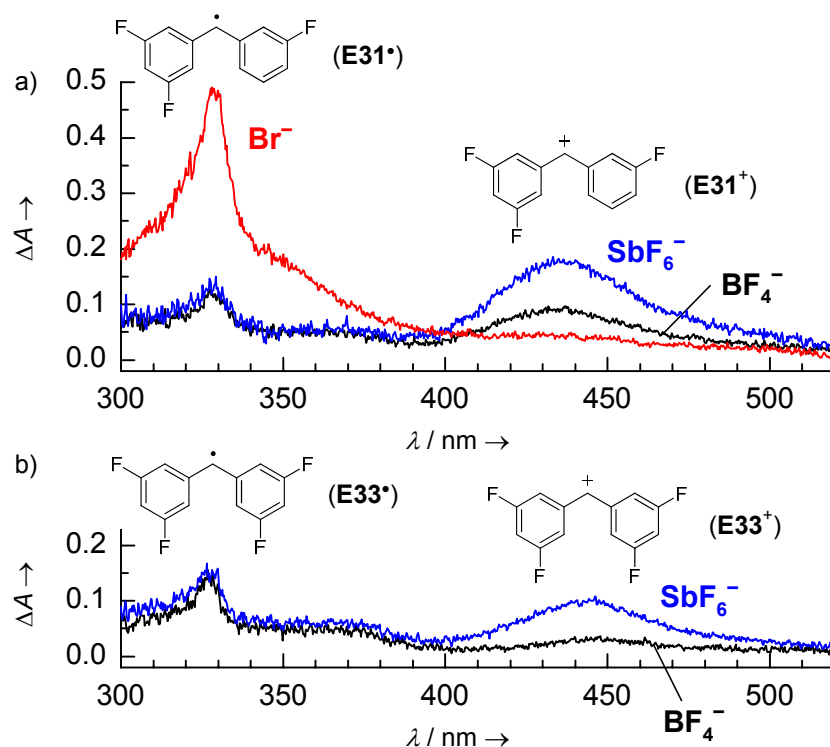


Figure 2.7. Transient spectra obtained after irradiation of CH_2Cl_2 solutions of benzhydryl tris(*p*-chlorophenyl)phosphonium salts with different counter-anions with a 7-ns laser pulse ($\lambda_{\text{exc}} = 266 \text{ nm}$, gate width: 10 ns): (a) $\mathbf{E31}\text{-P}(p\text{-Cl-C}_6\text{H}_4)_3^+ \text{X}^-$ with $\text{X}^- = \text{BF}_4^-$ (black, $A_{266 \text{ nm}} = 1.0$), $\text{X}^- = \text{SbF}_6^-$ (blue, $A_{266 \text{ nm}} = 1.0$) and $\text{X}^- = \text{Br}^-$ (red, $A_{266 \text{ nm}} = 1.0$); (b) $\mathbf{E33}\text{-P}(p\text{-Cl-C}_6\text{H}_4)_3^+ \text{X}^-$ with $\text{X}^- = \text{BF}_4^-$ (black, $A_{266 \text{ nm}} = 1.0$) and $\text{X}^- = \text{SbF}_6^-$ (blue, $A_{266 \text{ nm}} = 0.9$).

When we irradiated CH_2Cl_2 solutions of the phosphonium hexafluoroantimonate $\mathbf{E31}\text{-P}(p\text{-Cl-C}_6\text{H}_4)_3^+ \text{SbF}_6^-$, however, the intensity of the cation band was doubled compared with that obtained from the corresponding BF_4^- salt, while that of the radical band remained virtually unchanged (Figure 2.7a, blue line).

Similarly, the absorbance of $\mathbf{E33}^+$ more than tripled when we used the hexafluoroantimonate $\mathbf{E33}\text{-P}(p\text{-Cl-C}_6\text{H}_4)_3^+ \text{SbF}_6^-$ (Figure 2.7b, blue curve) instead of the corresponding

tetrafluoroborate (Figure 2.7b, black curve), while the yield of the benzhydryl radical **E33'** was unaffected. The combination of the P(*p*-Cl-C₆H₄)₃ photo-leaving group and the SbF₆⁻ counterion hence finally allowed us to generate **E33**⁺ in sufficient concentrations to study its kinetics with nucleophiles in CH₂Cl₂. Similarly, we could also obtain the highly electrophilic 4,4'-bis(trifluoromethyl)benzhydrylium ion **E32**⁺ from **E32**-P(*p*-Cl-C₆H₄)₃⁺ SbF₆⁻ (Figure 2.S.6 in section 2.S.6).

Apparently, the BF₄⁻ anions trap a significant portion of the carbocations **E(31-33)**⁺ within the [**E**⁺ BF₄⁻] ion pairs that are generated by the laser pulse. This is not the case for the parent benzhydryl cation **E25**⁺ which was obtained in similar concentrations from the hexafluoroantimonate and the tetrafluoroborate precursor (Figure 2.5b, black and blue curves); on the microsecond time scale we also see a faster decay with the BF₄⁻ counterion than with SbF₆⁻ (see below). The trapping of the carbocation by BF₄⁻ within the ion pair becomes less efficient as the electrophilicity of the carbocations is reduced. The higher reactivity of BF₄⁻ compared to SbF₆⁻ is in agreement with the calculated enthalpies of fluoride abstractions in the gas phase, which are 151 kJ mol⁻¹ more exothermic for BF₄⁻ than for SbF₆⁻.⁵⁴ Furthermore, the photoinitiation efficiencies of onium salts in cationic polymerizations generally depend on the nature of the anions and decrease in the order SbF₆⁻ > AsF₆⁻ > PF₆⁻ > BF₄⁻.²⁶ This is usually explained by the different nucleophilicities of the anions which are considered to be relevant for the stability of the active center in the propagation step of cationic polymerizations.²⁶

2.2.7 Lifetimes of Benzhydrylium Ions in CH₂Cl₂, CH₃CN, and CF₃CH₂OH. Not only the yields of the carbocations **E**⁺ on the ≤10 ns time scale but also their lifetimes on the μs time scale depend greatly on the experimental conditions. Figure 2.8 shows the time-dependent absorbances of the parent benzhydrylium ion **E25**⁺, which we observed when we generated this carbocation from precursors **E25**-PPh₃⁺ X⁻ with different counter-anions (X⁻ = BF₄⁻, SbF₆⁻, Br⁻, or Cl⁻) in CH₃CN or CH₂Cl₂. The lifetime of **E25**⁺ depends on the decay mechanism of the carbocation, which can be (i) recombination with the photo-leaving group PPh₃, (ii) reaction with the counter-anions X⁻ of the phosphonium salt precursor, or (iii) reaction with the solvent.

Recombination with the Photo-nucleofuge. A general limitation of the laser flash photolysis technique is entailed by the recombination reactions of the carbocations with the free (diffusionally separated) photo-nucleofuges. Photo-nucleofuges (e.g., Hal⁻, NR₃, PR₃, RCO₂⁻)

typically undergo diffusion-controlled recombination reactions with highly electrophilic carbocations ($E > 0$) in solvents of low nucleophilicity.⁵⁵ Exceptions to this rule are anionic photo-leaving groups in fluorinated alcohols which stabilize anions very well (e.g., acetate or *p*-cyanophenolate in $\text{CF}_3\text{CH}_2\text{OH}$).⁸ In our case, the triarylphosphines ($N \geq 12.58$, $s_N = 0.65$)³⁷ undergo diffusion-controlled or almost diffusion-controlled reactions with the benzhydrylium ions **E(13-33)**⁺.

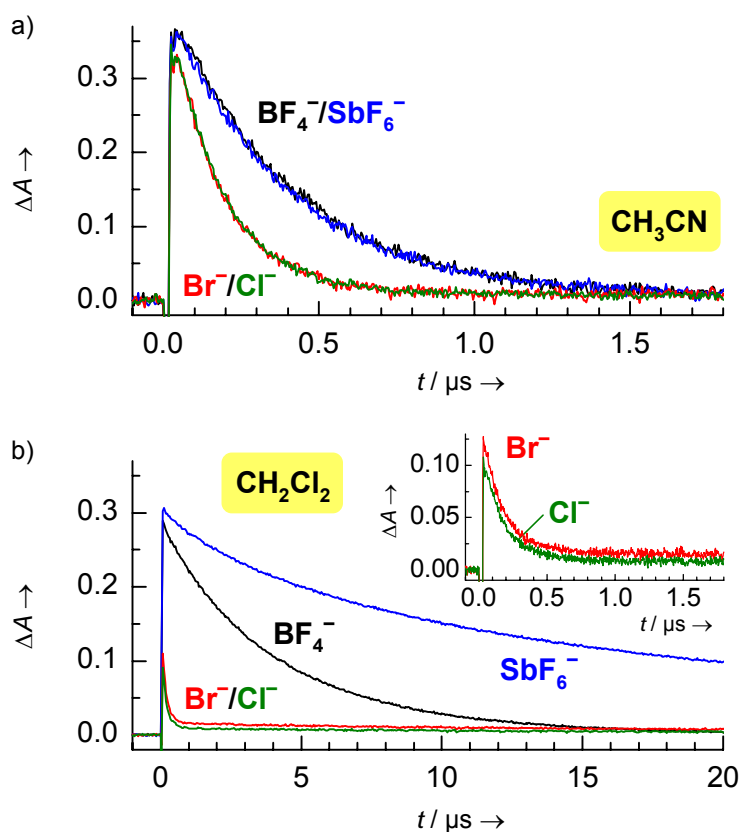


Figure 2.8. Time-dependent absorbances of **E25**⁺ obtained after 7-ns irradiation of **E25**– $\text{PPh}_3^+ \text{X}^-$ ($A_{266 \text{ nm}} = 0.5$, $(1.0\text{-}1.2) \times 10^{-4}$ M) with different counter-anions $\text{X}^- = \text{BF}_4^-$ (black), SbF_6^- (blue), Br^- (red) or Cl^- (green) with a 7-ns laser pulse: (a) in CH_3CN and (b) in CH_2Cl_2 (inset: enlarged decay curves for **E25**⁺ from precursors with halide counterions).

The blue curve in Figure 2.8b shows that the recombination reaction with PPh_3 can be observed when **E25**⁺ is generated by irradiation of **E25**– $\text{PPh}_3^+ \text{SbF}_6^-$ in CH_2Cl_2 . Since **E25**⁺ and PPh_3 are generated in equimolar amounts by the laser pulse, the observed decay of the absorbance is not mono-exponential. Using the software Gepasi,⁴³ we could fit the observed decay to a kinetic model which takes into account the second-order recombination reaction with PPh_3 and a general first-order reaction which summarizes all (pseudo-)first-order reactions which may occur (Figure 2.9). Details and more examples of such fits can be found

in section 2.S.7. As expected, second-order rate constants $k_{\text{PPh}_3} \approx 1 \times 10^{10} \text{ M}^{-1} \text{ s}^{-1}$ are found for the combinations of **E20**⁺, **E21**⁺, and **E25**⁺ with PPh₃, indicating diffusion-controlled reactions. The obtained rate constants k_0 (s⁻¹) for the first-order background decay reactions agree with the trends discussed below.

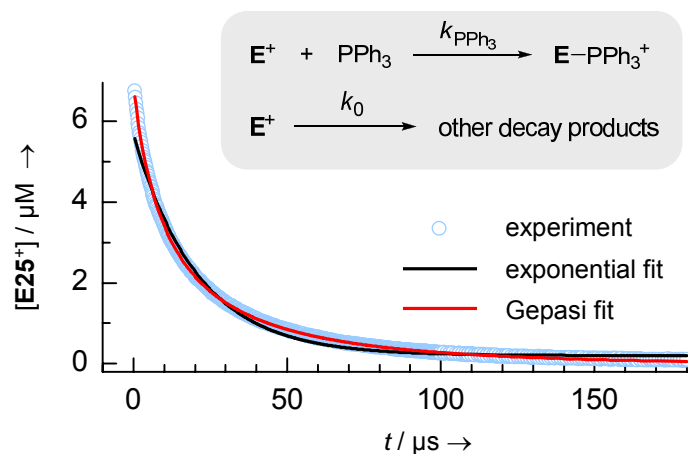


Figure 2.9. Decay of the concentration of **E25**⁺ observed after irradiation of **E25**–PPh₃⁺ SbF₆⁻ ($A_{266 \text{ nm}} = 0.53$, $1.03 \times 10^{-4} \text{ M}$) in CH₂Cl₂ with a 7-ns laser pulse: Superposition of experimental data (○), an exponential fit (black), and a fit calculated by Gepasi (red) according to the kinetic model with variable [PPh₃] shown in this Figure ($k_{\text{PPh}_3} = (1.31 \pm 0.003) \times 10^{10} \text{ M}^{-1} \text{ s}^{-1}$ and $k_0 = (6.49 \pm 0.02) \times 10^3 \text{ s}^{-1}$).

At typical concentrations of the photofragments **E**⁺ and PAr₃ in our experiments ($\sim 10^{-6}$ to 10^{-5} M), we find such nonexponential decay kinetics for all systems in which the benzhydryl cations **E**⁺ have lifetimes $> 10 \mu\text{s}$. The recombination reaction with the photo-leaving group thus sets a lower limit for measuring pseudo-first-order kinetics of the benzhydryl cations **E**⁺ with external nucleophiles: Only pseudo-first-order rate constants larger than $(1\text{-}5) \times 10^5 \text{ s}^{-1}$ can be determined reliably by fitting the data to an exponential decay curve; otherwise the decay kinetics will be dominated by the second-order reaction with the photo-leaving group.

Reaction with the Counter-anion of the Precursor Phosponium Salt. When precursors **E25**–PPh₃⁺ X⁻ with halide counter-anions were used for the generation of benzhydryl cations **E**⁺, we observed exponential decays of the carbocations which were significantly faster than the decays of carbocations generated from phosponium salts with X⁻ = BF₄⁻ or SbF₆⁻ (Figure 2.8). Halide ions undergo diffusion-controlled reactions with reactive carbocations ($E > -2$) in aprotic solvents⁷ and the reactions follow pseudo-first-order kinetics since $[\text{E}^+] \ll [\text{X}^-]$ (only a small fraction of Ar₂CH–PPh₃⁺ X⁻ is cleaved to the carbocations). For example, irradiation of $1.2 \times 10^{-4} \text{ M}$ solutions of **E25**–PPh₃⁺ X⁻ with X⁻ = Br⁻ or Cl⁻ in CH₃CN (Figure

2.8a, red and green curves) gave pseudo-first-order rate constants $k_{\text{obs}} \approx 6 \times 10^6 \text{ s}^{-1}$ for the decay of **E25**⁺. Irradiation of $1.0 \times 10^{-4} \text{ M}$ solutions of the same precursors in CH₂Cl₂ (Figure 2.8b, red and green curves) yielded similar rate constants ($k_{\text{obs}} \approx 7 \times 10^6 \text{ s}^{-1}$). These values correspond to second-order rate constants of $k_2 \approx 5 \times 10^{10} \text{ M}^{-1} \text{ s}^{-1}$ (CH₃CN) and $k_2 \approx 7 \times 10^{10} \text{ M}^{-1} \text{ s}^{-1}$ (CH₂Cl₂) for the diffusion-controlled reactions of **E25**⁺ with Br[−] and Cl[−].

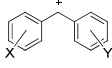
An almost mono-exponential decay of **E25**⁺ was also observed in CH₂Cl₂ when we irradiated **E25**–PPh₃⁺ X[−] with X[−] = BF₄[−] (Figure 2.8b, black curve, $k_{\text{obs}} \approx 2.6 \times 10^5 \text{ s}^{-1}$). This decay is much slower than the decays for X[−] = Cl[−] or Br[−] but significantly faster than the non-exponential decay observed for X[−] = SbF₆[−] (Figure 2.8b, blue curve) indicating that **E25**⁺ reacts with BF₄[−]. Similar mono-exponential decays were found for the benzhydrylium ions **E(22-30)**⁺ which were generated from the phosphonium tetrafluoroborates **E(22-30)**–PAr₃⁺ BF₄[−]; the decay rate constants increase with the electrophilicities *E* of the carbocations (see section 2.S.8 for details). As the yields of the more reactive benzhydryl cations **E(31-33)**⁺ obtained from the BF₄[−] salt precursors were lower than those from the SbF₆[−] salt precursors (see above), one can conclude that the reactions of **E(31-33)**⁺ with BF₄[−] already occur on time scales <10 ns. For the highly reactive carbocations **E(31-33)**⁺ we also observed mono-exponential decays when they were generated from the corresponding hexafluoroantimonate salts **E(31-33)**–P(*p*-Cl-C₆H₄)₃⁺ SbF₆[−]. As the background decay rates k_0 of the carbocations **E(31-33)**⁺ observed on the >10 ns time scale after irradiation of **E(31-33)**–P(*p*-Cl-C₆H₄)₃⁺ X[−] with X[−] = BF₄[−] and SbF₆[−] also become similar (Figure 2.S.8.2 in section 2.S.8), we assume that now the reactions of **E**⁺ with solvent impurities such as residual water in CH₂Cl₂ are dominating.

We have already discussed in section 2.2.5 that the benzhydrylium tetrafluoroborates **E**⁺ BF₄[−] predominantly exist as ion pairs in CH₂Cl₂ solutions (in the presence of $\sim 1 \times 10^{-4} \text{ M}$ phosphonium tetrafluoroborate). Accordingly, a further increase of the concentration of BF₄[−] has little effect on the kinetics. Thus, the decay rate constant of **E31**⁺ increased only slightly (factor 1.5) when we irradiated CH₂Cl₂ solutions of **E31**–P(*p*-Cl-C₆H₄)₃⁺ BF₄[−] in the presence of $1.4 \times 10^{-2} \text{ M}$ KBF₄/18-crown-6. The high concentration of BF₄[−] ions reduced the initial absorbance of **E31**⁺ by less than 30%, i.e., the effect is much smaller than when exchanging $5.7 \times 10^{-5} \text{ M}$ SbF₆[−] for the same concentration of BF₄[−] (Figure 2.7a).

Reactions with the Solvent. In CH₃CN or 2,2,2-trifluoroethanol (TFE), which are typical solvents for the laser-flashphotolytic generation of carbocations,¹ the characterization of highly electrophilic carbocations is hampered by the nucleophilicity of these solvents. In

CH₃CN, for example, the parent benzhydryl cation **E25**⁺ decays mono-exponentially with a first-order rate constant of $k_1 = 2.52 \times 10^6 \text{ s}^{-1}$ when it is generated from **E25**-PPh₃⁺ BF₄⁻ or SbF₆⁻ (Figure 2.8a), that is, it decays at least 1 order of magnitude faster than in CH₂Cl₂. A slightly larger value ($k_1 = 3.21 \times 10^6 \text{ s}^{-1}$) was observed for the decay of **E25**⁺ in trifluoroethanol (TFE). These rate constants are independent of the choice of the photo-leaving groups (Table 2.3). As solvation effects have a relatively small influence on the reactivities of carbocations,⁵⁶ the ~440-fold increase of the decay rate of **E25**⁺ in CH₃CN and TFE compared with CH₂Cl₂ ($k_0 \approx 6.5 \times 10^3 \text{ s}^{-1}$, Figure 2.9) must result from reactions of **E25**⁺ with these solvents.^{8,9,40}

Table 2.3. First-Order Rate Constants k_1 (s⁻¹) for the Decay of Benzhydryl Cations **E**⁺ in CH₃CN and 2,2,2-Trifluoroethanol (TFE) at 20 °C.

E ⁺			<i>E</i> ^a	k_1 (CH ₃ CN) / s ⁻¹	k_1 (TFE) / s ⁻¹
	X	Y			
E22 ⁺	4-F	4-F	5.01	1.1×10^6 ^b	5.82×10^5 ^c
E23 ⁺	4-F	H	5.20	1.8×10^6 ^b	^d
E25 ⁺	H	H	5.47	2.52×10^6 ^{c,e}	3.21×10^6 ^{c,f}
E26 ⁺	4-Cl	4-Cl	5.48	2.8×10^6 ^b	1.47×10^6 ^c
E27 ⁺	3-F	H	6.23	1.00×10^7 ^c	1.29×10^7 ^c
E28 ⁺	4-(CF ₃)	H	6.70	3.8×10^7 ^b	^d
E30 ⁺	3-F	3-F	6.87	3.49×10^7 ^c	4.6×10^7 ^c

^a Electrophilicity parameters *E* of the benzhydryl cations **E**⁺; see Table 2.1 for references. ^b Photolysis of **E**-Cl in CH₃CN.⁴⁰ ^c Photolysis of **E**-PPh₃⁺ BF₄⁻, this work. ^d Not determined. ^e Photolysis of **E25**-Cl in CH₃CN gave a value of $2.5 \times 10^6 \text{ s}^{-1}$.⁴⁰ ^f Photolysis of benzhydryl *p*-cyanophenyl ether in TFE gave a value of $3.2 \times 10^6 \text{ s}^{-1}$.⁸

The most reactive benzhydryl cations of this series, **E31**⁺, **E32**⁺, and **E33**⁺, decay too fast in CH₃CN or TFE ($\tau < 10 \text{ ns}$) to be observed with the nanosecond laser flash photolysis setup. It is possible, however, to generate the acceptor-substituted benzhydrylium ions **E(27-30)**⁺ in these solvents and to follow the exponential decays of their UV/vis absorbances. Since the first-order rate constants for their reactions with CH₃CN and TFE are $\geq 1 \times 10^7 \text{ s}^{-1}$ (Table 2.3), it is difficult to characterize the electrophilic reactivities of these benzhydrylium ions toward

other nucleophiles in these solvents, because only nucleophiles that react with rate constants close to the diffusion limit can efficiently compete with these solvents.

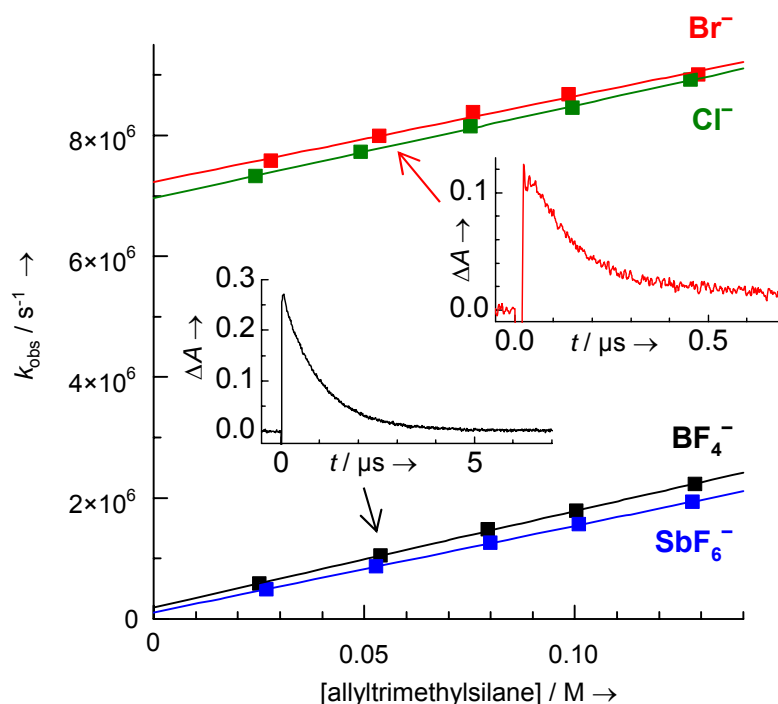
Dichloromethane is considerably less nucleophilic than CH₃CN or TFE. First-order decay rate constants of $\sim 2 \times 10^6 \text{ s}^{-1}$ (**E31**⁺) and $\sim 3 \times 10^6 \text{ s}^{-1}$ (**E33**⁺) were measured when these carbocations were generated from **E(31,33)**-P(*p*-Cl-C₆H₄)₃⁺ SbF₆⁻ (Figure 2.S.8.2 in section 2.S.8). However, these values are probably due to impurities and do not reflect the reactivity of CH₂Cl₂ (see above). They just represent an upper limit for the nucleophilic reactivity of CH₂Cl₂. Anyway, the lifetimes of the benzhydrylium ions in highly purified CH₂Cl₂ (see section 2.S.1) are much longer than in anhydrous CH₃CN and TFE and allow us to study the electrophilic reactivities of **E(27-33)**⁺ toward a variety of nucleophiles.

2.2.8 Counterion Effects on Bimolecular Reactions. As discussed in section 2.2.5, the usual assumption that only free ions are observed in nanosecond laser flash photolysis experiments^{1a,b} does not hold when the carbocations are generated by photolysis of certain onium salts with low-nucleophilicity counterions (e.g., BF₄⁻, SbF₆⁻). Consequently, the question arises whether bimolecular reactions of the photolytically generated carbocations are affected by the nature of the counter-anion in the precursor salt. Previous results already showed that the rate constants for the reactions of moderately stabilized benzhydrylium ions such as methoxy- or methyl substituted benzhydrylium ions **E(15-21)**⁺ with neutral nucleophiles like π -nucleophiles^{3d,56,57} or hydride donors⁵⁸ in CH₂Cl₂ are independent of the nature of the counter-anion and the degree of ion pairing. We now investigated the influence of the counter-anion on the reactions of the considerably more electrophilic benzhydrylium ions **E25**⁺ and **E31**⁺ with π -nucleophiles (Table 2.4).

When we generated the benzhydrylium ions **E**⁺ from different precursors **E**-PAR₃⁺ X⁻ with different counter-anions X⁻ in the presence of a large excess of π -nucleophiles, we observed exponential decays of the UV/vis absorbances of the benzhydryl cations **E**⁺ from which we obtained the pseudo-first-order rate constants k_{obs} (s⁻¹). Plots of k_{obs} versus the nucleophile concentrations were linear in all cases, as exemplified in Figure 2.10 for the reaction of **E25**⁺ with allyltrimethylsilane.

Table 2.4. Second-Order Rate Constants k_2 ($\text{M}^{-1} \text{s}^{-1}$) for the Reactions of π -Nucleophiles with Benzhydryl Cations E^+ Obtained from Different Precursors $\text{E-PAr}_3^+ \text{X}^-$ in CH_2Cl_2 at 20°C .

E^+	precursor E-PAr_3^+	X^-	$k_2 / \text{M}^{-1} \text{s}^{-1}$
E25⁺ Reaction with allyltrimethylsilane			
	PPh_3	BF_4^-	1.60×10^7
	PPh_3	SbF_6^-	1.43×10^7
	PPh_3	Br^-	1.42×10^7
	PPh_3	Cl^-	1.53×10^7
E31⁺ Reaction with 2,3-dimethyl-1-butene			
	PPh_3	BF_4^-	8.22×10^7
	$\text{P}(p\text{-Cl-C}_6\text{H}_4)_3$	BF_4^-	8.24×10^7
	$\text{P}(p\text{-Cl-C}_6\text{H}_4)_3$	SbF_6^-	8.27×10^7

**Figure 2.10.** Plots of the pseudo-first-order rate constants k_{obs} (s^{-1}) for the reactions of E25^+ with allyltrimethylsilane in CH_2Cl_2 when E25^+ was generated by irradiation of $1.0 \times 10^{-4} \text{ M}$ solutions of the precursors $\text{E25-PPh}_3^+ \text{X}^-$ with different counter-anions $\text{X}^- = \text{BF}_4^-$ (black squares), SbF_6^- (blue squares), Br^- (red squares), or Cl^- (green squares) against the concentration of allyltrimethylsilane. The small graphs show the absorbance decays of E25^+ in presence of $5.4 \times 10^{-2} \text{ M}$ allyltrimethylsilane (black curve, $\text{X}^- = \text{BF}_4^-$; red curve, $\text{X}^- = \text{Br}^-$).

The intercepts of these plots vary with the counter-anion X^- of the phosphonium salts and correspond to the rate constants k_0 for the background decay reactions discussed in section 2.2.7. For $X^- = Br^-$ and Cl^- , we find quite large intercepts of $k_0 \approx 7 \times 10^6 \text{ s}^{-1}$ due to the diffusion-controlled reactions of E^+ with the halide anions. For $X^- = BF_4^-$ and SbF_6^- , the intercepts are substantially lower and their origin has been discussed above. The slopes of the four plots are independent of the counter-anion and provide the second-order rate constants k_2 ($M^{-1} \text{ s}^{-1}$) for the reaction of $E25^+$ with allyltrimethylsilane listed in Table 2.4. We thus measured the same rate constants within experimental error for the reactions of $E25^+$ with allyltrimethylsilane when $E25^+$ was generated from different precursors $E25-PPh_3^+ X^-$ with $X^- = BF_4^-$, SbF_6^- , Br^- , or Cl^- (Table 2.4). As discussed in section 2.2.5, the benzhydryl cations obtained from precursors with halide ions are the free (unpaired) cations because $[E25^+ Hal^-]$ pairs collapse to covalent $E25-Hal$ in less than 10 ns. Since $E25^+ BF_4^-$ and $E25^+ SbF_6^-$ are significantly paired, on the other hand, we can conclude that paired and unpaired benzhydrylium ions $E25^+$ react with the same rate constants in bimolecular reactions and can be characterized by an anion-independent electrophilicity parameter ($E = 5.47$).

The same situation has been observed for the reactions of 2,3-dimethyl-1-butene with $E31^+$, which is the most electrophilic carbocation ($E = 7.52$) in our series that could be obtained from precursors with different counterions. When we generated $E31^+$ from either $E31-P(p-Cl-C_6H_4)_3^+ BF_4^-$ or $E31-P(p-Cl-C_6H_4)_3^+ SbF_6^-$, we again measured the same rate constants within experimental error (Table 2.4). Moreover, we also obtained the same rate constant when we used $E31-PPh_3^+ BF_4^-$ as precursor, which shows that the photo-leaving group does not have any effect on the carbocations' reactivities either. As discussed in section 2.2.6, we could not generate $E31^+$ from the phosphonium bromide precursor in CH_2Cl_2 (radical formation), and therefore we cannot compare the reactivities of free and paired carbocations in this case. The counterion independence of the experimental rate constants for carbocation alkene combination reactions implies that ion pairing stabilizes the transition states to about the same extent as the reactant carbocations.

2.3 Conclusion

The efficiencies of the photo-generation of benzhydrylium ions and benzhydryl radicals from phosphonium salts $E-PAr_3^+ X^-$ depend not only on the photo-electrofuge (E^+) and the

photoleaving group PAR_3 , but also on the counterion X^- , the solvent, and the concentration of the precursor molecules. Depending on the reaction conditions, benzhydryl radicals E^\bullet or benzhydryl cations E^+ may be obtained almost exclusively. The results presented in this work should also be relevant for the photochemistry of other onium salts. Spectroscopic investigations on the fs to ps time scale like those performed in this and related work^{4,5,16,45} provide a complete microscopic understanding of the photo-generation and the dynamics of reactive intermediates in the geminate solvent cage. With the knowledge of phosphonium salt photochemistry acquired from the present study, we can now select the proper precursor salts for the efficient generation of highly reactive carbocations which are not easily accessible by conventional methods. The method described in this work will subsequently be used to characterize the electrophilic reactivities of the acceptor-substituted benzhydrylium ions $\text{E}(\mathbf{27-33})^+$ in CH_2Cl_2 at 20 °C, which provides a further extension of our long-ranging electrophilicity scale.⁴¹

2.4 Acknowledgment

We thank Prof. Shinjiro Kobayashi for setting up the nanosecond laser flash working station, Dr. Armin Ofial, Dr. Igor Pugliesi, Sebastian Thallmair, and Konstantin Troshin for helpful discussions, Christoph Grill for early experimental work, and the Deutsche Forschungsgemeinschaft (SFB 749) for financial support.

2.5 References and Notes

- (1) Reviews: (a) McClelland, R. A. In *Reactive Intermediate Chemistry*; Moss, R. A., Platz, M. S., Jones, M. J., Eds.; Wiley: Hoboken, NJ, 2004, p 3–40. (b) McClelland, R. A. *Tetrahedron* **1996**, *52*, 6823–6858. (c) Fleming, S. A.; Pincock, J. A. *Mol. Supramol. Photochem.* **1999**, *3*, 211–281. (d) Das, P. K. *Chem. Rev.* **1993**, *93*, 119–144.
- (2) McClelland, R. A.; Chan, C.; Cozens, F. L.; Modro, A.; Steenken, S. *Angew. Chem.* **1991**, *103*, 1389–1391; *Angew. Chem., Int. Ed.* **1991**, *30*, 1337–1339.
- (3) (a) Bartl, J.; Steenken, S.; Mayr, H. *J. Am. Chem. Soc.* **1991**, *113*, 7710–7716. (b) Johnston, L. J.; Kwong, P.; Shelemay, A.; Lee-Ruff, E. *J. Am. Chem. Soc.* **1993**,

- 115, 1664–1669. (c) Kobayashi, S.; Hori, Y.; Hasako, T.; Koga, K.-i.; Yamataka, H. *J. Org. Chem.* **1996**, *61*, 5274–5279. (d) Mayr, H.; Schimmel, H.; Kobayashi, S.; Kotani, M.; Prabakaran, T. R.; Sipos, L.; Faust, R. *Macromolecules* **2002**, *35*, 4611–4615. (e) Phan, B. T.; Nolte, C.; Kobayashi, S.; Ofial, A. R.; Mayr, H. *J. Am. Chem. Soc.* **2009**, *131*, 11392–11401.
- (4) Sailer, C. F.; Fingerhut, B. P.; Thallmair, S.; Nolte, C.; Ammer, J.; Mayr, H.; de Vivie-Riedle, R.; Pugliesi, I.; Riedle, E., submitted.
- (5) Sailer, C. F.; Fingerhut, B. P.; Ammer, J.; Nolte, C.; Pugliesi, I.; Mayr, H.; de Vivie-Riedle, R.; Riedle, E. In *Ultrafast Phenomena XVII*; Chergui, M., Jonas, D., Riedle, E., Schoenlein, R. W., Taylor, A., Eds.; Oxford University Press: New York, **2011**; pp 427–429.
- (6) (a) McClelland, R. A.; Banait, N.; Steenken, S. *J. Am. Chem. Soc.* **1986**, *108*, 7023–7027. (b) McClelland, R. A.; Kanagasabapathy, V. M.; Banait, N. S.; Steenken, S. *J. Am. Chem. Soc.* **1989**, *111*, 3966–3972. (c) McClelland, R. A.; Kanagasabapathy, V. M.; Banait, N. S.; Steenken, S. *J. Am. Chem. Soc.* **1991**, *113*, 1009–1014. (d) McClelland, R. A.; Kanagasabapathy, V. M.; Banait, N.; Steenken, S. *J. Am. Chem. Soc.* **1992**, *114*, 1816–1823. (e) Van Pham, T.; McClelland, R. A. *Can. J. Chem.* **2001**, *79*, 1887–1897.
- (7) Minegishi, S.; Loos, R.; Kobayashi, S.; Mayr, H. *J. Am. Chem. Soc.* **2005**, *127*, 2641–2649.
- (8) McClelland, R. A.; Kanagasabapathy, V. M.; Steenken, S. *J. Am. Chem. Soc.* **1988**, *110*, 6913–6914.
- (9) Minegishi, S.; Kobayashi, S.; Mayr, H. *J. Am. Chem. Soc.* **2004**, *126*, 5174–5181.
- (10) (a) Hallett-Tapley, G.; Cozens, F. L.; Schepp, N. P. *J. Phys. Org. Chem.* **2009**, *22*, 343–348. (b) Horn, M.; Mayr, H. *Chem. Eur. J.* **2010**, *16*, 7478–7487. (c) Horn, M.; Mayr, H. *Eur. J. Org. Chem.* **2011**, 6470–6475.
- (11) Baidya, M.; Kobayashi, S.; Brotzel, F.; Schmidhammer, U.; Riedle, E.; Mayr, H. *Angew. Chem.* **2007**, *119*, 6288–6292; *Angew. Chem., Int. Ed.* **2007**, *46*, 6176–6179.
- (12) (a) Cozens, F.; Li, J.; McClelland, R. A.; Steenken, S. *Angew. Chem.* **1992**, *104*, 753–755; *Angew. Chem., Int. Ed.* **1992**, *31*, 743–745. (b) Mladenova, G.; Chen, L.; Rodriguez, C. F.; Siu, K. W. M.; Johnston, L. J.; Hopkinson, A. C.; Lee-Ruff, E. *J. Org. Chem.* **2001**, *66*, 1109–1114. (c) Loos, R.; Kobayashi, S.; Mayr, H. *J. Am. Chem. Soc.*

- 2003**, 125, 14126–14132. (d) Schaller, H. F.; Schmidhammer, U.; Riedle, E.; Mayr, H. *Chem. Eur. J.* **2008**, 14, 3866–3868.
- (13) See refs 14–18 for kinetic studies using quaternary triarylphosphonium salts and refs 18 and 19 for kinetic studies with other quaternary phosphonium salts as precursors.
- (14) Ammer, J.; Baidya, M.; Kobayashi, S.; Mayr, H. *J. Phys. Org. Chem.* **2010**, 23, 1029–1035 (CHAPTER 9 of this work).
- (15) Ammer, J.; Mayr, H. *Macromolecules* **2010**, 43, 1719–1723 (CHAPTER 6 of this work).
- (16) Sailer, C. F.; Singh, R. B.; Ammer, J.; Riedle, E.; Pugliesi, I. *Chem. Phys. Lett.* **2011**, 512, 60–65.
- (17) (a) Shi, L.; Horn, M.; Kobayashi, S.; Mayr, H. *Chem. Eur. J.* **2009**, 15, 8533–8541. (b) Troshin, K.; Schindele, C.; Mayr, H. *J. Org. Chem.* **2011**, 76, 9391–9408.
- (18) (a) Baidya, M.; Kobayashi, S.; Mayr, H. *J. Am. Chem. Soc.* **2010**, 132, 4796–4805. (b) Duan, X.-H.; Maji, B.; Mayr, H. *Org. Biomol. Chem.* **2011**, 9, 8046–8050. (c) Nigst, T. A.; Ammer, J.; Mayr, H. *Angew. Chem.* **2011**, 124, 1381–1385; *Angew. Chem., Int. Ed.* **2011**, 51, 1353–1356. (d) Nolte, C.; Ammer, J.; Mayr, H. *J. Org. Chem.* **2012**, 77, 3325–3335.
- (19) (a) Kanzian, T.; Lakhdar, S.; Mayr, H. *Angew. Chem.* **2010**, 121, 9717–9720; *Angew. Chem., Int. Ed.* **2010**, 49, 9526–9529. (b) Streidl, N.; Branzan, R.; Mayr, H. *Eur. J. Org. Chem.* **2010**, 4205–4210. (c) Lakhdar, S.; Ammer, J.; Mayr, H. *Angew. Chem.* **2011**, 123, 10127–10130; *Angew. Chem., Int. Ed.* **2011**, 50, 9953–9956 (CHAPTER 7 of this work).
- (20) For examples of carbocations generated by photolysis of phosphonium precursors acting as initiating species in carbocationic polymerizations, see: (a) Takata, T.; Takuma, K.; Endo, T. *Makromol. Chem., Rapid Commun.* **1993**, 14, 203–206. (b) Takuma, K.; Takata, T.; Endo, T. *J. Photopolym. Sci. Technol.* **1993**, 6, 67–74.
- (21) Examples of photoacid generation mechanisms with heterolytic cleavage of carbon-heteroatom bonds: (a) Pohlers, G.; Scaiano, J. C.; Step, E.; Sinta, R. *J. Am. Chem. Soc.* **1999**, 121, 6167–6175. (b) Sanrame, C. N.; Brandao, M. S. B.; Coenjarts, C.; Scaiano, J. C.; Pohlers, G.; Suzuki, Y.; Cameron, J. F. *Photochem. Photobiol. Sci.* **2004**, 3, 1052–1057.
- (22) Examples for the photogeneration of tertiary amines from benzhydryl derivatives: (a) Hanson, J. E.; Jensen, K. H.; Gargiulo, N.; Motta, D.; Pingor, D. A.; Novembre, A. E.; Mixon, D. A.; Kometani, J. M.; Knurek, C. In *Microelectronics Technology*.

- Polymers for Advanced Imaging and Packaging*; Reichmanis, E., Ober, C. K., MacDonald, S. A., Iwayanagi, T., Nishikubo, T., Eds.; ACS Symposium Series 614; American Chemical Society: Washington, DC, 1995. (b) Jensen, K. H.; Hanson, J. E. *Chem. Mater.* **2002**, *14*, 918–923.
- (23) Examples for the photogeneration of PPh₃ from quaternary phosphonium salts: (a) Önen, A.; Arsu, N.; Yagci, Y. *Angew. Makromol. Chem.* **1999**, *264*, 56–59. (b) Kasapoglu, F.; Aydin, M.; Arsu, N.; Yagci, Y. *J. Photochem. Photobiol., A* **2003**, *159*, 151–159.
- (24) For reviews about photoinitiators, see refs 25 and 26 and the following: (a) Yagci, Y.; Reetz, I. *Prog. Polym. Sci.* **1998**, *23*, 1485–1538. (b) Yagci, Y.; Durmaz, Y. Y.; Aydogan, B. *Chem. Rec.* **2007**, *7*, 78–90. (c) Allonas, X.; Croutxé-Barghorn, C.; Fouassier, J.-P.; Lalevée, J.; Malval, J.-P.; Morlet-Savary, F. In *Lasers in Chemistry*; Lackner, M., Ed.; Wiley-VCH: Weinheim, 2008; Vol. 2, pp 1001–1027. (d) Suyama, K.; Shirai, M. *Prog. Polym. Sci.* **2009**, *34*, 194–209. (e) Yagci, Y.; Jockusch, S.; Turro, N., J. *Macromolecules* **2010**, *43*, 6245–6260.
- (25) (a) Toba, Y. *J. Photopolym. Sci. Technol.* **2003**, *16*, 115–118. (b) Crivello, J. V. *J. Photopolym. Sci. Technol.* **2008**, *21*, 493–497.
- (26) (a) Fouassier, J.-P. In *Photoinitiation, Photopolymerization, and Photocuring: Fundamentals and Applications*; Hanser: Munich, 1995; pp 102–144. (b) Lazauskaite, R.; Grazulevicius, J. V. In *Handbook of Photochemistry and Photobiology*; Nalwa, H. S., Ed.; American Scientific Publishers: Stevenson Ranch, CA, 2003; Vol. 2, pp 335–392.
- (27) (a) Miranda, M. A.; Pérez-Prieto, J.; Font-Sanchis, E.; Scaiano, J. C. *Acc. Chem. Res.* **2001**, *34*, 717–726. (b) Kropp, P. J. In *CRC Handbook of Organic Photochemistry and Photobiology*, 2nd ed.; Horspool, W., Lenci, F., Eds.; CRC Press: Boca Raton, 2004; pp 1-1–1-32. (c) Kitamura, T. In *CRC Handbook of Organic Photochemistry and Photobiology*, 2nd ed.; Horspool, W., Lenci, F., Eds.; CRC Press: Boca Raton, 2004; pp 11-1–11-10. (d) Peters, K. S. *Chem. Rev.* **2007**, *107*, 859–873.
- (28) Pincock, J. A. *Acc. Chem. Res.* **1997**, *30*, 43–49.
- (29) Dektar, J. L.; Hacker, N. P. *J. Org. Chem.* **1991**, *56*, 1838–1844.
- (30) Dektar, J. L.; Hacker, N. P. *J. Am. Chem. Soc.* **1990**, *112*, 6004–6015.
- (31) Appleton, D. C.; Bull, D. C.; Givens, R. S.; Lillis, V.; McKenna, J.; McKenna, J. M.; Thackeray, S.; Walley, A. R. *J. Chem. Soc., Perkin Trans. 2* **1980**, 77–82.

- (32) Imrie, C.; Modro, T. A.; Rohwer, E. R.; Wagener, C. C. P. *J. Org. Chem.* **1993**, *58*, 5643–5649.
- (33) Alonso, E. O.; Johnston, L. J.; Scaiano, J. C.; Toscano, V. G. *Can. J. Chem.* **1992**, *70*, 1784–1794.
- (34) (a) Alonso, E. O.; Johnston, L. J.; Scaiano, J. C.; Toscano, V. G. *J. Am. Chem. Soc.* **1990**, *112*, 1270–1271. (b) Imrie, C.; Modro, T. A.; Wagener, C. C. P. *J. Chem. Soc., Perkin Trans. 2* **1994**, 1379–1382.
- (35) For general reviews, see refs 1 and 26. Similar photocleavage mechanisms were previously discussed for halides (refs 4 and 27), carboxylates (ref 28), halonium salts (ref 29), sulfonium salts (ref 30), ammonium salts (ref 31), and phosphonium salts (refs 32 and 33).
- (36) For equilibrium constants of stabilized benzhydryl cations with triarylphosphines, see ref 37. In cases where highly stabilized carbocations do not give stable triarylphosphonium salts, one may use a more Lewis-basic phosphine such as P(*n*-Bu)₃ as the photo-leaving group (refs 18 and 19).
- (37) Kempf, B.; Mayr, H. *Chem. Eur. J.* **2005**, *11*, 917–927.
- (38) For a review of the literature up to 1994, see: Dankowski, M. In *The chemistry of organophosphorus compounds*; Hartley, F. R., Ed.; Wiley: Chichester, 1994; Vol. 3, pp 325–343.
- (39) Megerle, U.; Pugliesi, I.; Schriever, C.; Sailer, C. F.; Riedle, E. *Appl. Phys. B: Laser Opt.* **2009**, *96*, 215–231.
- (40) Bartl, J.; Steenzen, S.; Mayr, H.; McClelland, R. A. *J. Am. Chem. Soc.* **1990**, *112*, 6918–6928.
- (41) (a) Mayr, H.; Bug, T.; Gotta, M. F.; Hering, N.; Irrgang, B.; Janker, B.; Kempf, B.; Loos, R.; Ofial, A. R.; Remennikov, G.; Schimmel, H. *J. Am. Chem. Soc.* **2001**, *123*, 9500–9512. (b) Mayr, H.; Kempf, B.; Ofial, A. R. *Acc. Chem. Res.* **2003**, *36*, 66–77. (c) For a comprehensive database of nucleophilicity and electrophilicity parameters, see: <http://www.cup.lmu.de/oc/mayr/DBintro.html>.
- (42) Syntheses, structural investigations, and ion-pairing phenomena of benzhydryl triarylphosphonium salts are reported in CHAPTER 1 of this work.
- (43) (a) Mendes, P. *Comput. Appl. Biosci.* **1993**, *9*, 563–571. (b) Mendes, P. *Trends Biochem. Sci.* **1997**, *22*, 361–363. (c) Mendes, P.; Kell, D. B. *Bioinformatics* **1998**, *14*, 669–883. (d) Further information about Gepasi: www.gepasi.org.

- (44) Alfassi, Z. B.; Neta, P.; Beaver, B. *J. Phys. Chem. A* **1997**, *101*, 2153–2158.
- (45) Fingerhut, B. P.; Sailer, C. F.; Ammer, J.; Riedle, E.; de Vivie-Riedle, R. *J. Phys. Chem. A* **2012**, DOI: 10.1021/jp300986t.
- (46) Exclusive formation of **E20**⁺ is observed after irradiation of **E20**–PPh₃⁺ BF₄[–] in CH₃CN; the plot for this system is shown in Figure S6 in the Supporting Information of ref 16.
- (47) (a) Nakamura, M.; Miki, M.; Majima, T. *J. Chem. Soc., Perkin Trans. 2* **2000**, 1447–1452. (b) Tojo, S.; Yasui, S.; Fujitsuka, M.; Majima, T. *J. Org. Chem.* **2006**, *71*, 8227–8232.
- (48) Fukuzumi, S.; Shimoosako, K.; Suenobu, T.; Watanabe, Y. *J. Am. Chem. Soc.* **2003**, *125*, 9074–9082.
- (49) Griffin, C. E.; Kaufman, M. L. *Tetrahedron Lett.* **1965**, *12*, 773–775.
- (50) Both groups have derived their conclusions from product studies after extended irradiation of benzyl triphenylphosphonium salts. It should be noted that product studies do not necessarily give the same results as transient measurements. Multiple irradiation of the same starting material molecules in preparative photolyses will distort the product ratios if the geminate recombination of one or both types of photofragment pair is a relevant process. Further complications arise if the photoproducts (e.g., arylmethyl halides) can undergo subsequent photolysis reactions.
- (51) The observed rate constant k_{obs} for formation of **E25**[•] is the sum of the rate constants for phosphoranyl radical dissociation and back electron transfer. The derivation of this relationship is analogous to the case of the carbocation dynamics in the geminate solvent cage, cf. section S5 in the Supporting Information of *J. Am. Chem. Soc.* **2012**, *134*, 11481–11494.
- (52) Schneider, R.; Mayr, H.; Plesch, P. H. *Ber. Bunsen-Ges.* **1987**, *91*, 1369–1374.
- (53) The absorbance maximum of the short-lived (<300 ps) [**E**⁺ Cl[–]] ion pairs is also blue-shifted compared to the free **E**⁺. The dependence of λ_{max} on the distance between **E**⁺ and Cl[–] is investigated in detail in ref 4.
- (54) Krossing, I.; Raabe, I. *Chem. Eur. J.* **2004**, *10*, 5017–5030.
- (55) For nucleophilicity parameters of common photo-nucleofuges such as halides, carboxylates, tertiary amines, pyridines, tertiary phosphines, and others, see ref 41c.
- (56) Mayr, H.; Schneider, R.; Schade, C.; Bartl, J.; Bederke, R. *J. Am. Chem. Soc.* **1990**, *112*, 4446–4454.

- (57) (a) Mayr, H.; Schneider, R.; Irrgang, B.; Schade, C. *J. Am. Chem. Soc.* **1990**, *112*, 4454–4459. (b) Hagen, G.; Mayr, H. *J. Am. Chem. Soc.* **1991**, *113*, 4954–4961. (c) Mayr, H.; Patz, M. *Macromol. Symp.* **1996**, *107*, 99–110. (d) Burfeindt, J.; Patz, M.; Müller, M.; Mayr, H. *J. Am. Chem. Soc.* **1998**, *120*, 3629–3634.
- (58) (a) Mayr, H.; Basso, N.; Hagen, G. *J. Am. Chem. Soc.* **1992**, *114*, 3060–3066. (b) Mayr, H.; Lang, G.; Ofial, A. R. *J. Am. Chem. Soc.* **2002**, *124*, 4076–4083.

2.S Supplementary Data and Experimental Section

2.S.1 Materials

Phosponium Salts and Reagents. The phosphonium salts $E-PAr_3^+ X^-$ were prepared by heating Ar_2CH-OH with $Ph_3PH^+ X^-$ or by treating Ar_2CH-Br with PAr_3 and subsequent anion metathesis.⁴² Allyltrimethylsilane (ABCR, 98%) and 2,3-dimethyl-1-butene (Aldrich, 97%) were used as received.

Solvents. For the nanosecond laser flash photolysis experiments, p.a. grade CH_2Cl_2 (Merck) was subsequently treated with concentrated sulfuric acid, water, 10% $NaHCO_3$ solution, and again water. After predrying with anhydrous $CaCl_2$, it was freshly distilled over CaH_2 . Acetonitrile (VWR or Sigma-Aldrich, HPLC grade) and 2,2,2-trifluoroethanol (TFE) (Apollo, 99%) were used as received.

2.S.2 Experimental procedures for laser flash photolysis measurements

2.S.2.1 Nanosecond laser flash photolysis

Instrumentation. The laser pulses (7-ns pulse length, $\lambda = 266$ nm, 30-60 mJ/pulse) from a Nd:YAG laser system (Innolas SpitLight 600, 1064 nm) with second (532 nm) and fourth (266 nm) harmonic generators were directed into a fluorescence flow cell (Starna 73.2-F/MCTC/Q/10/Z15, UV-quartz glass Spectrosil Q, 2 mm wide and 10 mm pathlength) containing the sample solution. Perpendicular to the laser pulse, we used the probe light from a xenon short-arc lamp (Osram XBO 150W/CR OFR in a Hamamatsu E7536 housing with Hamamatsu C8849 power supply) to record transient UV/vis spectra with an ICCD camera (PI Acton PI-MAX:1024) or follow the absorbance change at a specified wavelength with a photomultiplier (Hamamatsu H-7732-10 with Hamamatsu C7169 power supply and Stanford Research Systems SR445A amplifier). A 350 MHz oscilloscope (Tektronix DPO 4032) was used for data acquisition of the photomultiplier output. A shutter was used to prevent long

exposure of the sample to the light from the xenon lamp, and the sample solution in the fluorescence flow cell was replaced completely between subsequent laser pulses by a membrane dosage pump (KNF Stepdos 03RC). For the precise timing of the laser pulses and measurements we used a pulse/delay generator (Berkeley Nucleonics BNC 565). The wavelengths of the CCD output were calibrated using the emission lines of a Pen-Ray Hg(Ne) lamp (LOT-Oriel).

Transient spectra. Solutions of the precursor phosphonium salts with $A_{266\text{ nm}} \approx 0.2$ to 0.9 (ca. 10^{-5} to 10^{-4} M) were irradiated with a 7-ns laser pulse ($\lambda_{\text{exc}} = 266$ nm, 30-60 mJ/pulse) and transient spectra were obtained as difference spectra from subsequent determinations without and with laser irradiation using the ICCD camera with a gate width of 10 ns. Typically, four to eight such spectra were averaged to obtain the spectra published in this work.

Decay kinetics. Kinetics were measured by following the decay of the absorbance of the benzhydryl cations (see below for wavelengths). Typically, ≥ 64 individual runs were averaged for each measurement, and the (pseudo-)first-order rate constants k_{obs} (s^{-1}) were obtained by least-squares fitting to the single exponential curve $A_t = A_0 e^{-k_{\text{obs}}t} + C$. The second-order rate constants k_2 ($\text{M}^{-1} \text{s}^{-1}$) for the combination reactions with nucleophiles were obtained from the slopes of plots of k_{obs} versus the concentrations of the nucleophiles. The non-exponential decays were evaluated with the software Gepasi.⁴³

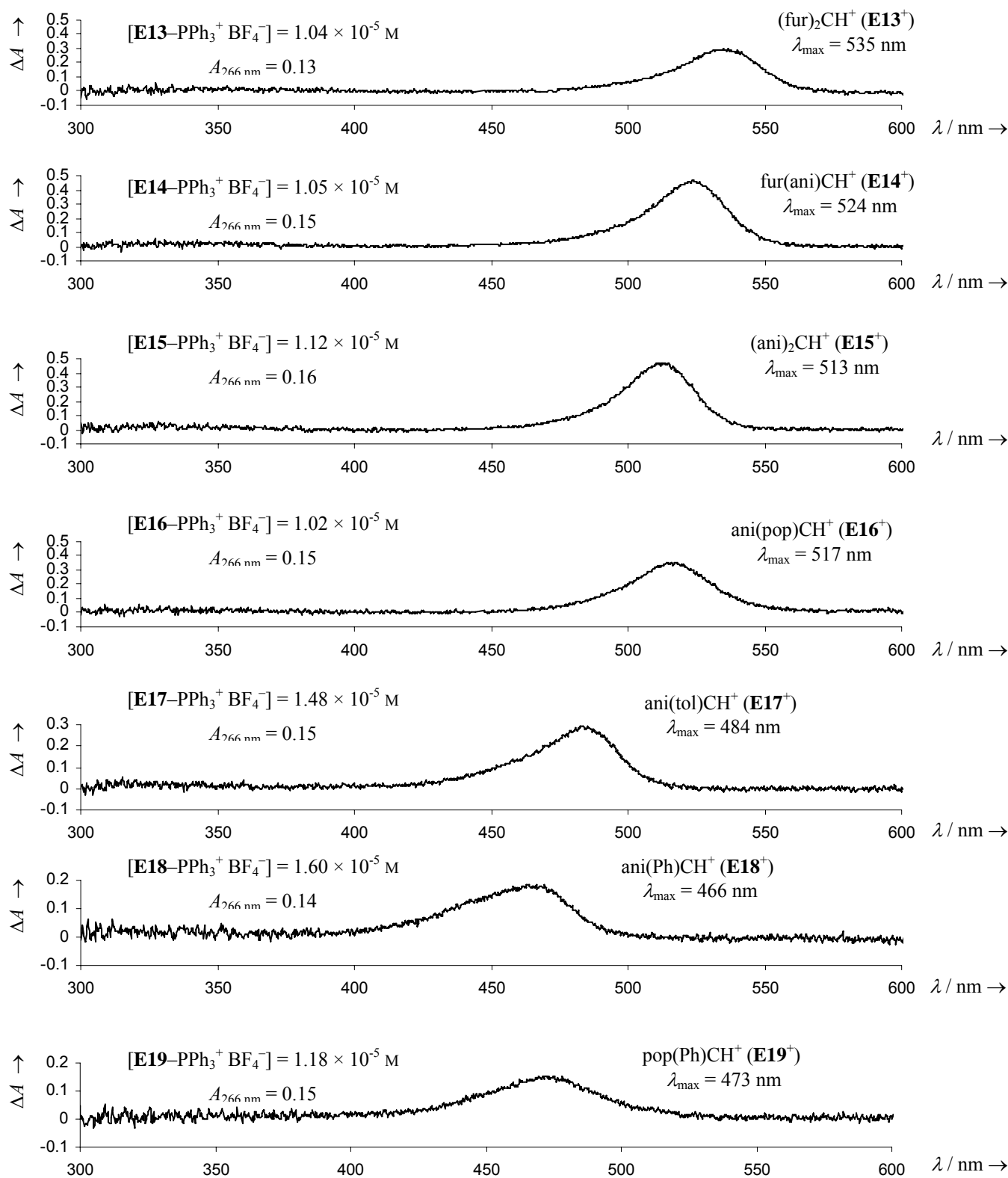
2.S.3 Transient spectra obtained by irradiation of E-PPh₃⁺ BF₄⁻ in CH₂Cl₂

Figure 2.S.3. Transient spectra of E⁺ and E^{*} obtained after irradiation of CH₂Cl₂ solutions of E-PPh₃⁺ BF₄⁻ with a 7-ns laser pulse ($\lambda_{\text{exc}} = 266 \text{ nm}$, gate width: 10 ns).

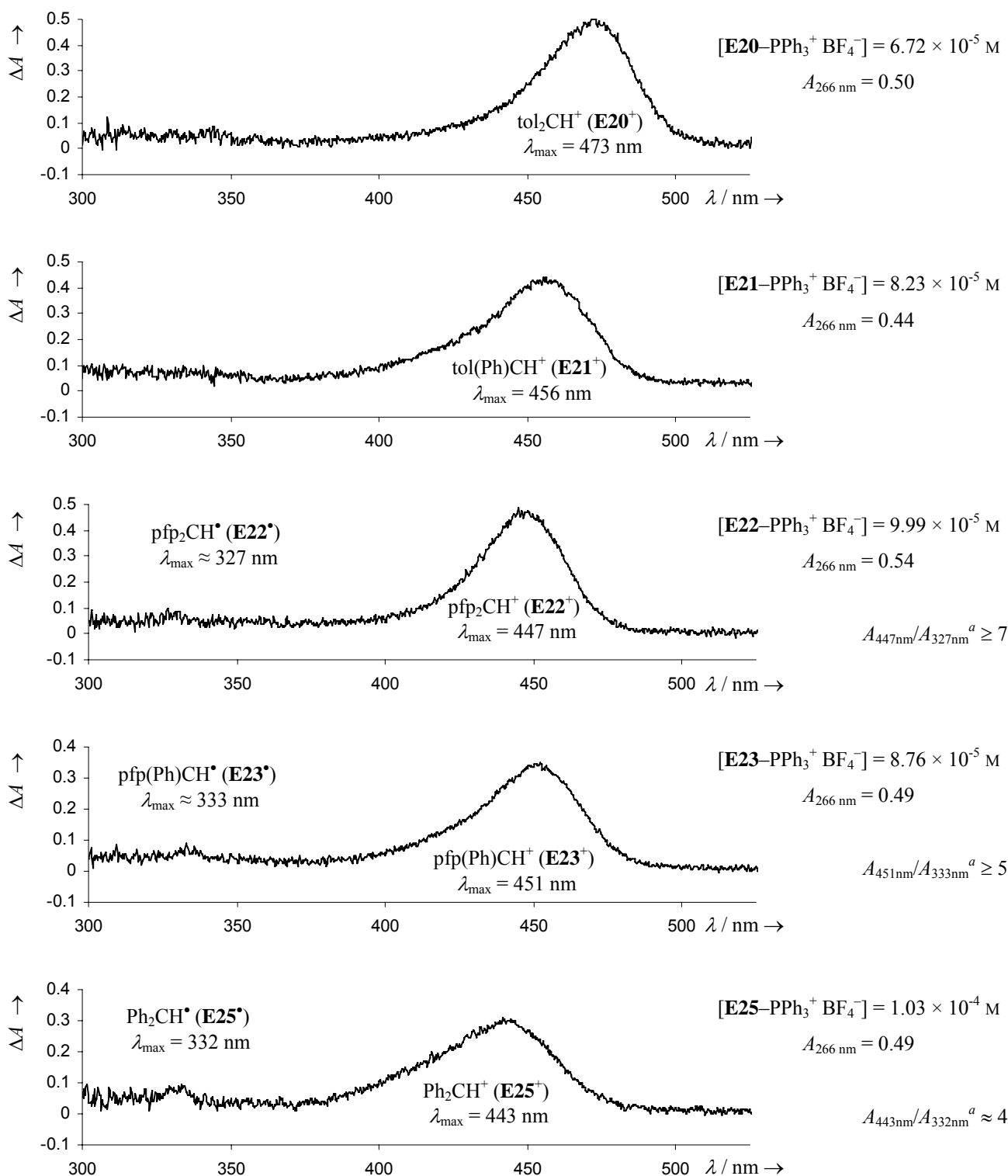


Figure 2.S.3 (continued). Transient spectra of E^+ and E^* obtained after irradiation of CH_2Cl_2 solutions of $\text{E-PPh}_3^+ \text{BF}_4^-$ with a 7-ns laser pulse ($\lambda_{\text{exc}} = 266 \text{ nm}$, gate width: 10 ns).

^a The absorbance maxima at the lower wavelengths can be assigned to the radicals E^* ,⁴⁰ but only approximate numeric values can be obtained from the spectra due to the overlap of the $\text{PPh}_3^{+\bullet}$ absorption band and the relatively large noise in this range of the spectrum.

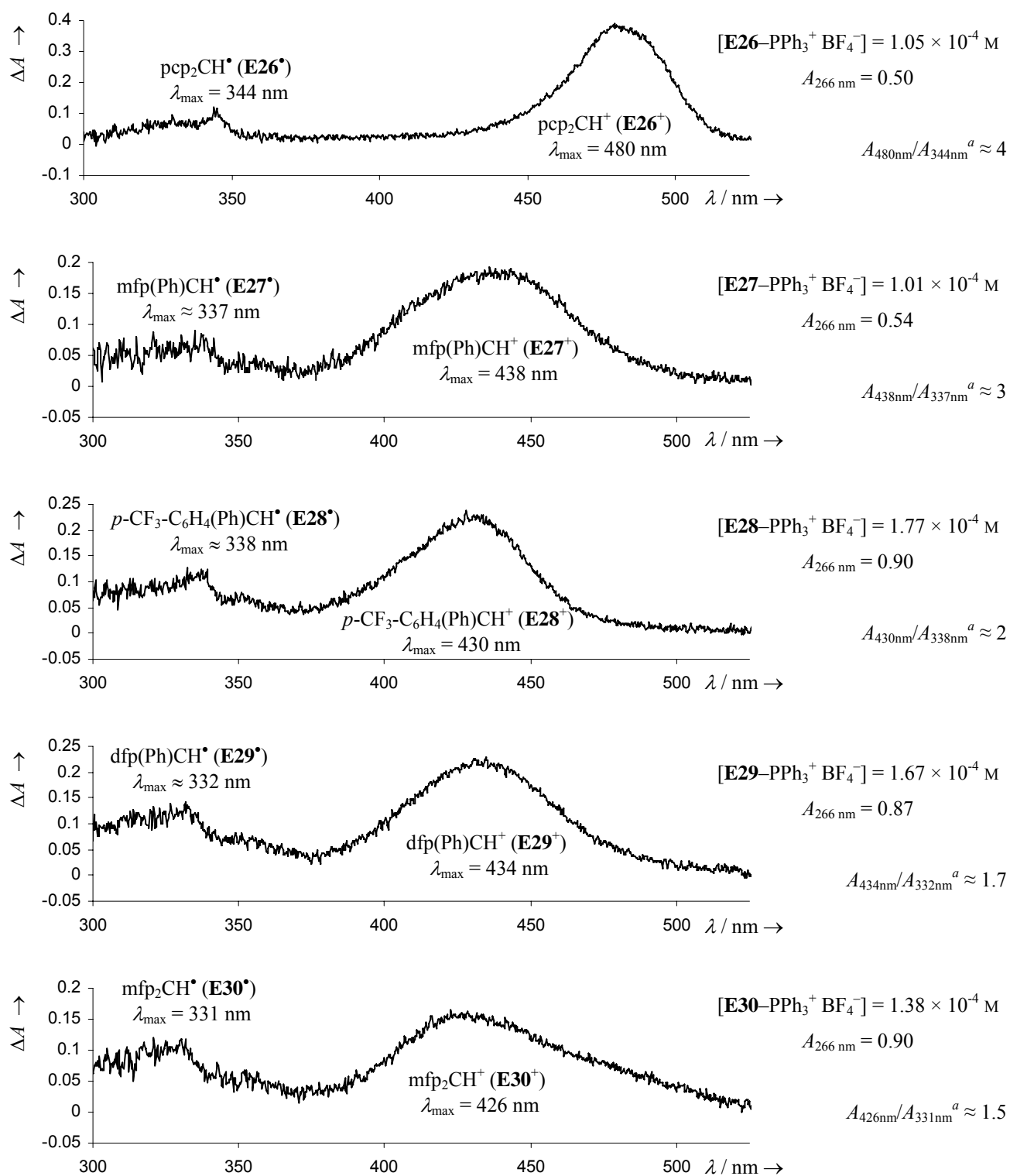


Figure 2.S.3 (continued). Transient spectra of \mathbf{E}^+ and \mathbf{E}^\bullet obtained after irradiation of CH_2Cl_2 solutions of $\mathbf{E}\text{-PPh}_3^+ \text{BF}_4^-$ with a 7-ns laser pulse ($\lambda_{\text{exc}} = 266 \text{ nm}$, gate width: 10 ns).

^a The absorbance maxima at the lower wavelengths can be assigned to the radicals \mathbf{E}^\bullet ,⁴⁰ but only approximate numeric values can be obtained from the spectra due to the overlap of the $\text{PPh}_3^{\bullet+}$ absorption band and the relatively large noise in this range of the spectrum.

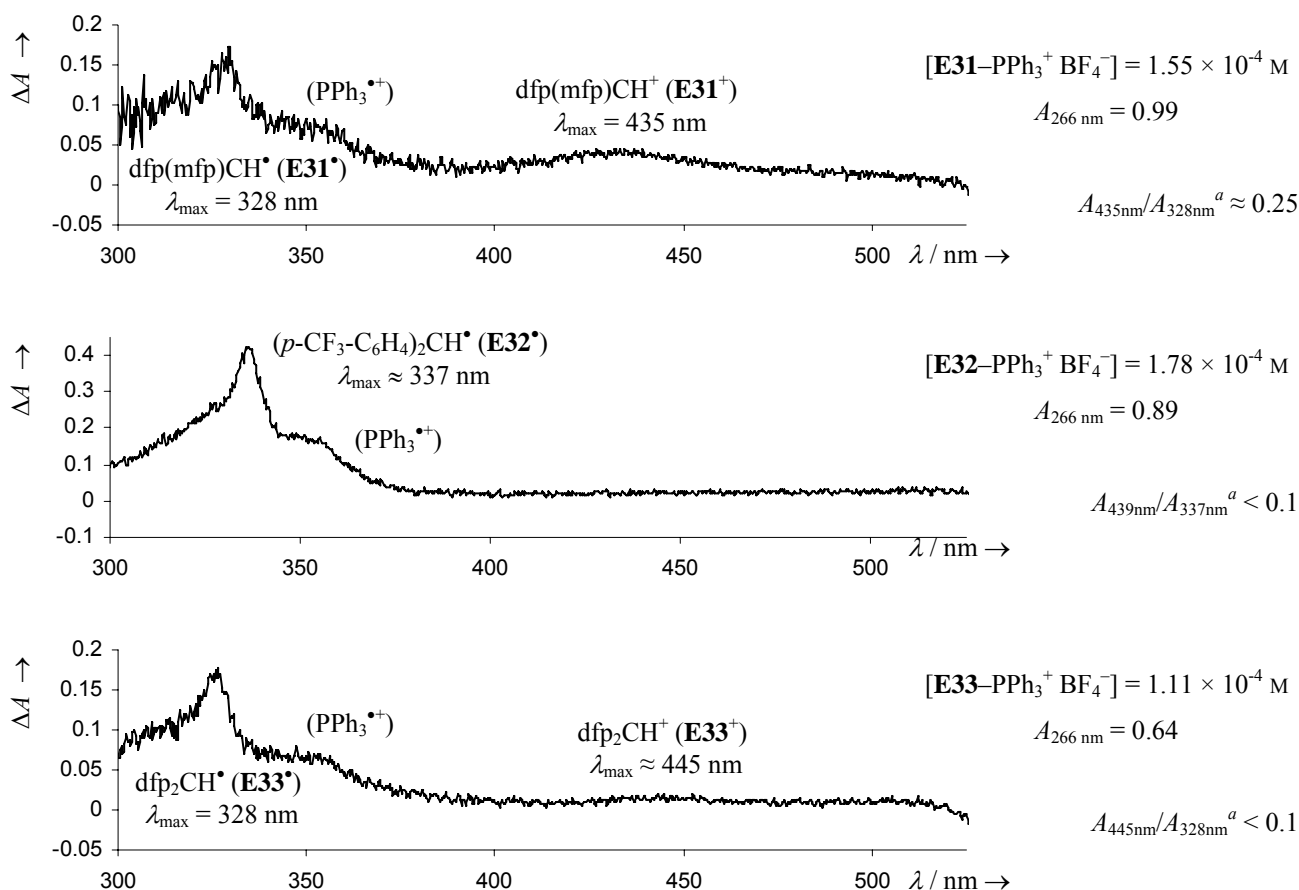


Figure 2.S.3 (continued). Transient spectra of E^+ and E^* obtained after irradiation of CH_2Cl_2 solutions of $\text{E-PPH}_3^+ \text{BF}_4^-$ with a 7-ns laser pulse ($\lambda_{\text{exc}} = 266 \text{ nm}$, gate width: 10 ns).

^a The absorbance maxima at the lower wavelengths can be assigned to the radicals E^* ,⁴⁰ but only approximate numeric values can be obtained from the spectra due to the overlap of the PPh_3^+ absorption band and the relatively large noise in this range of the spectrum.

2.S.4 Laser flash photolysis of $\mathbf{E25-PPh_3^+ BPh_4^-}$ in $\mathbf{CH_2Cl_2}$

We also tested the photobehavior of the tetraphenylborate salt $\mathbf{E25-PPh_3^+ BPh_4^-}$ in $\mathbf{CH_2Cl_2}$. With this precursor, the phosphonium ion and the tetraphenylborate anion can both be excited by the laser pulse. When a solution of $\mathbf{E25-PPh_3^+ BPh_4^-}$ ($A_{266\text{ nm}} = 0.5, 5.7 \times 10^{-5}$ M) in $\mathbf{CH_2Cl_2}$ was irradiated with a 7-ns laser pulse ($\lambda_{\text{exc}} = 266$ nm), we obtained the transient spectrum shown in Fig. 2.S.4.1 (pink curve). The spectrum features the absorption bands of $\mathbf{E25^+}$ and $\mathbf{E25^\bullet}$ together with a broad absorbance at $\lambda < 400$ nm. A similar band with $\lambda_{\text{max}} \approx 363$ nm was observed when we irradiated a $\mathbf{CH_2Cl_2}$ solution of $\mathbf{NaBPh_4/15-crown-5}$ with the same $\mathbf{BPh_4^-}$ concentration (Fig. 2.S.4.1a, purple curve). The difference spectrum (Fig. 2.S.4.1, grey curve) obtained from the two measurements resembles the transient spectrum obtained from the $\mathbf{E25-PPh_3^+ Cl^-}$ precursor (Fig. 2.S.4.1b).

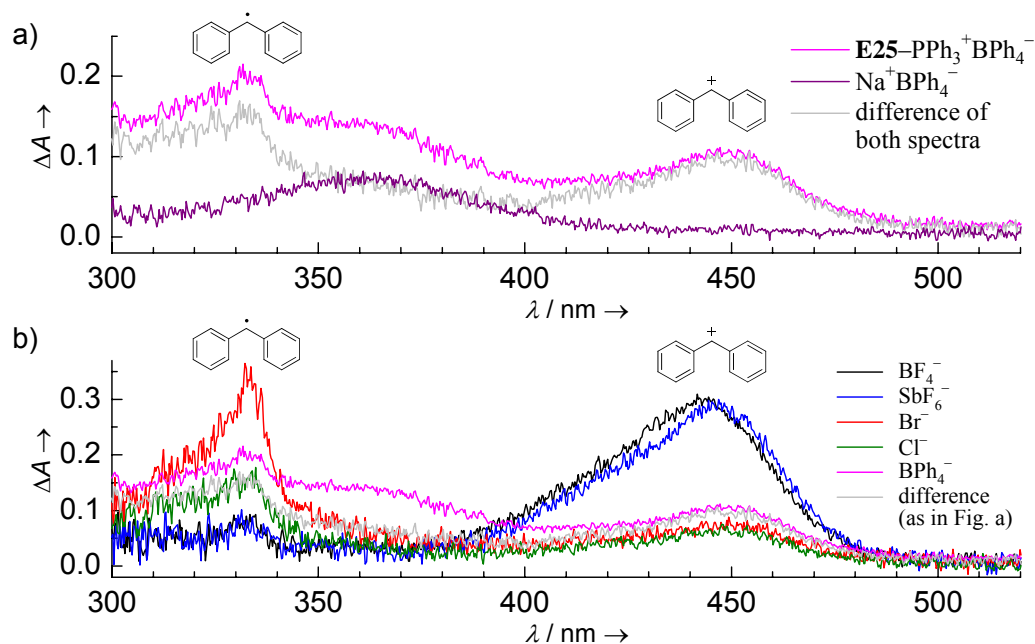


Figure 2.S.4.1. (a) Transient spectra obtained after irradiation of $\mathbf{E25-PPh_3^+ BPh_4^-}$ ($A_{266\text{ nm}} = 0.5, 5.7 \times 10^{-5}$ M) in $\mathbf{CH_2Cl_2}$ (pink) and after irradiation of a solution of $\mathbf{NaBPh_4}$ (5.7×10^{-5} M) and 15-crown-5 (1.7×10^{-3} M) in $\mathbf{CH_2Cl_2}$ (purple) with a 7-ns laser pulse ($\lambda_{\text{exc}} = 266$ nm, gate width: 10 ns). The difference between the two spectra is also shown (grey). (b) Comparison with the transient spectra obtained from $\mathbf{E25-PPh_3^+ X^-}$ ($A_{266\text{ nm}} = 0.5, (1.0-1.2) \times 10^{-4}$ M) with different counterions $\text{X}^- = \text{BF}_4^-$ (black), SbF_6^- (blue), Br^- (red), or Cl^- (green) (see Fig. 2.5b in the main part).

The data presented in Figure 2.S.4.1 are not in conflict with the general photocleavage mechanism outlined in the main part. However, we refrain from discussing the mechanism

because the situation is complicated by the fact that the anion BPh_4^- also absorbs at the excitation wavelength.

Irradiation of a 9.2×10^{-5} M solution of $\text{E25-PPH}_3^+ \text{BPh}_4^-$ gave a pseudo-first-order rate constant of $k_{\text{obs}} = 7.93 \times 10^6 \text{ s}^{-1}$ for the decay of E25^+ (Fig. 2.S.4.2). This value corresponds to a second-order rate constant of $k_2 \approx 9 \times 10^{10} \text{ M}^{-1} \text{ s}^{-1}$, indicating a diffusion-controlled reaction of E25^+ with BPh_4^- .

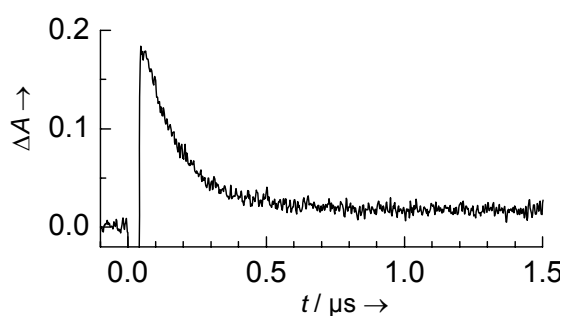


Figure 2.S.4.2. Absorbance decay of E25^+ obtained after irradiation of $\text{E25-PPH}_3^+ \text{BPh}_4^-$ ($A_{266 \text{ nm}} = 0.9$, 9.2×10^{-5} M) in CH_2Cl_2 with a 7-ns laser pulse ($\lambda_{\text{exc}} = 266 \text{ nm}$).

2.S.5 Ion pairing of $\mathbf{E25-PPH_3^+ BF_4^-}$ in CH_2Cl_2

As discussed in the main part, we assume that \mathbf{E}^+ exist as ion pairs with the BF_4^- counter-anions when they are obtained by laser flash photolysis of $\mathbf{E-PAr}_3^+ \text{BF}_4^-$. The nanosecond laser flash photolysis transient spectra of \mathbf{E}^+ published in this work were recorded immediately after the laser pulse (0 ns gate delay, 10 ns gate width). To confirm that the association equilibrium of $\mathbf{E}^+ \text{BF}_4^-$ is already established in our measurements, we measured additional spectra of $\mathbf{E25}^+$ at varying gate delays up to 15 μs after irradiation of $\mathbf{E25-PPH_3^+ BF_4^-}$ in CH_2Cl_2 (Fig. 2.S.5). The constant λ_{max} of $\mathbf{E25}^+$ in these spectra indicate that the degree of ion pairing does not change substantially during the lifetime of $\mathbf{E25}^+$, that is, the association equilibrium is already established in the first spectrum.

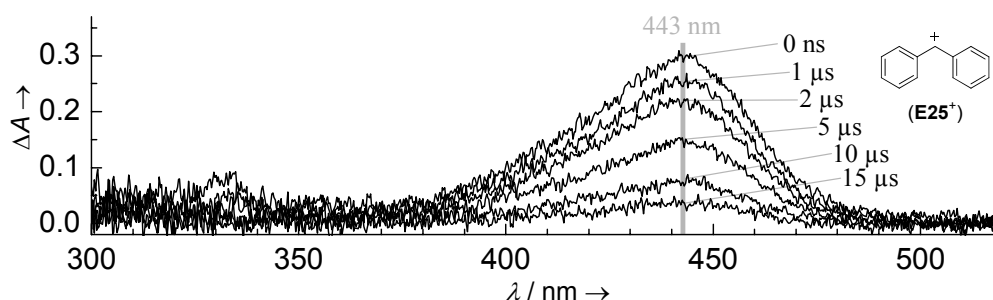


Figure 2.S.5. Transient spectra of $\mathbf{E25}^+$ recorded with varying ICCD gate delays after irradiation of a 1.01×10^{-4} M solution of $\mathbf{E25-PPH_3^+ BF_4^-}$ in CH_2Cl_2 ($A_{266 \text{ nm}} = 0.5$) with a 7-ns laser pulse ($\lambda_{\text{exc}} = 266 \text{ nm}$, gate width: 10 ns).

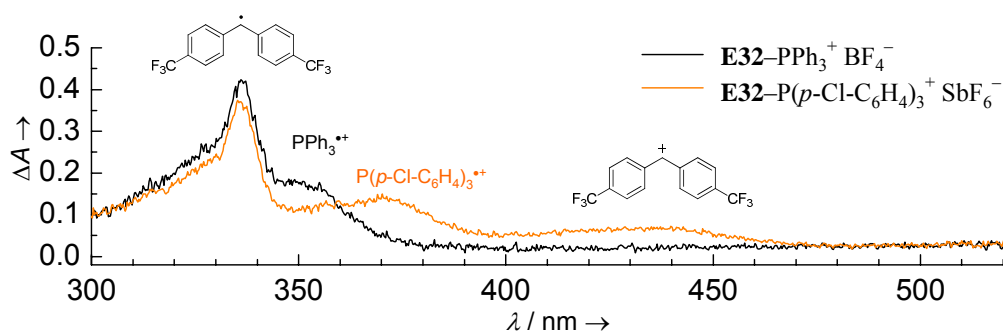
2.S.6 Transient spectra obtained by irradiation of $\mathbf{E32-PAr_3^+ X^-}$ in CH_2Cl_2 

Figure 2.S.6. Transient spectra of $\mathbf{E32^+}$ and $\mathbf{E32^\bullet}$ obtained after irradiation of CH_2Cl_2 solutions of $\mathbf{E32-PPh_3^+ BF_4^-}$ (black, 1.8×10^{-4} M, $A_{266 \text{ nm}} = 0.89$) and $\mathbf{E32-P(p-Cl-C_6H_4)_3^+ SbF_6^-}$ (orange, 5.9×10^{-5} M, $A_{266 \text{ nm}} = 0.90$) by a 7-ns laser pulse ($\lambda_{\text{exc}} = 266$ nm, gate width: 10 ns).

2.S.7 Evaluation of non-exponential decays of \mathbf{E}^+ in CH_2Cl_2

For benzhydryl cations \mathbf{E}^+ with lifetimes $> \sim 10 \mu\text{s}$, we observed non-exponential UV/vis absorption decays of the carbocations which we examined more closely in a few cases (Fig. 2.9 and Fig. 2.S.7).

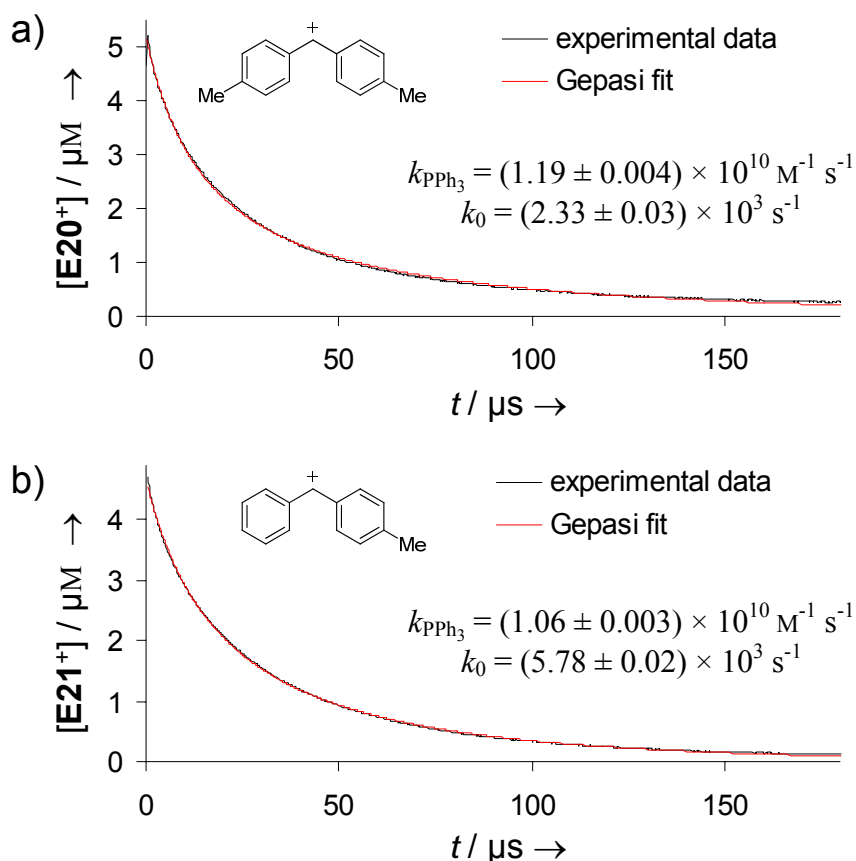
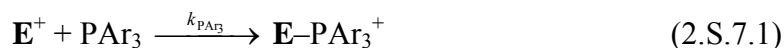


Figure 2.S.7. Decays of $\mathbf{E20}^+$ (a) and $\mathbf{E21}^+$ (b) observed after irradiation of $(4.2\text{--}4.7) \times 10^{-5} \text{ M}$ solutions of $\mathbf{E(29,21)}\text{--PPh}_3^+ \text{BF}_4^-$ in CH_2Cl_2 with a 7-ns laser pulse of $\lambda_{\text{exc}} = 266 \text{ nm}$. Experimental data (black) and fit according to the kinetic model discussed in the text (red).

The non-exponential decay kinetics result from a combination of second- and first-order processes. The second-order component is the combination reaction of the benzhydryl cations \mathbf{E}^+ with the photo-leaving group PAr_3 (eq. 2.S.7.1) which is generated by the laser pulse in the same initial concentration as the benzhydrylium ions.



However, second-order kinetics according to eq. 2.S.7.1 alone do not describe our experimental data satisfactorily. For that reason, we included a general first-order reaction (eq. 2.S.7.2) which summarizes all first-order reactions which may occur and which are discussed in section 2.2.7 of the main part.



The absorbances of \mathbf{E}^+ were converted to concentrations $[\mathbf{E}^+]$ by means of the published $\log \varepsilon$ (CH_3CN).⁴⁰ Using the software Gepasi,⁴³ the concentration data was then fitted according to the kinetic scheme indicated by equations 2.S.7.1 and 2.S.7.2, which yielded diffusion-controlled rate constants for the combination reaction with PAr_3 , $k_{\text{PAr}_3} \approx 1 \times 10^{10} \text{ M}^{-1} \text{ s}^{-1}$, and rate constants k_0 for the first-order background decay reaction. Direct determination of the second-order rate constants for the diffusion-controlled reactions of benzhydrylium ions \mathbf{E}^+ with PPh_3 was not attempted because PPh_3 absorbs at the excitation wavelength of the laser. Johnston, Scaiano and coworkers reported a rate constant of $5 \times 10^9 \text{ M}^{-1} \text{ s}^{-1}$ for the reaction of PPh_3 with the 2-naphthyl(phenyl)methyl cation in CH_3CN .³³

The Gepasi fits for the decays of $\mathbf{E}(\mathbf{20.21})^+$ obtained by irradiation of $\mathbf{E}(\mathbf{20.21})\text{-PPh}_3^+ \text{BF}_4^-$ in CH_2Cl_2 (Fig. 2.S.7) yielded k_0 values which probably reflect the reactions $\mathbf{E}(\mathbf{20.21})^+$ with BF_4^- . The obtained values are in good agreement with the directly measured background decay rate constants k_0 of the more electrophilic carbocations $\mathbf{E}(\mathbf{22-30})^+$ when these were generated from $\mathbf{E}(\mathbf{22-30})\text{-PPh}_3^+ \text{BF}_4^-$ precursors (see section 2.S.8). For the example of $\mathbf{E25}^+$ obtained by irradiation of $\mathbf{E25}\text{-PPh}_3^+ \text{SbF}_6^-$ in CH_2Cl_2 (Fig. 2.9 in the main part), the exact nature of the background decay reaction is not clear; as expected the determined k_0 value is considerably smaller than that for the tetrafluoroborate salt.

2.S.8 Reactions of E^+ with BF_4^- in CH_2Cl_2

Generally, the background decay rate constants k_0 (s^{-1}) measured for E^+ which were obtained by irradiation of $E-PAr_3^+ BF_4^-$ in CH_2Cl_2 correlate roughly with the electrophilicity parameters E of the benzhydryl cations E^+ (Fig. 2.S.8.1). However, the observed k_0 values vary considerably between different experiments which may be a result of varying precursor concentrations and/or varying concentrations of solvent impurities in the experiments. Since a large fraction of the carbocations are paired and the k_0 values partly reflect first-order reactions within the $E^+ BF_4^-$ ion pairs, we do not derive nucleophilicity parameters for BF_4^- in CH_2Cl_2 from these decay rate constants.

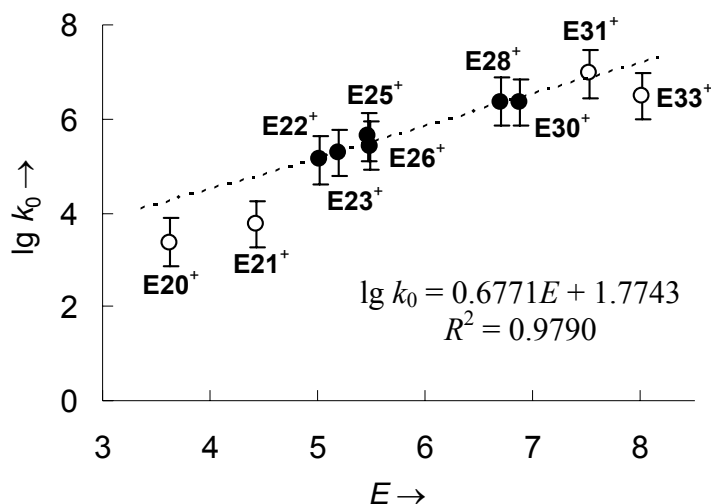


Figure 2.S.8.1. Typical background decay rate constants k_0 (s^{-1}) of E^+ observed after irradiation of $E-PAr_3^+ BF_4^-$ in CH_2Cl_2 with a 7-ns laser pulse ($\lambda_{exc} = 266$ nm) versus the electrophilicity parameters E of the benzhydryl cations E^+ . Arbitrary error bars (one logarithmic unit) symbolize the large uncertainties associated with the individual measurements. Open symbols: Data for $E(21,22)^+$ (obtained by Gepasi fits) and $E(31,33)^+$ (which show a lower dependence on the counter-anions) were not included in the fit.

Fig 2.S.8.2 clearly shows the lower initial absorbances of $E(31,33)^+$ when the benzhydryl cations were obtained by irradiation of $E(31,33)-P(p-Cl-C_6H_4)_3^+ X^-$ with $X^- = BF_4^-$ instead of precursors with $X^- = SbF_6^-$ (also see Fig. 2.7 in the main part). Again, this suggests that BF_4^- very quickly traps a significant fraction of $E(31,33)^+$ in the ion pairs generated by the laser pulse.

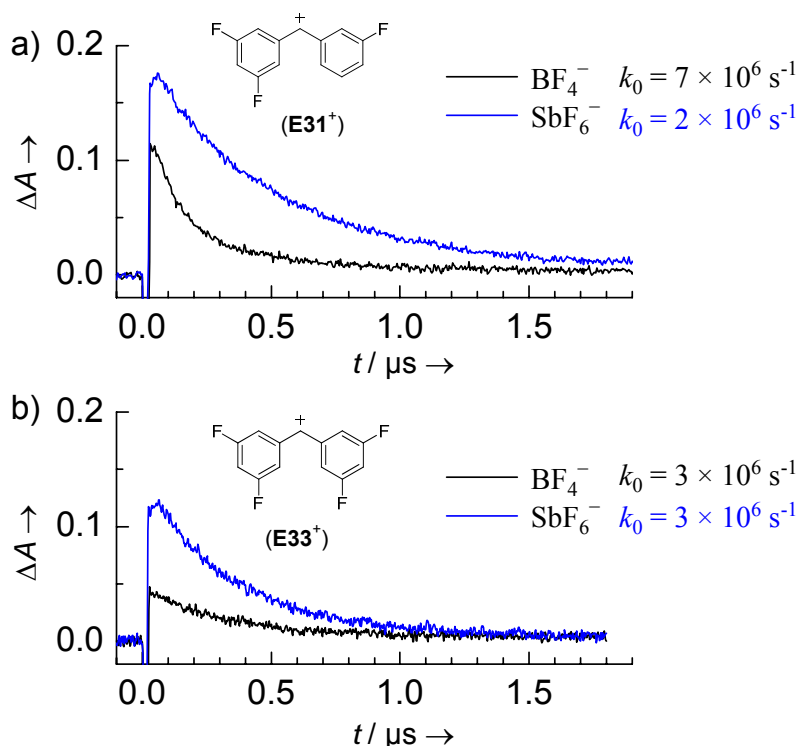
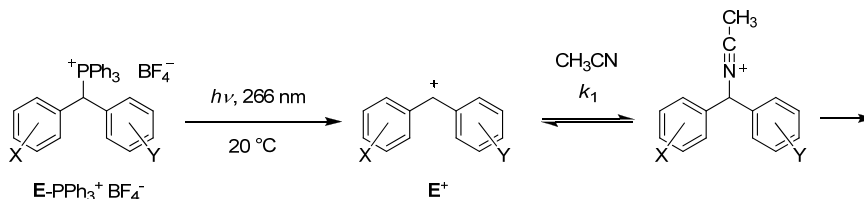


Figure 2.S.8.2. Absorbance decays of $\text{E}(31,33)^+$ obtained after irradiation of (a) $5.7 \times 10^{-5} \text{ M}$ solutions of $\text{E}31\text{-P}(p\text{-Cl-C}_6\text{H}_4)_3 \text{ X}^-$ or (b) $6.5 \times 10^{-5} \text{ M}$ solutions of $\text{E}33\text{-P}(p\text{-Cl-C}_6\text{H}_4)_3 \text{ X}^-$ with different counter-anions $\text{X}^- = \text{BF}_4^-$ (black) and SbF_6^- (blue) in CH_2Cl_2 with a 7-ns laser pulse.

We observed exponential decays of the carbocations $\text{E}(31,33)^+$ with similar rate constants k_0 when they were generated from precursors with $\text{X}^- = \text{BF}_4^-$ or SbF_6^- in CH_2Cl_2 (Fig 2.S.8.2). This suggests that the benzhydryl cations E^+ also undergo some additional decay reaction which is independent of the counterions and becomes more dominant with higher electrophilicity E of the carbocations. This additional decay pathway probably results from the reactions of E^+ with solvent impurities such as residual water in our CH_2Cl_2 , which also explains why we find slightly varying k_0 values in different experiments (different batches of CH_2Cl_2). Even small amounts of water may have a significant effect on carbocation lifetimes: 1 ppm water in CH_2Cl_2 corresponds to a $7.3 \times 10^{-5} \text{ M}$ solution of water in CH_2Cl_2 . From the N_1 and s parameters for pure water (ref.⁹) one can estimate that the rate constants for reactions of water with benzhydrylium ions $\text{E}(22-33)^+$ will only be a few orders of magnitude below the diffusion limit and the observed rate constants will be quite high in spite of the low water content.

2.S.9 Decay kinetics of benzhydryl cations in CH₃CN and TFE

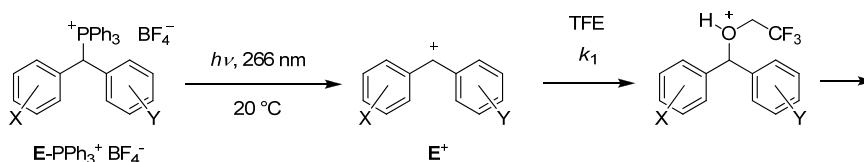
2.S.9.1 First-order decay rate constants of benzhydryl cations in acetonitrile



benzhydryl cation	[E-PPh ₃ ⁺ BF ₄ ⁻] / M	λ / nm	k ₁ / s ⁻¹
E25⁺ Ph ₂ CH ⁺	1.22 × 10 ⁻⁴	435	2.52 × 10 ⁶ ^a
E27⁺ mfp(Ph)CH ⁺	1.09 × 10 ⁻⁴	432	1.00 × 10 ⁷
E30⁺ (mfp) ₂ CH ⁺	1.39 × 10 ⁻⁴	435	3.49 × 10 ⁷ ^b

^a A value of 2.5 × 10⁶ was reported in ref.⁴⁰ ^b This rate constant is slightly above the limit which can be measured accurately with our instrument. To minimize the statistical error, 352 individual runs were averaged to obtain this *k*_{obs} value.

2.S.9.2 First-order decay rate constants of benzhydryl cations in 2,2,2-trifluoroethanol (TFE)

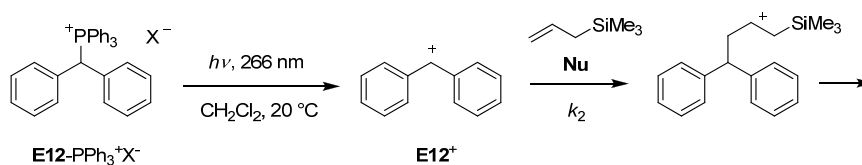


benzhydryl cation	[E-PPh ₃ ⁺ BF ₄ ⁻] / M	λ / nm	k ₁ / s ⁻¹
E22⁺ (pfp) ₂ CH ⁺	6.15 × 10 ⁻⁵	447	5.82 × 10 ⁵
E25⁺ (Ph) ₂ CH ⁺	1.13 × 10 ⁻⁴	440	3.21 × 10 ⁶ ^a
E26⁺ (pcp) ₂ CH ⁺	1.12 × 10 ⁻⁵	481	1.47 × 10 ⁶
E27⁺ mfp(Ph)CH ⁺	1.10 × 10 ⁻⁴	440	1.29 × 10 ⁷
E30⁺ (mfp) ₂ CH ⁺	(1.4 - 1.5) × 10 ⁻⁴	428	4.6 × 10 ⁷ ^b

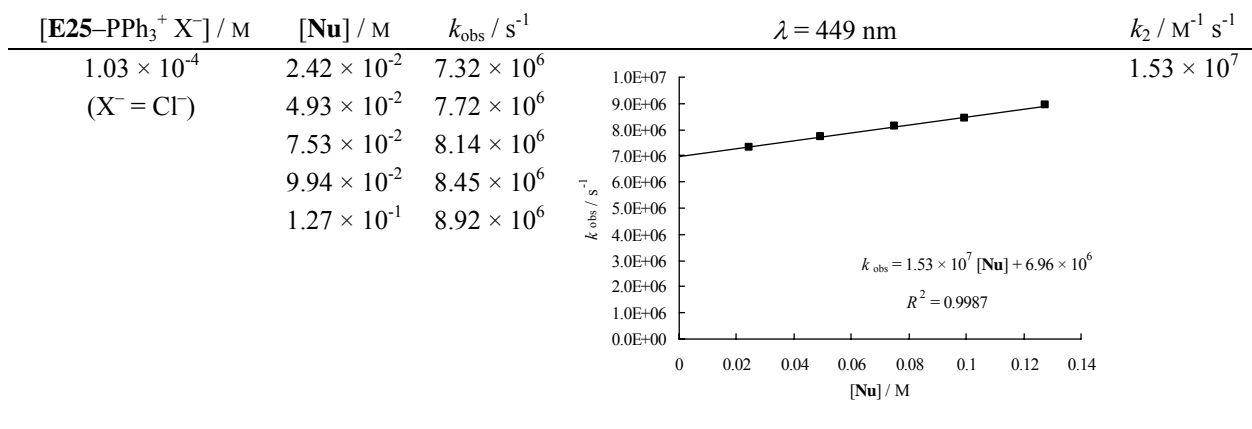
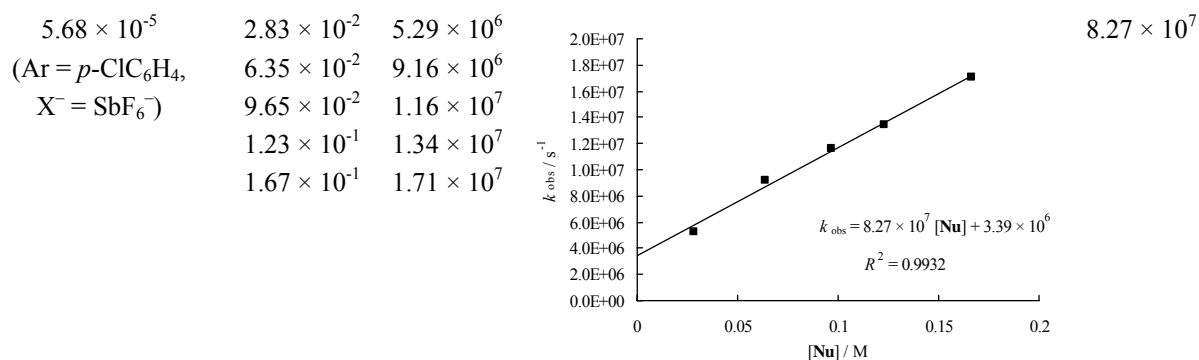
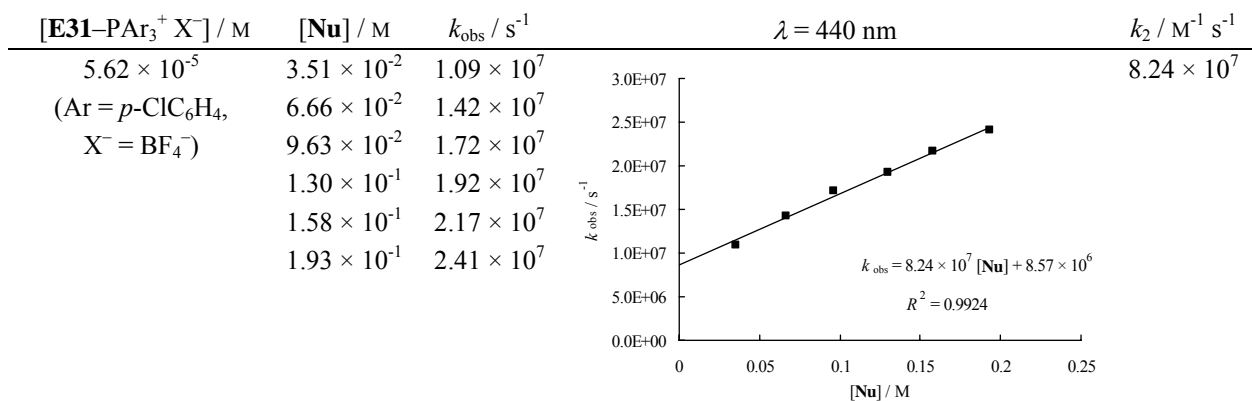
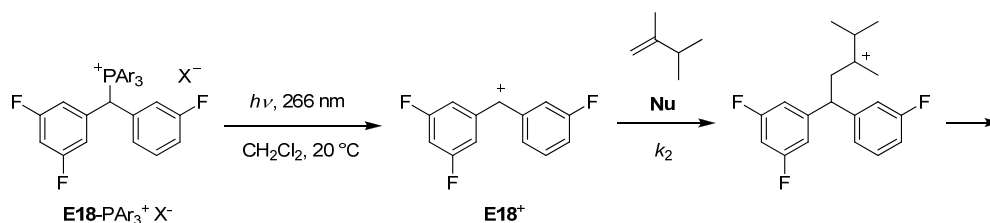
^a A value of 3.2 × 10⁶ was reported in ref.⁸ ^b Such high rate constants cannot be measured accurately with our instrument. To minimize the statistical error, 384 individual runs were averaged to obtain this *k*_{obs} value.

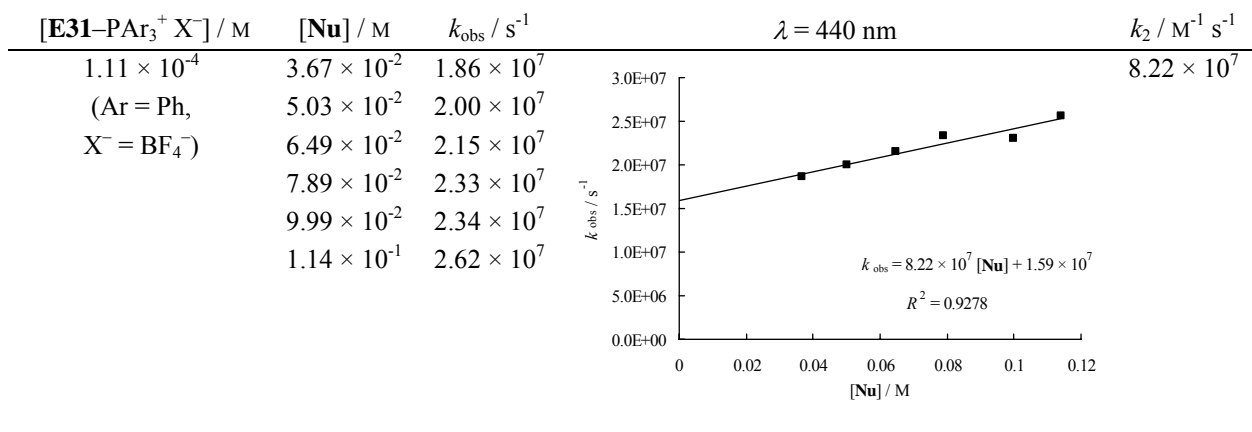
2.S.10 Counterion effects on the kinetics of bimolecular reactions of E⁺ with nucleophiles in CH₂Cl₂

2.S.10.1 Reactions of E25⁺ with allyltrimethylsilane in dichloromethane at 20 °C.



[E25-PPH ₃ ⁺ X ⁻]/M	[Nu]/M	k _{obs} /s ⁻¹	λ = 449 nm	k ₂ /M ⁻¹ s ⁻¹
1.02 × 10 ⁻⁴ (X ⁻ = BF ₄ ⁻)	2.52 × 10 ⁻²	5.78 × 10 ⁵		1.60 × 10 ⁷
	5.39 × 10 ⁻²	1.05 × 10 ⁶		
	7.94 × 10 ⁻²	1.48 × 10 ⁶		
	1.00 × 10 ⁻¹	1.79 × 10 ⁶		
	1.29 × 10 ⁻¹	2.23 × 10 ⁶		
1.02 × 10 ⁻⁴ (X ⁻ = SbF ₆ ⁻)	2.69 × 10 ⁻²	4.89 × 10 ⁵		1.43 × 10 ⁷
	5.29 × 10 ⁻²	8.66 × 10 ⁵		
	8.00 × 10 ⁻²	1.25 × 10 ⁶		
	1.01 × 10 ⁻¹	1.56 × 10 ⁶		
	1.28 × 10 ⁻¹	1.93 × 10 ⁶		
9.95 × 10 ⁻⁵ (X ⁻ = Br ⁻)	2.79 × 10 ⁻²	7.57 × 10 ⁶		1.42 × 10 ⁷
	5.37 × 10 ⁻²	7.99 × 10 ⁶		
	7.59 × 10 ⁻²	8.38 × 10 ⁶		
	9.86 × 10 ⁻²	8.67 × 10 ⁶		
	1.29 × 10 ⁻¹	9.00 × 10 ⁶		

2.S.10.2 Reactions of E31⁺ with 2,3-dimethyl-1-butene in dichloromethane at 20 °C.



Free Energy Relationships for Reactions of Substituted Benzhydrylium Ions: From Enthalpy over Entropy to Diffusion Control

Johannes Ammer, Christoph Nolte, and Herbert Mayr

J. Am. Chem. Soc. **2012**, *134*, 13902-13911

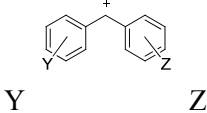
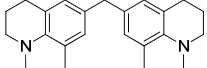
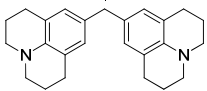
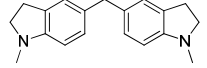
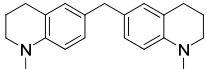
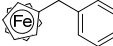
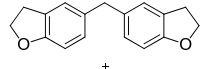
3.1 Introduction

Reactions of benzhydrylium ions (Ar_2CH^+) with a large variety of π -nucleophiles in CH_2Cl_2 have been used to construct the most wide-stretching linear free energy relationships presently known.¹ Using eq 1, it has become possible to predict second-order rate constants k_2 ($\text{M}^{-1} \text{s}^{-1}$) of reactions of electrophiles with nucleophiles by means of one electrophile-specific parameter E and two solvent-dependent nucleophile-specific parameters N and s_N .¹

$$\log k_2(20^\circ\text{C}) = s_N(N + E) \quad (1)$$

Since the beginning of this work,^{1a,b} the scope of electrophiles characterized by eq 1 has been extended considerably. Apart from the benzhydrylium ions **E(1-26)**⁺ which were employed as reference electrophiles in the original work (Table 3.1),^{1b,2} eq 1 has been applied to many other classes of electrophiles,^{1c-f} including allyl cations,^{1c,3} reactions of tritylium ions with sterically nondemanding nucleophiles,⁴ iminium ions,^{1c,5} carboxonium ions,^{1c} dithiocarbene ions,^{1c} and cationic metal- π -complexes.^{1c,6} Equation 1 is also applicable to reactions of neutral carbon electrophiles such as acceptor-substituted arenes,⁷ aldehydes,⁸ imines,⁸ and acceptor-substituted ethylenes such as quinone methides,^{9a,b} benzylidenemalononitriles,^{1f} 2-benzylideneindan-1,3-diones,^{1f} benzylidenebarbituric and -thiobarbituric acids,^{1f} benzylidene Meldrum's acids,^{9c} benzylidenemalonates,^{9d} 1,2-diaza-1,3-dienes,^{9e} *trans*- β -nitrostyrenes,^{9f} and bisulfonyl ethylenes.^{9g} Equation 1 has furthermore been employed to describe reactions of carbon nucleophiles with heteroatom electrophiles like diazonium ions,^{1c} azodicarboxylates,¹⁰ and chlorinating agents.¹¹ Currently, the electrophilicity scale defined by eq 1 encompasses a range of 30 orders of magnitude ($-24 \leq E \leq +6$).¹²

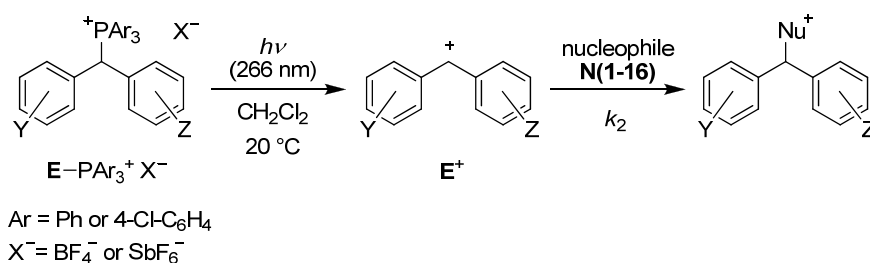
Table 3.1. Electrophiles **E(1-33)**⁺ and Their Electrophilicity Parameters *E*.

no.	abbreviation ^a		<i>E</i>
		Y Z	
E1 ⁺	(lil) ₂ CH ⁺		-10.04 ^b
E2 ⁺	(jul) ₂ CH ⁺		-9.45 ^b
E3 ⁺	(ind) ₂ CH ⁺		-8.76 ^b
E4 ⁺	(thq) ₂ CH ⁺		-8.22 ^b
E5 ⁺	(pyr) ₂ CH ⁺	Y = Z = 4-(<i>N</i> -pyrrolidino)	-7.69 ^b
E6 ⁺	(dma) ₂ CH ⁺	Y = Z = 4-N(Me) ₂	-7.02 ^b
E7 ⁺	(mpa) ₂ CH ⁺	Y = Z = 4-N(Me)(Ph)	-5.89 ^b
E8 ⁺	(mor) ₂ CH ⁺	Y = Z = 4-(<i>N</i> -morpholino)	-5.53 ^b
E9 ⁺	(dpa) ₂ CH ⁺	Y = Z = 4-N(Ph) ₂	-4.72 ^b
E10 ⁺	(mfa) ₂ CH ⁺	Y = Z = 4-N(Me)(CH ₂ CF ₃)	-3.85 ^b
E11 ⁺	(pfa) ₂ CH ⁺	Y = Z = 4-N(Ph)(CH ₂ CF ₃)	-3.14 ^b
E12 ⁺	fc(Ph)CH ⁺		-2.64 ^b
E13 ⁺	(fur) ₂ CH ⁺		-1.36 ^b
E14 ⁺	fur(ani)CH ⁺		-0.81 ^c
E15 ⁺	(ani) ₂ CH ⁺	4-MeO 4-MeO	0.00 ^b
E16 ⁺	ani(pop)CH ⁺	4-MeO 4-PhO	0.61 ^b
E17 ⁺	ani(tol)CH ⁺	4-MeO 4-Me	1.48 ^b
E18 ⁺	ani(Ph)CH ⁺	4-MeO H	2.11 ^b
E19 ⁺	pop(Ph)CH ⁺	4-PhO H	2.90 ^b
E20 ⁺	(tol) ₂ CH ⁺	4-Me 4-Me	3.63 ^b
E21 ⁺	tol(Ph)CH ⁺	4-Me H	4.43 ^c
E22 ⁺	(pfp) ₂ CH ⁺	4-F 4-F	5.01 ^c
E23 ⁺	pfp(Ph)CH ⁺	4-F H	5.20 ^c
E24 ⁺	–	3-F, 4-Me 3-F, 4-Me	5.24 ^c
E25 ⁺	Ph ₂ CH ⁺	H H	5.47 ^c
E26 ⁺	(pcp) ₂ CH ⁺	4-Cl 4-Cl	5.48 ^c
E27 ⁺	mfp(Ph)CH ⁺	3-F H	6.23 ^c
E28 ⁺	tfm(Ph)CH ⁺	4-(CF ₃) H	6.70 ^c
E29 ⁺	dfp(Ph)CH ⁺	3,5-F ₂ H	6.74 ^c
E30 ⁺	(mfp) ₂ CH ⁺	3-F 3-F	6.87 ^c
E31 ⁺	dfp(mfp)CH ⁺	3,5-F ₂ 3-F	7.52 ^c
E32 ⁺	(tfm) ₂ CH ⁺	4-(CF ₃) 4-(CF ₃)	(7.96) ^{c,d}
E33 ⁺	(dfp) ₂ CH ⁺	3,5-F ₂ 3,5-F ₂	(8.02) ^{c,d}

^a Abbreviations as introduced in ref 1b and three new abbreviations: mfp = 3-fluorophenyl, dfp = 3,5-difluorophenyl, tfm = 4-(trifluoromethyl)phenyl. ^b From ref 1b. ^c New or revised; this work. ^d Approximate values.

The most reactive electrophiles characterized so far were alkyl-substituted benzyl cations ($E \approx 5.7-9.6$)¹³ and tertiary alkyl cations ($E \approx 7.5-9.0$),¹⁴ but all electrophilicity parameters of highly reactive carbenium ions with $E > 6$ were only indirectly obtained by competition experiments. Direct measurements of rate constants for reactions of acceptor-substituted benzhydrylium ions ($E > 6$) with nucleophiles turned out to be a veritable challenge due to the low stabilities and high reactivities of these carbocations.¹⁴⁻¹⁷ We have recently reported an efficient method to generate the highly reactive benzhydrylium ions **E(27-33)**⁺ by laser flash photolysis of the triarylphosphonium salts **E-PAr₃⁺ X⁻** in CH₂Cl₂ (Scheme 3.1).¹⁸ This method will be used in this work to determine the second-order rate constants k_2 for the reactions of highly reactive benzhydrylium ions **E⁺** with a variety of nucleophiles **N** in order to provide quantitative information about their electrophilic reactivities. In this way, it has become possible to investigate free energy relationships in reaction series stretching from slow reactions proceeding within hours to the fastest bimolecular reactions, which are controlled by diffusion. The conclusions derived therefrom will be crucial for the development of theoretical models of polar organic reactivity.

Scheme 3.1. Generation of Benzhydrylium Ions **E⁺** by Laser Flash Irradiation of the Phosphonium Salts **E-PAr₃⁺ X⁻**.



3.2 Results and Discussion

3.2.1 Kinetics of the Reactions of Benzhydrylium Ions with π -Nucleophiles in CH₂Cl₂.

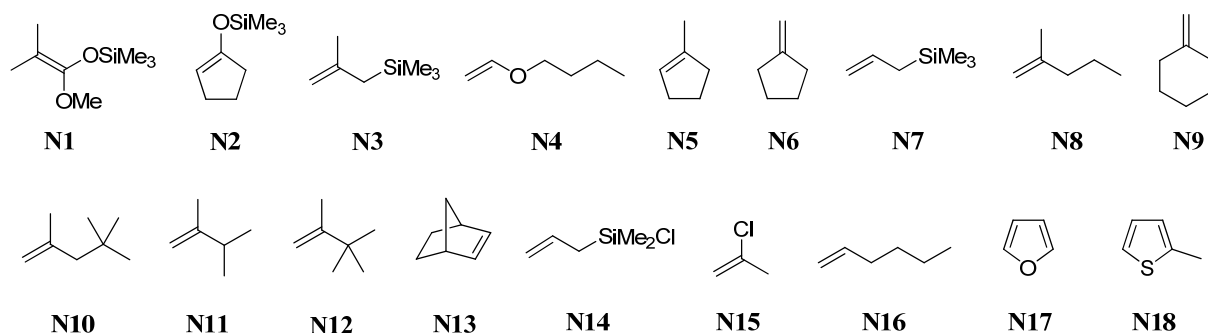
The presently available electrophilicity and nucleophilicity parameters (eq 1) were derived from the second-order rate constants of the reactions of the benzhydrylium ions **E(1-13)**⁺, **E(15-21)**⁺, **E23**⁺, **E25**⁺, and **E26**⁺ ($-10 \leq E \leq +6$, Table 3.1) with a variety of π -nucleophiles in dichloromethane solution.^{1b} For the inclusion of acceptor-substituted benzhydryl cations

into the electrophilicity scale, we now determined the second-order rate constants for the reactions of these carbocations with the same class of π -nucleophiles in CH_2Cl_2 at 20 °C.

Electrophiles. Indirectly determined estimates of electrophilicity parameters for two *m*-chloro-substituted benzhydrylium ions were previously published,¹⁴ but further use of these compounds has been discouraged because they may cause severe skin irritations.^{19a} For that reason, we now recommend the *m*-fluoro-substituted benzhydrylium ions **E(27,30,31,33)**⁺ as reference systems.²⁰ Other *m*-fluoro- (**E24**⁺ and **E29**⁺) and *p*-(trifluoromethyl)-substituted systems (**E28**⁺ and **E32**⁺) were investigated for comparison. We further included **E14**⁺ and **E22**⁺ as new reference electrophiles, and determined additional rate constants for the reactions of **E(21-23)**⁺ and **E(25,26)**⁺ because only limited data were available for each of these benzhydryl cations at the time of the original correlation analysis.^{1b}

Nucleophiles. Chart 3.1 shows the π -nucleophiles **N(1-18)** which were used for the kinetic investigations in this study. Some of them were already employed as reference nucleophiles in our prior work.^{1b} The characterization of electrophiles with $E > 4$ requires nucleophiles in the range of $N < 4$, but there are additional restrictions. Nucleophiles which absorb at the excitation wavelength of the laser (e.g., **N17**, **N18**, or compounds containing phenyl groups) were not used for the laser flash photolysis experiments because they interfere with the photogeneration of the carbocations. Many of the remaining well-characterized nucleophiles in the range of $N < 4$ were not recommended as reference nucleophiles in ref 1b owing to their volatility or their tendency to undergo side reactions. Therefore, we have also studied reactions of **E**⁺ with several other π -nucleophiles which have been characterized only poorly in our previous work. All π -nucleophiles used in this study could be obtained commercially, except **N12** which was prepared by a literature procedure.²¹

Chart 3.1. π -Nucleophiles Used in This Study.



Kinetic Measurements. The benzhydrylium ions $\mathbf{E}(\mathbf{13-30})^+$ ($-2 < E < 7$) were generated in CH_2Cl_2 solution by irradiation of the triphenylphosphonium tetrafluoroborates $\mathbf{E}(\mathbf{13-30})\text{-PPh}_3^+ \text{BF}_4^-$ (Scheme 3.1) with a 7-ns pulse from the fourth harmonic of a Nd/YAG laser ($\lambda_{\text{exc}} = 266 \text{ nm}$, 30-60 mJ/pulse).¹⁸ As previously reported, the highly electrophilic benzhydrylium ions $\mathbf{E}(\mathbf{31-33})^+$ with $E > 7$ could only be generated efficiently when $\text{P}(p\text{-Cl-C}_6\text{H}_4)_3$ instead of PPh_3 was employed as the photoleaving group.¹⁸ Since the highly reactive benzhydrylium ions $\mathbf{E32}^+$ and $\mathbf{E33}^+$ are consumed by reaction with BF_4^- so rapidly that they cannot be observed UV/vis-spectroscopically on the nanosecond time scale, the investigation of these carbocations additionally required the use of SbF_6^- as counteranion instead of BF_4^- .¹⁸

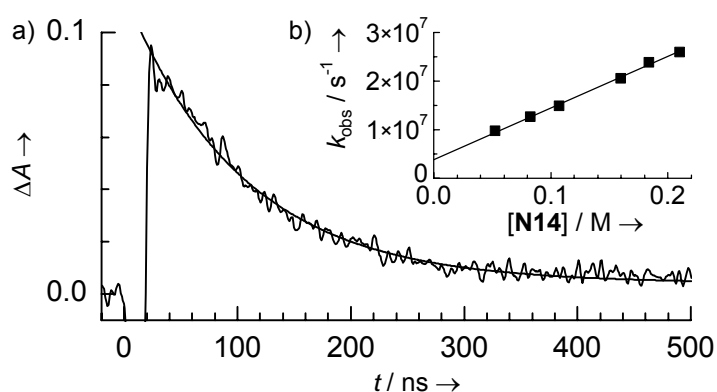


Figure 3.1. (a) Decay of the absorbance of $\mathbf{E33}^+$ at $\lambda = 445 \text{ nm}$ observed after irradiation of a $6.85 \times 10^{-5} \text{ M}$ solution of $\mathbf{E33}\text{-P}(p\text{-Cl-C}_6\text{H}_4)_3^+ \text{SbF}_6^-$ in CH_2Cl_2 in the presence of $5.26 \times 10^{-2} \text{ M}$ $\mathbf{N14}$ and exponential fit of the data ($k_{\text{obs}} = 9.68 \times 10^6 \text{ s}^{-1}$, $R^2 = 0.9873$). (b) Plot of the pseudo-first-order rate constants k_{obs} for the reactions of $\mathbf{E33}^+$ with $\mathbf{N14}$ in CH_2Cl_2 against the concentrations of $\mathbf{N14}$ ($k_{\text{obs}} = 1.06 \times 10^8 [\mathbf{N14}] + 3.88 \times 10^6$, $R^2 = 0.9979$).

When the benzhydrylium ions $\mathbf{E}(\mathbf{13-33})^+$ were generated by irradiation of $\mathbf{E}(\mathbf{13-33})\text{-PAR}_3^+ \text{X}^-$ ($\text{Ar} = \text{Ph}$ or $p\text{-Cl-C}_6\text{H}_4$, $\text{X}^- = \text{BF}_4^-$ or SbF_6^-) in the presence of a large excess of the nucleophiles $\mathbf{N}(\mathbf{1-16})$, we typically observed monoexponential decays of the absorbances of the benzhydrylium ions, as illustrated in Figure 3.1a for the most electrophilic benzhydrylium ion of this series, $\mathbf{E33}^+$, in the presence of $5.26 \times 10^{-2} \text{ M}$ allylchlorodimethylsilane ($\mathbf{N14}$). The pseudo-first-order rate constants k_{obs} (s^{-1}) were obtained by fitting exponential decay functions to the experimental data. Plots of k_{obs} versus the concentrations of the nucleophiles were linear (Figure 3.1b) in all cases, and the slopes of these plots provided the second-order rate constants k_2 ($\text{M}^{-1} \text{ s}^{-1}$) which are listed in Table 3.2. Although the benzhydrylium ions \mathbf{E}^+ generated by photolysis of $\mathbf{E}\text{-PAR}_3^+ \text{X}^-$ may exist as ion pairs $\mathbf{E}^+ \text{X}^-$ in CH_2Cl_2 solution, it

was shown that the rate constants k_2 for the reactions of \mathbf{E}^+ with added π -nucleophiles are independent of the nature of X^- and the degree of ion-pairing.¹⁸ Benzhydryl radicals which are formed as byproducts of the photolysis of the phosphonium salts do not affect the kinetics. The UV/vis absorption bands of the benzhydryl radicals ($\lambda_{\max} \approx 327$ - 344 nm) never overlap with those of the benzhydryl cations ($\lambda_{\max} > 420$ nm).¹⁸ Moreover, the reactions of radicals with π -systems are known to be much slower than the reactions of the structurally analogous carbocations^{19b} and, therefore, do not affect the effective concentrations of the π -nucleophiles.

Table 3.2. Second-Order Rate Constants k_2 ($\text{M}^{-1} \text{s}^{-1}$) for Reactions of Electrophiles \mathbf{E}^+ with π -Nucleophiles and Comparison with Rate Constants k_{calc} ($\text{M}^{-1} \text{s}^{-1}$) Calculated from Equation 1.^a

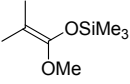
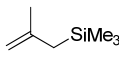
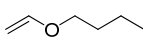
N	nucleophile		\mathbf{E}^+	electrophile abbreviation	E	experiment		correlation analysis	
	formula	N, s_N				$k_2^b / \text{M}^{-1} \text{s}^{-1}$	$k_{\text{calc}}^c / \text{M}^{-1} \text{s}^{-1}$	k_{calc}/k_2	
N1		$N = 9.00^d$ $s_N = 0.98^d$	$\mathbf{E13}^+$	(fur) ₂ CH ⁺	-1.36^d	1.86×10^7	3.07×10^7	1.65	
			$\mathbf{E14}^+$	fur(ani)CH ⁺	-0.81	4.47×10^7	1.06×10^8	2.38	
			$\mathbf{E15}^+$	(ani) ₂ CH ⁺	0.00^d	1.54×10^8	(6.61×10^8)	(4.29)	
			$\mathbf{E17}^+$	ani(tol)CH ⁺	1.48^d	4.15×10^8	(1.86×10^{10})	(44.9)	
			$\mathbf{E20}^+$	(tol) ₂ CH ⁺	3.63^d	1.02×10^9	(2.38×10^{12})	(2.3×10^3)	
			$\mathbf{E25}^+$	(Ph) ₂ CH ⁺	5.47	1.15×10^9	(1.52×10^{14})	(1.3×10^5)	
			$\mathbf{E30}^+$	(mfp) ₂ CH ⁺	6.87	1.52×10^9	(3.57×10^{15})	(2.3×10^6)	
N2		$N = 6.57^d$ $s_N = 0.93^d$	$\mathbf{E16}^+$	ani(pop)CH ⁺	0.61^d	5.34×10^6	4.76×10^6	0.89	
			$\mathbf{E18}^+$	ani(Ph)CH ⁺	2.11^d	6.64×10^7	1.18×10^8	1.78	
			$\mathbf{E20}^+$	(tol) ₂ CH ⁺	3.63^d	3.00×10^8	(3.06×10^9)	(10.2)	
			$\mathbf{E25}^+$	(Ph) ₂ CH ⁺	5.47	9.39×10^8	(1.57×10^{11})	(168)	
			$\mathbf{E30}^+$	(mfp) ₂ CH ⁺	6.87	1.73×10^9	(3.16×10^{12})	(1.8×10^3)	
N3		$N = 4.41^d$ $s_N = 0.96^d$	$\mathbf{E20}^+$	(tol) ₂ CH ⁺	3.63^d	2.81×10^7	5.23×10^7	1.86	
			$\mathbf{E21}^+$	tol(Ph)CH ⁺	4.43	1.23×10^8	(3.06×10^8)	(2.49)	
			$\mathbf{E25}^+$	(Ph) ₂ CH ⁺	5.47	3.97×10^8	(3.05×10^9)	(7.69)	
			$\mathbf{E30}^+$	(mfp) ₂ CH ⁺	6.87	1.14×10^9	(6.74×10^{10})	(59.1)	
			$\mathbf{E31}^+$	dfp(mfp)CH ⁺	7.52	1.21×10^9	(2.48×10^{11})	(243)	
N4		$N = 3.76$ $s_N = 0.91$	$\mathbf{E9}^+$	(dpa) ₂ CH ⁺	-4.72^d	1.06×10^{-1e}	1.34×10^{-1}	1.26	
			$\mathbf{E10}^+$	(mfa) ₂ CH ⁺	-3.85^d	7.49×10^{-1f}	8.28×10^{-1}	1.11	
			$\mathbf{E14}^+$	fur(ani)CH ⁺	-0.81	7.65×10^{2g}	4.84×10^2	0.63	
			$\mathbf{E20}^+$	(tol) ₂ CH ⁺	3.63^d	6.51×10^6	5.31×10^6	0.82	
			$\mathbf{E21}^+$	tol(Ph)CH ⁺	4.43	3.09×10^7	2.84×10^7	0.92	
			$\mathbf{E22}^+$	(pfp) ₂ CH ⁺	5.01	6.37×10^7	9.57×10^7	1.50	
			$\mathbf{E25}^+$	(Ph) ₂ CH ⁺	5.47	1.59×10^8	(2.51×10^8)	(1.58)	
			$\mathbf{E26}^+$	(pcp) ₂ CH ⁺	5.48	1.60×10^8	(2.56×10^8)	(1.60)	
			$\mathbf{E30}^+$	(mfp) ₂ CH ⁺	6.87	6.58×10^8	(4.71×10^9)	(8.82)	
			$\mathbf{E31}^+$	dfp(mfp)CH ⁺	7.52	1.35×10^9	(1.84×10^{10})	(13.6)	

Table 3.2 (continued).

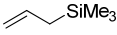
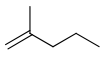
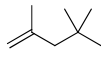
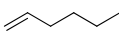
N	nucleophile		electrophile			experiment	correlation analysis	
	formula	N, s_N	E^+	abbreviation	E	$k_2^b / M^{-1} s^{-1}$	$k_{calc}^c / M^{-1} s^{-1}$	k_{calc}/k_2
N5		$N = 1.18$ $s_N = 1.17$	E20⁺	(tol) ₂ CH ⁺	3.63 ^d	5.6×10^5 ^h	4.24×10^5	0.76
			E21⁺	tol(Ph)CH ⁺	4.43	6.13×10^6	3.66×10^6	0.60
			E22⁺	(pfp) ₂ CH ⁺	5.01	1.53×10^7	1.75×10^7	1.14
			E23⁺	pfp(Ph)CH ⁺	5.20	3.49×10^7	2.91×10^7	0.84
			E24⁺	–	5.24	3.17×10^7	3.25×10^7	1.02
			E25⁺	(Ph) ₂ CH ⁺	5.47	5.91×10^7	6.03×10^7	1.02
			E26⁺	(pcp) ₂ CH ⁺	5.48	4.72×10^7	6.20×10^7	1.31
			E27⁺	mfp(Ph)CH ⁺	6.23	1.76×10^8	(4.67×10^8)	(2.66)
			E30⁺	(mfp) ₂ CH ⁺	6.87	5.87×10^8	(2.62×10^9)	(4.47)
			E31⁺	dfp(mfp)CH ⁺	7.52	1.33×10^9	(1.51×10^{10})	(11.4)
N6		$N = 2.82$ $s_N = 0.89$	E27⁺	mfp(Ph)CH ⁺	6.23	1.44×10^8	(1.13×10^8)	(0.79)
N7		$N = 1.68$ $s_N = 1.00$	E14⁺	fur(ani)CH ⁺	-0.81	9.95 ⁱ	7.41	0.75
			E21⁺	tol(Ph)CH ⁺	4.43	2.49×10^6	1.29×10^6	0.52
			E22⁺	(pfp) ₂ CH ⁺	5.01	5.68×10^6	4.90×10^6	0.86
			E23⁺	pfp(Ph)CH ⁺	5.20	1.06×10^7	7.59×10^6	0.72
			E24⁺	–	5.24	9.17×10^6	8.32×10^6	0.91
			E25⁺	(Ph) ₂ CH ⁺	5.47	1.50×10^7 ^j	1.41×10^7	0.94
			E26⁺	(pcp) ₂ CH ⁺	5.48	1.54×10^7	1.45×10^7	0.94
			E27⁺	mfp(Ph)CH ⁺	6.23	6.19×10^7	8.13×10^7	1.31
			E28⁺	tfm(Ph)CH ⁺	6.70	1.52×10^8	(2.40×10^8)	(1.58)
			E30⁺	(mfp) ₂ CH ⁺	6.87	2.13×10^8	(3.55×10^8)	(1.67)
N8		$N = 0.84$ $s_N = 1.06$	E22⁺	(pfp) ₂ CH ⁺	5.01	1.33×10^6	1.59×10^6	1.19
			E23⁺	pfp(Ph)CH ⁺	5.20	4.55×10^6	2.53×10^6	0.56
			E24⁺	–	5.24	2.79×10^6	2.78×10^6	1.00
			E25⁺	(Ph) ₂ CH ⁺	5.47	5.69×10^6	4.88×10^6	0.86
			E26⁺	(pcp) ₂ CH ⁺	5.48	5.00×10^6	5.00×10^6	1.00
			E27⁺	mfp(Ph)CH ⁺	6.23	2.95×10^7	3.12×10^7	1.06
			E28⁺	tfm(Ph)CH ⁺	6.70	9.51×10^7	9.83×10^7	1.03
			E29⁺	dfp(Ph)CH ⁺	6.74	9.16×10^7	1.08×10^8	1.18
			E30⁺	(mfp) ₂ CH ⁺	6.87	1.37×10^8	(1.49×10^8)	(1.09)
			N9		$N = 1.16$ $s_N = 1.04$	E22⁺	(pfp) ₂ CH ⁺	5.01
E25⁺	(Ph) ₂ CH ⁺	5.47				9.86×10^6	7.86×10^6	0.80
E27⁺	mfp(Ph)CH ⁺	6.23				4.68×10^7	4.85×10^7	1.04
E30⁺	(mfp) ₂ CH ⁺	6.87				1.47×10^8	(2.24×10^8)	(1.53)
E31⁺	dfp(mfp)CH ⁺	7.52				3.47×10^8	(1.06×10^9)	(3.07)
N10		$N = 0.79$ $s_N = 1.07$	E22⁺	(pfp) ₂ CH ⁺	5.01	1.50×10^6	1.61×10^6	1.07
			E25⁺	(Ph) ₂ CH ⁺	5.47	6.61×10^6	4.99×10^6	0.76
			E27⁺	mfp(Ph)CH ⁺	6.23	2.91×10^7	3.25×10^7	1.12
			E30⁺	(mfp) ₂ CH ⁺	6.87	1.82×10^8	(1.57×10^8)	(0.86)

Table 3.2 (continued).

N	nucleophile		E^+	electrophile		experiment		correlation analysis	
	formula	N, s_N		abbreviation	E	$k_2^b / M^{-1} s^{-1}$	$k_{\text{calc}}^c / M^{-1} s^{-1}$	k_{calc}/k_2	
N11		$N = 0.65$ $s_N = 1.00$	E25 ⁺	(Ph) ₂ CH ⁺	5.47	1.93×10^6	1.32×10^6	0.68	
			E26 ⁺	(pcp) ₂ CH ⁺	5.48	1.46×10^6	1.35×10^6	0.92	
			E27 ⁺	mfp(Ph)CH ⁺	6.23	1.11×10^7	7.59×10^6	0.68	
			E28 ⁺	tfm(Ph)CH ⁺	6.70	2.11×10^7	2.24×10^7	1.06	
			E29 ⁺	dfp(Ph)CH ⁺	6.74	2.35×10^7	2.45×10^7	1.04	
			E30 ⁺	(mfp) ₂ CH ⁺	6.87	4.11×10^7	3.31×10^7	0.81	
			E31 ⁺	dfp(mfp)CH ⁺	7.52	8.24×10^{7j}	1.48×10^8	1.80	
N12		$N = 0.06$ $s_N = 1.07$	E25 ⁺	(Ph) ₂ CH ⁺	5.47	2.16×10^6	8.26×10^5	0.38	
			E27 ⁺	mfp(Ph)CH ⁺	6.23	6.32×10^6	5.37×10^6	0.85	
			E30 ⁺	(mfp) ₂ CH ⁺	6.87	2.42×10^7	2.60×10^7	1.07	
			E31 ⁺	dfp(mfp)CH ⁺	7.52	7.52×10^7	1.29×10^8	1.72	
N13		$N = -0.25$ $s_N = 1.09$	E25 ⁺	(Ph) ₂ CH ⁺	5.47	6.96×10^5	4.90×10^5	0.70	
			E27 ⁺	mfp(Ph)CH ⁺	6.23	3.57×10^6	3.30×10^6	0.92	
			E28 ⁺	tfm(Ph)CH ⁺	6.70	1.20×10^7	1.07×10^7	0.89	
			E29 ⁺	dfp(Ph)CH ⁺	6.74	1.42×10^7	1.19×10^7	0.84	
			E30 ⁺	(mfp) ₂ CH ⁺	6.87	1.51×10^7	1.64×10^7	1.09	
			E31 ⁺	dfp(mfp)CH ⁺	7.52	5.24×10^7	8.40×10^7	1.60	
			E32 ⁺	(tfm) ₂ CH ⁺	(7.96) ^k	1.15×10^8	(2.53×10^8)	(2.20)	
E33 ⁺	(dfp) ₂ CH ⁺	(8.02) ^k	1.24×10^8	(2.95×10^8)	(2.38)				
N14		$N = -0.57$ $s_N = 1.06$	E31 ⁺	dfp(mfp)CH ⁺	7.52	3.94×10^7	2.33×10^7	0.59	
			E32 ⁺	(tfm) ₂ CH ⁺	(7.96) ^k	6.17×10^7	6.81×10^7	1.10	
			E33 ⁺	(dfp) ₂ CH ⁺	(8.02) ^k	1.06×10^8	(7.89×10^7)	(0.74)	
N15		$N = -3.65$ $s_N = 1.97$	E31 ⁺	dfp(mfp)CH ⁺	7.52	6.68×10^7	4.21×10^7	0.63	
			E32 ⁺	(tfm) ₂ CH ⁺	(7.96) ^k	1.20×10^8	(3.10×10^8)	(8.08)	
N16		$N = -2.77$ $s_N = 1.41$	E22 ⁺	(pfp) ₂ CH ⁺	5.01	1.95×10^{3l}	1.44×10^3	0.74	
			E31 ⁺	dfp(mfp)CH ⁺	7.52	5.77×10^6	4.98×10^6	0.86	
			E32 ⁺	(tfm) ₂ CH ⁺	(7.96) ^k	2.31×10^7	2.08×10^7	0.90	
			E33 ⁺	(dfp) ₂ CH ⁺	(8.02) ^k	2.54×10^7	^m	^m	
N17		$N = 1.33$ $s_N = 1.29$	E14 ⁺	fur(ani)CH ⁺	-0.81	3.41^f	4.69	1.37	
N18		$N = 1.35$ $s_N = 0.99$	E14 ⁺	fur(ani)CH ⁺	-0.81	6.18^f	3.42	0.55	

^a A complete list of rate constants used in the correlation analysis is given in Table 3.S.3.1 in section 3.S.3.

^b Unless noted otherwise: Laser flash photolysis of benzhydryl triarylphosphonium salts, this work; only rate constants with $\log k_2 \leq 8.0$ were used for the correlation analysis. ^c Calculated from eq 1. Calculated values for rate constants $k_2 > 1.0 \times 10^8 M^{-1} s^{-1}$ are shown in parentheses as eq 1 does not account for the limiting effect of diffusion. ^d These values were kept fixed to values obtained from the original correlation analysis.^{1b} ^e From ref 22. ^f Conventional UV/vis spectrophotometry, this work. ^g Stopped-flow UV/vis measurement, this work. ^h Determined from nonexponential decay curves as the reaction of E20⁺ with N5 does not follow pseudo-first-order kinetics due to recombination of E20⁺ with the photoleaving group PPh₃. See section 3.S.2.5 for details. ⁱ From ref 23a. ^j From ref 18. ^k These E parameters are based on only one or two rate constants, as reactions with $k_2 > 10^8 M^{-1} s^{-1}$ were not included in the correlations. ^l From ref 15. ^m $k_{\text{calc}} = k_2$ since this is the only rate constant used for determining the E parameter of E33⁺.

Background Reactions. The positive intercepts of the k_{obs} versus $[\mathbf{N}]$ plots correspond to the rate constants k_0 (s^{-1}) for the background reactions without added nucleophile, which may be reactions with the BF_4^- anions of the phosphonium salts or with impurities that are still present in the rigorously purified CH_2Cl_2 .¹⁸ With increasing electrophilicity of the carbocations \mathbf{E}^+ , these background reactions become faster, which sets a lower limit for the determination of the second-order rate constants k_2 by this method, because the bimolecular reactions of interest must be able to compete with the background reactions. For the most electrophilic benzhydrylium ions in our series, $\mathbf{E32}^+$ and $\mathbf{E33}^+$, k_0 is in the range of $(4-8) \times 10^6 \text{ s}^{-1}$ when the carbocations are generated from $\mathbf{E(32,33)}\text{-P}(p\text{-Cl-C}_6\text{H}_4)_3^+ \text{SbF}_6^-$ in CH_2Cl_2 . As a consequence of these fast background reactions, there is only a very limited group of nucleophiles \mathbf{N} which react fast enough to determine k_2 but slow enough to stay below the diffusion-controlled regime (see below). Moreover, reactions of \mathbf{E}^+ with suitable nucleophiles \mathbf{N} can only compete with the background reaction when the nucleophiles are employed in sufficiently high concentrations, since $k_2[\mathbf{N}]$ must be of comparable magnitude as k_0 .

Another restriction for the determination of rate constants with the laser flash photolysis technique is imposed by the recombination of the photogenerated carbocations \mathbf{E}^+ with the photoleaving group PAR_3 which occurs on time scales $\geq 10 \mu\text{s}$ at typical concentrations of the photofragments in our experiments.¹⁸ As \mathbf{E}^+ and PAR_3 are generated in equimolar amounts (10^{-6} - 10^{-5} M) by the laser pulse, the reaction of \mathbf{E}^+ with PAR_3 is not of first order, and a nonexponential decay of \mathbf{E}^+ is observed in these cases. Thus, even with moderately stabilized carbocations, such as $\mathbf{E(13-21)}^+$, there is a lower limit of $(1-5) \times 10^5 \text{ s}^{-1}$ for the pseudo-first-order rate constants k_{obs} that can be determined by a monoexponential fit of the experimental data, because slower reactions of \mathbf{E}^+ show more complicated decay kinetics due to the concurrent diffusion-controlled second-order reaction of \mathbf{E}^+ with PAR_3 .¹⁸ The second-order rate constant $k_2 = 5.6 \times 10^5 \text{ M}^{-1} \text{ s}^{-1}$ for the reaction of $\mathbf{E20}^+$ with $\mathbf{N5}$, for example, was obtained by fitting the decay of $[\mathbf{E20}^+]$ to a kinetic model consisting of two second-order processes for the reactions of $\mathbf{E20}^+$ with $\mathbf{N5}$ ($\mathbf{E20}^+ + \mathbf{N5}$, second-order rate constant k_2) and with PPh_3 ($\mathbf{E20}^+ + \text{PPh}_3 \rightarrow \mathbf{E20}\text{-PPh}_3^+$, second-order rate constant $k_{\text{phosphine}}$) using the software package Gepasi²⁴ (see section 3.S.2.5 for details). Second-order reactions of benzhydrylium ions ($E \geq 0$) which proceed slower than $\sim 5 \times 10^5 \text{ M}^{-1} \text{ s}^{-1}$ cannot be evaluated reliably, because even in the presence of high nucleophile concentrations the reaction with the photoleaving group PAR_3 is observed almost exclusively.

Diffusion Limit. Besides the experimental limits discussed above and the upper limit accessible by our instrumentation ($k_{\text{obs}} \approx 3 \times 10^7 \text{ s}^{-1}$), there is another more fundamental limitation that needs to be considered for a quantitative description of reactivities: In very fast reactions, the reaction rates are controlled by the rate of the diffusive approach of the reactants and not by the intrinsic reactivities of the reaction partners. Although **N1** reacts almost 40,000 times faster with stabilized benzhydrylium ions than **N3**,^{1b} we measured almost the same rate constants $k_2 \approx (1.1\text{-}1.7) \times 10^9 \text{ M}^{-1} \text{ s}^{-1}$ for the reactions of **N(1-3)** with the highly electrophilic carbocations **E(30,31)**⁺ (Table 3.2), indicating that these reactions are entirely controlled by diffusion. The diffusion rate constants for the reactions of **N1** and **N2** with benzhydrylium ions in CH_2Cl_2 are thus slightly smaller than the rate constants determined for the reactions of the same nucleophiles with **E26**⁺ in CH_3CN ($k_2 \approx 2.4 \times 10^9 \text{ M}^{-1} \text{ s}^{-1}$).²⁵ For the less nucleophilic compounds **N(4-16)**, the diffusion limit (plateau of $\log k_2$ vs E correlations) could not be determined due to the lack of a method to generate sufficiently electrophilic carbocations.

For reactions of **N(1-3)** that proceed with rate constants $k_2 < 1 \times 10^8 \text{ M}^{-1} \text{ s}^{-1}$, there is an excellent agreement between the experimental rate constants from the laser flash measurements (Table 3.2) and the rate constants calculated by eq 1 using the previously published E , N , and s_N parameters which were derived from reactions monitored by conventional and stopped-flow UV/vis spectrophotometry.^{1b} On the other hand, the rate constants for the reactions of **N(1-3)** in the range of $k_2 = (1\text{-}5) \times 10^8 \text{ M}^{-1} \text{ s}^{-1}$ show substantially larger deviations from the values predicted by eq 1, which indicates that the limiting effect of diffusion is already noticeable in reactions with second-order rate constants $k_2 > 1 \times 10^8 \text{ M}^{-1} \text{ s}^{-1}$. Relative reactivities derived from product ratios in CH_2Cl_2 had previously led to the same conclusion.¹⁴

3.2.2 New Electrophilicity Parameters. Data Set for the Correlation Analysis. The directly measured rate constants for the reactions of **E**⁺ with **N(1-3)** in CH_2Cl_2 which are presented in the preceding paragraphs confirm our previous practice to consider only rate constants $k_2 < 1.0 \times 10^8 \text{ M}^{-1} \text{ s}^{-1}$ for the correlation analysis, as the correlation lines are flattening when this rate constant is exceeded.^{1b} As reported before,^{1b,c,26} solvent effects on the rates of the reactions of benzhydrylium ions with neutral π -nucleophiles are small. This can be derived from the good agreement between the rate constants for the reactions in CH_2Cl_2 (Table 3.2) and the rate constants that were previously published for some of these electrophile-

nucleophile combinations in CH₃CN.²⁵ Although the differences between the two solvents are small (factor 1.2-5), the rate constants reported for CH₃CN are generally higher than those measured in CH₂Cl₂. As we can now also determine rate constants for fast reactions in CH₂Cl₂, i. e., in the same solvent which was employed for measuring the rate constants of the slower reactions ($k_2 < 10^6 \text{ M}^{-1} \text{ s}^{-1}$),^{1b} we restricted the correlation analysis in this work to data acquired in CH₂Cl₂ (Table 3.2), and we excluded the data for reactions in acetonitrile which were included in the original correlation analysis.^{1b}

The data determined by laser flash photolysis experiments in this work (Table 3.2) are supplemented by other previously reported^{1b,15,18,22,23a,27} and newly determined (Table 3.2) rate constants for the reactions of benzhydryl cations **E**⁺ with the π -nucleophiles **N(1-16)** in CH₂Cl₂ which were determined by conventional²⁶ or stopped-flow^{1b} UV/vis spectroscopic measurements. Although we have not determined additional rate constants for the reactions of (*E*)-propenylbenzene (**N19**), *m*-xylene (**N20**), and toluene (**N21**), their *N* and *s_N* parameters were also subjected to the correlation analysis because they are linked to the electrophilicities of the benzhydrylium ions **E(21-23,25,26)**⁺ ($E > 4$) which will be revised in this work.²⁸ A complete list of all rate constants used for the correlation analysis can be found in Table 3.S.3.1 in section 3.S.3.

Variables in the Correlation Analysis. One of the reasons why we selected benzhydrylium ions as reference electrophiles for deriving reactivity parameters of nucleophiles according to eq 1 was to avoid the need for a continuous reparametrization whenever we acquired reactivity parameters for previously uncharacterized compounds.^{1b,g} In this work, we have gathered a large number of new rate constants for a series of benzhydrylium ions which have not yet belonged to the reference electrophiles (Table 3.2), and there is no reason for treating these data differently from those for other benzhydrylium ions. In addition, Table 3.2 lists 18 new rate constants k_2 for reactions of **E(21,23,25,26)**⁺ with π -nucleophiles in CH₂Cl₂ at 20 °C which are below $10^8 \text{ M}^{-1} \text{ s}^{-1}$. As the *E* parameters for these benzhydrylium ions had previously been derived from 14 rate constants determined in CH₂Cl₂ and 8 rate constants from laser flash photolysis experiments in CH₃CN,^{1b} we have now revised the electrophilicity parameters of the four reference systems **E(21,23,25,26)**⁺ using only the rate constants for their reactions with π -nucleophiles in CH₂Cl₂ (from Table 3.2 and refs 1b, 27).

In order to avoid insignificant changes of all previously published reactivity parameters for the sake of introducing some new systems and updating a small section ($E > 4$) of our electrophilicity scale ($-24 \leq E \leq 6$), we kept the *E* parameters of **E(1-13)**⁺ and **E(15-20)**⁺ fixed

to the values obtained in the previous correlation (Table 3.1).^{1b} Thus, the only variables in the correlation analysis were the E parameters of $\mathbf{E}(21-33)^+$ ($E > 4$) and of $\mathbf{E14}^+$ (not reported previously), as well as the reactivity parameters N and s_N of $\mathbf{N}(4-21)$ which were derived from the reactions of the corresponding nucleophiles with $\mathbf{E}(21-33)^+$. The N and s_N parameters of the overwhelming number of other nucleophiles are not affected by the new correlation analysis, because they were derived exclusively from the reactivities toward less reactive electrophiles with unchanged E parameters.²⁹

Fixed points of our initial correlation were $E = 0.00$ for $\mathbf{E15}^+$ and $s_N = 1.00$ for $\mathbf{N8}$.^{1b} However, the inclusion of the rate constants listed in Table 3.2 in the correlation more than doubles the number of available rate constants for $\mathbf{N8}$, which now adopts a value of $s_N = 1.06$. In order to avoid extensive changes of published reactivity parameters, the slopes of the correlations are now defined by reactions of allyltrimethylsilane ($\mathbf{N7}$; $s_N = 1.00$).³⁰

Correlation Analysis. In analogy to our previous treatment,^{1b} the E parameters of $\mathbf{E}(21-33)^+$ and $\mathbf{E14}^+$ and the N and s_N parameters of $\mathbf{N}(4-21)$ were calculated by a leastsquares minimization. For that purpose, we minimized Δ^2 specified by eq 2 using the nonlinear solver program “What’sBest! 7.0 Industrial” by Lindo Systems Inc.³¹ with the constraints that were discussed in the previous section.

$$\Delta^2 = \sum (\lg k_2 - \lg k_{\text{calc}})^2 = \sum (\lg k_2 - s_N(N + E))^2 \quad (2)$$

A total of 116 rate constants for the reactions of 14 benzhydrylium ions with 19 π -nucleophiles were employed for this correlation analysis (see Table 3.S.3.1 in section 3.S.3). Tables 3.2 and 3.S.3.1 provide a comparison of the calculated rate constants k_{calc} obtained in this manner with the experimental values k_2 . The quality of the new correlation (standard deviation as defined in ref 1b: $\sigma = 1.36$) is slightly poorer than that of the previous correlation analysis ($\sigma = 1.19$).^{1b} The larger deviations may be due to the incorporation of more reactions with rate constants $k_2 > 10^7 \text{ M}^{-1} \text{ s}^{-1}$ and of more reactions for which the rate constants $k_2(20 \text{ }^\circ\text{C})$ were extrapolated from measurements at lower temperatures. These reactions also showed larger deviations in the previous correlation analysis.^{1b} Still, for 112 out of 116 reactions, the deviations between k_{calc} and k_{exp} are within the range observed in the previous analysis (deviation \leq factor 1.7).^{1b}

Figure 3.2 illustrates the correlations by plotting $\log k_2$ for the reactions of \mathbf{E}^+ with \mathbf{N} against the E parameters of the benzhydrylium ions. The figure also shows the good agreement of experimental (filled symbols) and calculated (lines) rate constants for the reactions of \mathbf{E}^+ with

N(1-3), whose N and s_N parameters were kept fixed in the correlation analysis. As discussed above, deviations from linearity are observed for reactions with $k_2 > 10^8 \text{ M}^{-1} \text{ s}^{-1}$, and these rate constants (open symbols) were excluded from the calculation of the E , N , and s_N parameters. The excellent linear correlations for reactions with $k_2 < 10^8 \text{ M}^{-1} \text{ s}^{-1}$ demonstrate the agreement of the different kinetic methods employed to measure the rate constants. These methods include conventional UV/vis spectrophotometry at 20 °C, extrapolation of $k_2(20 \text{ °C})$ from conventional UV/vis spectrophotometry at lower temperatures, stopped-flow UV/vis spectrophotometry (20 °C), and laser flash photolysis measurements (20 °C) from this work.

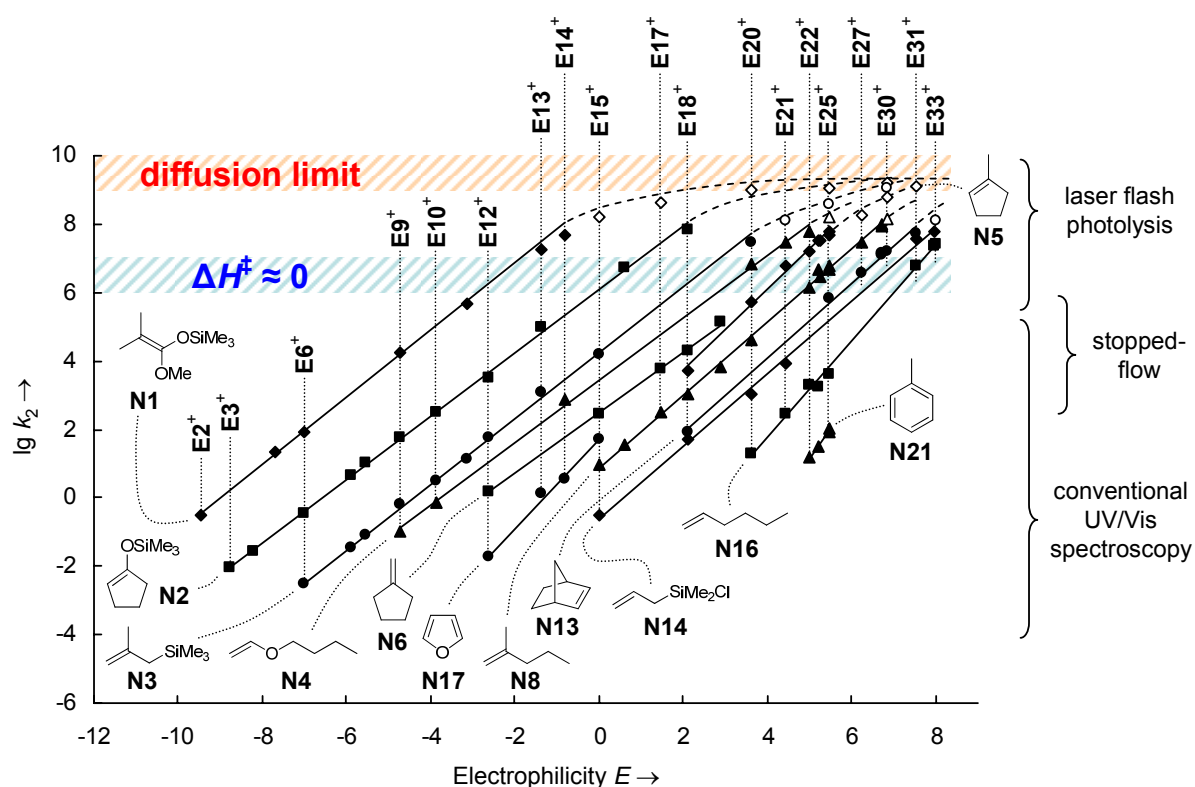


Figure 3.2. Plot of $\log k_2$ versus E for the reactions of benzhydryl cations with π -nucleophiles. Open symbols indicate rate constants $k_2 > 10^8 \text{ M}^{-1} \text{ s}^{-1}$. For the sake of clarity, only selected data are shown; complete plots for all correlations are compiled in sections 3.S.3.4 and 3.S.3.5. The blue-shaded area indicates the region where the activation enthalpy reaches the value $\Delta H^\ddagger = 0$ (see text).

For the sake of clarity, not all correlations are shown in Figure 3.2, and several rate constants $k_2 > 10^8 \text{ M}^{-1} \text{ s}^{-1}$ are omitted. Complete plots of $\log k_2$ versus E for all nucleophiles N are compiled in section 3.S.3.4. Equation 1 requires linear correlations with slopes of unity for plots of $(\log k_2)/s_N$ versus N . Such plots are shown for all electrophiles E^+ in section 3.S.3.5,

and the readers may convince themselves that the optimized slopes are indeed close to unity ($s_E = 1.00 \pm 0.14$).

The electrophilicity parameters E of **E(21-33)**⁺ and **E14**⁺ obtained from the new correlation analysis are summarized in Table 3.1. The values for **E(21-23)**⁺ and **E(25,26)**⁺ are 0.2-0.5 unit smaller than the previously published values.^{1b} Calculations based on the new values will yield rate constants that deviate by less than a factor of 3.5 from those obtained with the old E parameters. The largest change is found for **E26**⁺ ($E = 5.48$), which can be rationalized by the fact that the previously published value of $E = 6.02$ for **E26**⁺ was mostly based on reactions in CH₃CN, which are somewhat faster than in CH₂Cl₂ (see above).

Since only one or two rate constants $k_2 < 10^8 \text{ M}^{-1} \text{ s}^{-1}$ are available for the most electrophilic benzhydrylium ions **E32**⁺ and **E33**⁺, their E parameters have to be considered approximate. Although rate constants $k_2 > 1.0 \times 10^8 \text{ M}^{-1} \text{ s}^{-1}$ were not considered in the correlation analysis, the data in Table 3.2 show that in many cases eq 1 also provides good estimates for reactions with rate constants in the range of $(1.0\text{-}2.0) \times 10^8 \text{ M}^{-1} \text{ s}^{-1}$ or only slightly overestimates the rate constants of such reactions. The good agreement between k_{calc} and k_2 for reactions of **E32**⁺ and **E33**⁺ with rate constants $k_2 < 2.0 \times 10^8 \text{ M}^{-1} \text{ s}^{-1}$ thus substantiates the electrophilicity parameters of $E = 7.96$ for **E32**⁺ and $E = 8.02$ for **E33**⁺ that were derived from the few available rate constants $k_2 < 1.0 \times 10^8 \text{ M}^{-1} \text{ s}^{-1}$.

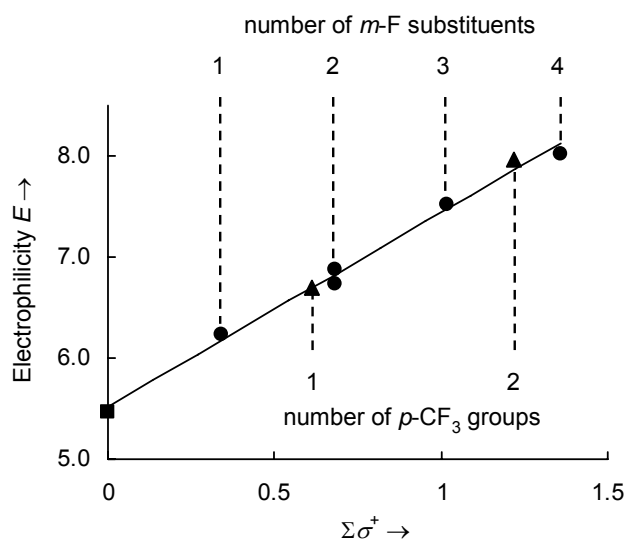


Figure 3.3. Plot of the E parameters for the parent (■), m -F-substituted (●), and p -CF₃-substituted (▲) benzhydrylium ions **E(25)**⁺ and **E(27-33)**⁺ against the sum of the σ^+ parameters of their substituents (linear fit: $E = 1.92\sigma^+ + 5.52$, $R^2 = 0.9927$, $n = 8$).

Figure 3.3 illustrates that the substituent effects of the *m*-F and *p*-CF₃ groups on the electrophilicities of the benzhydrylium ions **E**⁺ are additive: Each *p*-CF₃ substituent increases the *E* value by 1.2 units and each *m*-F substituent by ~0.7 unit. A comparison of the *E* parameters of **E24**⁺ and **E20**⁺ shows a similar increment of $\Delta E = 0.8$ per *m*-F substituent. Additivity of the *m*-F-effects has also been reported for the electrophilicities *E* of tritylium ions^{32a} and the electrofugalities *E*_f of benzhydrylium²⁰ and tritylium ions.^{32b} In contrast, the effects of donor substituents have generally been found to be nonadditive (saturation effect).^{1b,4}

3.2.3 Free Energy Relationships. As shown in Figure 3.2, all rate constants $k_2 < 10^8 \text{ M}^{-1} \text{ s}^{-1}$ correlate linearly with *E*, and curvature is only observed for $k_2 > 10^8 \text{ M}^{-1} \text{ s}^{-1}$ as the diffusion limit is approached. In previous work, we had determined activation parameters for the reactions of benzhydrylium ions with olefins in CH₂Cl₂.^{1b,27} Typically, variation of the electrophiles only affected the activation enthalpy ΔH^\ddagger while the activation entropy ΔS^\ddagger remained constant within experimental error for reactions with rate constants in the range $10^{-2} < k_2 < 5 \times 10^4 \text{ M}^{-1} \text{ s}^{-1}$.³³ Figure 3.4 (open symbols) illustrates this behavior for reactions of benzhydrylium ions with allyltrimethylsilane (**N7**) and 2-methylpent-1-ene (**N8**).

Extrapolation of the correlation lines, as indicated by the dashed lines in Figure 3.4, showed that for the investigated reactions ΔH^\ddagger might become 0 for carbocations of *E* = 5-6, and the question arose whether the rate constants would grow further when more electrophilic carbocations are employed. As it was not possible at that time (1995) to generate more electrophilic carbocations laser-flash-photolytically in CH₂Cl₂ solution (only investigations in CH₃CN were possible), we approached this question indirectly. From competition experiments with π -systems of different reactivity, we concluded that crossing the point $\Delta H^\ddagger = 0$ is not associated with a bend of the linear free energy relationship and that ΔS^\ddagger starts changing as ΔH^\ddagger becomes zero.³³

Using the recently introduced method to generate highly reactive carbocations in CH₂Cl₂ solution from benzhydryl triarylphosphonium salts with complex counterions,¹⁸ we have now been able to study also rates of the reactions of highly reactive carbocations with olefins in CH₂Cl₂, as listed in Table 3.2. Figure 3.4 shows that the correlation $\log k_2$ versus *E* does not experience a break when the extrapolated correlation line ΔH^\ddagger vs *E* arrives at $\Delta H^\ddagger = 0$.

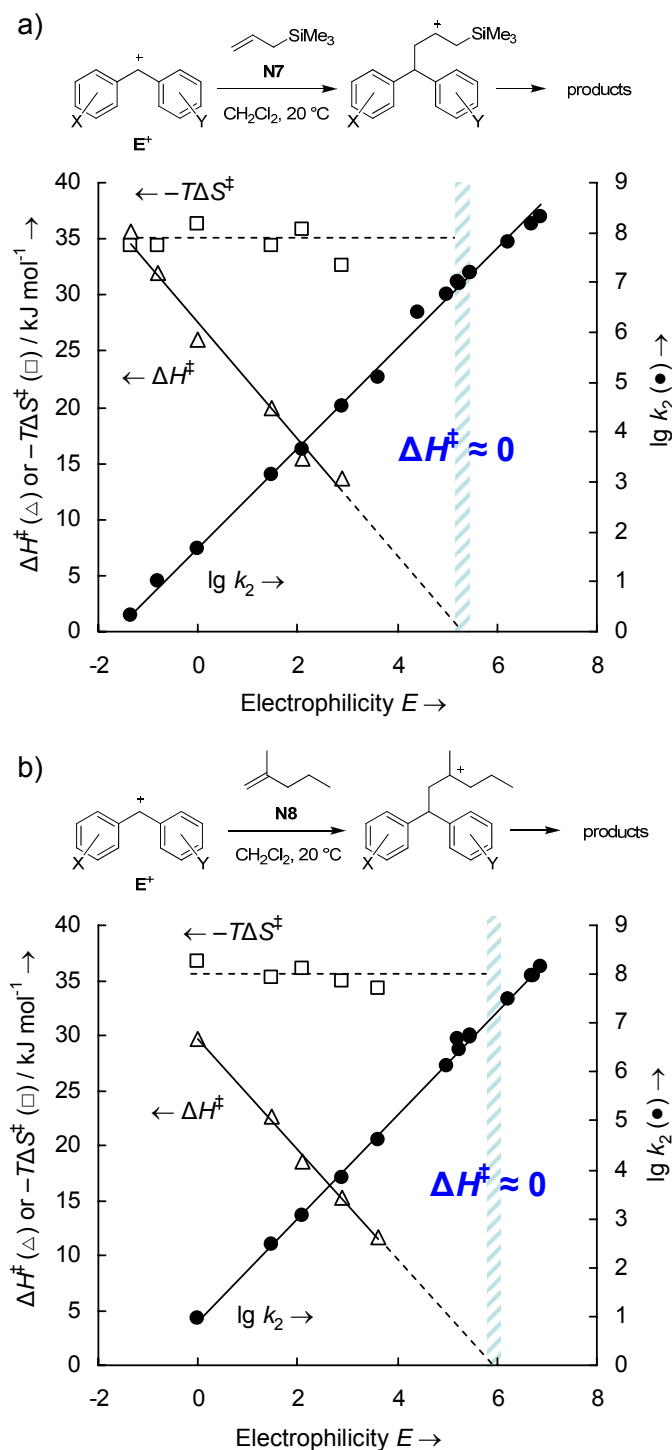


Figure 3.4. Correlations between the activation parameters ΔH^\ddagger (Δ) and $-T\Delta S^\ddagger$ (\square) for the reactions of benzhydrylium ions E^+ with (a) allyltrimethylsilane and (b) 2-methylpent-1-ene and the electrophilicity parameters E of the benzhydrylium ions. The correlations of $\lg k_2$ (\bullet) versus E remain linear well beyond the extrapolation to $\Delta H^\ddagger = 0$.

Table 3.S.4.1 in section 3.S.4 summarizes previously determined activation parameters for the reactions of **N7** and **N8** with benzhydrylium ions in CH_2Cl_2 . For these and other structurally related nucleophiles,^{1b,27} we typically found activation entropies ΔS^\ddagger in between -110 and

$-130 \text{ J mol}^{-1} \text{ K}^{-1}$ which correspond to second-order rate constants of $k_2 = (1-10) \times 10^6 \text{ M}^{-1} \text{ s}^{-1}$ for $\Delta H^\ddagger = 0$. Figure 3.2, where this range of rate constants is marked by a light-blue shading, shows that all correlation lines cross this range without noticeable bending. Bending only occurs for $k_2 > 10^8 \text{ M}^{-1} \text{ s}^{-1}$ when the diffusion limit is approached.

3.2.4 Kinetics of the Reactions of Benzhydrylium Ions with Other Classes of Nucleophiles. In the previous sections we have derived electrophilicity parameters for the acceptor-substituted benzhydrylium ions **E(27-33)**⁺ from the rate constants of their reactions with π -nucleophiles in CH_2Cl_2 . In the subsequent sections we will examine the applicability of these E parameters to other types of reactions such as reactions of benzhydrylium ions with hydride donors^{1b,34} and solvents.^{16,35-37}

Triethylsilane in CH_2Cl_2 . The second-order rate constants k_2 ($\text{M}^{-1} \text{ s}^{-1}$) for the reactions of benzhydrylium ions **E**⁺ with the hydride donor triethylsilane (**N22**) in CH_2Cl_2 at 20 °C, which are listed in Table 3.3, were determined in the same manner as described above for the π -nucleophiles. Figure 3.5a shows an excellent linear correlation of these rate constants with the electrophilicity parameters E of the benzhydrylium ions. From this correlation, we obtained the nucleophilicity parameters $N = 3.58$ and $s_N = 0.70$ for **N22**, in good agreement with the previously reported values ($N = 3.64$, $s_N = 0.65$)^{1b} that were based on only two rate constants.

Table 3.3. Second-Order Rate Constants k_2 for the Reactions of Electrophiles **E**⁺ with Triethylsilane (**N22**, H-SiEt_3 , $N = 3.58$, $s_N = 0.70$) in CH_2Cl_2 at 20 °C and Comparison with Rate Constants k_{calc} Calculated from Equation 1.

E ⁺	electrophile abbreviation	E	experiment		
			$k_2 / \text{M}^{-1} \text{ s}^{-1}$	$k_{\text{calc}}^a / \text{M}^{-1} \text{ s}^{-1}$	k_{calc}/k_2
E13 ⁺	(fur) ₂ CH ⁺	-1.36	3.76×10^1 ^b	3.58×10^1	0.95
E14 ⁺	fur(ani)CH ⁺	-0.81	7.94×10^1 ^c	8.69×10^1	1.09
E15 ⁺	(ani) ₂ CH ⁺	0.00	3.98×10^2 ^b	3.21×10^2	0.81
E17 ⁺	ani(tol)CH ⁺	1.48	4.87×10^3 ^b	3.48×10^3	0.72
E18 ⁺	ani(Ph)CH ⁺	2.11	5.29×10^3 ^d	9.62×10^3	1.82
E27 ⁺	mfp(Ph)CH ⁺	6.23	6.66×10^6 ^e	7.36×10^6	1.11
E30 ⁺	(mfp) ₂ CH ⁺	6.87	2.51×10^7 ^e	2.07×10^7	0.82
E31 ⁺	dfp(mfp)CH ⁺	7.52	6.04×10^7 ^e	5.89×10^7	0.97

^a Calculated from eq 1. ^b Stopped-flow UV/vis measurement, from ref 23b. ^c Conventional UV/vis spectrophotometry, from ref 23a. ^d Conventional UV/vis spectrophotometry, from ref 1b. ^e Laser flash photolysis of triarylphosphonium salts, this work.

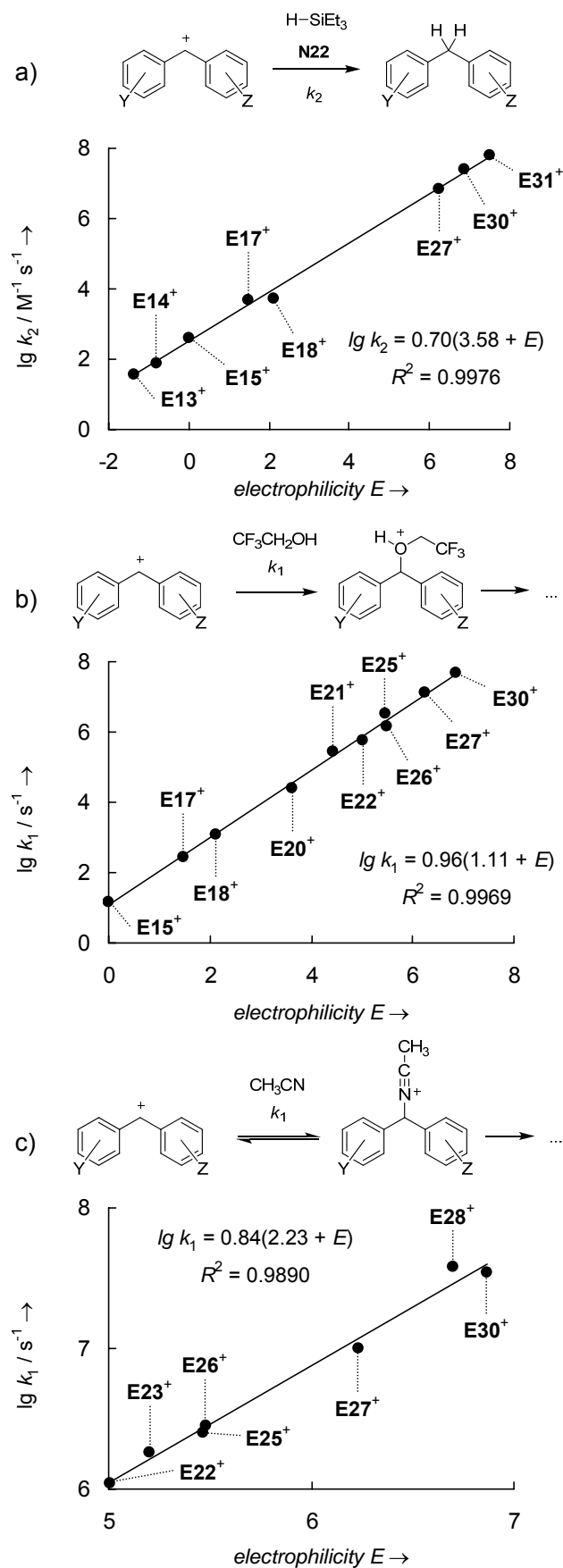


Figure 3.5. Plots of $\log k_2$ or $\log k_1$ for reactions of benzhydrylium ions E^+ with triethylsilane (a), 2,2,2-trifluoroethanol (b), and acetonitrile (c) versus the E parameters of E^+ .

Trifluoroethanol. Equation 1 can also predict first-order rate constants k_1 (s^{-1}) for reactions of carbocations with solvents when the solvent-specific nucleophilicity parameters N_1 and s_N are employed.³⁵ It was shown, for example, that the first-order rate constants k_1 for the decay of benzhydrylium ions \mathbf{E}^+ in 2,2,2-trifluoroethanol correlate with the E parameters of \mathbf{E}^+ .³⁵ Because trifluoroethanol stabilizes anions very well, the recombination reactions of the photofragments proceed with negligible rates when anionic photoleaving groups such as acetate or *p*-cyanophenolate are employed. Using this method, McClelland and Steenken were able to determine rate constants in the range $1 \times 10^1 < k_1 < 4 \times 10^6 \text{ s}^{-1}$ for the first-order decay reactions of the benzhydrylium ions $\mathbf{E}(\mathbf{15}, \mathbf{17}, \mathbf{18}, \mathbf{20}, \mathbf{21}, \mathbf{25})^+$ in trifluoroethanol.³⁷ Figure 3.5b illustrates that the rate constants for the reactions of $\mathbf{E22}^+$, $\mathbf{E26}^+$, $\mathbf{E27}^+$, and $\mathbf{E30}^+$ with trifluoroethanol¹⁸ nicely extend the correlation line and thus confirm the consistency of the E values determined in this work. The reactivity parameters of trifluoroethanol obtained from Figure 3.5b, $N_1 = 1.11$ and $s_N = 0.96$, are close to the previously reported values ($N_1 = 1.23$, $s_N = 0.92$).³⁵

Acetonitrile. The formation of nitrilium ions from carbenium ions and nitriles is a key step in the Ritter reaction.^{38,39} In dry CH_3CN ($\leq 2 \text{ mM H}_2\text{O}$), photolytically generated benzhydrylium ions (\mathbf{E}^+) with $E \geq 5$ were reported to decay via formation of nitrilium ions $\mathbf{E}-\text{N}^+\equiv\text{C}-\text{CH}_3$, which are subsequently hydrolyzed to *N*-(diarylmethyl)acetamides $\mathbf{E}-\text{NHC}(\text{O})\text{CH}_3$.⁴⁰ Photolytically generated benzhydrylium ions with $E < 5$ show nonexponential decay kinetics in CH_3CN due to the recombination of \mathbf{E}^+ with the photoleaving group.^{18,40} Therefore, the reactions of CH_3CN with these benzhydrylium ions cannot be followed with the laser flash photolysis technique.

The previously reported first-order rate constants for the decays of the highly electrophilic benzhydrylium ions $\mathbf{E}(\mathbf{22}-\mathbf{30})^+$ in anhydrous acetonitrile^{18,40} that proceed via formation of the nitrilium ions $\mathbf{E}-\text{N}^+\equiv\text{C}-\text{CH}_3$ can now be correlated with the electrophilicity parameters E of the benzhydrylium ions \mathbf{E}^+ from this work to characterize the solvent nucleophilicity of acetonitrile (Figure 3.5c). The resulting solvent nucleophilicity parameters for acetonitrile, $N_1 = 2.23$ and $s_N = 0.84$, are comparable to those of trifluoroethanol. As $\mathbf{E15}^+ \text{BF}_4^-$ ($E = 0.00$) can be dissolved in CH_3CN to give a persistent solution despite a calculated rate constant of 74.7 s^{-1} ($\tau_{1/2} < 10 \text{ ms}$) for its reaction with CH_3CN , one can conclude that CH_3CN is a weak Lewis base and its reaction with $\mathbf{E15}^+$ is highly reversible.

3.3 Conclusion

Second-order rate constants for the reactions of the benzhydrylium ions **E(13-33)**⁺ with π -nucleophiles in CH₂Cl₂ could be determined using benzhydryl triarylphosphonium salts as precursors for the laser flash photolytic generation of these carbocations.¹⁸ In this way, it became possible to determine electrophilicity parameters E for the highly reactive acceptor-substituted benzhydrylium ions **E(27-33)**⁺, which have previously not been accessible by laser flash photolysis.¹⁶ The consistency of the newly determined E values was demonstrated by showing that the electrophilicity parameters derived from reactions with π -nucleophiles are also applicable to reactions of these carbenium ions with other types of nucleophiles, such as triethylsilane, acetonitrile, or trifluoroethanol. This study thus presents an extension of our electrophilicity scale to the more reactive carbocations **E(27-33)**⁺, which will be employed in subsequent work to characterize the reactivities of further weak nucleophiles.

Most remarkable is that, in all series investigated, the linear correlations of $\log k_2$ versus E do not show any bending over the entire range of rate constants from 10^{-4} to 10^8 M⁻¹ s⁻¹, although this range encompasses reaction series with widely differing transition states, and leveling only occurs for $k_2 > 10^8$ M⁻¹ s⁻¹, when the diffusion limit [$(1.1-1.7) \times 10^9$ M⁻¹ s⁻¹ in CH₂Cl₂] is approached. Figure 3.4 shows that in slow reactions ($10^{-4} < k_2 < 5 \times 10^4$ M⁻¹ s⁻¹) of **N7** or **N8** with the alkoxy- and methyl-substituted benzhydrylium ions **E(13-20)**⁺, variation of the benzhydrylium ions exclusively changes the activation enthalpies ΔH^\ddagger while the activation entropies ΔS^\ddagger remain almost constant. One can extrapolate that ΔH^\ddagger will disappear for reactions with $k_2 > (1-10) \times 10^6$ M⁻¹ s⁻¹. Despite the fact that such fast reactions correspond to processes which proceed only downhill on a potential energy surface, $\log k_2$ continues to increase linearly with E . We are not aware of any other reaction series, where linear free energy relationships extend over such wide ranges, and only bend when the observed reaction constants exceed 10^8 M⁻¹ s⁻¹, i.e., get close to the diffusion rate constants.

The observation that, in all reaction series investigated, variation of a carbocation has exactly the same effect on the rate constants of enthalpy-controlled reactions as on rate constants of reactions where the reactants slide into each other without crossing an enthalpy barrier is of fundamental importance for our understanding of chemical reactivity. Though proportional changes of $\delta\Delta H^\ddagger$ and $\delta\Delta S^\ddagger$ have long been known (compensation effect),⁴¹ it is most surprising that the linearity of linear free energy relationships persists in the range of activation-less reactions, which challenges theoretical treatments.

3.4 Acknowledgment

We thank Prof. Shinjiro Kobayashi for installing the laser-flash working station, Dr. Armin R. Ofial for helpful discussions, and the Deutsche Forschungsgemeinschaft (SFB749) for financial support.

3.5 References and Notes

- (1) (a) Mayr, H.; Patz, M. *Angew. Chem.* **1994**, *106*, 990–1010; *Angew. Chem., Int. Ed. Engl.* **1994**, *33*, 938–957. (b) Mayr, H.; Bug, T.; Gotta, M. F.; Hering, N.; Irrgang, B.; Janker, B.; Kempf, B.; Loos, R.; Ofial, A. R.; Remennikov, G.; Schimmel, H. *J. Am. Chem. Soc.* **2001**, *123*, 9500–9512. (c) Mayr, H.; Kempf, B.; Ofial, A. R. *Acc. Chem. Res.* **2003**, *36*, 66–77. (d) Mayr, H.; Ofial, A. R. In *Carbocation Chemistry*; Olah, G. A., Prakash, G. K. S., Eds.; Wiley: Hoboken (NJ), 2004; pp 331–358. (e) Mayr, H.; Ofial, A. R. *Pure Appl. Chem.* **2005**, *77*, 1807–1821. (f) Mayr, H.; Ofial, A. R. *J. Phys. Org. Chem.* **2008**, *21*, 584–595. (g) Mayr, H. *Angew. Chem.* **2011**, *123*, 3692–3698; *Angew. Chem., Int. Ed.* **2011**, *50*, 3612–3618.
- (2) **E(14,22,24)⁺** were not used in the original work.
- (3) Troshin, K.; Schindele, C.; Mayr, H. *J. Org. Chem.* **2011**, *76*, 9391–9408.
- (4) Review: Horn, M.; Mayr, H. *J. Phys. Org. Chem.* **2012**, *25*, 979–988.
- (5) (a) Lakhdar, S.; Tokuyasu, T.; Mayr, H. *Angew. Chem.* **2008**, *120*, 8851–8854; *Angew. Chem., Int. Ed.* **2008**, *47*, 8723–8726. (b) Lakhdar, S.; Ammer, J.; Mayr, H. *Angew. Chem.* **2011**, *123*, 10127–10130; *Angew. Chem., Int. Ed.* **2011**, *50*, 9953–9956 (CHAPTER 7 of this work).
- (6) (a) Mayr, H.; Müller, K.-H.; Ofial, A. R.; Bühl, M. *J. Am. Chem. Soc.* **1999**, *121*, 2418–2424. (b) Dulich, F.; Müller, K.-H.; Ofial, A. R.; Mayr, H. *Helv. Chim. Acta* **2005**, *88*, 1754–1768. (c) Troshin, K.; Mayer, P.; Mayr, H. *Organometallics* **2012**, *31*, 2416–2424.
- (7) (a) Terrier, F.; Lakhdar, S.; Boubaker, T.; Goumont, R. *J. Org. Chem.* **2005**, *70*, 6242–6253. (b) Lakhdar, S.; Goumont, R.; Berionni, G.; Boubaker, T.; Kurbatov, S.;

- Terrier, F. *Chem. Eur. J.* **2007**, *13*, 8317–8324. (c) Seeliger, F.; Błażej, S.; Bernhardt, S.; Małosza, M.; Mayr, H. *Chem. Eur. J.* **2008**, *14*, 6108–6118. (d) Rodriguez-Dafonte, P.; Terrier, F.; Lakhdar, S.; Kurbatov, S.; Goumont, R. *J. Org. Chem.* **2009**, *74*, 3305–3315.
- (8) Appel, R.; Mayr, H. *J. Am. Chem. Soc.* **2011**, *133*, 8240–8251. (9) (a) Lucius, R.; Loos, R.; Mayr, H. *Angew. Chem.* **2002**, *114*, 97–102; *Angew. Chem., Int. Ed.* **2002**, *41*, 91–95. (b) Richter, D.; Hampel, N.; Singer, T.; Ofial, A. R.; Mayr, H. *Eur. J. Org. Chem.* **2009**, 3203–3211. (c) Kaumanns, O.; Mayr, H. *J. Org. Chem.* **2008**, *73*, 2738–2745. (d) Kaumanns, O.; Lucius, R.; Mayr, H. *Chem. Eur. J.* **2008**, *14*, 9675–9682. (e) Kanzian, T.; Nicolini, S.; De Crescentini, L.; Attanasi, O. A.; Ofial, A. R.; Mayr, H. *Chem. Eur. J.* **2010**, *16*, 12008–12016. (f) Zenz, I.; Mayr, H. *J. Org. Chem.* **2011**, *76*, 9370–9378. (g) Asahara, H.; Mayr, H. *Chem. Asian J.* **2012**, *7*, 1401–1407.
- (10) Kanzian, T.; Mayr, H. *Chem. Eur. J.* **2010**, *16*, 11670–11677.
- (11) Duan, X.-H.; Mayr, H. *Org. Lett.* **2010**, *12*, 2238–2241.
- (12) For a comprehensive database of nucleophilicity and electrophilicity parameters, see: <http://www.cup.lmu.de/oc/mayr/DBintro.html>.
- (13) (a) De, P.; Faust, R.; Schimmel, H.; Ofial, A. R.; Mayr, H. *Macromolecules* **2004**, *37*, 4422–4433. (b) Mayr, H.; Ofial, A. R.; Schimmel, H. *Macromolecules* **2005**, *38*, 33–40. (c) Ammer, J.; Mayr, H. *Macromolecules* **2010**, *43*, 1719–1723 (CHAPTER 6 of this work).
- (14) Roth, M.; Mayr, H. *Angew. Chem.* **1995**, *107*, 2428–2430; *Angew. Chem., Int. Ed. Engl.* **1995**, *34*, 2250–2252.
- (15) Streiter, A. Dissertation, Ludwig-Maximilians-Universität München, 2006.
- (16) McClelland, R. A.; Kanagasabapathy, V. M.; Banait, N. S.; Steenken, S. *J. Am. Chem. Soc.* **1989**, *111*, 3966–3972.
- (17) The generation of benzhydrylium ions by low-temperature electrolysis (“cation pool” method) also fails for highly reactive carbocations such as $\mathbf{E30}^+$: (a) Okajima, M.; Soga, K.; Nokami, T.; Suga, S.; Yoshida, J.-i. *Org. Lett.* **2006**, *8*, 5005–5007. (b) Okajima, M.; Soga, K.; Watanabe, T.; Terao, K.; Nokami, T.; Suga, S.; Yoshida, J.-i. *Bull. Chem. Soc. Jpn.* **2009**, *82*, 594–599.
- (18) Ammer, J.; Sailer, C. F.; Riedle, E.; Mayr, H. *J. Am. Chem. Soc.* **2012**, *134*, 11481–11494 (CHAPTER 2 of this work).

- (19) (a) Streidl, N.; Denegri, B.; Kronja, O.; Mayr, H. *Acc. Chem. Res.* **2010**, *43*, 1537–1549.
(b) Fischer, H.; Radom, L. *Angew. Chem.* **2001**, *113*, 1380–1414; *Angew. Chem., Int. Ed.* **2001**, *40*, 1340–1371.
- (20) Nolte, C.; Mayr, H. *Eur. J. Org. Chem.* **2010**, 1435–1439.
- (21) House, H. O.; Gaa, P. C.; Lee, J. H. C.; VanDerveer, D. *J. Org. Chem.* **1983**, *48*, 1670–1678.
- (22) Schimmel, H. Dissertation, Ludwig-Maximilians-Universität München, 2000.
- (23) (a) Funke, M.-A. Dissertation, Technische Hochschule Darmstadt: Darmstadt, 1997.
(b) Horn, M. Dissertation, Ludwig-Maximilians-Universität: München, 2011.
- (24) (a) Mendes, P. *Comput. Appl. Biosci.* **1993**, *9*, 563–571. (b) Mendes, P. *Trends Biochem. Sci.* **1997**, *22*, 361–363. (c) Mendes, P.; Kell, D. B. *Bioinformatics* **1998**, *14*, 669–883. (d) Further information about Gepasi: www.gepasi.org.
- (25) Bartl, J.; Steenken, S.; Mayr, H. *J. Am. Chem. Soc.* **1991**, *113*, 7710–7716.
- (26) Mayr, H.; Schneider, R.; Schade, C.; Bartl, J.; Bederke, R. *J. Am. Chem. Soc.* **1990**, *112*, 4446–4454.
- (27) (a) Mayr, H.; Schneider, R.; Irrgang, B.; Schade, C. *J. Am. Chem. Soc.* **1990**, *112*, 4454–4459. (b) Roth, M.; Schade, C.; Mayr, H. *J. Org. Chem.* **1994**, *59*, 169–172.
- (28) The revised reactivity parameters for these nucleophiles are: $N = -0.49$, $s_N = 1.18$ for (*E*)-propenylbenzene (**N19**); $N = -3.57$, $s_N = 2.08$ for *m*-xylene (**N20**); and $N = -4.36$, $s_N = 1.77$ for toluene (**N21**). See section 3.S.3 for details.
- (29) The N and s_N parameters of **N17** and **N18**, however, are also revised in this work because the previous values were based on only three rate constants for reactions of each of these nucleophiles with reference electrophiles.
- (30) We are aware of the fact that this is not strictly correct, because slightly different reactivity parameters would result if we subjected all E , N , and s_N parameters to a correlation analysis with fixed values only for **E15**⁺ ($E = 0.00$) and **N7** ($s_N = 1.00$). The inconsistencies introduced by this procedure are negligible, but in this way we can update some reactivity parameters without changing all previously published values.
- (31) *What's Best!*, 7.0; Industrial Lindo Systems Inc.: Chicago, IL, 2004.
- (32) (a) Horn, M.; Mayr, H. *Eur. J. Org. Chem.* **2011**, 6470–6475. (b) Horn, M.; Metz, C.; Mayr, H. *Eur. J. Org. Chem.* **2011**, 6476–6485.
- (33) (a) Patz, M.; Mayr, H.; Bartl, J.; Steenken, S. *Angew. Chem.* **1995**, *107*, 519–521; *Angew. Chem., Int. Ed. Engl.* **1995**, *34*, 490–492. (b) Mayr, H. In *Ionic Polymerizations*

- and Related Processes*; Puskas, J. E., Michel, A., Barghi, S., Paulo, C., Eds.; Kluwer Academic Publishers: Dordrecht, 1999; pp 99–115.
- (34) (a) Watt, C. I. F. *Adv. Phys. Org. Chem.* **1988**, *24*, 57–112. (b) Spange, S.; Eismann, U. *Macromol. Chem. Phys.* **2001**, *202*, 900–905.
- (35) Minegishi, S.; Kobayashi, S.; Mayr, H. *J. Am. Chem. Soc.* **2004**, *126*, 5174–5181.
- (36) Richard, J. P.; Amyes, T. L.; Toteva, M. M. *Acc. Chem. Res.* **2001**, *34*, 981–988.
- (37) McClelland, R. A.; Kanagasabapathy, V. M.; Steenken, S. *J. Am. Chem. Soc.* **1988**, *110*, 6913–6914.
- (38) Reviews: (a) Gridnev, I. D.; Gridneva, N. A. *Russ. Chem. Rev.* **1995**, *64*, 1021–1034. (b) Guérinot, A.; Reymond, S.; Cossy, J. *Eur. J. Org. Chem.* **2012**, 19–28.
- (39) Evidence for nitrilium ions as intermediates: (a) Kevill, D. N.; Kim, C.-B. *J. Org. Chem.* **1974**, *39*, 3085–3089. (b) Stepanov, A. G.; Luzgin, M. V. *Chem. Eur. J.* **1997**, *3*, 47–56. (c) Gerasimova, N. P.; Nozhnin, N. A.; Ermolaeva, V. V.; Ovchinnikova, A. V.; Moskvichev, Y. A.; Alov, E. M.; Danilova, A. S. *Mendeleev Commun.* **2003**, *13*, 82–83.
- (40) Bartl, J.; Steenken, S.; Mayr, H.; McClelland, R. A. *J. Am. Chem. Soc.* **1990**, *112*, 6918–6928.
- (41) Liu, L.; Guo, Q.-X. *Chem. Rev.* **2001**, *101*, 673–696.
- (S1) Friedrich, E. C.; DeLucca, G. *J. Org. Chem.* **1983**, *48*, 1678–1682.
- (S2) (a) Mayr, H.; Pock, R. *Chem. Ber.* **1986**, *119*, 2473–2496. (b) Pock, R.; Mayr, H. *Chem. Ber.* **1986**, *119*, 2497–2509. (c) Mayr, H.; Striepe, W. *J. Org. Chem.* **1983**, *48*, 1159–1165. (d) Mayr, H.; Schneider, R.; Grabis, U. *J. Am. Chem. Soc.* **1990**, *112*, 4460–4467. (e) Burfeindt, J.; Patz, M.; Müller, M.; Mayr, H. *J. Am. Chem. Soc.* **1998**, *120*, 3629–3634. (f) Hagen, G.; Mayr, H. *J. Am. Chem. Soc.* **1991**, *113*, 4954–4961. (g) Mayr, H.; Striepe, W. *J. Org. Chem.* **1985**, *50*, 2995–2998. (h) Pock, R.; Klein, H.; Mayr, H. *Chem. Ber.* **1986**, *119*, 929–942. (i) Gotta, M. F.; Mayr, H. *J. Org. Chem.* **1998**, *63*, 9769–9775. (j) Roth, M. Dissertation, Technische Hochschule Darmstadt, 1996. (k) Hagen, G. Dissertation, Medizinische Universität zu Lübeck, 1990.

3.S Supplementary Data and Experimental Section

3.S.1 Details of the kinetic experiments

3.S.1.1 Materials

Solvents. For the kinetic experiments, p.a. grade CH_2Cl_2 (Merck) was subsequently treated with concentrated sulfuric acid, water, 10% NaHCO_3 solution, and again water. After predrying with anhydrous CaCl_2 , it was freshly distilled over CaH_2 .

Phosphonium salts. The phosphonium salts $\text{E(13-33)-PAR}_3^+ \text{X}^-$ (Ar = Ph or *p*-Cl- C_6H_4 , $\text{X}^- = \text{BF}_4^-$ or SbF_6^-) were prepared by heating E(13-33)-OH with $\text{Ph}_3\text{PH}^+ \text{BF}_4^-$ or by treating E(13-33)-Br with PAR_3 and subsequent anion metathesis. Details of the synthetic procedures are reported in CHAPTER 1 of this work.

3.S.1.2 Laser flash photolysis experiments

Procedure. For the laser-flash-photolytic generation of the benzhydryl cations, solutions of the precursor phosphonium salts with $A_{266 \text{ nm}} \approx 0.2$ to 0.9 (ca. 10^{-5} to 10^{-4} M) were irradiated with a 7-ns laser pulse (fourth harmonic of a Nd:YAG laser, $\lambda_{\text{exc}} = 266 \text{ nm}$, 40-60 mJ/pulse). A xenon lamp was used as probe light for UV/Vis detection. The system is equipped with a fluorescence flow cell and a dosage pump which allows replacing the sample cell volume completely between subsequent laser pulses. The setup is described in detail in ref.¹⁸

Kinetics were measured by following the decay of the absorbance of the benzhydryl cations (see below for wavelengths) in the nucleophilic solvent mixtures or in CH_2Cl_2 solution in presence of varying concentrations of nucleophiles. For each (pseudo-)first-order rate constant, ≥ 64 individual runs were averaged. All measurements were performed in an air-conditioned laboratory at 20 ± 1 °C.

Spectra of the benzhydryl cations were obtained as difference spectra from subsequent determinations without and with laser irradiation using an ICCD camera with a gate width of 10 ns. Four to eight such spectra were averaged for noise reduction.

Transient spectra of the carbocations. The benzhydryl cations **E(13-23)**⁺ and **E(25-33)**⁺ were identified by their previously reported UV/vis spectra.¹⁸ The transient spectrum obtained by irradiating a solution of **E24**–PPh₃⁺ BF₄[−] in CH₂Cl₂ is shown in Fig. 3.S.1.1.

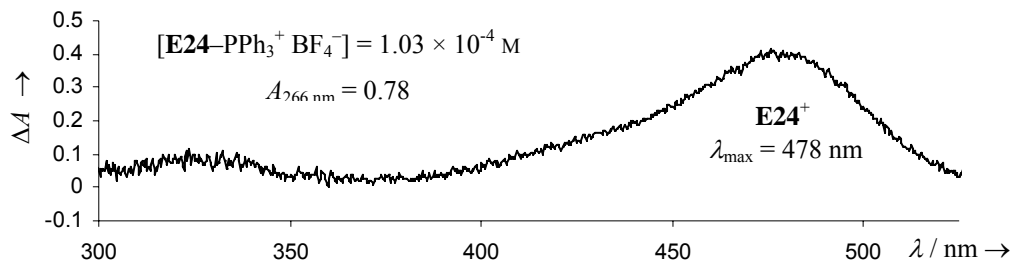


Figure 3.S.1.1. Transient spectrum obtained after irradiation of a CH₂Cl₂ solution of **E24**–PPh₃⁺ BF₄[−] with a 7-ns laser pulse of $\lambda_{\text{exc}} = 266$ nm.

3.S.1.3 Evaluation of the kinetics

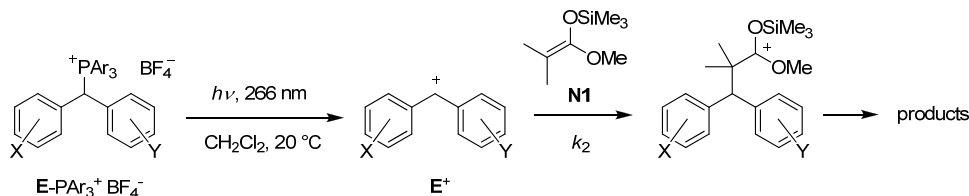
The rate constants k_{obs} (s^{−1}) were obtained by least-squares fitting of the absorbance decays of the benzhydryl cations to the single exponential curve $A_t = A_0 e^{-k_{\text{obs}} t} + C$. Non-exponential kinetics were evaluated using the software Gepasi.²⁴ The second-order rate constants k_2 (M^{−1} s^{−1}) for the combination reactions with nucleophiles were obtained from the slopes of plots of the k_{obs} for each nucleophile concentration versus the nucleophile concentrations.

3.S.1.4 Reaction products

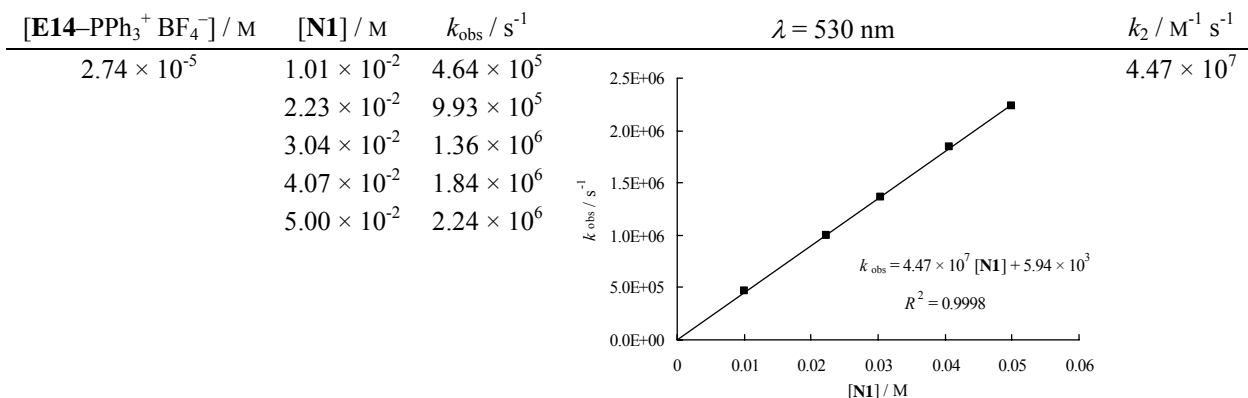
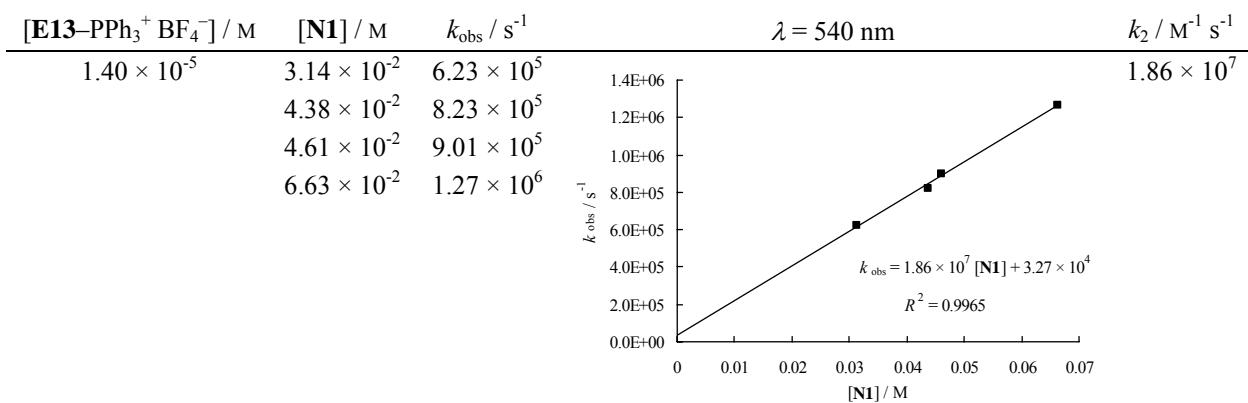
We did not attempt to isolate products from the photo-S_N1 reaction of benzhydryl triarylphosphonium salts with nucleophiles because multiple irradiations of the precursor molecules and reaction products cannot be avoided when the conditions of our kinetic experiments are scaled up for product analysis.

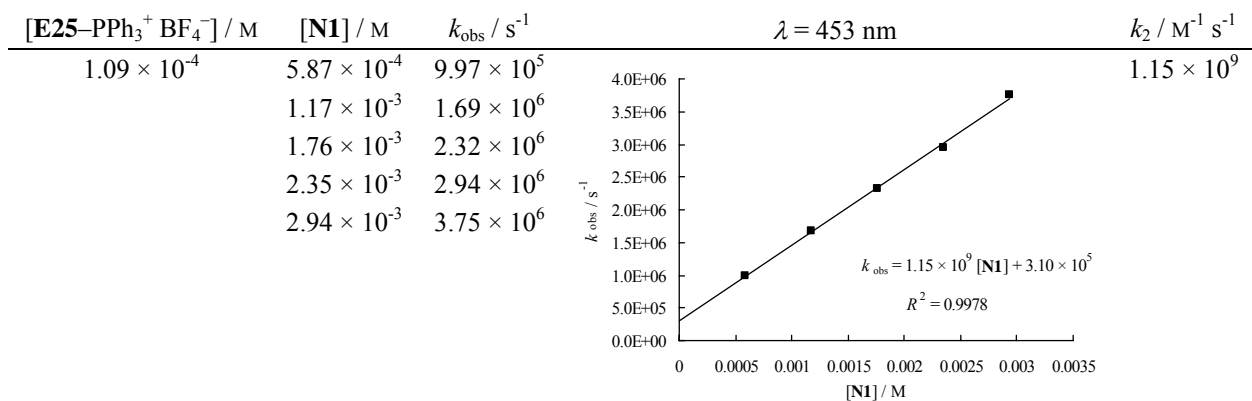
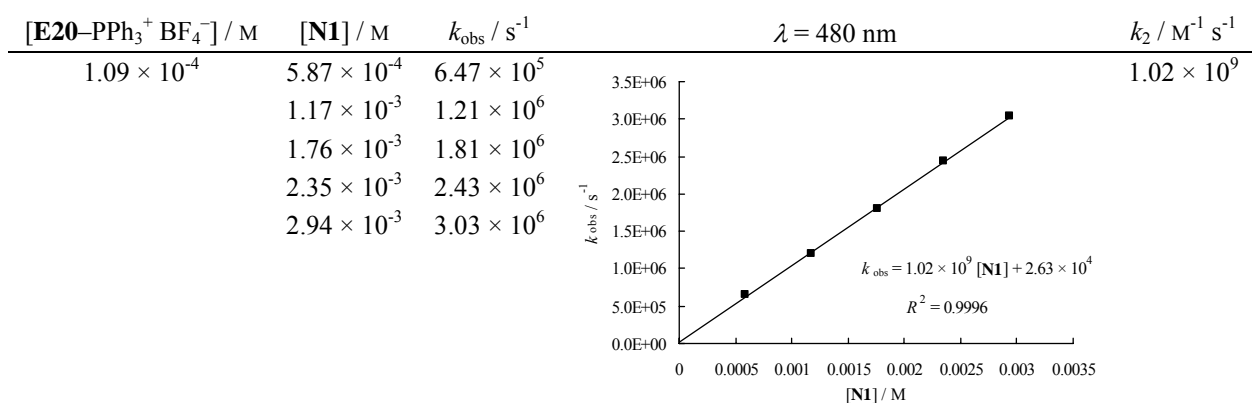
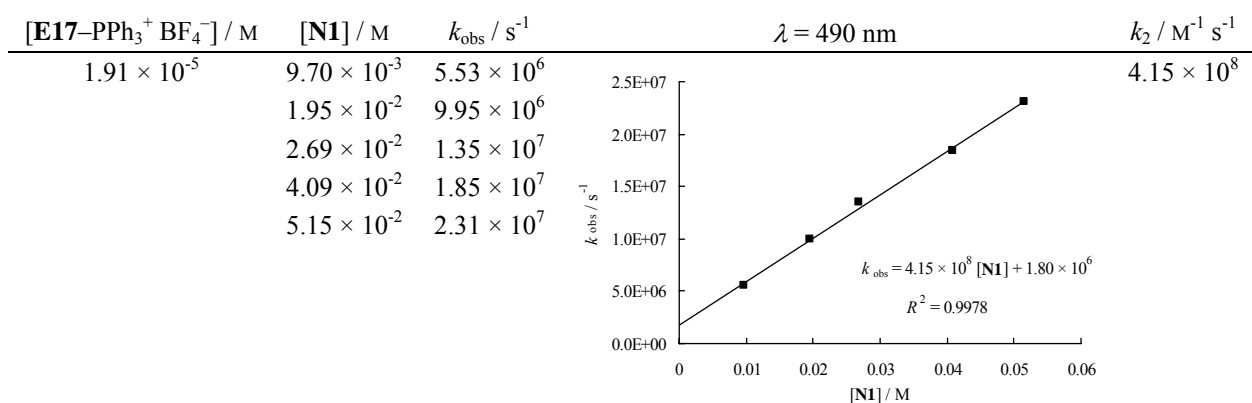
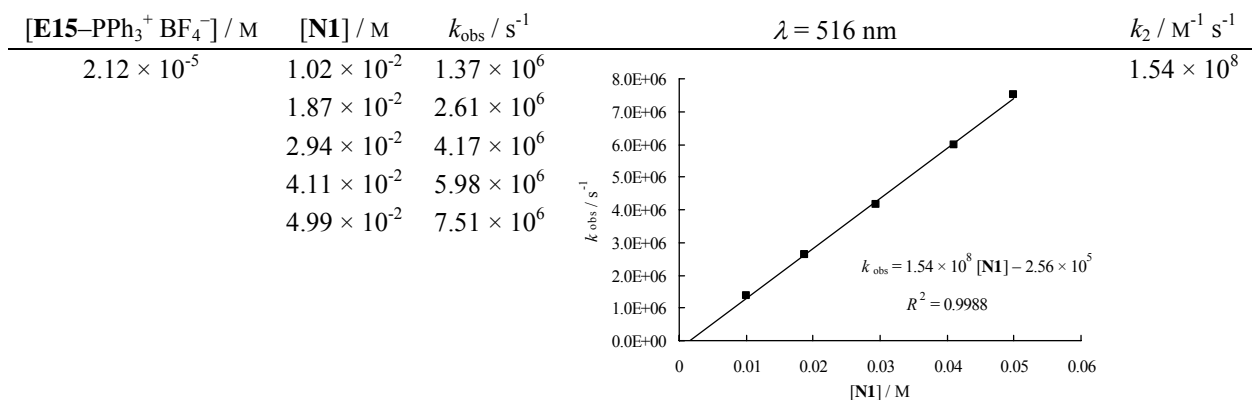
Reactions of benzhydrylium ions **E**⁺ with all of the nucleophiles employed in this work (except *n*-butyl vinyl ether) and many structurally analogous nucleophiles (including ethyl vinyl ether) have been studied extensively in previous work by our group.^{1b,15,22,23a,26,27,S2} In the presence of complex counterions which can act as halide donors, 1:1 products are usually obtained quantitatively. Asymmetric alkenes are attacked in such a way that the most

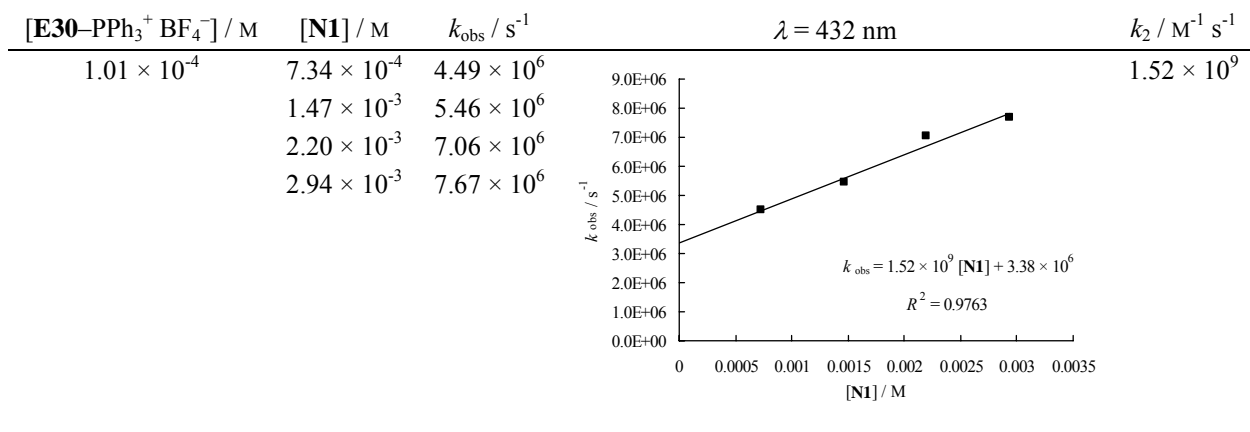
stabilized carbenium ion is formed. Reactions of *m*-chloro-substituted benzhydryl cations with alkenes in the presence of chloride donors also gave the expected chloride-trapped 1:1 adducts¹⁵ and reactions of *m*-chloro-substituted benzhydryl cations with allylsilanes gave the expected 1,1-diarylbutenes.^{S2j}

3.S.2 Kinetics of the reactions of electrophiles with π -nucleophiles in CH_2Cl_2 3.S.2.1 Reactions of benzhydrylium ions (E^+) with 1-methoxy-2-methyl-1-(trimethylsilyloxy)propene (**N1**) in dichloromethane at 20 °C.

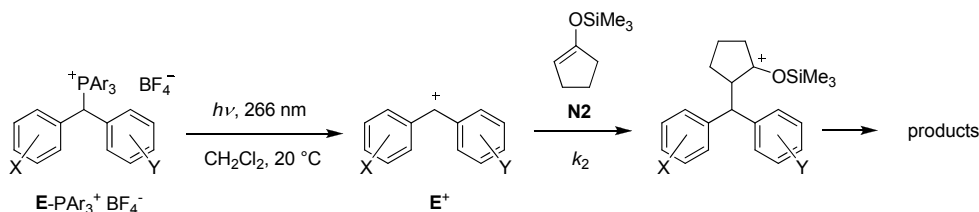
Reactions of $(\text{pfa})_2\text{CH}^+$ (**E11**⁺), $(\text{dpa})_2\text{CH}^+$ (**E9**⁺), $(\text{dma})_2\text{CH}^+$ (**E6**⁺), $(\text{pyr})_2\text{CH}^+$ (**E5**⁺), and $(\text{jul})_2\text{CH}^+$ (**E2**⁺) tetrafluoroborate salts with **N1** have previously been reported to yield methyl 3,3-diaryl-2,2-dimethylpropionates as the final products.^{1b,S2e}



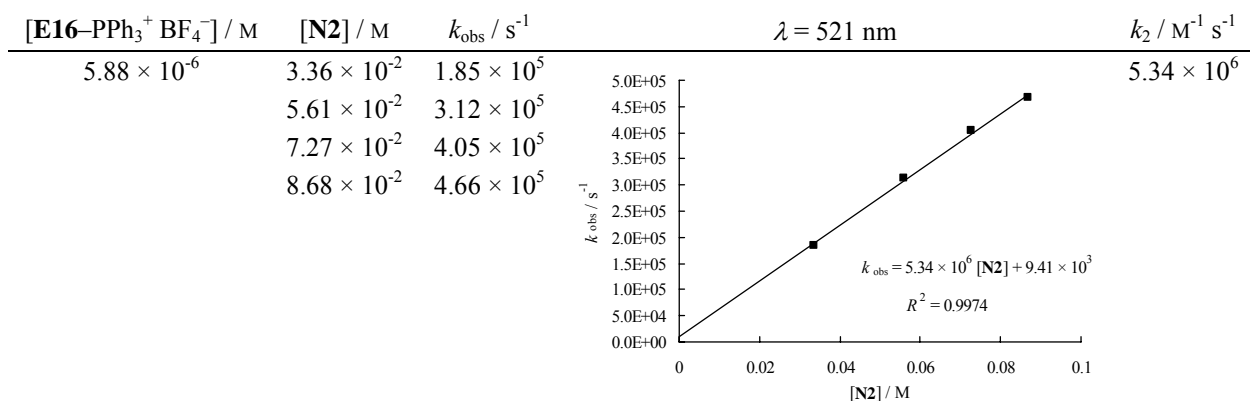


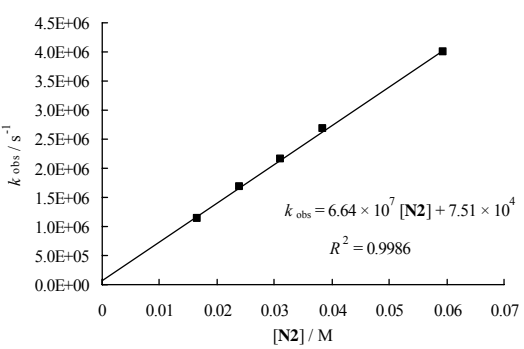
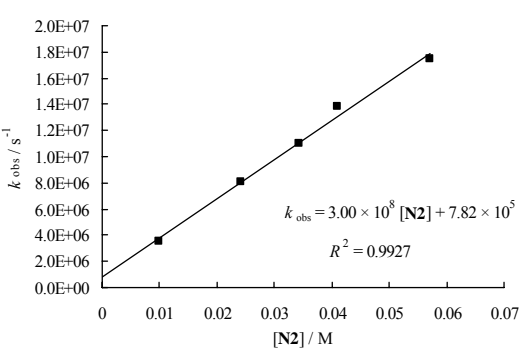
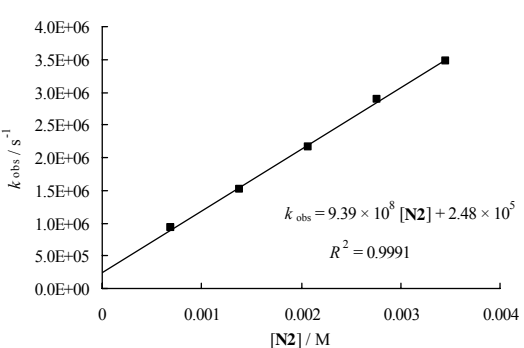
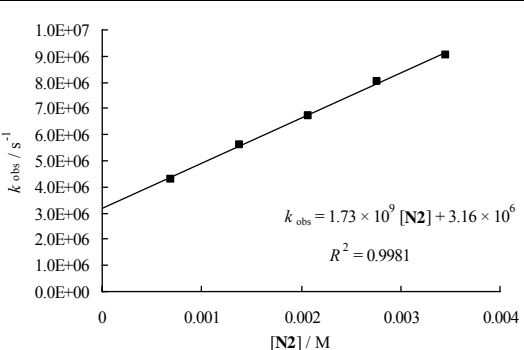


3.S.2.2 Reactions of benzhydrylium ions (\mathbf{E}^+) with 1-(trimethylsiloxy)cyclopentene ($\mathbf{N2}$) in dichloromethane at 20 °C.

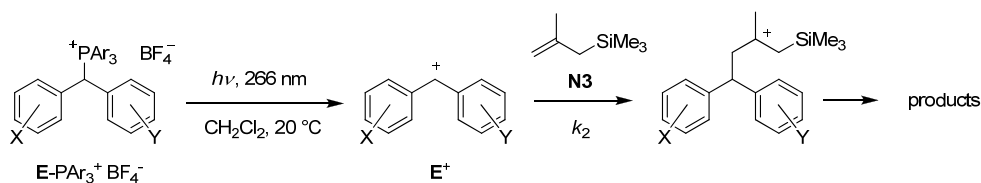


Reactions of $(\text{mfa})_2\text{CH}^+$ ($\mathbf{E10}^+$), $(\text{dpa})_2\text{CH}^+$ ($\mathbf{E9}^+$), $(\text{mor})_2\text{CH}^+$ ($\mathbf{E8}^+$), $(\text{dma})_2\text{CH}^+$ ($\mathbf{E6}^+$), and $(\text{ind})_2\text{CH}^+$ ($\mathbf{E3}^+$) tetrafluoroborate salts with $\mathbf{N2}$ have previously been reported to yield 2-(diarylmethyl)cyclopentanones as the final products.^{1b,S2e}

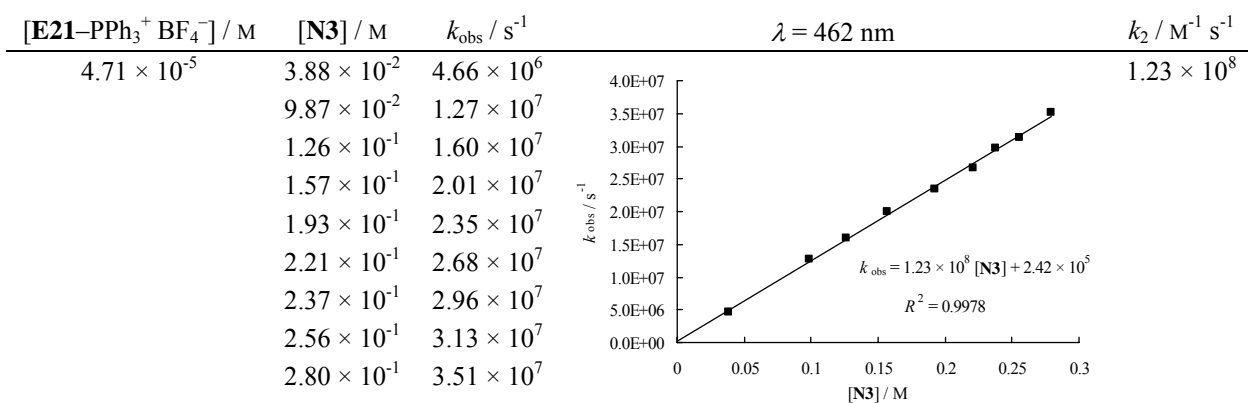
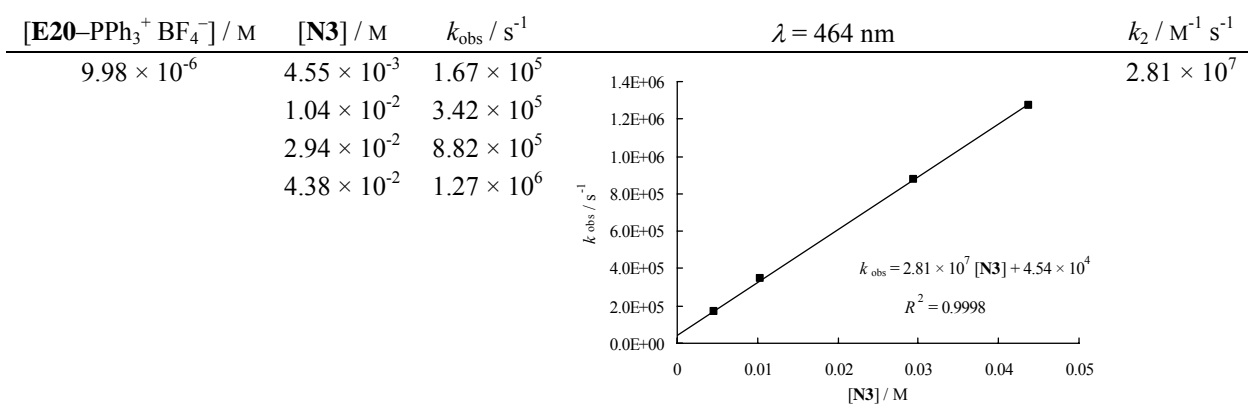


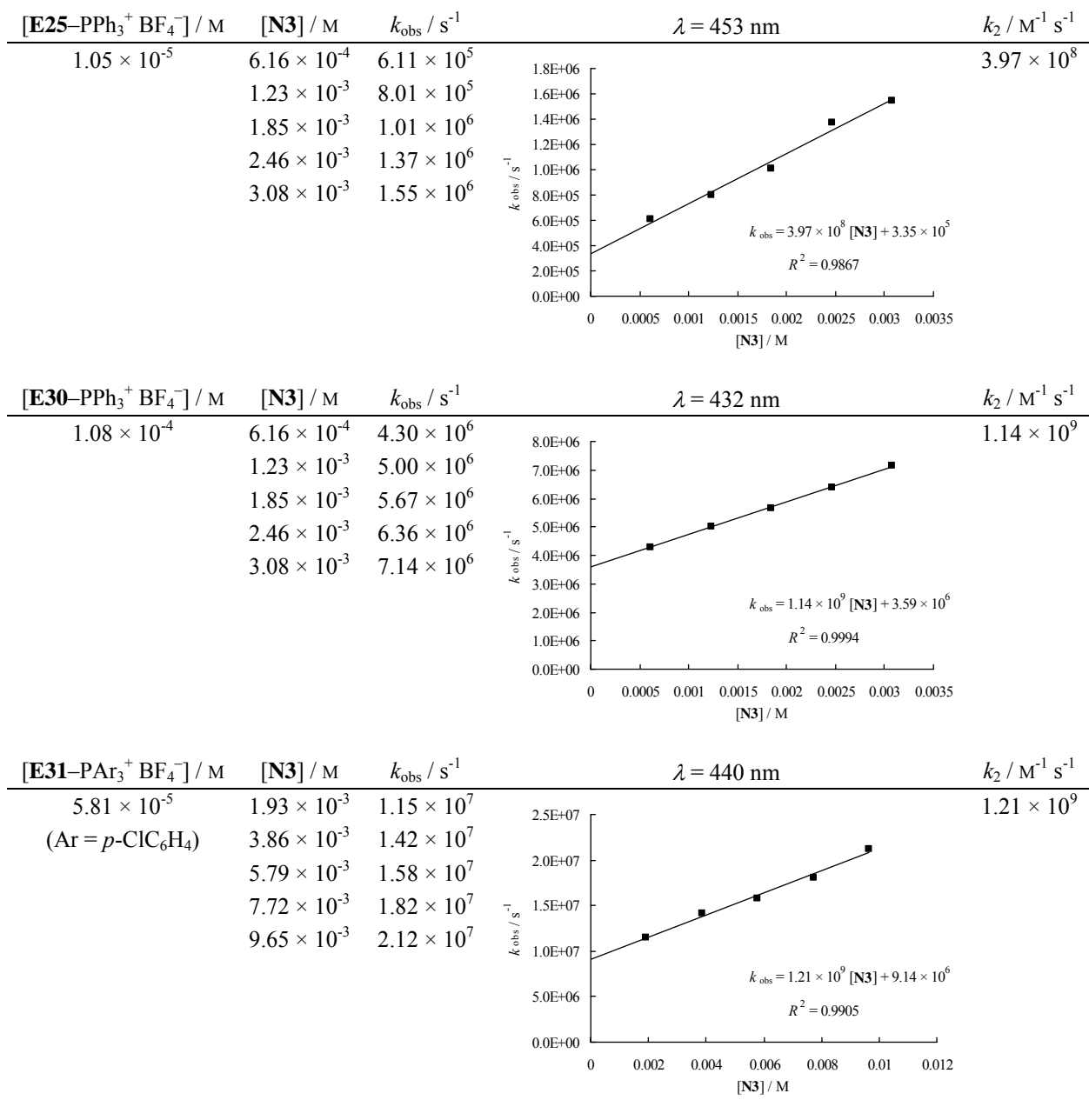
[E18-PPh ₃ ⁺ BF ₄ ⁻]/M	[N ₂]/M	$k_{\text{obs}}/\text{s}^{-1}$	$\lambda = 471 \text{ nm}$	$k_2/\text{M}^{-1}\text{s}^{-1}$
1.90×10^{-5}	1.66×10^{-2}	1.13×10^6		6.64×10^7
	2.39×10^{-2}	1.67×10^6		
	3.10×10^{-2}	2.17×10^6		
	3.85×10^{-2}	2.67×10^6		
	5.95×10^{-2}	3.99×10^6		
[E20-PPh ₃ ⁺ BF ₄ ⁻]/M	[N ₂]/M	$k_{\text{obs}}/\text{s}^{-1}$	$\lambda = 480 \text{ nm}$	$k_2/\text{M}^{-1}\text{s}^{-1}$
5.71×10^{-5}	9.82×10^{-3}	3.52×10^6		3.00×10^8
	2.41×10^{-2}	8.04×10^6		
	3.44×10^{-2}	1.10×10^7		
	4.10×10^{-2}	1.38×10^7		
	5.72×10^{-2}	1.75×10^7		
[E25-PPh ₃ ⁺ BF ₄ ⁻]/M	[N ₂]/M	$k_{\text{obs}}/\text{s}^{-1}$	$\lambda = 453 \text{ nm}$	$k_2/\text{M}^{-1}\text{s}^{-1}$
1.09×10^{-4}	6.91×10^{-4}	9.19×10^5		9.39×10^8
	1.38×10^{-3}	1.53×10^6		
	2.07×10^{-3}	2.19×10^6		
	2.76×10^{-3}	2.88×10^6		
	3.45×10^{-3}	3.48×10^6		
[E30-PPh ₃ ⁺ BF ₄ ⁻]/M	[N ₂]/M	$k_{\text{obs}}/\text{s}^{-1}$	$\lambda = 432 \text{ nm}$	$k_2/\text{M}^{-1}\text{s}^{-1}$
1.11×10^{-4}	6.91×10^{-4}	4.30×10^6		1.73×10^9
	1.38×10^{-3}	5.60×10^6		
	2.07×10^{-3}	6.72×10^6		
	2.76×10^{-3}	8.05×10^6		
	3.45×10^{-3}	9.04×10^6		

3.S.2.3 Reactions of benzhydrylium ions (E^+) with (2-methylallyl)trimethylsilane (**N3**) in dichloromethane at 20 °C.



Reactions of (pfa)₂CH⁺ (**E11**⁺), (mfa)₂CH⁺ (**E10**⁺), (dpa)₂CH⁺ (**E9**⁺), (mor)₂CH⁺ (**E8**⁺), (mpa)₂CH⁺ (**E7**⁺), (dma)₂CH⁺ (**E6**⁺), (pyr)₂CH⁺ (**E5**⁺), (ani)₂CH⁺ (**E15**⁺), ani(Ph)CH⁺ (**E18**⁺), (tol)₂CH⁺ (**E20**⁺), (Ph)₂CH⁺ (**E25**⁺), (pcp)₂CH⁺ (**E26**⁺), the 3-chlorobenzhydrylium ion, and the 3,3'-dichlorobenzhydrylium ion with **N3** have previously been reported to yield 4,4-diaryl-2-methyl-1-butenes as the final products.^{1b,S2f,S2j}





3.S.2.4 Reactions of benzhydrylium ions (E^+) with *n*-butyl vinyl ether (**N4**) in dichloromethane at 20 °C.

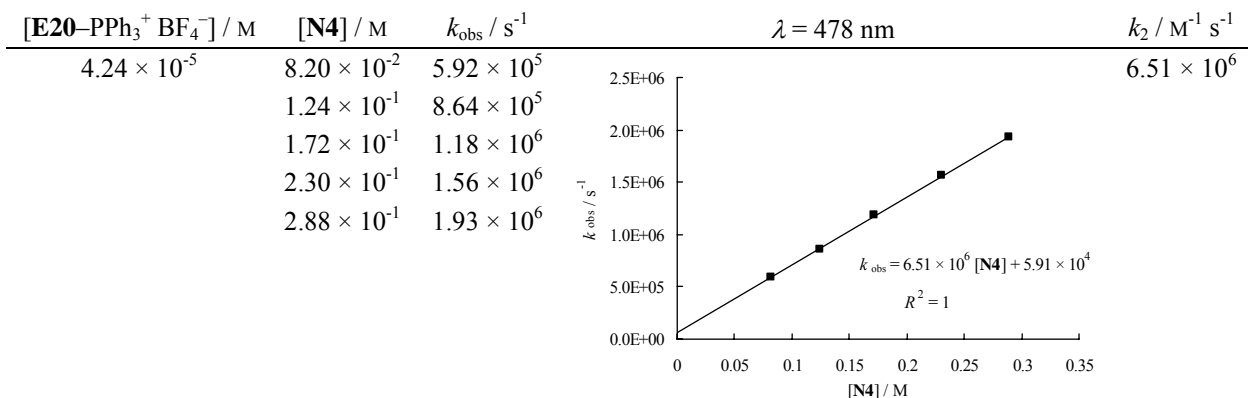
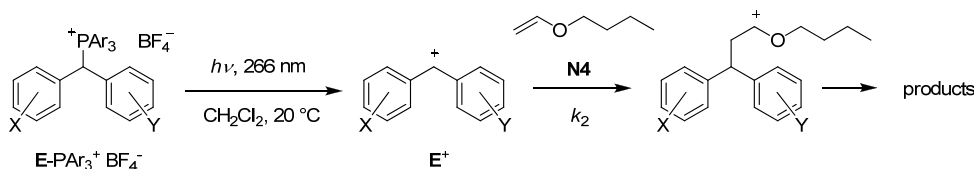
The reactivity of vinyl ethers does not depend much on the alkyl rest,²² and *n*-butyl vinyl ether (**N4**) can be expected to have a similar reactivity as ethyl vinyl ether ($N = 3.92$, $s_N = 0.90$).^{1c} Due to its lower vapor pressure, we preferred the *n*-butyl derivative for the kinetic experiments in this study.

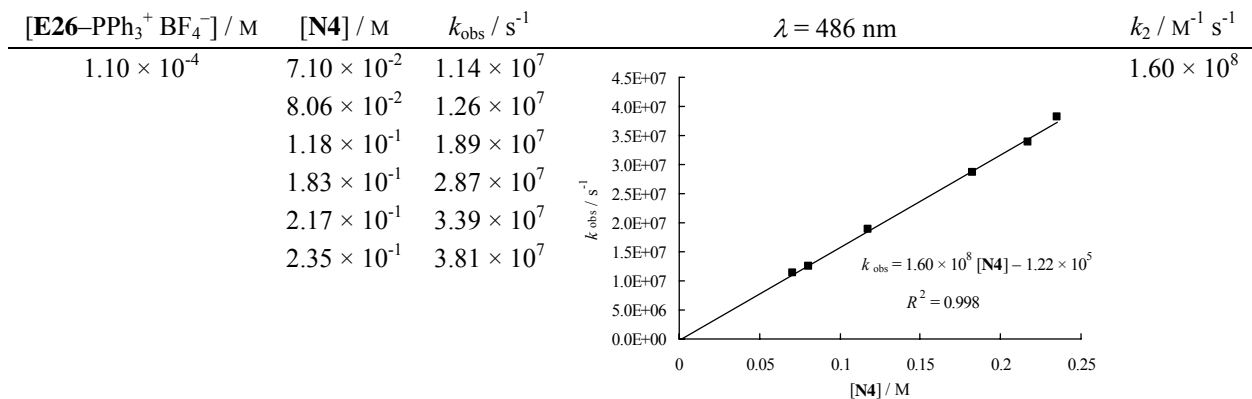
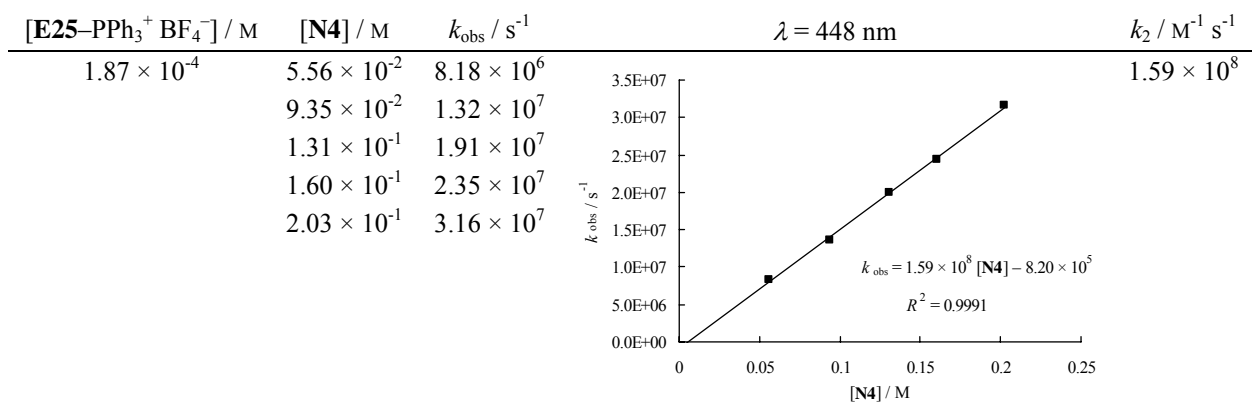
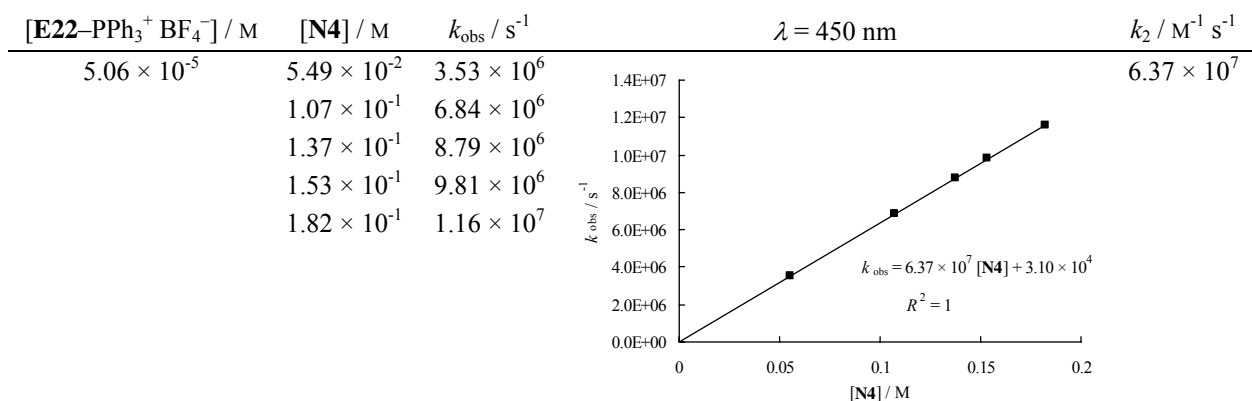
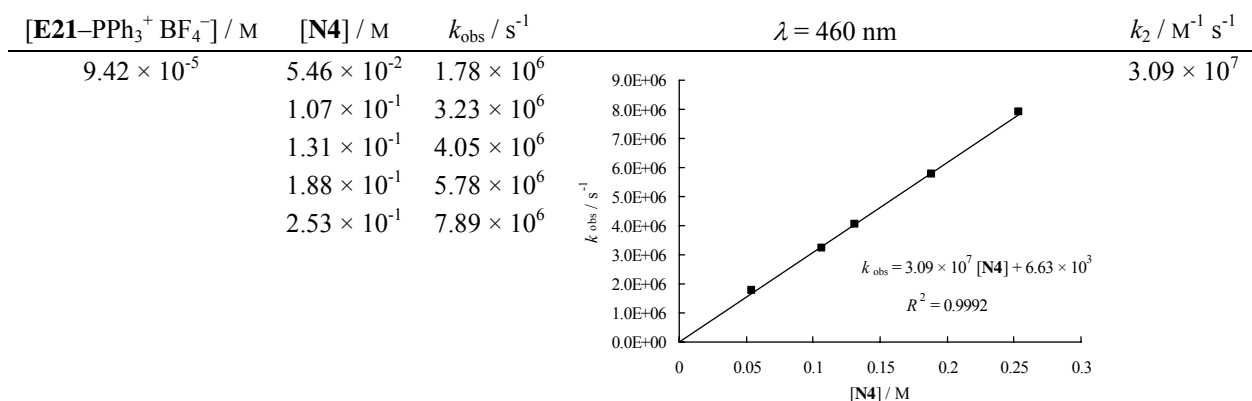
Reactions of benzhydryl cations with vinyl ethers yield alkoxy carbenium ions which are prone to oligomerization reactions and the final products depend on the exact reaction conditions.^{S2c,S2e} When (ani)₂CH–Cl (**E15–Cl**) was ionized by ZnBr₂·(OEt₂)₂ and reacted with ethyl vinyl ether in CH₂Cl₂ at –78 to –40 °C, the 1:1 adduct could be trapped by the halozincate counterion and 3,3-bis(*p*-methoxyphenyl)propanal was obtained after aqueous workup.^{S2e} On the other hand, the reaction of (dma)₂CH⁺ BF₄[–] (**E6**⁺ BF₄[–]) with ethyl vinyl ether at 20 °C gave rise to the formation of polymeric products,^{S2e} because the intermediate alkoxy carbenium ion is considerably more electrophilic than (dma)₂CH⁺.

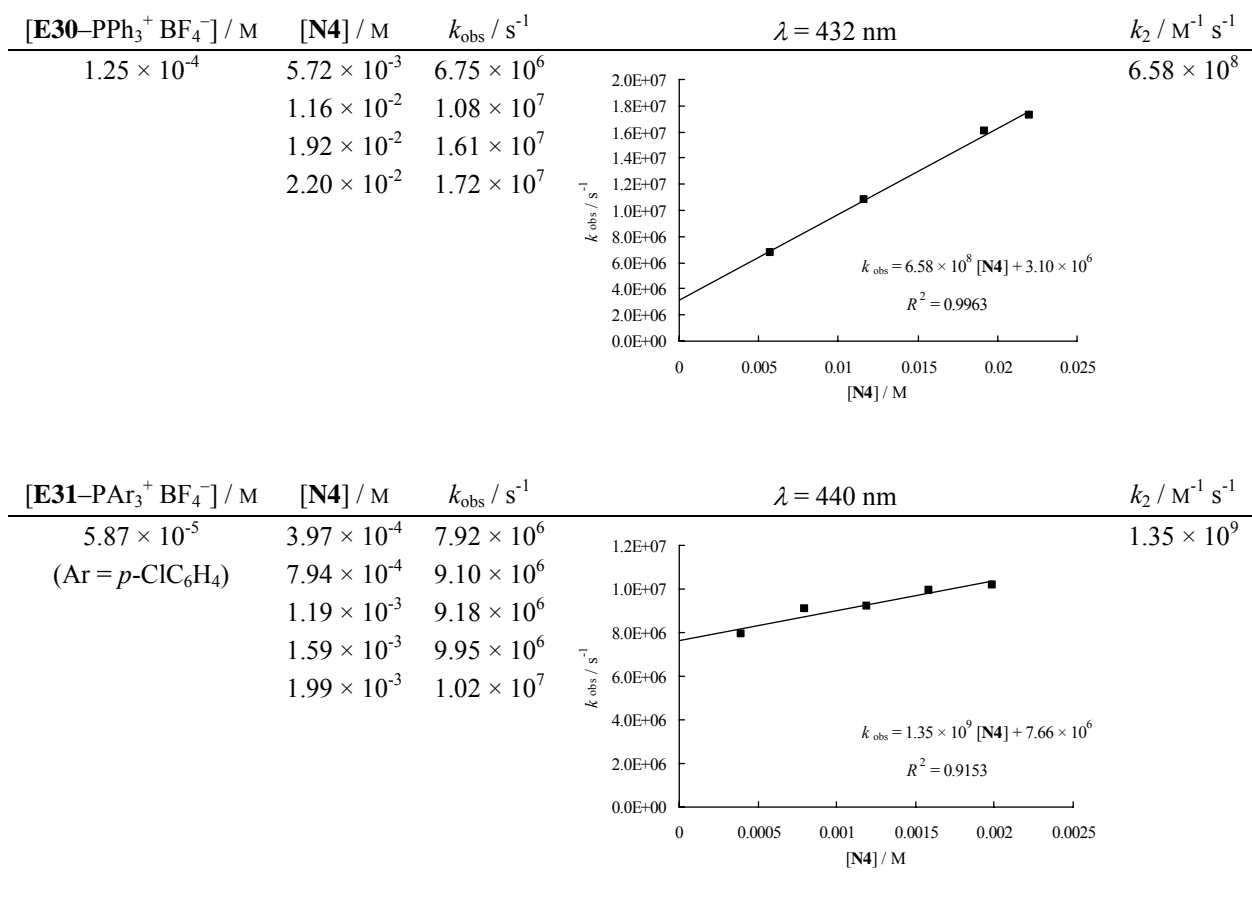
Similarly, it was reported that the kinetics of reactions of (dpa)₂CH⁺ BF₄[–] (**E9**⁺ BF₄[–]) with excess ethyl vinyl ether or *n*-butyl vinyl ether (**N4**) showed pseudo-first-order behavior only for the first 20-30% conversion, because the nucleophile was consumed by oligomerization reactions.²²

For the reactions of (mfa)₂CH⁺ BF₄[–] (**E10**⁺ BF₄[–]), fur(ani)CH⁺ BF₄[–] (**E14**⁺ BF₄[–]), and more reactive benzhydryl cations with *n*-butyl vinyl ether (**N4**) reported in this work, however, we observed good pseudo-first-order kinetics for the decay of the benzhydryl cations when we employed **N4** in a >20-fold excess. Apparently, these reactions were sufficiently fast so that the subsequent oligomerization reactions did not affect the pseudo-first-order conditions.

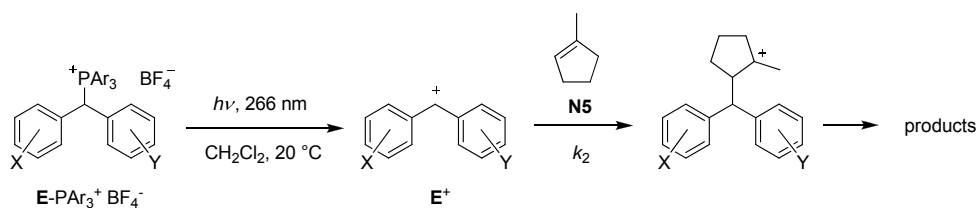
Laser-flash kinetics







3.S.2.5 Reactions of benzhydrylium ions (E^+) with 1-methylcyclopentene (**N5**) in dichloromethane at 20 °C.

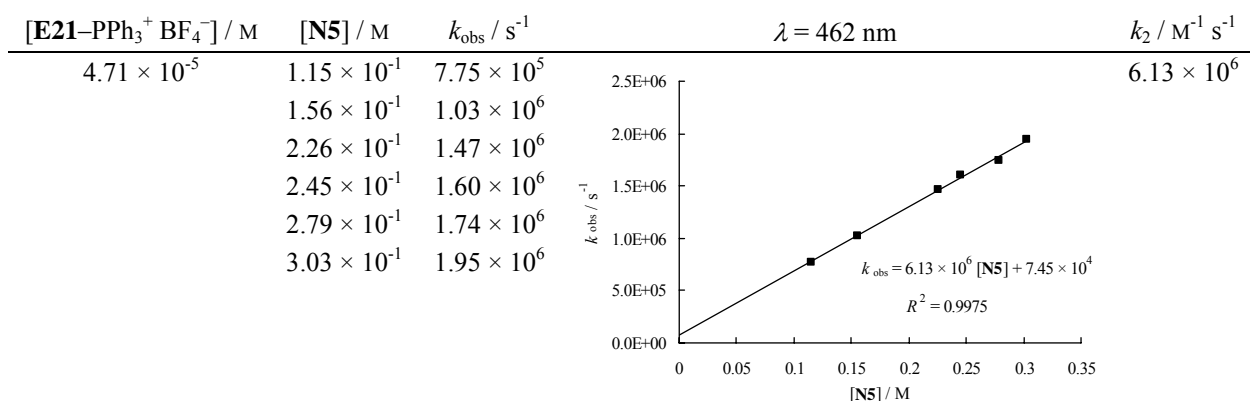


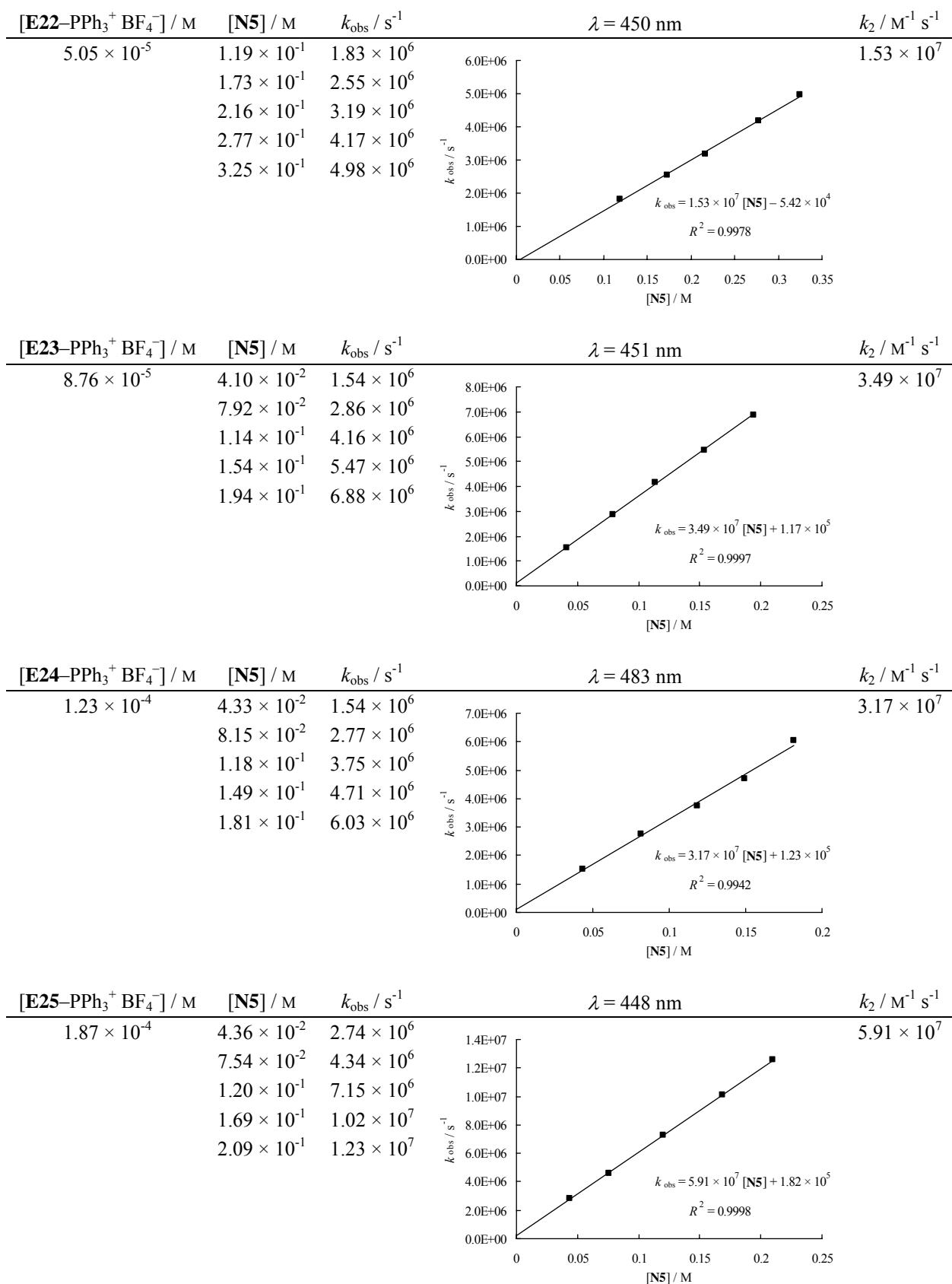
When ani(Ph)CH–Cl (**E18–Cl**) was ionized with BCl_3 at -70°C and reacted with **N5** in CH_2Cl_2 , the resulting 1:1 adducts were trapped by the BCl_4^- counter-ion yielding the 1-chloro-1-methyl-2-(diarylmethyl)cyclopentane, accompanied by formation of indanes through an intramolecular reaction with one of the aryl rings.^{27a}

When we irradiated $\text{E20–PPh}_3^+ \text{BF}_4^-$ in the presence of variable concentrations of **N5**, the decays of E20^+ ($\lambda = 462\text{ nm}$) did not follow pseudo-first order kinetics due to recombination of E20^+ with the photo-leaving group PPh_3 .¹⁸ A second-order rate constant of $k_{\text{phosphine}} \approx 1.19 \times 10^{10}\text{ M}^{-1}\text{ s}^{-1}$ (average of three published values in ref. ¹⁸) was previously determined for the diffusion of PPh_3 in CH_2Cl_2 . The second-order rate constant k_2 for the reaction of E20^+ with **N5** was then obtained by fitting the decay of $[\text{E20}^+]$ to a kinetic model consisting of two second-order processes for the reactions of E20^+ with **N5** ($\text{E20}^+ + \text{N5} \rightarrow 1:1\text{ adduct}$, rate constant k_2) and with PPh_3 ($\text{E20}^+ + \text{PPh}_3 \rightarrow \text{E20–PPh}_3^+$, rate constant $k_{\text{phosphine}} = 1.19 \times 10^{10}\text{ M}^{-1}\text{ s}^{-1}$) using the software package Gepasi.²⁴

$[\text{E20–PPh}_3^+ \text{BF}_4^-] / \text{M}$	$[\text{N5}]_0 / \text{M}$	$[\text{E20}^+]_0 / \text{M}^a$	$k_2 / \text{M}^{-1}\text{ s}^{-1}$
4.24×10^{-5}	7.92×10^{-2}	5.02×10^{-6}	5.81×10^5
	1.11×10^{-1}	5.09×10^{-6}	5.24×10^5
	1.41×10^{-1}	5.02×10^{-6}	5.59×10^5
	1.92×10^{-1}	5.00×10^{-6}	5.38×10^5
	2.22×10^{-1}	4.94×10^{-6}	5.83×10^5
	3.13×10^{-1}	4.89×10^{-6}	5.90×10^5
average:			$5.6 (\pm 0.3) \times 10^5$

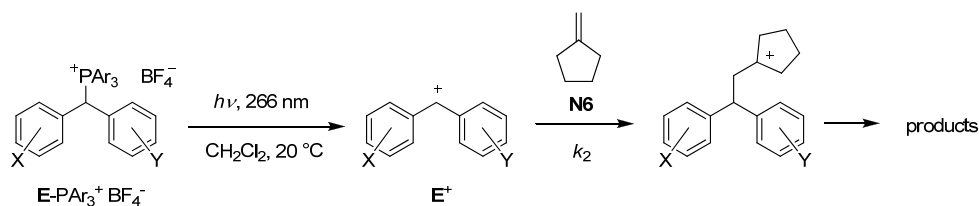
^a $[\text{E20}^+]_0 = [\text{PPh}_3]_0$ calculated from the initial absorbance A_0 and $\epsilon = 74100\text{ M}^{-1}\text{ cm}^{-1}$ (H_2SO_4).⁴⁰



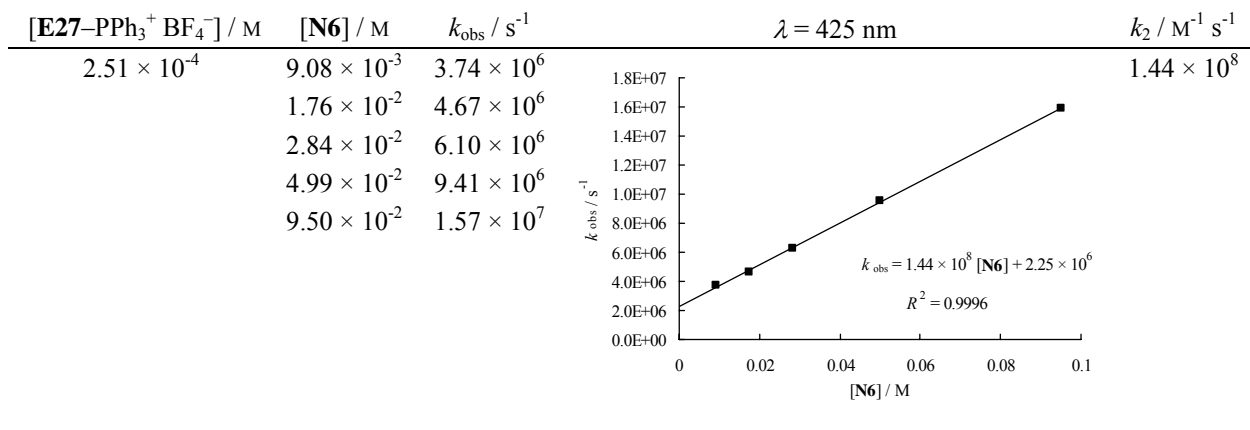


$[\text{E26-PPh}_3^+ \text{BF}_4^-] / \text{M}$	$[\text{N5}] / \text{M}$	$k_{\text{obs}} / \text{s}^{-1}$	$\lambda = 486 \text{ nm}$	$k_2 / \text{M}^{-1} \text{s}^{-1}$
1.10×10^{-4}	1.08×10^{-1}	5.90×10^6		4.72×10^7
	1.52×10^{-1}	8.00×10^6		
	1.92×10^{-1}	9.82×10^6		
	2.29×10^{-1}	1.14×10^7		
	2.73×10^{-1}	1.38×10^7		
$[\text{E27-PPh}_3^+ \text{BF}_4^-] / \text{M}$	$[\text{N5}] / \text{M}$	$k_{\text{obs}} / \text{s}^{-1}$	$\lambda = 450 \text{ nm}$	$k_2 / \text{M}^{-1} \text{s}^{-1}$
2.51×10^{-4}	5.60×10^{-3}	3.07×10^6		1.76×10^8
	1.34×10^{-2}	4.38×10^6		
	2.26×10^{-2}	6.62×10^6		
	3.50×10^{-2}	8.36×10^6		
	4.87×10^{-2}	1.05×10^7		
	7.48×10^{-2}	1.61×10^7		
$[\text{E30-PPh}_3^+ \text{BF}_4^-] / \text{M}$	$[\text{N5}] / \text{M}$	$k_{\text{obs}} / \text{s}^{-1}$	$\lambda = 432 \text{ nm}$	$k_2 / \text{M}^{-1} \text{s}^{-1}$
1.12×10^{-4}	8.29×10^{-4}	7.32×10^6		5.87×10^8
	1.66×10^{-3}	7.78×10^6		
	2.49×10^{-3}	8.51×10^6		
	3.32×10^{-3}	8.80×10^6		
	4.15×10^{-3}	9.25×10^6		
$[\text{E31-PAr}_3^+ \text{BF}_4^-] / \text{M}$	$[\text{N5}] / \text{M}$	$k_{\text{obs}} / \text{s}^{-1}$	$\lambda = 440 \text{ nm}$	$k_2 / \text{M}^{-1} \text{s}^{-1}$
5.60×10^{-5}	3.76×10^{-4}	6.93×10^6		1.33×10^9
(Ar = <i>p</i> -ClC ₆ H ₄)	7.53×10^{-4}	7.56×10^6		
	1.13×10^{-3}	7.46×10^6		
	1.51×10^{-3}	8.22×10^6		
	1.88×10^{-3}	9.11×10^6		

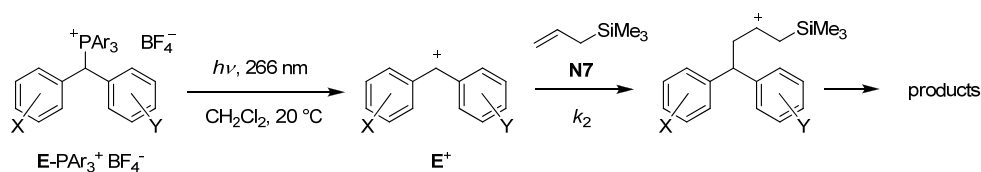
3.S.2.6 Reaction of benzhydrylium ions (E^+) with methylenecyclopentane (**N6**) in dichloromethane at 20 °C.



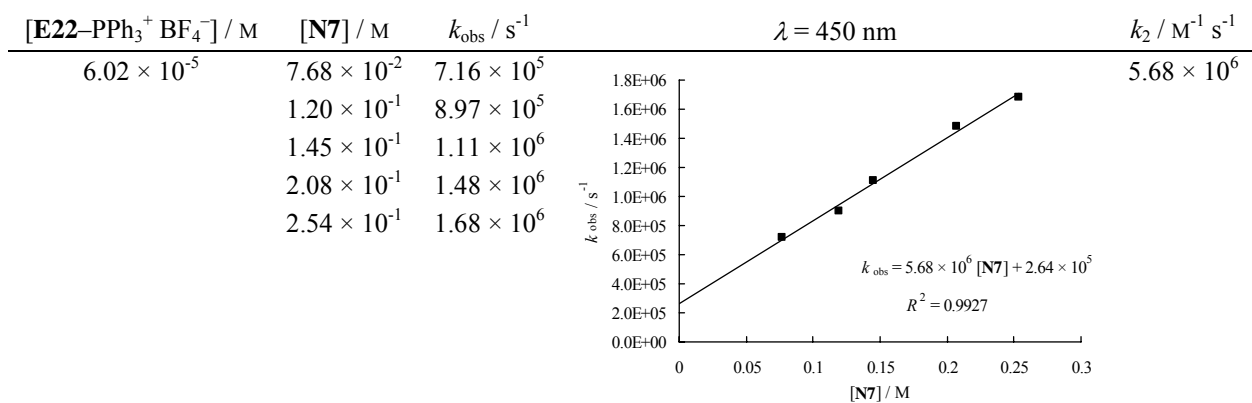
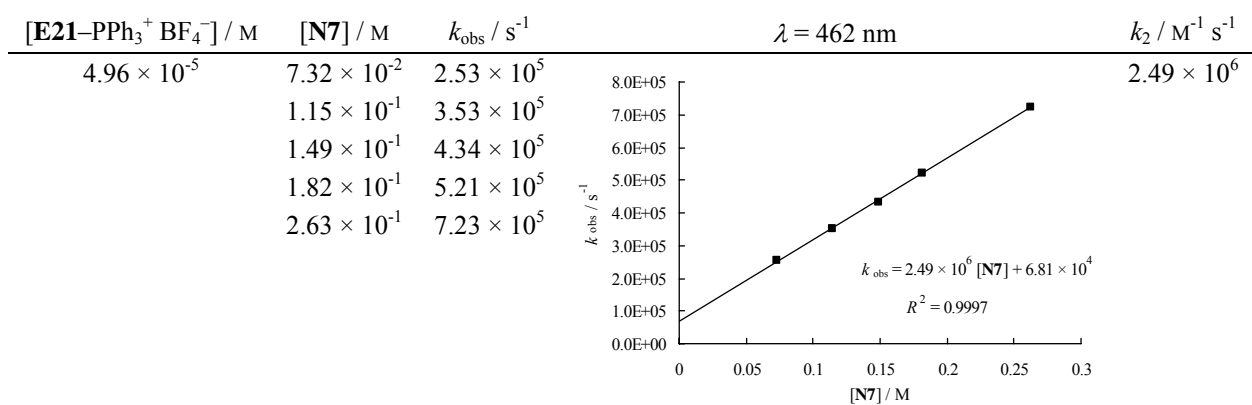
When ani(Ph)CH^+ (**E18**⁺) tetrachloroborate salt or $(\text{tol})_2\text{CH}^+$ (**E20**⁺) trichlorozincate salt were reacted with **N6** in CH_2Cl_2 at -78°C , the 1:1-adducts were trapped by the complex counterions and 1-[2,2-diarylethyl]-1-chlorocyclopentanes were isolated as the main products.^{27b,S2a}

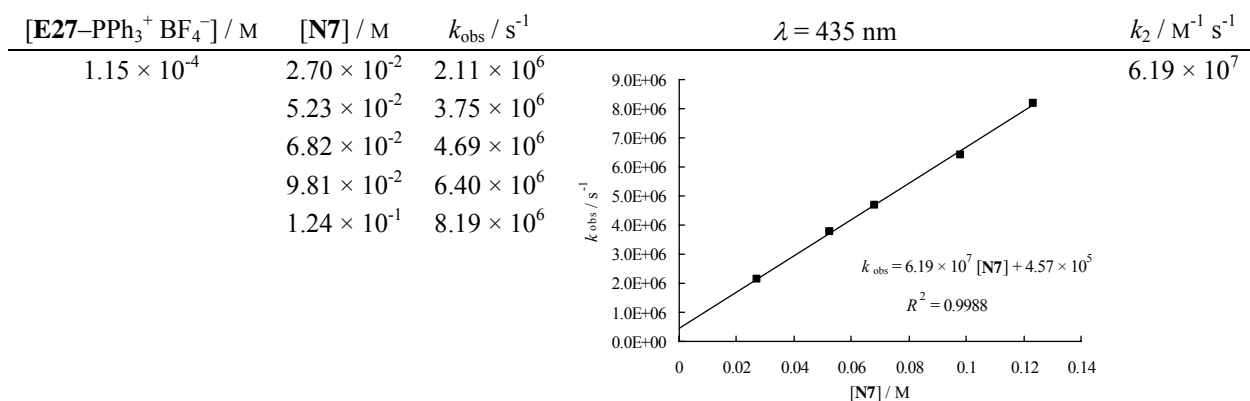
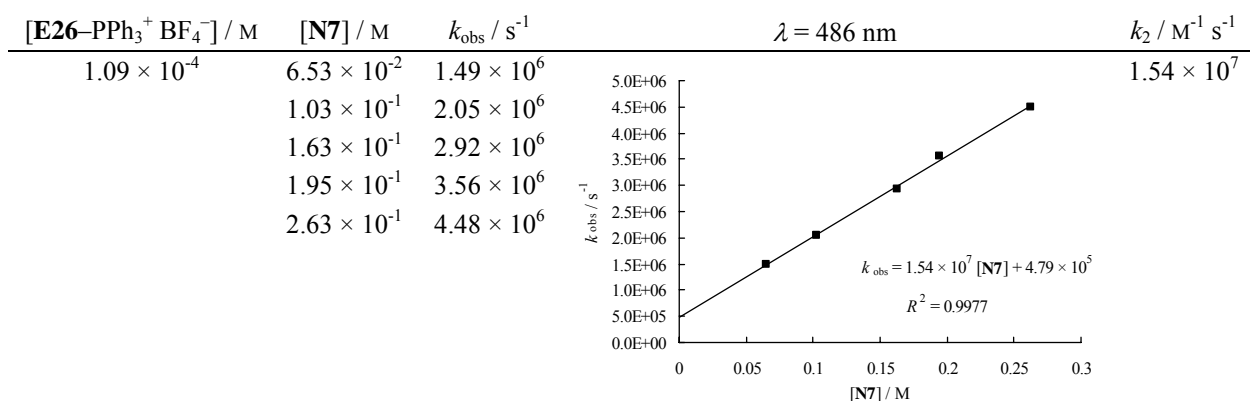
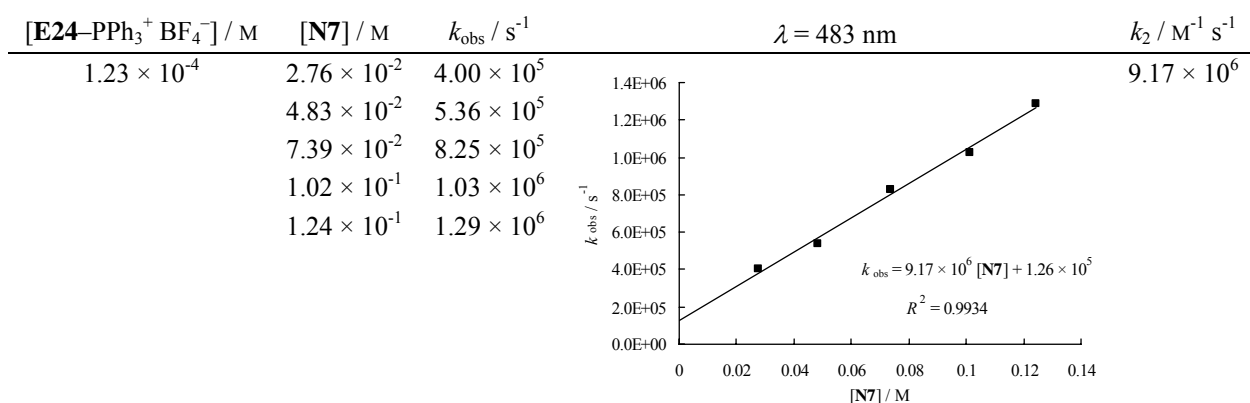
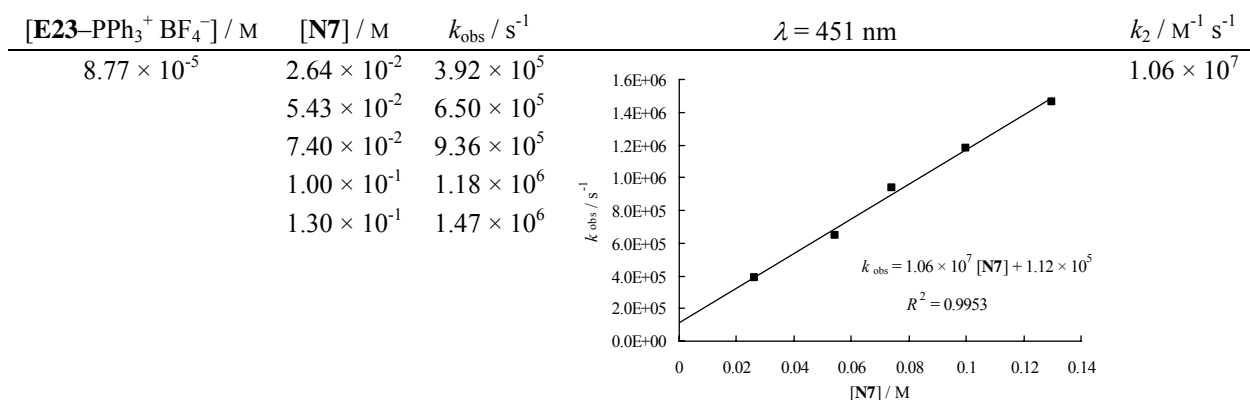


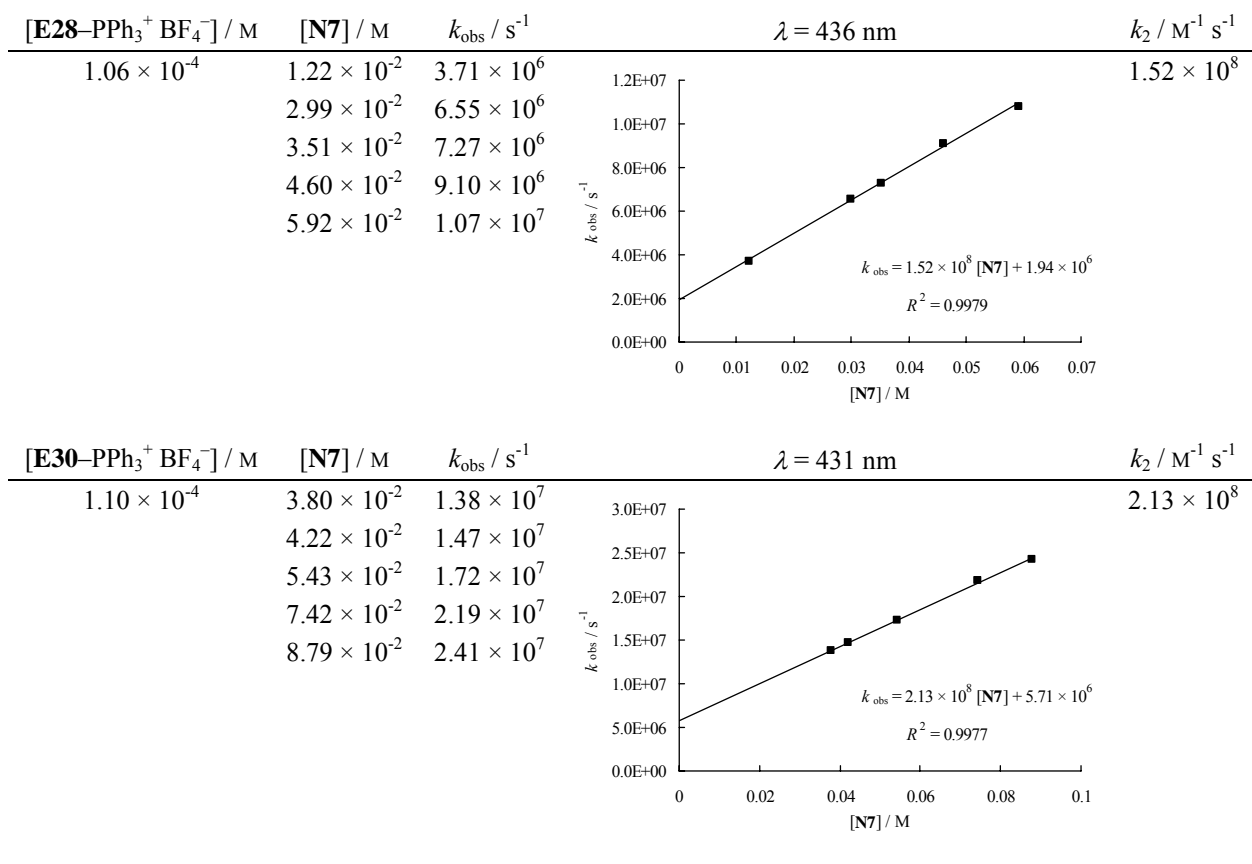
3.S.2.7 Reactions of benzhydrylium ions (E^+) with allyltrimethylsilane (**N7**) in dichloromethane at 20 °C.

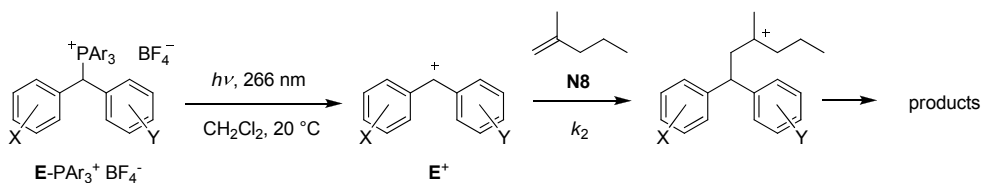


Reactions of $(fur)_2CH^+$ (**E13**⁺), $fur(ani)CH^+$ (**E14**⁺), $(ani)_2CH^+$ (**E15**⁺), $ani(tol)CH^+$ (**E17**⁺), $ani(Ph)CH^+$ (**E18**⁺), $pop(Ph)CH^+$ (**E19**⁺), $(tol)_2CH^+$ (**E20**⁺), $(Ph)_2CH^+$ (**E25**⁺), $(pcp)_2CH^+$ (**E26**⁺), the 3-chlorobenzhydrylium ion and the 3,3'-dichlorobenzhydrylium ion with **N7** in CH_2Cl_2 have previously been reported to yield 4,4-diaryl-1-butenes as the final products.^{23a,S2f,S2j}

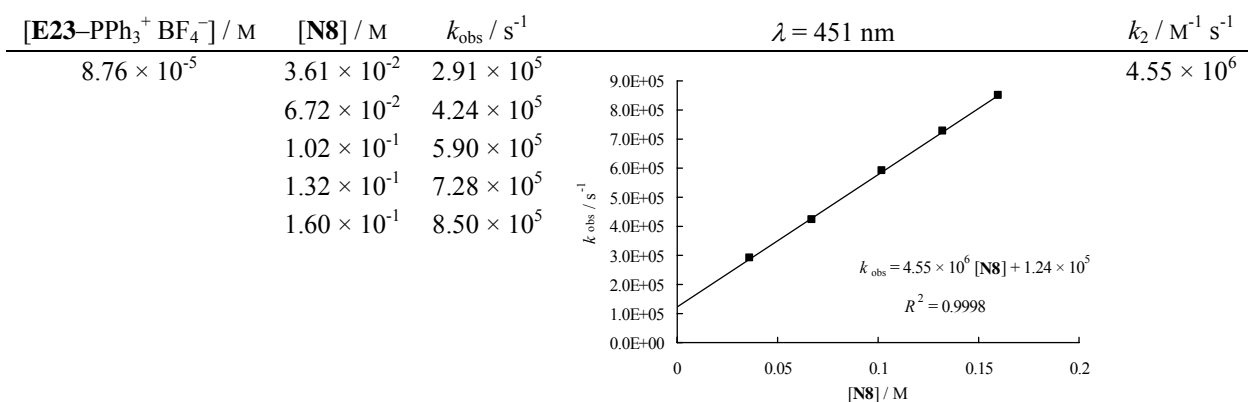
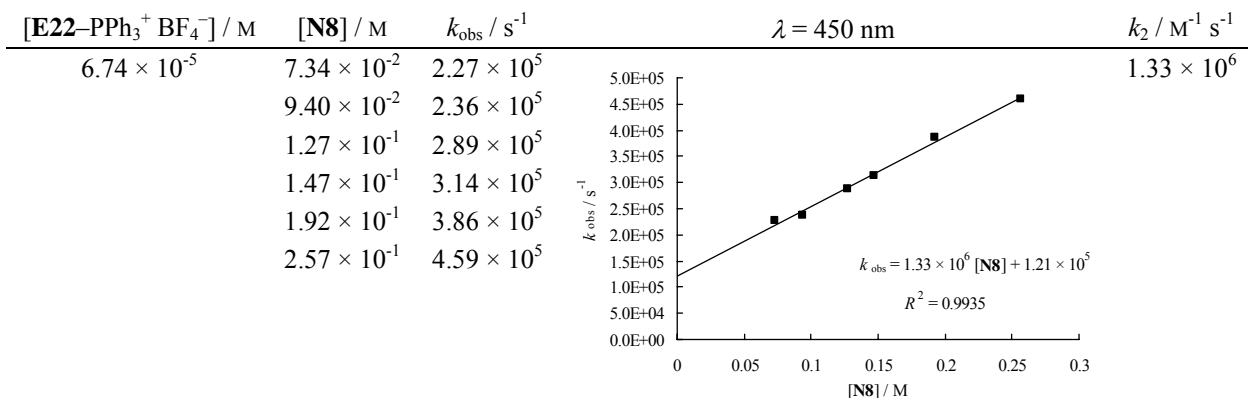


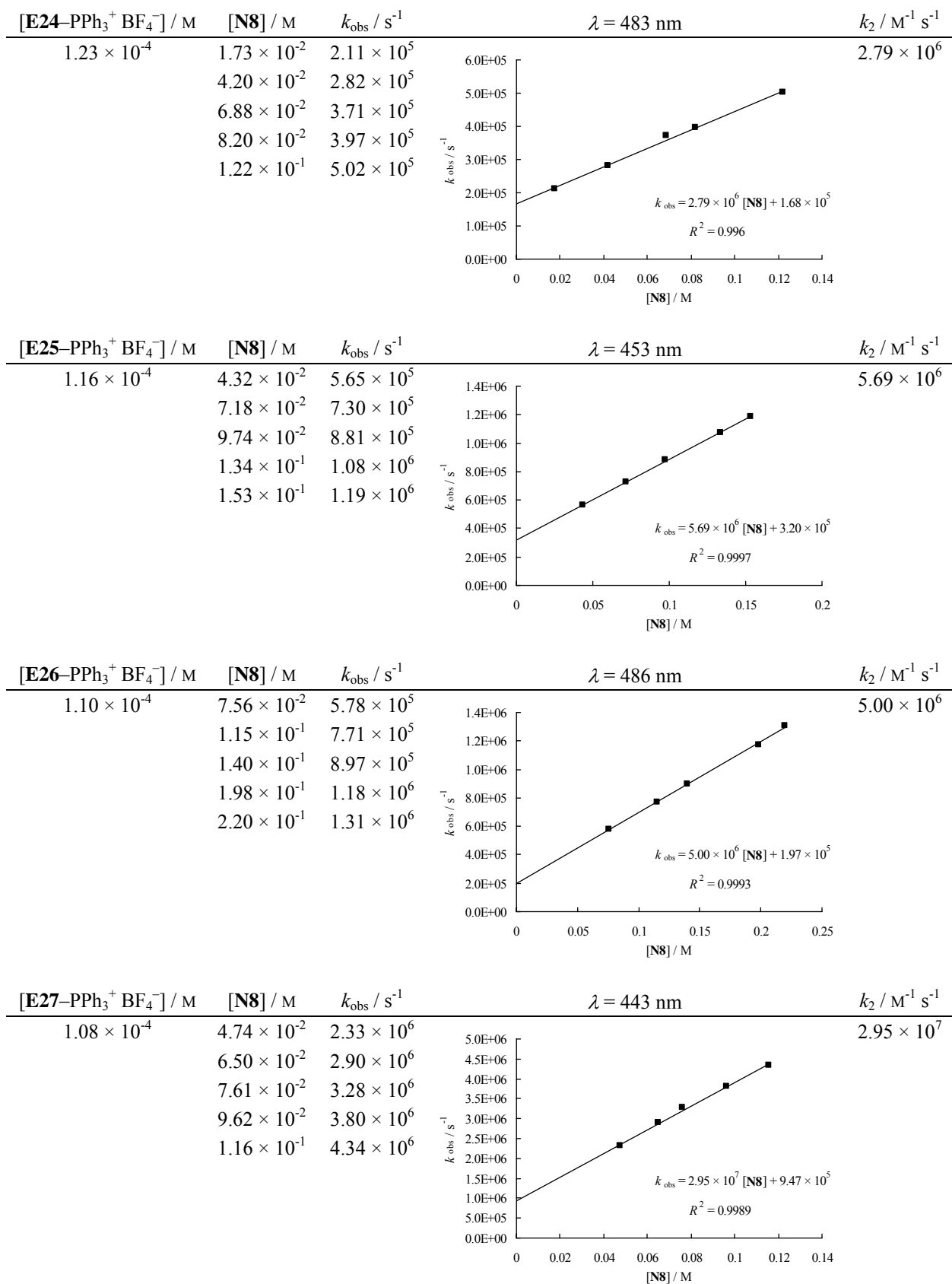


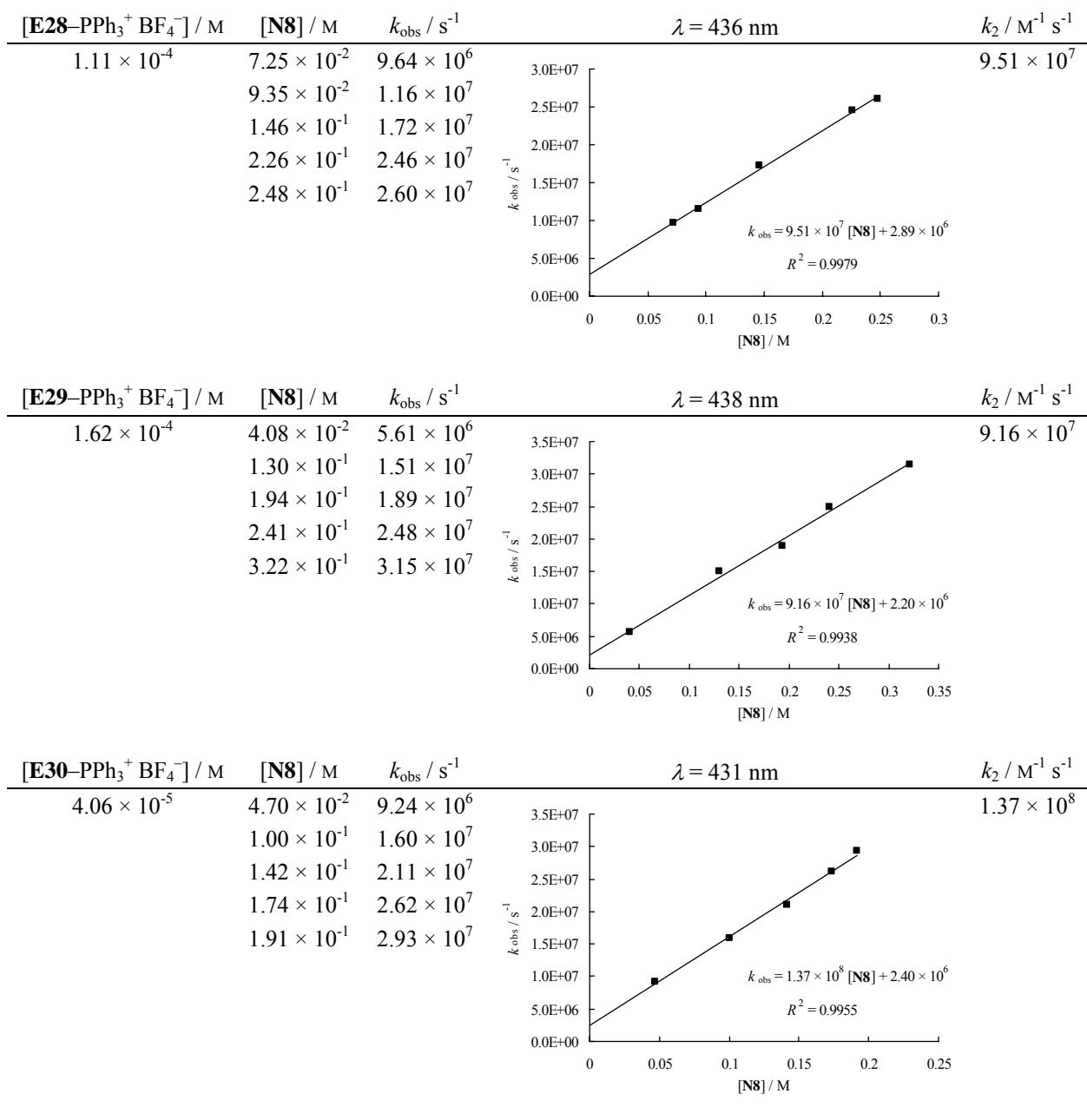


3.S.2.8 Reactions of benzhydrylium ions (E^+) with 2-methyl-1-pentene (**N8**) in dichloromethane at 20 °C.

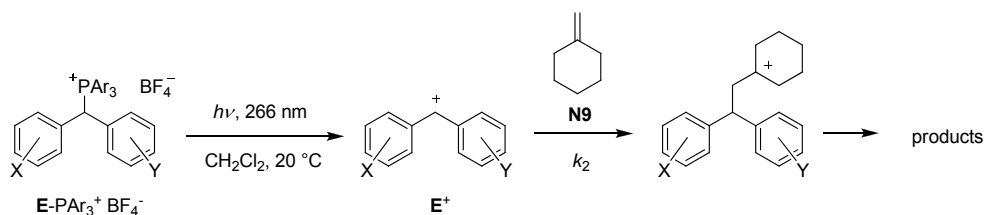
When ani(Ph)CH–Cl (**E18–Cl**), (tol)₂CH–Cl (**E20–Cl**) or Ph₂CH–Cl (**E25–Cl**) were ionized with BCl₃ or ZnCl₂·(OEt₂)₂ at low temperature and reacted with **N8** in CH₂Cl₂, the 1:1-adducts were trapped by the complex counterions and 3-chloro-1,1-diaryl-3-methylhexanes were isolated as the main products.^{26,S2a,S2g}



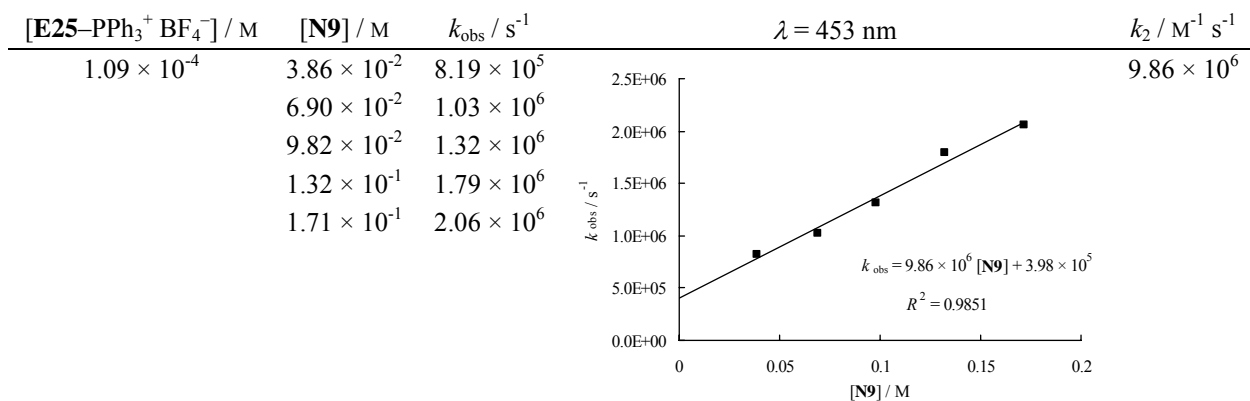
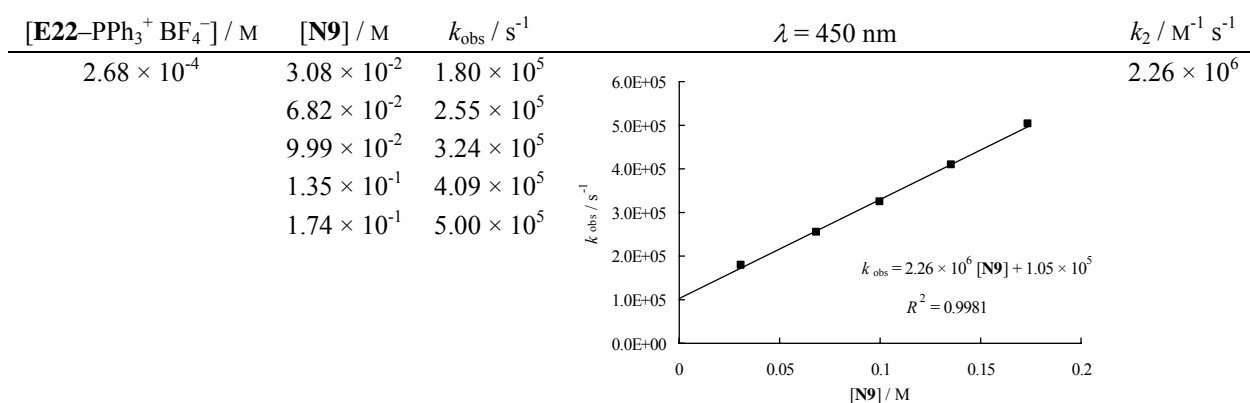




3.S.2.9 Reactions of benzhdrylium ions (E^+) with methylenecyclohexane (**N9**) in dichloromethane at 20 °C.

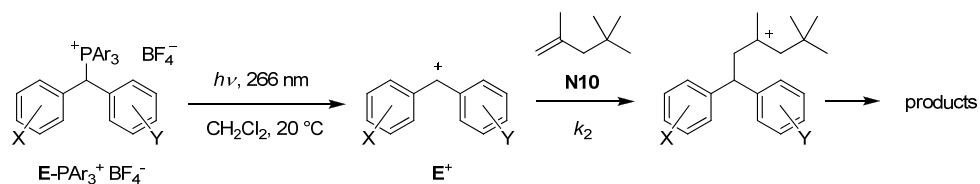


When ani(Ph)CH⁺ (**E18**⁺) tetrachloroborate or (tol)₂CH⁺ (**E20**⁺) trichlorozincate were reacted with **N9** in CH₂Cl₂ at -78 °C, the 1:1-adducts were trapped by the complex counterions and 1-[2,2-diarylethyl]-1-chlorocyclohexanes were isolated as the main products.^{27b,S2a}

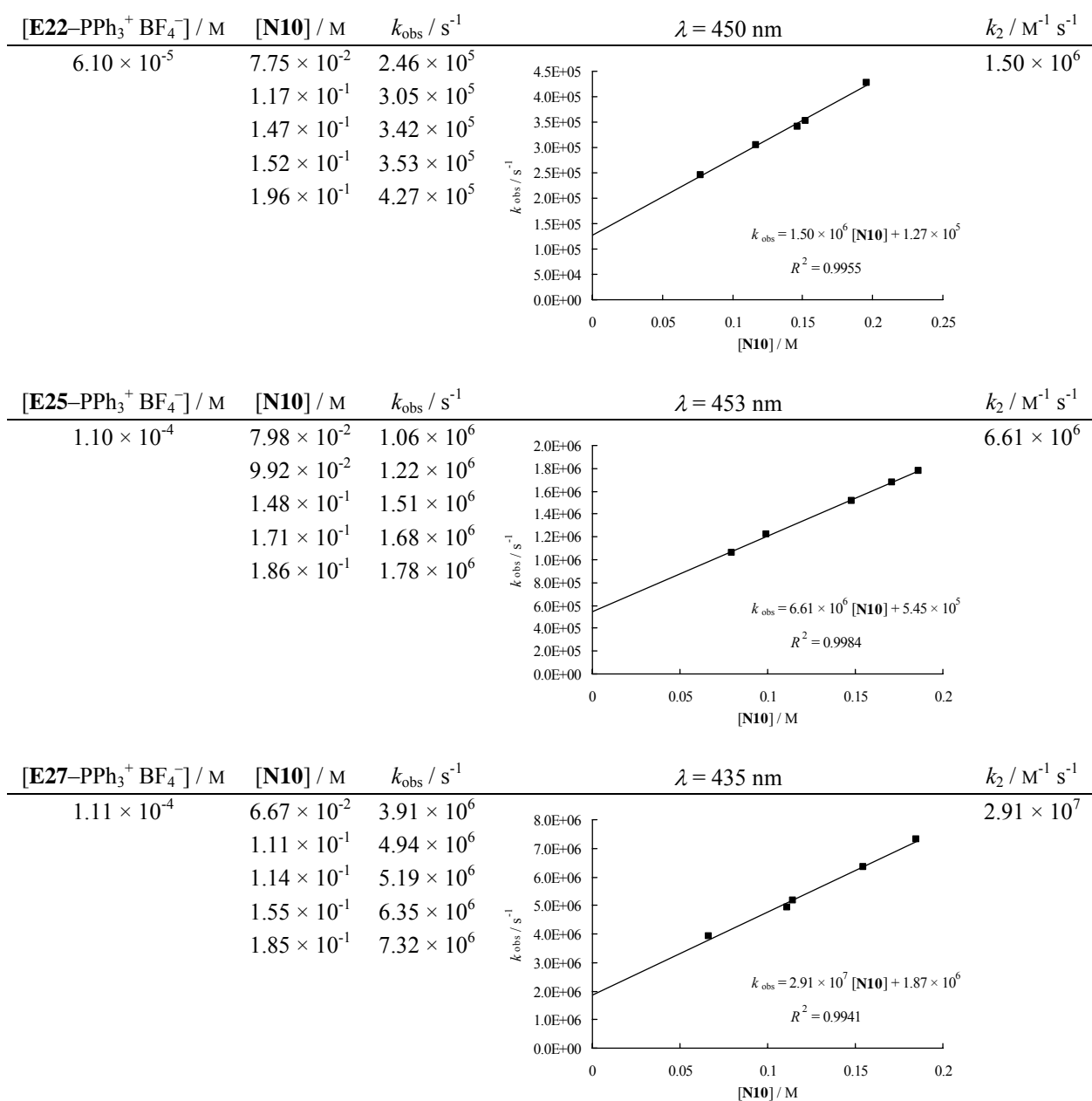


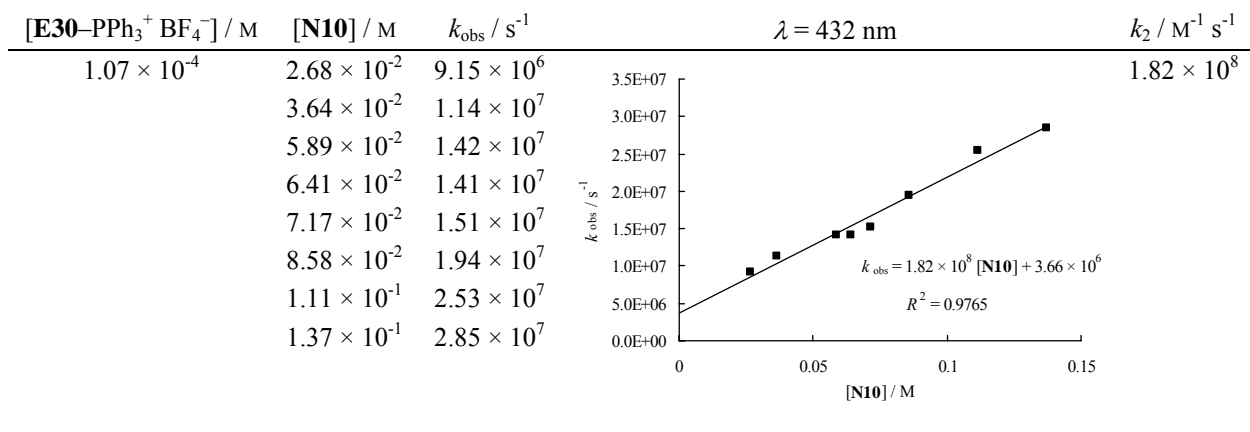
$[\text{E27-PPh}_3^+ \text{BF}_4^-] / \text{M}$	$[\text{N9}] / \text{M}$	$k_{\text{obs}} / \text{s}^{-1}$	$\lambda = 435 \text{ nm}$	$k_2 / \text{M}^{-1} \text{s}^{-1}$
1.08×10^{-4}	3.68×10^{-2}	2.52×10^6		4.68×10^7
	7.03×10^{-2}	4.14×10^6		
	9.88×10^{-2}	5.55×10^6		
	1.34×10^{-1}	6.96×10^6		
	1.70×10^{-1}	8.79×10^6		
$[\text{E30-PPh}_3^+ \text{BF}_4^-] / \text{M}$	$[\text{N9}] / \text{M}$	$k_{\text{obs}} / \text{s}^{-1}$	$\lambda = 432 \text{ nm}$	$k_2 / \text{M}^{-1} \text{s}^{-1}$
1.11×10^{-4}	1.71×10^{-2}	7.39×10^6		1.47×10^8
	3.53×10^{-2}	1.04×10^7		
	5.00×10^{-2}	1.28×10^7		
	6.71×10^{-2}	1.44×10^7		
	8.63×10^{-2}	1.78×10^7		
$[\text{E31-PAr}_3^+ \text{BF}_4^-] / \text{M}$	$[\text{N9}] / \text{M}$	$k_{\text{obs}} / \text{s}^{-1}$	$\lambda = 440 \text{ nm}$	$k_2 / \text{M}^{-1} \text{s}^{-1}$
5.57×10^{-5}	1.03×10^{-2}	1.38×10^7		3.47×10^8
(Ar = <i>p</i> -ClC ₆ H ₄)	1.91×10^{-2}	1.75×10^7		
	2.41×10^{-2}	1.98×10^7		
	3.12×10^{-2}	2.15×10^7		
	4.17×10^{-2}	2.44×10^7		

3.S.2.10 Reactions of benzhydrylium ions (E^+) with 2,3,3-trimethyl-1-pentene (**N10**) in dichloromethane at 20 °C.

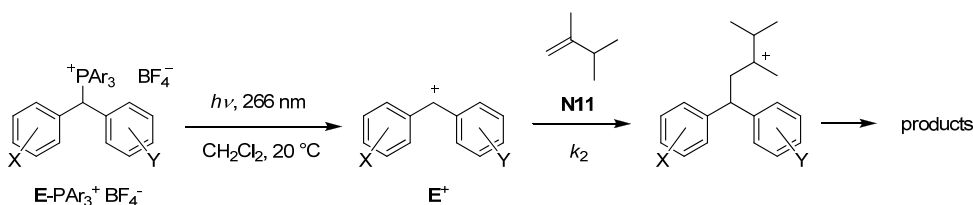


When ani(Ph)CH–Cl (**E18–Cl**) was ionized with BCl_3 at -70°C and reacted with **N10** in CH_2Cl_2 , the 1:1-adduct was trapped by the complex counterion and 3-chloro-1,1-diaryl-3,5,5-trimethylhexane were isolated as the main product.^{27a}

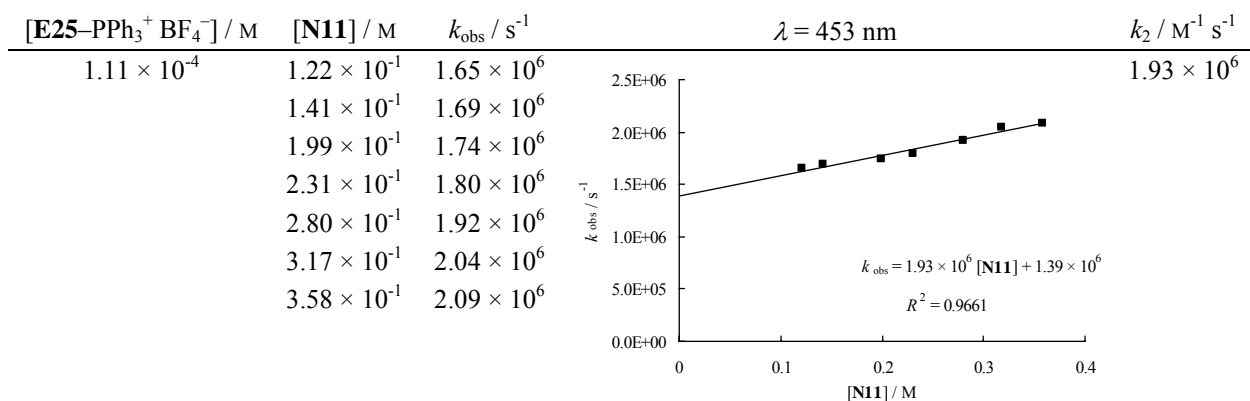


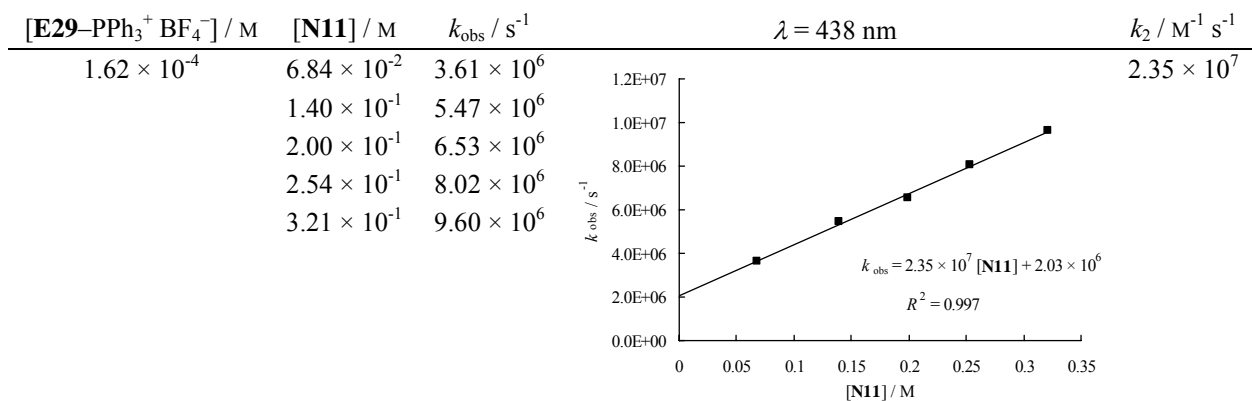
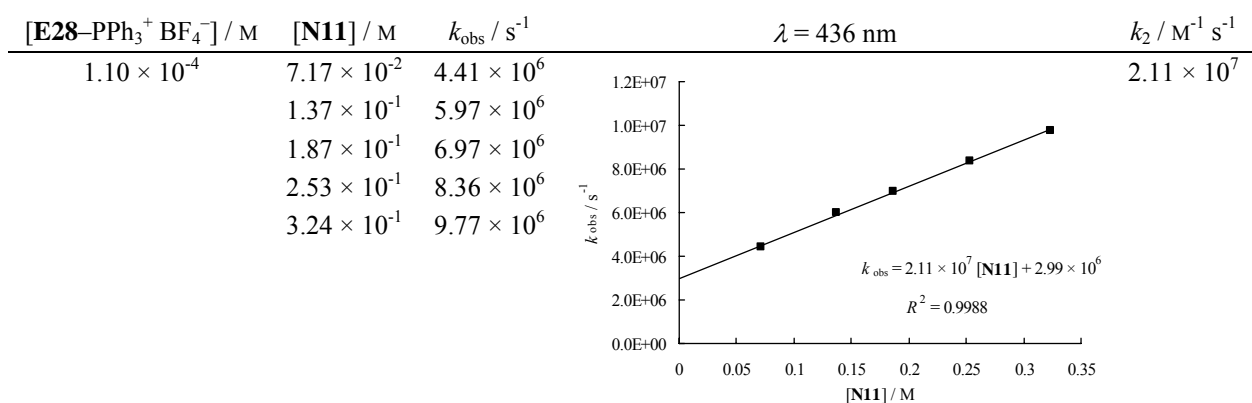
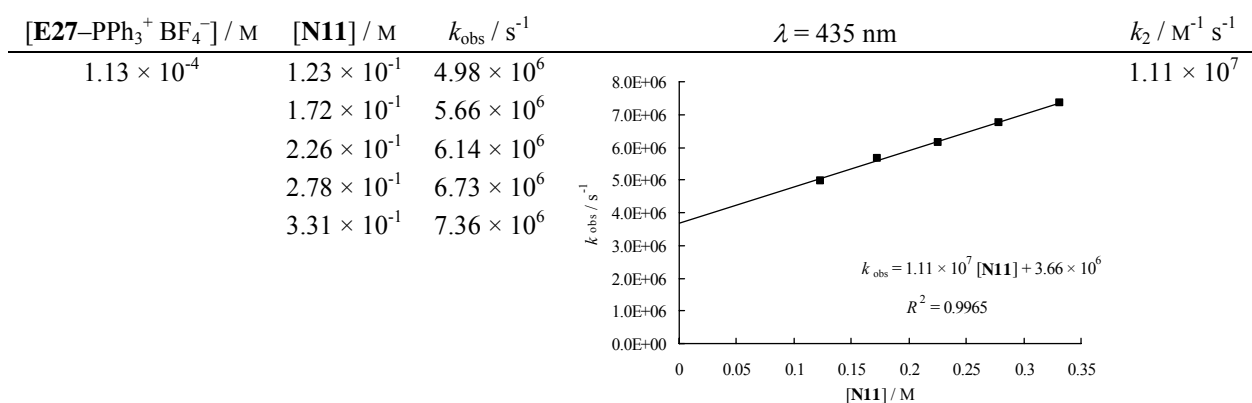
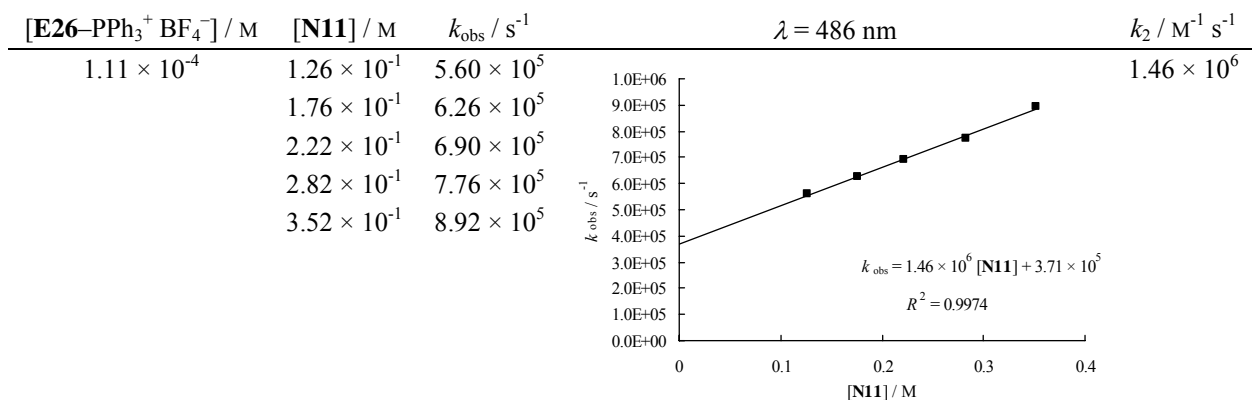


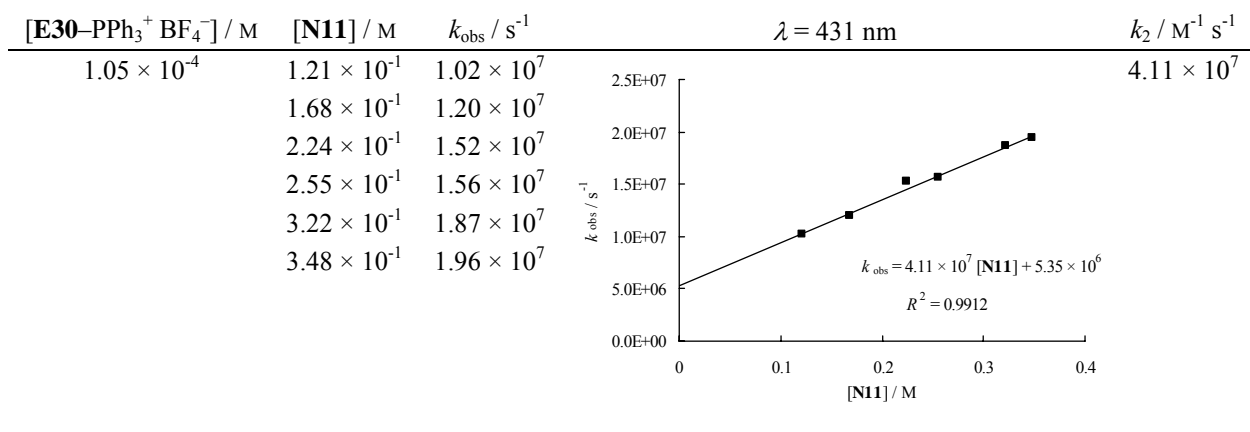
3.S.2.11 Reactions of benzhydrylium ions (E^+) with 2,3-dimethyl-1-butene (**N11**) in dichloromethane at 20 °C.



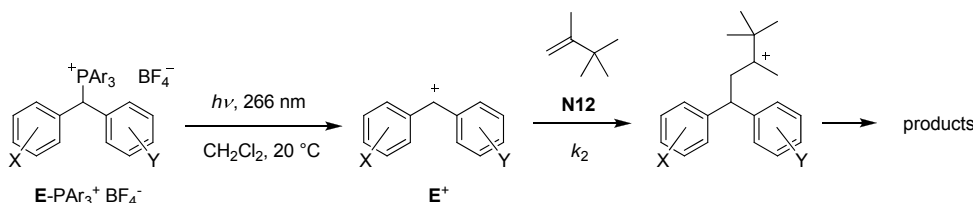
When ani(Ph)CH-Cl (**E18-Cl**) was ionized with BCl_3 at -70°C and reacted with **N11** in CH_2Cl_2 , the resulting 1:1 adduct was partly trapped by the BCl_4^- counter-ion yielding the 3-chloro-3,4-dimethyl-1,1-diarylpentane or the rearranged product 2-chloro-2,3-dimethyl-5,5-diarylpentane, accompanied by formation of tetrahydronaphthalenes through an intramolecular reaction of the rearranged carbocation with one of the aryl rings.^{27a}



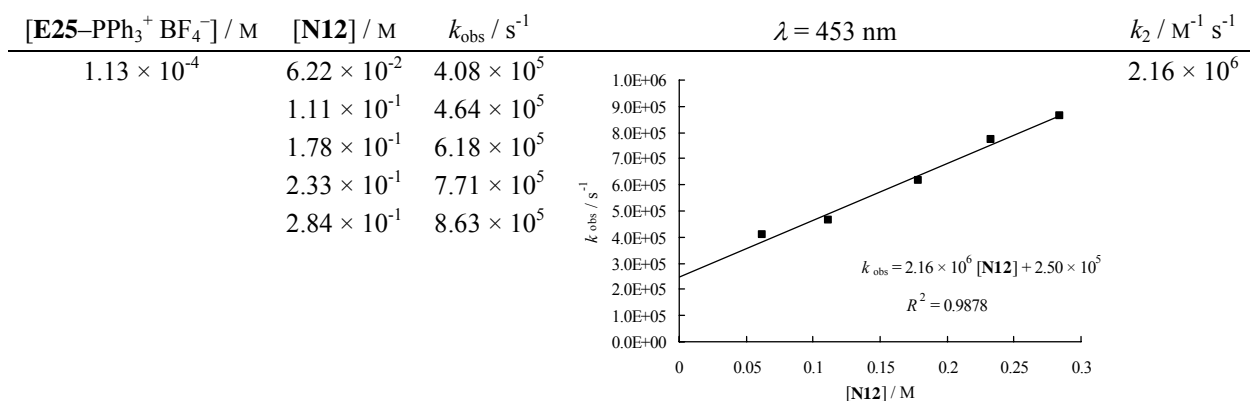


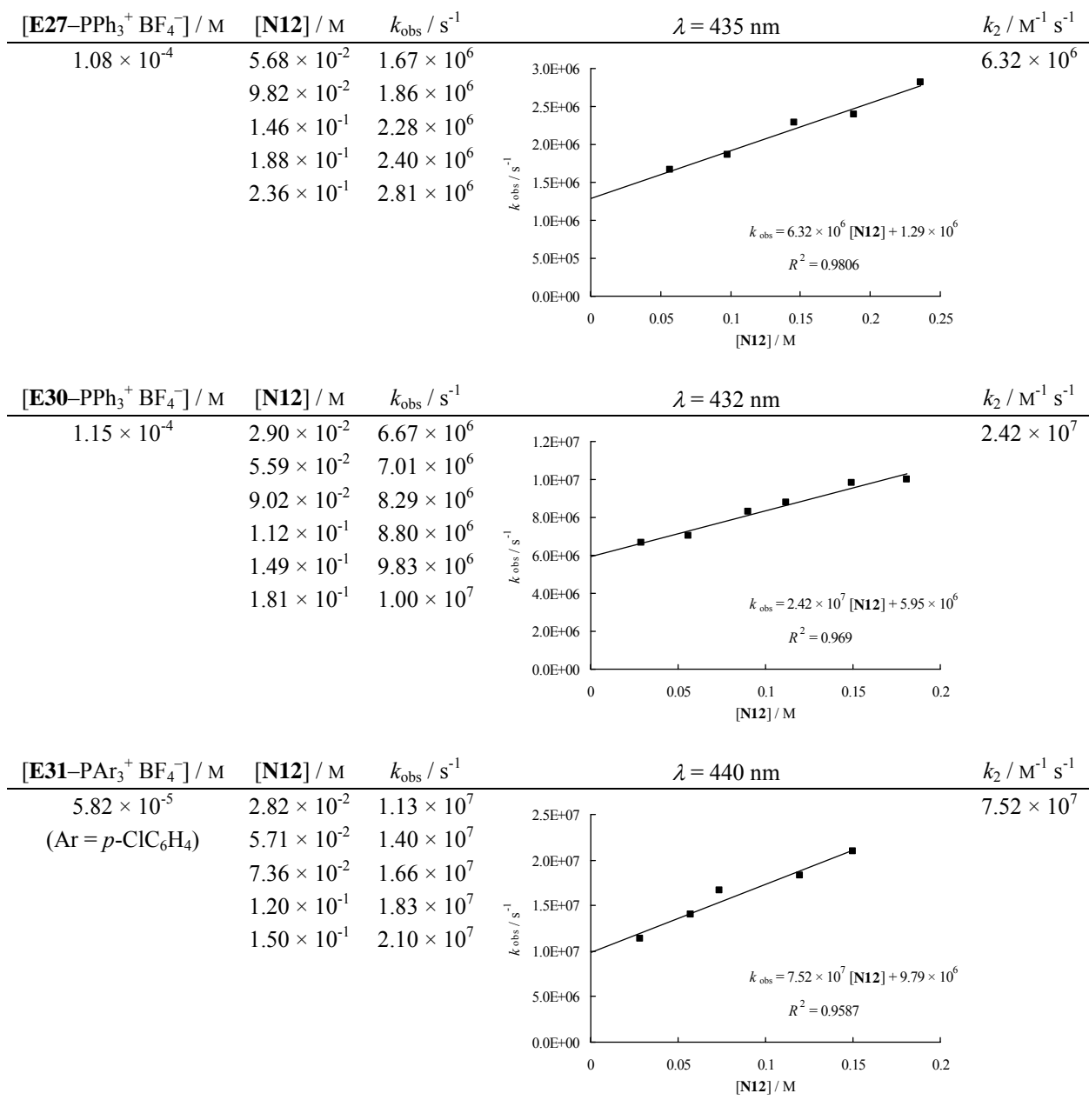


3.S.2.12 Reactions of benzhydrylium ions (E^+) with 2,3,3-trimethyl-1-butene (**N12**) in dichloromethane at 20 °C.

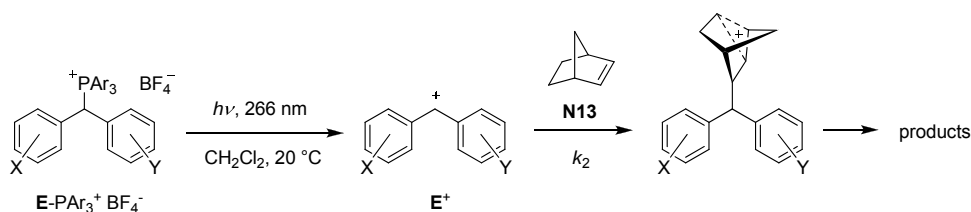


When $\text{ani}(\text{Ph})\text{CH}-\text{Cl}$ (**E18-Cl**) was ionized with BCl_3 at -70°C and reacted with **N12** in CH_2Cl_2 , the resulting 1:1 adduct was partly trapped by the BCl_4^- counter-ion yielding the 3-chloro-2,2,3-trimethyl-5,5-diarylpentane or the rearranged product 2-chloro-2,3,3-trimethyl-5,5-diarylpentane, accompanied by formation of tetrahydronaphthalenes through an intramolecular reaction of the rearranged carbocation with one of the aryl rings.^{27a}

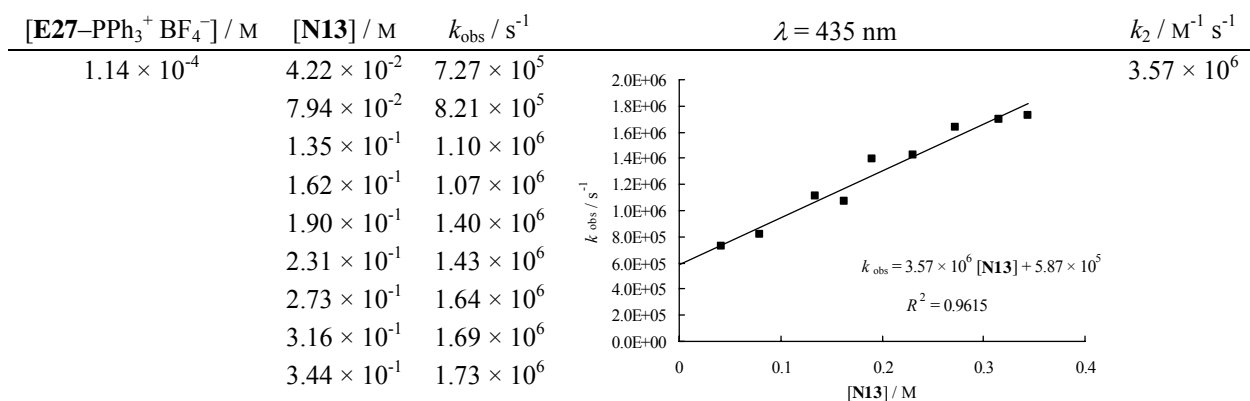
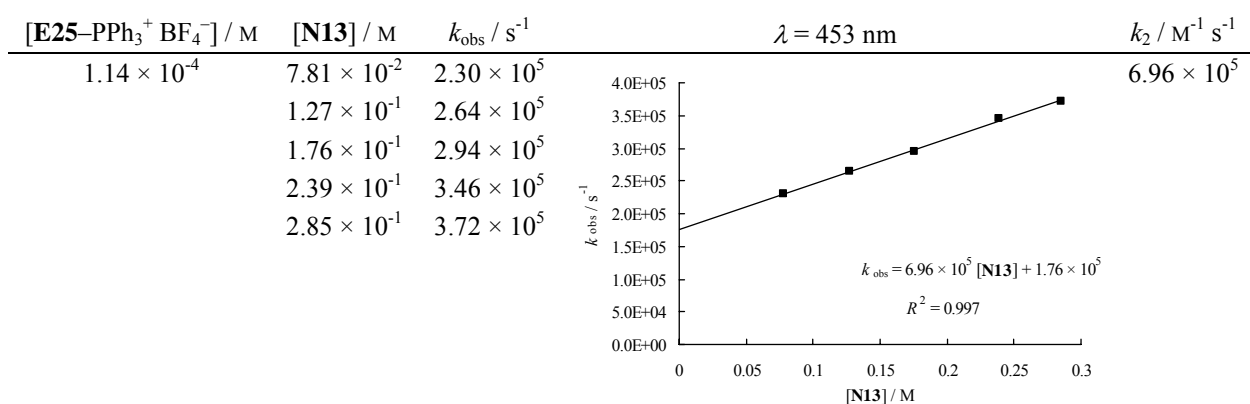


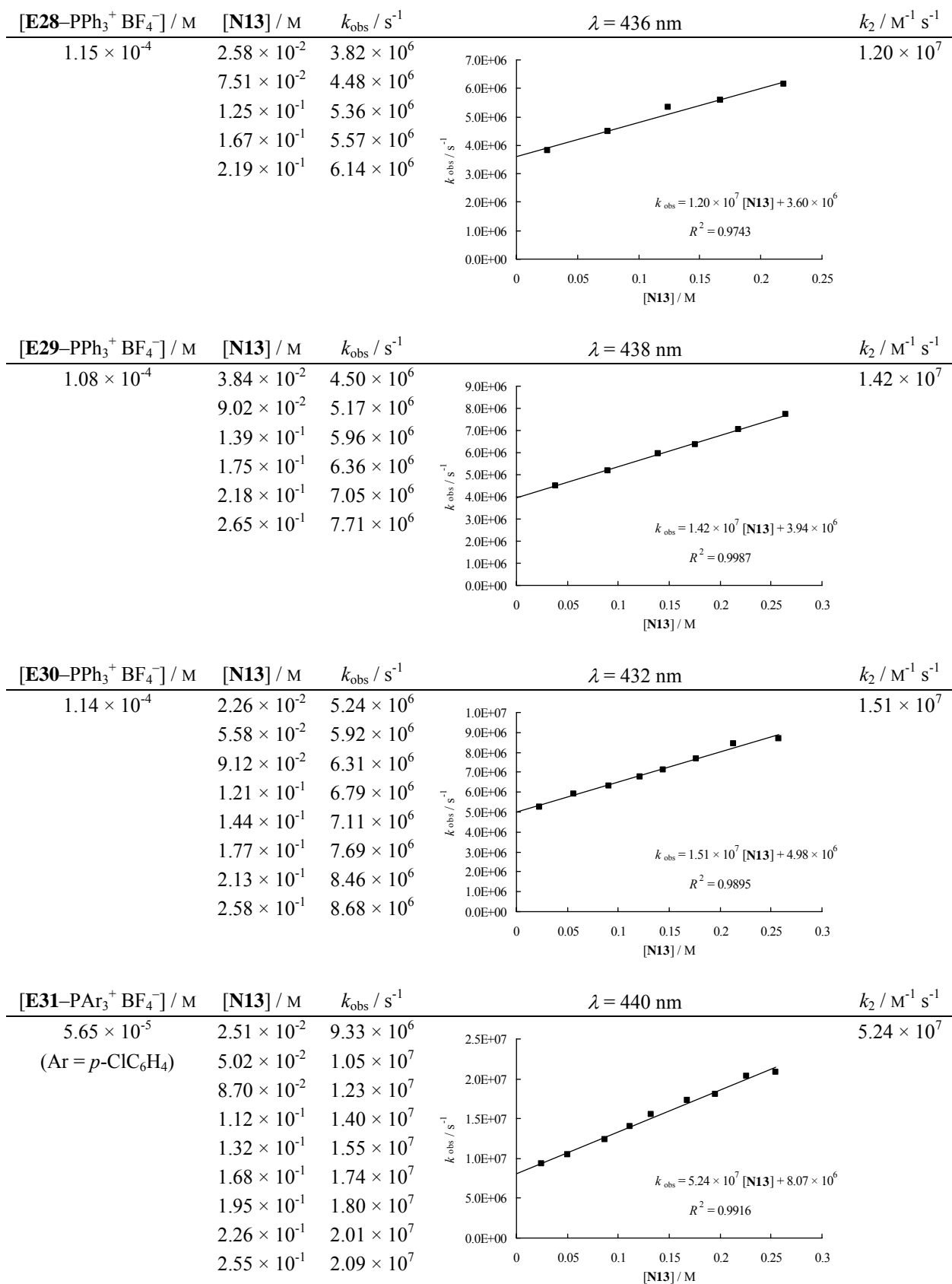


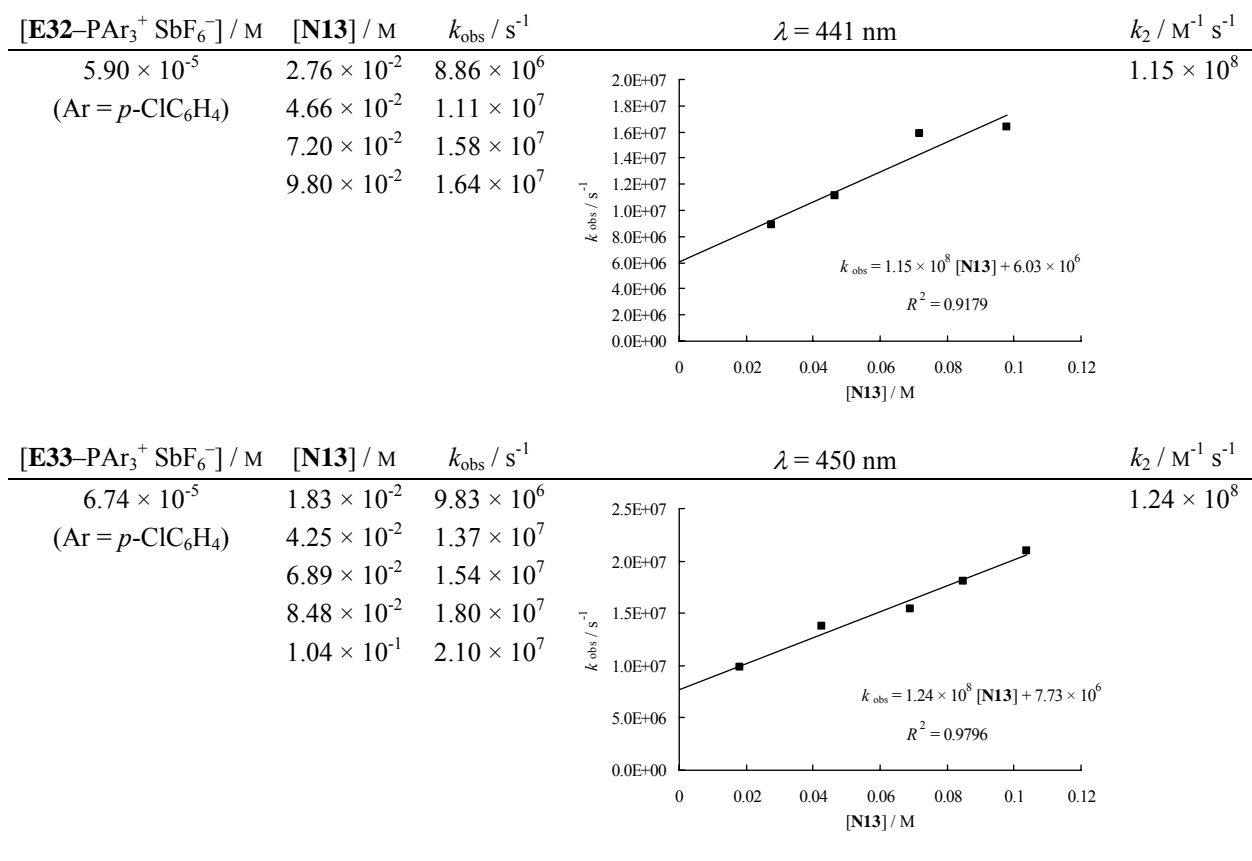
3.S.2.13 Reactions of benzhydrylium ions (E^+) with 2-norbornene (**N13**) in dichloromethane at 20 °C.



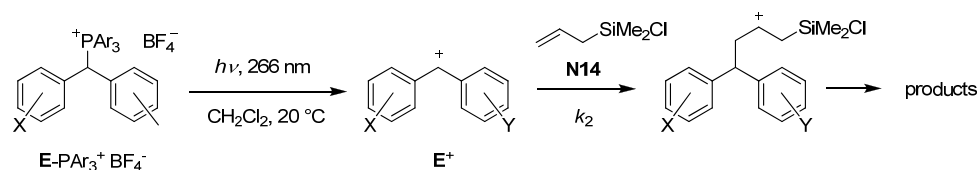
When ani(Ph)CH–Cl (**E18–Cl**), (tol)₂CH–Cl (**E20–Cl**) or Ph₂CH–Cl (**E25–Cl**) were ionized with BCl₃, ZnCl₂·(OEt₂)₂ or SnCl₄ at low temperature and reacted with **N13** in CH₂Cl₂, the 1:1-adducts were trapped by the complex counterions, yielding *exo*-2-chloro-*syn*-7-(diarylmethyl)norbornanes as the final products.^{27a,S2h}







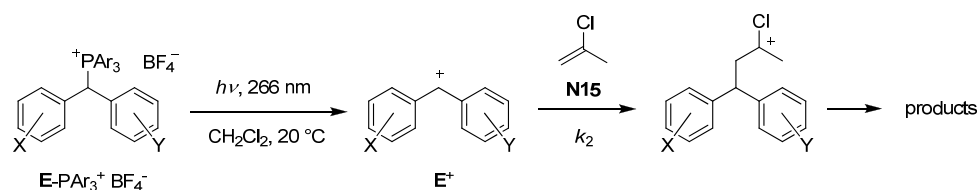
3.S.2.14 Reactions of benzhydrylium ions (E^+) with allylchlorodimethylsilane (**N14**) in dichloromethane at 20 °C.



When ani(Ph)CH–Cl (**E18–Cl**) was ionized with BCl_3 at $-78^\circ C$ and reacted with **N14** in CH_2Cl_2 , quantitative formation of 4-(*p*-anisyl)-4-phenyl-1-butene was observed.^{S2f}

$[E31-PAr_3^+ BF_4^-] / M$	$[N14] / M$	k_{obs} / s^{-1}	$\lambda = 440\text{ nm}$	$k_2 / M^{-1} s^{-1}$
5.68×10^{-5} (Ar = <i>p</i> -ClC ₆ H ₄)	5.18×10^{-2}	4.41×10^6		3.94×10^7
	1.07×10^{-1}	7.44×10^6		
	1.57×10^{-1}	8.98×10^6		
	2.13×10^{-1}	1.15×10^7		
	2.68×10^{-1}	1.30×10^7		
$[E32-PAr_3^+ SbF_6^-] / M$	$[N14] / M$	k_{obs} / s^{-1}	$\lambda = 441\text{ nm}$	$k_2 / M^{-1} s^{-1}$
5.91×10^{-5} (Ar = <i>p</i> -ClC ₆ H ₄)	1.54×10^{-2}	4.94×10^6		6.17×10^7
	2.23×10^{-2}	5.33×10^6		
	3.86×10^{-2}	6.17×10^6		
	5.24×10^{-2}	7.49×10^6		
	7.00×10^{-2}	8.17×10^6		
$[E33-PAr_3^+ SbF_6^-] / M$	$[N14] / M$	k_{obs} / s^{-1}	$\lambda = 445\text{ nm}$	$k_2 / M^{-1} s^{-1}$
6.85×10^{-5} (Ar = <i>p</i> -ClC ₆ H ₄)	5.26×10^{-2}	9.69×10^6		1.06×10^8
	8.28×10^{-2}	1.26×10^7		
	1.07×10^{-1}	1.49×10^7		
	1.60×10^{-1}	2.06×10^7		
	1.84×10^{-1}	2.38×10^7		
	2.10×10^{-1}	2.60×10^7		

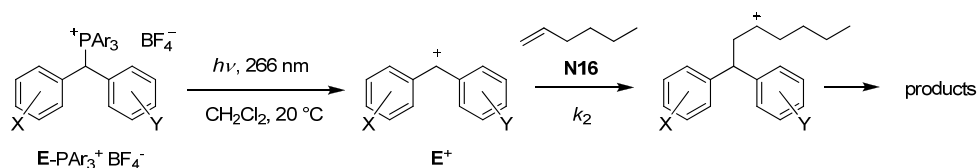
3.S.2.15 Reactions of benzhydrylium ions (E^+) with 2-chloropropene (**N15**) in dichloromethane at 20 °C.



When $(tol)_2CH-Cl$ (**E20-Cl**), $pfp(Ph)CH-Cl$ (**E23-Cl**), Ph_2CH-Cl (**E25-Cl**), or 3-chlorobenzhydryl chloride were ionized with $TiCl_4$ or $GaCl_3$ at $-78^\circ C$ and reacted with **N15** in CH_2Cl_2 , the 1:1-adducts were trapped by the complex counterions, yielding 3,3-dichloro-1,1-diarylbutanes.^{1b,15}

$[E31-PAr_3^+ BF_4^-] / M$	$[N15] / M$	k_{obs} / s^{-1}	$\lambda = 440\text{ nm}$	$k_2 / M^{-1} s^{-1}$
5.79×10^{-5}	1.11×10^{-2}	2.49×10^6		6.68×10^7
(Ar = <i>p</i> -ClC ₆ H ₄)	2.21×10^{-2}	3.19×10^6		
	3.32×10^{-2}	4.04×10^6		
	4.42×10^{-2}	4.78×10^6		
	5.53×10^{-2}	5.39×10^6		
$[E32-PAr_3^+ SbF_6^-] / M$	$[N15] / M$	k_{obs} / s^{-1}	$\lambda = 441\text{ nm}$	$k_2 / M^{-1} s^{-1}$
5.88×10^{-5}	1.19×10^{-2}	6.35×10^6		1.20×10^8
(Ar = <i>p</i> -ClC ₆ H ₄)	2.37×10^{-2}	7.81×10^6		
	3.56×10^{-2}	9.24×10^6		
	4.75×10^{-2}	1.08×10^7		
	5.93×10^{-2}	1.20×10^7		

3.S.2.16 Reactions of benzhydrylium ions (E^+) with 1-hexene (**N16**) in dichloromethane at 20 °C.



When $tol(Ph)CH^+$ (**E21**⁺), $pfp(Ph)CH^+$ (**E23**⁺), or Ph_2CH^+ (**E25**⁺) were generated from the corresponding benzhydryl chlorides using $TiCl_4$ as Lewis acid and combined with **N16** in CH_2Cl_2 , the 1:1-adducts were trapped by $TiCl_5^-$, yielding 3-chloro-1,1-diarylheptanes.^{S2d}

$[E31-PAr_3^+ BF_4^-] / M$	$[N16] / M$	k_{obs} / s^{-1}	$\lambda = 440\text{ nm}$	$k_2 / M^{-1} s^{-1}$
5.73×10^{-5} (Ar = <i>p</i> -ClC ₆ H ₄)	9.16×10^{-2}	2.16×10^6		5.77×10^6
	1.98×10^{-1}	3.26×10^6		
	3.05×10^{-1}	3.40×10^6		
	4.17×10^{-1}	4.20×10^6		
$[E32-PAr_3^+ SbF_6^-] / M$	$[N16] / M$	k_{obs} / s^{-1}	$\lambda = 441\text{ nm}$	$k_2 / M^{-1} s^{-1}$
5.80×10^{-5} (Ar = <i>p</i> -ClC ₆ H ₄)	6.40×10^{-2}	7.55×10^6		2.31×10^7
	1.30×10^{-1}	9.11×10^6		
	1.91×10^{-1}	1.01×10^7		
	2.41×10^{-1}	1.14×10^7		
3.21×10^{-1}	1.36×10^7			
$[E33-PAr_3^+ SbF_6^-] / M$	$[N16] / M$	k_{obs} / s^{-1}	$\lambda = 450\text{ nm}$	$k_2 / M^{-1} s^{-1}$
5.40×10^{-5} (Ar = <i>p</i> -ClC ₆ H ₄)	6.43×10^{-2}	7.00×10^6		2.54×10^7
	1.31×10^{-1}	9.02×10^6		
	1.95×10^{-1}	1.07×10^7		
	2.57×10^{-1}	1.19×10^7		
3.20×10^{-1}	1.36×10^7			

3.S.3 Correlation analysis for the reactions of electrophiles with π -nucleophiles in CH_2Cl_2

3.S.3.1 Data set

Table 3.S.3.1 lists the experimental second-order rate constants $k_2(20\text{ }^\circ\text{C})$ determined in this work, supplemented by relevant literature data for the reactions of benzhydryl cations \mathbf{E}^+ with the π -nucleophiles $\mathbf{N(1-18)}$ ^{1b,15,18,22,23a,27} and with further previously used reference nucleophiles.^{1b} As discussed in the article, only reactions with $k_2(20\text{ }^\circ\text{C}) \leq 1.0 \times 10^8\text{ M}^{-1}\text{ s}^{-1}$ were used for the correlation analysis. Rate constants determined in acetonitrile, which were included in the original correlation analysis,^{1b} were excluded from the correlation in this work.

Some rate constants $k_2(T)$ taken from the literature were determined at lower temperatures than $20\text{ }^\circ\text{C}$ and converted to $T = 293.16\text{ K}$ using the Eyring equation (eq. 3.S.3.1) and the relationship $\Delta G^\ddagger = \Delta H^\ddagger - T\Delta S^\ddagger$. By substituting the $k_2(T)$ and the activation entropies ΔS^\ddagger into eq. 3.S.3.1, we calculated ΔH^\ddagger from which we obtained the rate constants $k_2(293.16\text{ K})$ from eq. 3.S.3.1.

$$k = \frac{k_{\text{B}}T}{h} \cdot e^{\frac{-\Delta G^\ddagger}{RT}} \quad (3.S.3.1)$$

In some cases, the activation entropies ΔS^\ddagger were not available and we estimated the ΔS^\ddagger values based on known ΔS^\ddagger for structurally analogous systems (see footnotes in Table 3.S.3.1; note that this procedure is only applicable for reactions in the isoentropic regime³³).

Table 3.S.3.1. Experimental second-order rate constants k_2 ($\text{M}^{-1} \text{s}^{-1}$) for reactions of electrophiles E^+ with π -nucleophiles and comparison with rate constants k_{calc} ($\text{M}^{-1} \text{s}^{-1}$) calculated from eq. 1.

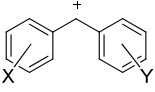
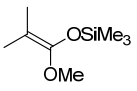
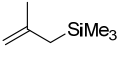
nucleophile N , s_N		experiment			correlation analysis			
		E^+	abbreviation	E	$k_2 / \text{M}^{-1} \text{s}^{-1}$	ref.	used? ^a	$k_{\text{calc}}^b / \text{M}^{-1} \text{s}^{-1}$
 N1 $N = 9.00, {}^c s_N = 0.98^c$	E2^+	(jul) ₂ CH ⁺	-9.45 ^c	3.16×10^{-1}	1b	●	3.62×10^{-1}	1.15
	E5^+	(pyr) ₂ CH ⁺	-7.69 ^c	2.32×10^1	1b	●	1.92×10^1	0.83
	E6^+	(dma) ₂ CH ⁺	-7.02 ^c	7.96×10^1	1b	●	8.72×10^1	1.10
	E9^+	(dpa) ₂ CH ⁺	-4.72 ^c	1.66×10^4	1b	●	1.56×10^4	0.94
	E11^+	(pfa) ₂ CH ⁺	-3.14 ^c	4.80×10^5	1b	●	5.53×10^5	1.15
	E13^+	(fur) ₂ CH ⁺	-1.36 ^c	1.86×10^7	<i>d</i>	●	3.07×10^7	1.65
	E14^+	fur(ani)CH ⁺	-0.81	4.47×10^7	<i>d</i>	✓	1.06×10^8	2.38
	E15^+	(ani) ₂ CH ⁺	0.00 ^c	1.54×10^8	<i>d</i>	●	(6.61×10^8)	(4.29)
	E17^+	ani(tol)CH ⁺	1.48 ^c	4.14×10^8	<i>d</i>	●	(1.86×10^{10})	(44.9)
	E20^+	(tol) ₂ CH ⁺	3.63 ^c	1.02×10^9	<i>d</i>	●	(2.38×10^{12})	(2.3×10^3)
E25^+	(Ph) ₂ CH ⁺	5.47	1.15×10^9	<i>d</i>	✗	(1.52×10^{14})	(1.3×10^5)	
E30^+	(mfp) ₂ CH ⁺	6.87	1.52×10^9	<i>d</i>	✗	(3.57×10^{15})	(2.3×10^6)	
 N2 $N = 6.57, {}^c s_N = 0.93^c$	E3^+	(ind) ₂ CH ⁺	-8.76 ^c	9.44×10^{-3}	1b	●	9.19×10^{-3}	0.97
	E4^+	(thq) ₂ CH ⁺	-8.22 ^c	2.68×10^{-2}	1b	●	2.92×10^{-2}	1.09
	E6^+	(dma) ₂ CH ⁺	-7.02 ^c	3.61×10^{-1}	1b	●	3.82×10^{-1}	1.06
	E7^+	(mpa) ₂ CH ⁺	-5.89 ^c	4.52	1b	●	4.29	0.95
	E8^+	(mor) ₂ CH ⁺	-5.53 ^c	1.05×10^1	1b	●	9.27	0.88
	E9^+	(dpa) ₂ CH ⁺	-4.72 ^c	5.80×10^1	1b	●	5.25×10^1	0.91
	E10^+	(mfa) ₂ CH ⁺	-3.85 ^c	3.20×10^2	1b	●	3.39×10^2	1.06
	E12^+	fc(Ph)CH ⁺	-2.64 ^c	3.31×10^3	1b	●	4.52×10^3	1.36
	E13^+	(fur) ₂ CH ⁺	-1.36 ^c	9.36×10^4	1b	●	7.00×10^4	0.75
	E16^+	ani(pop)CH ⁺	0.61 ^c	5.34×10^6	<i>d</i>	●	4.76×10^6	0.89
	E18^+	ani(Ph)CH ⁺	2.11 ^c	6.64×10^7	<i>d</i>	●	1.18×10^8	1.78
	E20^+	(tol) ₂ CH ⁺	3.63 ^c	3.00×10^8	<i>d</i>	●	(3.06×10^9)	(10.2)
	E25^+	(Ph) ₂ CH ⁺	5.47	9.39×10^8	<i>d</i>	✗	(1.57×10^{11})	(168)
E30^+	(mfp) ₂ CH ⁺	6.87	1.73×10^9	<i>d</i>	✗	(3.16×10^{12})	(1.8×10^3)	
 N3 $N = 4.41, {}^c s_N = 0.96^c$	E6^+	(dma) ₂ CH ⁺	-7.02 ^c	3.04×10^{-3}	1b	●	3.12×10^{-3}	1.03
	E7^+	(mpa) ₂ CH ⁺	-5.89 ^c	3.64×10^{-2}	1b	●	3.79×10^{-2}	1.04
	E8^+	(mor) ₂ CH ⁺	-5.53 ^c	8.54×10^{-2}	1b	●	8.41×10^{-2}	0.98
	E9^+	(dpa) ₂ CH ⁺	-4.72 ^c	6.13×10^{-1}	1b	●	5.04×10^{-1}	0.82
	E10^+	(mfa) ₂ CH ⁺	-3.85 ^c	2.97	1b	●	3.45	1.16
	E11^+	(pfa) ₂ CH ⁺	-3.14 ^c	1.35×10^1	1b	●	1.66×10^1	1.23
	E12^+	fc(Ph)CH ⁺	-2.64 ^c	5.45×10^1	1b	●	5.00×10^1	0.92
	E13^+	(fur) ₂ CH ⁺	-1.36 ^c	1.16×10^3	1b	●	8.47×10^2	0.73
	E15^+	(ani) ₂ CH ⁺	0.00 ^c	1.53×10^4	1b, e	●	1.71×10^4	1.12
	E20^+	(tol) ₂ CH ⁺	3.63 ^c	2.81×10^7	<i>d</i>	●	5.23×10^7	1.86
	E21^+	tol(Ph)CH ⁺	4.43	1.23×10^8	<i>d</i>	✗	(3.06×10^8)	(2.49)
	E25^+	(Ph) ₂ CH ⁺	5.47	3.97×10^8	<i>d</i>	✗	(3.05×10^9)	(7.69)
	E30^+	(mfp) ₂ CH ⁺	6.87	1.14×10^9	<i>d</i>	✗	(6.74×10^{10})	(59.1)
E31^+	dfp(mfp)CH ⁺	7.52	1.21×10^9	<i>d</i>	✗	(2.48×10^{11})	(243)	

Table 3.S.3.1 (continued).

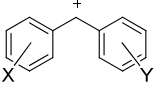
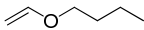
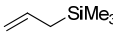
nucleophile N, s_N		experiment				correlation analysis		
		E^+	abbreviation	E	$k_2 / M^{-1} s^{-1}$	ref.	used? ^a	$k_{\text{calc}}^b / M^{-1} s^{-1}$
 N4 $N = 3.76, s_N = 0.91$	E9⁺	(dpa) ₂ CH ⁺	-4.72 ^c	1.06×10^{-1}	22	✓	1.34×10^{-1}	1.26
	E10⁺	(mfa) ₂ CH ⁺	-3.85 ^c	7.49×10^{-1}	<i>f</i>	✓	8.28×10^{-1}	1.11
	E14⁺	fur(ani)CH ⁺	-0.81	7.65×10^2	<i>g</i>	✓	4.84×10^2	0.63
	E20⁺	(tol) ₂ CH ⁺	3.63 ^c	6.51×10^6	<i>d</i>	✓	5.31×10^6	0.82
	E21⁺	tol(Ph)CH ⁺	4.43	3.09×10^7	<i>d</i>	✓	2.84×10^7	0.92
	E22⁺	(pfp) ₂ CH ⁺	5.01	6.37×10^7	<i>d</i>	✓	9.57×10^7	1.50
	E25⁺	(Ph) ₂ CH ⁺	5.47	1.59×10^8	<i>d</i>	✗	(2.51×10^8)	(1.58)
	E26⁺	(pcp) ₂ CH ⁺	5.48	1.60×10^8	<i>d</i>	✗	(2.56×10^8)	(1.60)
	E30⁺	(mfp) ₂ CH ⁺	6.87	6.58×10^8	<i>d</i>	✗	(4.71×10^9)	(8.82)
	E31⁺	dfp(mfp)CH ⁺	7.52	1.35×10^9	<i>d</i>	✗	(1.84×10^{10})	(13.6)
 N5 $N = 1.18, s_N = 1.17$	E18⁺	ani(Ph)CH ⁺	2.11 ^c	5.46×10^3 ^h	27a	✓	7.07×10^3	1.29
	E20⁺	(tol) ₂ CH ⁺	3.63 ^c	2.5×10^5 ⁱ	<i>d</i>	✓	4.24×10^5	0.76
	E21⁺	tol(Ph)CH ⁺	4.43	6.13×10^6	<i>d</i>	✓	3.66×10^6	0.60
	E22⁺	(pfp) ₂ CH ⁺	5.01	1.53×10^7	<i>d</i>	✓	1.75×10^7	1.14
	E23⁺	pfp(Ph)CH ⁺	5.20	3.49×10^7	<i>d</i>	✓	2.91×10^7	0.84
	E24⁺	–	5.24	3.17×10^7	<i>d</i>	✓	3.25×10^7	1.02
	E25⁺	(Ph) ₂ CH ⁺	5.47	5.91×10^7	<i>d</i>	✓	6.03×10^7	1.02
	E26⁺	(pcp) ₂ CH ⁺	5.48	4.72×10^7	<i>d</i>	✓	6.20×10^7	1.31
	E27⁺	mfp(Ph)CH ⁺	6.23	1.76×10^8	<i>d</i>	✗	(4.67×10^8)	(2.66)
	E30⁺	(mfp) ₂ CH ⁺	6.87	5.87×10^8	<i>d</i>	✗	(2.62×10^9)	(4.47)
	E31⁺	dfp(mfp)CH ⁺	7.52	1.33×10^9	<i>d</i>	✗	(1.51×10^{10})	(11.4)
 N6 $N = 2.82, s_N = 0.89$	E12⁺	fc(Ph)CH ⁺	-2.64 ^c	1.51	1b	✓	1.45	0.96
	E15⁺	(ani) ₂ CH ⁺	0.00 ^c	2.96×10^2	1b, e	✓	3.23×10^2	1.09
	E17⁺	ani(tol)CH ⁺	1.48 ^c	6.15×10^3	1b, e	✓	6.71×10^3	1.09
	E18⁺	ani(Ph)CH ⁺	2.11 ^c	2.04×10^4	1b	✓	2.44×10^4	1.20
	E19⁺	pop(Ph)CH ⁺	2.90 ^c	1.35×10^5	1b, e	✓	1.23×10^5	0.91
	E27⁺	mfp(Ph)CH ⁺	6.23	1.44×10^8	<i>d</i>	✗	(1.13×10^8)	(0.79)
 N7 $N = 1.68, s_N = 1.00$	E13⁺	(fur) ₂ CH ⁺	-1.36 ^c	2.14	1b	✓	2.09	0.98
	E14⁺	fur(ani)CH ⁺	-0.81	9.95	23a	✓	7.41	0.75
	E15⁺	(ani) ₂ CH ⁺	0.00 ^c	4.69×10^1	1b	✓	4.79×10^1	1.02
	E17⁺	ani(tol)CH ⁺	1.48 ^c	1.41×10^3	1b	✓	1.45×10^3	1.03
	E18⁺	ani(Ph)CH ⁺	2.11 ^c	4.48×10^3	1b	✓	6.17×10^3	1.38
	E19⁺	pop(Ph)CH ⁺	2.90 ^c	3.31×10^4	1b	✓	3.80×10^4	1.15
	E20⁺	(tol) ₂ CH ⁺	3.63 ^c	1.22×10^5	1b, e	✓	2.04×10^5	1.67
	E21⁺	tol(Ph)CH ⁺	4.43	2.49×10^6	<i>d</i>	✓	1.29×10^6	0.52
	E22⁺	(pfp) ₂ CH ⁺	5.01	5.68×10^6	<i>d</i>	✓	4.90×10^6	0.86
	E23⁺	pfp(Ph)CH ⁺	5.20	1.06×10^7	<i>d</i>	✓	7.59×10^6	0.72
	E24⁺	–	5.24	9.17×10^6	<i>d</i>	✓	8.32×10^6	0.91
	E25⁺	(Ph) ₂ CH ⁺	5.47	1.50×10^7	18	✓	1.41×10^7	0.94
	E26⁺	(pcp) ₂ CH ⁺	5.48	1.54×10^7	<i>d</i>	✓	1.45×10^7	0.94
	E27⁺	mfp(Ph)CH ⁺	6.23	6.19×10^7	<i>d</i>	✓	8.13×10^7	1.31
E28⁺	tfm(Ph)CH ⁺	6.70	1.52×10^8	<i>d</i>	✗	(2.40×10^8)	(1.58)	
E30⁺	(mfp) ₂ CH ⁺	6.87	2.13×10^8	<i>d</i>	✗	(3.55×10^8)	(1.67)	

Table 3.S.3.1 (continued).

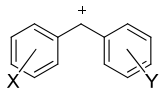
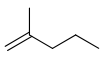
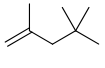
nucleophile N, s_N		experiment				correlation analysis		
		E^+	abbreviation	E	$k_2 / M^{-1} s^{-1}$	ref.	used? ^a	$k_{\text{calc}}^b / M^{-1} s^{-1}$
 N8 $N = 0.84, s_N = 1.06$	E15⁺	(ani) ₂ CH ⁺	0.00 ^c	9.35	1b	✓	7.77	0.83
	E16⁺	ani(pop)CH ⁺	0.61 ^c	3.65×10^1	1b, e	✓	3.44×10^1	0.94
	E17⁺	ani(tol)CH ⁺	1.48 ^c	2.99×10^2	1b	✓	2.88×10^2	0.96
	E18⁺	ani(Ph)CH ⁺	2.11 ^c	1.12×10^3	1b	✓	1.34×10^3	1.20
	E19⁺	pop(Ph)CH ⁺	2.90 ^c	6.65×10^3	1b	✓	9.21×10^3	1.39
	E20⁺	(tol) ₂ CH ⁺	3.63 ^c	4.01×10^4	1b	✓	5.47×10^4	1.36
	E22⁺	(pfp) ₂ CH ⁺	5.01	1.33×10^6	d	✓	1.59×10^6	1.19
	E23⁺	pfp(Ph)CH ⁺	5.20	4.55×10^6	d	✓	2.53×10^6	0.56
	E24⁺	–	5.24	2.79×10^6	d	✓	2.78×10^6	1.00
	E25⁺	(Ph) ₂ CH ⁺	5.47	5.69×10^6	d	✓	4.88×10^6	0.86
	E26⁺	(pcp) ₂ CH ⁺	5.48	5.00×10^6	d	✓	5.00×10^6	1.00
	E27⁺	mfp(Ph)CH ⁺	6.23	2.95×10^7	d	✓	3.12×10^7	1.06
	E28⁺	tfm(Ph)CH ⁺	6.70	9.51×10^7	d	✓	9.83×10^7	1.03
E29⁺	dfp(Ph)CH ⁺	6.74	9.16×10^7	d	✓	1.08×10^8	1.18	
E30⁺	(mfp) ₂ CH ⁺	6.87	1.37×10^8	d	✗	(1.49×10^8)	(1.09)	
 N9 $N = 1.16, s_N = 1.04$	E18⁺	ani(Ph)CH ⁺	2.11 ^c	2.56×10^3	27b	✓	2.52×10^3	0.98
	E22⁺	(pfp) ₂ CH ⁺	5.01	2.26×10^6	d	✓	2.61×10^6	1.16
	E25⁺	(Ph) ₂ CH ⁺	5.47	9.86×10^6	d	✓	7.86×10^6	0.80
	E27⁺	mfp(Ph)CH ⁺	6.23	4.68×10^7	d	✓	4.85×10^7	1.04
	E30⁺	(mfp) ₂ CH ⁺	6.87	1.47×10^8	d	✗	(2.24×10^8)	(1.53)
	E31⁺	dfp(mfp)CH ⁺	7.52	3.47×10^8	d	✗	(1.06×10^9)	(3.07)
 N10 $N = 0.79, s_N = 1.07$	E18⁺	ani(Ph)CH ⁺	2.11 ^c	1.26×10^3	27a	✓	1.27×10^3	1.01
	E22⁺	(pfp) ₂ CH ⁺	5.01	1.50×10^6	d	✓	1.61×10^6	1.07
	E25⁺	(Ph) ₂ CH ⁺	5.47	6.61×10^6	d	✓	4.99×10^6	0.76
	E27⁺	mfp(Ph)CH ⁺	6.23	2.91×10^7	d	✓	3.25×10^7	1.12
	E30⁺	(mfp) ₂ CH ⁺	6.87	1.82×10^8	d	✗	(1.57×10^8)	(0.86)
 N11 $N = 0.65, s_N = 1.00$	E18⁺	ani(Ph)CH ⁺	2.11 ^c	4.51×10^2	27a	✓	5.75×10^2	1.28
	E25⁺	(Ph) ₂ CH ⁺	5.47	1.93×10^6	d	✓	1.32×10^6	0.68
	E26⁺	(pcp) ₂ CH ⁺	5.48	1.46×10^6	d	✓	1.35×10^6	0.92
	E27⁺	mfp(Ph)CH ⁺	6.23	1.11×10^7	d	✓	7.59×10^6	0.68
	E28⁺	tfm(Ph)CH ⁺	6.70	2.11×10^7	d	✓	2.24×10^7	1.06
	E29⁺	dfp(Ph)CH ⁺	6.74	2.35×10^7	d	✓	2.45×10^7	1.04
	E30⁺	(mfp) ₂ CH ⁺	6.87	4.11×10^7	d	✓	3.31×10^7	0.81
E31⁺	dfp(mfp)CH ⁺	7.52	8.24×10^7	18	✓	1.48×10^8	1.80	
 N12 $N = 0.06, s_N = 1.07$	E18⁺	ani(Ph)CH ⁺	2.11 ^c	1.48×10^2	27a	✓	2.10×10^2	1.42
	E25⁺	(Ph) ₂ CH ⁺	5.47	2.16×10^6	d	✓	8.26×10^5	0.38
	E27⁺	mfp(Ph)CH ⁺	6.23	6.32×10^6	d	✓	5.37×10^6	0.85
	E30⁺	(mfp) ₂ CH ⁺	6.87	2.42×10^7	d	✓	2.60×10^7	1.07
	E31⁺	dfp(mfp)CH ⁺	7.52	7.52×10^7	d	✓	1.29×10^8	1.72

Table 3.S.3.1 (continued).

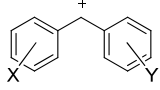
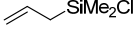
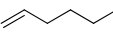
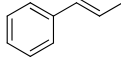
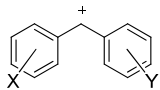
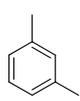
nucleophile N, s_N		experiment			correlation analysis			
		E^+	abbreviation	E	$k_2 / M^{-1} s^{-1}$	ref.	used? ^a	$k_{\text{calc}}^b / M^{-1} s^{-1}$
 N13 $N = -0.25, s_N = 1.09$	E18 ⁺	ani(Ph)CH ⁺	2.11 ^c	8.83×10^1	27a	✓	1.07×10^2	1.21
	E25 ⁺	(Ph) ₂ CH ⁺	5.47	6.96×10^5	<i>d</i>	✓	4.90×10^5	0.70
	E27 ⁺	mfp(Ph)CH ⁺	6.23	3.57×10^6	<i>d</i>	✓	3.30×10^6	0.92
	E28 ⁺	tfm(Ph)CH ⁺	6.70	1.20×10^7	<i>d</i>	✓	1.07×10^7	0.89
	E29 ⁺	dfp(Ph)CH ⁺	6.74	1.42×10^7	<i>d</i>	✓	1.19×10^7	0.84
	E30 ⁺	(mfp) ₂ CH ⁺	6.87	1.51×10^7	<i>d</i>	✓	1.64×10^7	1.09
	E31 ⁺	dfp(mfp)CH ⁺	7.52	5.24×10^7	<i>d</i>	✓	8.40×10^7	1.60
	E32 ⁺	(tfm) ₂ CH ⁺	(7.96) ^k	1.15×10^8	<i>d</i>	✗	(2.53×10^8)	(2.20)
	E33 ⁺	(dfp) ₂ CH ⁺	(8.02) ^k	1.24×10^8	<i>d</i>	✗	(2.95×10^8)	(2.38)
 N14 $N = -0.57, s_N = 1.06$	E15 ⁺	(ani) ₂ CH ⁺	0.00 ^c	3.15×10^{-1}	1b, e	✓	2.49×10^{-1}	0.79
	E18 ⁺	ani(Ph)CH ⁺	2.11 ^c	5.37×10^1	1b, e	✓	4.29×10^1	0.80
	E20 ⁺	(tol) ₂ CH ⁺	3.63 ^c	1.04×10^3	1b	✓	1.75×10^3	1.68
	E21 ⁺	tol(Ph)CH ⁺	4.43	8.84×10^3	1b, e	✓	1.23×10^4	1.40
	E31 ⁺	dfp(mfp)CH ⁺	7.52	3.94×10^7	<i>d</i>	✓	2.33×10^7	0.59
	E32 ⁺	(tfm) ₂ CH ⁺	(7.96) ^k	6.17×10^7	<i>d</i>	✓	6.81×10^7	1.10
	E33 ⁺	(dfp) ₂ CH ⁺	(8.02) ^k	1.06×10^8	<i>d</i>	✗	(7.89×10^7)	(0.74)
 N15 $N = -3.65, s_N = 1.97$	E20 ⁺	(tol) ₂ CH ⁺	3.63 ^c	2.32	1b	✓	9.13×10^{-1}	0.39
	E21 ⁺	tol(Ph)CH ⁺	4.43	1.85×10^1	1b	✓	3.44×10^1	1.86
	E23 ⁺	pfp(Ph)CH ⁺	5.20	8.95×10^2	1b	✓	1.13×10^3	1.26
	E25 ⁺	(Ph) ₂ CH ⁺	5.47	2.23×10^3	1b	✓	3.85×10^3	1.73
	E31 ⁺	dfp(mfp)CH ⁺	7.52	6.68×10^7	<i>d</i>	✓	4.21×10^7	0.63
	E32 ⁺	(tfm) ₂ CH ⁺	(7.96) ^k	1.20×10^8	<i>d</i>	✗	(3.10×10^8)	(8.08)
 N16 $N = -2.77, s_N = 1.41$	E20 ⁺	(tol) ₂ CH ⁺	3.63 ^c	1.93×10^1	1b	✓	1.63×10^1	0.85
	E21 ⁺	tol(Ph)CH ⁺	4.43	2.75×10^2	1b, e	✓	2.19×10^2	0.80
	E22 ⁺	(pfp) ₂ CH ⁺	5.01	1.95×10^3	15	✓	1.44×10^3	0.74
	E23 ⁺	pfp(Ph)CH ⁺	5.20	1.69×10^3	1b, e	✓	2.67×10^3	1.58
	E25 ⁺	(Ph) ₂ CH ⁺	5.47	3.96×10^3	1b, e	✓	6.41×10^3	1.62
	E31 ⁺	dfp(mfp)CH ⁺	7.52	5.77×10^6	<i>d</i>	✓	4.98×10^6	0.86
	E32 ⁺	(tfm) ₂ CH ⁺	(7.96) ^k	2.31×10^7	<i>d</i>	✓	2.08×10^7	0.90
 N17 $N = 1.33, s_N = 1.29$	E12 ⁺	fc(Ph) ₂ CH ⁺	-2.64 ^c	1.83×10^{-2}	1b	✓	2.04×10^{-2}	1.12
	E13 ⁺	(fur) ₂ CH ⁺	-1.36 ^c	1.32	1b	✓	9.15×10^{-1}	0.69
	E14 ⁺	fur(ani)CH ⁺	-0.81	3.41	<i>f</i>	✓	4.69	1.37
	E15 ⁺	(ani) ₂ CH ⁺	0.00 ^c	5.43×10^1	1b	✓	5.20×10^1	0.96
 N18 $N = 1.35, s_N = 0.99$	E12 ⁺	fc(Ph) ₂ CH ⁺	-2.64 ^c	6.51×10^{-2}	1b	✓	5.28×10^{-2}	0.81
	E13 ⁺	(fur) ₂ CH ⁺	-1.36 ^c	4.59×10^{-1}	1b	✓	9.77×10^{-1}	2.13
	E14 ⁺	fur(ani)CH ⁺	-0.81	6.18	<i>f</i>	✓	3.42	0.55
	E15 ⁺	(ani) ₂ CH ⁺	0.00 ^c	2.13×10^1	1b	✓	2.17×10^1	1.02
 N19 $N = -0.49, s_N = 1.18$	E17 ⁺	ani(tol)CH ⁺	1.48 ^c	1.16×10^1	1b, e	✓	1.47×10^1	1.27
	E18 ⁺	ani(Ph)CH ⁺	2.11 ^c	9.41×10^1	1b	✓	8.16×10^1	0.87
	E19 ⁺	pop(Ph)CH ⁺	2.90 ^c	9.03×10^2	1b, e	✓	6.98×10^2	0.77
	E20 ⁺	(tol) ₂ CH ⁺	3.63 ^c	4.41×10^3	1b, e	✓	5.07×10^3	1.15
	E21 ⁺	tol(Ph)CH ⁺	4.43	4.00×10^4	1b, e	✓	4.46×10^4	1.11

Table 3.S.3.1 (continued).

nucleophile N, s_N			experiment			correlation analysis		
	E^+	abbreviation	E	$k_2 / M^{-1} s^{-1}$	ref.	used? ^a	$k_{\text{calc}}^b / M^{-1} s^{-1}$	k_{calc} / k_2
 N20 $N = -3.57, s_N = 2.08$	E20⁺	(tol) ₂ CH ⁺	3.63 ^c	1.19	^{1b}	✓	1.33	1.12
	E21⁺	tol(Ph)CH ⁺	4.43	6.38×10^1	^{1b}	✓	6.15×10^1	0.96
	E22⁺	(pfp) ₂ CH ⁺	5.01	1.20×10^3	^{1b}	✓	9.89×10^2	0.82
	E25⁺	(Ph) ₂ CH ⁺	5.47	6.45×10^3	^{1b}	✓	8.95×10^3	1.39
	E26⁺	(pcp) ₂ CH ⁺	5.48	1.01×10^4	^{1b}	✓	9.39×10^3	0.93
 N21 $N = -4.36, s_N = 1.77$	E22⁺	(pfp) ₂ CH ⁺	5.01	1.43×10^1	^{1b}	✓	1.41×10^1	0.99
	E23⁺	pfp(Ph)CH ⁺	5.20	2.98×10^1	^{1b}	✓	3.07×10^1	1.03
	E25⁺	(Ph) ₂ CH ⁺	5.47	8.53×10^1	^{1b}	✓	9.22×10^1	1.08
	E26⁺	(pcp) ₂ CH ⁺	5.48	1.04×10^2	^{1b}	✓	9.60×10^1	0.92

^a Only rate constants $k_2 \leq 1.0 \times 10^8 M^{-1} s^{-1}$ were used for the correlation analysis (✓), larger rate constants were not used (✗). Electrophile/nucleophile combinations for which all E , N , and s_N parameters were kept constant are marked with a dot (●) and were also not used in the correlation analysis. ^b Calculated from eq. 1. Data points with $k_2 > 1.0 \times 10^8 M^{-1} s^{-1}$ are shown in parentheses as eq. 1 does not account for the limiting effect of diffusion. ^c These values were kept fixed to values obtained from the original correlation analysis. ^{1b, d} This work; laser flash photolysis. ^e Estimated activation entropies ΔS^\ddagger were used to calculate $k_2(20^\circ C)$ values in the original work. ^{1b, f} This work (C. Nolte); conventional UV/Vis spectrophotometry. ^g This work (C. Nolte); stopped-flow UV/Vis spectrophotometry. ^h An estimated activation entropy of $\Delta S^\ddagger = -136 J mol^{-1} K^{-1}$ was used to calculate $k_2(20^\circ C)$. ⁱ Determined from non-exponential decay curves as the reaction of **E20⁺** with **N5** does not follow pseudo-first-order kinetics due to recombination of **E20⁺** with the photo-leaving group PPh₃. See Section 3.S.2.5 for details. ^j An estimated activation entropy of $\Delta S^\ddagger = -120 J mol^{-1} K^{-1}$ was used to calculate $k_2(20^\circ C)$. ^k These E parameters are based on only 1 or 2 rate constants. ^l $k_{\text{calc}} = k_2$ since this is the only rate constant used for determining the E parameter of **E33⁺**.

3.S.3.2 Variables

Electrophilicity parameters. The electrophilicity parameters E of the electrophiles **E(1-20)⁺** were kept fixed at the values obtained in the previous correlation,^{1b} except for that of fur(ani)CH⁺ (**E14⁺**) which was not reported previously. The E parameters of **E(21-23)⁺** and **E(25,26)⁺** are revised in this work. The acceptor-substituted benzhydryl cations **E24⁺** and **E(27-33)⁺**, which have not been characterized previously, were included in the correlation analysis.

Nucleophilicity parameters. The N and s_N parameters of most π -systems that were employed as reference nucleophiles in the original correlation^{1b} are not affected by the new correlation analysis, because they were only characterized by reactions with **E(1-13)⁺** and **E(15-20)⁺** whose E parameters were kept constant. The N and s_N parameters of **N(1-3)** were also kept

constant, as these nucleophiles were only used to measure reactions close to the diffusion limit ($\lg k_2(20\text{ °C}) > 8.0$) and to characterize the electrophilicity of fur(ani)CH⁺ (**E14**⁺).

The N and s_N values of the nucleophiles **N(4-16)** as well as those of (*E*)-propenylbenzene, *m*-xylene and toluene were variable in the correlation analysis. The N and s_N parameters of **N17** and **N18** were also revised in this work because the previous values were based on only three rate constants $k_2(20\text{ °C})$ for reactions of each of these nucleophiles with reference electrophiles.

3.S.3.3 Least squares optimization

As in our previous treatment,^{1b} the reactivity parameters E , N and s_N , as defined by eq. 1,

$$\lg k_{\text{calc}}(20\text{ °C}) = s_N(N + E) \quad (1)$$

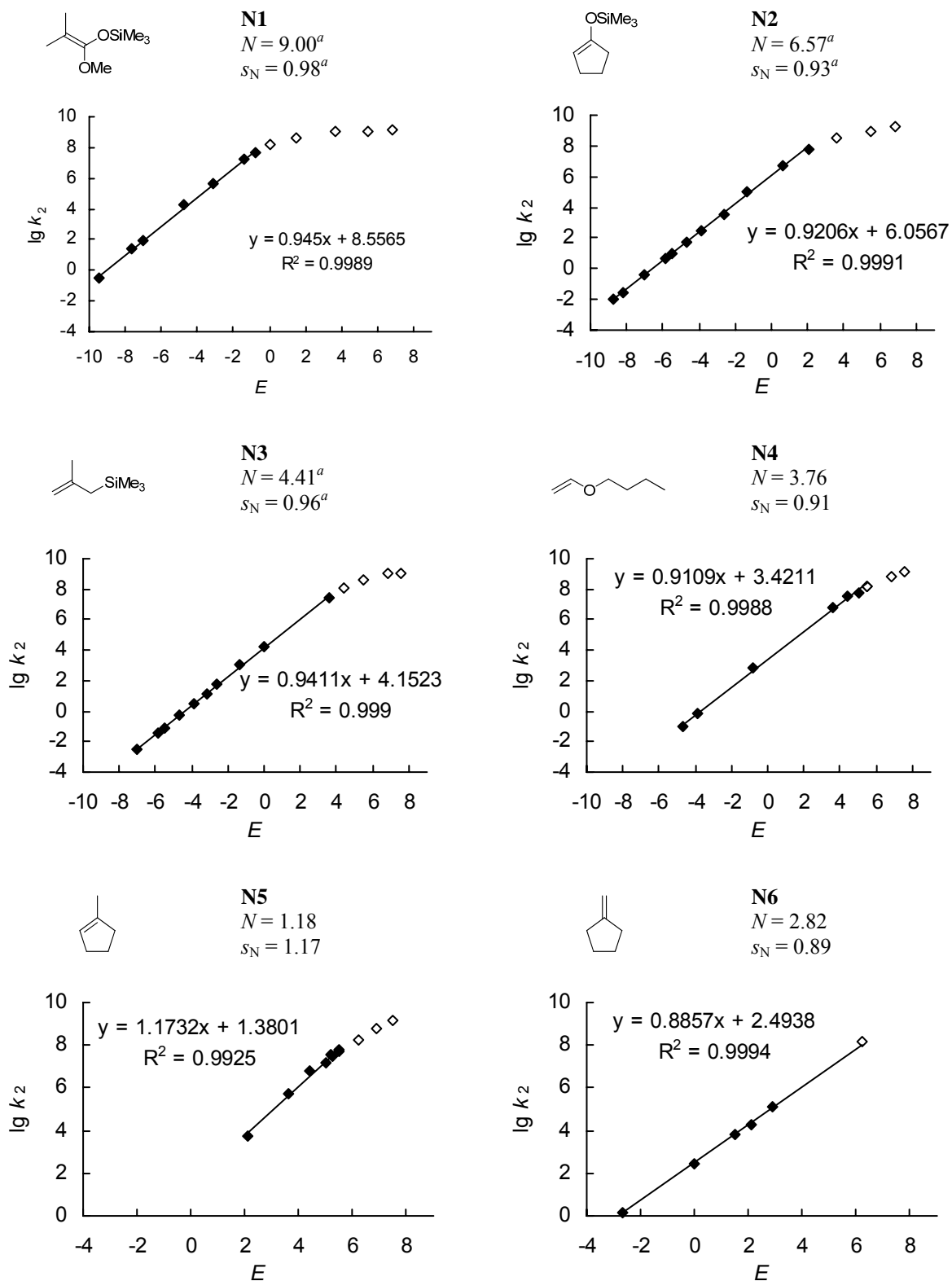
were calculated by a least squares optimization, minimizing Δ^2 as specified by eq. 2,

$$\Delta^2 = \sum (\lg k_2 - \lg k_{\text{calc}})^2 = \sum (\lg k_2 - s_N(N + E))^2 \quad (2)$$

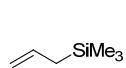
using the nonlinear solver program “What’sBest! 7.0 Industrial” by Lindo Systems Inc.³¹

Table 3.S.3.1 features a comparison of the experimental rate constants k_2 with the calculated rate constants k_{calc} obtained from the least squares optimization.

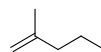
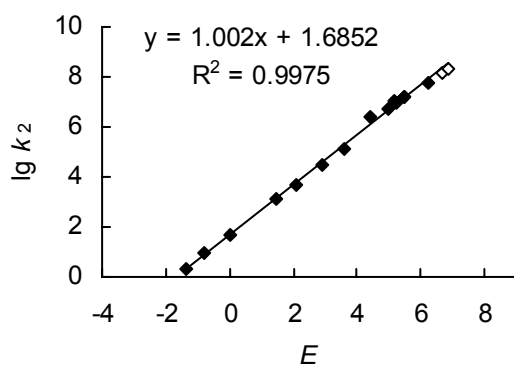
3.S.3.4 Plots of $\lg k_2$ versus E for nucleophiles N(1-18)



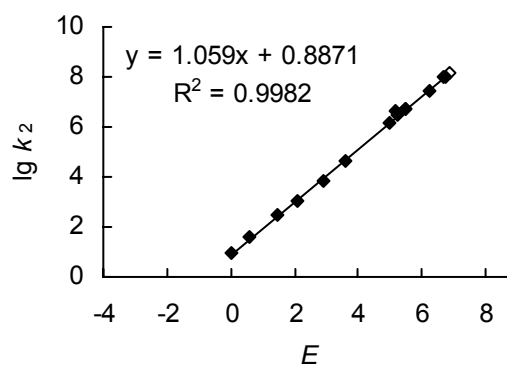
^a These N and s_N parameters from ref. 1b were not changed.



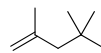
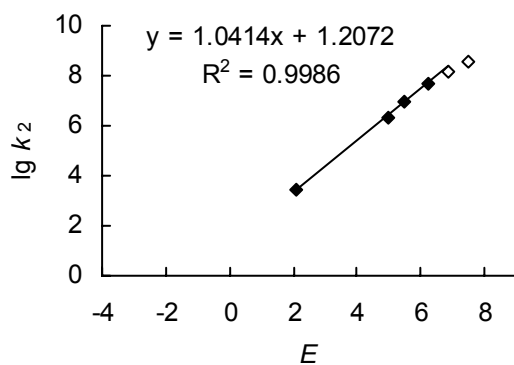
N7
 $N = 1.68$
 $s_N = 1.00$



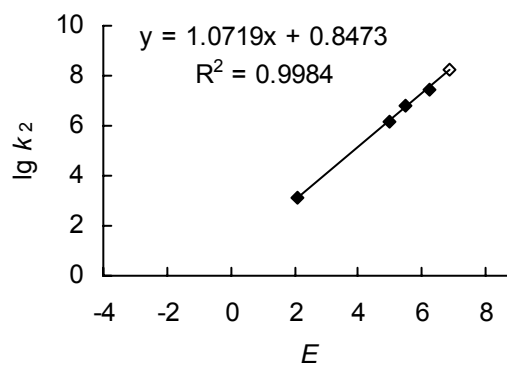
N8
 $N = 0.84$
 $s_N = 1.06$



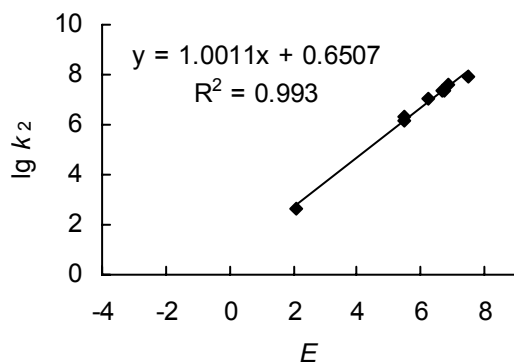
N9
 $N = 1.16$
 $s_N = 1.04$



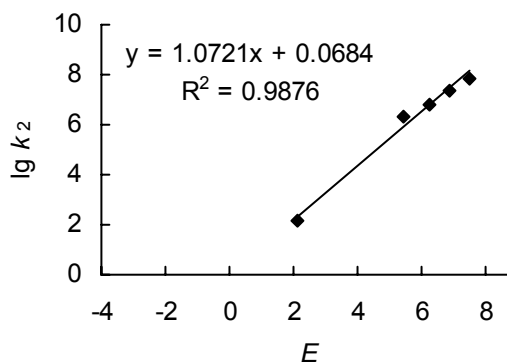
N10
 $N = 0.79$
 $s_N = 1.07$



N11
 $N = 0.65$
 $s_N = 1.00$



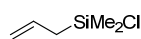
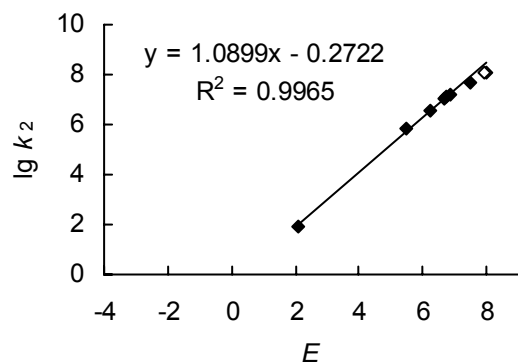
N12
 $N = 0.06$
 $s_N = 1.07$





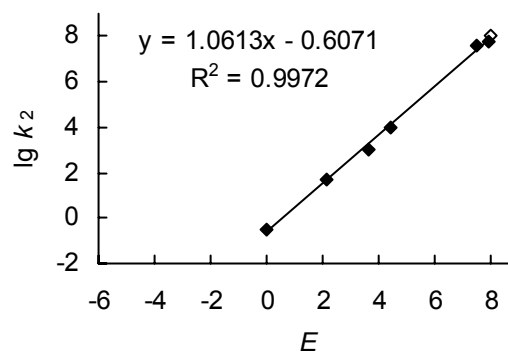
N13

$N = -0.25$
 $s_N = 1.09$



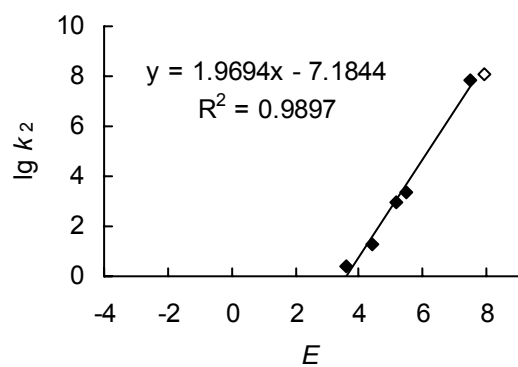
N14

$N = -0.57$
 $s_N = 1.06$



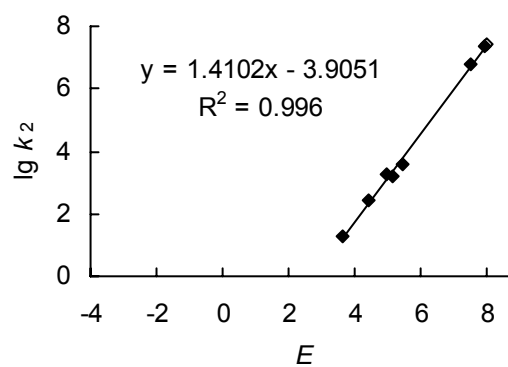
N15

$N = -3.65$
 $s_N = 1.97$



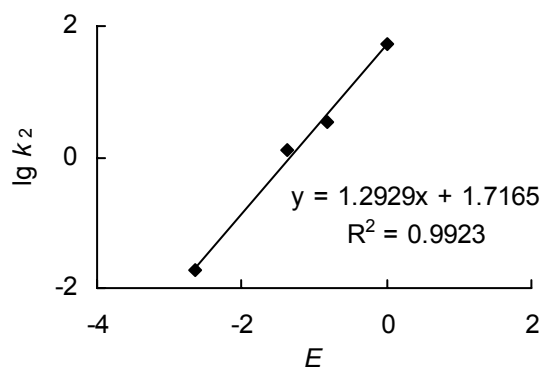
N16

$N = -2.77$
 $s_N = 1.41$



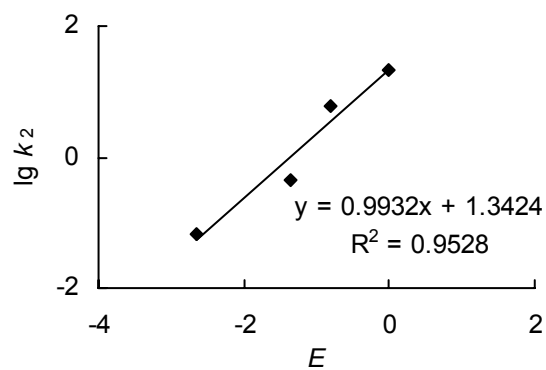
N17

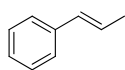
$N = 1.33$
 $s_N = 1.29$



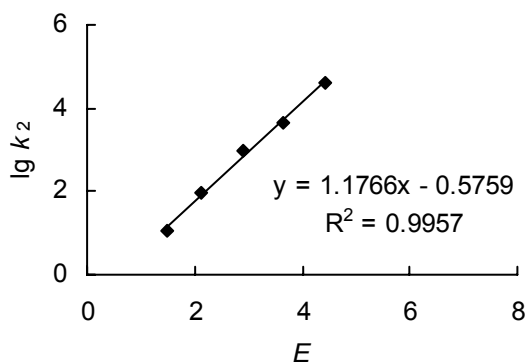
N18

$N = 1.35$
 $s_N = 0.99$

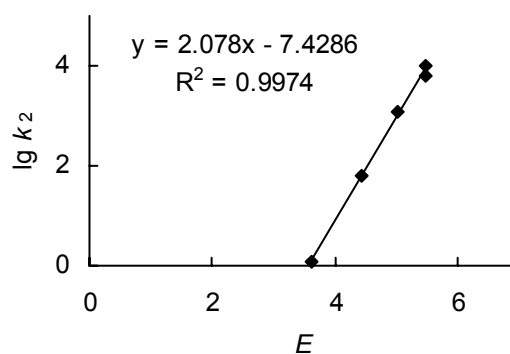




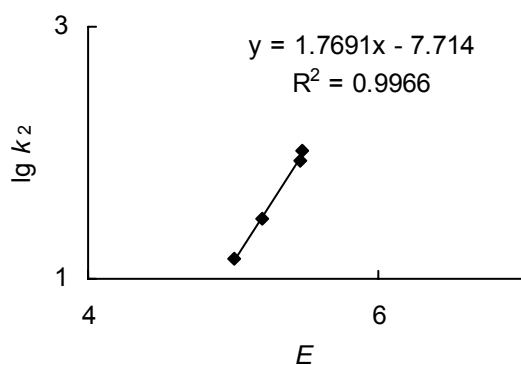
N19
 $N = -0.49$
 $s_N = 1.18$



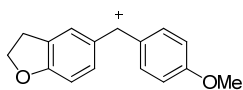
N20
 $N = -3.57$
 $s_N = 2.08$



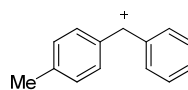
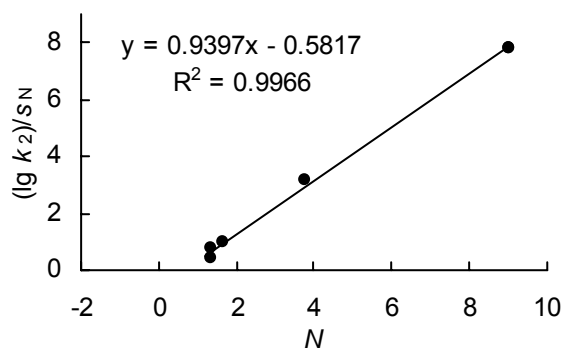
N21
 $N = -4.36$
 $s_N = 1.77$



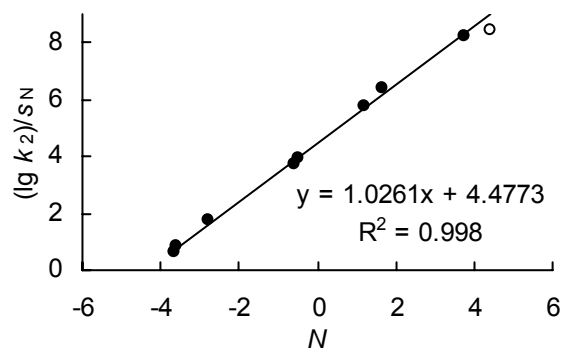
3.S.3.5 Plots of $(\lg k_2)/s_N$ versus N for electrophiles $E14^+$ and $E(21-33)^+$

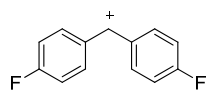


E14⁺
 $E = -0.81$

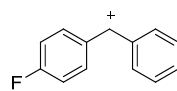
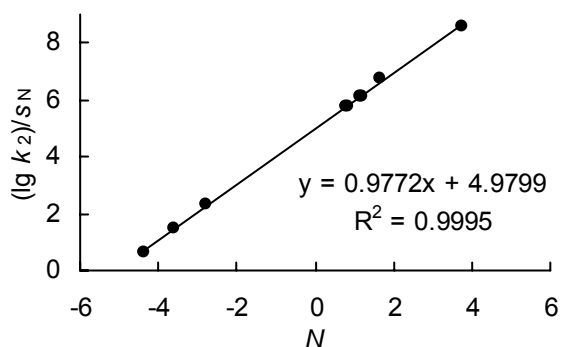


E21⁺
 $E = 4.43$

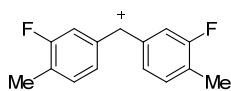
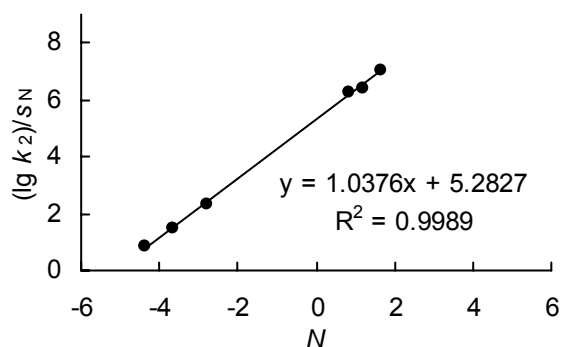




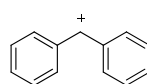
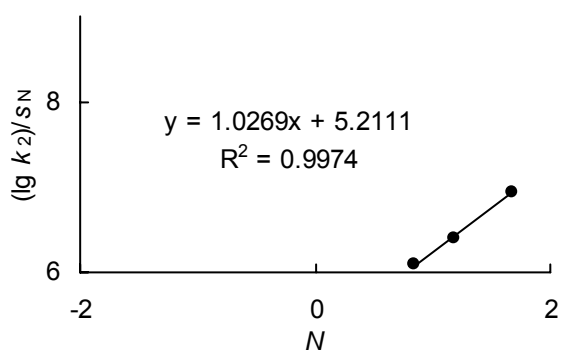
E22⁺
E = 5.01



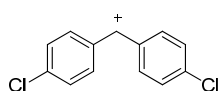
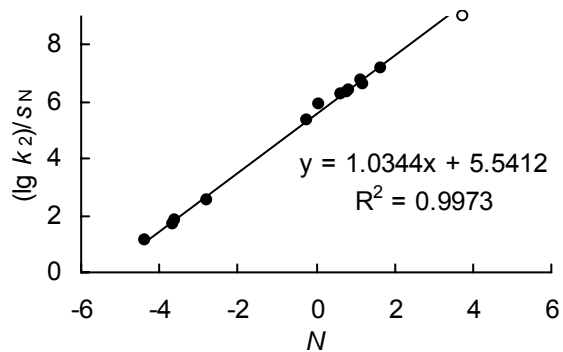
E23⁺
E = 5.20



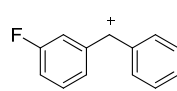
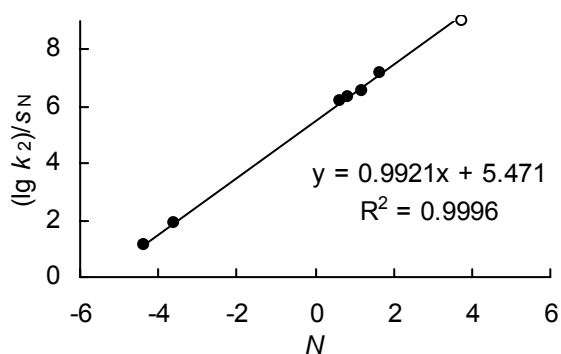
E24⁺
E = 5.24



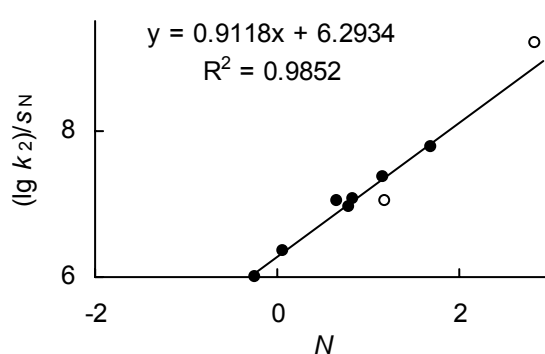
E25⁺
E = 5.47

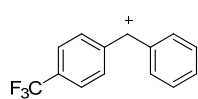


E26⁺
E = 5.48

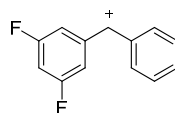
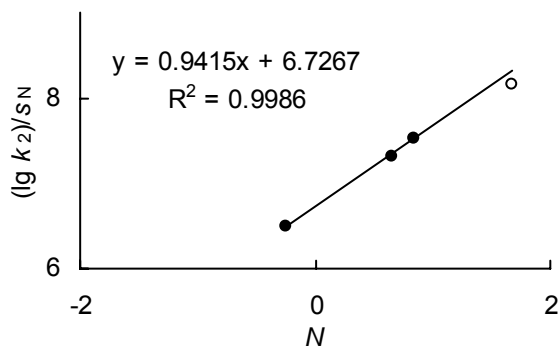


E27⁺
E = 6.23

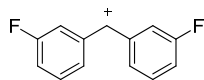
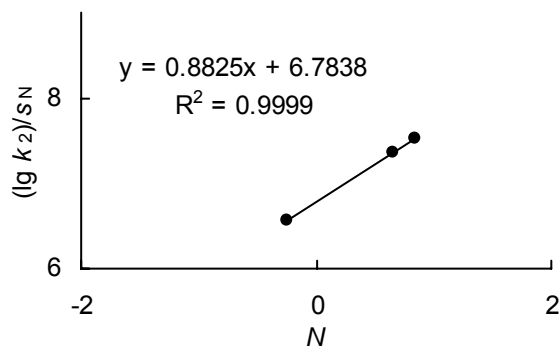




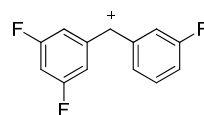
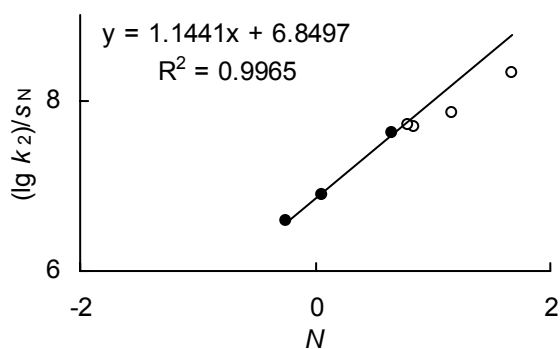
E28⁺
E = 6.70



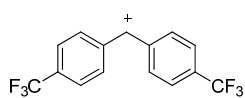
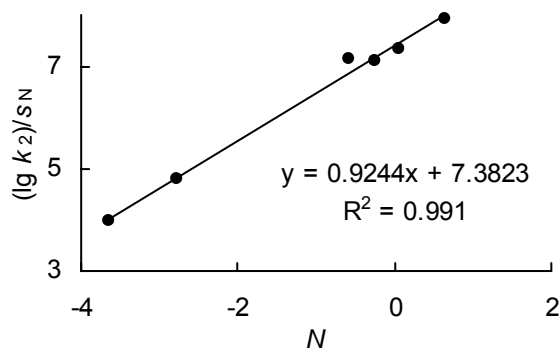
E29⁺
E = 6.74



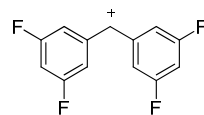
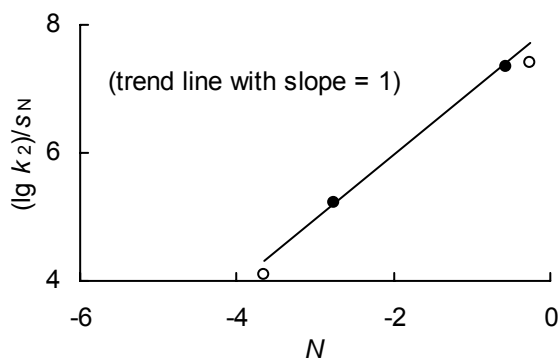
E30⁺
E = 6.87



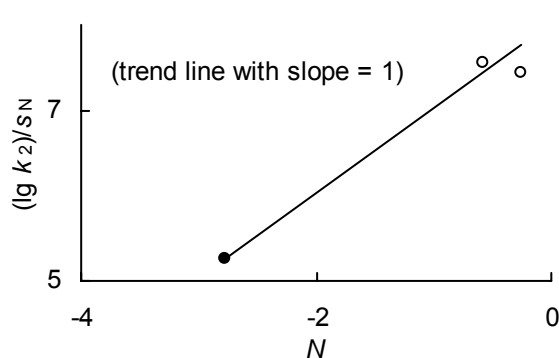
E31⁺
E = 7.52



E32⁺
E = 7.96

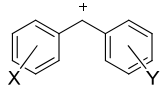
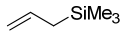
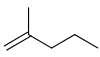


E33⁺
E = 8.02



3.S.4 Activation parameters for reactions of benzhydrylium ions with N7 and N8 in CH₂Cl₂

Table 3.S.4.1. Activation enthalpies ΔH^\ddagger and activation entropies ΔS^\ddagger for the reactions of benzhydrylium ions with N7 and N8 in CH₂Cl₂.

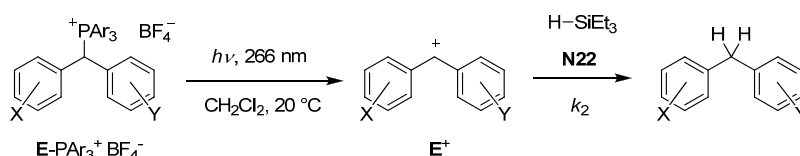
nucleophile N, s_N		E ⁺ abbreviation	E	activation parameters	
				ΔH^\ddagger ^a / kJ mol ⁻¹	ΔS^\ddagger ^a / J mol ⁻¹ K ⁻¹
		E13 ⁺ (fur) ₂ CH ⁺	-1.36	35.6	-117
		E14 ⁺ fur(ani)CH ⁺	-0.81	31.9 ^b	-117 ^b
		E15 ⁺ (ani) ₂ CH ⁺	0.00	26.1	-124
N7		E17 ⁺ ani(tol)CH ⁺	1.48	19.9	-117
$N = 1.68, s_N = 1.00$		E18 ⁺ ani(Ph)CH ⁺	2.11	15.5	-122
		E19 ⁺ pop(Ph)CH ⁺	2.90	13.7	-111
		E15 ⁺ (ani) ₂ CH ⁺	0.00	29.7	-125
		E17 ⁺ ani(tol)CH ⁺	1.48	22.7	-120
		E18 ⁺ ani(Ph)CH ⁺	2.11	18.6	-123
N8		E19 ⁺ pop(Ph)CH ⁺	2.90	15.3	-119
$N = 0.84, s_N = 1.06$		E20 ⁺ (tol) ₂ CH ⁺	3.63	11.6	-117

^a From ref.^{1b} unless noted otherwise. ^b From ref.^{23a}

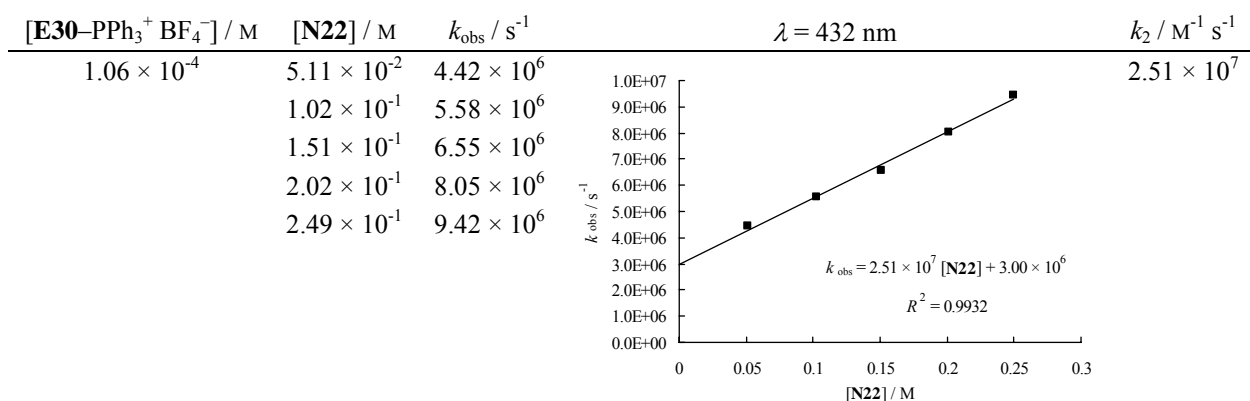
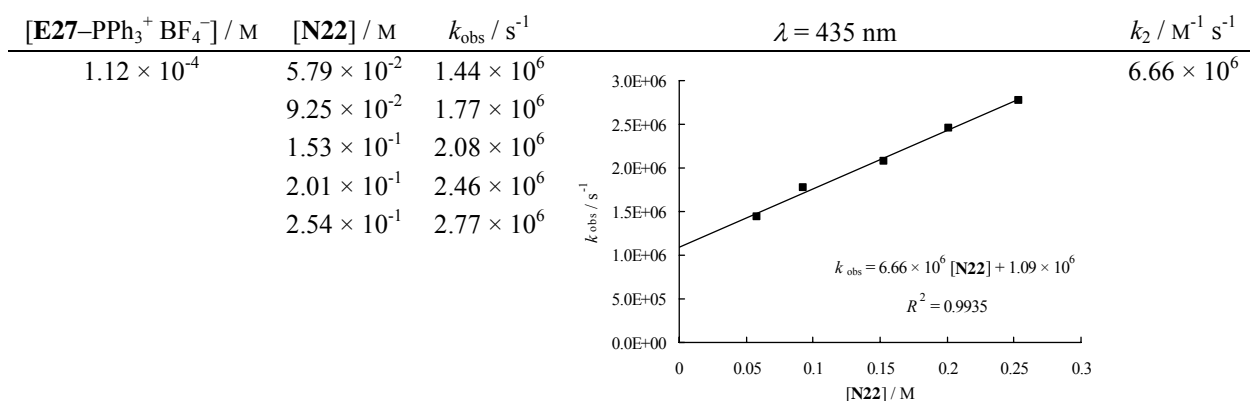
3.S.5 Kinetics of the reactions of benzhydrylium ions with other classes of nucleophiles

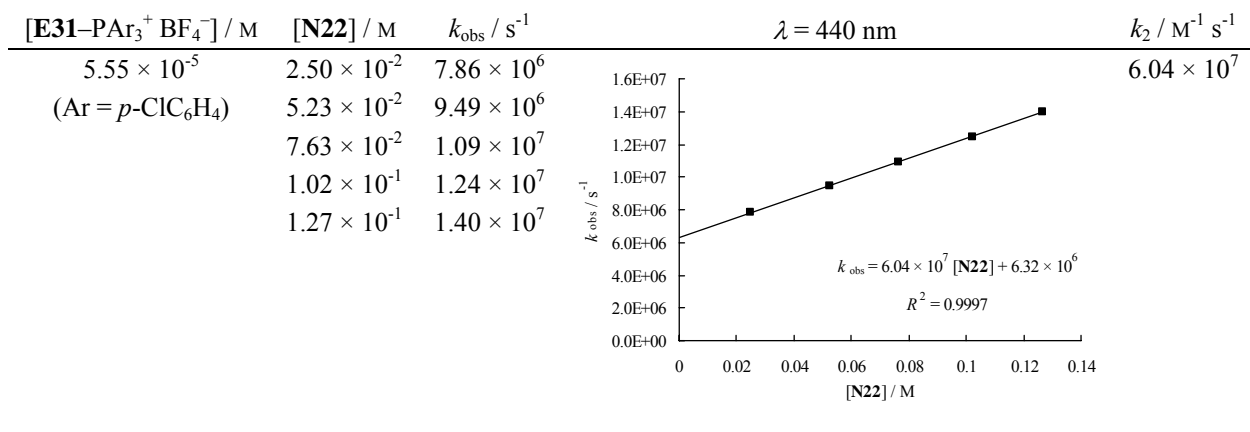
3.S.5.1 Triethylsilane (N22)

3.S.5.1.1 Reactions of benzhydrylium ions (E^+) with triethylsilane (N22) in dichloromethane at 20 °C.



Reactions of $(fur)_2CH^+$ (**E13**⁺), $fur(ani)CH^+$ (**E14**⁺), and $ani(Ph)CH^+$ (**E18**⁺) with N22 have previously been reported to yield diarylmethanes as the final products.^{23a,S2k}



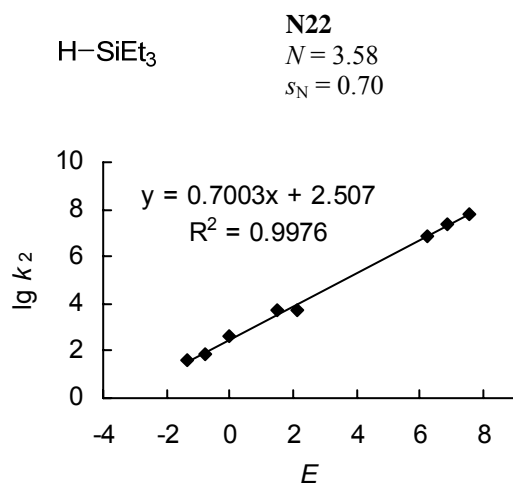


3.S.5.1.2 Revised nucleophilicity parameter for triethylsilane (N22)

nucleophile N, s_N		experiment			calculated	
		E^a	$k_2 / \text{M}^{-1} \text{s}^{-1}$	ref.	$k_{\text{calc}}^b / \text{M}^{-1} \text{s}^{-1}$	k_{calc} / k_2
H-SiEt ₃	E13 ⁺ (fur) ₂ CH ⁺	-1.36	3.76×10^1	23b	3.58×10^1	0.95
	E14 ⁺ fur(ani)CH ⁺	-0.81	7.94×10^1	23a	8.69×10^1	1.09
	E15 ⁺ (ani) ₂ CH ⁺	0.00	3.98×10^2	23b	3.21×10^2	0.81
N22 $N = 3.58, s_N = 0.70^c$	E17 ⁺ ani(tol)CH ⁺	1.48	4.87×10^3	23b	3.48×10^3	0.72
	E18 ⁺ ani(Ph)CH ⁺	2.11	5.29×10^3	1b	9.62×10^3	1.82
	E27 ⁺ mfp(Ph)CH ⁺	6.23	6.66×10^6	<i>d</i>	7.36×10^6	1.11
	E30 ⁺ (mfp) ₂ CH ⁺	6.87	2.51×10^7	<i>d</i>	2.07×10^7	0.82
	E31 ⁺ dfp(mfp)CH ⁺	7.52	6.04×10^7	<i>d</i>	5.89×10^7	0.97

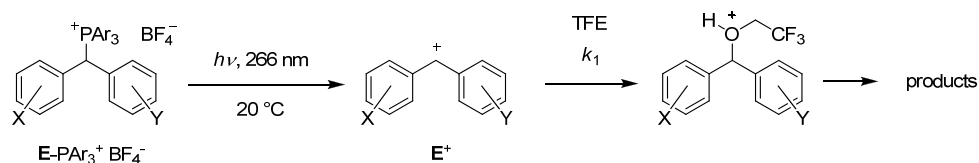
^a E parameters derived from data for reactions of π -nucleophiles in CH₂Cl₂. ^b Calculated from eq. 1. ^c The previously published nucleophilicity parameters ($N = 3.64, s_N = 0.65$) were based on kinetics with only two reference electrophiles.^{1b} ^d This work; laser flash photolysis.

3.S.5.1.3 Plot of $\lg k_2$ versus E for triethylsilane (N22)



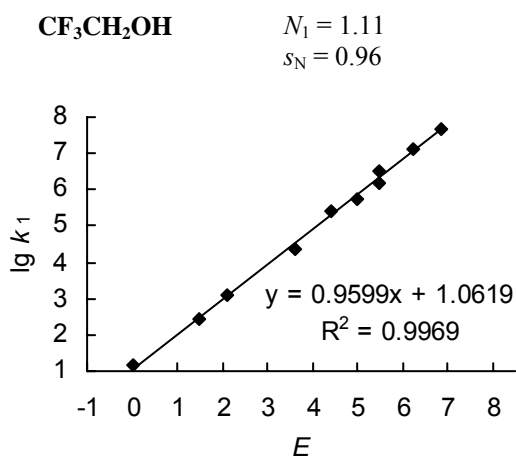
3.S.5.2 Trifluoroethanol

3.S.5.2.1 Revised solvent nucleophilicity parameter for 2,2,2-trifluoroethanol (TFE)



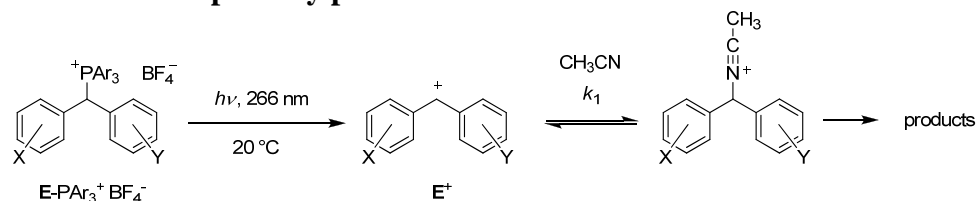
solvent N_1, s_N			experiment			calculated	
	E^+	abbreviation	E^a	k_1 / s^{-1}	ref.	$k_{\text{calc}}^b / \text{s}^{-1}$	k_{calc} / k_1
$\text{CF}_3\text{CH}_2\text{OH}$ $N_1 = 1.11, s_N = 0.96$	E15⁺	(ani) ₂ CH ⁺	0.00	1.4×10^1	37	1.16×10^1	0.8
	E17⁺	ani(tol)CH ⁺	1.48	2.8×10^2	37	3.06×10^2	1.1
	E18⁺	ani(Ph)CH ⁺	2.11	1.2×10^3	37	1.23×10^3	1.0
	E20⁺	(tol) ₂ CH ⁺	3.63	2.4×10^4	37	3.55×10^4	1.5
	E21⁺	tol(Ph)CH ⁺	4.43	2.7×10^5	37	2.08×10^5	0.8
	E22⁺	(pfp) ₂ CH ⁺	5.01	5.82×10^5	18	7.50×10^5	1.29
	E25⁺	(Ph) ₂ CH ⁺	5.47	3.21×10^6	18,37	2.07×10^6	0.65
	E26⁺	(pcp) ₂ CH ⁺	5.48	1.47×10^6	18	2.12×10^6	1.44
	E27⁺	mfp(Ph)CH ⁺	6.23	1.29×10^7	18	1.11×10^7	0.86
	E30⁺	(mfp) ₂ CH ⁺	6.87	4.6×10^7	18	4.58×10^7	1.0

^a E parameters derived from data for reactions of π -nucleophiles in CH_2Cl_2 . ^b Calculated from eq. 1.

3.S.5.2.3 Plot of $\lg k_1$ versus E for 2,2,2-trifluoroethanol (TFE)

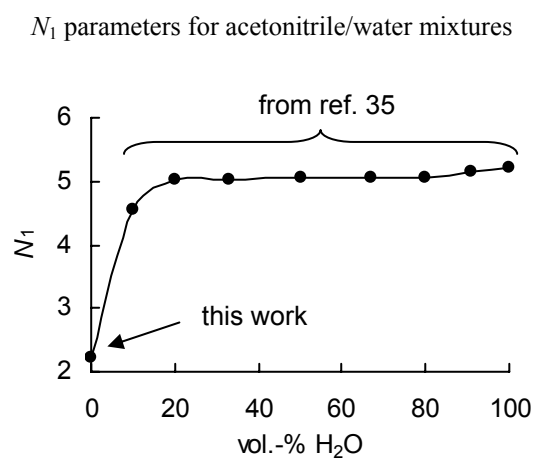
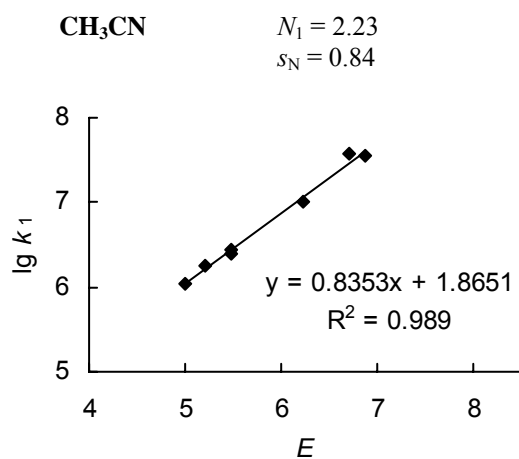
3.S.5.3 Acetonitrile

3.S.5.3.1 Solvent nucleophilicity parameters for acetonitrile



solvent N_1, s_N	 E^+ abbreviation		E^a	experiment		calculated	
	k_1 / s^{-1}	ref.		$k_{\text{calc}}^b / \text{s}^{-1}$	k_{calc} / k_1		
CH₃CN $N_1 = 2.23, s_N = 0.84$	E22⁺	(pfp) ₂ CH ⁺	5.01	1.1×10^6	40	1.21×10^6	1.1
	E23⁺	pfp(Ph)CH ⁺	5.20	1.8×10^6	40	1.74×10^6	1.0
	E25⁺	(Ph) ₂ CH ⁺	5.47	2.52×10^6	18,40	2.94×10^6	1.17
	E26⁺	(pcp) ₂ CH ⁺	5.48	2.8×10^6	40	3.00×10^6	1.1
	E27⁺	mfp(Ph)CH ⁺	6.23	1.00×10^7	18	1.28×10^7	1.28
	E28⁺	tfm(Ph)CH ⁺	6.70	3.8×10^7	40	3.17×10^7	0.8
	E30⁺	(mfp) ₂ CH ⁺	6.87	3.49×10^7	18	4.41×10^7	1.26

^a E parameters derived from data for reactions of π -nucleophiles in CH_2Cl_2 . ^b Calculated from eq. 1.

3.S.5.3.2 Plot of $\lg k_1$ versus E for acetonitrile and plot of N_1 versus water content for acetonitrile/water mixtures

Solvent Nucleophilicities of Hexafluoroisopropanol/Water Mixtures

Johannes Ammer and Herbert Mayr

J. Phys. Org. Chem. **2013**, 26, 59-63

4.1 Introduction

Because of their unique solvating properties, 1,1,1,3,3,3-hexafluoro-2-propanol (HFIP) and HFIP/water mixtures have been employed as solvents for synthetic transformations^[1-7] and for the study of protein structures.^[8,9] HFIP/water mixtures have also played a key role in solvolytic studies due to their high ionizing powers and low nucleophilicities,^[10-14] which allowed one to investigate S_N1 reactions of substrates which solvolyze with nucleophilic solvent assistance in other media.^[15] However, also in HFIP/water mixtures, a change from S_N1 to S_N2 processes is occurring, when the S_N1 process would lead to poorly stabilized carbocations. In order to predict this change of mechanism from S_N1 to S_N2, the nucleophilic reactivity of the solvent must be known.^[16]

We have recently reported that highly reactive acceptor-substituted benzhydrylium ions can be generated by laser flash photolysis of phosphonium salts^[17] and employed this method to determine the empirical electrophilicity parameters E of these benzhydrylium ions^[18] as defined by Eqn 1. This linear free energy relationship relates the second-order rate constants k_2 (M⁻¹ s⁻¹) of bimolecular reactions of electrophiles with nucleophiles to the electrophile-specific parameter E and the nucleophile-specific parameters N and s_N .^[19-21]

$$\log k_2(20\text{ }^\circ\text{C}) = s_N(N + E) \quad (1)$$

Equation 1 can also be used to predict the first-order rate constants k_1 (s⁻¹) for the reactions of electrophiles with solvents, when the solvent-specific parameters N_1 and s_N are employed (Eqn 1a).^[22]

$$\log k_1(20\text{ }^\circ\text{C}) = s_N(N_1 + E) \quad (1a)$$

With the aid of our recently determined electrophilicity parameters E for the highly reactive acceptor-substituted benzhydrylium ions,^[18] we can now provide quantitative reactivity parameters for the weakly nucleophilic HFIP/water mixtures.

4.2 Results and Discussion

Irradiation of ca. 10^{-4} M solutions of the phosphonium salts $\mathbf{E-PAr}_3^+ \text{BF}_4^-$ (Ar = Ph or *p*-Cl-C₆H₄) in mixtures of HFIP and water (W) ranging from 50HFIP50W to 99HFIP1W (*w/w*) yielded the benzhydrylium ions \mathbf{E}^+ (Scheme 4.1 and Table 4.1).

Scheme 4.1. Generation of benzhydrylium ions \mathbf{E}^+ by laser flash irradiation of the phosphonium salts $\mathbf{E-PAr}_3^+ \text{BF}_4^-$ (Ar = Ph or *p*-Cl-C₆H₄).

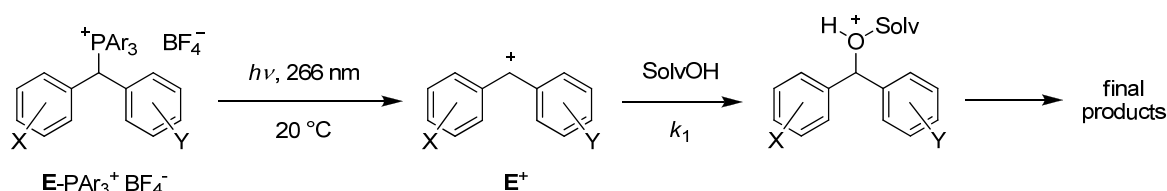


Table 4.1. Electrophiles \mathbf{E}^+ and their electrophilicity parameters E .

no.			E^a
	X	Y	
E18⁺	4-MeO	H	2.11
E20⁺	4-Me	4-Me	3.63
E21⁺	4-Me	H	4.43
E22⁺	4-F	4-F	5.01
E24⁺	3-F, 4-Me	3-F, 4-Me	5.24
E25⁺	H	H	5.47
E26⁺	4-Cl	4-Cl	5.48
E27⁺	3-F	H	6.23
E28⁺	4-(CF ₃)	H	6.70
E29⁺	3,5-F ₂	H	6.74
E30⁺	3-F	3-F	6.87
E31⁺	3,5-F ₂	3-F	7.52
E33⁺	3,5-F ₂	3,5-F ₂	(8.02) ^b

^a From ref. [18] ^b Approximate value.

In those cases where the reactions of \mathbf{E}^+ with the solvent were faster than the recombination with the photo-leaving group PAR_3 , exponential decays of the UV/Vis absorbances of \mathbf{E}^+ can be observed, as illustrated in Fig. 4.1a for the decay of the most electrophilic carbocation in our series, $\mathbf{E33}^+$, in 99HFIP1W. From the exponential decays, we derived the first-order rate constants k_1 (s^{-1}) listed in Table 4.2 for the reactions of \mathbf{E}^+ with the HFIP/water mixtures.

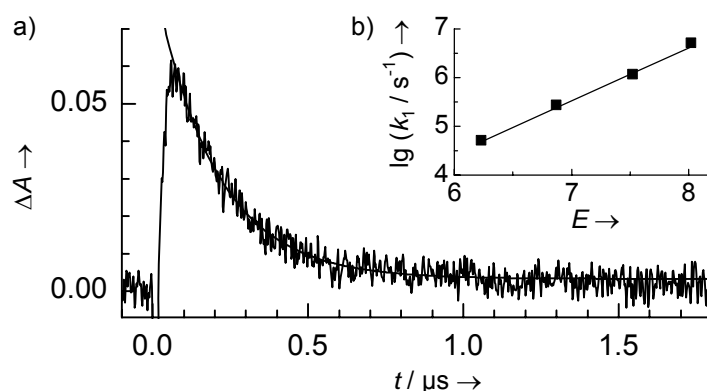


Figure 4.1. (a) Decay of the absorbance of $\mathbf{E33}^+$ at $\lambda = 439$ nm observed after irradiation of a 8.52×10^{-5} M solution of $\mathbf{E33-P}(p\text{-Cl-C}_6\text{H}_4)_3^+ \text{BF}_4^-$ in 99HFIP1W and exponential fit of the data ($k_1 = 5.11 \times 10^6 \text{ s}^{-1}$, $R^2 = 0.9685$). (b) Plot of $\lg k_1$ obtained from reactions of $\mathbf{E27}^+$, $\mathbf{E30}^+$, $\mathbf{E31}^+$, and $\mathbf{E33}^+$ with 99HFIP1W against the electrophilicity parameters E of these benzhydrylium ions ($\lg k_1 = 1.09(-1.93 + E)$, $R^2 = 0.9973$).

Table 4.2. First-order rate constants k_1 (s^{-1}) for reactions of electrophiles \mathbf{E}^+ with HFIP/water mixtures and comparison with rate constants k_{calc} (s^{-1}) calculated from Eqn 1a.

nucleophile solvent ^a	N_1, s_N	\mathbf{E}^+	electrophile abbreviation	E^b	experiment k_1^c / s^{-1}	calculated $k_{\text{calc}}^d / \text{s}^{-1}$	k_{calc}/k_2
50HFIP50W 38.5% (v/v) $x_{\text{HFIP}} = 0.097$	$N_1 = 1.50$ $s_N = 1.03$	E18 ⁺	ani(Ph)CH ⁺	2.11	5.56×10^3 ^e	5.23×10^3	0.94
		E20 ⁺	(tol) ₂ CH ⁺	3.63	1.50×10^5	1.92×10^5	1.28
		E21 ⁺	tol(Ph)CH ⁺	4.43	1.20×10^6	1.28×10^6	1.07
		E22 ⁺	(pfp) ₂ CH ⁺	5.01	5.32×10^6	5.07×10^6	0.95
70HFIP30W 59.3% (v/v) $x_{\text{HFIP}} = 0.200$	$N_1 = 1.65$ $s_N = 0.96$	E20 ⁺	(tol) ₂ CH ⁺	3.63	1.13×10^5	1.17×10^5	1.04
		E21 ⁺	tol(Ph)CH ⁺	4.43	8.06×10^5	6.87×10^5	0.85
		E22 ⁺	(pfp) ₂ CH ⁺	5.01	3.25×10^6	2.48×10^6	0.76
		E24 ⁺	–	5.24	3.32×10^6	4.12×10^6	1.24
90HFIP10W 84.9% (v/v) $x_{\text{HFIP}} = 0.491$	$N_1 = 0.96$ $s_N = 0.93$	E25 ⁺	(Ph) ₂ CH ⁺	5.47	7.52×10^6	6.84×10^6	0.91
		E21 ⁺	tol(Ph)CH ⁺	4.43	1.10×10^5	1.03×10^5	0.94
		E22 ⁺	(pfp) ₂ CH ⁺	5.01	3.74×10^5	3.57×10^5	0.95
		E25 ⁺	(Ph) ₂ CH ⁺	5.47	1.01×10^6	9.55×10^5	0.95
		E27 ⁺	mfp(Ph)CH ⁺	6.23	5.21×10^6	4.86×10^6	0.93
		E29 ⁺	dfp(Ph)CH ⁺	6.74	1.55×10^7	1.45×10^7	0.93
E30 ⁺	(mfp) ₂ CH ⁺	6.87	2.10×10^7	1.91×10^7	0.91		

Table 4.2 (continued). First-order rate constants k_1 (s^{-1}) for reactions of electrophiles \mathbf{E}^+ with HFIP/water mixtures and comparison with rate constants k_{calc} (s^{-1}) calculated from Eqn 1a.

nucleophile		\mathbf{E}^+	electrophile		experiment	calculated	
solvent ^a	N_1, s_N		abbreviation	E^b	k_1^c / s^{-1}	$k_{\text{calc}}^d / \text{s}^{-1}$	k_{calc}/k_2
93HFIP7W 89.3% (v/v) $x_{\text{HFIP}} = 0.588$	$N_1 = 0.34$ $s_N = 0.96$	E21⁺	tol(Ph)CH ⁺	4.43	3.88×10^4	3.79×10^4	0.98
		E22⁺	(pfp) ₂ CH ⁺	5.01	1.39×10^5	1.37×10^5	0.98
		E25⁺	(Ph) ₂ CH ⁺	5.47	3.99×10^5	3.78×10^5	0.95
		E26⁺	(pcp) ₂ CH ⁺	5.48	2.61×10^5	3.87×10^5	1.48
		E27⁺	mfp(Ph)CH ⁺	6.23	1.96×10^6	2.03×10^6	1.04
		E28⁺	tfm(Ph)CH ⁺	6.70	6.26×10^6	5.73×10^6	0.92
		E30⁺	(mfp) ₂ CH ⁺	6.87	9.10×10^6	8.35×10^6	0.92
		E31⁺	dfp(mfp)CH ⁺	7.52	2.92×10^7	3.51×10^7	1.20
95HFIP5W 92.2% (v/v) $x_{\text{HFIP}} = 0.671$	$N_1 = -0.10$ $s_N = 0.97$	E21⁺	tol(Ph)CH ⁺	4.43	1.67×10^4	1.59×10^4	0.95
		E22⁺	(pfp) ₂ CH ⁺	5.01	5.78×10^4	5.79×10^4	1.00
		E25⁺	(Ph) ₂ CH ⁺	5.47	1.70×10^5	1.62×10^5	0.95
		E27⁺	mfp(Ph)CH ⁺	6.23	8.61×10^5	8.83×10^5	1.03
		E30⁺	(mfp) ₂ CH ⁺	6.87	4.53×10^6	3.69×10^6	0.81
		E31⁺	dfp(mfp)CH ⁺	7.52	1.55×10^7	1.58×10^7	1.02
97HFIP3W 95.3% (v/v) $x_{\text{HFIP}} = 0.776$	$N_1 = -1.19$ $s_N = 1.08$	E22⁺	(pfp) ₂ CH ⁺	5.01	1.52×10^4	1.34×10^4	0.88
		E25⁺	(Ph) ₂ CH ⁺	5.47	5.01×10^4	4.19×10^4	0.84
		E26⁺	(pcp) ₂ CH ⁺	5.48	3.00×10^4	4.30×10^4	1.43
		E27⁺	mfp(Ph)CH ⁺	6.23	2.68×10^5	2.77×10^5	1.04
		E29⁺	dfp(Ph)CH ⁺	6.74	1.11×10^6	9.86×10^5	0.89
		E30⁺	(mfp) ₂ CH ⁺	6.87	1.46×10^6	1.36×10^6	0.93
		E31⁺	dfp(mfp)CH ⁺	7.52	6.48×10^6	6.86×10^6	1.06
98HFIP2W 96.8% (v/v) $x_{\text{HFIP}} = 0.840$	$N_1 = -1.62$ $s_N = 1.10$	E22⁺	(pfp) ₂ CH ⁺	5.01	6.17×10^3	5.36×10^3	0.87
		E25⁺	(Ph) ₂ CH ⁺	5.47	2.04×10^4	1.72×10^4	0.84
		E26⁺	(pcp) ₂ CH ⁺	5.48	1.24×10^4	1.76×10^4	1.42
		E27⁺	mfp(Ph)CH ⁺	6.23	1.14×10^5	1.18×10^5	1.03
		E30⁺	(mfp) ₂ CH ⁺	6.87	6.54×10^5	5.96×10^5	0.91
		E31⁺	dfp(mfp)CH ⁺	7.52	2.60×10^6	3.09×10^6	1.19
		E33⁺	(dfp) ₂ CH ⁺	(8.02) ^f	1.20×10^7	1.10×10^7	0.91
99HFIP1W 98.4% (v/v) $x_{\text{HFIP}} = 0.914$	$N_1 = -1.93$ $s_N = 1.09$	E27⁺	mfp(Ph)CH ⁺	6.23	5.18×10^4	4.86×10^4	0.94
		E30⁺	(mfp) ₂ CH ⁺	6.87	2.72×10^5	2.42×10^5	0.89
		E31⁺	dfp(mfp)CH ⁺	7.52	1.15×10^6	1.24×10^6	1.08
		E33⁺	(dfp) ₂ CH ⁺	(8.02) ^f	5.11×10^6	4.35×10^6	0.85

^a Solvent mixtures are given as w/w. Abbreviations: HFIP = 1,1,1,3,3,3-hexafluoro-2-propanol, W= water. To accommodate literature conventions in other fields, we also provide the v/v percentages and molar fractions. ^b E parameters derived from kinetic data for reactions of \mathbf{E}^+ with π -nucleophiles in CH_2Cl_2 ; from ref. [18] ^c Laser flash photolysis of triarylphosphonium salts, this work. ^d Calculated from Eqn 1a. ^e Determined from a non-exponential decay curve as the reaction of **E18⁺** with 50HFIP50W does not follow first-order kinetics due to recombination of **E18⁺** with the photo-leaving group PPh_3 . See section 4.S.3 for details. ^f This E parameter is based on only one rate constant.

Reactions which proceed with rate constants lower than ca. 10^4 s^{-1} were not investigated, because the kinetics of these reactions are complicated by the recombination of \mathbf{E}^+ with the photo-leaving group PAR_3 which proceeds on a similar time scale.^[17] To determine the rate

constants of slower reactions, one might employ anionic photo-leaving groups such as *p*-cyanophenolate, which can be expected to undergo significantly slower recombination reactions with the photogenerated carbocations due to the exceptionally good solvation of anions by fluorinated alcohols.^[23] Since a major goal of this investigation was the characterization of the electrophilic reactivities of acceptor-substituted benzhydrylium ions towards relatively weak nucleophiles such as HFIP/water mixtures, we have not included *p*-cyanophenolates in this study.

Plots of $\lg k_1$ for the reactions of \mathbf{E}^+ with the HFIP/water mixtures versus the E parameters of \mathbf{E}^+ were linear (Fig. 4.2) and allowed us to derive the solvent nucleophilicity parameters N_1 and s_N listed in Table 4.2. Figure 4.2 illustrates the excellent correlations of k_1 with the E parameters that were derived from reactions of \mathbf{E}^+ with π -nucleophiles in CH_2Cl_2 . Only very small deviations are found for the most electrophilic benzhydrylium ion in the series, $\mathbf{E33}^+$, although the electrophilicity parameter of this carbocation had been derived from only one rate constant because of its extremely high reactivity.^[18] The kinetic data from this work thus corroborate the electrophilicity parameter $E = 8.02$ ^[18] for $\mathbf{E33}^+$.

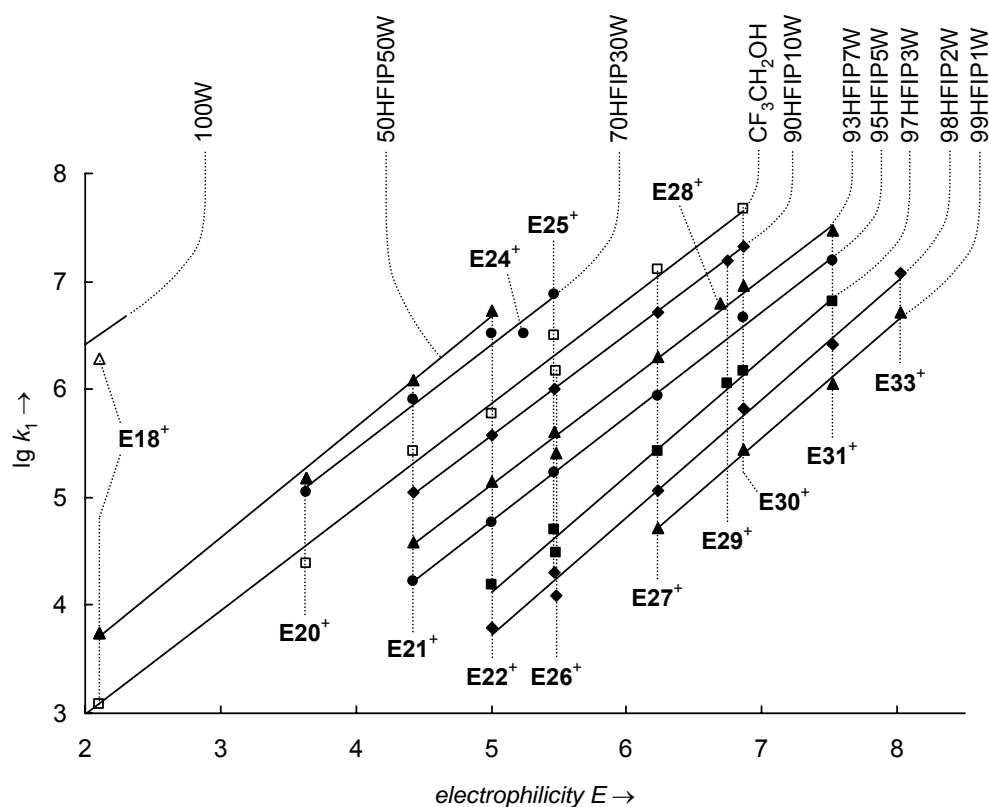


Figure 4.2. Plot of $\lg k_1$ versus E for the reactions of benzhydryl cations with HFIP/water mixtures (filled symbols). For comparison, data for 100W and trifluoroethanol are also shown (open symbols; only a part of the correlation lines is shown).^[22]

The 4,4-dichlorobenzhydrylium ion $\mathbf{E26}^+$ deviates slightly from these correlations. Although $\mathbf{E26}^+$ has the same electrophilicity as $\mathbf{E25}^+$ in CH_2Cl_2 , the rate constants for reactions of $\mathbf{E26}^+$ in trifluoroethanol and HFIP/water mixtures are lower than those of $\mathbf{E25}^+$ by a factor of 1.5 to 2.2 (Fig. 4.2).

The nucleophilic reactivities of the HFIP/water mixtures increase with increasing water content, which is particularly pronounced for the mixtures with low water content. Figure 4.3 compares $\lg k_1$ for the reaction of $\mathbf{E27}^+$ with HFIP/water mixtures of varying water content, which is similar to a N_1 versus % H_2O plot as the s_N parameters are closely similar.

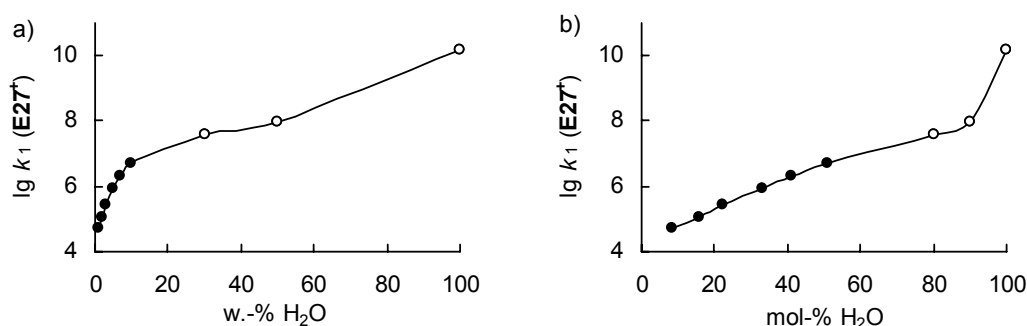


Figure 4.3. Plots of $\lg k_1$ for the decay of $\mathbf{E27}^+$ in HFIP/water mixtures against the water content of the mixtures in weight-% (a) or mol-% (b). Filled circles: experimental data; open circles: calculated from Eqn 1a.

It has been reported that the microscopic structures of HFIP/water mixtures change when the water content is varied. The structures of the solvent mixtures investigated in this work range from micelle-like assemblies of HFIP molecules in water (50HFIP50W; 38.5 vol.-% HFIP, $x_{\text{HFIP}} = 0.097$) over a poorly characterized complex intermediate structure of small HFIP associates (70HFIP30W to 95HFIP5W; 59-92 vol.-% HFIP, $0.200 \leq x_{\text{HFIP}} \leq 0.671$) to short helical chains of HFIP molecules as in neat HFIP (97HFIP3W to 99HFIP1W; >95 vol.-% HFIP, $x_{\text{HFIP}} \geq 0.776$).^[24] Despite these large structural variations, $\lg k_1$ for the reactions of $\mathbf{E27}^+$ with the HFIP/water mixtures increases almost linearly with the molar fraction of water over the entire range from 99HFIP1W to 50HFIP50W (Fig. 4.3b). A similar effect is also found for the ionizing powers Y_{OTs} of the HFIP/water mixtures, which decrease almost linearly with increasing water content for compositions with 0-90 mol-% water.^[12] The inverse linear correlation between $\lg k_1$ ($\mathbf{E27}^+$) and Y_{OTs} in this range indicates that nucleophilicity as well as solvent ionizing power of HFIP/water mixtures are affected in a similar manner by changes in solvent structure.

Between 90 mol-% water (50HFIP50W) and 100 mol-% water, however, there is a further substantial increase in nucleophilicity (Fig 4.3b), indicating that the nucleophilicity of pure water is reduced significantly by the presence of only 10 mol-% of the good hydrogen bond donor HFIP. A sharp increase between 90 and 100 mol-% water is also found in the ionizing powers Y_{OTs} of the HFIP/water mixtures.^[12] These observations are in agreement with another structural transition of the binary solvent system, which exists as dilute single HFIP molecules in water for compositions with more than ~95 mol-% water (35HFIP65W, 25 vol.-% HFIP).^[24] Large water clusters that are not influenced by HFIP may also explain why we could not observe $\mathbf{E21}^+$ after irradiation of $\mathbf{E21-PAr}_3^+ \text{BF}_4^-$ in 25HFIP75W (calculated lifetime of $\mathbf{E21}^+$ in pure water: 2.7 ns).

As the nucleophilicity parameters for mixtures with low water content are highly sensitive to the water content (Fig. 4.3a), we did not attempt to determine N_1 and s_N of pure HFIP. Literature values of k_1 for the decay of $\mathbf{E25}^+$ in HFIP range from “around 10^2 s^{-1} ” (meticulously dried HFIP but inaccurate measurement)^[25] to $2.2 \times 10^4 \text{ s}^{-1}$ (commercial HFIP, >99.8%, used as received).^[26] The latter value is slightly larger than the calculated rate constant for the reaction of $\mathbf{E25}^+$ with HFIP containing 1% water ($k_{\text{calc}} = 7.2 \times 10^3 \text{ s}^{-1}$). It thus seems problematic to derive accurate quantitative information about the electrophilic reactivities of carbocations from their decay rate constants in neat HFIP as traces of water may strongly affect the results.

The N_1 parameters for HFIP/water mixtures determined in this work (Table 4.2) agree within 1.5 units with our previous estimates for some of these solvents that were derived from a correlation with Kevill’s N_T parameters.^[22] However, the s_N parameters of the HFIP/water mixtures are somewhat larger than for other alcoholic and aqueous solvents.^[22]

The low nucleophilicity of HFIP/water mixtures has previously been utilized to study solvolysis reactions under conditions where nucleophilic solvent assistance is reduced. For example, the solvolysis of 2-propyl tosylate in 97% aqueous HFIP proceeds by an S_N1 mechanism, whereas the same reaction in 97% aqueous trifluoroethanol already proceeds with measurable nucleophilic solvent assistance (factor 15).^[15] It has been argued that an intermediate can only exist if its lifetime is at least as long as the duration of a bond vibration ($\sim 10^{-13} \text{ s}$).^[27-30] Thus, S_N1 reactions leading to carbocations with lifetimes shorter than ca. 10^{-13} s cannot occur, and only S_N2 reactions are possible in these cases.

We have previously investigated the borderline between S_N1 and S_N2 mechanisms for nucleophilic substitution reactions in DMSO ($N_1 = 11.3$, $s_N = 0.74$).^[16] Equation 1a predicts a

lifetime near the theoretical limit (5×10^{-14} s) for **E28⁺** ($E = 6.70$) in DMSO, and no significant nucleophilic solvent participation was observed for reactions of the corresponding bromide (i.e., DMSO only reacts via S_N1 and not via S_N2 mechanism).^[16] On the other hand, significant nucleophilic solvent participation was found for reactions of bis[4-(trifluoromethyl)phenyl]methyl bromide,^[16] in agreement with a calculated lifetime of 6×10^{-15} s for the corresponding carbocation ($E = 7.96$)^[18] in DMSO, which is shorter than the period of a bond vibration ($\sim 10^{-13}$ s).

The N_1 and s_N parameters for the HFIP/water mixtures from Table 4.2 can now be employed to predict when a change from S_N1 to S_N2 mechanism can be expected in these solvents. The limiting lifetime of ca. 10^{-13} s will thus be reached for carbocations with $E \geq 11$ in 50HFIP50W and for carbocations with $E \geq 12$ in 70HFIP30W. Carbocations with higher electrophilicity parameters cannot exist in these solvents. As the decreasing N_1 parameters are compensated by slightly increasing s_N parameters in the series 90HFIP10W to 99HFIP1W, we calculate a limiting value of $E \approx (13 \text{ to } 14)$ for all HFIP/water mixtures with $\leq 10\%$ water content. These limiting E parameters are well beyond those of the most electrophilic carbocations which have so far been characterized by Eqn 1.^[18] It can thus be concluded that nucleophilic solvent assistance will generally not be observed in HFIP/water mixtures with $\leq 10\%$ water content.

4.3 Conclusion

The excellent linear correlations of $\lg k_1$ for the reactions of benzhydrylium ions with HFIP/water mixtures with the electrophilicity parameters E of these benzhydrylium ions (Fig. 4.2) once again demonstrate that Eqn 1 adequately describes the decay rate constants of benzhydrylium ions in nucleophilic solvents and solvent mixtures.^[18,22]

In the future, the reactivity parameters of the HFIP/water mixtures may be of interest for characterizing the electrophilic reactivities of further highly reactive electrophiles ($E > 7$) which cannot be studied in trifluoroethanol or acetonitrile due to the high nucleophilicity of these solvents.^[17] The decay rate constants of carbocations in many less nucleophilic solvents such as CH_2Cl_2 , on the other hand, do not reflect the reactivities of these solvents but result from reactions with impurities or with the precursor molecules.^[17] Mixtures of HFIP and

water with $\geq 90\%$ (w/w) HFIP combine the two advantages that they are less nucleophilic than trifluoroethanol and acetonitrile but still have a clearly defined nucleophilic reactivity.

4.4 Acknowledgment

We thank Dr. Armin R. Ofial for discussions and the Deutsche Forschungsgemeinschaft (SFB 749) for financial support.

4.5 References and Notes

- [1] J.-P. Bégue, D. Bonnet-Delpon, B. Crousse, *Synlett* **2004**, 18–29.
- [2] A. Berkessel, in *Modern Oxidation Methods*, 2nd ed. (Ed: J.-E. Baeckvall), Wiley-VCH, Weinheim, **2010**, 117–145.
- [3] S. Panchenko, P. S. A. Runichina, V. V. Tumanov, *Mendeleev Commun.* **2011**, *21*, 226–228.
- [4] A. V. Miroshnichenko, V. V. Tumanov, V. M. Menshov, W. A. Smit, *J. Polymer Res.* **2012**, *19*, 1–4.
- [5] M. O. Ratnikov, V. V. Tumanov, W. A. Smit, *Angew. Chem.* **2008**, *120*, 9885–9888; *Angew. Chem. Int. Ed.* **2008**, *47*, 9739–9742.
- [6] A. Berkessel, J. A. Adrio, *J. Am. Chem. Soc.* **2006**, *128*, 13412–13420.
- [7] I. A. Shuklov, N. V. Dubrovina, A. Börner, *Synthesis* **2005**, 2925–2943.
- [8] D. Hamada, Y. Goto, in *Protein Folding Handbook*, Vol. 1 (Eds: J. Buchner, T. Kiefhaber), Wiley-VCH, Weinheim, **2005**, 884–915.
- [9] C. Chatterjee, G. Hovagimyan, J. T. Gerig, in *Current Fluoroorganic Chemistry* (Eds: V. A. Soloshonok, K. Mikami, T. Yamazaki, J. T. Welch, J. F. Honek), American Chemical Society, Washington DC, **2007**, 379–392.
- [10] T. W. Bentley, G. Llewellyn, in *Progress in Physical Organic Chemistry*, Vol. 17 (Ed.: R. W. Taft), Wiley, New York, **1990**, 121–158.
- [11] F. L. Schadt, P. v. R. Schleyer, T. W. Bentley, *Tetrahedron Lett.* **1974**, *15*, 2335–2338.
- [12] B. Allard, E. Casadevall, *Nouv. J. Chim.* **1983**, *7*, 569–574.
- [13] P. H. Ferber, G. E. Gream, *Aust. J. Chem.* **1981**, *34*, 2217–2223.

- [14] D. N. Kevill, Z. H. Ryu, *Int. J. Mol. Sci.* **2006**, *7*, 451–455.
- [15] F. L. Schadt, T. W. Bentley, P. v. R. Schleyer, *J. Am. Chem. Soc.* **1976**, *98*, 7667–7674.
- [16] B. T. Phan, C. Nolte, S. Kobayashi, A. R. Ofial, H. Mayr, *J. Am. Chem. Soc.* **2009**, *131*, 11392–11401.
- [17] J. Ammer, C. F. Sailer, E. Riedle, H. Mayr, *J. Am. Chem. Soc.* **2012**, *134*, 11481–11494 (CHAPTER 2 of this work).
- [18] J. Ammer, C. Nolte, H. Mayr, *J. Am. Chem. Soc.* **2012**, *134*, 13902–13911 (CHAPTER 3 of this work).
- [19] H. Mayr, T. Bug, M. F. Gotta, N. Hering, B. Irrgang, B. Janker, B. Kempf, R. Loos, A. R. Ofial, G. Remennikov, H. Schimmel, *J. Am. Chem. Soc.* **2001**, *123*, 9500–9512.
- [20] H. Mayr, B. Kempf, A. R. Ofial, *Acc. Chem. Res.* **2003**, *36*, 66–77.
- [21] H. Mayr, *Angew. Chem.* **2011**, *123*, 3692–3698; *Angew. Chem. Int. Ed.* **2011**, *50*, 3612–3618.
- [22] S. Minegishi, S. Kobayashi, H. Mayr, *J. Am. Chem. Soc.* **2004**, *126*, 5174–5181.
- [23] For example, rate constants $k_1 \geq 10^1 \text{ s}^{-1}$ could be determined for the first-order decay reactions of benzhydrylium ions in trifluoroethanol: R. A. McClelland, V. M. Kanagasabapathy, S. Steenken, *J. Am. Chem. Soc.* **1988**, *110*, 6913–6914.
- [24] B. Czarnik-Matuszewicz, S. Pilorz, L.-P. Zhang, Y. Wu, *J. Mol. Struct.* **2008**, *883–884*, 195–202.
- [25] E. MacKnight, R. A. McClelland, *Can. J. Chem.* **1996**, *74*, 2518–2527.
- [26] G. Hallett-Tapley, F. L. Cozens, N. P. Schepp, *J. Phys. Org. Chem.* **2009**, *22*, 343–348.
- [27] W. P. Jencks, *Acc. Chem. Res.* **1980**, *13*, 161–169.
- [28] W. P. Jencks, *Chem. Soc. Rev.* **1981**, *10*, 345–375.
- [29] J. P. Richard, W. P. Jencks, *J. Am. Chem. Soc.* **1984**, *106*, 1373–1383.
- [30] J. P. Richard, W. P. Jencks, *J. Am. Chem. Soc.* **1984**, *106*, 1383–1396.
- [31] T. W. Bentley, C. T. Bowen, W. Parker, C. I. F. Watt, *J. Chem. Soc., Perkin Trans. 2* **1980**, 1244–1252.
- [32] P. Mendes, *Comput. Appl. Biosci.* **1993**, *9*, 563–571.
- [33] P. Mendes, *Trends Biochem. Sci.* **1997**, *22*, 361–363.
- [34] P. Mendes, D. B. Kell, *Bioinformatics* **1998**, *14*, 669–883.
- [35] Further information about Gepasi: www.gepasi.org
- [S1] J. Bartl, S. Steenken, H. Mayr, R. A. McClelland, *J. Am. Chem. Soc.* **1990**, *112*, 6918–6928.

4.S Supplementary Data and Experimental Section

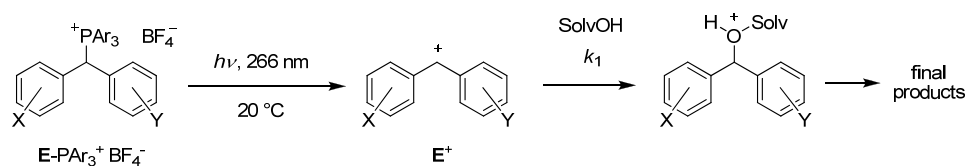
4.S.1 Materials. *Solvents.* HFIP (1,1,1,3,3,3-hexafluoro-2-propanol, Apollo, 99%) was refluxed with CaH_2 for 30 minutes and then distilled under nitrogen (CAUTION: oil bath temperature $\leq 80\text{ }^\circ\text{C}$).^[31] Doubly distilled water (Impedance $18.2\ \Omega$) was prepared with a water purification system (Milli-Q Plus machine from Millipore). The appropriate amounts of HFIP and water were combined to obtain the HFIP/water mixtures, which are given as (w/w).

Phosphonium salts. The phosphonium salts $\mathbf{E}\text{-PAr}_3^+ \text{BF}_4^-$ (Ar = Ph or *p*-Cl-C₆H₄) were prepared by heating $\mathbf{E}\text{-OH}$ with $\text{Ph}_3\text{PH}^+ \text{BF}_4^-$ or by treating $\mathbf{E}\text{-Br}$ with PAr_3 and subsequent anion metathesis. Details of the synthetic procedures are reported in CHAPTER 1 of this work.

4.S.2 Laser flash photolysis experiments. *Procedure.* For the laser-flash-photolytic generation of the benzhydryl cations, solutions of the precursor phosphonium salts with $A_{266\text{ nm}} \approx 0.2$ to 0.9 (ca. 10^{-4} M) were irradiated with a 7-ns laser pulse (fourth harmonic of Nd/YAG laser, $\lambda_{\text{exc}} = 266\text{ nm}$, 40-60 mJ/pulse). A xenon lamp was used as probe light for UV/vis detection. The system is equipped with a fluorescence flow cell and a dosage pump which allows replacing the sample cell volume completely between subsequent laser pulses. The setup is described in detail in ref.^[17]

Kinetics were measured by following the decay of the absorbances of the benzhydryl cations (see below for wavelengths) in the HFIP/water solvent mixtures. For each first-order rate constant, ≥ 64 individual runs were averaged. All measurements were performed in an air-conditioned laboratory at $20 \pm 1\text{ }^\circ\text{C}$.

The rate constants k_1 (s^{-1}) were obtained by least-squares fitting of the time-dependent absorbances of the benzhydryl cations to the single exponential curve $A_t = A_0 e^{-k_1 t} + C$. Non-exponential kinetics were evaluated using the software Gepasi.^[32-35]

4.S.3 Reactions of benzhydrylium ions (E^+) with HFIP/water mixtures at 20 °C

According to literature conventions, hexafluoroisopropanol/water mixtures are given as *w/w*. The following abbreviations are used: HFIP = 1,1,1,3,3,3-hexafluoro-2-propanol, W = water.

50HFIP50W (*w/w*) ($x_{\text{HFIP}} = 0.097$; 38.5 vol.-% HFIP)

		$[\text{E-PAr}_3^+ \text{BF}_4^-] / \text{M}$	Ar	λ / nm	k_1 / s^{-1}
E18⁺	ani(Ph)CH ⁺	6.30×10^{-5}	Ph	455	5.56×10^3 ^a
E20⁺	(tol) ₂ CH ⁺	6.60×10^{-5}	Ph	464	1.50×10^5
E21⁺	tol(Ph)CH ⁺	1.07×10^{-4}	Ph	450	1.20×10^6
E22⁺	(pfp) ₂ CH ⁺	1.04×10^{-4}	Ph	444	5.32×10^6

^a) The decay of **E18⁺** in 50HFIP50W does not follow first-order kinetics due to the recombination reaction with PPh₃.^[17] This k_1 value was therefore obtained by fitting the decay of [**E18⁺**] to a kinetic model consisting of a first-order process ($E^+ + \text{SolvOH} \rightarrow E\text{-OHSolv}^+$, rate constant k_1) and a second-order process ($E^+ + \text{PPh}_3 \rightarrow E\text{-PPh}_3^+$, rate constant $k_{\text{phosphine}}$) using the software package Gepasi.^[32-35] [**E18⁺**]₀ = [PPh₃]₀ = 1.42×10^{-6} M was calculated from the initial absorbance A_0 and $\epsilon = 6.17 \times 10^4 \text{ M}^{-1} \text{ cm}^{-1}$ (H₂SO₄).^[S1] The fit yielded the first-order rate constant $k_1 = 5.56 \times 10^3 \text{ s}^{-1}$ for the reaction of **E18⁺** with the solvent and the second-order rate constant $k_{\text{phosphine}} = 1.21 \times 10^{10} \text{ M}^{-1} \text{ s}^{-1}$ for the recombination reaction of **E18⁺** with PPh₃.

70HFIP30W (*w/w*) ($x_{\text{HFIP}} = 0.200$; 59.3 vol.-% HFIP)

		$[\text{E-PAr}_3^+ \text{BF}_4^-] / \text{M}$	Ar	λ / nm	k_1 / s^{-1}
E20⁺	(tol) ₂ CH ⁺	4.86×10^{-5}	Ph	464	1.13×10^5
E21⁺	tol(Ph)CH ⁺	7.28×10^{-5}	Ph	450	8.06×10^5
E22⁺	(pfp) ₂ CH ⁺	1.00×10^{-4}	Ph	444	3.25×10^6
E24⁺	Ar ₂ CH ⁺ ^a	1.09×10^{-4}	Ph	479	3.32×10^6
E25⁺	(Ph) ₂ CH ⁺	1.05×10^{-4}	Ph	435	7.52×10^6

^a) Ar = 3-fluoro-4-methylphenyl.

90HFIP10W (*w/w*) ($x_{\text{HFIP}} = 0.491$; 84.9 vol.-% HFIP)

		$[\text{E-PAr}_3^+ \text{BF}_4^-] / \text{M}$	Ar	λ / nm	k_1 / s^{-1}
E21⁺	tol(Ph)CH ⁺	5.28×10^{-5}	Ph	450	1.10×10^5
E22⁺	(pfp) ₂ CH ⁺	9.81×10^{-5}	Ph	444	3.74×10^5
E25⁺	(Ph) ₂ CH ⁺	1.05×10^{-4}	Ph	435	1.01×10^6
E27⁺	mfp(Ph)CH ⁺	1.09×10^{-4}	Ph	430	5.21×10^6
E29⁺	dfp(Ph)CH ⁺	1.42×10^{-4}	Ph	435	1.55×10^7
E30⁺	(mfp) ₂ CH ⁺	1.05×10^{-4}	Ph	425	2.10×10^7

93HFIP7W (w/w) ($x_{\text{HFIP}} = 0.588$; 89.3 vol.-% HFIP)

		[E-PAr ₃ ⁺ BF ₄ ⁻] / M	Ar	λ / nm	k_1 / s ⁻¹
E21 ⁺	tol(Ph)CH ⁺	6.82×10^{-5}	Ph	450	3.88×10^4
E22 ⁺	(pfp) ₂ CH ⁺	1.02×10^{-4}	Ph	444	1.39×10^5
E25 ⁺	(Ph) ₂ CH ⁺	1.19×10^{-4}	Ph	435	3.99×10^5
E26 ⁺	(pcp) ₂ CH ⁺	1.09×10^{-4}	Ph	472	2.61×10^5
E27 ⁺	mfp(Ph)CH ⁺	1.06×10^{-4}	Ph	435	1.96×10^6
E28 ⁺	tfm(Ph)CH ⁺	1.16×10^{-4}	Ph	430	6.26×10^6
E30 ⁺	(mfp) ₂ CH ⁺	1.14×10^{-4}	Ph	425	9.10×10^6
E31 ⁺	dfp(mfp)CH ⁺	1.18×10^{-4}	Ph	425	2.92×10^7

95HFIP5W (w/w) ($x_{\text{HFIP}} = 0.671$; 92.2 vol.-% HFIP)

		[E-PAr ₃ ⁺ BF ₄ ⁻] / M	Ar	λ / nm	k_1 / s ⁻¹
E21 ⁺	tol(Ph)CH ⁺	6.27×10^{-5}	Ph	450	1.67×10^4
E22 ⁺	(pfp) ₂ CH ⁺	6.74×10^{-5}	Ph	444	5.78×10^4
E25 ⁺	(Ph) ₂ CH ⁺	1.15×10^{-4}	Ph	435	1.70×10^5
E27 ⁺	mfp(Ph)CH ⁺	1.10×10^{-4}	Ph	430	8.61×10^5
E30 ⁺	(mfp) ₂ CH ⁺	1.06×10^{-4}	Ph	425	4.53×10^6
E31 ⁺	dfp(mfp)CH ⁺	1.07×10^{-4}	Ph	425	1.55×10^7

97HFIP3W (w/w) ($x_{\text{HFIP}} = 0.776$; 95.3 vol.-% HFIP)

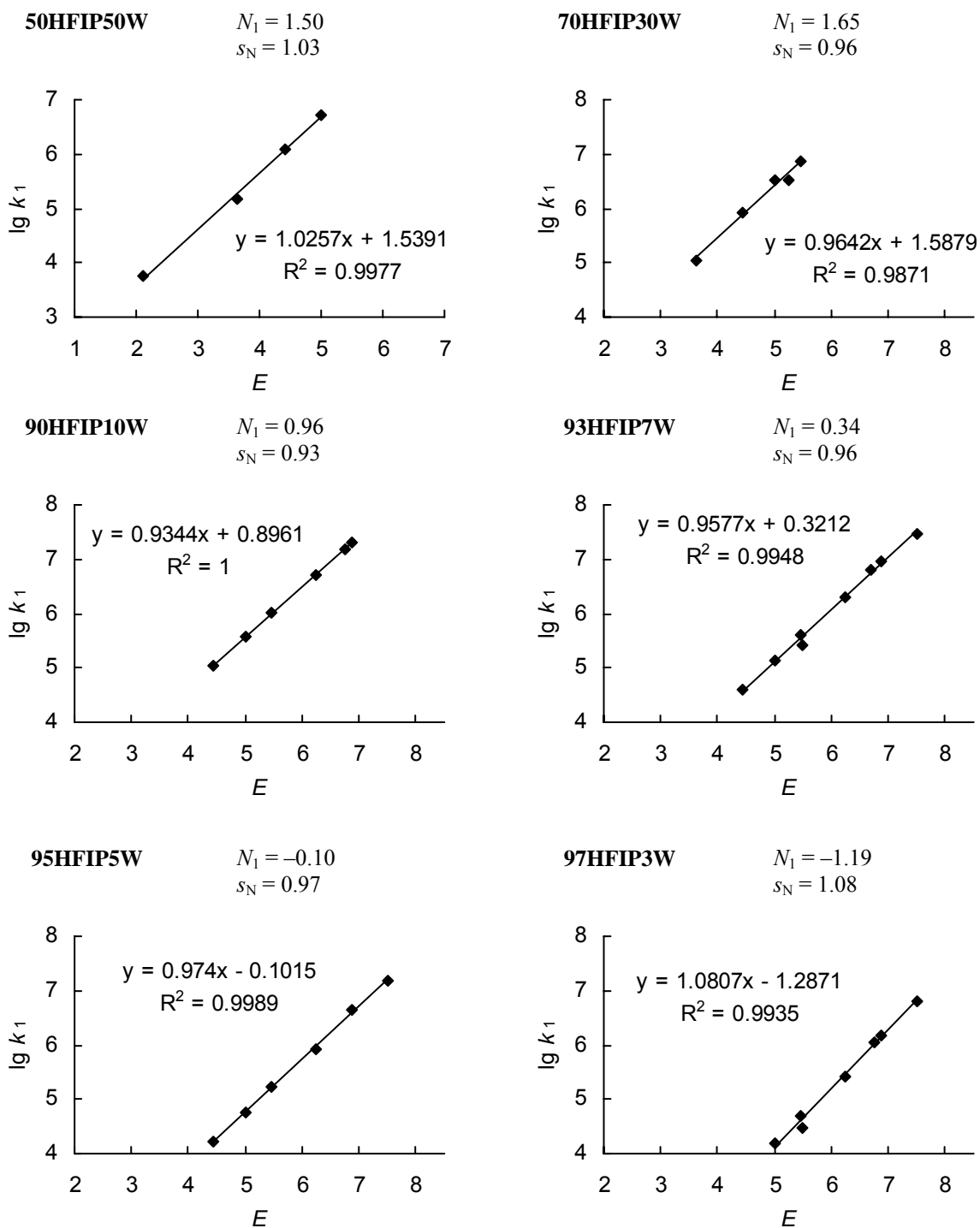
		[E-PAr ₃ ⁺ BF ₄ ⁻] / M	Ar	λ / nm	k_1 / s ⁻¹
E22 ⁺	(pfp) ₂ CH ⁺	1.04×10^{-4}	Ph	444	1.52×10^4
E25 ⁺	(Ph) ₂ CH ⁺	1.03×10^{-4}	Ph	435	5.01×10^4
E26 ⁺	(pcp) ₂ CH ⁺	1.05×10^{-4}	Ph	472	3.00×10^4
E27 ⁺	mfp(Ph)CH ⁺	1.05×10^{-4}	Ph	430	2.68×10^5
E29 ⁺	dfp(Ph)CH ⁺	1.10×10^{-4}	Ph	425	1.11×10^6
E30 ⁺	(mfp) ₂ CH ⁺	1.00×10^{-4}	Ph	425	1.46×10^6
E31 ⁺	dfp(mfp)CH ⁺	1.01×10^{-4}	Ph	425	6.48×10^6

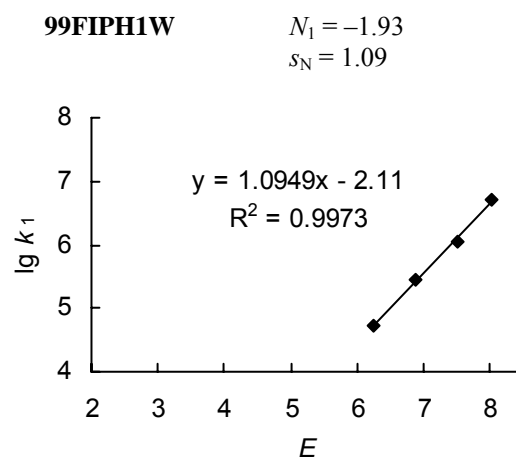
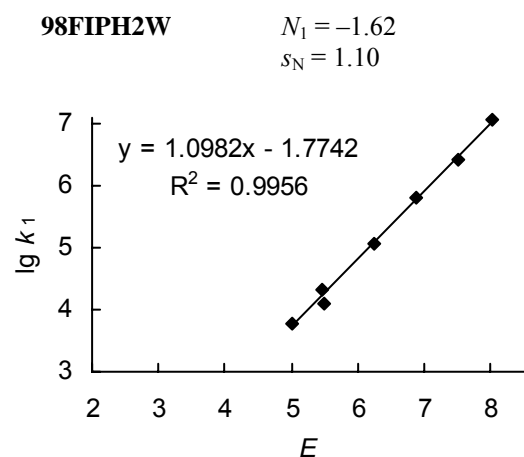
98HFIP2W (w/w) ($x_{\text{HFIP}} = 0.840$; 96.8 vol.-% HFIP)

		[E-PAr ₃ ⁺ BF ₄ ⁻] / M	Ar	λ / nm	k_1 / s ⁻¹
E22 ⁺	(pfp) ₂ CH ⁺	1.01×10^{-4}	Ph	444	6.17×10^3
E25 ⁺	(Ph) ₂ CH ⁺	1.14×10^{-4}	Ph	435	2.04×10^4
E26 ⁺	(pcp) ₂ CH ⁺	1.12×10^{-4}	Ph	472	1.24×10^4
E27 ⁺	mfp(Ph)CH ⁺	1.04×10^{-4}	Ph	430	1.14×10^5
E30 ⁺	(mfp) ₂ CH ⁺	1.07×10^{-4}	Ph	425	6.54×10^5
E31 ⁺	dfp(mfp)CH ⁺	1.04×10^{-4}	Ph	425	2.60×10^6
E33 ⁺	(dfp) ₂ CH ⁺	8.61×10^{-5}	<i>p</i> -Cl-C ₆ H ₄	439	1.20×10^7

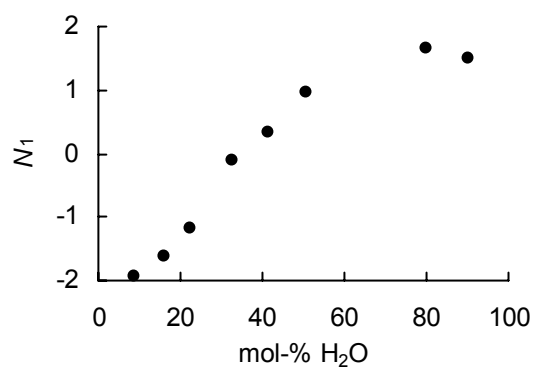
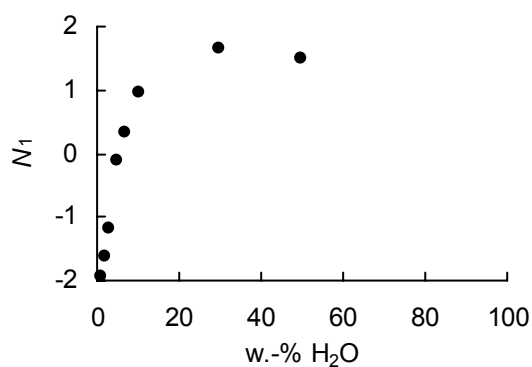
99HFIP1W (w/w) ($x_{\text{HFIP}} = 0.914$; 98.4 vol.-% HFIP)

		[E-PAr ₃ ⁺ BF ₄ ⁻] / M	Ar	λ / nm	k_1 / s ⁻¹
E27 ⁺	mfp(Ph)CH ⁺	1.01×10^{-4}	Ph	430	5.18×10^4
E30 ⁺	(mfp) ₂ CH ⁺	1.08×10^{-4}	Ph	425	2.72×10^5
E31 ⁺	dfp(mfp)CH ⁺	1.06×10^{-4}	Ph	425	1.15×10^6
E33 ⁺	(dfp) ₂ CH ⁺	8.52×10^{-5}	<i>p</i> -Cl-C ₆ H ₄	439	5.11×10^6

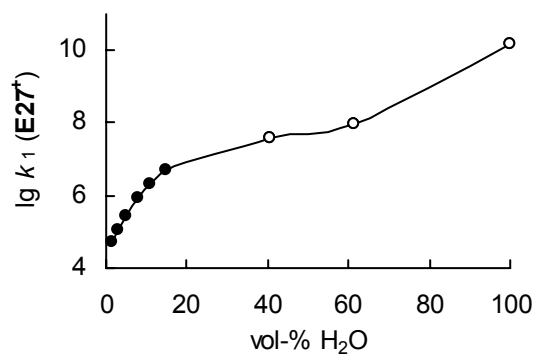
4.S.4 Plots of $\lg k_1$ versus E for all HFIP/water mixtures



4.S.5 Additional plots of N_1 and $\lg k_1$ (E_{27}^+) versus water content



The scatter in the plots is a result of the slightly differing slopes of the correlation lines. The point for 100W is not shown because of the different s_N parameter.



Closed symbols: Directly measured rate constants. Open symbols: Values calculated from eq. 1a (N_1 and s_N for 100W from ref.^[22]).

Substituent Effects on Intrinsic Barriers: A Closer Look at the Basic Principles Behind Linear Free Energy Relationships

Johannes Ammer, Thomas Singer, Tobias A. Nigst, Christoph Nolte, and Herbert Mayr

5.1 Introduction

Benzhydrylium ions \mathbf{E}^+ (Table 5.1) serve as reference compounds for empirical electrophilicity¹⁻⁴ and electrofugality scales.^{5,6} The rates of combination reactions of electrophiles with nucleophiles can be described by eq. 1, which relates the second-order rate constants k_2 ($\text{M}^{-1} \text{s}^{-1}$) to one electrophile-specific parameter E and two nucleophile-specific parameters N and s_N .¹⁻⁴

$$\lg k_2(20 \text{ }^\circ\text{C}) = s_N(N + E) \quad (1)$$

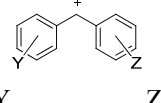
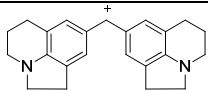
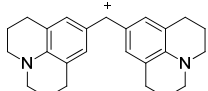
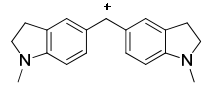
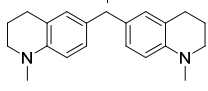
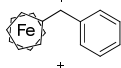
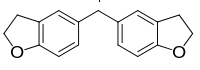
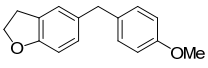
Analogously, heterolysis rate constants k_s (s^{-1}) of substrates R-X ($\text{X}^- = \text{Cl}^-, \text{Br}^-, \text{AcO}^-, \text{TsO}^-$, etc.) can be obtained from eq. 2 using one electrofuge-specific parameter E_f and two nucleofuge-specific parameters N_f and s_f .^{5,6}

$$\lg k_s(25 \text{ }^\circ\text{C}) = s_f(N_f + E_f) \quad (2)$$

In equations 1 and 2, the parameters E and E_f are defined as solvent-independent, while the nucleophile-specific parameters N and s_N , as well as the nucleofuge-specific parameters N_f and s_f , are defined with respect to a certain solvent.

Though theoretical approaches have been reported,⁷ the reason for the long-stretching linearity of these correlations is still not clear.^{3,8} We and other research groups have examined several rate-rate and rate-equilibrium relationships: Thus, the electrophilicity parameters E of the benzhydrylium ions \mathbf{E}^+ were reported to correlate linearly with the Hammett-Brown σ^+ constants,¹ the one-electron reduction potentials E_{red}^0 of the benzhydrylium ions \mathbf{E}^+ ,⁹ their $\text{p}K_{\text{R}^+}$ values,¹⁰ the calculated methyl anion affinities of \mathbf{E}^+ in the gas phase,¹¹ and the calculated hydride anion affinities of \mathbf{E}^+ in the gas phase and in CH_3CN solution.¹² The

Table 5.1. Reference electrophiles **E(1-33)⁺** with their electrophilicity parameters E , electrofugality parameters E_f , and calculated methyl anion affinities ΔG_{MA} .

no.		E^a	E_f^b	$\Delta G_{\text{MA}}^{c,d}$ / kJ mol ⁻¹
E1⁺		-10.04	5.05	-639.8
E2⁺		-9.45	5.61	-642.2
E3⁺		-8.76	4.83	-654.5
E4⁺		-8.22	5.22	-654.0
E5⁺	Y = Z = 4-(<i>N</i> -pyrrolidino)	-7.69	5.35	-658.3
E6⁺	Y = Z = 4-N(Me) ₂	-7.02	4.84	-670.7
E7⁺	Y = Z = 4-N(Me)(Ph)	-5.89	3.46	-667.1
E8⁺	Y = Z = 4-(<i>N</i> -morpholino)	-5.53	3.03	-688.2
E9⁺	Y = Z = 4-N(Ph) ₂	-4.72	1.78	-689.9
E10⁺	Y = Z = 4-N(Me)(CH ₂ CF ₃)	-3.85	3.13	-711.9
E11⁺	Y = Z = 4-N(Ph)(CH ₂ CF ₃)	-3.14	1.79	-708.5
E12⁺		-2.64	^e	^e
E13⁺		-1.36	1.07	-728.8
E14⁺		-0.81	0.61	^e
E15⁺	4-MeO 4-MeO	0.00	0.00	-747.2
E16⁺	4-MeO 4-PhO	0.61	-0.86	-747.6
E17⁺	4-MeO 4-Me	1.48	-1.32	-765.3
E18⁺	4-MeO H	2.11	-2.09	-781.7
E19⁺	4-PhO H	2.90	-3.52	-782.5
E20⁺	4-Me 4-Me	3.63	-3.44	-789.8
E21⁺	4-Me H	4.43	-4.63	-807.0
E22⁺	4-F 4-F	5.01	^e	-834.3
E23⁺	4-F H	5.20	-5.72	-828.9
E24⁺	3-F, 4-Me 3-F, 4-Me	5.24	-6.37 ^d	-823.9
E25⁺	H H	5.47	-6.03	-827.6
E26⁺	4-Cl 4-Cl	5.48	-6.91	-836.1
E27⁺	3-F H	6.23	-7.53	-844.7
E28⁺	4-(CF ₃) H	6.70	-8.66 ^d	-859.5
E29⁺	3,5-F ₂ H	6.74	-9.00 ^f	-863.0
E30⁺	3-F 3-F	6.87	-9.26	-865.0
E31⁺	3,5-F ₂ 3-F	7.52	-10.88	-882.2
E32⁺	4-(CF ₃) 4-(CF ₃)	7.96	^e	-891.8
E33⁺	3,5-F ₂ 3,5-F ₂	8.02	-12.60	-904.1

^a Electrophilicity parameters E from ref.⁴ ^b Electrofugality parameters E_f from ref.⁶ unless noted otherwise.
^c Methyl anion affinities of the benzhydrylium ions calculated on the B3LYP/6-311++G(3df,2pd)//B3LYP/6-31G(d,p) level of theory. ^d This work. ^e Not determined. ^f From ref.¹³

observation that correlations of the electrophilicity parameters E with various gas phase and solution phase thermodynamic parameters are more or less linear over the entire range of $-10 \leq E \leq 6$ led Zhu *et al.* to the statement that it was “reasonable to deduce that the E values are thermodynamic data but not kinetic data”.¹²

Based on a limited set of data, we initially reported an inverse relationship between the electrophilicities E and the electrofugalities E_f of the benzhydrylium ions \mathbf{E}^+ .^{5,14} However, it was later shown that this inverse relationship does not hold for highly stabilized benzhydrylium ions ($E < -6$) because the ionization rates (and thus the E_f parameters) of these systems are largely controlled by differences in intrinsic barriers and not by the stabilization (Lewis acidities) of the carbocations.^{6,15,16}

The observation that a plot of the rate constants k_s for the reactions of donor- and acceptor-substituted tritylium ions with an acetonitrile/water mixture (1:2 v/v) versus σ^+ is curved¹⁷ has been taken as an indication of an imbalance between resonance and polar effects in the transition state.^{17,18a} An analogous series of benzhydrylium ions could not be investigated at the time due to the high reactivity of the acceptor-substituted systems, but it was noted that the behavior of the donor-substituted benzhydrylium ions is comparable to that of analogously substituted tritylium ions.¹⁷

Only recently, we have developed a method to generate highly reactive carbenium ions by laser flash photolysis of benzhydryl triarylphosphonium salts with complex counter-anions¹⁹ and employed it to characterize the electrophilic reactivities of acceptor-substituted benzhydrylium ions.⁴ One remarkable result of these studies was that fast reactions without enthalpic barriers ($\Delta H^\ddagger = 0$, i. e., entropy-controlled reactions) follow eq. 1 equally well as slower reactions where reactivity differences result from variations of the activation enthalpies ΔH^\ddagger ,⁴ and presently we do not understand the reasons for this behavior.

Figure 5.1 illustrates another result of our recent work:^{4,20} We investigated reactions of benzhydrylium ions with different kinds of nucleophiles, including various π -systems,⁴ triethyl silane (hydride donor),⁴ trifluoroethanol,⁴ and different hexafluoroisopropanol/water mixtures.²⁰ Despite the large structural variations of the nucleophiles, we always found linear correlations of $\lg k_2$ or $\lg k_1$ versus E in reaction series which included reactions of both donor- and acceptor-substituted systems (Fig. 5.1). This finding is quite remarkable as it is in conflict with at least one of the literature statements discussed above – either with Zhu’s view that the E parameters are “thermodynamic” parameters,¹² or with the expected^{17,18} transition state imbalance between resonance and polar effects.

Clearly, there is a problem in our present understanding of chemical reactivity, and a closer look on how substituents affect the free energy barriers ΔG^\ddagger for the reactions of benzhydrylium ions with nucleophiles is now warranted.

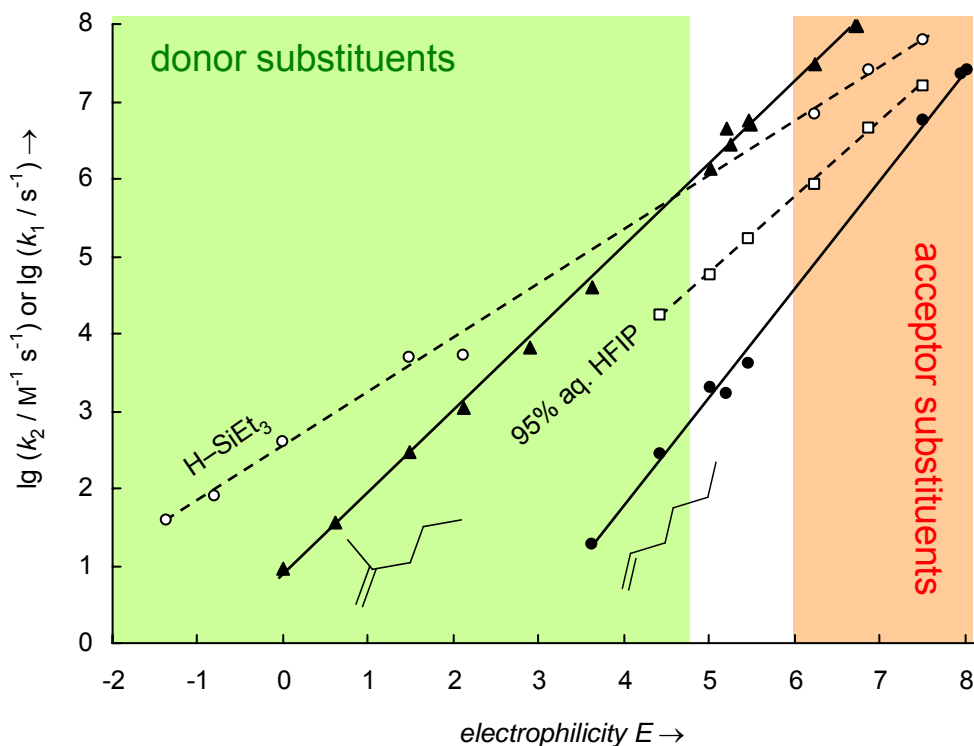


Figure 5.1. Plots of $\lg k$ for the reactions of benzhydrylium ions with the π -nucleophiles 2-methylpent-1-ene (closed triangles) and 1-hexene (closed circles), and the hydride donor triethylsilane (open circles), as well as for the first-order decays of benzhydrylium ions in 95% aqueous hexafluoroisopropanol (HFIP; open squares) against the electrophilicity parameters E of the benzhydrylium ions. Green: Benzhydrylium ions with donor substituents such as *p*-methyl or *p*-alkoxy. Red: Benzhydrylium ions with acceptor substituents such as *m*-fluoro or *p*-(trifluoromethyl). In between: Parent compound and benzhydrylium ions with substituents that combine electron-donating resonance effects with electron-withdrawing inductive effects (e.g., *p*-fluoro).

5.2 Results and Discussion

5.2.1 Correlation of Electrophilicity Parameters E with Other Thermodynamic and Kinetic Data. *Hammett analysis.* A linear correlation between electrophilicities E of symmetrically substituted E^+ and the Hammett-Brown σ^+ constants for the substituents was previously reported.¹ Inclusion of acceptor-substituted benzhydrylium ions⁴ reduces the quality of the linear correlation considerably (Figure 5.S.1.1 in section 5.S.1). The correlation

now shows a slight downward curvature indicating that the σ^+ constants underestimate the retarding effect of the *p*-alkoxy and *p*-amino groups on the reactions of benzhydrylium ions \mathbf{E}^+ with nucleophiles. However, solvolyses of *tert*-cumyl chlorides, from which the σ^+ constants were derived, may not be the best choice of reference reactions for discussing the reactivities of \mathbf{E}^+ towards π -nucleophiles.

Electrofugality. As the ionization of $\mathbf{E-LG}$ is just the reverse of the combination reaction of \mathbf{E}^+ with the anionic nucleophile LG^- , it is tempting to assume an inverse relationship between E_f and E . In our first report on this topic, we indeed found $E_f \approx -E$ for $\mathbf{E(15-25)}^+$ ($0 \leq E < 6$),^{5,14} although we had emphasized that the unity slope is only a consequence of the arbitrary definitions of the sensitivity parameters for nucleophiles ($s_N = 1.00$ for 2-methylpent-1-ene)¹ and for nucleofuges ($s_f = 1.00$ for Cl^- in ethanol).^{5,14} However, later investigations showed that solvolyses leading to the better stabilized carbocations $\mathbf{E(1-11)}^+$ ($E < -3$) were slower than expected from the E parameters of the resulting benzhydrylium ions, and even the order of reactivities was different: For example, $\mathbf{E5}^+$ is a better electrofuge than $\mathbf{E1}^+$ although $\mathbf{E5}^+$ is ~220 times more electrophilic.¹⁵ The different behavior of the amino-substituted benzhydrylium ions $\mathbf{E(1-11)}^+$ in relative rates of reactions with nucleophiles and relative rates of formation by heterolytic cleavage reactions was explained by the fact that the heterolysis reactions are not controlled by the relative thermodynamic stabilities of the carbocations but by the different intrinsic barriers. Solvolysis reactions yielding less stable carbocations such as $\mathbf{E(20-33)}^+$, on the other hand, are mainly controlled by the differences in the thermodynamic stabilities of the carbocations.^{6,15,16}

Deviations from the linear electrofugality vs electrophilicity correlation are also observed for the acceptor-substituted benzhydrylium ions $\mathbf{E(27-33)}^+$. The most reactive benzhydrylium ion of this series, $\mathbf{E33}^+$ ($E = 8.02$), is only ~350 times more electrophilic than $\mathbf{E25}^+$ ($E = 5.47$)⁴ although the heterolytic generation of $\mathbf{E25}^+$ ($E_f = -6.03$) is over three million times faster than that of $\mathbf{E33}^+$ ($E_f = -12.60$).⁶ When we include the acceptor-substituted benzhydrylium ions $\mathbf{E(27-33)}^+$ in a plot of E_f versus E , which now spans 18 orders of magnitude in E and in E_f , it becomes apparent that the plot is curved (Fig. 5.2).

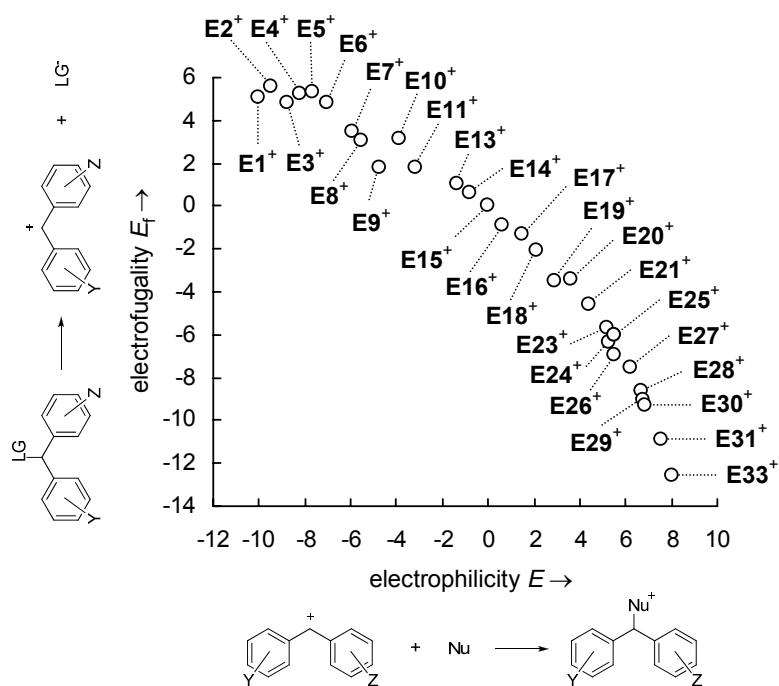


Figure 5.2. Plot of electrofugality E_f versus electrophilicity E of benzhydrylium ions E^+ .

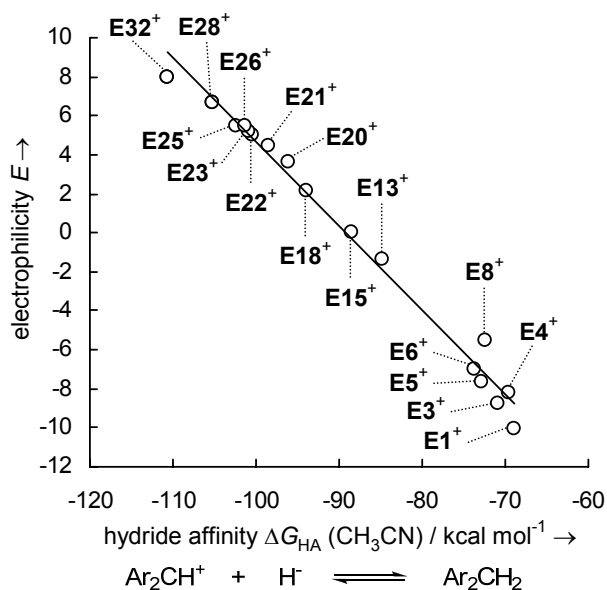


Figure 5.3. Plot of E versus Zhu's calculated hydride affinities in CH_3CN solution ($E = -0.4322\Delta G_{\text{HA}} - 38.567$, $R^2 = 0.9858$).

Hydride affinities. In order to elucidate the origin of the substituent effects on the electrophilic reactivities of the benzhydrylium ions E^+ , we now relate the electrophilicity parameters E of E^+ to a scale of relative thermodynamic stabilities of the benzhydrylium ions. Zhu *et al.* reported a linear correlation of E with calculated hydride affinities ΔG_{HA} of the

benzhydrylium ions \mathbf{E}^+ in CH_3CN solution.¹² After including the E parameters for the $p\text{-CF}_3$ -substituted systems $\mathbf{E28}^+$ ($E = 6.70$) and $\mathbf{E32}^+$ ($E = 7.96$) and updating the values for $\mathbf{E(21-26)}^+$,⁴ we still observe a moderately linear correlation of E with the hydride affinities reported by Zhu *et al.*¹² (Fig. 5.3). A slight curvature again indicates that the gradient is smaller for acceptor-substituted systems.

Methyl anion affinities. In previous work, we had calculated the methyl anion affinities ΔG_{MA} in the gas phase for a number of benzhydrylium ions according to eq. 3 at the B3LYP/6-31G-(d,p) level of theory.¹¹



We found a linear correlation of the E parameters of 11 benzhydrylium ions in the range $-10 \leq E < +6$ with their methyl anion affinities ΔG_{MA} in the gas phase, and only $\mathbf{E26}^+$ deviated slightly from this correlation.¹¹ In order to provide a thermodynamic stability scale for the benzhydrylium ions, we now calculated the methyl anion affinities ΔG_{MA} (eq. 3) in the gas phase for 31 benzhydrylium ions on the B3LYP/6-311++G(3df,2pd)//B3LYP/6-31G(d,p) level. The obtained methyl anion affinities ΔG_{MA} are listed in Table 5.1. Figure 5.S.2.1a in section 5.S.2 shows a linear correlation with unity slope between the gas phase methyl anion affinities ΔG_{MA} from this work and the hydride affinities ΔG_{HA} of the benzhydrylium ions \mathbf{E}^+ in the gas phase which were calculated by Zhu *et al.* on the BLYP/6-311++G (2df, 2p) level,¹² in line with previous observations that structural variation of the benzhydrylium ions affects their affinities toward different anions in the same manner.^{11,12}

When we plotted the electrophilicity parameters E of the benzhydrylium ions $\mathbf{E(1-33)}^+$ covering the whole range of $-10 \leq E \leq +8$ against the gas phase methyl anion affinities ΔG_{MA} determined in this work, we again observed a curved plot (see Fig. 5.8 in section 5.2.4) similar to the correlation between E and ΔG_{HA} (Fig. 5.3). We will come back to this curved plot in section 5.2.4.

Are the curvatures in these plots caused by solvation effects? All comparisons made so far have in common that we correlated the electrophilicity parameters E , which were derived from reactions of \mathbf{E}^+ towards π -nucleophiles in CH_2Cl_2 , with some other quantity which was derived from data in a different solvent or in the gas phase. Although the E parameters were defined independent of the solvent,¹ one may thus wonder whether the curvatures in Figures

5.2 (E vs E_f), 5.3 (E vs ΔG_{HA}), 5.8 (E vs ΔG_{MA}), and 5.S.1.1 (E vs σ^+) result from a differential solvation of acceptor-substituted benzhydrylium ions with respect to the donor-substituted systems. However, this possibility can be ruled out by the excellent linear correlations between the rate constants for reactions of donor- and acceptor-substituted benzhydrylium ions \mathbf{E}^+ in acetonitrile and trifluoroethanol,⁴ as well as in different hexafluoroisopropanol/water mixtures,²⁰ with the E parameters of the benzhydrylium ions which were derived from reactions in CH_2Cl_2 . Similar linear correlations have also been reported between solution phase and gas phase thermodynamic stabilities of the benzhydrylium ions¹² (also see Fig. 5.S.2.1b in section 5.S.2). Consequently, the curvatures in Figures 5.2, 5.3, 5.8 and 5.S.1.1 cannot be explained by differential solvation effects.

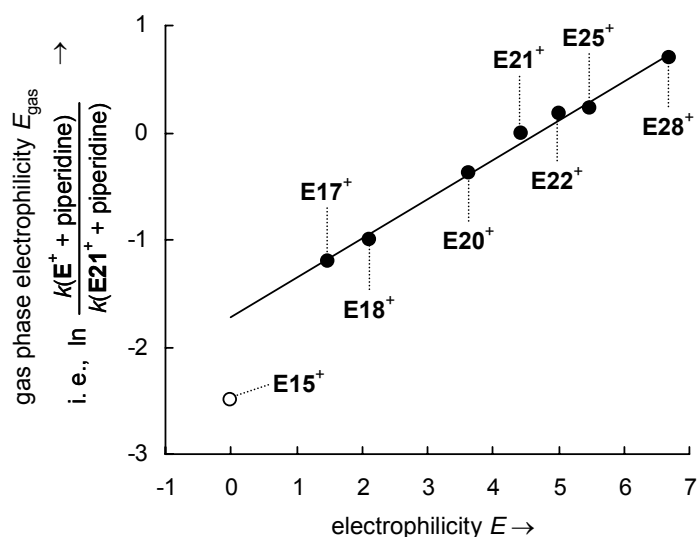


Figure 5.4. Plot of Denekamp's gas phase electrophilicity parameters E_{gas} , i. e., $\ln [k(\mathbf{E}^+ + \text{piperidine})/k(\mathbf{E21}^+ + \text{piperidine})]$, versus solution phase electrophilicity parameters E ($E_{\text{gas}} = 0.3684E - 1.7286$; $R^2 = 0.9917$; note that the use of \ln instead of \lg on the ordinate results in a 2.303 times larger slope). The point for $\mathbf{E15}^+$ (open symbol) was not used for the correlation (see ref.²¹).

Gas phase electrophilicity parameters. That the effect of solvation on the rates of the reactions of benzhydrylium ions with nucleophiles changes linearly with the intrinsic reactivities of the benzhydrylium ions is also illustrated by a comparison of solution phase and gas phase reactivities of the benzhydrylium ions $\mathbf{E(17-28)}^+$. Denekamp *et al.* have derived gas phase electrophilicity parameters E_{gas} for these benzhydrylium ions based on the gas phase reactions of \mathbf{E}^+ with various amines and demonstrated a linear correlation of E_{gas} with the solution phase electrophilicity parameters E that were derived from reactions of \mathbf{E}^+ with

π -nucleophiles in CH_2Cl_2 .²¹ Figure 5.4 shows an update of this correlation using the revised E parameters for **E21**⁺ and **E25**⁺ and including the E values of **E22**⁺ and the p - CF_3 -substituted benzhydrylium ion **E28**⁺.⁴ Like Denekamp *et al.*,²¹ we did not include **E15**⁺ in the correlation due to experimental uncertainties in the determination of E_{gas} . The excellent correlation between the gas phase (E_{gas}) and solution phase electrophilic reactivities (E) of **E**⁺ also holds for highly electrophilic carbocations such as **E28**⁺ ($E = 6.70$). This demonstrates again the absence of differential solvation effects in reactions of donor- and acceptor-substituted benzhydrylium ions with nucleophiles, and confirms our previous finding that the influence of ion pairing on the electrophilic reactivities of **E**⁺ in CH_2Cl_2 solution is negligible also for such highly electrophilic carbocations.^{4,19}

5.2.2 Quantitative Free-energy Profiles for Combination Reactions of Benzhydrylium Ions with Nucleophiles. Before we examine the reasons for the curved correlations between the E parameters and other thermodynamic and kinetic parameters discussed in section 5.2.1, let us go one step back and have a look at the behavior of donor- and acceptor-substituted benzhydrylium ions **E**⁺ in reactions with π -nucleophiles, which were employed to derive the E parameters of **E**⁺.¹⁻⁴

2-Methylpent-1-ene. Using the recently published rate constants for reactions of the benzhydrylium ions **E(25-30)**⁺ with 2-methylpent-1-ene (**N8**),⁴ we can construct free-energy profiles for these reactions. Analogous free-energy profiles have previously been drawn for the reactions of **N8** with **E(15-20)**⁺,^{22,23} it will be interesting to compare the behavior of the acceptor-substituted systems (Fig. 5.5).

In Fig. 5.5, the substituted benzhydryl chlorides **E(15-30)**-Cl are positioned at the same level. The Gibbs free energies of the carbocations **E(15-30)**⁺ are then given by the free ionization energies ΔG_{i}^0 of **E(15-30)**-Cl in CH_2Cl_2 according to eq. 4.



The values of the free ionization energies ΔG_{i}^0 (eq. 4) were obtained as follows: As reactions of **E(15-30)**⁺ with Cl^- in CH_3CN are diffusion controlled,²⁴ one can conclude that there is also no barrier for the combination of **E(15-30)**⁺ with Cl^- in CH_2Cl_2 solution. Therefore, the free energies of activation $\Delta G_{\text{i}}^\ddagger$ for the ionization reactions of **E(15-30)**-Cl reflect the free ionization energies ΔG_{i}^0 of **E(15-30)**-Cl in CH_2Cl_2 (eq. 4). Substituting the electrofugality

parameters E_f^6 of \mathbf{E}^+ and the nucleofugality parameters $N_f = -0.57$ and $s_f = 1.28$ for Cl^- in CH_2Cl_2 ²⁵ into eq. 2 yields the rate constants for the ionization of $\mathbf{E}-\text{Cl}$ to \mathbf{E}^+ and Cl^- , which are converted to the free energies of activation ΔG_i^\ddagger for the ionization reaction by the Eyring equation (eq. 5).

$$k = \frac{k_B T}{h} \cdot e^{-\frac{\Delta G^\ddagger}{RT}} \quad (5)$$

These ΔG_i^\ddagger values provide the relative thermodynamic stabilities ΔG_i^0 of the carbocations $\mathbf{E}(\mathbf{15-30})^+$ with respect to the covalent benzhydryl chlorides in CH_2Cl_2 , which are plotted in Fig. 5.5. Figure 5.S.3.1 in section 5.S.3 illustrates that the ΔG_i^0 values calculated by this method agree well with the few $\Delta \Delta G_i^0$ values which have been derived from equilibrium constants in CH_2Cl_2 .^{26,27}

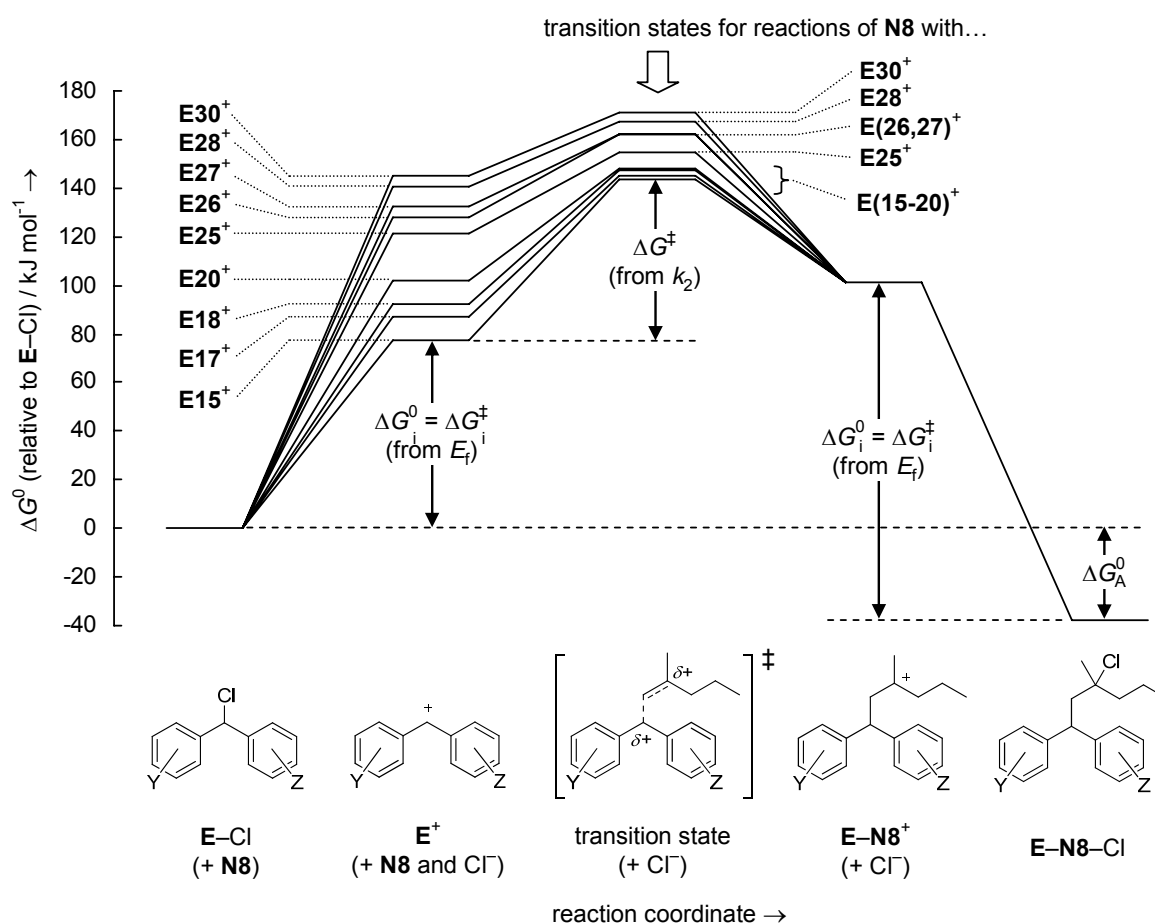


Figure 5.5. Gibbs free energy profiles for the reactions of benzhydrylium ions \mathbf{E}^+ with 1 M 2-methylpent-1-ene (**N8**) in CH_2Cl_2 at 20 °C.

The positions of the transition states in Fig. 5.5 are defined by the free energies of activation ΔG^\ddagger for the reactions of **E(15-30)**⁺ with **N8** which are calculated from the Eyring equation (eq. 5) and the experimental rate constants k_2 from refs.^{1,4} The products of the combination reactions are the tertiary alkyl cations **E(15-30)-N8**⁺ (Fig. 5.5). The thermodynamic stabilities of these carbocations are more or less independent of the remote aryl groups. Rate constants of $(0.9 - 2.4) \times 10^{-4} \text{ s}^{-1}$ were measured for solvolyses of **E(15,20,25,26)-N8-Cl** in 80% aqueous ethanol at 50 °C,²⁸ from which one can estimate electrofugalities $E_f \approx (-8.7 \text{ to } -8.2)$ for **E-N8**⁺ (Table 5.S.3.2 in section 5.S.3) which are similar to that of the structurally related *tert*-butyl cation ($E_f \approx -8.21$).²⁹ In analogy to the procedure for the benzhydryl chlorides, we can calculate the ionization rate constant of **E-N8-Cl** in CH₂Cl₂ and thus $\Delta G^\ddagger_i = \Delta G^0_i$ from eq. 2. To place **E-N8**⁺ in the free-energy profile, we have to know the position of **E-N8-Cl** relative to **E-Cl + N8** which is given by the free energy of addition ΔG^0_A of **N8** to **E-Cl**. The heats of addition ΔH^0_A of **N8** to **E(17-25)-Cl** have been measured as $-86.5 \text{ kJ mol}^{-1}$ independent of the aryl substituents.²⁶ In analogy to our previous treatment,²² ΔH^0_A can be combined with the estimated $\Delta S^0_A \approx -164 \text{ J mol}^{-1} \text{ K}^{-1}$ to obtain ΔG^0_A . The numeric values obtained from these calculations are compiled in section 5.S.3.

The alkoxy- and methyl-substituted benzhydrylium ions **E(15-20)**⁺ exhibit the previously described behavior: The separations of the energy levels in the transition states are much smaller than the stability differences of the benzhydryl cations (Fig. 5.5).^{22,23} However, the reactions of **E(25-30)**⁺ with **N8** show a completely different behavior: For these reactions, the separations of the energy levels in the transition states are almost as large as the stability differences between the benzhydrylium ions (Fig. 5.5), indicating that the substituent effects in the transition states are of comparable magnitude as those in the benzhydrylium ions. Relatively high ΔG^0 values of the transition states with respect to the ground states are found for the reactions of **E26**⁺ (Fig. 5.5) as well as **E19**⁺ and **E24**⁺ (not shown).

Other nucleophiles. Figure 5.6 shows additional Gibbs free energy profiles for the reactions of benzhydrylium ions with other nucleophiles. The ΔG^0 values of the benzhydrylium ions **E**⁺ in Fig. 5.6 were calculated with respect to the covalent benzhydryl chlorides **E-Cl** as described above, and the ΔG^0 values of the transition states were obtained from the Eyring equation (eq 5) and the rate constants for these reactions published in ref.⁴ The energies of the products are not known, but they can again be expected to be virtually independent of the substituents on the phenyl rings. For the series of the donor-substituted benzhydrylium ions,

$\mathbf{E(13-25)}^+$, the separations of the transition states are much smaller than the stability differences of the carbocations. In the series of the acceptor-substituted benzhydrylium ions, $\mathbf{E(25-33)}^+$, on the other hand, the separations of the transition states are comparably large and almost of the same magnitude as the stability differences of the carbocations. Again, $\mathbf{E19}^+$ (Fig. 5.6a) and $\mathbf{E26}^+$ (Fig. 5.6c) show relatively high ΔG^0 values of the transition states with respect to the ground states.

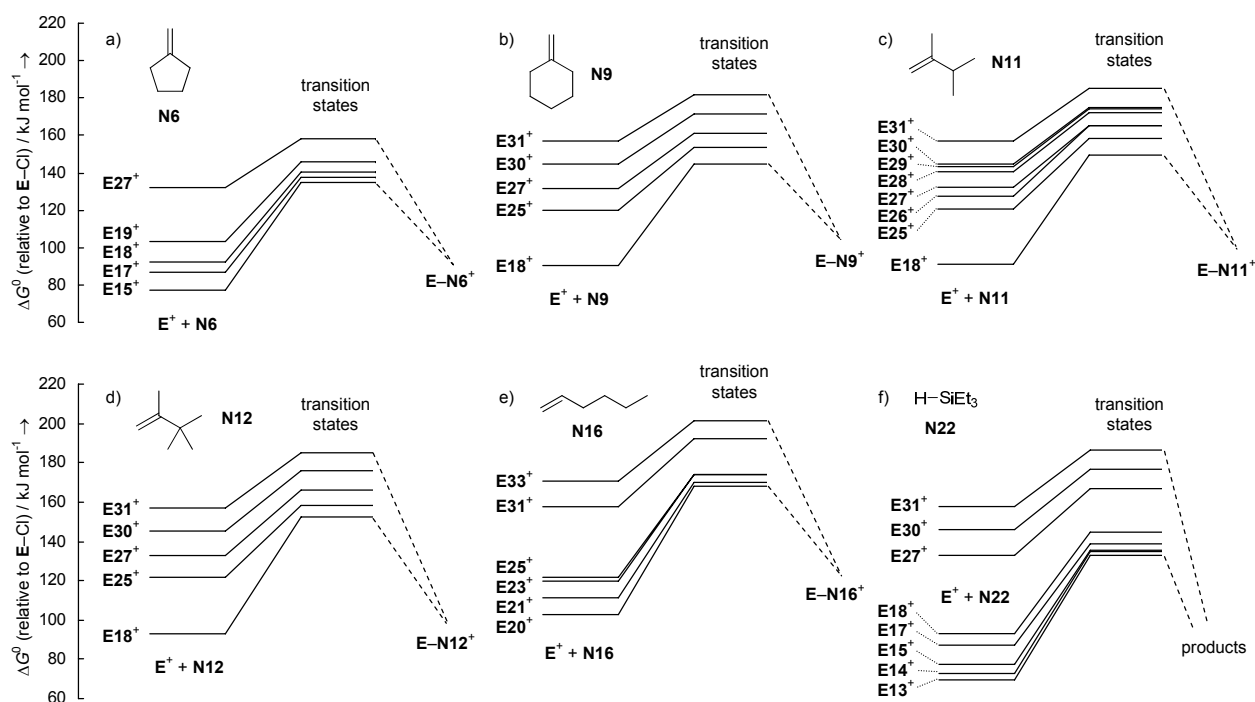


Figure 5.6. Gibbs free energy profiles for reactions of benzhydrylium ions \mathbf{E}^+ with (a) methylenecyclopentane, (b) methylenecyclohexane, (c) 2,3-dimethylbut-1-ene, (d) 2,3,3-trimethylbut-1-ene, (e) hex-1-ene, and (f) triethylsilane (1 M, CH_2Cl_2 , 20 °C).

We have thus demonstrated a close analogy between the Gibbs free energy profiles for the reactions of benzhydrylium ions \mathbf{E}^+ with different alkenes (Figures 5.5 and 5.6a-e) and the hydride donor triethylsilane (Fig. 5.6f). From the excellent correlations of $\lg k_2$ for numerous reactions of \mathbf{E}^+ with different nucleophiles with the E parameters of \mathbf{E}^+ (Fig. 5.1 and refs.^{4,20}), we conclude that the observed substituent effects on the reaction kinetics must be a general phenomenon. Most remarkable are the far-stretching series of rate constants for the reactions of donor- and acceptor-substituted benzhydrylium ions \mathbf{E}^+ with trifluoroethanol⁴ and hexafluoroisopropanol/water mixtures²⁰ that were found to correlate linearly with the E parameters derived from reactions of \mathbf{E}^+ in CH_2Cl_2 .

5.2.3 The Role of Intrinsic Barriers in Combination Reactions. A different treatment of the data shown in Fig. 5.5 is provided by Fig. 5.7a which plots ΔG^\ddagger for the reactions of **E(15-30)⁺** with **N8** versus ΔG_i^0 for the ionization of **E(15-30)–Cl**. Following the classic interpretation of such plots by Leffler, the slope $0 < \alpha < 1$ provides information about the structure of the transition state,³⁰⁻³² but we will show in the following that this interpretation is not correct in our case.

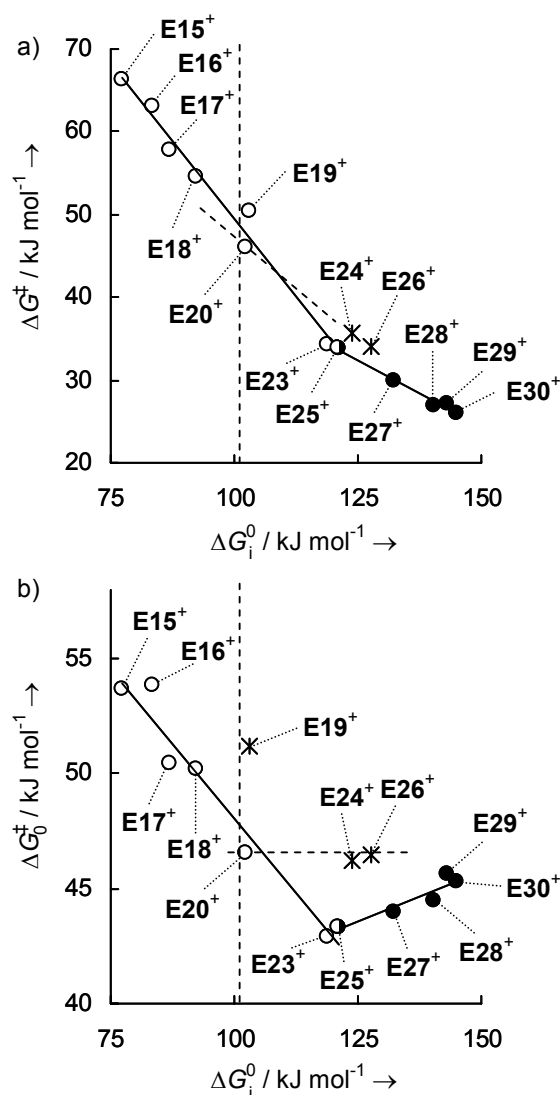


Figure 5.7. (a) Correlations between experimental ΔG^\ddagger for the reactions of **E⁺** with **N8** and ΔG_i^0 for ionization of **E–Cl**. Open symbols: **E(15-25)⁺** ($\Delta G^\ddagger = -0.7472\Delta G_i^0 + 124.15$; $R^2 = 0.9837$); filled symbols: **E(25-30)⁺** ($\Delta G^\ddagger = -0.3238\Delta G_i^0 + 72.922$; $R^2 = 0.9871$); data for **E24⁺** and **E26⁺** (*) were not used for the fits. (b) Correlations between the intrinsic barriers ΔG_0^\ddagger for the reactions of **E⁺** with **N8** and ΔG_i^0 for ionization of **E–Cl**. Open symbols: **E(15-25)⁺** ($\Delta G_0^\ddagger = -0.2576\Delta G_i^0 + 73.833$; $R^2 = 0.9612$); filled symbols: **E(25-30)⁺** ($\Delta G_0^\ddagger = 0.0895\Delta G_i^0 + 32.354$; $R^2 = 0.8730$); data for **E19⁺**, **E24⁺** and **E26⁺** (*) were not used for the fits. The vertical dashed lines indicate a reaction with $\Delta G^0 = 0$; the diagonal dashed line in Fig. a indicates a slope of $\alpha = 0.5$, which would be expected for reactions with $\Delta G^0 \approx 0$ and constant intrinsic barriers ΔG_0^\ddagger .

The Marcus equation^{34,35} (eq. 6, the work terms are neglected) relates ΔG^\ddagger to the reaction free energy ΔG^0 and the intrinsic barrier ΔG_0^\ddagger of a reaction, which is defined as the activation free energy of a process with $\Delta G^0 = 0$.

$$\Delta G^\ddagger = \Delta G_0^\ddagger + 0.5\Delta G^0 + \frac{(\Delta G^0)^2}{16\Delta G_0^\ddagger} \quad (6)$$

We can thus use eq. 6 to separate ΔG^\ddagger into a thermodynamic component and the intrinsic barrier ΔG_0^\ddagger which corresponds to ΔG^\ddagger of a reaction with $\Delta G^0 = 0$ and is associated with the reorganization that is required for a reaction. The intrinsic barriers ΔG_0^\ddagger for the reactions of **E(15-30)**⁺ with **N8** are plotted in Fig. 5.7b against the thermodynamic stabilities of the carbocations (ΔG^0_i). The experiment where we come closest to the direct observation of ΔG_0^\ddagger is the reaction of **E20**⁺ with **N8** which is exergonic by only 1.2 kJ mol⁻¹ but has a barrier of $\Delta G^\ddagger = 45.9$ kJ mol⁻¹ (Fig. 5.5).

For constant intrinsic barriers, differentiation of eq. 6 with respect to ΔG^0 yields the Leffler parameter α according to eq. 7.^{31,33-37}

$$\alpha = \frac{\partial \Delta G^\ddagger}{\partial \Delta G^0} = \frac{1}{2} \left(1 + \frac{\Delta G^0}{4\Delta G_0^\ddagger} \right) \quad (7)$$

Eq. 7 predicts $\alpha = 1/2$ for reactions with $\Delta G^0 = 0$ (indicated by the vertical dashed lines in Fig. 5.7), values of $\alpha > 1/2$ for endergonic reactions and $\alpha < 1/2$ for exergonic reactions. Although ΔG^0 for the reaction with **E20**⁺ is almost zero, Figure 5.7a (open symbols) shows that $\alpha = 0.75$ for the reactions of **N8** with **E(15-25)**⁺. The large slope for this series is a consequence of the variations of the intrinsic barriers (Fig. 5.7b) and does not provide information about Leffler-Hammond type variations of transition state structure with respect to ΔG^0 .^{33,37}

As ΔG_0^\ddagger is large compared to ΔG^0 for the series **E(15-25)**⁺, the quadratic term in eq. 6 is negligible. As a consequence, the linear dependence of the intrinsic barriers ΔG_0^\ddagger for **E(15-25)**⁺ on the thermodynamic stabilities of **E(15-25)**⁺ (Fig. 5.7b, open symbols) entails a linear dependence of ΔG^\ddagger (Fig. 5.7a, open symbols) on the thermodynamic stabilities of the benzhydrylium ions (the reason why **E19**⁺, **E24**⁺ and **E26**⁺ were not considered for the fit will be explained later). The intrinsic barriers for the reactions of **N8** with **E(25-30)**⁺, on the other hand, are almost constant ($\Delta G_0^\ddagger \approx 45 \pm 2$ kJ mol⁻¹) – if anything, there is a slight increase of

ΔG_0^\ddagger with ΔG_i^0 of \mathbf{E}^+ (Fig. 5.7b, filled symbols). For a reaction series with constant ΔG_0^\ddagger , eq. 7 is applicable, which predicts that the linear free energy relationship should be curved when ΔG^0 is varied over a sufficiently wide range.^{31,34} However, the slight curvature will not be noticed within the small range of $\mathbf{E}(\mathbf{25-30})^+$ (Fig. 5.7a, open symbols).

As reactions of benzhydrylium ions with other nucleophiles show similar variations in ΔG^\ddagger (see section 5.2.2), which is linearly correlated with $\lg k_2$ (eq. 5), these effects must be accounted for by the reactivity parameters E , N , and s_N in eq. 1. The N and s_N parameters describe the contributions of the nucleophile and the solvent to ΔG^\ddagger . The E parameters of the benzhydrylium ions \mathbf{E}^+ contain those contributions to the activation free energy ΔG^\ddagger which depend on the electrophile, which are the thermodynamic stabilities of the carbocations (ΔG_i^0) and those contributions to the intrinsic barriers ΔG_0^\ddagger which are affected by the structural properties of \mathbf{E}^+ . How substituent variations in \mathbf{E}^+ influence the activation free energies ΔG^\ddagger for the reactions of \mathbf{E}^+ with $\mathbf{N8}$ will thus find expression in the E parameters.

5.2.4 Effect of Intrinsic Barriers on Electrophilicity and Electrofugality Parameters.

Figure 5.8 plots the electrophilicity parameters E of the benzhydrylium ions $\mathbf{E}(\mathbf{1-33})^+$ against their gas phase methyl anion affinities ΔG_{MA} (from Table 5.1). The electrophilicities of the acceptor-substituted benzhydrylium ions (filled symbols) are affected to a lower extent by differences in the thermodynamic stabilities of \mathbf{E}^+ than those of the donor-substituted systems. As discussed above, the filled symbols in Figure 5.8 represent a series of benzhydrylium ions \mathbf{E}^+ where ΔG_0^\ddagger is almost constant ($\Delta G_0^\ddagger \approx 45 \text{ kJ mol}^{-1}$). The solid line in Figure 5.8 is an extrapolation of this series to better stabilized carbocations assuming constant ΔG_0^\ddagger (see section 5.S.4 for details of the calculation). As required by Marcus theory,^{31,34} the extrapolated line is slightly curved (“Marcus curvature”). When we go to the better stabilized methyl- and alkoxy-substituted benzhydrylium ions in Fig. 5.8, the data points deviate downward from the extrapolated line for constant ΔG_0^\ddagger due to the higher intrinsic barriers ΔG_0^\ddagger . A downward curvature with respect to the extrapolation line results as the intrinsic barriers increase with increasing stabilities of the benzhydrylium ions. An almost linear correlation between E and ΔG_{MA} is observed for the benzhydrylium ions $\mathbf{E}(\mathbf{13-25})^+$, which is a consequence of the linear dependence of ΔG_0^\ddagger on ΔG_i^0 in this range (cf. Fig. 5.7b). According to Fig. 5.8, the increase of the intrinsic barriers with increasing carbocation stability is then continued by the amino-substituted benzhydrylium ions. The scatter in the

plot increases with the magnitude of the intrinsic barriers (i.e., from left to right in Fig. 5.8), to such an extent that the orders of E^+ on the E and ΔG_{MA} scales may become different for the amino-substituted benzhydrylium ions.

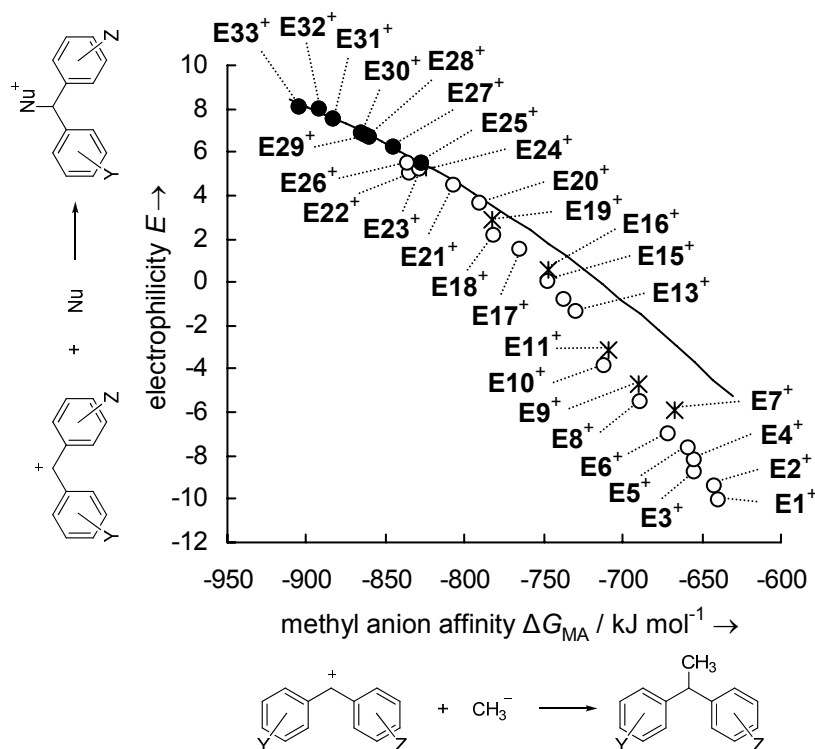


Figure 5.8. Plot of electrophilicity E versus methyl anion affinity ΔG_{MA} of benzhydrylium ions E^+ . Filled symbols: parent and acceptor-substituted benzhydrylium ions. Asterisks: phenoxy- and phenylamino-substituted compounds. Solid line: Estimated plot for reactions with constant intrinsic barriers.

Figure 5.9 shows the correlation of the electrofugality parameters E_f of the benzhydrylium ions $E(1-33)^+$ with their gas phase methyl anion affinities ΔG_{MA} . The heterolytic cleavage of a substrate $R-X$ is nothing but the reverse of a combination of a carbocation R^+ with an anionic nucleophile X^- . According to the principle of microscopic reversibility, ionization reactions must therefore have the same intrinsic barriers as the corresponding reverse reactions. Those systems which show downward deviations in the E vs ΔG_{MA} plot (Fig. 5.8) due to larger intrinsic barriers must therefore also show downward deviations in the E_f vs ΔG_{MA} plot (Fig. 5.9). However, there is one peculiarity of ionization reactions leading to highly reactive carbocations, which is worth discussing here: Ionizations of $E(20-33)-X$ that proceed with measurable rates typically require nucleofuges (e. g., $X^- = Cl^-, Br^-$ in hydroxylic solvents) which recombine with $E(20-33)^+$ with diffusion-controlled rates.^{6,15,16} As the combination

reactions do not have any barrier, the transition states for the ionization reactions correspond to the Gibbs free energies of the generated carbocations and the E_f parameters of these benzhydrylium ions only reflect changes in ΔG^0 . Accordingly, Figure 5.9 shows an excellent linear correlation between the electrofugalities E_f of $\mathbf{E(20-33)}^+$ and their methyl anion affinity ΔG_{MA} . For the better stabilized alkoxy-substituted benzhydrylium ions $\mathbf{E(13-19)}^+$, the linear correlation between E_f and ΔG_{MA} is still good (Fig. 5.9). However, it breaks down for the amino-substituted benzhydrylium ions $\mathbf{E(1-11)}^+$, in agreement with previous reports that the ionization rates of these systems are controlled by differences in intrinsic barriers.^{6,15,16}

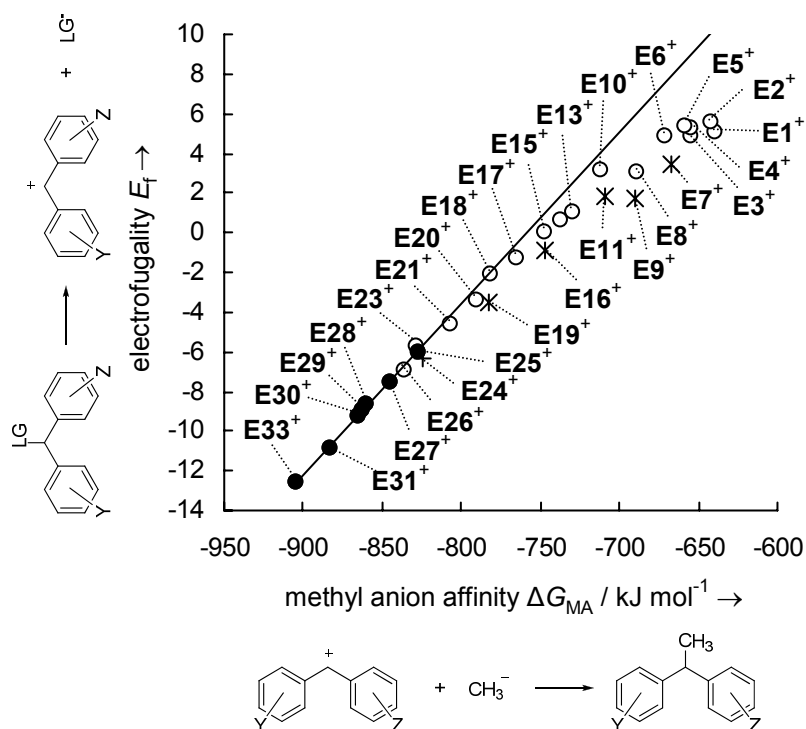


Figure 5.9. Plot of electrofugality E_f of versus methyl anion affinity ΔG_{MA} of benzhydrylium ions E^+ . Filled symbols: parent and acceptor-substituted benzhydrylium ions. Asterisks: phenoxy- and phenylamino-substituted compounds. Solid line: Linear correlation between E_f and ΔG_{MA} for $\mathbf{E25}^+$ and $\mathbf{E(27-33)}^+$ (filled symbols; $E_f = 0.0866\Delta G_{MA} + 65.685$; $R^2 = 0.9987$) extrapolated to better stabilized benzhydrylium ions.

5.2.5 Substituent Effects on Intrinsic Barriers. How can there be such a remarkably uniform variation in ΔG_0^\ddagger for the donor-substituted benzhydrylium ions over such a wide range? From Figures 5.5 and 5.6 it is evident that a large extent of the stabilization which $\mathbf{E(15-20)}^+$ experience from the resonance or hyperconjugation effects of their alkoxy and methyl substituents is lost in the transition states. In contrast, the inductive and field effects of the acceptor substituents in $\mathbf{E(27-30)}^+$ are largely preserved in the transition states. Thus, the

loss of the resonance stabilization occurs earlier on the reaction coordinate than the loss of the destabilization by the inductive substituent effects, and there is a so-called transition state imbalance³⁸ between resonance and inductive substituent effects. The same conclusion is also obtained if we separate the resonance and inductive effects of the substituents using Jencks' modification³⁹ of the Yukawa-Tsuno equation⁴⁰ (see section 5.S.5).

In fact, it is inevitable that the loss of resonance stabilization is ahead of the loss of inductive effect destabilization.⁴¹ At any point during the course of the reaction, there is a certain degree of new bond formation between the benzhydrylium ion \mathbf{E}^+ and the nucleophile \mathbf{N} , which is associated with a certain degree of sp^3 hybridization at the former sp^2 carbon atom of \mathbf{E}^+ , and with a certain degree of positive charge that is transferred from \mathbf{E}^+ to \mathbf{N} . Only the positive charge remaining on the benzhydryl moiety can profit from the resonance stabilization by a substituent on the aryl group. However, the percentage of charge delocalized to the substituent by resonance is a function of the π -bond order of the bond between the benzylic carbon and the aryl group, which is already lost to some extent. Therefore, the resonance effect for the stabilization of the remaining charge on the benzhydryl fragment can only be a fraction of the original resonance effect in the benzhydryl cation \mathbf{E}^+ . On the other hand, the inductive and field effects operate irrespective of π -bond order through the σ -bond framework or through space and exert their whole influence on the benzhydryl fragment. The disappearance of the inductive effect is thus better synchronized with the transfer of the positive charge from \mathbf{E}^+ to \mathbf{N} than the disappearance of the resonance effect.

According to the principle of non-perfect synchronization, a reactant stabilizing factor such as the resonance stabilization in \mathbf{E}^+ which is lost early compared to the main bond changes leads to an increased intrinsic barrier.¹⁸ The better thermodynamic stabilization of benzhydrylium ions \mathbf{E}^+ by resonance effect substituents is thus accompanied by increased intrinsic barriers for the combination reactions of \mathbf{E}^+ with nucleophiles (Fig. 5.7b, open symbols) that result from the early loss of these resonance effects. There are plenty of examples in the literature where intrinsic barriers for carbocation nucleophile combinations were shown to increase with stronger contributions of resonance effects; many of them are given in reviews by Richard⁴² and Bernasconi.¹⁸ McClelland and coworkers have discussed a transition state imbalance between inductive and resonance substituent effects for reactions of tritylium ions with acetonitrile/water mixtures but failed to generate benzhydrylium ions containing only electron-withdrawing groups.¹⁷ Plotting the data obtained with our new laser flash photolytic

method for the generation of these carbocations,¹⁹ we can now illustrate this effect for a series of benzhydrylium ions covering 18 orders of magnitude in reactivity (Fig. 5.8).

As the inductive effects are better balanced with the main bond changes, the intrinsic barriers for a series of reactions of the acceptor-substituted benzhydrylium ions are almost constant and we only find a slight increase of ΔG_0^\ddagger when going from **E25**⁺ to **E30**⁺ in Fig. 5.7b (filled symbols). This slight increase of ΔG_0^\ddagger may be rationalized by the fact that also in **E(27-33)**⁺ there is some delocalization of positive charge into the aryl rings due to resonance which is lost early in reactions of **E(27-33)**⁺ with nucleophiles. Relative to the overall reaction, the inductive effect thus disappears a little later, and a reactant destabilizing factor which is lost late also results in a higher intrinsic barrier.¹⁸

The benzhydrylium ions **E24**⁺ and **E26**⁺ were not included in the linear fits shown in Fig. 5.7b. These two systems are special since their substituents compensate inductive electron acceptor character (*m*-F or *p*-Cl substituents) with resonance/hyperconjugation electron donor properties (*p*-Me or *p*-Cl). The involvement of resonance effects may explain why these compounds have higher intrinsic barriers than benzhydrylium ions of comparable thermodynamic stabilities (Fig. 5.7b).²⁷

5.2.6 Solvent Effects. As a result of the higher energy of reorganization of polar solvents and the early loss of resonance which requires a concomitant early solvent response to the charge redistribution, the intrinsic barriers for reactions of benzhydrylium ions with nucleophiles increase with solvent polarity.¹⁵ However, these effects of the solvent are included in the solvent-dependent nucleophilicity and nucleofugality parameters, not in the *E* and *E_f* parameters, which are solvent independent. It has already been discussed in section 5.2.1 that the overall curvature in Figure 5.8 cannot be a result of differential solvation by CH₂Cl₂ for benzhydrylium ions of differing reactivities.

There is generally no differential solvation of **E**⁺ in the ground state, i. e., solvation changes linearly with the thermodynamic stabilities of the carbocations.^{1,2,22} Exceptions to this rule are the *p*-phenoxy-substituted benzhydrylium ions **E16**⁺ and **E19**⁺ and the *p*-phenylamino-substituted compounds **E7**⁺, **E9**⁺, and **E11**⁺, which are marked by asterisks in Figures 5.8 and 5.9. The electrophilicities *E* of these benzhydrylium ions are somewhat higher (Fig. 5.8) while their electrofugalities *E_f* are lower (Fig. 5.9) than those of structurally related compounds which have similar methyl anion affinities ΔG_{MA} in the gas phase. This suggests a less efficient solvation of the phenyl-substituted benzhydrylium ions in the ground state compared

to benzhydrylium ions without additional phenyl groups. The methyl anion affinities ΔG_{MA} in the gas phase would then overestimate the thermodynamic stabilities of the phenyl-substituted benzhydrylium ions in solution relative to the other benzhydrylium ions, and one would observe deviations to the right for these compounds in Figures 5.8 and 5.9. Indeed, an unusual solvent dependence of the reactivities of the *p*-phenylamino-substituted benzhydrylium ions was already noted previously: The reactions of **E9**⁺ and related phenyl-substituted benzhydrylium ions in acetonitrile are systematically faster than predicted on the basis of their reactivities towards π -nucleophiles in CH₂Cl₂.⁴³

As a consequence of these small ground state solvation effects, ΔG_i^0 (CH₂Cl₂) for the *p*-phenoxy-substituted **E19**⁺ cannot be determined accurately from the E_f parameters of these benzhydrylium ions, which were derived from solvolyses in hydroxylic solvents. The anomalous ΔG_0^\ddagger values for these benzhydrylium ions (Fig. 5.7b) are thus at least in part due to inaccuracies in the determination of ΔG_i^0 (CH₂Cl₂). This conclusion is supported by the deviation of **E19**⁺ from the linear correlation of ΔG_i^0 (from E_f) with experimental data²⁶ on ionization equilibria of **E**-Cl in CH₂Cl₂ at -70 °C (Fig. 5.S.3.1 in section 5.S.3).

5.2.7 Why Do the Linear Free Energy Relationships Work? Section 5.S.6 illustrates graphically how the activation free energy ΔG^\ddagger (and thus k_2) of a reaction can be related to the quantities ΔG_0^\ddagger and ΔG^0 by the Marcus equation (eq. 6). The sections of the parabola $\lg k_2$ vs ΔG^0 which are located in the experimentally accessible range of $10^{-4} \leq k_2 \leq 10^8 \text{ M}^{-1} \text{ s}^{-1}$ have only a small curvature for realistic values of ΔG^0 and ΔG_0^\ddagger .

The curvature becomes almost negligible when the intrinsic barriers ΔG_0^\ddagger increase linearly with ΔG^0 . For a series of different combination reactions of carbocations with nucleophiles featuring such $\lg k_2$ vs ΔG^0 plots with negligible curvatures, it will be possible to describe $\lg k_2$ for each of these reactions as a linear function of the relative thermodynamic stabilities of the electrophiles **E**⁺. The linear increase of the intrinsic barriers ΔG_0^\ddagger with the thermodynamic stabilities ΔG_i^0 of **E**⁺ within the series **E(15-25)**⁺ (Fig. 5.7b, open circles) thus explains the existence of linear free energy relationships *within* this series.

Obviously, the activation free enthalpy ΔG^\ddagger of a reaction of **E**⁺ with one nucleophile may be influenced in a different way by thermodynamic effects and by variations of the intrinsic barriers which are induced by substituents on the benzhydryl system than ΔG^\ddagger of a reaction of **E**⁺ with another nucleophile. The resulting varying relative importances of substituent effects

on ΔG_0^\ddagger and on ΔG^0 for the activation free energies ΔG^\ddagger of the reactions are expressed in the nucleophile-specific parameters N and s_N .

However, the discussion in section 5.2.3 makes it clear that the acceptor-substituted systems **E(25-30)**⁺ behave differently. In this series, the intrinsic barriers are almost constant (Fig. 5.7b, closed circles). In a reaction series including both donor- and acceptor-substituted benzhydrylium ions, there is a break in ΔG_0^\ddagger vs ΔG^0 (such as in Fig. 5.7b), and the same break will also be found in $\lg k_2$ vs ΔG^0 (see Figure 5.S.6.1 for a graphical illustration). It is therefore quite surprising, that eq. 1 holds for reaction series which include reactions of both donor- and acceptor-substituted benzhydrylium ions.^{4,20}

For the different reactions investigated in CH_2Cl_2 solution, the similar behavior may be explained by the fact that we could only determine rate constants for reactions of **E(27-33)**⁺ within a small experimental window, which is defined by the approach to the diffusion limit ($k_2 \leq 10^8 \text{ M}^{-1} \text{ s}^{-1}$; validity limit of eq. 1) and by the fact that the reactions must be fast enough to compete with the fast background reactions ($k_2 \geq \sim 10^6 \text{ M}^{-1} \text{ s}^{-1}$).⁴ If we further assume that reactions of **E(27-33)**⁺ with nucleophiles are generally exergonic, the activation free energies of $\Delta G^\ddagger \approx 27\text{-}38 \text{ kJ mol}^{-1}$ which are defined by the range of rate constants $10^6 \leq k_2 \leq 10^8 \text{ M}^{-1} \text{ s}^{-1}$ indicate substantial intrinsic barriers ΔG_0^\ddagger (roughly $40\text{-}50 \text{ kJ mol}^{-1}$ for reactions with $\Delta G^0 \approx -50$ to -10 kJ mol^{-1}).

However, linear correlations of $\lg k_2$ with E are not only found for reactions of **E**⁺ with π -nucleophiles in CH_2Cl_2 , but also for reactions of **E**⁺ with other classes of nucleophiles such as triethylsilane, acetonitrile, trifluoroethanol, and hexafluoroisopropanol/water mixtures.^{4,20}

The linear correlations of $\lg k_2$ vs E imply that, for all these nucleophiles, the slopes in the regions before (donor-substituted systems) and after (acceptor-substituted systems) the break in the $\lg k_2$ vs ΔG^0 plots are affected in the same way by variation of the electrophile: If the slope of the $\lg k_2$ vs ΔG^0 plot for the reactions of the donor-substituted benzhydrylium ions with one nucleophile is s_N times that of the slope of the plot for another nucleophile, the same factor of s_N must also apply between the slopes of the $\lg k_2$ vs ΔG^0 plots for the reactions of the acceptor-substituted benzhydrylium ions with these two nucleophiles.

Such a behavior is only possible if the contribution of the nucleophile reorganization to ΔG^\ddagger linearly depends on ΔG^0 of the reaction. That is, the transition state imbalances resulting from the resonance effects of the substituents in the benzhydryl moiety do not affect the reorganization energy of the nucleophile, but only that of the benzhydryl moiety. With this

reasonable assumption, the existence of linear free energy relationships for both donor- and acceptor-substituted benzhydrylium ions can be rationalized.

5.3 Conclusion

The recently reported⁴ quantitative data on the electrophilic reactivities of **E(27-33)**⁺ made it possible to discern the roles of inductive and resonance substituent effects on the electrophilic reactivities of benzhydryl cations. The understanding of these effects in reactions of benzhydrylium ions with nucleophiles provides a glimpse on the physical principles behind linear free energy relationships such as eq. 1.

As for other carbocation nucleophile combinations,^{17,18,42} resonance effects cause transition state imbalances and increase the intrinsic barriers for the reactions. Thus, the resonance effect substituents induce a linear increase of the intrinsic barriers for reactions of **E**⁺ with nucleophiles (ΔG_0^\ddagger) with the thermodynamic driving forces of the reactions (ΔG^0). Inductive substituent effects are better balanced with the overall reaction progress than resonance effects, and the intrinsic barriers ΔG_0^\ddagger remain almost constant in a reaction series involving only acceptor-substituted benzhydrylium ions. Therefore, variations of the thermodynamic stabilities of the acceptor-benzhydrylium ions result in smaller changes of the electrophilic reactivities compared to a series of donor-substituted benzhydrylium ions.

The Marcus equation^{34,35} relates $\lg k_2$ for reactions of **E**⁺ with nucleophiles to ΔG_0^\ddagger on ΔG^0 of these reactions and explains the existence of linear free energy relationships within each of the series of donor- or acceptor-substituted benzhydrylium ions. However, the intrinsic barriers behave differently in the two series, and it is remarkable that linear correlations of $\lg k_2$ versus E (eq. 1) are also found for so many reaction series which include both donor- and acceptor-substituted benzhydrylium ions (Fig. 5.1).^{4,20} From this observation, we conclude that the transition state imbalances resulting from the resonance effects of the substituents only affect the reorganization energy of the carbocation, and have only little effect on the reorganization of the nucleophile. The same must be true for the reactions of nucleophiles towards the many other structurally different electrophiles, which can be described by eq. 1. It can be expected that eq. 1 will not hold for reactions, where there is a resonance interaction between the electrophile and nucleophile moieties in the transition state.

5.4 Acknowledgment

We thank Konstantin Troshin for helpful discussions and the Deutsche Forschungsgemeinschaft for financial support.

5.5 References and Notes

- (1) Mayr, H.; Bug, T.; Gotta, M. F.; Hering, N.; Irrgang, B.; Janker, B.; Kempf, B.; Loos, R.; Ofial, A. R.; Remennikov, G.; Schimmel, H. *J. Am. Chem. Soc.* **2001**, *123*, 9500-9512.
- (2) Mayr, H.; Kempf, B.; Ofial, A. R. *Acc. Chem. Res.* **2003**, *36*, 66-77.
- (3) Mayr, H.; Ofial, A. R. *J. Phys. Org. Chem.* **2008**, *21*, 584-595.
- (4) Ammer, J.; Nolte, C.; Mayr, H. *J. Am. Chem. Soc.* **2012**, *134*, 13902-13911 (CHAPTER 3 of this work).
- (5) Denegri, B.; Streiter, A.; Jurić, S.; Ofial, A. R.; Kronja, O.; Mayr, H. *Chem. Eur. J.* **2006**, *12*, 1648-1656, 5415.
- (6) Streidl, N.; Denegri, B.; Kronja, O.; Mayr, H. *Acc. Chem. Res.* **2010**, *43*, 1537-1549.
- (7) (a) Pérez, P.; Toro-Labbé, A.; Aizman, A.; Contreras, R. *J. Org. Chem.* **2002**, *67*, 4747-4752; (b) Aizman, A.; Contreras, R.; Pérez, P. *Tetrahedron* **2005**, *61*, 889-895; (c) Ormazábal-Toledo, R.; Campodónico, P. R.; Contreras, R. *Org. Lett.* **2010**, *13*, 822-824; (d) Wang, C.; Fu, Y.; Guo, Q.-X.; Liu, L. *Chem. Eur. J.* **2010**, *16*, 2586-2598.
- (8) (a) Mayr, H.; Ofial, A. R. *Angew. Chem.* **2006**, *118*, 1876-1886; *Angew. Chem. Int. Ed.* **2006**, *45*, 1844-1854; (b) Mayr, H. *Angew. Chem.* **2011**, *123*, 3692-3698; *Angew. Chem. Int. Ed.* **2011**, *50*, 3612-3618.
- (9) Ofial, A. R.; Ohkubo, K.; Fukuzumi, S.; Lucius, R.; Mayr, H. *J. Am. Chem. Soc.* **2003**, *125*, 10906-10912.
- (10) Mayr, H.; Patz, M.; Gotta, M. F.; Ofial, A. R. *Pure Appl. Chem.* **1998**, *70*, 1993-2000.
- (11) Schindele, C.; Houk, K. N.; Mayr, H. *J. Am. Chem. Soc.* **2002**, *124*, 11208-11214.
- (12) Zhu, X.-Q.; Wang, C.-H. *J. Phys. Chem. A* **2010**, *114*, 13244-13256.
- (13) Nolte, C.; Mayr, H. *Eur. J. Org. Chem.* **2010**, 1435-1439.

- (14) Denegri, B.; Minegishi, S.; Kronja, O.; Mayr, H. *Angew. Chem.* **2004**, *116*, 2353-2356; *Angew. Chem. Int. Ed.* **2004**, *43*, 2302-2305.
- (15) Schaller, H. F.; Tishkov, A. A.; Feng, X.; Mayr, H. *J. Am. Chem. Soc.* **2008**, *130*, 3012-3022.
- (16) Mayr, H.; Ofial, A. R. *Pure Appl. Chem.* **2009**, *81*, 667-683.
- (17) McClelland, R. A.; Kanagasabapathy, V. M.; Banait, N. S.; Steenken, S. *J. Am. Chem. Soc.* **1989**, *111*, 3966-3972.
- (18) (a) Bernasconi, C. F. *Adv. Phys. Org. Chem.* **1992**, *27*, 119-238; (b) Bernasconi, C. F. *Adv. Phys. Org. Chem.* **2010**, *44*, 223-324.
- (19) Ammer, J.; Sailer, C. F.; Riedle, E.; Mayr, H. *J. Am. Chem. Soc.* **2012**, *134*, 11481-11494 (CHAPTER 2 of this work).
- (20) Ammer, J.; Mayr, H. *J. Phys. Org. Chem.* **2012**, accepted (CHAPTER 4 of this work).
- (21) Denekamp, C.; Sandler, Y. *Angew. Chem.* **2006**, *118*, 2147-2150; *Angew. Chem. Int. Ed.* **2006**, *45*, 2093-2096.
- (22) Mayr, H.; Schneider, R.; Schade, C.; Bartl, J.; Bederke, R. *J. Am. Chem. Soc.* **1990**, *112*, 4446-4454.
- (23) Mayr, H. *Angew. Chem.* **1990**, *102*, 1415-1574; *Angew. Chem. Int. Ed.* **1990**, *29*, 1371-1384.
- (24) Minegishi, S.; Loos, R.; Kobayashi, S.; Mayr, H. *J. Am. Chem. Soc.* **2005**, *127*, 2641-2649.
- (25) Streidl, N.; Mayr, H. *Eur. J. Org. Chem.* **2011**, 2498-2506.
- (26) Schade, C.; Mayr, H.; Arnett, E. M. *J. Am. Chem. Soc.* **1988**, *110*, 567-571.
- (27) Figure 5.S.3.2 in section 5.S.3 shows that the ΔG_i^0 values for the benzhydrylium ions **E(15-30)**⁺ which were calculated from the E_f parameters via eq. 2 also correlate linearly with the gas phase methyl anion affinities ΔG_{MA} of these benzhydrylium ions. Note that the points for **E24**⁺ and **E26**⁺ also lie on the correlation line, which illustrates that a different solvation in the ground state is absent also for these benzhydrylium ions.
- (28) Schade, C., dissertation, Medizinische Universität zu Lübeck, 1988.
- (29) Denegri, B.; Ofial, A. R.; Jurić, S.; Streiter, A.; Kronja, O.; Mayr, H. *Chem. Eur. J.* **2006**, *12*, 1657-1666.
- (30) (a) Leffler, J. E. *Science* **1953**, *117*, 340-341; (b) Williams, A. *Acc. Chem. Res.* **1984**, *17*, 425-430; (c) Jencks, W. P. *Bull. Soc. Chim. Fr.* **1988**, 218-224; (d) Leffler, J. E.; Grunwald, E. *Rates and Equilibria of Organic Reactions*; Wiley: New York, 1963.

- (31) Williams, A. *Free Energy Relationships in Organic and Bio-Organic Chemistry*; Royal Society of Chemistry: Cambridge, 2003.
- (32) For a criticism of this interpretation, see ref. 33 and: (a) Pross, A.; Shaik, S. S. *J. Am. Chem. Soc.* **1982**, *104*, 1129-1130; (b) Pross, A. In *Theoretical and Physical Principles of Organic Reactivity*; John Wiley & Sons: New York, 1995, p 159-182.
- (33) Pross, A.; Shaik, S. S. *New J. Chem.* **1989**, *13*, 427-433.
- (34) Marcus, R. A. *J. Phys. Chem.* **1968**, *72*, 891-899.
- (35) Albery, W. J. *Annu. Rev. Phys. Chem.* **1980**, *31*, 227-263.
- (36) Lewis, E. S. *J. Phys. Org. Chem.* **1990**, *3*, 1-8.
- (37) Marcus, R. A. *J. Am. Chem. Soc.* **1969**, *91*, 7224-7225.
- (38) Jencks, W. P. *Chem. Rev.* **1985**, *85*, 511-527.
- (39) Young, P. R.; Jencks, W. P. *J. Am. Chem. Soc.* **1977**, *99*, 8238-8248.
- (40) (a) Tsuno, Y.; Fujio, M. *Chem. Soc. Rev.* **1996**, *25*, 129-139; (b) Tsuno, Y.; Fujio, M. *Adv. Phys. Org. Chem.* **1999**, *32*, 267-385.
- (41) Our explanation follows a line of arguments previously employed by Kresge (Kresge, A. J. *Can. J. Chem.* **1974**, *52*, 1897-1903) and Bernasconi (ref. 18) for other types of reactions..
- (42) (a) Richard, J. P. *Tetrahedron* **1995**, *51*, 1535-1573; (b) Richard, J. P.; Amyes, T. L.; Toteva, M. M. *Acc. Chem. Res.* **2001**, *34*, 981-988.
- (43) (a) Nigst, T. A.; Westermaier, M.; Ofial, A. R.; Mayr, H. *Eur. J. Org. Chem.* **2008**, 2369-2374; (b) Kędziołek, M.; Mayer, P.; Mayr, H. *Eur. J. Org. Chem.* **2009**, 1202-1206; (c) Ammer, J.; Baidya, M.; Kobayashi, S.; Mayr, H. *J. Phys. Org. Chem.* **2010**, *23*, 1029-1035 (CHAPTER 9 of this work).
- (S1) Hansch, C.; Leo, A.; Taft, R. W. *Chem. Rev.* **1991**, *91*, 165-195.
- (S2) Brown, H. C.; Rao, C. G.; Ravindranathan, M. *J. Am. Chem. Soc.* **1977**, *99*, 7663-7667.
- (S3) *What'sBest! 7.0 Industrial*, Lindo Systems Inc. 2004.
- (S4) Stewart, R.; Teo, K. C. *Can. J. Chem.* **1980**, *58*, 2491-2496.

5.S Supplementary Data and Experimental Section

5.S.1 Hammett analysis

Figure 5.S.1.1a shows a plot of the E parameters for symmetrically substituted benzhydrylium ions \mathbf{E}^+ (Ar_2CH^+) from ref.⁴ against the sums of the σ^+ constants of their substituents. The σ^+ and σ_m constants were taken from ref. S1, except $\sigma^+ = -0.98^{\text{S}2}$ for the fused dihydrofuran in $\mathbf{E13}^+$ and $\mathbf{E14}^+$ ($\text{Ar} = 5\text{-coumaranyl}$). If one ignores the p -alkoxy and p -amino substituted compounds, the slope of the Hammett plot becomes significantly smaller (Fig. 5.S.1.1a, filled symbols, $E = 2.2312\Sigma\sigma^+ + 5.2309$, $R^2 = 0.9843$, correlation line not shown in the diagram). The different behavior of the p -alkoxy- and p -amino-substituted systems is even more noticeable in a Hammett plot that includes the unsymmetrically substituted \mathbf{E}^+ (Fig. 5.S.1.1b).

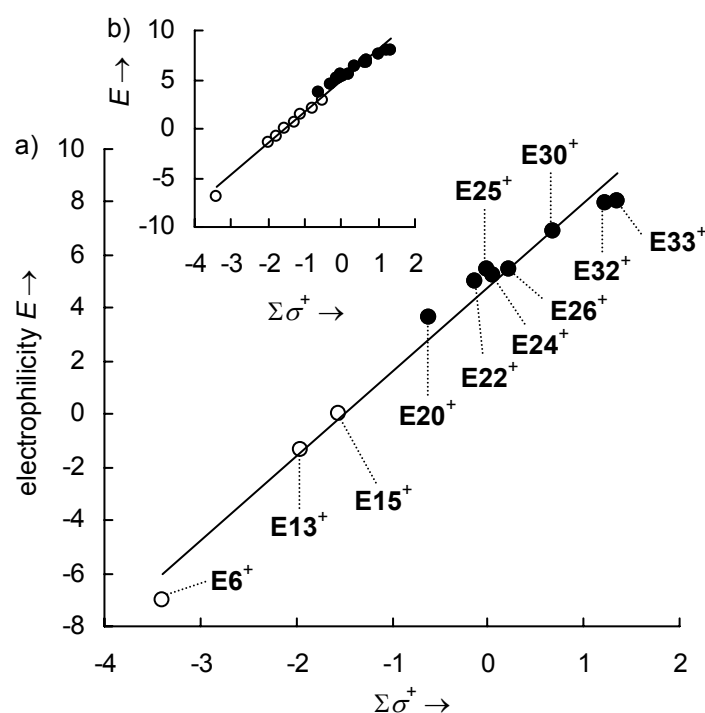


Figure 5.S.1.1 (a) Plot of E versus $\Sigma\sigma^+$ for (a) symmetrically substituted benzhydrylium ions ($E = 3.1745\Sigma\sigma^+ + 4.7675$, $R^2 = 0.9793$) or (b) all benzhydrylium ions ($E = 3.1628\Sigma\sigma^+ + 4.7925$, $R^2 = 0.9802$). Empty symbols indicate p -alkoxy- and p -amino-substituted benzhydrylium ions.

5.S.2 Correlations of hydride and methyl anion affinities

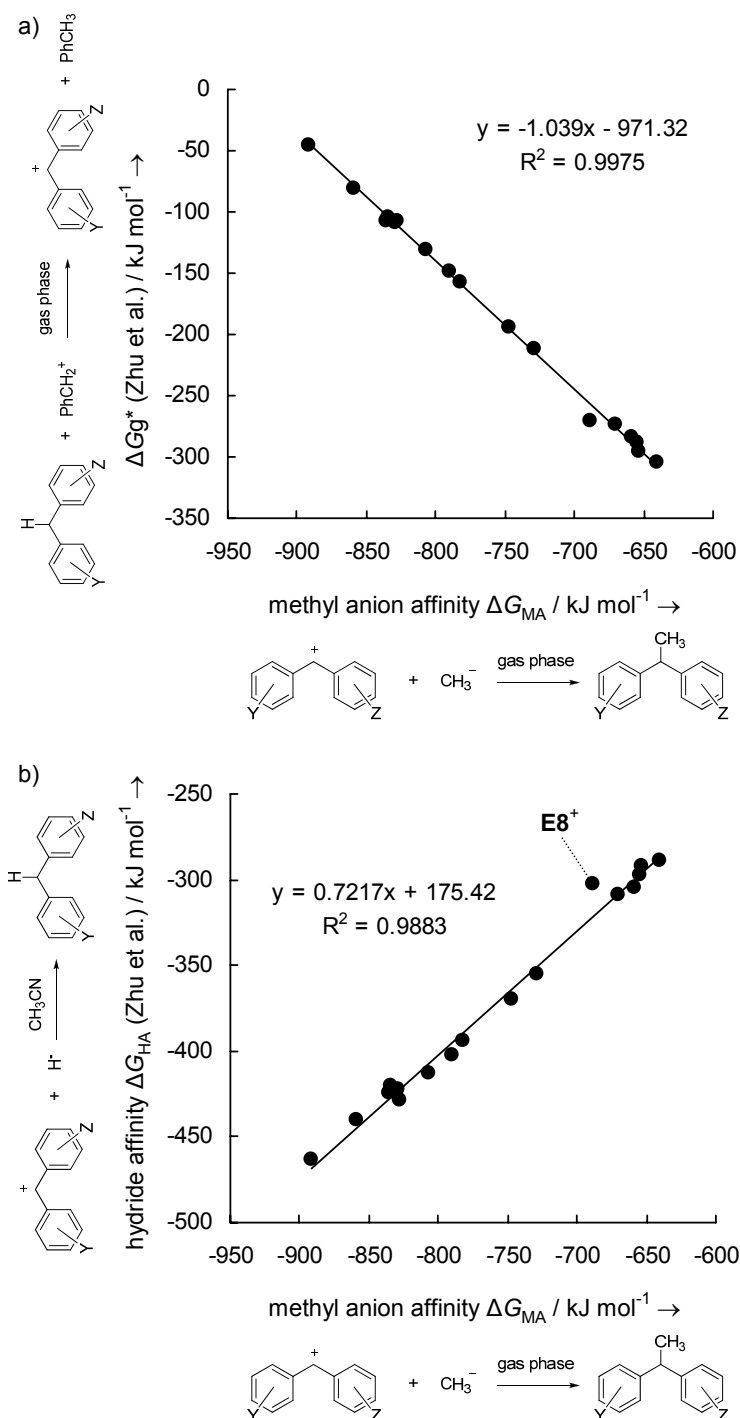


Figure 5.S.2.1. Correlation of calculated relative gas phase hydride affinities ΔG_{g^*} (kJ mol^{-1}) of the benzhydrylium ions E^+ in the gas phase (a) and solution phase hydride affinities ΔG_{HA} of the benzhydrylium ions E^+ in CH_3CN solution (b) reported by Zhu *et al.*¹² with the calculated methyl anion affinities ΔG_{MA} (kJ mol^{-1}) of the benzhydrylium ions E^+ in the gas phase from this work (T. Singer, T. A. Nigst).

5.S.3 Gibbs free energy profiles and intrinsic barriers

Table 5.S.3.1 lists the numeric data plotted in Figure 5.5 for the carbocations and transition states. As discussed in section 5.2.2, we substituted the E_f parameters of \mathbf{E}^+ and the nucleofugality parameters of Cl^- in CH_2Cl_2 ($N_f = -0.57$, $s_f = 1.28$)²⁵ into eq. 2 to calculate ΔG_i^0 of \mathbf{E}^+ (Table 5.S.3.1) because there are only limited experimental data available. The temperature difference between the rate constants $k_2(20\text{ }^\circ\text{C})$ for the combination reactions and the solvolysis rate constants $k_s(25\text{ }^\circ\text{C})$ obtained from eq. 2 is neglected.

Table 5.S.3.1. Data for free energy profiles and intrinsic barriers for the reactions of \mathbf{E}^+ with **N8**.

cation	relative thermodynamic stabilities of \mathbf{E}^+				combination reactions of \mathbf{E}^+ with N8			
	E_f^a	k_s^b / s^{-1}	$\Delta G_i^\ddagger = \Delta G_i^0$ / kJ mol^{-1}		ΔG^0 / kJ mol^{-1}	k_2^c / $\text{M}^{-1} \text{s}^{-1}$	ΔG^\ddagger / kJ mol^{-1}	ΔG_0^\ddagger / kJ mol^{-1}
			relative to $\mathbf{E}-\text{Cl}$	relative to $\mathbf{E15}^+$				
E15 ⁺	0.00	1.86×10^{-1}	77.2	0	23.9	9.35^d	66.3	53.7
E16 ⁺	-0.86	1.48×10^{-2}	83.5	6.3	17.6	3.65×10^{1d}	63.0	53.8
E17 ⁺	-1.32	3.81×10^{-3}	86.8	9.6	14.3	2.99×10^{2d}	57.9	50.5
E18 ⁺	-2.09	3.94×10^{-4}	92.5	15.3	8.6	1.12×10^{3d}	54.6	50.2
E19 ⁺	-3.52	5.82×10^{-6}	102.9	25.7	-1.8	6.65×10^{3d}	50.3	51.2
E20 ⁺	-3.44	7.37×10^{-6}	102.3	25.1	-1.2	4.01×10^{4d}	45.9	46.5
E23 ⁺	-5.72	8.89×10^{-9}	119.0	41.8	-17.9	4.55×10^6	34.4	42.9
E24 ⁺	-6.37 ^e	1.31×10^{-9}	123.7	46.5	-22.6	2.79×10^6	35.6	46.2
E25 ⁺	-6.03	3.56×10^{-9}	121.3	44.1	-21.7	5.69×10^6	33.8	43.3
E26 ⁺	-6.91	2.66×10^{-10}	127.7	50.5	-20.2	5.00×10^6	34.2	46.5
E27 ⁺	-7.53	4.29×10^{-11}	132.2	55.0	-31.1	2.95×10^7	29.8	42.9
E28 ⁺	-8.66 ^e	1.53×10^{-12}	140.5	63.3	-39.4	9.51×10^7	27.0	44.5
E29 ⁺	-9.00 ^f	5.63×10^{-13}	143.0	65.8	-41.9	9.16×10^7	27.1	45.6
E30 ⁺	-9.26	2.62×10^{-13}	144.9	67.7	-43.8	1.37×10^8	26.1	45.3
E33 ⁺	-12.60	1.39×10^{-17}	169.3	92.1	–	–	–	–

^a From ref.⁶ unless noted otherwise. ^b Calculated from eq. 2 using $N_f = -0.57$ and $s_f = 1.28$ for Cl^- in CH_2Cl_2 from ref.²⁵. ^c Experimental rate constants (20 °C) from ref.⁴ unless noted otherwise. ^d From ref.¹ ^e This work (C. Nolte). ^f From ref.¹³

Figure 5.S.3.1 shows a good agreement between the calculated ΔG_i^0 via eq. 2 (25 °C) and experimental data from equilibrium measurements in $\text{CH}_2\text{Cl}_2/\text{BCl}_3$ at -70 °C from ref.²⁶ The choice of the E_f parameters for the calculation of ΔG_i^0 via eq. 2 is also justified by the good correlation of the calculated ΔG_i^0 values with the calculated methyl anion affinities ΔG_{MA} of the benzhydrylium ions \mathbf{E}^+ (Fig. 5.S.3.2).

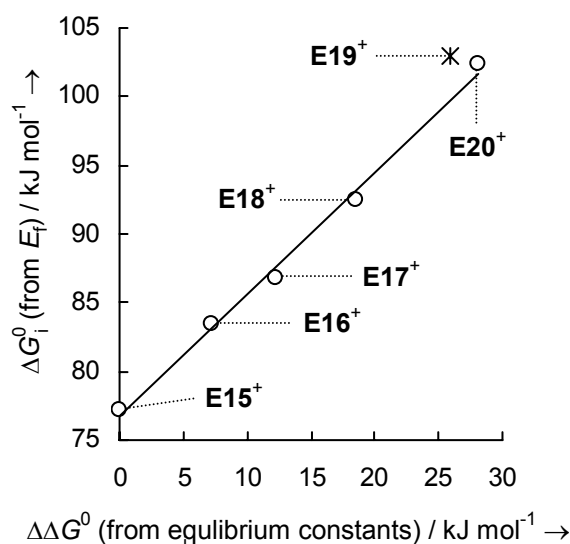


Figure 5.S.3.1. Comparison of ΔG_i^0 calculated from E_f parameters of \mathbf{E}^+ (eq. 2) with experimental data from equilibrium measurements in $\text{CH}_2\text{Cl}_2/\text{BCl}_3$ at -70 °C from ref.²⁶ ($\Delta G_i^0(\text{calc}) = 0.8846\Delta\Delta G_i^0(\text{exp}) + 76.764$; $R^2 = 0.9948$). The point for $\mathbf{E19}^+$ (*) was not used for the correlation.

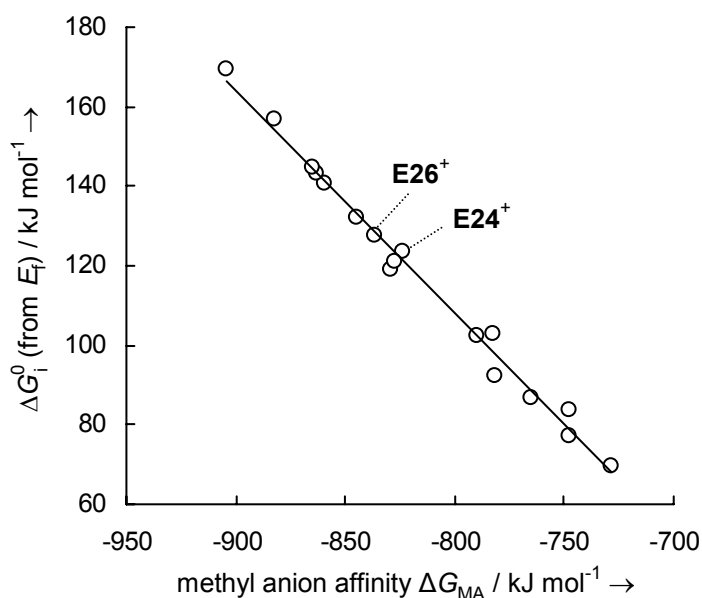


Figure 5.S.3.2. Correlation of ΔG_i^0 calculated from E_f parameters of \mathbf{E}^+ (eq. 2) with calculated methyl anion affinities ΔG_{MA} of \mathbf{E}^+ ($\Delta G_i^0(\text{calc}) = -0.5613\Delta G_{\text{MA}} - 341.03$; $R^2 = 0.9901$).

The rate constants for solvolyses of **E–N8–Cl** in 80% aqueous ethanol were found to be almost independent of the substituents on the aryl rings (Table 5.S.3.2).²⁸ These data can be used to estimate the E_f parameters of **E–N8⁺** (Table 5.S.3.2), which are comparable to the previously published electrofugality parameter for the *tert*-butyl cation ($E_f = -8.21$).²⁹ In analogy to the procedure for the benzhydrylium ions (see above), we used the E_f parameters of **E–N8⁺** to calculate the activation free energies ΔG_i^\ddagger for the ionization of **E–N8–Cl** (Table 5.S.3.2), which reflect the thermodynamic stabilities ΔG_i^0 of **E–N8⁺** relative to **E–N8–Cl** because the reverse reactions (**E–N8⁺** + Cl⁻ → **E–N8–Cl**) are diffusion-controlled.

Table 5.S.3.2. First-order rate constants for the solvolyses of **E–N8–Cl** in 80% aqueous ethanol (v/v) at 50 °C and thermodynamic stabilities of **E–N8⁺** relative to **E–N8–Cl**.

cation	80E20W		E_f^c	k_s^d / s ⁻¹	CH ₂ Cl ₂
	$k_{s, \text{EtOH}}(50 \text{ °C})^a$ / s ⁻¹	$k_{s, \text{EtOH}}(25 \text{ °C})^b$ / s ⁻¹			$\Delta G_i^\ddagger = \Delta G_i^0$ / kJ mol ⁻¹ relative to E–N8–Cl
E15–N8⁺	2.400×10^{-4}	1.13×10^{-5}	-8.2	5.9×10^{-12}	137
E20–N8⁺	2.114×10^{-4}	9.86×10^{-6}	-8.3	4.4×10^{-12}	138
E25–N8⁺	1.448×10^{-4}	6.54×10^{-6}	-8.5	2.5×10^{-12}	139
E26–N8⁺	0.891×10^{-4}	3.87×10^{-6}	-8.7	1.4×10^{-12}	141
(CH ₃) ₃ C ⁺	–	–	-8.21 ^e	5.8×10^{-12}	137

^a Rate constant for solvolysis of the corresponding chloride in 80% aqueous ethanol (v/v) from ref.²⁸ ^b For the temperature correction, we estimated $\Delta S^\ddagger \approx -20 \text{ J K}^{-1} \text{ mol}^{-1}$, a value which was also determined for solvolyses of similar compounds.²⁸ ^c Calculated by substituting $k_s(25 \text{ °C})$ and the reactivity parameters $N_f = 3.24$ and $s_f = 0.99$ for chloride in 80E20W⁶ into eq. 2. ^d Calculated from eq. 2 using $N_f = -0.57$ and $s_f = 1.28$ for Cl⁻ in CH₂Cl₂ from ref.²⁵. ^e From ref.²⁹

The free energy of addition $\Delta G_A^0(25 \text{ °C}) = -37.6 \text{ kJ mol}^{-1}$ for the reaction of **N8** with **E–Cl** to **E–N8–Cl** is calculated from $\Delta G_A^0 = \Delta H_A^0 - T \Delta S_A^0$ using the experimental $\Delta H_A^0 = -86.5 \text{ kJ mol}^{-1}$ from ref.²⁶ and the estimated $\Delta S_A^0 \approx -164 \text{ J mol}^{-1} \text{ K}^{-1}$ from ref.²²

In combination with the average ΔG_i^0 for **E–N8–Cl** (138.7 kJ mol⁻¹) from Table 5.S.3.1, we arrive at $\Delta G_{\text{rel}}^0 = \Delta G_A^0 + \Delta G_i^0(\text{E–N8–Cl}) = 101.1 \text{ kJ mol}^{-1}$ as an estimate for the Gibbs free energy of **E–N8⁺** relative to **E–Cl**.

These data are then used to calculate the free energies ΔG^0 for the reactions of **E⁺** with **N8** (Table 5.S.3.1). The activation free energies ΔG^\ddagger for these reactions are obtained from the second-order rate constants k_2 by the Eyring equation (eq. 5). With the Marcus equation (eq. 6) we can then calculate the intrinsic barriers ΔG_0^\ddagger from ΔG^0 and ΔG^\ddagger (Table 5.S.3.1).

5.S.4 Extrapolated E vs ΔG_{MA} plot for constant intrinsic barriers

This section explains how we calculated the solid line in Fig. 5.8, which is an extrapolation of a reaction series with constant $\Delta G_0^\ddagger = 45 \text{ kJ mol}^{-1}$ to better stabilized carbocations.

Using $\Delta G_{\text{rel}}^0 = 101.1 \text{ kJ mol}^{-1}$ for $\mathbf{E-N8}^+$ (relative to $\mathbf{E-Cl}$) as determined in Section 5.S.3, we can calculate the reaction free energies ΔG^0 for the reactions specified in eq. 5.S.4.1 as a function of ΔG_i^0 for the benzhydryl chlorides $\mathbf{E-Cl}$ (eq. 5.S.4.2).



$$\Delta G^0 = \Delta G_{\text{rel}}^0(\mathbf{E-N8}^+) - \Delta G_i^0(\mathbf{E-Cl}) \quad (5.S.4.2)$$

Assuming constant $\Delta G_0^\ddagger = 45 \text{ kJ mol}^{-1}$, we can use the Marcus equation (eq. 6) to calculate the activation free energies ΔG^\ddagger for these reactions which are converted to rate constants by the Eyring equation (eq. 5). The resulting $\lg k_2$ values for the combination reactions (eq. 5.S.4.1) are plotted against the thermodynamic stabilities (ΔG_i^0) of \mathbf{E}^+ in Fig. 5.S.4.1.

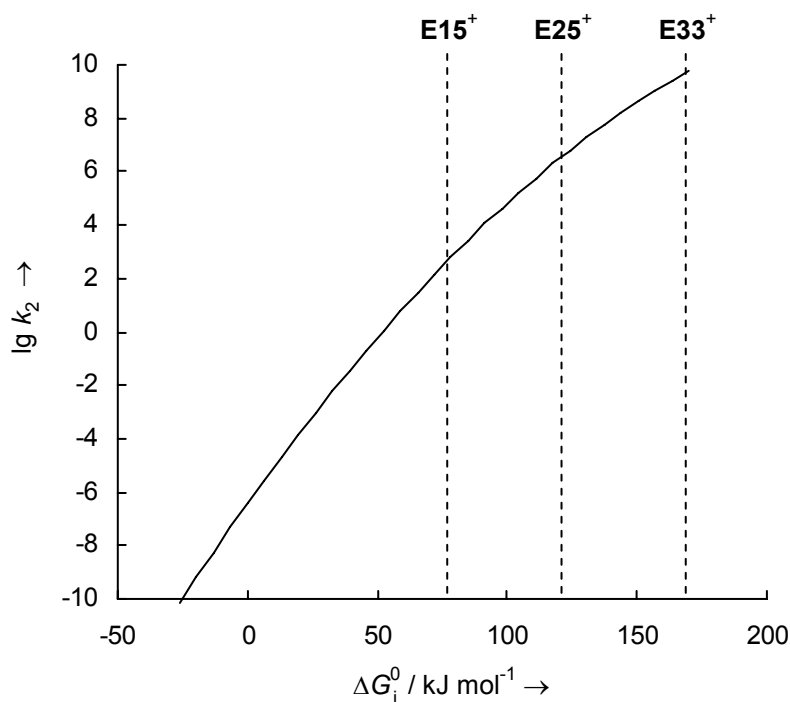


Figure 5.S.4.1. Plot of hypothetical $\lg k$ values for the combination reactions of \mathbf{E}^+ with $\mathbf{N8}$ to $\mathbf{E-N8}^+$ ($\lg k_2$) and the ionization reactions of $\mathbf{E-N8}^+$ to \mathbf{E}^+ and $\mathbf{N8}$ ($\lg k_s$) which were calculated from the Marcus equation assuming constant $\Delta G_0^\ddagger = 45 \text{ kJ mol}^{-1}$ against the free ionization energies ΔG_i^0 of $\mathbf{E-Cl}$ in CH_2Cl_2 . The dashed lines indicate the ΔG_i^0 values of $\mathbf{E15-Cl}$, $\mathbf{E25-Cl}$, and $\mathbf{E33-Cl}$ as determined in Section 5.S.3.

Using the correlation in Fig. 5.S.3.2 to replace ΔG_i^0 by the methyl anion affinities ΔG_{MA} , we obtain Figure 5.S.4.2a ($\lg k_2$ vs ΔG_{MA}), which can be converted into Figure 5.S.4.2b (E vs ΔG_{MA}) by eq. 1 and the nucleophilicity parameters of $\mathbf{N8}$ ($N = 0.84$, $s_N = 1.06$).⁴ This curve is plotted in Fig. 5.8 in section 5.2.4.

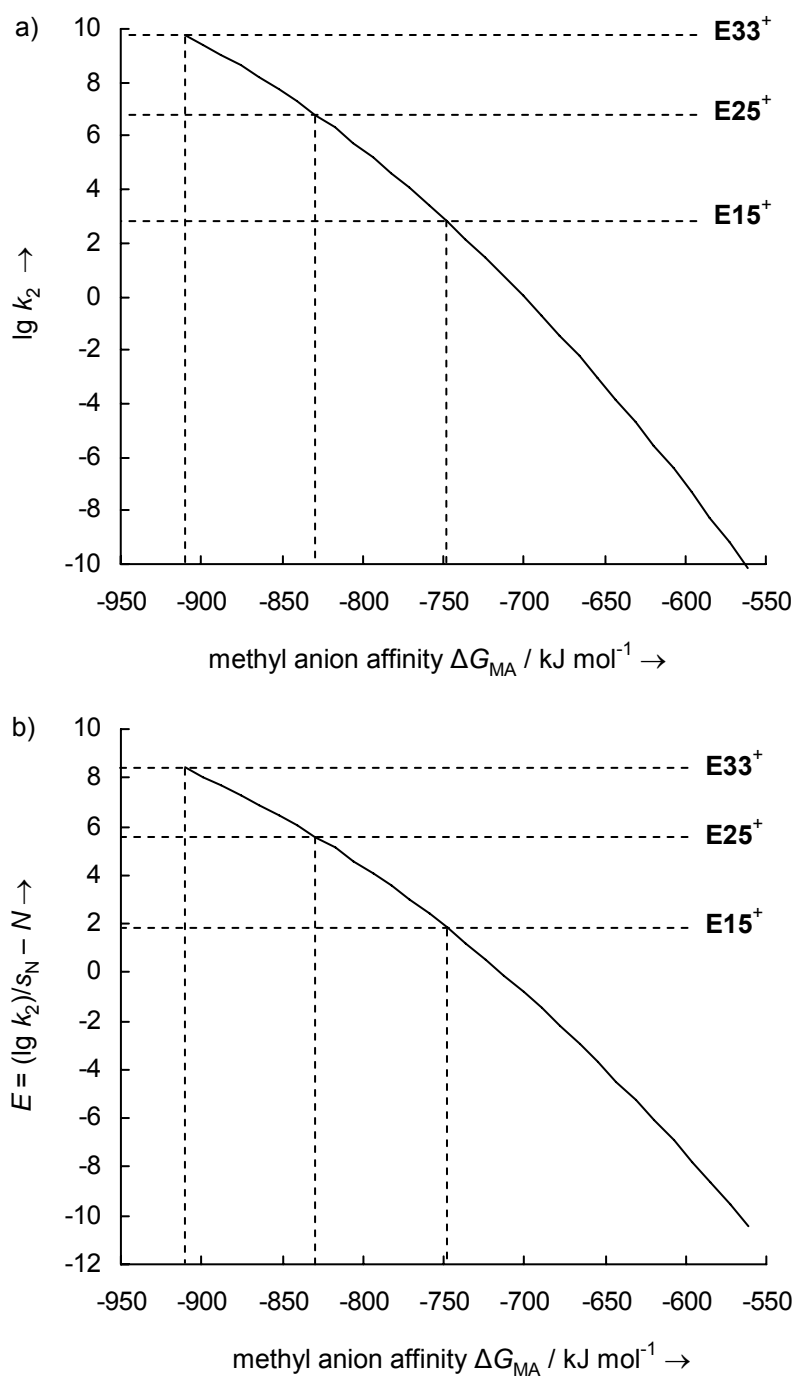


Figure 5.S.4.2. (a) Plot of $\lg k_2$ for the combination reactions of \mathbf{E}^+ with $\mathbf{N}8$ to $\mathbf{E-N}8^+$ assuming constant $\Delta G_0^\ddagger = 45 \text{ kJ mol}^{-1}$ against the methyl anion affinities ΔG_{MA} of \mathbf{E}^+ . The dashed lines indicate the rate constants for reactions of hypothetical benzhydrylium ions which have the same thermodynamic stabilities as $\mathbf{E}15^+$, $\mathbf{E}25^+$ or $\mathbf{E}33^+$ but constant $\Delta G_0^\ddagger = 45 \text{ kJ mol}^{-1}$ for their reactions with $\mathbf{N}8$. (b) Plot of $E = (\lg k_2)_{s_N} - N$ derived from the $\lg k_2$ data from Fig. (a) against the methyl anion affinities ΔG_{MA} of \mathbf{E}^+ .

5.S.5 Yukawa-Tsuno analysis

Following the approach of Jencks,³⁹ we used a modified Yukawa-Tsuno equation⁴⁰ (eq. 5.S.5.1) to separate the inductive and resonance substituent effects in the E parameters (eq. 5.S.5.2).

$$\lg \frac{k}{k_0} = \rho^n \sigma + \rho^r (\sigma^+ - \sigma) \quad (5.S.5.1)$$

$$E = \rho^n \sigma + \rho^r (\sigma^+ - \sigma) + c \quad (5.S.5.2)$$

The ρ^n and ρ^r parameters were determined from the E parameters of the symmetrically substituted benzhydrylium ions by a least-squares minimization using the the nonlinear solver program “What’sBest! 7.0 Industrial” by Lindo Systems Inc.^{S3} The σ and σ^+ constants were taken from ref.² except for $\sigma = -0.38$ ^{S4} and $\sigma^+ = -0.98$ ^{S2} for the fused dihydrofuran in **E13**⁺. The quality of the correlation is illustrated by Fig. 5.S.5.1, which also plots the data for the unsymmetrically substituted systems (open symbols).

Table 5.S.5.1. Structure-reactivity coefficients separating inductive (ρ^n) and resonance effects (ρ^r) in electrophilicity parameters E and electrofugality parameters E_f .

	ρ^n	ρ^r	c^a	R^2	r^b
parameters for E	1.86	5.08	5.67	0.9921	2.73
normalized parameters for E^c	0.29	0.69	–	–	–
parameters for E_f	–4.61	–2.31	–5.80	0.9870	0.50
normalized parameters for E_f^d	0.71	0.31	–	–	–

^a Constant c from eq. 5.S.5.2 was also allowed to vary because otherwise the electrophilicity or electrofugality parameters of **E25**⁺ ($E = 5.47$, $E_f = -6.03$) would have received infinite weight in the correlation analysis. ^b In the classical form of the Yukawa-Tsuno-equation, $r = \rho^r/\rho^n$ indicates the degree of resonance interaction between the aryl group and the reaction site in the rate-determining transition state. A value of $r > 1$ indicates that the resonance demand in the transition state is larger than in the reference reaction (solvolyses of *tert*-cumyl chlorides).⁴⁰ ^c Normalized values ρ_{nor} as defined by eq. 5.S.5.3. ^d $\rho_{\text{nor}}(E_f) = 1 - \rho_{\text{nor}}(E)$.

An analogous treatment was employed to obtain ρ^n and ρ^r for the E_f parameters (Table 5.S.5.1, Fig. 5.S.5.2). Using the relationship $\rho_{\text{equilibrium}} = \rho_{\text{forward}} - \rho_{\text{reverse}}$,³⁹ the normalized parameters ρ_{nor}^n and ρ_{nor}^r were then calculated by eq. 5.S.5.3.

$$\rho_{\text{nor}} = \frac{\rho_{\text{forward}}}{\rho_{\text{equilibrium}}} = \frac{\rho(E)}{\rho(E) - \rho(E_f)} \quad (5.S.5.3)$$

For a combination reaction of **E**⁺ and a hypothetical nucleophile with $s_N = s_f = 1$, the normalized ρ parameters obtained from eq. 5.S.5.3 indicate that 29% of the inductive effect and 69% of the resonance effect are lost in the transition state (Table 5.S.5.1). Thus, there is

an imbalance between inductive effects and resonance effects in the transition state. Variations of s_N and s_f in the usual range will change the numeric values of ρ_{nor}^n and ρ_{nor}^f but do not lead to a different conclusion.

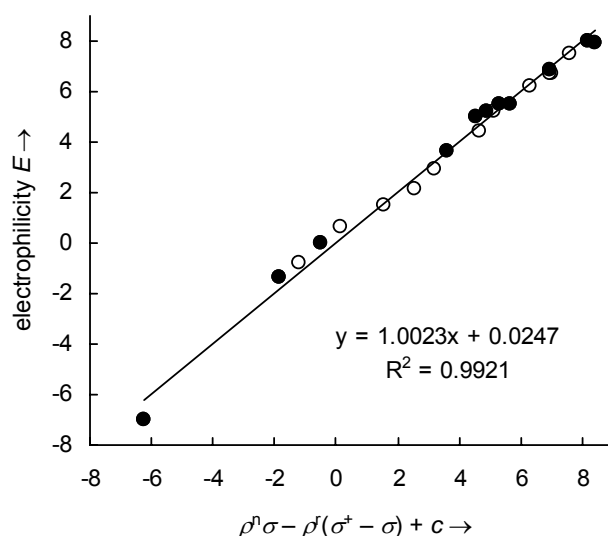


Figure 5.S.5.1. Plot of E versus $\rho^n \sigma - \rho^f (\sigma^+ - \sigma) + c$. Filled symbols: Symmetrically substituted benzhydrylium ions; open symbols: Unsymmetrically substituted systems (not used for the calculation of ρ^n and ρ^f).

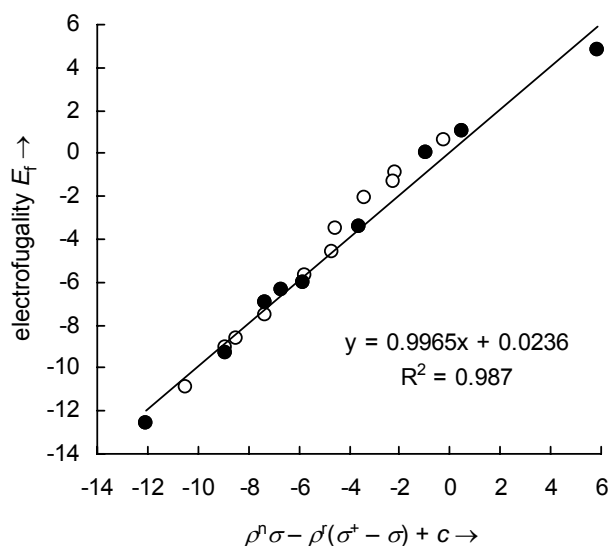
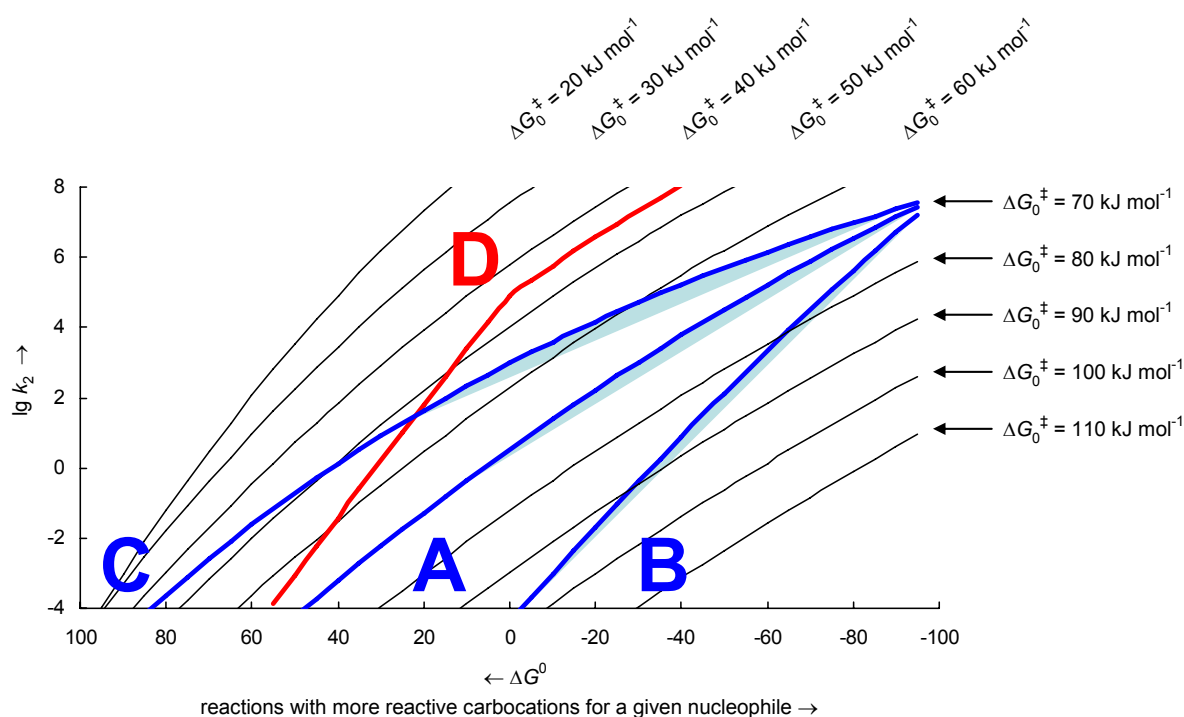
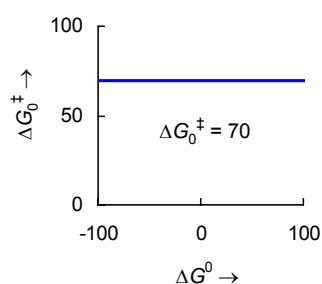


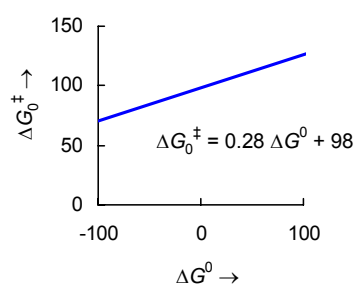
Figure 5.S.5.2. Plot of E_f versus $\rho^n \sigma - \rho^f (\sigma^+ - \sigma) + c$. Filled symbols: Symmetrically substituted benzhydrylium ions; open symbols: Unsymmetrically substituted systems (not used for the calculation of ρ^n and ρ^f).

5.S.6 Effect of ΔG_0^\ddagger on the linearity of $\lg k_2$ vs ΔG^0 plots

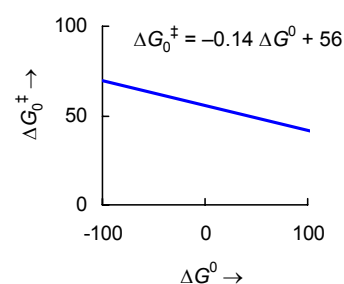
Line A:



Line B:



Line C:



Line D:

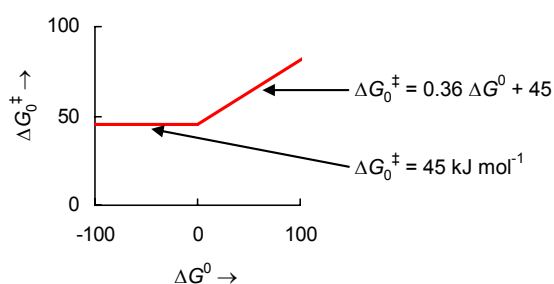


Figure 5.S.6.1. Series of parabola sections calculated by the Marcus equation (eq. 6); each of the thin lines is a plot of $\lg k_2$ versus ΔG^0 for a constant ΔG_0^\ddagger as specified in the Figure. Line **A**: constant intrinsic barriers ΔG_0^\ddagger . Line **B**: intrinsic barriers ΔG_0^\ddagger increase linearly with ΔG^0 . Line **C**: intrinsic barriers ΔG_0^\ddagger decrease linearly with ΔG^0 . Line **D**: the intrinsic barriers ΔG_0^\ddagger were assumed to be constant for reactions with $\Delta G^0 < 0$ and to increase linearly with ΔG^0 for reactions with $\Delta G^0 > 0$.

Figure 5.S.6.1 illustrates that the curvature of parabola sections calculated by the Marcus equation (eq. 6) is quite small in the experimentally accessible range of $\sim -4 \leq \lg k_2 \leq 8$ (= validity limit of eq. 1). If the intrinsic barriers ΔG_0^\ddagger increase linearly with ΔG^0 (line **B**), the curvature becomes even more negligible.

Line **D** in Fig. 5.S.6.1 shows a mixed behavior, where the intrinsic barriers ΔG_0^\ddagger are constant for reactions with $\Delta G^0 < 0$ and increase linearly with ΔG^0 for reactions with $\Delta G^0 > 0$. As a consequence, we observe a break between two separate linear correlations of $\lg k_2$ versus ΔG^0 .

Electrophilic Reactivity of the α,α -Dimethylbenzyl (Cumyl) Cation

Johannes Ammer and Herbert Mayr

Macromolecules **2010**, *43*, 1719-1723

6.1 Introduction

Whereas there are numerous investigations about the rate of formation of the cumyl cation under solvolytic conditions¹ as well as about its heat of formation² and spectral identification under stable-ion conditions,^{3,4} information about its electrophilic reactivity is rare.⁵

McClelland and Steenken generated the cumyl cation by laser-flash-induced photoprotonation of α -methylstyrene in 1,1,1,3,3,3-hexafluoroisopropanol (HFIP) and measured the rates of its reactions with this solvent as well as with Br^- and alcohols in HFIP solution.^{6,7} The failure to observe directly the cumyl cation by the same method in 2,2,2-trifluoroethanol (TFE) was explained by its estimated lifetime of <20 ns, which is below the experimental limit of the instrumentation used.⁷ Steenken reported that photoprotonation of bicumene in HFIP and subsequent fragmentation also yields the cumyl cation.⁸ Second-order rate constants close to the diffusion limit were reported for the reactions of the cumyl cation with N_3^- or halide ions in HFIP.⁸ Indirect evidence of the formation of the cumyl cation in TFE via a biphotonic pathway involving an intermediate bicumene radical cation has been obtained from the analysis of the resulting products.⁸ Cozens generated the cumyl cation by irradiation of bicumene incorporated in a zeolite and measured the rate of its decay in zeolite cavities.⁹

The cumyl cation is of particular importance in macromolecular chemistry. On the one side, it is the active electrophile in Kennedy's INIFER process,^{10,11} and on the other side, it is closely related to the propagating species in the carbocationic polymerization of α -methylstyrene. To characterize the electrophilic reactivity of the cumyl cation, we have now measured the rates of the reactions of the cumyl cation with various π -systems in CH_2Cl_2 solution. These rate constants will then be used to calculate the electrophilicity parameter, E , of the cumyl cation according to eq 1

$$\log k_2(20\text{ }^\circ\text{C}) = s_N(N + E) \quad (1)$$

where E is an electrophilicity parameter, N is a nucleophilicity parameter, and s_N is a nucleophile-specific slope parameter, which is usually close to 1.^{12,13}

A large body of data provides evidence that reactions of carbocations with CC double bonds follow eq 1.¹³ The applicability of the linear free energy relationship approach (eq 1) for the prediction of propagation rate constants¹⁴ has been demonstrated for the carbocationic polymerization of isobutylene,¹⁵ *N*-vinylcarbazole,¹⁶ styrene,¹⁷ and 2,4,6-trimethylstyrene.¹⁸

In the accompanying paper, Dimitrov and Faust derived the propagation rate constant for the carbocationic polymerization of α -methylstyrene from competition experiments, where the dimer of the cumyl cation selected between different π -systems.¹⁹ This article reports a fully independent approach to the same question, and from the agreement between the two methods, one can derive the reliability of the resulting rate constants.

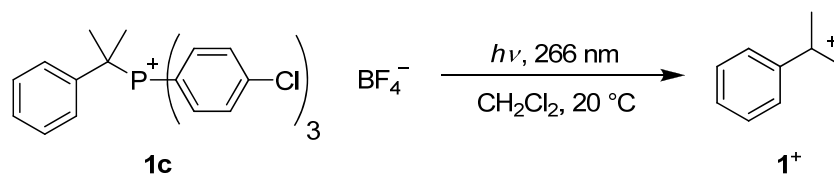
6.2 Results and Discussion

6.2.1 Laser-Flash-Photolytic Generation of the Cumyl Cation in Dichloromethane.

Photolyses of carbon-halogen bonds have extensively been studied,^{21,22} and Steenken reported that halide anions are excellent photoleaving groups for the laser-flash-photolytic generation of benzhydryl cations Ph_2CH^+ from various benzhydryl derivatives.^{22a} However, photoheterolysis of neutral precursors requires polar solvents, such as acetonitrile or TFE,²³ whereas in nonpolar solvents such as CH_2Cl_2 , only radicals are obtained.^{22a} An alternative way to generate carbocations by photoheterolysis is the irradiation of phosphonium ions.²⁴ This method can also be employed in dichloromethane.²⁵

When trying to generate the cumyl cation from cumyl chloride (**1a**) in acetonitrile or from cumyl triphenylphosphonium tetrafluoroborate (**1b**) in acetonitrile, TFE, or dichloromethane, we have not been able to obtain sufficient concentrations of the cumyl cation (in all cases $A_{\sim 330\text{nm}} < 0.04$).

In contrast, laser flash photolysis (266 nm, 40-60 mJ/pulse) of the cumyl tris(*p*-chlorophenyl)-phosphonium tetrafluoroborate (**1c**) gave the cumyl cation (**1⁺**) in dichloromethane solution in a concentration that is sufficient for measuring its reactivity (Scheme 6.1).

Scheme 6.1. Photolytic Generation of the Cumyl Cation

Identification. The transient spectrum (Figure 6.1, $\lambda_{\text{max}} \approx 335$ nm) is very similar to the reported spectra of the cumyl cation in HFIP ($\lambda_{\text{max}} \approx 325$ nm)⁶⁻⁸ and zeolite cavities ($\lambda_{\text{max}} \approx 330$ nm).⁹ Rapid mixing of α -methylstyrene and excess $\text{CF}_3\text{SO}_3\text{H}$ in dichloroethane also yielded a spectrum with $\lambda_{\text{max}} \approx 336$ nm, which was attributed to the cumyl cation.²⁶ Furthermore, λ_{max} of 335 nm is in good agreement with the absorption maximum observed after treatment of cumyl chloride with SbF_5 in CH_2Cl_2 at -72 °C ($\lambda_{\text{max}} = 333$ nm; $\epsilon_{333\text{ nm}} > 26\,300\text{ M}^{-1}\text{ cm}^{-1}$).⁴ The absorption maxima in $\text{FSO}_3\text{H-SbF}_5$ ($\lambda_{\text{max}} = 326$ nm)^{3b} and in 98% H_2SO_4 ($\lambda_{\text{max}} = 324$ nm)^{3c} were found to be at slightly lower wavelengths. An analogous bathochromic shift of 5-15 nm was observed for benzhydrylium ions when going from solutions in acetonitrile or strong mineral acids to dichloromethane solution.^{22a}

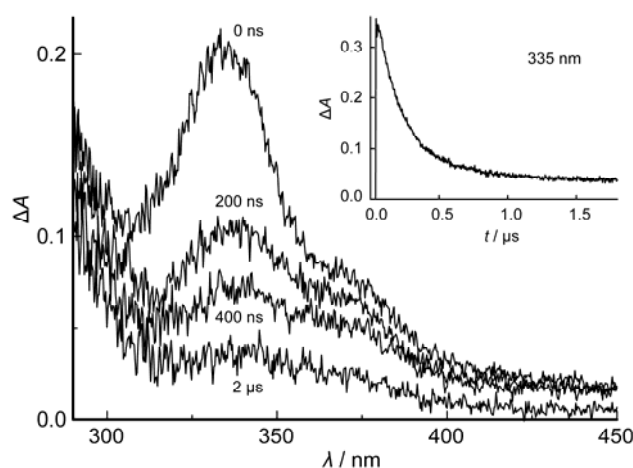


Figure 6.1. Transient spectra obtained 0 ns, 200 ns, 400 ns, and 2 μs after 266 nm irradiation of cumyl tris(4-chlorophenyl)phosphonium tetrafluoroborate (8.9×10^{-5} M, $A_{266\text{nm}} = 0.9$) in CH_2Cl_2 . The inset shows the decay at 335 nm during the first 1.8 μs .

The lifetime of the 335 nm transient in CH_2Cl_2 is ~ 0.2 μs . Its cationic nature is in line with the fact that it was not observable when the photolysis was carried out in the presence of 1.0×10^{-3} M tetrabutylammonium bromide. Under these conditions, the collapse of the

resulting cumyl cation bromide ion pair proceeds so fast that the carbocation cannot be detected with the instrumentation used (limit ≈ 10 -20 ns).

The fast decay of the transient with $\lambda_{\text{max}} = 335$ nm is superimposed by a slower decay ($1/k \approx 7$ to 8 μs) of a broad absorption band in the range of 330-380 nm. The rate of decay of this species (measured at 335 nm) is not affected by bromide, which suggests a radical species. Steenken reported that the spectrum of the cumyl radical obtained by pulse radiolysis in CH_2Cl_2 shows λ_{max} at 265 nm and two smaller absorption maxima at 308 and 320 nm.⁸ Furthermore, $\text{Ph}_3\text{P}^{+\bullet}$ and $(p\text{-Cl-C}_6\text{H}_4)_3\text{P}^{+\bullet}$ have been reported to absorb in this range.²⁷ Therefore, the formation of cumyl radicals and phosphinium radical cations by homolytic photocleavage of the precursor are considered to be a plausible explanation for the residual absorption.

We had problems observing the cumyl cation in TFE or in acetonitrile, which is rationalized by the higher nucleophilicity and basicity of these solvents compared with CH_2Cl_2 ; the appearance of a weak absorbance at ~ 330 nm in TFE will be discussed below.

Influence of the Photoleaving Group. It is interesting that the cumyl cation is much more efficiently generated from the precursor with the $(p\text{-Cl-C}_6\text{H}_4)_3\text{P}$ than with the Ph_3P photoleaving group. Because both phosphines can be expected to undergo diffusion-controlled reactions with carbocations of high electrophilicity ($E > 3$),²⁸ one can conclude that the difference in the efficiency of carbocation formation from $\text{PhC}(\text{CH}_3)_2\text{-PPh}_3^+ \text{BF}_4^-$ (**1b**) and $\text{PhC}(\text{CH}_3)_2\text{-P}(p\text{-Cl-C}_6\text{H}_4)_3^+ \text{BF}_4^-$ (**1c**) is not due to external return of Ar_3P but results from different behavior within the geminate solvent cage. $(p\text{-Cl-C}_6\text{H}_4)_3\text{P}$ is less nucleophilic than Ph_3P ($\Delta N = 1.75$),²⁸ less basic ($\Delta pK_{\text{AH}} = 1.7$ in H_2O),²⁹ and less easily oxidized ($\Delta E^0_{\text{ox}} = 0.22$ V in CH_3CN).³⁰

If one assumes that the photolytic generation of the carbocation proceeds via initial homolytic cleavage and subsequent electron transfer,^{21,23,24b} then the higher yield of **1**⁺ from **1c** might be rationalized by the higher reduction potential of $(p\text{-Cl-C}_6\text{H}_4)_3\text{P}^{+\bullet}$. This explanation is unlikely, however, because the benzhydryl cation Ph_2CH^+ can readily be generated from $\text{Ph}_2\text{CH-PPh}_3^+ \text{BF}_4^-$ though the oxidation potential of $\text{Ph}_2\text{CH}^\bullet$ is even higher than that of the cumyl radical.³¹ Because carbocations can only be observed on this time scale if they escape from the geminate solvent cage faster than they recombine with the photoleaving group, the different nucleophilicity of the phosphines may account for the increased efficiency with the $(p\text{-Cl-C}_6\text{H}_4)_3\text{P}$ leaving group. However, as stated above, the parent benzhydryl cation can be

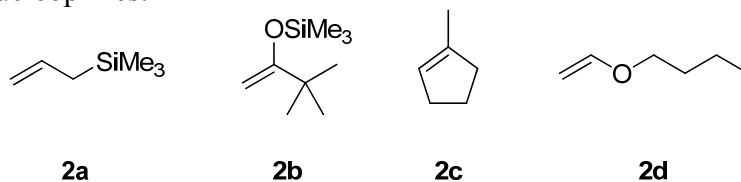
generated from $\text{Ph}_2\text{CH}-\text{PPh}_3^+ \text{BF}_4^-$, although its electrophilicity is comparable to that of the cumyl cation. (See below.)

We therefore assume that it is the higher Brønsted basicity of triphenylphosphine compared with $(p\text{-Cl-C}_6\text{H}_4)_3\text{P}$ that rapidly deprotonates the cumyl cation and thus is responsible for the failure to generate the cumyl cation by photolysis of $\text{PhC}(\text{CH}_3)_2-\text{PPh}_3^+ \text{BF}_4^-$ (**1b**).

This interpretation is in agreement with observations by Thibblin, who investigated the solvolyses of cumyl derivatives in 25% (v/v) aqueous acetonitrile, which proceed via intermediate cumyl cations.^{5d} Because the ratio α -methylstyrene/cumyl alcohol increases with the basicity of the leaving group, it was concluded that a significant amount of the elimination product is generated in the initial ion pair.

6.2.2 Rates of the Reactions of Cumyl Cations with π -Systems. When the laser flash photolysis of **1c** (Scheme 6.1) was carried out in the presence of a high excess of the π -nucleophiles **2a-d** (Scheme 6.2), exponential decays of the cumyl cations' absorbance at 335 nm were observed, from which the pseudo-first-order rate constants k_{obs} were obtained. Plots of k_{obs} against the concentrations of the nucleophiles were linear, as shown for a typical example in Figure 6.2.

Scheme 6.2. π -Nucleophiles.



The large intercepts of these plots ($(5\text{-}8) \times 10^6 \text{ s}^{-1}$) reflect the fast decay of the cumyl cation in CH_2Cl_2 solution. The magnitude of the intercept varied somewhat between different experiments, reflecting variable concentrations of water and other impurities in different batches of dichloromethane. The slopes of these plots represent the second-order rate constants k_2 that are reported in Table 6.1.

Only nucleophiles within a narrow range of reactivity could be employed to characterize the electrophilic reactivity of the cumyl cation: Because of the fast decay, the rate constant had to be greater than $\sim 10^7 \text{ M}^{-1} \text{ s}^{-1}$, but it had to be less than $\sim 2 \times 10^8 \text{ M}^{-1} \text{ s}^{-1}$ not to approach the limit of diffusion control where eq 1 cannot be employed.

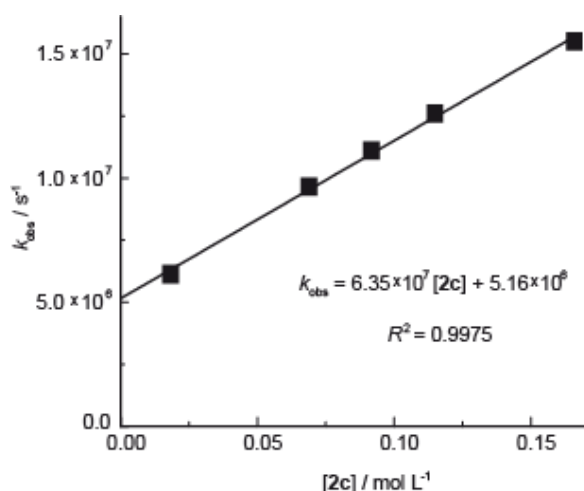
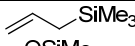
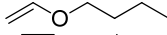
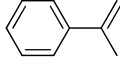


Figure 6.2. Plot of the pseudo-first-order rate constants k_{obs} obtained from reaction of the cumyl cation $\mathbf{1}^+$ with 1-methylcyclopentene ($\mathbf{2c}$) in CH_2Cl_2 against the concentration of $\mathbf{2c}$.

Table 6.1. Experimental Rate Constants ($\text{M}^{-1} \text{s}^{-1}$) for the Reactions of $\mathbf{1}^+$ with π -Nucleophiles $\mathbf{2a-d}$ in CH_2Cl_2 (Laser Flash Photolysis, 20 °C) and Comparison with Values Calculated from Equation 1.

nucleophile	$N (s_N)^a$	$k_2 / \text{M}^{-1} \text{s}^{-1}$	$k_{\text{calc}}^b / \text{M}^{-1} \text{s}^{-1}$
2a 	1.79 (0.94)	1.22×10^7	1.20×10^7
2b 	3.78 (0.79)	3.46×10^7	3.32×10^7
2c 	1.37 (1.10)	6.35×10^7	6.62×10^7
2d 	3.92 (0.90) ^c	1.18×10^8	4.94×10^8 ^c
2e 	2.35 (1.00)	– ^d	1.23×10^8

^a From ref 13. ^b From eq 1 using $E = 5.74$. ^c N , s_N parameters and k_{calc} for ethyl vinyl ether. ^d Not determined because the nucleophile absorbs at the wavelength of the excitation.

Allyltrimethylsilane (**2a**) is the least reactive nucleophile for which a reliable rate constant could be determined: Even at the highest concentration used ($[\mathbf{2a}] = 0.25 \text{ M}$), only one-third of the measured pseudo-first-order rate constant k_{obs} is due to the reaction with allyltrimethylsilane, whereas two-thirds correspond to the background reaction. For less reactive nucleophiles, the slope of the k_{obs} versus $[\mathbf{2}]$ plot is so small that a large error of the second-order rate constant will result.

According to eq 1, the electrophilicity parameter $E = 5.74$ for the cumyl cation ($\mathbf{1}^+$) is obtained from a plot of $(\log k_2)/s_N$ versus the nucleophilicity parameter N of **2a-c** (Figure 6.3). As expected from the good correlation in Figure 6.3, Table 6.1 shows that the calculated rate constants for $\mathbf{1}^+ + \mathbf{2a}$, **2b**, and **2c** agree well with experimental values. The calculated value

for the reaction of $\mathbf{1}^+$ with ethyl vinyl ether is 4 times larger than that measured for the reaction of $\mathbf{1}^+$ with *n*-butyl vinyl ether (Table 6.1).

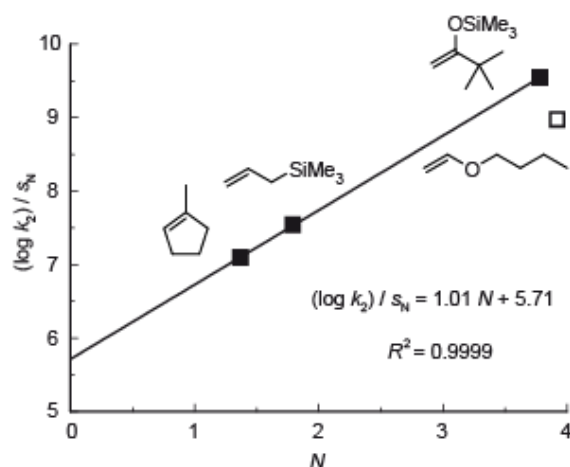


Figure 6.3. Plot of $(\log k_2)/s_N$ versus N for the reactions of the cumyl cation ($\mathbf{1}^+$) with the π -systems **2a-c** (■). When the slope is set to unity as required by eq 1, one obtains $E = 5.74$. For *n*-butyl vinyl ether (□), the N , s_N parameters are not known, and those of ethyl vinyl ether were used. This value was not used for the correlation.

The similarity of the E parameters of the cumyl cation $\mathbf{1}^+$ ($E = 5.74$) and the benzhydryl cation Ph_2CH^+ ($E = 5.90$)¹³ is another example for the rule-of-thumb that one phenyl group has a similar stabilizing effect on carbocations as two methyl groups.³²

Parr's global electrophilicity index, ω ,³³ which has previously been determined for the cumyl (12.8) and the benzhydryl cation (13.0),³⁴ also predicts similar electrophilic reactivities of these two carbenium ions. From ω_C , the local electrophilicity at the carbocation site,^{34a} one would predict that the cumyl cation ($\omega_C = 5.57$) is considerably more electrophilic than the benzhydryl cation Ph_2CH^+ ($\omega_C = 4.61$),³⁴ in contrast with our observations.

6.2.3 Comparison with Other Kinetic and Thermodynamic Data. Reactions with Solvents.

Equation 1 can also be employed for reactions of carbocations with solvents; first-order rate constants k_1 are obtained when the solvent-specific parameters N_1 and s_N are substituted in eq 1.³⁵ As shown in Table 6.2, a first-order rate constant of $2.5 \times 10^6 \text{ s}^{-1}$ is calculated for the reaction of the cumyl cation ($\mathbf{1}^+$) with the solvent trifluoroethanol.

Table 6.2. First-Order Rate Constants (s^{-1}) for the Reaction of the Cumyl Cation ($\mathbf{1}^+$) with Solvents and Comparison with Values Calculated from Equation 1.

solvent ^a	$N_1 (s_N)$ ^b	k_1 / s^{-1}	$k_{\text{calc}}^c / \text{s}^{-1}$
TFE	1.23 (0.92)	$(> 5 \times 10^7)^d$	2.5×10^6
25AN75W	5.04 (0.89) ^e	$\sim 5 \times 10^9$ ^f	3.9×10^9
50T50W	3.57 (0.89)	1.7×10^{10} ^g	1.9×10^8

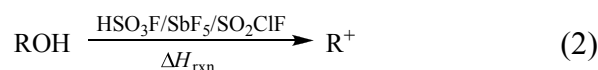
^a Mixtures of solvents are given as (v/v). AN: acetonitrile, T: TFE, W: water. ^b From ref 35. ^c Calculated from eq 1. ^d Laser flash photoprotonation of α -methylstyrene;^{7,8} lower limit derived from the fact that the lifetime was less than the experimental limit of 20 ns. ^e Interpolated; solvent nucleophilicity parameters are virtually constant for solvent mixtures 20AN80W to 50AN50W.^{35f} By azide clock method.^{5d} ^g By azide clock method.^{5a,b}

Previous investigations^{7,8} indicated a fast decay of the cumyl cation in TFE solution, and a decay rate constant $>5 \times 10^7 \text{ s}^{-1}$ has been suggested.⁷ In our experiments, laser flash photolysis of $\mathbf{1c}$ in TFE gave rise to a small absorbance at $\lambda \approx 330 \text{ nm}$, but because of the low absorbance ($A < 0.04$), it was not possible to obtain a spectrum or measure its decay rate reliably. A rough estimate for the decay of this absorbance gives a rate constant ($5 \times 10^6 \text{ s}^{-1}$) close to the calculated value.

Using the azide clock method, Thibblin determined a first-order rate constant of $\sim 5 \times 10^9 \text{ s}^{-1}$ for the reaction of the cumyl cation ($\mathbf{1}^+$) with 25AN75W^{5d} close to the calculated value of $3.9 \times 10^9 \text{ s}^{-1}$ (Table 6.2). Because of the lower nucleophilicity of 50T50W,³⁵ we would expect a considerably slower decay of the cumyl cation ($\mathbf{1}^+$) in this solvent ($k_{\text{calc}} = 1.9 \times 10^8 \text{ s}^{-1}$), and we cannot explain why the azide clock method gave a higher decay rate constant for the cumyl cation in 50T50W ($k_1 = 1.7 \times 10^{10} \text{ s}^{-1}$)^{5a,b} than in 25AN75W.

Comparison with Solvolysis Rates. Solvolysis rate constants, k_s , of cumyl chloride have been measured by Brown^{1a} and Liu^{1b} in different solvents. From the reported k_s values, an estimate for the electrofugality of the cumyl cation $E_f \approx -4.99$ has been derived,^{36b} indicating that cumyl derivatives solvolyze ~ 10 times faster than the corresponding benzhydryl derivatives (for Ph_2CH^+ , $E_f = -6.05$).³⁶ The difference in the solvolysis rates of $\text{PhC}(\text{CH}_3)_2\text{Cl}$ and Ph_2CHCl in various solvents is not reflected by the almost equal electrophilicities of the resulting carbenium ions.

Comparison with Thermodynamic Parameters. Arnett and Hofelich have established a carbenium ion stability scale based on the heats of reaction, ΔH_{rxn} , of alcohols with $\text{HSO}_3\text{F}/\text{SbF}_5/\text{SO}_2\text{ClF}$ at $-55 \text{ }^\circ\text{C}$ (eq 2).^{2b}



By this method, the cumyl cation ($\Delta H_{\text{rxn}} = -168.7 \text{ kJ mol}^{-1}$) turns out to be slightly more stabilized than the parent benzhydryl cation ($\Delta H_{\text{rxn}} = -164.5 \text{ kJ mol}^{-1}$), in line with the relative solvolysis rate constants.

Only crude estimates of the $\text{p}K_{\text{R}}$ value for the reaction of water with the cumyl cation are available (-10.1 to -12.3),^{5b,31a} and we refrain from comparing it with that of the benzhydryl cation.

6.2.4 Rate Constant for the Addition of the Cumyl Cation to α -Methylstyrene. A direct kinetic determination of the first step of the carbocationic polymerization of α -methylstyrene, that is, the reaction of the cumyl cation ($\mathbf{1}^+$) with α -methylstyrene ($\mathbf{2e}$) to form the dimeric cation, was not attempted because α -methylstyrene absorbs at the excitation wavelength of the laser and interferes with the photolytic generation of the cumyl cation. Furthermore, the UV-absorption spectra of the cumyl ($\lambda_{\text{max}} = 335 \text{ nm}$) and the dimeric cation ($\lambda_{\text{max}} = 348 \text{ nm}$)³⁷ are very similar, which complicates measuring the rate of consumption or formation of the carbocations.

Using the known nucleophilicity parameter of α -methylstyrene ($N = 2.35$, $s_{\text{N}} = 1.00$)¹³ and the E value of 5.74 for the cumyl cation determined in this work, eq 1 yields $k_{\text{calc}, 20^\circ\text{C}} = 1.2 \times 10^8 \text{ M}^{-1} \text{ s}^{-1}$ for the rate of the reaction of the cumyl cation with α -methylstyrene. Because bimolecular reactions of such high rates do not have enthalpic barriers,^{14a,38} this rate constant can be considered to be almost independent of temperature.

The rate constant calculated in this way is 400 times higher than the value reported previously by the Paris laboratory for the addition of the cumyl cation to α -methylstyrene at -65°C , which was obtained from the initial slopes of appearance of a 348 nm absorbance band ascribed to the dimeric cation.³⁷

Although previous investigations on styrene derivatives showed similar electrophilic reactivities of monomeric and dimeric cations,^{17,18} we cannot generalize this observation. Because we were not able to synthesize suitable precursors for the laser flash photolytic generation of the dimeric cation, we leave the investigation of the oligomeric cations to the following paper.¹⁹

6.3 Note Added After Publication

After the publication of this work, we have reported slightly modified electrophilicity parameters for our highly electrophilic reference electrophiles ($E > 4$) and revised the N and s_N parameters of several weak π -nucleophiles.^{25b} Figure 6.4 shows an updated plot of $(\log k_2)/s_N$ versus N for the reactions of the cumyl cation ($\mathbf{1}^+$) with the π -systems **2a-c** using the revised nucleophilicity parameters from ref. 25b. The resulting electrophilicity parameter of the cumyl cation ($\mathbf{1}^+$), $E = 5.42$, is again very similar to that of the benzhydryl cation (Ph_2CH^+ , $E = 5.47$).^{25b} As the deviation is small, a revision of the published value of $E = 5.74$ for $\mathbf{1}^+$ is unnecessary.

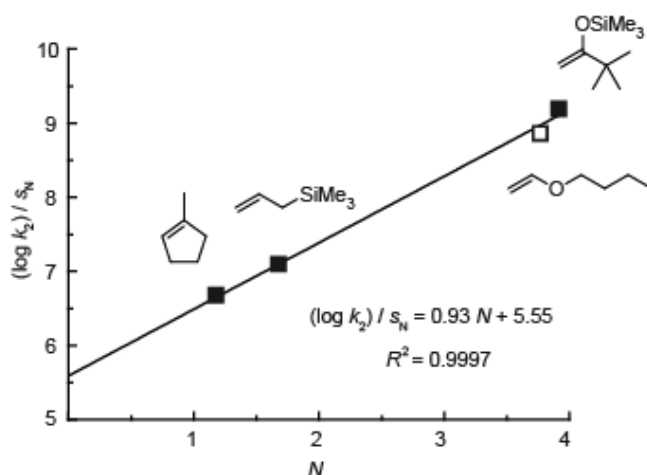


Figure 6.4. Plot of $(\log k_2)/s_N$ versus N for the reactions of the cumyl cation ($\mathbf{1}^+$) with the π -systems **2a-c** (■) using the revised nucleophilicity parameters from ref. 25b.^a When the slope is set to unity as required by eq 1, one obtains $E = 5.42$. The rate constant for *n*-butyl vinyl ether (□) was not used for the correlation, as the rate constant is above the limit of $10^8 \text{ M}^{-1} \text{ s}^{-1}$.

^a The reactivity parameters $N = 3.91$ and $s_N = 0.82$ for **2b** are obtained, when the rate constants for the reactions of **2b** with benzhydrylium ions^{12b} and the updated E parameters of the benzhydrylium ions^{25b} are substituted into eq 1.

The failure to generate $\mathbf{1}^+$ from cumyl tris(*p*-chlorophenyl)phosphonium tetrafluoroborate (**1c**) in the presence of $1.0 \times 10^{-3} \text{ M}$ tetrabutylammonium bromide could also be explained by a photo-electron transfer in the phosphonium bromide ion pair.^{25a}

6.4 Acknowledgment

Dedicated to Professor Oskar Nuyken on the occasion of his 70th birthday. We thank Professor R. Faust for stimulating this investigation and the Deutsche Forschungsgemeinschaft for financial support.

6.5 References and Notes

- (1) (a) Okamoto, Y.; Inukai, T.; Brown, H. C. *J. Am. Chem. Soc.* **1958**, *80*, 4972–4976. (b) Liu, K.-T.; Chen, P.-S.; Chiu, P.-F.; Tsao, M.-L. *Tetrahedron Lett.* **1992**, *33*, 6499–6502. (c) Liu, K.-T.; Chang, L.-W.; Chen, P.-S. *J. Org. Chem.* **1992**, *57*, 4791–4793. (d) Liu, K.-T.; Lee, J.-K.; Chen, H.-I. *J. Org. Chem.* **1990**, *55*, 3662–3664. (e) Brown, H. C.; Peters, E. N. *J. Am. Chem. Soc.* **1977**, *99*, 1712–1716. (f) Creary, X. *J. Org. Chem.* **1985**, *50*, 5080–5084. (g) Creary, X.; Wang, Y.-X. *J. Org. Chem.* **1992**, *57*, 4761–4765.
- (2) (a) Arnett, E. M.; Petro, C. *J. Am. Chem. Soc.* **1978**, *100*, 5408–5416. (b) Arnett, E. M.; Hofelich, T. C. *J. Am. Chem. Soc.* **1983**, *105*, 2889–2895.
- (3) (a) Olah, G. A. *J. Am. Chem. Soc.* **1964**, *86*, 932–934. (b) Olah, G. A.; Pittman, C. U.; Waack, R.; Doran, M. *J. Am. Chem. Soc.* **1966**, *88*, 1488–1495. (c) Bertoli, V.; Plesch, P. H. *J. Chem. Soc. B* **1968**, 1500–1516.
- (4) Matyjaszewski, K.; Sigwalt, P. *Macromolecules* **1987**, *20*, 2679–2689.
- (5) For applications of the azide clock method, see: (a) Richard, J. P.; Amyes, T. L.; Vontor, T. *J. Am. Chem. Soc.* **1991**, *113*, 5871–5873. (b) Amyes, T. L.; Richard, J. P.; Novak, M. *J. Am. Chem. Soc.* **1992**, *114*, 8032–8041. (c) Richard, J. P.; Jagannadham, V.; Amyes, T. L.; Mishima, M.; Tsuno, Y. *J. Am. Chem. Soc.* **1994**, *116*, 6706–6712. (d) Thibblin, A. *J. Phys. Org. Chem.* **1989**, *2*, 15–25.
- (6) (a) McClelland, R. A.; Chan, C.; Cozens, F. L.; Modro, A.; Steenken, S. *Angew. Chem.* **1991**, *103*, 1389–1391; *Angew. Chem., Int. Ed.* **1991**, *30*, 1337–1339. (b) Cozens, F. L.; McClelland, R. A.; Steenken, S. *J. Am. Chem. Soc.* **1993**, *115*, 5050–5055.
- (7) Cozens, F. L.; Kanagasabapathy, V. M.; McClelland, R. A.; Steenken, S. *Can. J. Chem.* **1999**, *77*, 2069–2082.
- (8) Faria, J. L.; Steenken, S. *J. Phys. Chem.* **1992**, *96*, 10869–10874.

- (9) Cozens, F. L.; O'Neil, M.; Schepp, N. P. *J. Am. Chem. Soc.* **1997**, *119*, 7583–7584.
- (10) (a) Kennedy, J. P.; Smith, R. A. *Polym. Prepr.* **1979**, *20*, 316–319. (b) Kennedy, J. P.; Smith, R. A. *J. Polym. Sci., Polym. Chem. Ed.* **1980**, *18*, 1523–1537.
- (11) Reviews: (a) Kennedy, J. P.; Maréchal, E. Carbocationic Polymerization; Wiley: New York, 1982; pp 204-449. (b) Nuyken, O.; Pask, S. D.; Vischer, A.; Walter, M. *Makromol. Chem., Macromol. Symp.* **1986**, *3*, 129–152. (c) Freyer, C. V.; M€uhlbauer, H.-P.; Nuyken, O. *Angew. Makromol. Chem.* **1986**, *145/146*, 69–87.
- (12) (a) Mayr, H.; Patz, M. *Angew. Chem.* **1994**, *106*, 990–1010; *Angew. Chem., Int. Ed.* **1994**, *33*, 938-957. (b) Mayr, H.; Bug, T.; Gotta, M. F.; Hering, N.; Irrgang, B.; Janker, B.; Kempf, B.; Loos, R.; Ofial, A. R.; Remennikov, G.; Schimmel, H. *J. Am. Chem. Soc.* **2001**, *123*, 9500–9512. (c) Lucius, R.; Loos, R.; Mayr, H. *Angew. Chem.* **2002**, *114*, 97–102; *Angew. Chem., Int. Ed.* **2002**, *41*, 91-95. (d) Mayr, H.; Ofial, A. R. In Carbocation Chemistry, Olah, G. A., Prakash, G. K. S., Eds.; Wiley: Hoboken, NJ, 2004; pp 331-358. (e) Mayr, H.; Ofial, A. R. *Pure Appl. Chem.* **2005**, *77*, 1807–1821. (f) Mayr, H.; Ofial, A. R. *J. Phys. Org. Chem.* **2008**, *21*, 584–595.
- (13) Mayr, H.; Kempf, B.; Ofial, A. R. *Acc. Chem. Res.* **2003**, *36*, 66–77.
- (14) (a) Mayr, H. In Ionic Polymerizations and Related Processes; Puskas, J. E., Michel, A., Barghi, S., Paulo, C., Eds.; Kluwer Academic Publishers: Dordrecht, The Netherlands, 1999; pp 99-115. (b) Ofial, A. R.; Mayr, H. *Macromol. Symp.* **2004**, *215*, 353–367.
- (15) Roth, M.; Mayr, H. *Macromolecules* **1996**, *29*, 6104–6109.
- (16) Schimmel, H.; Ofial, A. R.; Mayr, H. *Macromolecules* **2002**, *35*, 5454–5458.
- (17) De, P.; Faust, R.; Schimmel, H.; Ofial, A. R.; Mayr, H. *Macromolecules* **2004**, *37*, 4422–4433.
- (18) Mayr, H.; Ofial, A. R.; Schimmel, H. *Macromolecules* **2005**, *38*, 33–40.
- (19) Dimitrov, P.; Faust, R. *Macromolecules* **2010**, *43*, 1724–1729.
- (20) Okuma, K.; Izaki, T. *Bull. Chem. Soc. Jpn.* **2005**, *78*, 1831–1833.
- (21) (a) Kitamura, T. In CRC Handbook of Organic Photochemistry and Photobiology, 2nd ed.; Horspool, W., Lenci, F., Eds.; CRC Press: Boca Raton, FL, 2004; pp 11-1-11-10. (b) Kropp, P. J. In CRC Handbook of Organic Photochemistry and Photobiology, 2nd ed.; Horspool, W., Lenci, F., Eds.; CRC Press: Boca Raton, FL, 2004; pp 1-1-1-32.
- (22) For generation of benzhydryl cations from benzhydryl halides, see: (a) Bartl, J.; Steenken, S.; Mayr, H.; McClelland, R. A. *J. Am. Chem. Soc.* **1990**, *112*, 6918–6928. (b) Bartl, J.; Steenken, S.; Mayr, H. *J. Am. Chem. Soc.* **1991**, *113*, 7710–7716.

- (c) Peters, K. S.; Li, B. *J. Phys. Chem.* **1994**, *98*, 401–403. (d) Mayr, H.; Schimmel, H.; Kobayashi, S.; Kotani, M.; Prabakaran, T. R.; Sipos, L.; Faust, R. *Macromolecules* **2002**, *35*, 4611–4615. (e) Phan, B. T.; Nolte, C.; Kobayashi, S.; Ofial, A. R.; Mayr, H. *J. Am. Chem. Soc.* **2009**, *131*, 11392–11401.
- (23) (a) McClelland, R. A. *Tetrahedron* **1996**, *52*, 6823–6858. (b) McClelland, R. A. In *Reactive Intermediate Chemistry*; Moss, R. A., Platz, M. S., Jones, M., Jr., Eds.; Wiley: Hoboken, NJ, 2004; pp 3-40.
- (24) (a) Alonso, E. O.; Johnston, L. J.; Scaiano, J. C.; Toscano, V. G. *J. Am. Chem. Soc.* **1990**, *112*, 1270–1271. (b) Alonso, E. O.; Johnston, L. J.; Scaiano, J. C.; Toscano, V. G. *Can. J. Chem.* **1992**, *70*, 1784–1794. (c) Imrie, C.; Modro, T. A.; Wagener, C. C. P. *J. Chem. Soc., Perkin Trans. 2* **1994**, 1379–1382. (d) Imrie, C.; Modro, T. A.; Rohwer, E. R.; Wagener, C. C. P. *J. Org. Chem.* **1993**, *58*, 5643–5649. (e) Shi, L.; Horn, M.; Kobayashi, S.; Mayr, H. *Chem. – Eur. J.* **2009**, *15*, 8533–8541.
- (25) (a) Ammer, J.; Sailer, C. F.; Riedle, E.; Mayr, H. *J. Am. Chem. Soc.* **2012**, *134*, 11481–11494 (CHAPTER 2 of this work). (b) Ammer, J.; Nolte, C.; Mayr, H. *J. Am. Chem. Soc.* **2012**, *134*, 13902–13911 (CHAPTER 3 of this work).
- (26) Takarabe, K.; Kunitake, T. *Makromol. Chem.* **1981**, *182*, 1587–1593.
- (27) (a) Alfassi, Z. B.; Neta, P.; Beaver, B. *J. Phys. Chem. A* **1997**, *101*, 2153–2158. (b) Tojo, S.; Yasui, S.; Fujitsuka, M.; Majima, T. *J. Org. Chem.* **2006**, *71*, 8227–8232.
- (28) Kempf, B.; Mayr, H. *Chem. – Eur. J.* **2005**, *11*, 917–927.
- (29) Allman, T.; Goel, R. G. *Can. J. Chem.* **1982**, *60*, 716–722.
- (30) Fukuzumi, S.; Shimoosako, K.; Suenobu, T.; Watanabe, Y. *J. Am. Chem. Soc.* **2003**, *125*, 9074–9082.
- (31) (a) Wayner, D. D. M.; McPhee, D. J.; Griller, D. *J. Am. Chem. Soc.* **1988**, *110*, 132–137. (b) Sim, B. A.; Milne, P. H.; Griller, D.; Wayner, D. D. M. *J. Am. Chem. Soc.* **1990**, *112*, 6635–6638.
- (32) Streitwieser, A., Jr. *Solvolytic Displacement Reactions*; McGraw-Hill: New York, 1962; p 43.
- (33) Chattaraj, P. K.; Sarkar, U.; Roy, D. R. *Chem. Rev.* **2006**, *106*, 2065–2091.
- (34) (a) Pérez, P.; Toro-Labbé, A.; Aizman, A.; Contreras, R. *J. Org. Chem.* **2002**, *67*, 4747–4752. (b) Aizman, A.; Contreras, R.; Pérez, P. *Tetrahedron* **2005**, *61*, 889–895.
- (35) Minegishi, S.; Kobayashi, S.; Mayr, H. *J. Am. Chem. Soc.* **2004**, *126*, 5174–5181.

- (36) (a) Denegri, B.; Streiter, A.; Jurić, S.; Ofial, A. R.; Kronja, O.; Mayr, H. *Chem. – Eur. J.* **2006**, *12*, 1648-1656; 5415. (b) Denegri, B.; Ofial, A. R.; Jurić, S.; Streiter, A.; Kronja, O.; Mayr, H. *Chem. – Eur. J.* **2006**, *12*, 1657–1666.
- (37) Russell, R.; Moreau, M.; Charleux, B.; Vairon, J.-P.; Matyjaszewski, K. *Macromolecules* **1998**, *31*, 3775–3782.
- (38) Patz, M.; Mayr, H.; Bartl, J.; Steenken, S. *Angew. Chem.* **1995**, *107*, 519-521; *Angew. Chem., Int. Ed.* **1995**, *34*, 490-492.

6.S Supplementary Data and Experimental Section

6.S.1 Materials. *Solvents.* For the laser flash photolysis experiments, p.a. grade dichloromethane (Merck) was subsequently treated with concentrated sulfuric acid, water, 10% NaHCO₃ solution, and again water. After predrying with anhydrous CaCl₂, it was freshly distilled over CaH₂. Acetonitrile (HPLC grade, VWR) and TFE (99%, Apollo) were used as received.

Precursors for Laser Flash Photolysis. α,α -Dimethylbenzyl chloride (97%, Apollo) was used as received. The phosphonium salts Ph(CH₃)₂CPAr₃⁺ BF₄⁻ were prepared by reaction of α -methylstyrene with the corresponding triarylphosphonium tetrafluoroborate Ar₃PH⁺ BF₄⁻ (see below).²⁰

Nucleophiles. Allyltrimethylsilane (97%, Acros), 1-methylcyclopentene (98%, ABCR), (2,2-dimethyl-1-methylenepropoxy) trimethylsilane (98%, Aldrich), and *n*-butyl vinyl ether (98%, Aldrich) were used as received. Tetrabutylammonium bromide (99%, Aldrich) was dried under high vacuum for several hours and then handled in the glovebox.

6.S.2 Synthetic procedures. *General.* Triphenylphosphine (99%, Acros), tris(4-chlorophenyl)-phosphine (98%, ABCR), α -methylstyrene (99%, Riedel-de Haën), aqueous HBF₄ (~50% in H₂O, purum, Fluka) and HBF₄·Et₂O (95-98%, BASF) were used as received.

Yields are not optimized. NMR-signal assignment was aided by HSQC and HMBC experiments.

(1-Methyl-1-phenylethyl)triphenylphosphonium tetrafluoroborate (1b). Following the procedure by Okuma *et al.*,²⁰ 0.79 g (3.0 mmol) of triphenylphosphine and 0.34 ml (2.7 mmol) of 8.0 M aqueous HBF₄ was heated to 120 °C for 1 h. Then, 0.35 ml (0.32 g, 2.7 mmol) α -methylstyrene was added, and the mixture was heated to 145 °C for 1 h. The residue was recrystallized from ethanol (12 ml), yielding 0.41 g (0.88 mmol, 33%) of a colorless solid, m.p. 188-189 °C (ethanol).

¹H NMR (400 MHz, CD₂Cl₂): δ 2.06 (d, 6 H, ³J_{H,P} = 17.6 Hz, CH₃), 6.98-7.02 (m, 2 H, *o*-C₆H₅), 7.26-7.31 (m, 2 H, *m*-C₆H₅), 7.37-7.43 (m, 1 H, *p*-C₆H₅), 7.49-7.55 (m, 6 H, *m*-PPh₃), 7.65-7.71 (m, 6 H, *o*-PPh₃), 7.85-7.90 (m, 3 H, *p*-PPh₃);

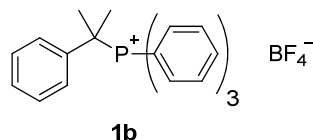
¹³C NMR (100 MHz, CD₂Cl₂): δ 25.8 (s, CH₃), 44.1 (d, ¹J_{C,P} = 38.7 Hz, CMe₂), 117.4 (d, ¹J_{C,P} = 78.8 Hz, *i*-PPh₃), 128.8 (d, ⁴J_{C,P} = 2.8 Hz, *m*-C₆H₅), 128.9 (d, ³J_{C,P} = 4.8 Hz, *o*-C₆H₅),

129.5 (d, $^5J_{C,P} = 3.3$ Hz, p -C₆H₅), 130.3 (d, $^3J_{C,P} = 11.9$ Hz, m -PPh₃), 135.1 (d, $^2J_{C,P} = 8.5$ Hz, o -PPh₃), 135.4 (d, $^4J_{C,P} = 3.1$ Hz, p -PPh₃), 137.0 (d, $^2J_{C,P} = 2.8$ Hz, i -C₆H₅);

^{31}P NMR (162 MHz, CD₂Cl₂): δ 31.6.

HR-MS (ESI, positive): Calcd m/z for C₂₇H₂₆P⁺: 381.1766, Found: 381.1753.

Elemental analysis: Calcd for C₂₇H₂₆BF₄P: C, 69.25; H, 5.60, Found: C, 68.99; H, 5.46.



Tris(4-chlorophenyl)(1-methyl-1-phenylethyl)phosphonium tetrafluoroborate (1c). The tertiary phosphonium salt was prepared by adding 0.30 ml (0.36 g, 2.2 mmol) HBF₄ · Et₂O to 0.80 g (2.2 mmol) tris(4-chlorophenyl)phosphine in ether (20 ml) and removing the solvent under reduced pressure. Then, 0.60 ml (0.55 g, 4.6 mmol) α -methylstyrene were added, and the mixture was heated to 145 °C for 1 h. The residue was recrystallized from CH₂Cl₂/ethanol, washed with ethanol, and dried, yielding 0.62 g (1.1 mmol, 50%) of a colorless solid, m.p. 198-200 °C (CH₂Cl₂/ethanol).

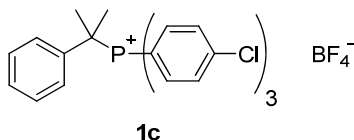
The product still contains small amounts (< 10 mol% by ^1H NMR) of a compound with an ethyl moiety, which was also present in the starting material phosphine. This is not considered problematic because the compound was used as the minor component in the kinetic experiments.

^1H NMR (400 MHz, CD₂Cl₂): δ 2.05 (d, 6 H, $^3J_{H,P} = 18.3$ Hz, CH₃), 7.00-7.05 (m, 2 H, o -C₆H₅), 7.30-7.35 (m, 2 H, m -C₆H₅), 7.41-7.48 (m, 1 H + 6 H, p -C₆H₅ + o -PAr₃), 7.66-7.71 (m, 6 H, m -PAr₃);

^{13}C NMR (100 MHz, CD₂Cl₂): δ 25.6 (d, $^2J_{C,P} = 0.8$ Hz, CH₃), 44.5 (d, $^1J_{C,P} = 37.9$ Hz, CMe₂), 115.2 (d, $^1J_{C,P} = 81.6$ Hz, i -PAr₃), 128.9 (d, $^3J_{C,P} = 5.0$ Hz, o -C₆H₅), 129.2 (d, $^4J_{C,P} = 2.9$ Hz, m -C₆H₅), 129.9 (d, $^5J_{C,P} = 3.5$ Hz, p -C₆H₅), 131.0 (d, $^3J_{C,P} = 12.7$ Hz, m -PAr₃), 136.37 (d, $^2J_{C,P} = 2.8$ Hz, i -C₆H₅), 136.38 (d, $^2J_{C,P} = 9.5$ Hz, o -PAr₃), 142.9 (d, $^4J_{C,P} = 3.7$ Hz, p -PAr₃);

^{31}P NMR (162 MHz, CD₂Cl₂): δ 31.3.

HR-MS (ESI, positive): Calcd m/z for C₂₇H₂₃(^{35}Cl)₃P⁺: 483.0597, Found: 483.0587.



6.S.3 Laser Flash Photolysis. *Experimental procedure.* Solutions of the precursor with $A_{266\text{ nm}} \approx 0.9$ (ca. 9×10^{-5} M) were irradiated with a 7-ns pulse from a quadrupled Nd:YAG laser (266 nm, 40-60 mJ/pulse), and a xenon lamp was used as probe light for UV/vis detection. The system is equipped with a fluorescence flow cell which allows to replace the sample volume completely between subsequent laser pulses.

Kinetics were measured by following the decay of the cumyl cation at 335 nm. For each concentration, ≥ 64 individual runs were averaged, and the pseudo-first order rate constants k_{obs} were obtained by least-squares fitting to the single-exponential curve $A_t = A_0 e^{-k_{\text{obs}} t} + C$.

The slope of a plot of k_{obs} versus concentration yields the second order rate constant k_2 .

Spectra of 1^+ were obtained as difference spectra from subsequent determinations without and with laser irradiation using an ICCD camera with a gate width of 10 ns and varying gate delay.

Reactions with nucleophiles. The high decay rate of the cumyl cation even without added nucleophile forced us to use quite high concentrations of nucleophiles in the kinetic experiments. Thus, as one reviewer pointed out, nucleophilic impurities in the reagents could be a problem. We exclude the possibility that impurities have an effect on the observed rate constants in the following way:

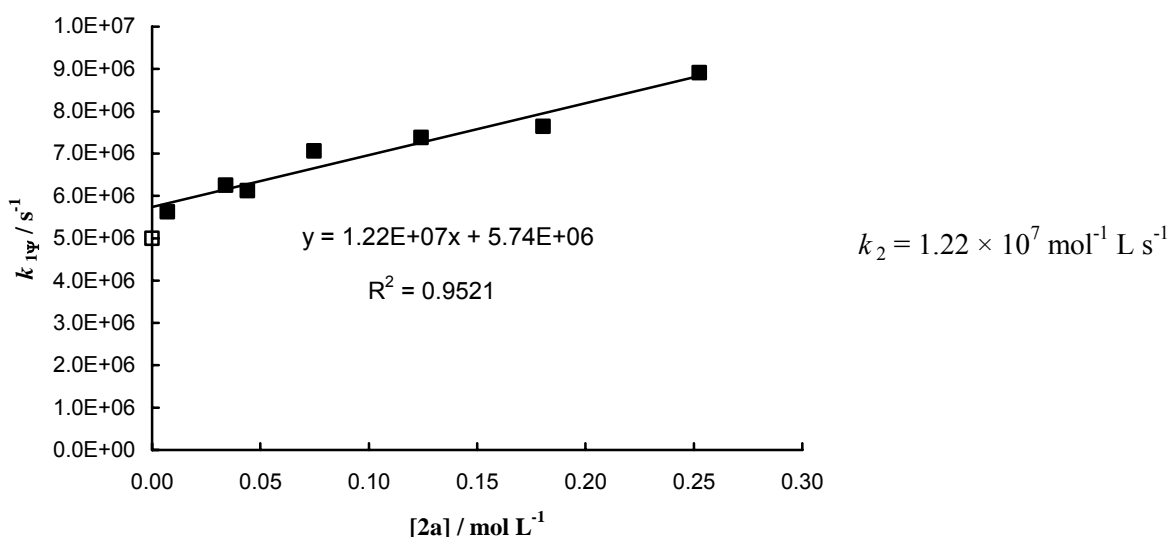
- a) Impurities of lower nucleophilicity are irrelevant because they only lower the rate constants by 1-3%.
- b) Impurities of higher nucleophilicity may effect the pseudo-first-order rate constants if the nucleophiles are used in high excess (e.g. 10^3 equivalents) because then also the concentration of a more reactive nucleophile present in 1% may stay constant during the reaction and give rise to an exponential decay of the cumyl cation. However, we have used the same samples of **2a-d** for studying reactions of benzhydryl cations of variable reactivity, where a small excess as well as a large excess of nucleophile was used. The consistency of these data shows that the impurities are not nucleophiles of high reactivity.
- c) Furthermore, the consistency of the reactivities of different nucleophiles shown in Figure 3 indicates the reliability of our data.

Details of the kinetic experiments.

Pseudo-first order rate constants for the reactions of the cumyl cation (1^+) with allyltrimethylsilane (**2a**) in CH_2Cl_2 (laser flash photolysis, 20 °C)

no.	$[1c]_0 / \text{mol L}^{-1}$	$[2a]_0 / \text{mol L}^{-1}$	$k_{1\Psi} / \text{s}^{-1}$
1	8.92×10^{-5}	0	5.00×10^6 ^a
2	8.92×10^{-5}	7.03×10^{-3}	5.63×10^6
3	8.92×10^{-5}	3.41×10^{-2}	6.25×10^6
4	8.92×10^{-5}	4.40×10^{-2}	6.12×10^6
5	8.92×10^{-5}	7.48×10^{-2}	7.06×10^6
6	8.92×10^{-5}	1.24×10^{-1}	7.38×10^6
7	8.92×10^{-5}	1.81×10^{-1}	7.64×10^6
8	8.92×10^{-5}	2.53×10^{-1}	8.91×10^6

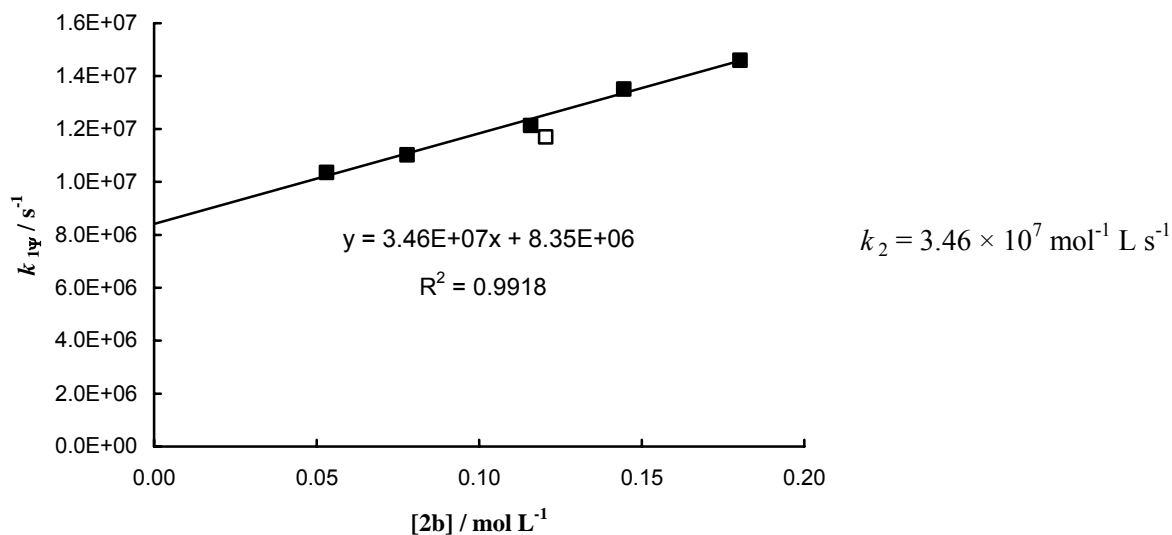
^a) Not used for calculation of k_2 .



Pseudo-first order rate constants for the reactions of the cumyl cation (1^+) with (2,2-dimethyl-1-methylene-propoxy)-trimethylsilane (**2b**) in CH_2Cl_2 (laser flash photolysis, 20 °C)

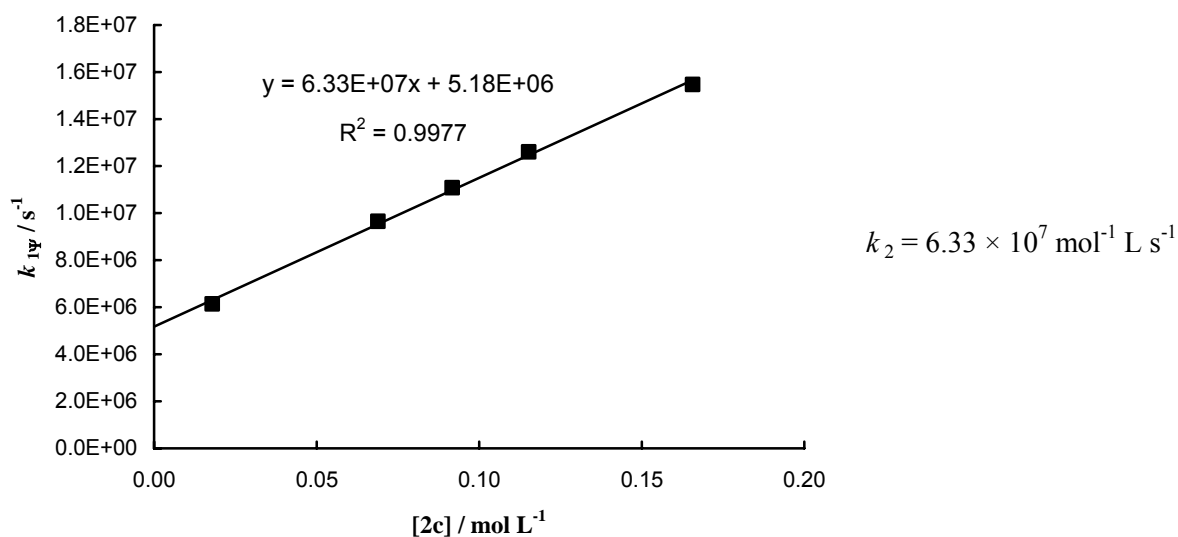
no.	$[1c]_0 / \text{mol L}^{-1}$	$[2b]_0 / \text{mol L}^{-1}$	$k_{1\Psi} / \text{s}^{-1}$
1	9.15×10^{-5}	5.31×10^{-2}	1.03×10^7
2	9.15×10^{-5}	7.78×10^{-2}	1.10×10^7
3	9.15×10^{-5}	1.16×10^{-1}	1.21×10^7
4	9.15×10^{-5}	1.21×10^{-1}	1.17×10^7 ^a
5	9.15×10^{-5}	1.45×10^{-1}	1.35×10^7
6	9.15×10^{-5}	1.80×10^{-1}	1.46×10^7

^a) Not used for calculation of k_2 .



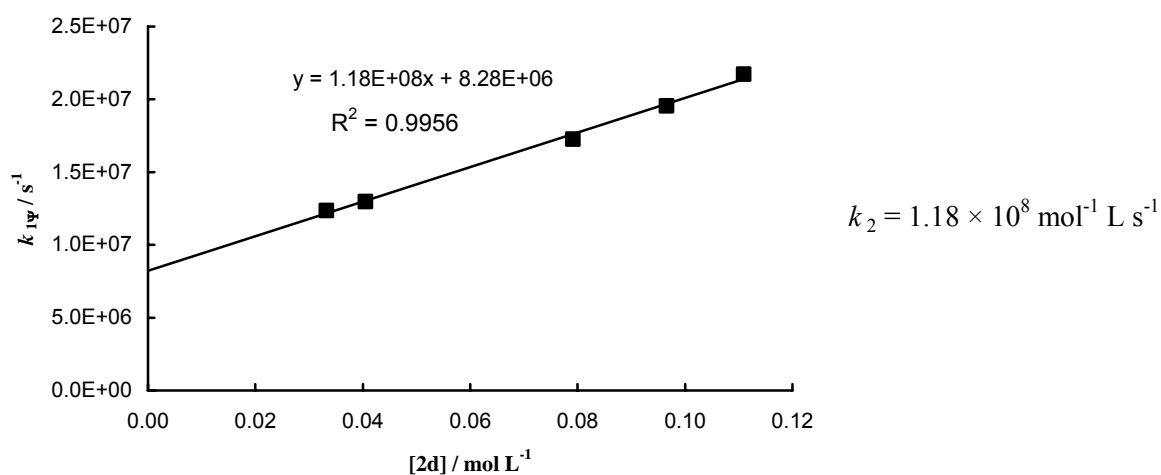
Pseudo-first order rate constants for the reactions of the cumyl cation (1^+) with 1-methylcyclopentene (2c) in CH_2Cl_2 (laser flash photolysis, 20°C)

no.	$[1c]_0 / \text{mol L}^{-1}$	$[2c]_0 / \text{mol L}^{-1}$	$k_{1\Psi} / s^{-1}$
1	8.92×10^{-5}	1.79×10^{-2}	6.13×10^6
2	8.92×10^{-5}	6.89×10^{-2}	9.65×10^6
3	8.92×10^{-5}	9.17×10^{-2}	1.11×10^7
4	8.92×10^{-5}	1.15×10^{-1}	1.26×10^7
5	8.92×10^{-5}	1.66×10^{-1}	1.55×10^7



Pseudo-first order rate constants for the reactions of the cumyl cation (1^+) with *n*-butyl vinyl ether (**2d**) in CH_2Cl_2 (laser flash photolysis, 20 °C)

no.	$[1c]_0 / \text{mol L}^{-1}$	$[2d]_0 / \text{mol L}^{-1}$	$k_{1\Psi} / \text{s}^{-1}$
1	8.94×10^{-5}	3.32×10^{-2}	1.24×10^7
2	8.94×10^{-5}	4.05×10^{-2}	1.30×10^7
3	8.94×10^{-5}	7.91×10^{-2}	1.73×10^7
4	8.94×10^{-5}	9.66×10^{-2}	1.95×10^7
5	8.94×10^{-5}	1.11×10^{-1}	2.17×10^7



Generation of α,β -Unsaturated Iminium Ions by Laser Flash Photolysis

Sami Lakhdar, Johannes Ammer and Herbert Mayr

Angew. Chem. **2011**, *123*, 10127-10130; *Angew. Chem. Int. Ed.* **2011**, *50*, 9953-9956

7.1 Introduction

Iminium activation has become one of the most important methods in enantioselective synthesis.^[1] For the optimization and the rational design of organocatalytic cycles, knowledge of the mechanism of these reactions is crucial.^[2] In previous work, we have shown that the rate constants for the reactions of unsaturated iminium ions with ketene acetals,^[2d] sulfur ylides,^[3] and pyrroles^[4] can be determined by UV/vis spectroscopy employing conventional spectrometers or stopped-flow equipment. Both methods require the mixing of the reactants, and therefore are not applicable to reactions that proceed on the sub-millisecond time scale.

We now report on the in situ laser-flash-photolytic generation of iminium ions derived from cinnamaldehyde and imidazolidinones, which allowed us to measure rate constants for the reactions of iminium ions with strong nucleophiles. This method along with previously reported kinetic procedures have been employed to directly compare the electrophilic reactivities of iminium ions derived from different imidazolidinones.

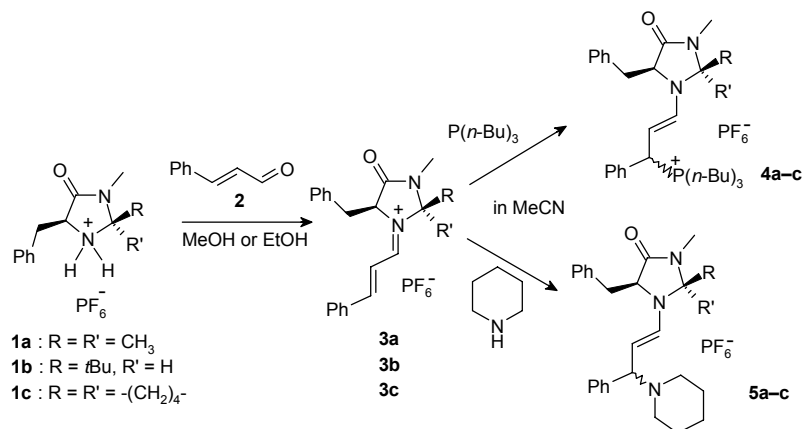
7.2 Results and Discussion

Treatment of the imidazolidinonium salts **1a-c** with cinnamaldehyde (**2**) in methanol or ethanol following literature procedures^[5,6] gave precipitates of the iminium salts **3a-c** (Scheme 7.1), which were previously analyzed by X-ray crystallography.^[5a,6c] When these crystals were dissolved in acetonitrile, only the *E* isomers of **3a-c** were observed by NMR spectroscopy.^[7]

Combination of the iminium salts **3a-c** with one equivalent of tributylphosphine gave the (*E*)-enaminophosphonium salts **4a-c** as mixtures of two diastereoisomers (2:1 for **4a** and **4c**

and 1:1 for **4b**; Scheme 7.1). Selective formation of the (*E*)-enamines **5a-c** (1:1 ratio of two diastereoisomers) was observed when solutions of **3a-c** in acetonitrile were treated with excess piperidine (Scheme 7.1).^[8]

Scheme 7.1.



As organocatalytic processes involving **3a-c** are often highly enantioselective,^[9] we have to conclude that the low stereoselectivities of the stoichiometric reactions with PBu_3 and piperidine in Scheme 7.1 are due to reversible reactions under the conditions employed.

Tri-*n*-butylphosphine has previously been reported to be an effective photo-leaving group for the laser-flash-photolytic generation of stabilized carbocations.^[10] Irradiation of acetonitrile solutions of the phosphonium salts **4a-c** with 7 ns laser pulses from the fourth harmonic of a Nd/YAG laser (266 nm, 30-60 mJ/pulse) yielded the iminium ions **3a-c** which showed the same UV/vis absorption maxima λ_{max} as solutions of the isolated iminium salts in acetonitrile (Figure 7.1a).

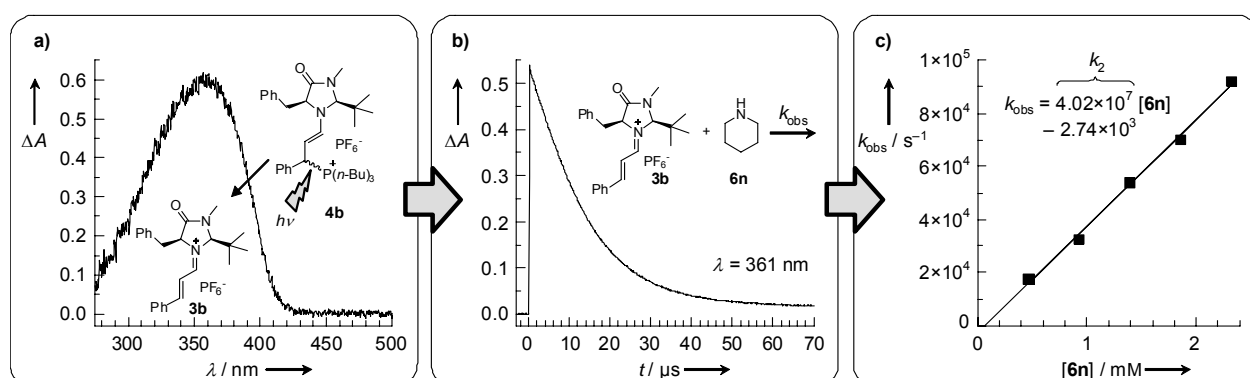


Figure 7.1. (a) UV/vis spectrum of **3b** immediately after the laser pulse in CH₃CN. (b) Decay of the absorbance of **3b** obtained after irradiation of a 1.51×10^{-4} M solution of **4b** in CH₃CN in the presence of piperidine (**6n**; 1.86×10^{-3} M). (c) Plot of the pseudo-first-order rate constants k_{obs} (s^{-1}) versus the concentration of piperidine.

When salts **3a-c** were generated in the presence of a large excess of the nucleophiles **6j** or **6l-o**, we observed monoexponential decays of their absorbances, from which the rate constants k_{obs} (s^{-1}) were obtained (Figure 7.1b). Plots of k_{obs} versus the nucleophile concentrations were linear (Figure 7.1c) and provided the second-order rate constants k_2 ($\text{M}^{-1} \text{s}^{-1}$) which are listed in Table 7.1.

Table 7.1. Second-order rate constants (k_2) for the reactions of the iminium ions **3a-c** with the nucleophiles **6a-o** (20 °C, MeCN).

Nucleophile		$N^{[a]}$	$s_N^{[a]}$	k_2 (3a) [$\text{M}^{-1} \text{s}^{-1}$]	k_2 (3b) [$\text{M}^{-1} \text{s}^{-1}$]	k_2 (3c) [$\text{M}^{-1} \text{s}^{-1}$]
pyrrole	6a	4.63	1.00	6.8×10^{-4} ^[b]	–	–
<i>N</i> -methylpyrrole	6b	5.85	1.03	7.2×10^{-3} ^[b]	–	–
1-(trimethylsiloxy)pentene	6c	6.57	0.93	–	5.18×10^{-1}	4.28×10^{-2}
2,5-dimethylpyrrole	6d	8.01	0.96	3.6 ^[b]	1.34×10^3 ^[c]	–
1,2,5-trimethylpyrrole	6e	8.69	1.07	5.3 ^[b]	–	–
2-(trimethylsiloxy)-5,6-dihydro-4 <i>H</i> -pyran	6f	10.61	0.86	5.23×10^2 ^[d]	–	–
2,4-dimethylpyrrole	6g	10.67	0.91	3.5×10^3 ^[b]	6.87×10^4 ^[c]	–
kryptopyrrole	6h	11.63	0.95	1.3×10^4 ^[b]	1.33×10^5 ^[c]	5.20×10^3 ^[c]
2-(trimethylsiloxy)-4,5-dihydrofuran	6i	12.56	0.70	1.14×10^4 ^[b,e]	1.12×10^5	–
$\text{H}_2\text{NCH}_2\text{CH}_2\text{OH}$	6j	14.11	0.71	7.56×10^5	5.27×10^7	–
$\text{P}(\text{Ph})_3$	6k	14.33	0.65	2.40×10^5	9.91×10^5	1.53×10^4
1,8-diazabicyclo[5.4.0]-undec-7-ene (DBU)	6l	15.29	0.70	6.81×10^5	7.54×10^7	–
$\text{P}(n\text{-Bu})_3$	6m	15.49	0.69	3.69×10^5	1.96×10^7	2.86×10^5
piperidine	6n	17.35	0.68	1.86×10^7	4.02×10^7	1.51×10^7
1,4-diazabicyclo[2.2.2]-octane (DABCO)	6o	18.80	0.70	4.95×10^8	5.88×10^8	4.86×10^8

^[a] See reference [11] for the origin of the nucleophilicity parameters N and s_N determined in MeCN or CH_2Cl_2 .

^[b] From reference [4]. ^[c] These rate constants were derived in the presence of potassium trifluoroacetate (as base) from plots of $1/k_{\text{obs}}$ versus $1/[\text{base}]$ as described in reference [4] because the initial C–C bond-forming step is reversible. ^[d] Second-order rate constant k_2 for the reaction of **3a**-OTf with **6f** in CH_2Cl_2 , from reference [2d].

^[e] In CH_2Cl_2 .

In order to provide a broader experimental basis for the comparison of the electrophilicities of iminium ions derived from different imidazolidinones we have also determined rate constants of the reactions of **3a**, **3b**, and **3c** with weaker nucleophiles using conventional UV spectrometers and stopped-flow techniques. The rate of the reaction of **3a** with DBU (**6l**) has been determined in two ways, with laser-flash-photolytically generated iminium ions as well as with solutions of isolated iminium salts, and the values differed by less than 6%. This agreement is remarkable in view of Seebach's hypothesis that (*E*)-iminium ions are more reactive than their *Z* isomers.^[6e] As we do not know the configuration of the photolytically generated iminium ions, the monoexponential decays of the photolytically generated iminium ions and the identical reactivities of the iminium ions generated in different ways either imply that only the *E* isomers are formed by the photolytic process or that the *E* and *Z* isomers have the same reactivities.

In previous work, we have shown that the reactions of carbocations and Michael acceptors with σ , *n*, and π nucleophiles follow Equation (1), in which electrophiles are described by *E* (electrophilicity parameter) and nucleophiles are described by *N* (nucleophilicity parameter) and s_N (nucleophile-specific sensitivity parameter).^[12]

$$\log k_2(20\text{ }^\circ\text{C}) = s_N(N + E) \quad (1)$$

In this way, we were able to set up comprehensive electrophilicity and nucleophilicity scales, covering more than 30 orders of magnitude.^[13] These scales have found wide application for the design of polar organic reactions, in particular in organocatalysis.^[14]

Figure 7.2, in which $(\lg k_2)/s_N$ is plotted versus the nucleophilicity parameter *N*, demonstrates not only that the rate constants obtained with different kinetic methods are consistent, but also that the *N* and s_N parameters of nucleophiles,^[11,12] which were derived from their reactions with benzhydrylium ions such as **7**, are suitable for predicting the rates of the reactions of these nucleophiles with the iminium ions **3**. Therefore, the electrophilicity parameters *E* of **3a-c** were determined by a least-squares fit, that is, by minimization of $\Delta^2 = \Sigma[\lg k_2 - s_N(N + E)]^2$, using k_2 , *N*, and s_N from Table 7.1.

Apart from the rate constants for DABCO (**6o**) which are close to the diffusion limit, only the second-order rate constants for the reactions of ethanolamine (**6j**) were excluded from these correlations. For unknown reasons, the observed rate constants for the reactions of **6j** with **3a** and **3b** are 11 and 44 times larger, respectively, than the values calculated by Equation (1). As

these deviations are still within the confidence interval of Equation (1), we will not speculate about their origin.

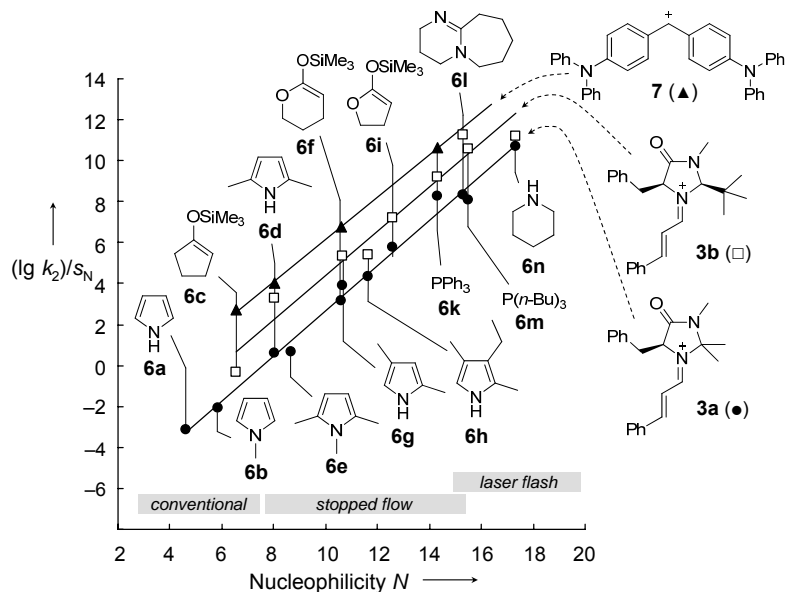


Figure 7.2. Correlation of $(\lg k_2)/s_N$ against the nucleophilicity parameters N of the nucleophiles **6a-n** for their reactions with the iminium ions **3a** and **3b** and the benzhydrylium ion **7** (correlation for **3c** is omitted for the sake of clarity; it is shown in section 7.S.3).

The electrophilicity parameters of the α,β -unsaturated iminium ions **3a-c** in Table 7.2 show that **3b** is about 10^2 times more reactive than **3a** and **3c**, which have quite similar electrophilicities. This finding is in line with Larsen's observation that **1b**- CF_3CO_2^- is a more active catalyst in Diels-Alder reactions of cinnamaldehyde than **1a**- CF_3CO_2^- , despite the fact that the equilibrium concentration of the iminium salt **3b**- CF_3CO_2^- is only half of that of **3a**- CF_3CO_2^- .^[15,16] The greater scope of reactions accessible with MacMillan's second-generation catalyst **1b**^[17] can now be unambiguously attributed to the significantly higher electrophilicity of the iminium ion **3b**.

Table 7.2. Electrophilicity parameters E of **3a-c**.

Electrophile	3a	3b	3c
$E^{[a]}$	-7.37	-5.52	-7.67

^[a] Determined from data in Table 7.1 by minimization of $\Delta^2 = \Sigma[\lg k_2 - s_N(N + E)]^2$.

What is the origin of the high electrophilicity of **3b**? Seebach's structural studies of iminium ions by X-ray analysis, NMR spectroscopy, and DFT calculations have shown that the

benzylic phenyl group of **3a** resides preferentially over the heterocyclic ring, while in the case of **3b** benzyl is sitting above the iminium π system and blocking the approach of nucleophiles from the *Re* face. An X-ray crystal structure of **3c**^[6g] shows that its conformation resembles that of **3a**. While the preferred *Si* approach to **3a** and **3c** is slowed down by the steric shielding of a methyl group and the cyclopentane ring, respectively, the reactive *Si* face of **3b** is free from any steric hindrance and, therefore, exhibits higher electrophilicity.

7.3 Conclusion

In conclusion, we have shown that the laser-flash-photolytic generation of iminium ions has allowed us to extend our kinetic investigations over the whole conceivable reactivity range, from the slowest to diffusion-controlled bimolecular reactions. We have also determined the first quantitative data on the extraordinarily high electrophilicities of iminium ions derived from MacMillan's second-generation catalyst **1b** and finally demonstrated the applicability of the benzhydrylium-derived nucleophilicity parameters *N* and s_N for analyzing scope and limitations of iminium-activated reactions.

7.4 Acknowledgment

We thank the Alexander von Humboldt Foundation (research fellowship for S.L.) and the Deutsche Forschungsgemeinschaft (Ma 673/21-3) for support of this work, Dr. P. Mayer for the X-ray structure determination, Prof. S. Kobayashi for installing the laser flash photolysis working station, and Dr. A. R. Ofial and Prof. D. Seebach for helpful comments.

7.5 References and Notes

- [1] a) P. I. Dalko, L. Moisan, *Angew. Chem.* **2004**, *116*, 5248 – 5286; *Angew. Chem. Int. Ed.* **2004**, *43*, 5138 – 5175; b) A. Berkessel, H. Gröger, *Asymmetric Organocatalysis*, Wiley-VCH, Weinheim, 2004; c) A. M. Walji, D.W. C. MacMillan, *Synlett* **2007**, 1477

- 1489; d) D. W. C. MacMillan, *Nature* **2008**, *455*, 304 – 308; e) A. Dondoni, A. Massi, *Angew. Chem.* **2008**, *120*, 4716 – 4739; *Angew. Chem. Int. Ed.* **2008**, *47*, 4638 – 4660; f) P. Melchiorre, M. Marigo, A. Carlone, G. Bartoli, *Angew. Chem.* **2008**, *120*, 6232 – 6265; *Angew. Chem. Int. Ed.* **2008**, *47*, 6138 – 6171; g) S. Bertelsen, K. A. Jørgensen, *Chem. Soc. Rev.* **2009**, *38*, 2178 – 2189; h) M. Nielsen, D. Worgull, T. Zweifel, B. Gschwend, S. Bertelsen, K. A. Jørgensen, *Chem. Commun.* **2011**, *47*, 632 – 649.
- [2] a) R. Gordillo, K. N. Houk, *J. Am. Chem. Soc.* **2006**, *128*, 3543 – 3553; b) P. Dinér, M. Nielsen, M. Marigo, K. A. Jørgensen, *Angew. Chem.* **2007**, *119*, 2029 – 2033; *Angew. Chem. Int. Ed.* **2007**, *46*, 1983 – 1987; c) G. Evans, T. J. K. Gibbs, R. L. Jenkins, S. J. Coles, M. B. Hursthouse, J. A. Platts, N. C. O. Tomkinson, *Angew. Chem.* **2008**, *120*, 2862 – 2865; *Angew. Chem. Int. Ed.* **2008**, *47*, 2820 – 2823; d) S. Lakhdar, T. Tokuyasu, H. Mayr, *Angew. Chem.* **2008**, *120*, 8851 – 8854; *Angew. Chem. Int. Ed.* **2008**, *47*, 8723 – 8726; e) S. Lakhdar, A. R. Ofial, H. Mayr, *J. Phys. Org. Chem.* **2010**, *23*, 886 – 892.
- [3] S. Lakhdar, R. Appel, H. Mayr, *Angew. Chem.* **2009**, *121*, 5134 – 5137; *Angew. Chem. Int. Ed.* **2009**, *48*, 5034 – 5037.
- [4] S. Lakhdar, H. Mayr, *Chem. Commun.* **2011**, *47*, 1866 – 1868.
- [5] a) J. B. Brazier, G. Evans, T. J. K. Gibbs, S. J. Coles, M. B. Hursthouse, J. A. Platts, N. C. O. Tomkinson, *Org. Lett.* **2009**, *11*, 133 – 136; b) J. B. Brazier, K. M. Jones, J. A. Platts, N. C. O. Tomkinson, *Angew. Chem.* **2011**, *123*, 1651 – 1654; *Angew. Chem. Int. Ed.* **2011**, *50*, 1613 – 1616.
- [6] For comprehensive studies on the isolation and X-ray structures of iminium salts derived from imidazolidinones see: a) D. Seebach, U. Grošelj, D. M. Badine, W. B. Schweizer, A. K. Beck, *Helv. Chim. Acta* **2008**, *91*, 1999 – 2034; b) U. Grošelj, D. Seebach, D. M. Badine, W. B. Schweizer, A. K. Beck, I. Krossing, P. Klose, Y. Hayashi, T. Uchimaru, *Helv. Chim. Acta* **2009**, *92*, 1225 – 1259; c) U. Grošelj, W. B. Schweizer, M.-O. Ebert, D. Seebach, *Helv. Chim. Acta* **2009**, *92*, 1 – 13; d) D. Seebach, U. Grošelj, W. B. Schweizer, S. Grimme, C. Mück-Lichtenfeld, *Helv. Chim. Acta* **2010**, *93*, 1 – 16; e) D. Seebach, R. Gilmour, U. Grošelj, G. Deniau, C. Sparr, M.-O. Ebert, A. K. Beck, L. B. McCusker, D. Šišak, T. Uchimaru, *Helv. Chim. Acta* **2010**, *93*, 603 – 634; f) C. Sparr, R. Gilmour, *Angew. Chem.* **2010**, *122*, 6670 – 6673; *Angew. Chem. Int. Ed.* **2010**, *49*, 6520 – 6523; g) for the X-ray structure of **3c** see: page S5 of the Supporting Information of *Angew. Chem. Int. Ed.* **2011**, *50*, 9953-9956. CCDC 827498 (**3c**) contains the

supplementary crystallographic data for this paper. These data can be obtained free of charge from The Cambridge Crystallographic Data Centre via www.ccdc.cam.ac.uk/data_request/cif.

- [7] While the presence of *Z* isomers could not be detected in the solutions of **3b,c**, a small, nonintegrable peak at $\delta = 8.5$ ppm in the ^1H NMR spectrum of **3a** might be assigned to (*Z*)-**3a**. *E/Z* isomerization of **3b** as observed by Seebach et al. (Ref. [6e]) during the formation of **3b** from **1b** and **2** was not detected under our conditions.
- [8] For NMR characterization of chiral enamines see: a) T. J. Peelen, Y. Chi, S. H. Gellman, *J. Am. Chem. Soc.* **2005**, *127*, 11598 – 11599; b) M. B. Schmid, K. Zeitler, R. M. Gschwind, *Angew. Chem.* **2010**, *122*, 5117 – 5123; *Angew. Chem. Int. Ed.* **2010**, *49*, 4997 – 5003; c) M. B. Schmid, K. Zeitler, R. M. Gschwind, *J. Org. Chem.* **2011**, *76*, 3005 – 3015; d) M. B. Schmid, K. Zeitler, R. M. Gschwind, *J. Am. Chem. Soc.* **2011**, *133*, 7065 – 7074; e) K. Patora-Komisarska, M. Benohoud, H. Ishikawa, D. Seebach, Y. Hayashi, *Helv. Chim. Acta* **2011**, *94*, 719 – 745.
- [9] a) K. A. Ahrendt, C. J. Borths, D. W. C. MacMillan, *J. Am. Chem. Soc.* **2000**, *122*, 4243 – 4244; b) N. A. Paras, D. W. C. MacMillan, *J. Am. Chem. Soc.* **2001**, *123*, 4370 – 4371; c) A. B. Northrup, D. W. C. MacMillan, *J. Am. Chem. Soc.* **2002**, *124*, 2458 – 2460; d) J. F. Austin, D. W. C. MacMillan, *J. Am. Chem. Soc.* **2002**, *124*, 1172 – 1173; e) N. A. Paras, D. W. C. MacMillan, *J. Am. Chem. Soc.* **2002**, *124*, 7894 – 7895; f) S. P. Brown, N. C. Goodwin, D. W. C. MacMillan, *J. Am. Chem. Soc.* **2003**, *125*, 1192 – 1194; g) S. G. Ouellet, J. B. Tuttle, D. W. C. MacMillan, *J. Am. Chem. Soc.* **2005**, *127*, 32 – 33; h) Y. K. Chen, M. Yoshida, D. W. C. MacMillan, *J. Am. Chem. Soc.* **2006**, *128*, 9328 – 9329; i) J. B. Tuttle, S. G. Ouellet, D. W. C. MacMillan, *J. Am. Chem. Soc.* **2006**, *128*, 12662 – 12663; j) G. Lelais, D. W. C. MacMillan, *Aldrichimica Acta* **2006**, *39*, 79 – 87.
- [10] For the photolysis of quaternary phosphonium salts see: a) E. O. Alonso, L. Johnston, J. C. Scaiano, V. G. Toscano, *J. Am. Chem. Soc.* **1990**, *112*, 1270 – 1271; b) E. O. Alonso, L. J. Johnston, J. C. Scaiano, V. G. Toscano, *Can. J. Chem.* **1992**, *70*, 1784 – 1794; c) C. Imrie, T. A. Modro, E. R. Rohwer, C. C. P. Wagener, *J. Org. Chem.* **1993**, *58*, 5643 – 5649; d) C. Imrie, T. A. Modro, C. C. P. Wagener, *J. Chem. Soc. Perkin Trans. 2* **1994**, 1379 – 1382; e) L. Shi, M. Horn, S. Kobayashi, H. Mayr, *Chem. Eur. J.* **2009**, *15*, 8533 – 8541; f) J. Ammer, H. Mayr, *Macromolecules* **2010**, *43*, 1719 – 1723 (CHAPTER 6 of this work); For the generation of benzhydryl cations from

- tri-*n*-butylphosphonium tetrafluoroborates see: g) T. Kanzian, S. Lakhdar, H. Mayr, *Angew. Chem.* **2010**, *122*, 9717 – 9720; *Angew. Chem. Int. Ed.* **2010**, *49*, 9526 – 9529; h) N. Streidl, R. Branzan, H. Mayr, *Eur. J. Org. Chem.* **2010**, 4205 – 4210; i) M. Baidya, S. Kobayashi, H. Mayr, *J. Am. Chem. Soc.* **2010**, *132*, 4796 – 4805.
- [11] Nucleophilicity parameters N and s_N a) for **6d**, **6e**, **6g**, and **6h**: T. A. Nigst, M. Westermaier, A. R. Ofial, H. Mayr, *Eur. J. Org. Chem.* **2008**, 2369 – 2374; b) for **6a-c**, **6f**, and **6i**: H. Mayr, T. Bug, M. F. Gotta, N. Hering, B. Irrgang, B. Janker, B. Kempf, R. Loos, A. R. Ofial, G. Remennikov, H. Schimmel, *J. Am. Chem. Soc.* **2001**, *123*, 9500 – 9512; c) for **6j** and **6n**: T. Kanzian, T. A. Nigst, A. Maier, S. Pichl, H. Mayr, *Eur. J. Org. Chem.* **2009**, 6379 – 6385; d) for **6k** and **6m**: B. Kempf, H. Mayr, *Chem. Eur. J.* **2005**, *11*, 917 – 927; e) for **6l**: M. Baidya, H. Mayr, *Chem. Commun.* **2008**, 1792 – 1794; f) for **6o**: M. Baidya, S. Kobayashi, F. Brotzel, U. Schmidhammer, E. Riedle, H. Mayr, *Angew. Chem.* **2007**, *119*, 6288 – 6292; *Angew. Chem. Int. Ed.* **2007**, *46*, 6176 – 6179.
- [12] a) H. Mayr, M. Patz, *Angew. Chem.* **1994**, *106*, 990 – 1010; *Angew. Chem. Int. Ed. Engl.* **1994**, *33*, 938 – 957; b) H. Mayr, B. Kempf, A. R. Ofial, *Acc. Chem. Res.* **2003**, *36*, 66 – 77; c) H. Mayr, A. R. Ofial, *Pure Appl. Chem.* **2005**, *77*, 1807 – 1821; d) H. Mayr, A. R. Ofial, *J. Phys. Org. Chem.* **2008**, *21*, 584 – 595.
- [13] For a comprehensive database of nucleophilicity and electrophilicity parameters, see: <http://www.cup.lmu.de/oc/mayr/DBintro.html>.
- [14] For selected examples on the use of Equation (1) in organocatalysis see: a) P. G. Cozzi, F. Benfatti and L. Zoli, *Angew. Chem.* **2009**, *121*, 1339 – 1342; *Angew. Chem. Int. Ed.* **2009**, *48*, 1313 – 1316; b) F. Benfatti, E. Benedetto, P. G. Cozzi, *Chem. Asian J.* **2010**, *5*, 2047 – 2052; c) M. G. Capdevila, F. Benfatti, L. Zoli, M. Stenta, P. G. Cozzi, *Chem. Eur. J.* **2010**, *16*, 11237 – 11241; d) L. Zhang, L. Cui, X. Li, J. Li, S. Luo, J.-P. Cheng, *Chem. Eur. J.* **2010**, *16*, 2045 – 2049; e) A. R. Brown, W.-H. Kuo, E. N. Jacobsen, *J. Am. Chem. Soc.* **2010**, *132*, 9286 – 9288; f) G. Bergonzini, S. Vera, P. Melchiorre, *Angew. Chem.* **2010**, *122*, 9879 – 9882; *Angew. Chem. Int. Ed.* **2010**, *49*, 9685 – 9688.
- [15] C. H.-M. Larsen, PhD Thesis, California Institute of Technology, 2005, pp. 41 – 42. We thank Professor D. W. C. MacMillan for bringing this work to our attention.
- [16] A quantitative comparison of the overall rates of imidazolidinone and diarylprolinol ether catalyzed reactions has recently been published: J. B. Brazier, G. P. Hopkins, M.

Jirari, S. Mutter, R. Pommereuil, L. Samulis, J. A. Platts, N. C. O. Tomkinson, *Tetrahedron Lett.* **2011**, 52, 2783 – 2785.

[17] (2*S*,5*S*)-5-Benzyl-2-*tert*-butyl-3-methyl-imidazolidin-4-one (**1b**) was first described in: R. Naef, D. Seebach, *Helv. Chim. Acta* **1985**, 68, 135 – 143.

7.S Supplementary Data and Experimental Section

7.S.1 Laser flash photolytic generation of iminium ions

Solutions of the precursor phosphonium salts with $A_{266\text{ nm}} \approx 0.5\text{-}1.0$ (ca. 1×10^{-4} M) were irradiated with a 7 ns pulse (266 nm, 30-60 mJ/pulse) from a quadrupled Nd/YAG laser using a xenon short-arc lamp as probe light. The system is equipped with a fluorescence flow cell and a dosage pump which allows to replace the sample volume completely between subsequent laser pulses.

Transient UV/vis spectra were recorded as difference spectra of subsequent determinations with and without laser irradiation using an ICCD camera with 10 ns gate width, and eight such spectra were averaged. The obtained transient spectra of the iminium ions **3a**, **3b**, and **3c** shown in Fig. S1 closely resemble the UV/Vis spectra of the isolated iminium salts.

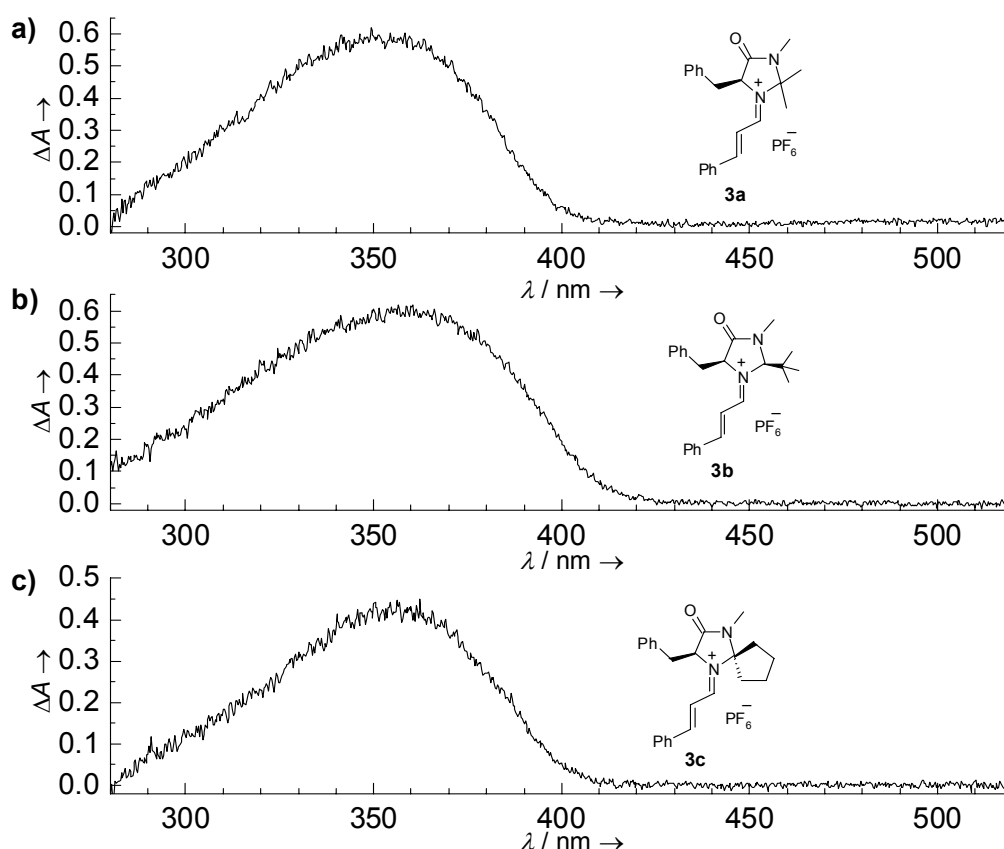


Figure 7.S.1. Transient UV/Vis spectra of photolytically generated iminium ions in CH₃CN. (a) **3a** obtained by irradiation of a 1.00×10^{-4} M solution of **4a**; (b) **3b** obtained by irradiation of a 1.51×10^{-4} M solution of **4b**; (c) **3c** obtained by irradiation of a 6.22×10^{-5} M solution of **4c**.

When the iminium ions **3a**, **3b**, and **3c** were generated in presence of a large excess of nucleophiles, we observed exponential decays of the UV/Vis absorbances of the iminium ions at their absorption maxima. Typically, 64 or more individual decay curves were averaged for noise reduction.

7.S.2 Kinetics of the reactions of iminium ions with nucleophiles

The rate constants k_{obs} (s^{-1}) which were obtained by least-squares fitting to the single exponential curve $A_t = A_0 e^{-k_{\text{obs}} t} + C$ depended linearly on the nucleophile concentration. The second-order rate constants k_2 ($\text{M}^{-1} \text{s}^{-1}$) for the combination reactions with nucleophiles were derived from the slopes of plots of k_{obs} for each nucleophile concentration versus the nucleophile concentrations.

Table 7.S.2.1. Rate constants for the reaction of **6j** with **3a** (precursor: **4a**) in acetonitrile (laser flash photolysis, 20 °C, $\lambda = 355$ nm).

[4a] (M)	[6j] (M)	k_{obs} (s^{-1})
1.00×10^{-4}	1.82×10^{-2}	8.17×10^3
1.00×10^{-4}	2.67×10^{-2}	1.32×10^4
1.00×10^{-4}	5.67×10^{-2}	3.51×10^4
1.00×10^{-4}	6.71×10^{-2}	4.41×10^4
1.00×10^{-4}	7.73×10^{-2}	5.30×10^4
$k_2 = 7.56 \times 10^5 \text{ M}^{-1} \text{ s}^{-1}$		

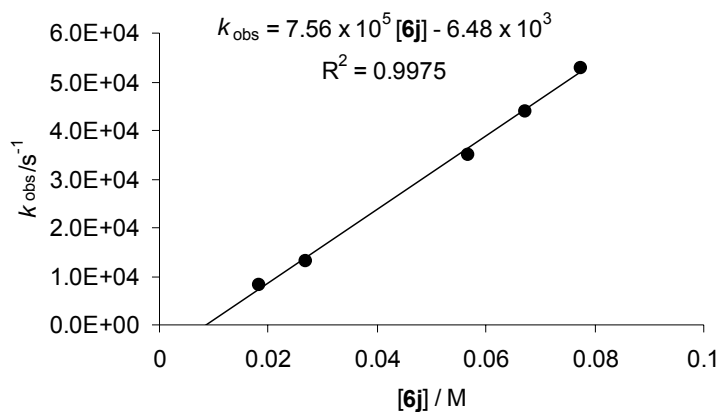
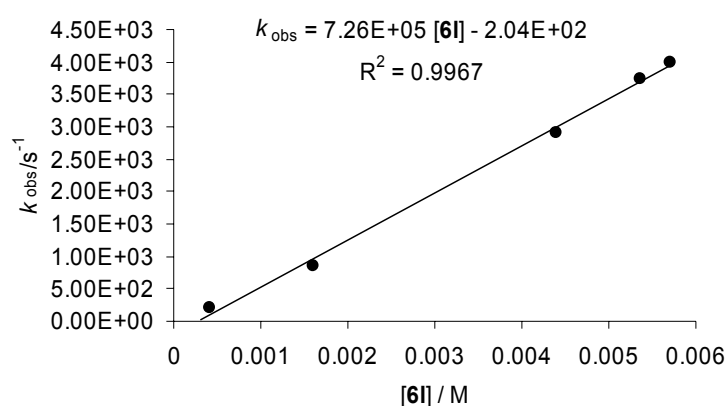
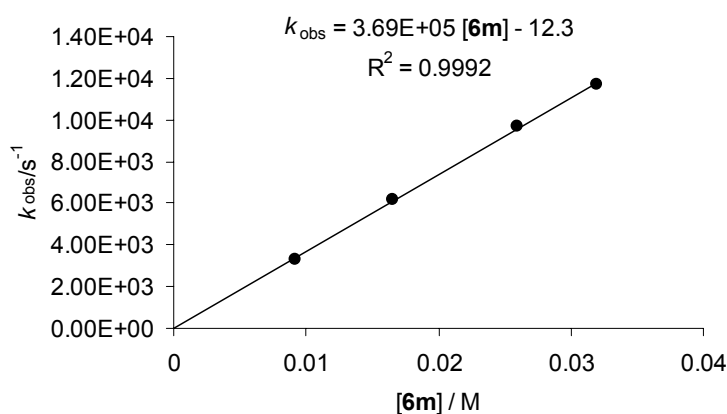


Table 7.S.2.2. Rate constants for the reaction of **6l** with **3a** (precursor: **4a**) in acetonitrile (laser flash photolysis, 20 °C, $\lambda = 355$ nm).

[4a] / M	[6l] / M	$k_{\text{obs}} / \text{s}^{-1}$
1.00×10^{-4}	4.20×10^{-4}	2.08×10^2
1.00×10^{-4}	1.61×10^{-3}	8.56×10^2
1.00×10^{-4}	4.40×10^{-3}	2.90×10^3
1.00×10^{-4}	5.37×10^{-3}	3.74×10^3
1.00×10^{-4}	5.71×10^{-3}	4.00×10^3
$k_2 = 7.26 \times 10^5 \text{ M}^{-1} \text{ s}^{-1}$		

**Table 7.S.2.3.** Rate constants for the reaction of **6m** with **3a** (precursor: **4a**) in acetonitrile (laser flash photolysis, 20 °C, $\lambda = 355$ nm).

[4a] / M	[6m] / M	$k_{\text{obs}} / \text{s}^{-1}$
1.00×10^{-4}	9.20×10^{-3}	3.31×10^3
1.00×10^{-4}	1.65×10^{-2}	6.14×10^3
1.00×10^{-4}	2.60×10^{-2}	9.66×10^3
1.00×10^{-4}	3.20×10^{-2}	1.17×10^4
$k_2 = 3.69 \times 10^5 \text{ M}^{-1} \text{ s}^{-1}$		

**Table 7.S.2.4.** Rate constants for the reaction of **6n** with **3a** (precursor: **4a**) in acetonitrile (laser flash photolysis, 20 °C, $\lambda = 355$ nm).

[4a] / M	[6n] / M	$k_{\text{obs}} / \text{s}^{-1}$
1.00×10^{-4}	9.28×10^{-4}	1.54×10^4
1.00×10^{-4}	1.86×10^{-3}	3.23×10^4
1.00×10^{-4}	2.78×10^{-3}	5.17×10^4
1.00×10^{-4}	3.71×10^{-3}	6.78×10^4
1.00×10^{-4}	4.64×10^{-3}	8.37×10^4
$k_2 = 1.86 \times 10^7 \text{ M}^{-1} \text{ s}^{-1}$		

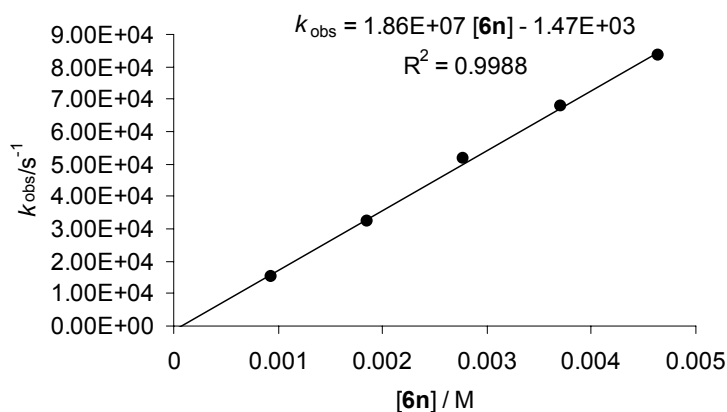
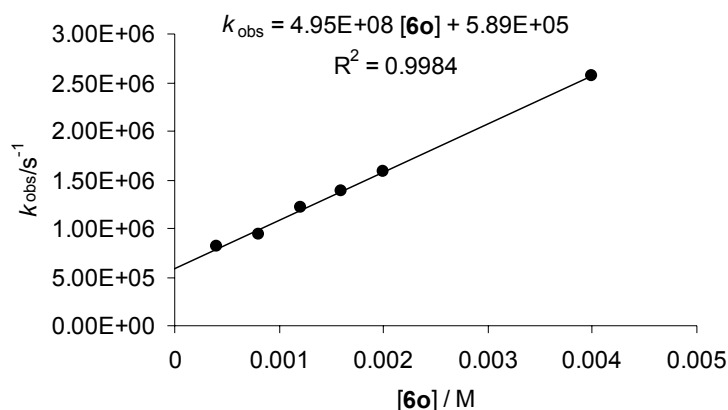


Table 7.S.2.5. Rate constants for the reaction of **6o** with **3a** (precursor: **4a**) in acetonitrile (laser flash photolysis, 20 °C, $\lambda = 355$ nm).

[4a] / M	[6o] / M	$k_{\text{obs}} / \text{s}^{-1}$
1.00×10^{-4}	4.00×10^{-4}	8.08×10^5
1.00×10^{-4}	8.00×10^{-4}	9.38×10^5
1.00×10^{-4}	1.20×10^{-3}	1.21×10^6
1.00×10^{-4}	1.60×10^{-3}	1.39×10^6
1.00×10^{-4}	2.00×10^{-3}	1.58×10^6
1.00×10^{-4}	4.00×10^{-3}	2.57×10^6
$k_2 = 4.95 \times 10^8 \text{ M}^{-1} \text{ s}^{-1}$		

**Table 7.S.2.6.** Rate constants for the reaction of **6j** with **3b** (precursor: **4b**) in acetonitrile (laser flash photolysis, 20 °C, $\lambda = 361$ nm).

[4b] / M	[6j] / M	$k_{\text{obs}} / \text{s}^{-1}$
1.22×10^{-4}	1.38×10^{-2}	6.27×10^5
1.22×10^{-4}	3.01×10^{-2}	1.51×10^6
1.22×10^{-4}	5.79×10^{-2}	3.11×10^6
1.22×10^{-4}	5.99×10^{-2}	3.06×10^6
1.22×10^{-4}	7.25×10^{-2}	3.76×10^6
1.22×10^{-4}	8.67×10^{-2}	4.44×10^6
$k_2 = 5.27 \times 10^7 \text{ M}^{-1} \text{ s}^{-1}$		

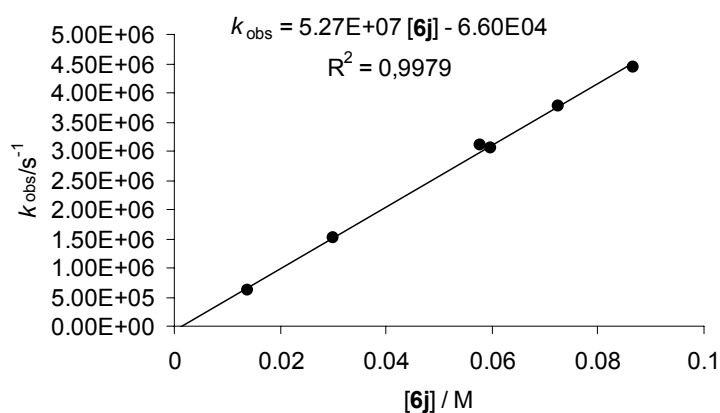
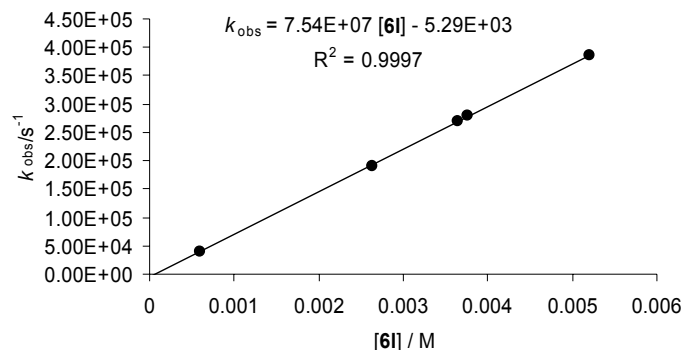
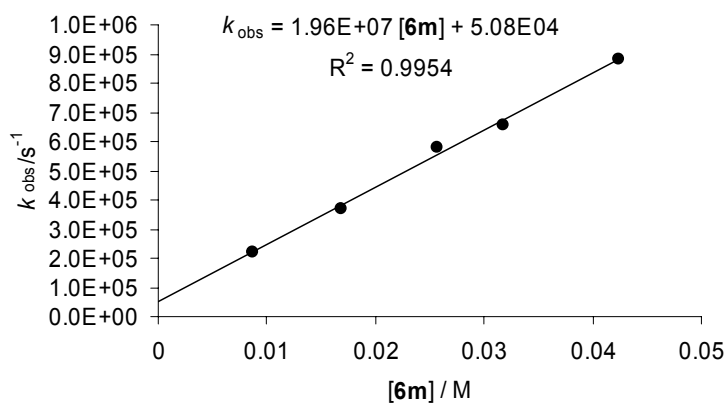


Table 7.S.2.7. Rate constants for the reaction of **6l** with **3b** (precursor: **4b**) in acetonitrile (laser flash photolysis, 20 °C, $\lambda = 361$ nm).

[4b] / M	[6l] / M	$k_{\text{obs}} / \text{s}^{-1}$
1.10×10^{-4}	5.91×10^{-4}	4.04×10^4
1.10×10^{-4}	2.64×10^{-3}	1.90×10^5
1.10×10^{-4}	3.65×10^{-3}	2.70×10^5
1.10×10^{-4}	3.76×10^{-3}	2.80×10^5
1.10×10^{-4}	5.20×10^{-3}	3.86×10^5
$k_2 = 7.54 \times 10^7 \text{ M}^{-1} \text{ s}^{-1}$		

**Table 7.S.2.8.** Rate constants for the reaction of **6m** with **3b** (precursor: **4b**) in acetonitrile (laser flash photolysis, 20 °C, $\lambda = 361$ nm).

[4b] / M	[6m] / M	$k_{\text{obs}} / \text{s}^{-1}$
1.22×10^{-4}	8.70×10^{-3}	2.23×10^5
1.22×10^{-4}	1.68×10^{-2}	3.68×10^5
1.22×10^{-4}	2.57×10^{-2}	5.80×10^5
1.22×10^{-4}	3.18×10^{-2}	6.55×10^5
1.22×10^{-4}	4.24×10^{-2}	8.83×10^5
$k_2 = 1.96 \times 10^7 \text{ M}^{-1} \text{ s}^{-1}$		

**Table 7.S.2.9.** Rate constants for the reaction of **6n** with **3b** (precursor: **4b**) in acetonitrile (laser flash photolysis, 20 °C, $\lambda = 361$ nm).

[4b] / M	[6n] / M	$k_{\text{obs}} / \text{s}^{-1}$
1.51×10^{-4}	4.64×10^{-4}	1.76×10^4
1.51×10^{-4}	9.28×10^{-4}	3.25×10^4
1.51×10^{-4}	1.39×10^{-3}	5.40×10^4
1.51×10^{-4}	1.86×10^{-3}	7.02×10^4
1.51×10^{-4}	2.32×10^{-3}	9.21×10^4
$k_2 = 4.02 \times 10^7 \text{ M}^{-1} \text{ s}^{-1}$		

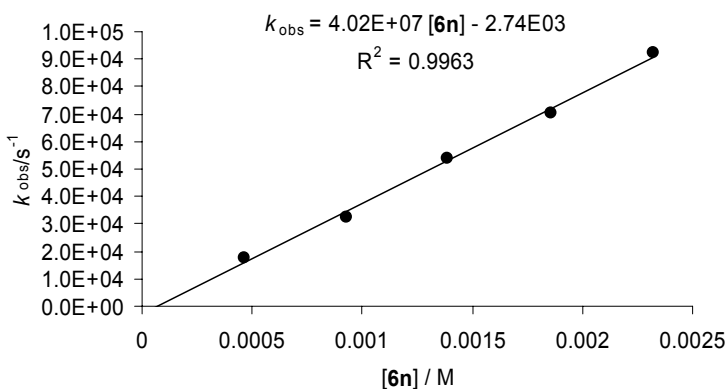
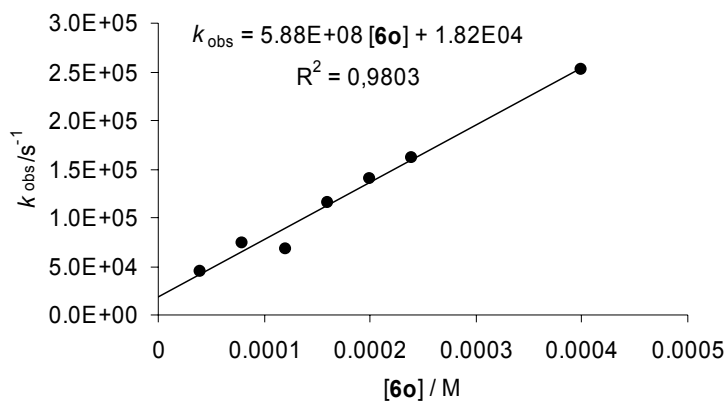


Table 7.S.2.10. Rate constants for the reaction of **6o** with **3b** (precursor: **4b**) in acetonitrile (laser flash photolysis, 20 °C, $\lambda = 361$ nm).

[4b] / M	[6o] / M	$k_{\text{obs}} / \text{s}^{-1}$
1.22×10^{-4}	4.00×10^{-5}	4.44×10^4
1.22×10^{-4}	8.00×10^{-5}	7.45×10^4
1.22×10^{-4}	1.20×10^{-4}	6.71×10^4
1.22×10^{-4}	1.60×10^{-4}	1.16×10^5
1.22×10^{-4}	2.00×10^{-4}	1.40×10^5
1.22×10^{-4}	2.40×10^{-4}	1.61×10^5
1.22×10^{-4}	4.00×10^{-4}	2.53×10^5
$k_2 = 5.88 \times 10^8 \text{ M}^{-1} \text{ s}^{-1}$		

**Table 7.S.2.11.** Rate constants for the reaction of **6m** with **3c** (precursor: **4c**) in acetonitrile (laser flash photolysis, 20 °C, $\lambda = 358$ nm).

[4c] / M	[6m] / M	$k_{\text{obs}} / \text{s}^{-1}$
6.22×10^{-5}	6.48×10^{-3}	1.28×10^3
6.22×10^{-5}	1.64×10^{-2}	3.91×10^3
6.22×10^{-5}	2.45×10^{-2}	6.50×10^3
6.22×10^{-5}	3.19×10^{-2}	8.54×10^3
6.22×10^{-5}	4.03×10^{-2}	1.08×10^4
$k_2 = 2.86 \times 10^5 \text{ M}^{-1} \text{ s}^{-1}$		

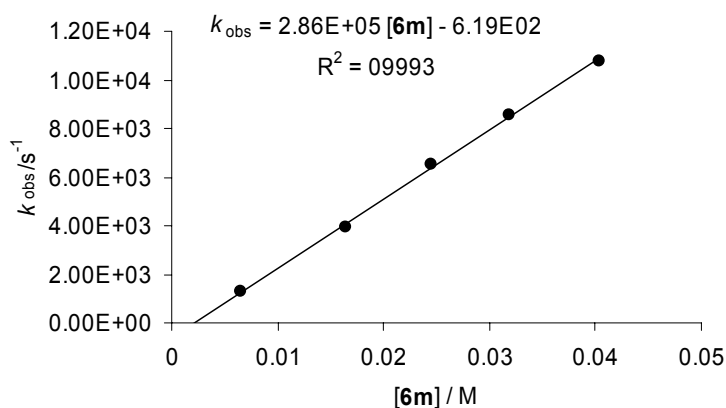
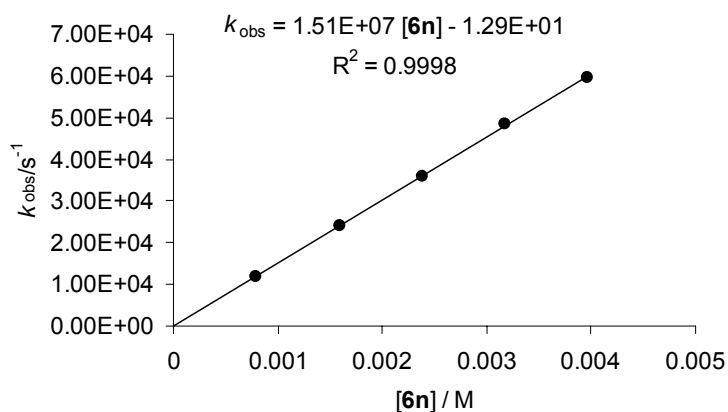
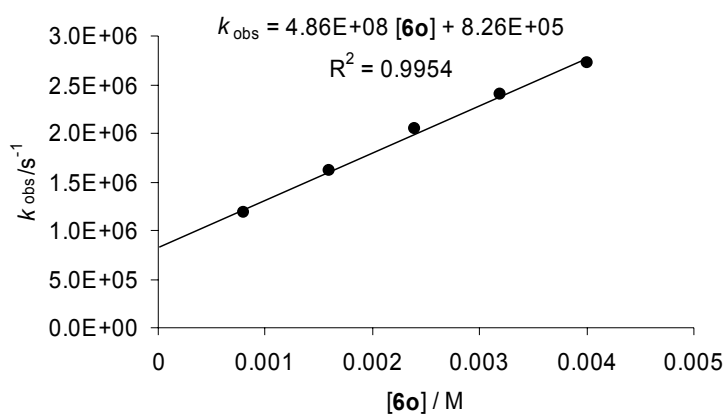


Table 7.S.2.12. Rate constants for the reaction of **6n** with **3c** (precursor: **4c**) in acetonitrile (laser flash photolysis, 20 °C, $\lambda = 358$ nm).

[4c] / M	[6n] / M	$k_{\text{obs}} / \text{s}^{-1}$
6.22×10^{-5}	7.92×10^{-4}	1.18×10^4
6.22×10^{-5}	1.59×10^{-3}	2.41×10^4
6.22×10^{-5}	2.38×10^{-3}	3.59×10^4
6.22×10^{-5}	3.17×10^{-3}	4.83×10^4
6.22×10^{-5}	3.96×10^{-3}	5.96×10^4
$k_2 = 1.51 \times 10^7 \text{ M}^{-1} \text{ s}^{-1}$		

**Table 7.S.2.13.** Rate constants for the reaction of **6o** with **3c** (precursor: **4c**) in acetonitrile (laser flash photolysis, 20 °C, $\lambda = 358$ nm).

[4c] / M	[6o] / M	$k_{\text{obs}} / \text{s}^{-1}$
6.22×10^{-5}	8.00×10^{-4}	1.18×10^6
6.22×10^{-5}	1.60×10^{-3}	1.61×10^6
6.22×10^{-5}	2.40×10^{-3}	2.05×10^6
6.22×10^{-5}	3.20×10^{-3}	2.40×10^6
6.22×10^{-5}	4.00×10^{-3}	2.72×10^6
$k_2 = 4.86 \times 10^8 \text{ M}^{-1} \text{ s}^{-1}$		



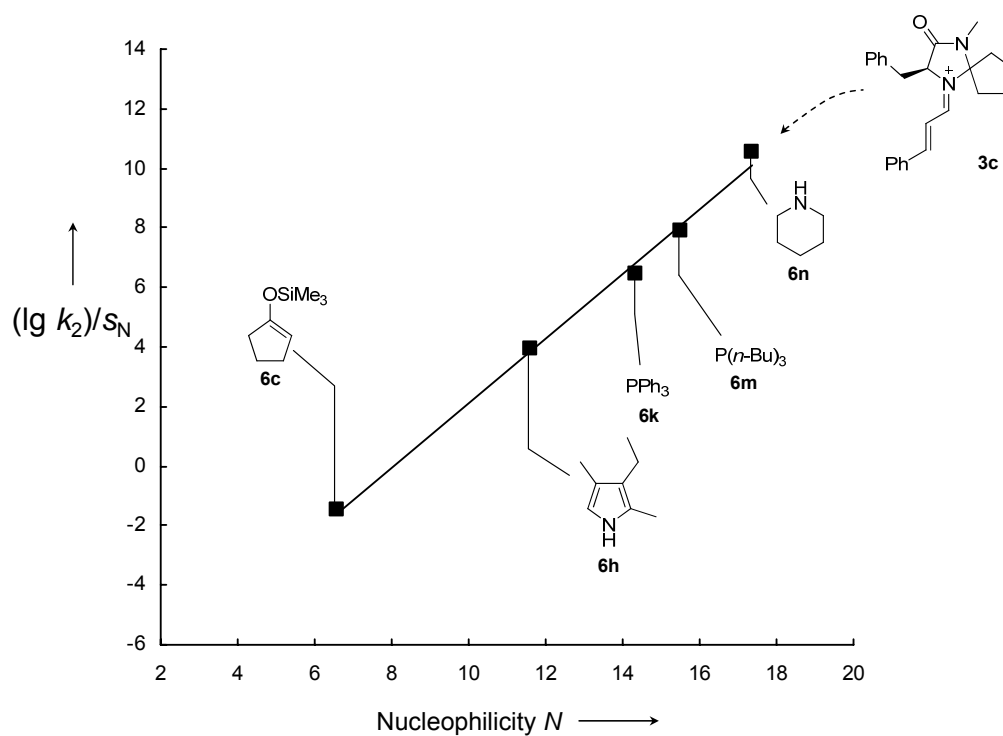
7.S.3 Plot of $(\lg k_2)/s_N$ versus N for the iminium ion **3c**

Figure 7.S.2. Correlation of $(\lg k_2)/s_N$ against the corresponding nucleophilicity parameters N of the nucleophiles **6c**, **6h**, **6k**, **6m** and **6n** for their reactions with the iminium ion **3c**.

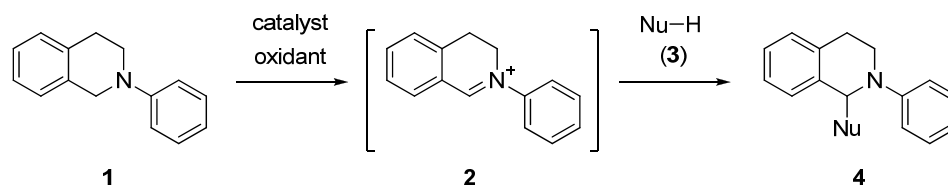
Electrophilic Reactivity of the 2-Phenyl-3,4-dihydroisoquinolinium Ion

Sami Lakhdar and Johannes Ammer
in collaboration with
Johannes Franz, Matthias Neumann and Kirsten Zeitler

8.1 Introduction

The oxidative coupling of tertiary amines with different nucleophiles presents an elegant method for the formation of C–C, C–N and C–P bonds.¹ A prominent example is the coupling of *N*-phenyl tetrahydroisoquinoline **1** with nucleophiles, which is believed to proceed via the intermediate iminium ion **2** (Scheme 8.1).^{1,2}

Scheme 8.1. Oxidative coupling of *N*-phenyl tetrahydroisoquinoline (**1**) with nucleophiles (**3**).



Recently, Klussmann and coworkers have investigated the mechanism of the copper-catalyzed oxidative coupling reactions of **1** with various nucleophiles.² When they employed $\text{CuCl}_2 \cdot 2 \text{H}_2\text{O}$ as catalyst and O_2 as oxidant (Scheme 8.2), they could directly observe the iminium ion **2** by NMR spectroscopy; the scope of nucleophiles for this coupling reaction was shown to be limited by the electrophilic reactivity of **2**.²

We have previously reported that reactions of σ -, n -, and π -nucleophiles with numerous carbon-centered electrophiles can be described by eq. 1,^{3-5,6}

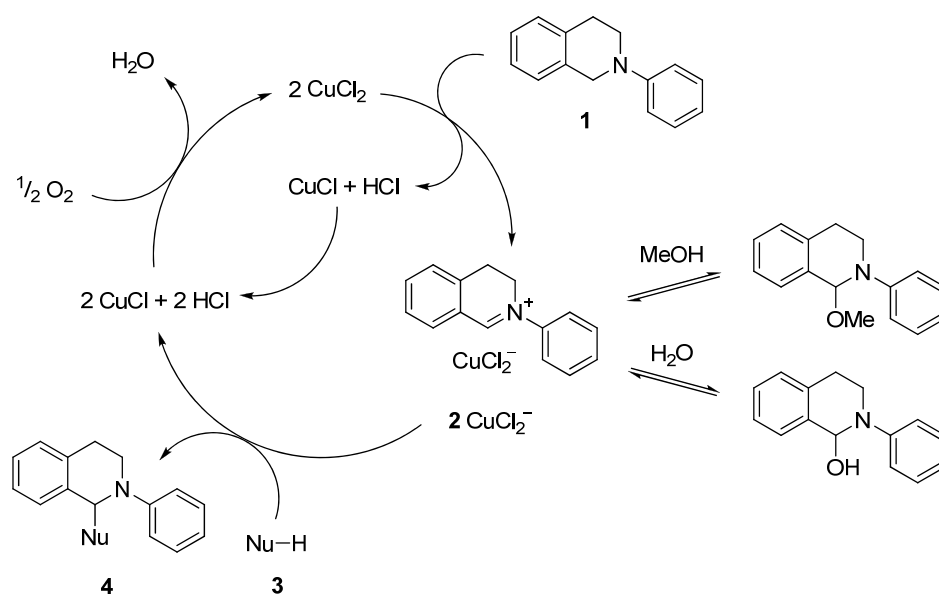
$$\log k_2(20^\circ\text{C}) = s_N(N + E) \quad (1)$$

in which electrophiles are described by E (electrophilicity parameter) and nucleophiles are described by N (nucleophilicity parameter) and s_N (nucleophile-specific sensitivity

parameter). The reactions of iminium ions with nucleophiles have also been shown to follow eq. 1.^{4,7-10}

Based on the nucleophilicity parameters N of the nucleophiles **3** which were found to react with **1** according to Scheme 8.2, Klusmann and coworkers estimated the electrophilicity parameter E of the iminium ion **2** to be “around -8 and -9 ”, adding the caveat that the true value may actually be somewhat higher.² In this work, we report kinetic investigations to determine the E parameter of **2**.

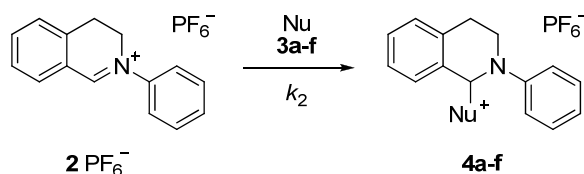
Scheme 8.2. Mechanism of the aerobic Cu-catalyzed oxidative coupling of **1** with nucleophiles (**3**).²



8.2 Kinetic Investigations

Stopped-flow measurements. The kinetics of the reactions of $\mathbf{2} \text{ PF}_6^-$ with nucleophiles **3a-f** in CH_3CN (Scheme 8.3) were investigated by stopped-flow photometry. A first-order rate constant $k_1 = 7.03 \times 10^{-1} \text{ s}^{-1}$ for the reaction of $\mathbf{2} \text{ PF}_6^-$ with a methanol/acetonitrile (1:1 v/v) mixture (**3a**) was determined by following the decay of the UV absorbance of **2** at $\lambda_{\text{max}} = 320 \text{ nm}$ after mixing a solution of $\mathbf{2} \text{ PF}_6^-$ in CH_3CN with an equal volume of CH_3OH in a stopped-flow spectrophotometer.

Scheme 8.3. Reactions of **2** PF₆[−] with nucleophiles **3a-f** (see Table 8.1 for the structures of the nucleophiles).



The second-order rate constants of the reactions of **2** PF₆[−] with the ketene acetal **3b** and the enamines **3c-e** were also determined with the stopped-flow method as described previously.³ When **2** PF₆[−] was treated with a high excess of the nucleophiles **3b-e**, we observed exponential decays of the absorbance of **2** (Fig. 8.1), from which we derived the pseudo-first-order rate constants k_{obs} (s^{−1}). Plots of k_{obs} versus [**3**] were linear (Fig. 8.1), and the second-order rate constants k_2 (M^{−1} s^{−1}) for the reactions of **2** with **3b-e** listed in Table 8.1 were obtained from the slopes of these plots.

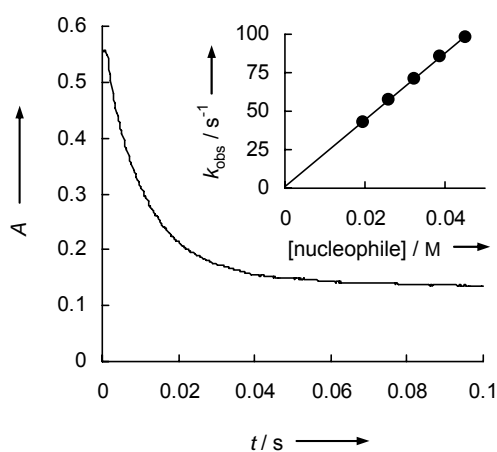
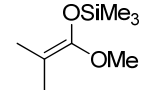
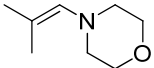
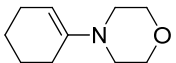
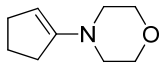


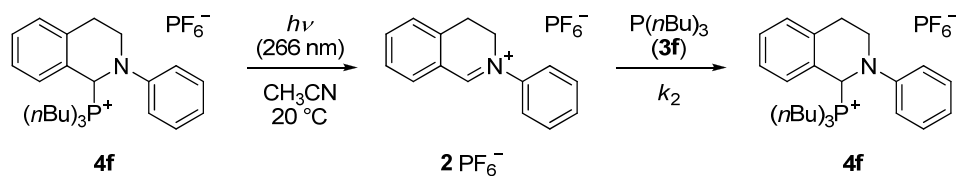
Figure 8.1. Decay of the absorbance of **2** at 320 nm in the presence of 4-cyclohexenyl-morpholine (**3d**, 4.53×10^{-2} M). The end absorbance at $t > 0.1$ s is due to the UV/vis band of the product **4d**. Inset: Plot of k_{obs} versus [**3d**]: $k_{\text{obs}} = 2.14 \times 10^3 [\text{3d}] + 1.55$ ($R^2 = 0.9994$).

Table 8.1. Second-order rate constants k_2 ($\text{M}^{-1} \text{s}^{-1}$) for the reactions of **2** with nucleophiles **3a-f** in CH_3CN at 20°C .

	nucleophile	N (s_N)	$k_2 / \text{M}^{-1} \text{s}^{-1}$	$k_{\text{calc}}^a / \text{M}^{-1} \text{s}^{-1}$
3a	50M50AN ^b	6.67 (0.90) ^c	2.50 ^d	7.75×10^{-1d}
3b		9.00 (0.98) ^{e,f}	5.55	1.46×10^{2e}
3c		10.04 (0.82) ^{e,g}	7.98×10^2	4.60×10^{2e}
3d		11.40 (0.83) ^{e,f}	2.14×10^3	6.67×10^{3e}
3e		13.41 (0.82) ^{e,g}	1.60×10^6	2.67×10^{5e}
3f	$\text{P}(\text{nBu})_3$	15.49 (0.69) ^{e,h}	$8.42 \times 10^7 i$	1.00×10^{6e}

^a Calculated from eq. 1 using $E(\mathbf{2}) = -6.79$. ^b Solvent mixture of methanol and acetonitrile 50:50 (v/v). ^c Solvent nucleophilicity parameter N_1 referring to first-order rate constant k_1 (s^{-1}); from ref.¹¹ ^d First-order rate constant k_1 (s^{-1}). ^e Solvent: CH_2Cl_2 . ^f From ref.³ ^g From ref.¹² ^h From ref.¹³ ⁱ The iminium ion **2** was generated by laser flash photolysis of **4f**.

Laser flash photolysis. Quaternary phosphonium salts are excellent precursors for the photogeneration of carbocations.¹⁴ In previous work, we have successfully used tri-*n*-butylphosphine (**3f**) as a photo-leaving group for the laser flash photolytic generation of iminium ions.⁹ Therefore, we also tested the use of the phosphonium salt **4f**, which we obtained by reaction of **2** PF_6^- with $\text{P}(\text{nBu})_3$, as a substrate for the photolytic generation of **2** (Scheme 8.4).

**Scheme 8.4.** Photogeneration of **2** by irradiation of **4f** in CH_3CN and reaction of **2** with $\text{P}(\text{nBu})_3$ (**3f**) to regenerate the phosphonium salt **4f**.

Irradiation of CH_3CN solutions of **4f** with 7-ns laser pulses from the fourth harmonic of a Nd/YAG laser ($\lambda_{\text{exc}} = 266 \text{ nm}$, 30-60 mJ/pulse) yielded the 2-phenyl-3,4-dihydroisoquinolinium ion (**2**) which shows the same absorbance maximum as solutions of the

isolated iminium salts (Fig. 8.2a). When we generated **2** by irradiation of **4f** in the presence of excess $P(nBu)_3$, we observed mono-exponential decays of the absorbance of **2**, from which we determined the pseudo-first-order rate constants k_{obs} (s^{-1}) (Fig. 8.2b). A plot of k_{obs} versus the concentration of $P(nBu)_3$ was linear (Fig. 8.2b, inset) and provided the second-order rate constant $k_2 = 8.42 \times 10^7 \text{ M}^{-1} \text{ s}^{-1}$ for the reaction of **2** with $P(nBu)_3$ (Table 8.1).

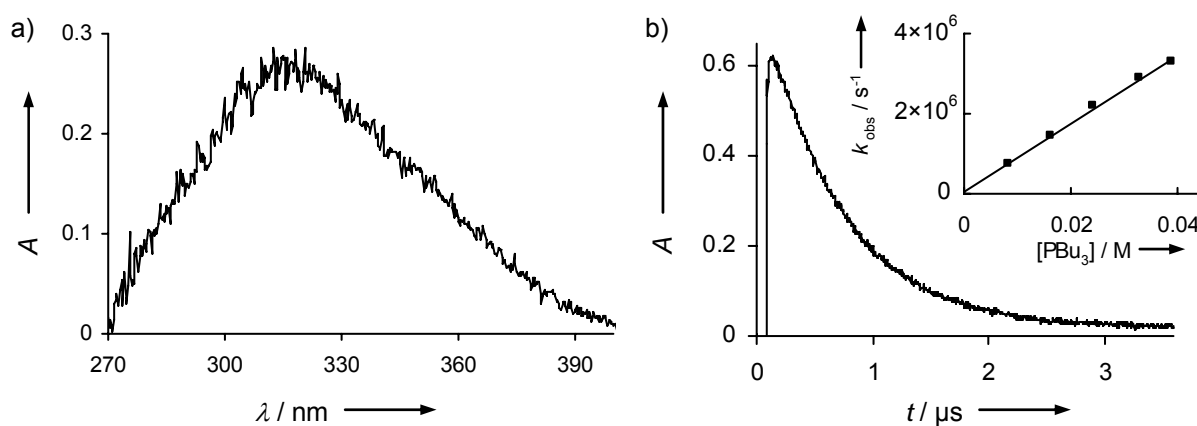


Figure 8.2. (a) Transient UV/vis spectrum of **2** obtained by irradiation of a $1.0 \times 10^{-4} \text{ M}$ solution of **4f** in CH_3CN with a 7-ns laser pulse ($\lambda_{exc} = 266 \text{ nm}$). (b) Absorbance decay of **2** at 320 nm after irradiation of a $1.8 \times 10^{-4} \text{ M}$ solution of **4f** in the presence of tri-*n*-butylphosphine (**3f**, $1.64 \times 10^{-4} \text{ M}$). Inset: Plot of k_{obs} versus $[P(\text{Bu})_3]$ with linear fit: $k_{obs} = 8.42 \times 10^7 [P(\text{Bu})_3] + 7.32 \times 10^4$ ($R^2 = 0.9972$).

However, we could not generate the iminium ion **2** when we irradiated the precursor **4f** in the presence of an excess of other nucleophiles such as 1,8-diazabicyclo[5.4.0]undec-7-ene (DBU), 1-cyclopentenylpyrrolidine, or cyanide. Presumably, small equilibrium concentrations of **2** are present in solutions of the phosphonium salt **4f** and therefore **4f** is not stable in the presence of other nucleophiles than $P(nBu)_3$ (**3f**). Considering this remarkably low Lewis acidity of **2**, it seems to be a necessary condition for the photo-generation of **2** that the nucleophile employed in the kinetic investigation must be identical with the photo-leaving group. Unfortunately, **4f** was the only compound we could identify that was suitable as precursor for the photogeneration of **2** and could be obtained by combination of **2** with nucleophiles having appropriate nucleophilicity parameters for the kinetic experiments.¹⁵

Electrophilic reactivity of the 2-phenyl-3,4-dihydroisoquinolinium ion (2). When $(\lg k_2)/s_N$ for the rate constants listed in Table 8.1 is plotted against the nucleophilicity parameters N of the nucleophiles, a linear plot is obtained (Figure 8.3). As required by eq. 1, the slope of the plot

is close to unity (1.23), and therefore we could derive the electrophilicity parameter of $E = -6.79$ for **2** from eq. 1 by least-squares minimization of $\Delta^2 = \Sigma[\lg k_2 - s_N(N+E)]^2$. Despite the large structural differences between **2** and the reference systems (benzhydryl cations), all rate constants k_{calc} which are calculated from eq. 1 (Table 8.1) are within the postulated error limit for eq. 1 (factor 100).

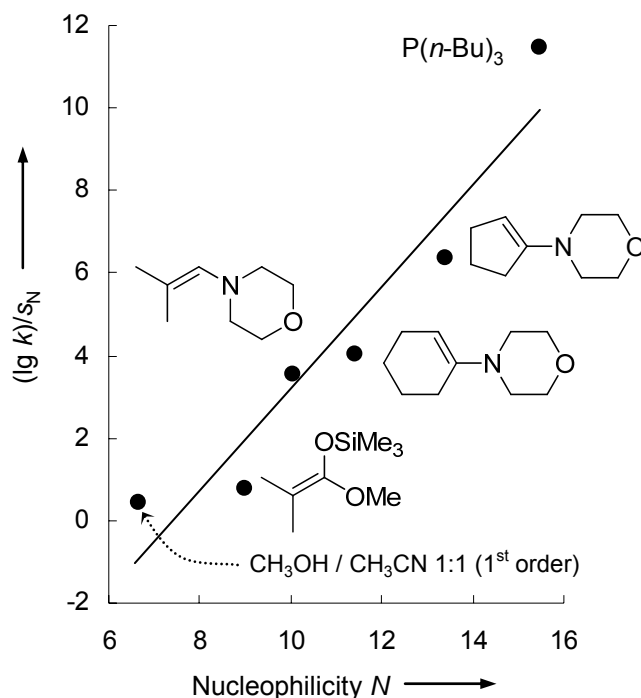
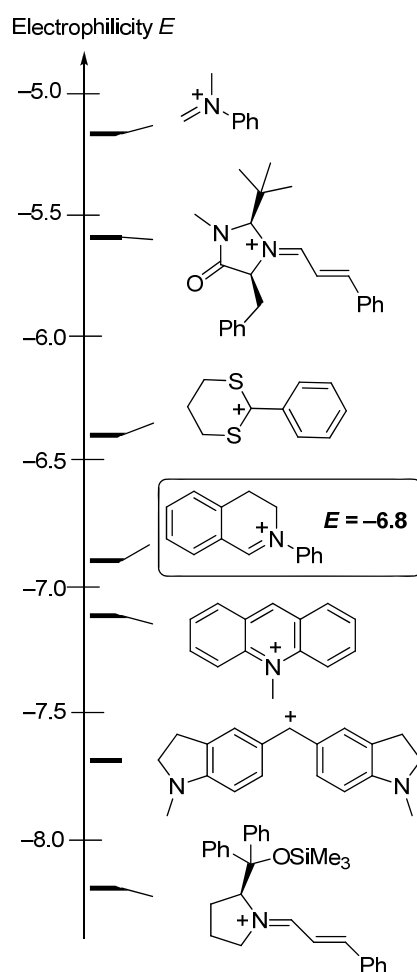


Figure 8.3. Plot of $(\lg k_2)/s_N$ versus N for reactions of **2** with nucleophiles **3a-f** and linear fit: $(\lg k_2)/s_N = 1.2369N - 9.1772$; $R^2 = 0.9092$. If the slope is set to unity as required by eq. 1, one obtains an electrophilicity parameter of $E = -6.79$.

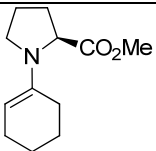
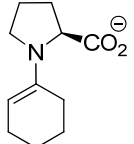
The electrophilicity parameter of $E = -6.79$ derived for **2** from the kinetic experiments in this work is somewhat higher than Klusmann's previous estimate (-8 to -9).² Scheme 8.5 compares the E parameter of the iminium ion **2** with those of other electrophiles and shows that the electrophilicity of **2** is comparable to that of the *N*-methyl acridinium ion.⁴ Thus, the 2-phenyl-3,4-dihydroisoquinolinium ion (**2**) is less reactive than the methyl phenyl methaniminium ion⁴ or the iminium ion derived from cinnamaldehyde and MacMillan's second generation catalyst⁹ (top two formulas in Scheme 8.5), but it is more reactive than most other cinnamaldehyde-derived iminium ions we have studied.^{7,9} The relatively high electrophilicity of **2** explains its reactions with a wide range of nucleophiles which have nucleophilicity parameters of $N \approx 2$ or higher.

Scheme 8.5. Comparison of the E parameters for the iminium ion **2** and other electrophiles.

This agrees well with the scope of nucleophiles that could be employed in coupling reactions with **1** by Klusmann and coworkers.² The low Lewis acidity of **2** may explain why it was not possible to obtain products from 2-methylfuran ($N = 3.61$)³ or 1,3-dimethoxybenzene ($N = 2.48$)³ in the aerobic Cu-catalyzed oxidative coupling reactions.²

Reactions of 2 with chiral enamines. We have also determined the rate constants for the reactions of **2** with the enantiopure enamine **3g** using the stopped-flow method (Table 8.2). The experimental data agree within the typical error limit (factor 10-100) with the value predicted from eq. 1 using the electrophilicity parameter of **2** ($E = -6.79$) determined in this work and the reactivity parameters of **3g** ($N = 14.96$, $s_N = 0.68$).¹⁶

Table 8.2. Second-order rate constants k_2 ($\text{M}^{-1} \text{s}^{-1}$) for the reactions of **2** with nucleophiles **3g-h** in CH_3CN at 20 °C.

nucleophile	N (s_N)	$k_2 / \text{M}^{-1} \text{s}^{-1}$	$k_{\text{calc}}^a / \text{M}^{-1} \text{s}^{-1}$
3g 	14.96 (0.68) ^b	4.93×10^4	3.58×10^5
3h 	18.86 (0.70) ^b	$(> 5 \times 10^6)^c$	2.80×10^8

^a Calculated from eq. 1 using $E = -6.79$. ^b From ref.¹⁶ ^c Too fast for stopped-flow technique.

The rate constant for the reaction of **2** with **3h** was too fast to be measured with the stopped-flow technique ($k_2 > 5 \times 10^6 \text{ M}^{-1} \text{ s}^{-1}$), and laser flash photolysis of **4f** in the presence of enamines did not yield the desired iminium ion **2** (see above). For this reaction, the rate constant of $k_{\text{calc}} = 2.80 \times 10^8 \text{ M}^{-1} \text{ s}^{-1}$ calculated from eq. 1 using the reactivity parameters of **3h** ($N = 18.86$, $s_N = 0.70$)¹⁶ and the electrophilicity parameter of **2** ($E = -6.79$) determined in this work cannot be compared with the experimental value. As shown by Klussmann and coworkers,¹⁷ the use of proline as organocatalyst for the addition of ketones to **2** leads to almost racemic products. This might be explained by the high second-order rate constant for the reaction of **3h** with **2**, which does not favor control of selectivity.

8.3 Acknowledgment

We thank the Deutsche Forschungsgemeinschaft for financial support.

8.4 References and Notes

- (a) Campos, K. R., *Chem. Soc. Rev.* **2007**, *36*, 1069-1084; (b) Jones, K. M.; Klussmann, M., *Synlett* **2012**, *23*, 159-162.
- Boess, E.; Schmitz, C.; Klussmann, M., *J. Am. Chem. Soc.* **2012**, *134*, 5317-5325.

3. Mayr, H.; Bug, T.; Gotta, M. F.; Hering, N.; Irrgang, B.; Janker, B.; Kempf, B.; Loos, R.; Ofial, A. R.; Remennikov, G.; Schimmel, H., *J. Am. Chem. Soc.* **2001**, *123*, 9500-9512.
4. Mayr, H.; Kempf, B.; Ofial, A. R., *Acc. Chem. Res.* **2003**, *36*, 66-77.
5. (a) Mayr, H.; Ofial, A. R., *J. Phys. Org. Chem.* **2008**, *21*, 584-595; (b) Mayr, H., *Angew. Chem.* **2011**, *123*, 3692-3698; *Angew. Chem. Int. Ed.* **2011**, *50*, 3612-3618; (c) Ammer, J.; Nolte, C.; Mayr, H., *J. Am. Chem. Soc.* **2012**, *134*, 13902-13911.
6. For a comprehensive database of nucleophilicity and electrophilicity parameters, see: <http://www.cup.lmu.de/oc/mayr/DBintro.html>.
7. Lakhdar, S.; Tokuyasu, T.; Mayr, H., *Angew. Chem.* **2008**, *120*, 8851-8854; *Angew. Chem. Int. Ed.* **2008**, *47*, 8723-8726.
8. (a) Lakhdar, S.; Appel, R.; Mayr, H., *Angew. Chem.* **2009**, *121*, 5134-5137; *Angew. Chem. Int. Ed.* **2009**, *48*, 5034-5037; (b) Lakhdar, S.; Mayr, H., *Chem. Commun.* **2011**, *47*, 1866-1868; (c) Maji, B.; Lakhdar, S.; Mayr, H., *Chem. Eur. J.* **2012**, *18*, 5732 – 5740; (d) Lakhdar, S.; Baidya, M.; Mayr, H., *Chem. Commun.* **2012**, *48*, 4504-4506.
9. Lakhdar, S.; Ammer, J.; Mayr, H., *Angew. Chem.* **2011**, *123*, 10127-10130; *Angew. Chem. Int. Ed.* **2011**, *50*, 9953-9956.
10. Reviews: (a) Lakhdar, S.; Ofial, A. R.; Mayr, H., *J. Phys. Org. Chem.* **2010**, *23*, 886-892; (b) Mayr, H.; Lakhdar, S.; Maji, B.; Ofial, A. R., *Beilstein J. Org. Chem.* **2012**, *8*, 1458-1478.
11. Minegishi, S.; Kobayashi, S.; Mayr, H., *J. Am. Chem. Soc.* **2004**, *126*, 5174-5181.
12. Kempf, B.; Hampel, N.; Ofial, A. R.; Mayr, H., *Chem. Eur. J.* **2003**, *9*, 2209-2218.
13. Kempf, B.; Mayr, H., *Chem. Eur. J.* **2005**, *11*, 917-927.
14. (a) Alonso, E. O.; Johnston, L. J.; Scaiano, J. C.; Toscano, V. G., *Can. J. Chem.* **1992**, *70*, 1784-1794; (b) Imrie, C.; Modro, T. A.; Rohwer, E. R.; Wagener, C. C. P., *J. Org. Chem.* **1993**, *58*, 5643-5649; (c) Ammer, J.; Baidya, M.; Kobayashi, S.; Mayr, H., *J. Phys. Org. Chem.* **2010**, *23*, 1029-1035; (d) Ammer, J.; Sailer, C. F.; Riedle, E.; Mayr, H., *J. Am. Chem. Soc.* **2012**, *134*, 11481-11494.
15. We could not obtain reproducible results using triscyclohexylphosphine as photo-leaving group and nucleophile, which probably results from the fact that this phosphine is very prone to oxidation reactions. Aromatic phosphines, on the other hand, have the disadvantage that they absorb at the excitation wavelength. Although tertiary amines are also good photo-leaving groups (ref. 14c), we could not obtain **2** by this method, since

the equilibrium mixtures obtained from the reaction of **2** with DABCO or *N*-methylpyrrolidine underwent subsequent decomposition reactions. A similar behavior was reported for the adducts of tertiary amines with other stabilized carbocations (ref. 14c).

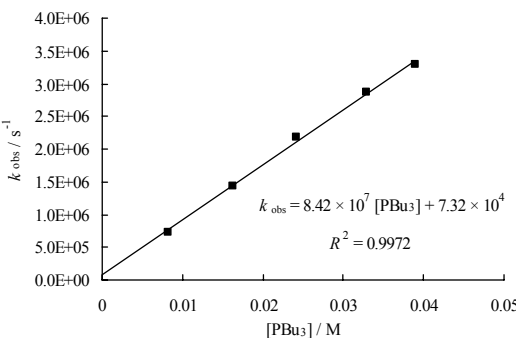
16. Kanzian, T.; Lakhdar, S.; Mayr, H., *Angew. Chem.* **2010**, *122*, 9717-9720; *Angew. Chem. Int. Ed.* **2010**, *49*, 9526-9529.
17. Sud, A.; Sureshkumar, D.; Klusmann, M., *Chem. Commun.* **2009**, 3169–3171.

8.S Supplementary Data and Experimental Section

Laser flash photolytic generation of 2. Solutions of $(1-2) \times 10^{-4}$ M **4f** in CH₃CN were irradiated with a 7-ns pulse (266 nm, 30-60 mJ/pulse) from a quadrupled Nd/YAG laser using a xenon short-arc lamp as probe light. The system is equipped with a fluorescence flow cell and a dosage pump which allows to replace the sample volume completely between subsequent laser pulses. The transient UV/vis spectrum was recorded as difference spectrum of subsequent determinations with and without laser irradiation using an ICCD camera with 10 ns gate width, and eight such spectra were averaged to obtain the spectrum shown in Fig. 8.2a. When **2** was generated in presence of a large excess of P(*n*Bu)₃ (**3f**), we observed exponential decays of the UV/vis absorbance of **2** at the absorption maximum. Typically, 64 or more individual decay curves were averaged for noise reduction.

Evaluation of the kinetics. The rate constants k_{obs} (s⁻¹) which were obtained by least-squares fitting to the single exponential curve $A_t = A_0 e^{-k_{\text{obs}}t} + C$ depended linearly on the nucleophile concentration. The second-order rate constants k_2 (M⁻¹ s⁻¹) for the combination reaction of **2** with **3f** was derived from the slope of plot of k_{obs} for each nucleophile concentration versus the nucleophile concentrations.

Table 8.S.1. Rate constants for the reaction of PBu₃ (**3f**) with **2** (generated from **4f**) in acetonitrile (laser flash photolysis, 20 °C, $\lambda = 320$ nm).

[4f] / M	[3f] / M	$k_{\text{obs}} / \text{s}^{-1}$	$\lambda = 320$ nm	$k_2 / \text{M}^{-1} \text{s}^{-1}$
1.76×10^{-4}	8.15×10^{-3}	7.26×10^5		8.42×10^7
	1.64×10^{-2}	1.44×10^6		
	2.42×10^{-2}	2.19×10^6		
	3.29×10^{-2}	2.88×10^6		
	3.90×10^{-2}	3.30×10^6		

Nucleophilic Reactivities of Tertiary Alkylamines

Johannes Ammer, Mahiuddin Baidya, Shinjiro Kobayashi, and Herbert Mayr

J. Phys. Org. Chem. **2010**, 23, 1029-1035

9.1 Introduction

Tertiary alkylamines are generally used as Brønsted bases in organic synthesis.^[1-2] On the other hand, many reactions are known, where tertiary amines act as nucleophilic catalysts.^[3-32] 1,4-Diazabicyclo[2.2.2]octane (DABCO, **1e**) and quinuclidine (**1f**), for example, are common catalysts in Baylis-Hillman reactions^[7] and in cyclopropanations of Michael acceptors.^[8] *N*-Methylpiperidine (**1c**) and *N*-methylnorpholine (**1d**) have been reported to function as nucleophilic catalysts in Baylis-Hillman reactions,^[9,10] and *N*-methylnorpholine (**1d**) served as a catalyst for the aziridination of α,β -unsaturated carbonyl compounds.^[11-13] Though acylations are commonly catalyzed by pyridines, in particular 4-dimethylaminopyridine (DMAP),^[14-18] triethylamine (**1a**),^[19-27] and the cyclic amines **1b**^[27] and **1c**^[23] have also been employed as acylation catalysts. Analogously, the hydrolyses of esters, imides, and amides are catalyzed by tertiary amines, including **1d**,^[28] through a nucleophilic mechanism.^[28-30] Nucleophilic substitution reactions of aromatic heterocycles have also been catalyzed by tertiary amines, including **1a** and **1c**.^[31,32]

Because the nucleophilic activities of amines are known to correlate only poorly with their Brønsted basicities (pK_{aH}),^[33-35] we now set out to include the tertiary amines **1(a-d)** (Chart 9.1) in our comprehensive nucleophilicity scales^[36-40] by studying the rates of their reactions with benzydrylium ions.^[36]

Chart 9.1. Tertiary alkylamines.

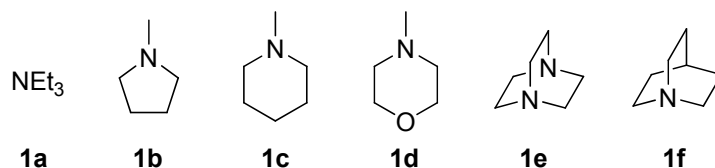
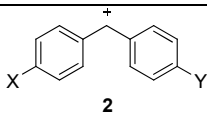
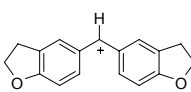
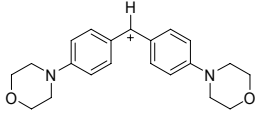
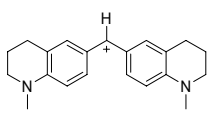
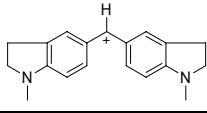


Table 9.1. Abbreviations and electrophilicity parameters (E) of the reference electrophiles employed in this work.

Ar_2CH^+	 2		E^a
Ph_2CH^+	H	H	5.90
tol(Ph)CH^+	H	CH_3	4.59
$(\text{tol})_2\text{CH}^+$	CH_3	CH_3	3.63
ani(Ph)CH^+	H	OCH_3	2.11
$(\text{ani})_2\text{CH}^+$	OCH_3	OCH_3	0.00
$(\text{fur})_2\text{CH}^+$			-1.36
$(\text{pfa})_2\text{CH}^+$	$\text{N(Ph)CH}_2\text{CF}_3$	$\text{N(Ph)CH}_2\text{CF}_3$	-3.14
$(\text{mfa})_2\text{CH}^+$	$\text{N(CH}_3\text{)CH}_2\text{CF}_3$	$\text{N(CH}_3\text{)CH}_2\text{CF}_3$	-3.85
$(\text{dpa})_2\text{CH}^+$	NPh_2	NPh_2	-4.72
$(\text{mor})_2\text{CH}^+$			-5.53
$(\text{mpa})_2\text{CH}^+$	N(Ph)CH_3	N(Ph)CH_3	-5.89
$(\text{dma})_2\text{CH}^+$	$\text{N(CH}_3\text{)}_2$	$\text{N(CH}_3\text{)}_2$	-7.02
$(\text{pyr})_2\text{CH}^+$	$\text{N(CH}_2\text{)}_4$	$\text{N(CH}_2\text{)}_4$	-7.69
$(\text{thq})_2\text{CH}^+$			-8.22
$(\text{ind})_2\text{CH}^+$			-8.76

^a From Reference [36].

Numerous kinetic investigations have shown that the rate constants for the reactions of n -, π -, and σ -nucleophiles with carbocations can be described by Eqn (1),^[36-40]

$$\log k_2(20\text{ }^\circ\text{C}) = s_N(N + E) \quad (1)$$

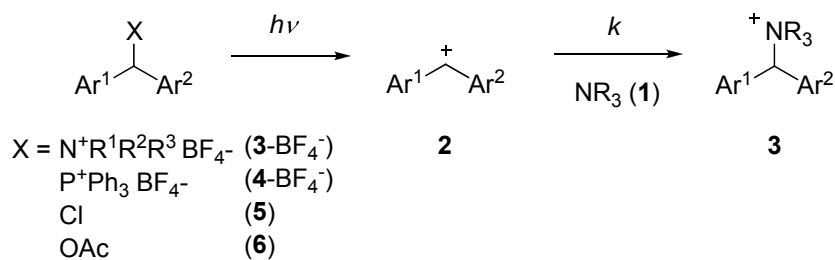
where nucleophiles are characterized by two parameters (N , s_N) and electrophiles are characterized by one parameter (E). By employing benzhydrylium ions (**2**, Table 9.1)^[36] and structurally related quinone methides^[40] as reference electrophiles, it became possible to compare reactivities of a large number of nucleophiles in a single scale.^[36-40] With this methodology, we have previously quantified the nucleophilicities of numerous n -, π -, and σ -nucleophiles,^[41] including primary and secondary amines,^[42] pyridines,^[43] amidines,^[44]

cinchona alkaloids,^[45] as well as the tertiary alkylamines **1e,f**.^[46] In this work, we will report on the nucleophilic reactivities of amines **1a-d**.

9.2 Results and Discussion

As the benzhydrylium ions (Ar_2CH^+ , **2**) are colored and their reactions with the amines **1a-d** yield colorless adducts, the progress of the reactions can be monitored by UV/vis spectroscopy. However, formation of quaternary ammonium salts from **1a-d** and the more stabilized benzhydrylium ions ($E < -9$ to -4) is thermodynamically unfavorable. Similar to previous observations for **1e,f**,^[46] those benzhydryl cations, which do combine with the tertiary amines **1a-d**, react very rapidly ($k > 5 \times 10^5 \text{ M}^{-1} \text{ s}^{-1}$ at 20°C). Conventional UV/vis spectroscopy, even in combination with stopped-flow techniques, was thus not suitable for following the rates of these reactions because they are completed during the mixing time of the stopped-flow instrument. For this reason, we have studied the reactions of **1a-d** with Ar_2CH^+ in CH_3CN and CH_2Cl_2 by laser-flash photolytic techniques (Scheme 9.1).

Scheme 9.1. Laser-flash-induced heterolytic cleavage of suitable precursors yields benzhydryl cations **2** which combine with the amines **1** to yield ammonium ions **3**.



9.2.1 Laser-flash-photolytic Generation of Benzhydryl Cations. *In acetonitrile.* In polar solvents like acetonitrile, numerous photo-leaving groups can be employed to generate benzhydryl cations **2** by photoheterolysis of the respective precursors.^[77-79] If the corresponding benzhydrylium ion is available as a stable tetrafluoroborate^[36] and the nucleophile to be studied can act as a photo-leaving group, the corresponding benzhydrylium precursor can be generated in solution by combining $\text{Ar}_2\text{CH}^+ \text{BF}_4^-$ with the corresponding nucleophile. We have previously applied this approach to study the nucleophilicities of thiocyanate,^[47] halide,^[48] nitrite,^[49] and cyanate^[50] ions, as well as the tertiary amines **1e,f**.^[46]

In this work, we will use it to determine the nucleophilic reactivities of the tertiary amines **1a-d**. This procedure is simple because the quaternary ammonium salts **3**-BF₄⁻ which serve as precursors for laser flash photolysis can be prepared in solution by adding a high excess (>10 equivalents) of the tertiary amine which is required for the kinetic experiment to a 10⁻⁵ to 10⁻⁴ M solution of the benzhydrylium tetrafluoroborate **2**-BF₄⁻. Due to the low concentration of **2**-BF₄⁻, the concentration of the tertiary amine remains virtually unchanged. This method has the further advantage that photolysis of the resulting precursors only regenerates the benzhydrylium ion and the tertiary amine.

The choice of photo-leaving group becomes more critical for less stabilized benzhydryl cations because photolysis gets less favorable with decreasing cation stability. For the generation of benzhydryl cations with $E > -2$, which cannot readily be isolated as stable salts, we usually use precursors which are known to have a high efficiency of photolysis, such as chlorides (**5**),^[51-53] acetates (**6**),^[54-58] and phosphonium salts (**4**).^[59-63] The concentrations of Cl⁻, AcO⁻, and R₃P generated by photolysis, which can be calculated from the absorbances and known extinction coefficients^[51] of the benzhydrylium ions, are so small that the rate of external return with the photo-leaving group is usually negligible.

In dichloromethane. Phosphonium tetrafluoroborates (**4**-BF₄⁻) are particularly interesting precursors for laser flash photolysis, because they allow us to generate reactive carbocations efficiently in low polarity solvents such as dichloromethane.^[63] Photolyses of neutral precursors, for example chlorides (**5**) or acetates (**6**), on the other hand, yield only radicals in dichloromethane if the aryl rests have *p*-MeO or less electron-donating substituents.^[51] An important reason for the high efficiency of phosphonium salts **4**-BF₄⁻ as precursors in apolar solvents is the fact that they already bear a positive charge and no net charge is generated during the separation of the carbocation and the neutral phosphine. A similar argument could be made for quaternary ammonium salts, and therefore we were also interested in the laser flash photolysis of the ammonium salts **3**-BF₄⁻ in dichloromethane. As far as we are aware of, the photolysis of quaternary ammonium salts^[64-66,80] has only been described in more polar solvents.

Photolysis of the quaternary ammonium bromide **3e**-Br⁻ with Ar¹ = Ar² = Ph^[67] in CH₂Cl₂ did not give rise to any absorbance of the benzhydryl cation (Ph₂CH⁺). This is not surprising because the Br⁻ anion undergoes a diffusion-controlled reaction with Ph₂CH⁺,^[48] and in CH₂Cl₂, the Br⁻ anion would presumably form contact ion pairs with the ammonium ions, i.e., it can intercept the carbocation within the geminate solvent cage. We then prepared the

corresponding ammonium tetrafluoroborate $\mathbf{3e}\text{-BF}_4^-$ ($\text{Ar}^1 = \text{Ar}^2 = \text{Ph}$) from the bromide by salt exchange with AgBF_4 in CH_3CN . When we photolyzed $\mathbf{3e}\text{-BF}_4^-$ ($\text{Ar}^1 = \text{Ar}^2 = \text{Ph}$) in CH_2Cl_2 , we could indeed observe the benzhydryl cation Ph_2CH^+ and identify it by its spectrum.

9.2.2 Thermodynamics of the Combination Reactions. As mentioned above, combinations of the tertiary amines **1a-d** with the highly stabilized benzhydryl cations are thermodynamically unfavorable and their solutions remain colored even when a high excess of the amines is added. In some cases, partial combinations occur, and we have previously reported on photometric determinations of equilibrium constants for the combination reactions of benzhydrylium ions with the tertiary amines **1e,f** in acetonitrile^[46] as well as for tertiary phosphines in dichloromethane.^[68] Attempts to determine equilibrium constants for the combinations of **1a-d** with Ar_2CH^+ in this work were unsuccessful because the fast combination of benzhydrylium ions with the amines was followed by an unknown subsequent reaction so that the end absorptions were not constant.

Qualitatively, the thermodynamic stabilities of the quaternary ammonium salts in CH_3CN decrease for a given benzhydrylium ion in the order $\text{DMAP} \gg \text{quinuclidine} > \text{DABCO} \approx \text{N-methylpyrrolidine} > \text{N-methylpiperidine} > \text{N-methylmorpholine} > \text{NEt}_3$. In CH_2Cl_2 , the formation of ammonium salts from benzyhydrylium ions and tertiary amines is thermodynamically less favorable than in CH_3CN .

9.2.3 Kinetics of the Reactions of Tertiary Amines with Benzhydryl Cations. The benzhydryl cations were generated by laser flash photolysis (7 ns pulse, 266 nm, 40-60 mJ/pulse) of suitable precursors (see above and footnotes in Table 9.2) in the presence of a high excess of the amines **1a-d** in CH_3CN or CH_2Cl_2 (Scheme 9.1). The kinetics of the reactions of the benzhydrylium ions **2** with the tertiary amines **1a-d** were then followed by monitoring the decrease of the absorbance of Ar_2CH^+ at λ_{max} . Unlike primary and secondary amines, tertiary amines react only very slowly with dichloromethane,^[69] which allowed us to study their reactivity also in CH_2Cl_2 solution.

In some cases, where the amines **1a-d** form only moderately stable adducts with the benzhydryl cations, we did not observe the expected pseudo-first-order kinetics due to an unidentified side or subsequent reaction on a similar timescale.

In cases, where the combination reactions of the benzhydrylium ions with the tertiary amines are fast, the absorbances of the benzhydrylium ions decrease mono-exponentially (Fig. 9.1) and the pseudo-first-order rate constants k_{obs} were obtained by fitting the decays of the absorbances to the mono-exponential functions $A_t = A_0 e^{-k_{\text{obs}} t} + C$. Plots of k_{obs} versus [amine] are linear and the second-order rate constants k_2 (Table 9.2) were derived from the slopes of such plots (Fig. 9.1).

Table 9.2. Second-order rate constants for the reactions of **1a-d** with benzhydrylium ions (Ar_2CH^+ , **2**) in CH_3CN and CH_2Cl_2 at 20 °C.^a

2	$k_2 / \text{M}^{-1} \text{s}^{-1}$							
	1a		1b		1c		1d	
	CH_3CN	CH_2Cl_2	CH_3CN	CH_2Cl_2	CH_3CN	CH_2Cl_2	CH_3CN	CH_2Cl_2
Ph_2CH^+ ^b	1.45×10^9		4.65×10^9		3.71×10^9		2.56×10^9	
$\text{tol}(\text{Ph})\text{CH}^+$ ^b				3.66×10^9				
$(\text{tol})_2\text{CH}^+$ ^b	1.64×10^9		4.06×10^9	3.55×10^9	2.97×10^9	2.00×10^9	2.66×10^9	
$\text{ani}(\text{Ph})\text{CH}^+$ ^b	7.31×10^8							
$(\text{ani})_2\text{CH}^+$ ^b	4.66×10^8			3.05×10^9	1.68×10^9	1.27×10^9	8.38×10^8	
$(\text{fur})_2\text{CH}^+$ ^b	1.91×10^8	1.96×10^8	2.31×10^9	1.65×10^9	8.32×10^8	5.96×10^8	2.71×10^8	7.10×10^7
$(\text{pfa})_2\text{CH}^+$	$(1.4 \times 10^7)^c$		9.24×10^8	6.31×10^8	1.53×10^8	1.45×10^8	1.63×10^7	
$(\text{mfa})_2\text{CH}^+$	^d		3.28×10^8	4.86×10^8	4.00×10^7	7.79×10^7	4.36×10^6	
$(\text{dpa})_2\text{CH}^+$			3.04×10^8	1.87×10^8	4.07×10^7	$(3 \times 10^7)^c$	5.06×10^6	
$(\text{mor})_2\text{CH}^+$			6.39×10^7	6.53×10^7	5.08×10^6		6.73×10^5	
$(\text{mpa})_2\text{CH}^+$			8.55×10^7	5.29×10^7	6.61×10^6		^d	
$(\text{dma})_2\text{CH}^+$			1.22×10^7		$(1.4 \times 10^6)^c$			
$(\text{pyr})_2\text{CH}^+$			7.19×10^6					
$(\text{thq})_2\text{CH}^+$			2.08×10^6					
$(\text{ind})_2\text{CH}^+$			^d					

^a Generated from the corresponding ammonium salts $\mathbf{3}\text{-BF}_4^-$, if not mentioned otherwise. ^b Generated from **5**, **6**, or $\mathbf{4}\text{-BF}_4^-$ in CH_3CN , and from $\mathbf{4}\text{-BF}_4^-$ in CH_2Cl_2 ; for details see Experimental Section. ^c Fits of the time-dependent absorbances of the benzhydryl cations to an exponential curve are not very good, and these rate constants have to be considered approximate. ^d Reactions do occur when higher concentrations of amines are used, but the reactions are not of pseudo-first order.

Figure 9.2 and the data in Table 9.2 show that the rate constants of the reactions of the benzhydrylium ions with the amines increase with increasing electrophilicity parameter E until the diffusion limit is reached, i.e., $(3\text{--}5) \times 10^9 \text{ M}^{-1} \text{ s}^{-1}$ for **1b-d** in acetonitrile. The fact

that the diffusion-controlled rate constants for the reactions of NEt_3 (**1a**) are 2-3 times smaller than for the cyclic amines **1b-d** can be rationalized by the greater steric demand of NEt_3 .

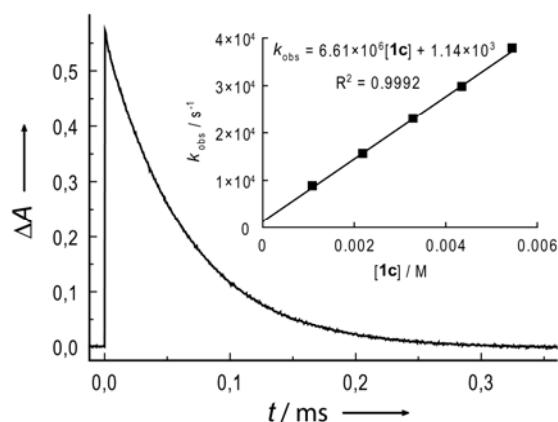


Figure 9.1. Exponential decay of the absorbance ΔA at 613 nm and linear correlation of the pseudo-first-order rate constants k_{obs} versus $[1c]$ for the reaction of $(\text{mpa})_2\text{CH}^+$ with **1c** in CH_3CN at 20 °C.

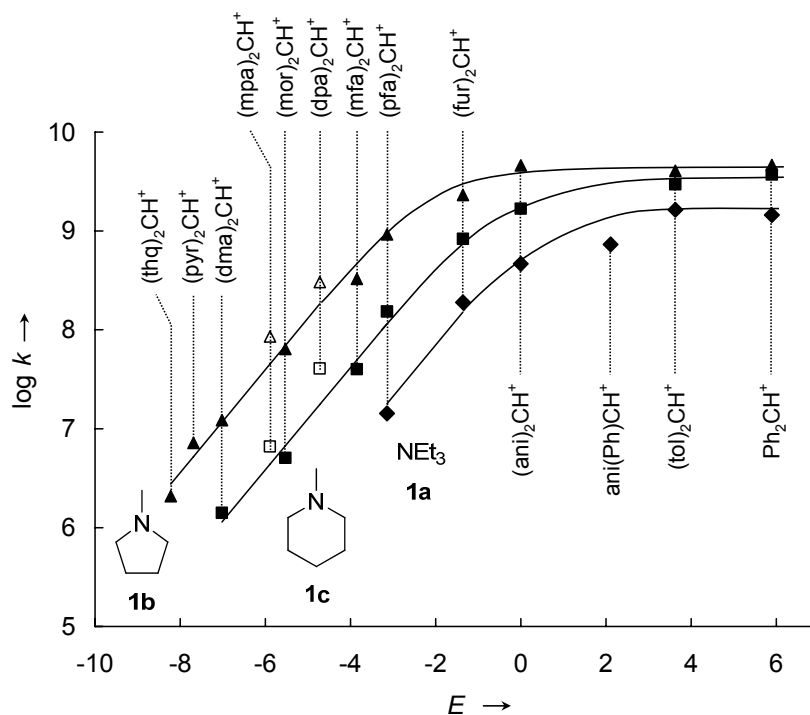


Figure 9.2. Correlation of $\log k_2$ for the reactions of triethylamine (**1a**, \blacklozenge), *N*-methylpyrrolidine (**1b**, \blacktriangle), and *N*-methylpiperidine (**1c**, \blacksquare) with benzhydrylium ions **2** in CH_3CN at 20 °C with electrophilicity parameters E – rate constants for $(\text{mpa})_2\text{CH}^+$ and $(\text{dpa})_2\text{CH}^+$ (open symbols) were not used for the determination of the N and s_N parameters. *N*-Methylmorpholine (**1d**) is not shown because the data points overlap with the line for **1a**.

Typically, plots of $\log k_2$ versus E show linear correlations from which the nucleophile-specific parameters N and s_N can be obtained (Eqn (1)). However, Eqn (1) is only valid for rate constants up to $\sim 2 \times 10^8 \text{ M}^{-1} \text{ s}^{-1}$,^[36] because then the correlation lines start to flatten as the rate constants approach the diffusion limit, which is also evident from Fig. 9.2. As a consequence, the suitable reactivity range to determine N and s_N parameters for **1a-d** is very narrow, limited by thermodynamic stability of the combination products on the lower end, and limited by diffusion control on the upper end. For that reason, only few rate constants can be used for the determination of N and s_N for triethylamine (**1a**) and *N*-methyldmorpholine (**1d**) in acetonitrile, as well as for **1a-d** in dichloromethane (Table 9.2).

Moreover, in acetonitrile, combination reactions of *N*-phenyl substituted benzhydrylium ions, particularly $(\text{dpa})_2\text{CH}^+$ and $(\text{mpa})_2\text{CH}^+$, with nucleophiles are usually faster than one would predict based on their E parameters.^[70] Reactions of **1b-d** with these cations in CH_3CN have similar or even higher rate constants than cations with somewhat higher E values (Table 9.2 and Fig. 9.2). This deviation indicates small differential solvent effects on the reactivities of these electrophiles with the consequence that the E -parameters of benzhydrylium ions which were derived from rate constants determined in dichloromethane^[36] are not applicable in CH_3CN . Therefore, we did not consider rate constants measured with $(\text{dpa})_2\text{CH}^+$ and $(\text{mpa})_2\text{CH}^+$ in CH_3CN for the determination of the N and s_N parameters.

Table 9.3. Reactivity parameters N of amines **1a-d** in CH_3CN and CH_2Cl_2 (with $s_N = 0.52$)

Amines	$N(\text{CH}_3\text{CN})$	$N(\text{CH}_2\text{Cl}_2)$
1a	17.1 ^a	17.3 ^a
1b	20.59	20.6 ^a
1c	18.72	18.9 ^a
1d	16.8 ^a	16.5 ^a

^a Estimated using $s_N = 0.52$.

Due to these limitations, only two series in Table 9.2 contain enough data points to derive the nucleophilicity parameters from Eqn (1), yielding $N = 20.59$, $s_N = 0.52$ for **1b** and $N = 18.72$, $s_N = 0.52$ for **1c** (Table 9.3). Assuming that the slope $s_N = 0.52$ also holds for the other reaction series, nucleophilicity parameters for **1a,d** in CH_3CN and **1a-d** in CH_2Cl_2 have been estimated from 1 to 3 reliable rate constants in the supposedly linear range of the correlations. From the N parameters in Table 3, and from the rate constants in Table 9.2, it can be seen that the tertiary amines **1a-d** have almost equal nucleophilicities in CH_2Cl_2 and in CH_3CN . The

nucleophilicity of DMAP also differs by less than one order of magnitude in these solvents.^[43] However, due to the paucity of data, the N and s_N parameters published in this work have to be considered approximate.

We can now compare the nucleophilic reactivities of **1a-d** with those of other N- and P-nucleophiles. Because reactions of the tertiary alkylamines **1a-f** with electrophiles which would react with second-order rate constants of $k_2 = 1 \text{ M}^{-1} \text{ s}^{-1}$ are thermodynamically unfavorable, N values (which reflect the relative reactivities toward such electrophiles) are less suitable for comparing these nucleophiles than relative reactivities toward an electrophile which does combine with these compounds. Therefore, we have plotted $\log k_2$ of the combination reactions with $(\text{dma})_2\text{CH}^+$ in Fig. 9.3.

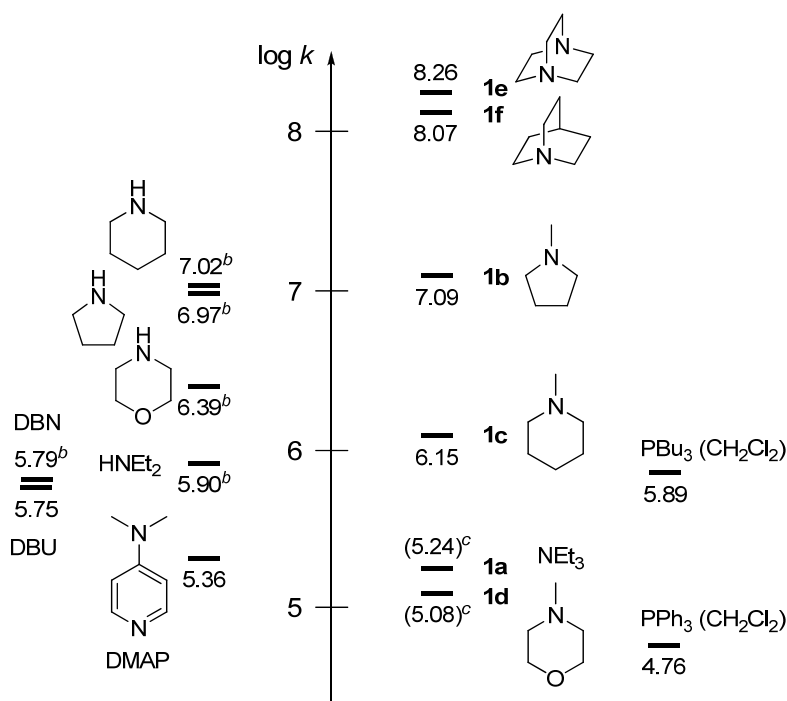


Figure 9.3. $\log k_2$ for reactions of $(\text{dma})_2\text{CH}^+$ ($E = -7.02$) with different N and P nucleophiles in CH_3CN .^{a,b,c}

^a Rate constants for **1e,f**,^[46] DMAP,^[43] DBU,^[44] and the phosphines^[68] were reported previously; rate constants for **1b,c** from this work. ^b Rate constants of reactions of secondary amines and DBN with $(\text{dma})_2\text{CH}^+$ have not been measured and were calculated from Eqn (1) using N and s_N parameters from References [42,44]. ^c **1a** and **1d** do not react with $(\text{dma})_2\text{CH}^+$, and rate constants for these reactions were calculated from Eqn (1).

As discussed previously,^[46] the higher reactivity of DABCO (**1e**) compared with quinuclidine (**1f**) is due to the fact that both rate constants are close to diffusion control, and attack at the diazacomound **1e** is favored statistically. The monocyclic compounds **1b** and **1c** are one (**1b**) and two orders of magnitude less reactive. Remarkably, the five-membered ring compound **1b**

is almost one order of magnitude more reactive than **1c**, while the corresponding secondary amines pyrrolidine and piperidine show very similar reactivities toward $(\text{dma})_2\text{CH}^+$ in acetonitrile (Fig. 9.3) as well as in methanol and water.^[42,71,72] The increase of steric hindrance, which may explain the reduction of reactivity from the bicyclic compounds **1e,f** to the monocyclic compounds **1b,c** may also account for the further reduction of nucleophilicity from **1b,c** to triethylamine (**1a**) which is so severe that the rate constant for the reaction of NEt_3 with $(\text{dma})_2\text{CH}^+$ had to be calculated by Eqn (1) because this reaction is highly reversible and cannot be directly measured. An analogous effect was found in the series of secondary amines, as shown by the comparison of piperidine, pyrrolidine, and diethylamine on the left side of Fig. 9.3. Introduction of an oxygen in *N*-methylpiperidine also reduces the nucleophilicity, and *N*-methylmorpholine (**1d**) is calculated to react one order of magnitude more slowly than **1c**; again, the rate constant for the reaction $(\text{dma})_2\text{CH}^+ + \mathbf{1d}$ could not be measured directly because the equilibrium does not favor the formation of the quaternary ammonium ion.

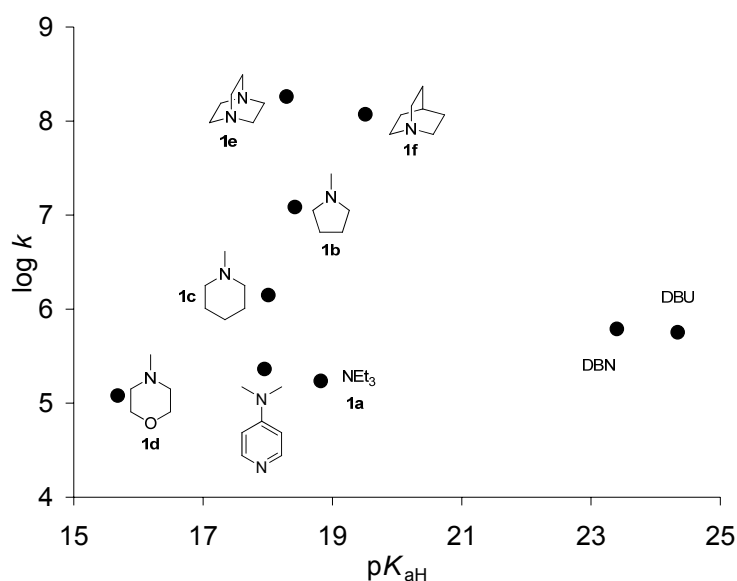


Figure 4. Correlation of $\log k_2$ for reactions of $(\text{dma})_2\text{CH}^+$ ($E = -7.02$) in CH_3CN with different N-nucleophiles and their pK_{aH} values in CH_3CN .^[73–76]

We have repeatedly commented that the relative nucleophilicities of amines cannot be determined from the corresponding basicities (pK_{aH}). Figure 9.4 shows that the newly determined nucleophilic reactivities of **1a–d** support this statement. Triethylamine ($pK_{aH} = 18.82$ in CH_3CN),^[73] though being a slightly stronger base than *N*-methylpyrrolidine (**1b**) and *N*-methylpiperidine (**1c**),^[74] is the weakest nucleophile of the three. In subsequent work, it

will be shown how the N and s_N parameters reported in this work can be used to rationalize the efficiency of these compounds in organocatalytic reactions.

9.3 Acknowledgments

The authors thank Nathalie Hampel for technical assistance and the Deutsche Forschungsgemeinschaft (Ma673/21-3) for financial support.

9.4 References and Notes

- [1] J. W. Smith, in *The Chemistry of the Amino Group* (Ed.: S. Patai), Interscience Publishers, London, **1968**, pp. 161–204.
- [2] M. Morgenthaler, E. Schweizer, A. Hoffmann-Röder, F. Benini, R. E. Martin, G. Jaeschke, B. Wagner, H. Fischer, S. Bendels, D. Zimmerli, J. Schneider, F. Diederich, M. Kansy, K. Müller, *ChemMedChem* **2007**, *2*, 1100–1115.
- [3] For reviews, see References 4-6.
- [4] S. E. Denmark, G. L. Beutner, *Angew. Chem.* **2008**, *120*, 1584–1663; *Angew. Chem. Int. Ed.* **2008**, *47*, 1560–1638.
- [5] A. Berkessel, H. Gröger, *Asymmetric Organocatalysis*, Wiley-VCH, Weinheim, **2005**.
- [6] P. I. Dalko, *Enantioselective Organocatalysis*, Wiley-VCH, Weinheim, **2007**.
- [7] D. Basavaiah, A. J. Rao, T. Satyanarayana, *Chem. Rev.* **2003**, *103*, 811–892.
- [8] C. D. Papageorgiou, S. V. Ley, M. J. Gaunt, *Angew. Chem.* **2003**, *115*, 852–855; *Angew. Chem. Int. Ed.* **2003**, *42*, 828–831.
- [9] S.-H. Zhao, Z.-B. Chen, *Synth. Commun.* **2005**, *35*, 3045–3053.
- [10] P. R. Krishna, E. R. Sekhar, V. Kannan, *Synthesis* **2004**, 857–860.
- [11] Y.-M. Shen, M.-X. Zhao, J. Xu, Y. Shi, *Angew. Chem.* **2006**, *118*, 8173–8176; *Angew. Chem. Int. Ed.* **2006**, *45*, 8005–8008.
- [12] A. Armstrong, D. R. Carbery, S. G. Lamont, A. R. Pape, R. Winiewicz, *Synlett* **2006**, 2504–2506.
- [13] A. Armstrong, C. A. Baxter, S. G. Lamont, A. R. Pape, R. Winiewicz, *Org. Lett.* **2007**, *9*, 351–353.

- [14] L. M. Litvinenko, A. I. Kirichenko, *Dokl. Akad. Nauk SSSR* **1967**, 176, 97–100.
- [15] G. Höfle, W. Steglich, H. Vorbrüggen, *Angew. Chem.* **1978**, 90, 602–615; *Angew. Chem. Int. Ed.* **1978**, 17, 569–583.
- [16] E. F. V. Scriven, *Chem. Soc. Rev.* **1983**, 12, 129–161.
- [17] U. Ragnarsson, L. Grehn, *Acc. Chem. Res.* **1998**, 31, 494–501.
- [18] G. C. Fu, *Acc. Chem. Res.* **2000**, 33, 412–420.
- [19] J. Burkus, C. F. Eckert, *J. Am. Chem. Soc.* **1958**, 80, 5948–5950.
- [20] V. A. Fedorova, *Dopovidi Natsional'noi Akad. Nauk Ukraini* **1998**, 155–157.
- [21] P. Y. Bruice, *J. Am. Chem. Soc.* **1983**, 105, 4982–4996.
- [22] H. Kasprzyk, S. Kinastowski, *React. Kinet. Catal. Lett.* **2002**, 77, 3–12.
- [23] R. Samtleben, H. Pracejus, *J. Prakt. Chem.* **1972**, 314, 157–169.
- [24] For applications in polymer chemistry, see References 25–27.
- [25] D. J. Brunelle, *J. Polym. Sci., Part A: Polym. Chem.* **2008**, 46, 1151–1164.
- [26] S. V. Vinogradova, V. Vasnyev, T. I. Mitaishvili, A. V. Vasil'yev, *J. Polym. Sci., Part A: Polym. Chem.* **1971**, 9, 3321–3325.
- [27] M. H. Kailani, C. S. P. Sung, *Macromolecules* **1998**, 31, 5779–5784.
- [28] Y.-L. Sim, A. Ariffin, M. N. Khan, *J. Org. Chem.* **2007**, 72, 8452–8458.
- [29] W. P. Jencks, M. Gilchrist, *J. Am. Chem. Soc.* **1968**, 90, 2622–2637.
- [30] M. J. Gresser, W. P. Jencks, *J. Am. Chem. Soc.* **1977**, 99, 6963–6970.
- [31] G. Ostrogovich, E. Fliegl, R. Bacaloglu, *Tetrahedron* **1971**, 27, 2885–2891.
- [32] B. Bitter, H. Zollinger, *Helv. Chim. Acta* **1961**, 44, 812–823.
- [33] J. M. Harris, S. P. McManus, *Nucleophilicity*, American Chemical Society, Washington, **1987**.
- [34] J. E. Leffler, E. Grunwald, *Rates and Equilibria of Organic Reactions*, Wiley, New York, **1963**.
- [35] A. Williams, *Free Energy Relationships in Organic and Bio-Organic Chemistry*, Royal Society of Chemistry, Cambridge, **2003**.
- [36] H. Mayr, T. Bug, M. F. Gotta, N. Hering, B. Irrgang, B. Janker, B. Kempf, R. Loos, A. R. Ofial, G. Remennikov, H. Schimmel, *J. Am. Chem. Soc.* **2001**, 123, 9500–9512.
- [37] H. Mayr, B. Kempf, A. R. Ofial, *Acc. Chem. Res.* **2003**, 36, 66–77.
- [38] H. Mayr, A. R. Ofial, *Pure Appl. Chem.* **2005**, 77, 1807–1821.
- [39] H. Mayr, A. R. Ofial, *J. Phys. Org. Chem.* **2008**, 21, 584–595.

- [40] D. Richter, N. Hampel, T. Singer, A. R. Ofial, H. Mayr, *Eur. J. Org. Chem.* **2009**, 3203–3211.
- [41] For a comprehensive data base for nucleophilicity parameters, see: www.cup.lmu.de/oc/mayr/DBintro.html.
- [42] T. Kanzian, T. A. Nigst, A. Maier, S. Pichl, H. Mayr, *Eur. J. Org. Chem.* **2009**, 6379–6385.
- [43] F. Brotzel, B. Kempf, T. Singer, H. Zipse, H. Mayr, *Chem. Eur. J.* **2007**, *13*, 336–345.
- [44] M. Baidya, H. Mayr, *Chem. Commun.* **2008**, 1792–1794.
- [45] M. Baidya, M. Horn, H. Zipse, H. Mayr, *J. Org. Chem.* **2009**, *74*, 7157–7164.
- [46] M. Baidya, S. Kobayashi, F. Brotzel, U. Schmidhammer, E. Riedle, H. Mayr, *Angew. Chem.* **2007**, *119*, 6288–6292; *Angew. Chem. Int. Ed.* **2007**, *46*, 6176–6179.
- [47] R. Loos, S. Kobayashi, H. Mayr, *J. Am. Chem. Soc.* **2003**, *125*, 14126–14132.
- [48] S. Minegishi, R. Loos, S. Kobayashi, H. Mayr, *J. Am. Chem. Soc.* **2005**, *127*, 2641–2649.
- [49] A. A. Tishkov, U. Schmidhammer, S. Roth, E. Riedle, H. Mayr, *Angew. Chem.* **2005**, *117*, 4699–4703; *Angew. Chem. Int. Ed.* **2005**, *44*, 4623–4626.
- [50] H. F. Schaller, U. Schmidhammer, E. Riedle, H. Mayr, *Chem. Eur. J.* **2008**, *14*, 3866–3868.
- [51] J. Bartl, S. Steenken, H. Mayr, R. A. McClelland, *J. Am. Chem. Soc.* **1990**, *112*, 6918–6928.
- [52] J. Bartl, S. Steenken, H. Mayr, *J. Am. Chem. Soc.* **1991**, *113*, 7710–7716.
- [53] K. N. Peters, B. Li, *J. Phys. Chem.* **1994**, *98*, 401–403.
- [54] J. A. Pincock, *Acc. Chem. Res.* **1997**, *30*, 43–49.
- [55] G. Hallett-Tapley, F. L. Cozens, N. P. Schepp, *J. Phys. Org. Chem.* **2009**, *22*, 343–348.
- [56] G. V. Rao, M. J. R. Reddy, K. Srinivas, M. J. R. Reddy, K. M. Bushan, V. J. Rao, *Photochem. Photobiol.* **2002**, *76*, 29–34.
- [57] S. A. Fleming, L. Renault, E. C. Grundy, J. A. Pincock, *Can. J. Chem.* **2006**, *84*, 1146–1154.
- [58] L. R. Heeb, K. N. Peters, *J. Am. Chem. Soc.* **2008**, *130*, 1711–1717.
- [59] E. O. Alonso, L. J. Johnston, J. C. Scaiano, V. G. Toscano, *J. Am. Chem. Soc.* **1990**, *112*, 1270–1271.
- [60] E. O. Alonso, L. J. Johnston, J. C. Scaiano, V. G. Toscano, *Can. J. Chem.* **1992**, *70*, 1784–1794.

- [61] C. Imrie, T. A. Modro, C. C. P. Wagener, *J. Chem. Soc., Perkin Trans. 2* **1994**, 1379–1382.
- [62] C. Imrie, T. A. Modro, E. R. Rohwer, C. C. P. Wagener, *J. Org. Chem.* **1993**, 58, 5643–5649.
- [63] J. Ammer, H. Mayr, *Macromolecules* **2010**, 43, 1719–1723 (CHAPTER 6 of this work).
- [64] K. H. Jensen, J. E. Hanson, *Chem. Mater.* **2002**, 14, 918–923.
- [65] Y. Itoh, S. Horiuchi, K. Yamamoto, *Photochem. Photobiol. Sci.* **2005**, 4, 835–839.
- [66] D. C. Appleton, D. C. Bull, R. S. Givens, V. Lillis, J. McKenna, J. M. McKenna, S. Thackeray, A. R. Walley, *J. Chem. Soc., Perkin Trans. 2* **1980**, 77–82.
- [67] E. Hilhorst, T. B. R. A. Chen, A. S. Iskander, U. K. Pandit, *Tetrahedron* **1994**, 50, 7837–7848.
- [68] B. Kempf, H. Mayr, *Chem. Eur. J.* **2005**, 11, 917–927.
- [69] G. O. Nevstad, J. Songstad, *Acta Chem. Scand. B* **1984**, 38, 469–477.
- [70] Similar deviations have previously been reported: T. A. Nigst, M. Westermaier, A. R. Ofial, H. Mayr, *Eur. J. Org. Chem.* **2008**, 2369–2374.
- [71] B. T. Phan, M. Breugst, H. Mayr, *Angew. Chem.* **2006**, 118, 3954–3959; *Angew. Chem. Int. Ed.* **2006**, 45, 3869–3874.
- [72] F. Brotzel, Y. C. Chu, H. Mayr, *J. Org. Chem.* **2007**, 72, 3679–3688.
- [73] pK_{aH} values for **1a**, DMAP, and DBU: I. Kaljurand, A. Kütt, L. Sooväli, T. Rodima, V. Mäemets, I. Leito, I. A. Koppel, *J. Org. Chem.* **2005**, 70, 1019–1028.
- [74] pK_{aH} values for **1c-d** and DBN: K. T. Leffek, P. Pruszyński, K. Thanapaalasingham, *Can. J. Chem.* **1989**, 67, 590–595.
- [75] pK_{aH} value for **1e**: J. F. Coetzee, G. R. Padmanabhan, *J. Am. Chem. Soc.* **1965**, 87, 5005–5010.
- [76] pK_{aH} value for **1f**: P. Beltrame, G. Gelli, A. Loi, *Gazz. Chim. Ital.* **1980**, 110, 491–494.
- [77] For reviews, see References 78 and 79.
- [78] R. A. McClelland, in *Reactive Intermediate Chemistry* (Eds: R. A. Moss, M. S. Platz, M. J. Jones), John Wiley & Sons, Ltd, New York, **2004**.
- [79] R. A. McClelland, *Tetrahedron* **1996**, 52, 6823–6858.
- [80] M. A. Ratcliff, J. K. Kochi, *J. Org. Chem.* **1971**, 36, 3112–3120.
- [S1] R. A. McClelland, V. M. Kanagasabapathy, N. S. Banait, S. Steenken, *J. Am. Chem. Soc.* **1989**, 111, 3966–3972.

9.S Supplementary Data and Experimental Section

Materials. *Solvents.* For the laser flash photolysis experiments, p.a. grade dichloromethane (Merck) was subsequently treated with concentrated sulfuric acid, water, 10% NaHCO₃ solution, and again water. After pre-drying with anhydrous CaCl₂, it was freshly distilled over CaH₂. Acetonitrile (HPLC-grade, VWR) was used as received.

Nucleophiles. Triethylamine (**1a**, Riedel-de-Haën, >99%), *N*-methylpyrrolidine (**1b**, Aldrich, 97%), *N*-methylpiperidine (**1c**, Acros, 99%), and *N*-methylmorpholine (**1d**, Acros, 99%) were distilled over LiAlH₄ to remove any secondary amine impurities.

Precursors for laser flash photolysis. Syntheses of the benzhydryl chlorides (**5**) and benzhydryl acetates (**6**) were reported previously.^[S1] 1-Benzhydryl-1-azonia-4-azabicyclo[2.2.2]octane tetrafluoroborate (**3e**-BF₄⁻, Ar¹ = Ar² = Ph) was prepared by anion metathesis from the corresponding bromide^[29] with AgBF₄ in CH₃CN. The other ammonium tetrafluoroborates were prepared in solution by adding the amines **1a-d** to solutions of the benzhydrylium tetrafluoroborates^[13a] immediately before the experiment, which gave completely or almost completely decolorized solutions. The synthesis of the phosphonium tetrafluoroborates (**4**-BF₄⁻) is described in CHAPTER 1 of this work. The precursors and their concentrations used for the individual experiments are indicated in Tables 9.S.1-9.S.8.

Laser flash photolysis. *Experimental procedure.* Solutions of the precursor with $A_{266\text{ nm}} = 0.3$ to 0.9 were irradiated with a 7 ns pulse from a quadrupled Nd/YAG laser (266 nm, 40-60 mJ/pulse), and a xenon lamp was used as probe light for UV/vis detection. The system is equipped with a fluorescence flow cell which allows to replace the sample volume completely between subsequent laser pulses.

Kinetics were measured by following the decay of the benzhydryl cations at their absorption maxima. For each concentration, ≥ 50 irradiation experiments were averaged, and the pseudo-first order rate constants k_{obs} were obtained by least-squares fitting to the single-exponential curve $A_t = A_0 e^{-k_{\text{obs}} t} + C$. The slope of a plot of k_{obs} versus concentration yields the second order rate constant k_2 .

Details of the kinetic experiments. The majority of the measurements in this section was performed by M. B. and S. K., but properly evaluated and interpreted by me. Several measurements were repeated by me in order to confirm or reject the data determined by my

coworkers. The rate constants for the reactions of **1a,d** in CH₂Cl₂ were determined exclusively by me.

Table 9.S.1. Kinetics of the reactions of triethylamine (**1a**) with Ar₂CH⁺ in CH₃CN at 20 °C.

Cation	[cation] / M	[1a] / M	$k_{\text{obs}} / \text{s}^{-1}$	$\lambda = 592 \text{ nm}$	$k_2 / \text{M}^{-1}\text{s}^{-1}$
(pfa) ₂ CH ⁺	[2-BF ₄] = 2.00×10^{-5}	2.00×10^{-3}	5.14×10^4		$(1.4 \times 10^7)^{\text{a}}$
		3.00×10^{-3}	6.67×10^4		
		4.00×10^{-3}	8.17×10^4		
		5.00×10^{-3}	9.41×10^4		
Cation	[precursor] / M	[1a] / M	$k_{\text{obs}} / \text{s}^{-1}$	$\lambda = 523 \text{ nm}$	$k_2 / \text{M}^{-1}\text{s}^{-1}$
(fur) ₂ CH ⁺	[4-BF ₄] = 1.37×10^{-5}	1.32×10^{-3}	2.21×10^5		1.91×10^8
		2.63×10^{-3}	4.51×10^5		
		3.95×10^{-3}	7.14×10^5		
		5.26×10^{-3}	1.02×10^6		
		6.58×10^{-3}	1.18×10^6		
Cation	[precursor] / M	[1a] / M	$k_{\text{obs}} / \text{s}^{-1}$	$\lambda = 500 \text{ nm}$	$k_2 / \text{M}^{-1}\text{s}^{-1}$
(ani) ₂ CH ⁺	[6] = 4.87×10^{-5}	1.14×10^{-3}	9.89×10^5		4.66×10^8
		2.28×10^{-3}	1.51×10^6		
		3.42×10^{-3}	2.03×10^6		
		4.55×10^{-3}	2.70×10^6		
		5.69×10^{-3}	3.04×10^6		
Cation	[precursor] / M	[1a] / M	$k_{\text{obs}} / \text{s}^{-1}$	$\lambda = 455 \text{ nm}$	$k_2 / \text{M}^{-1}\text{s}^{-1}$
(Ph)(ani)CH ⁺	[5] = 6.39×10^{-5}	1.14×10^{-3}	1.50×10^6		7.31×10^8
		2.28×10^{-3}	2.39×10^6		
		3.42×10^{-3}	3.19×10^6		
		4.55×10^{-3}	4.17×10^6		
		5.69×10^{-3}	4.76×10^6		

Table 9.S.1 (Continued). Kinetics of the reactions of triethylamine (**1a**) with Ar_2CH^+ in CH_3CN at 20 °C.

Cation	[precursor] / M	[1a] / M	$k_{\text{obs}} / \text{s}^{-1}$	$\lambda = 464 \text{ nm}$	$k_2 / \text{M}^{-1}\text{s}^{-1}$
$(\text{tol})_2\text{CH}^+$	[5] = 5.00×10^{-4}	1.00×10^{-3}	2.81×10^6		1.64×10^9
		2.00×10^{-3}	4.39×10^6		
		3.00×10^{-3}	6.05×10^6		
		4.00×10^{-3}	7.85×10^6		
		5.00×10^{-3}	9.29×10^6		
Ph_2CH^+	[5] = 1.00×10^{-3}	1.00×10^{-3}	5.29×10^6		1.45×10^9
		2.00×10^{-3}	6.35×10^6		
		3.00×10^{-3}	7.94×10^6		
		4.00×10^{-3}	9.56×10^6		

^b) Some non-monoexponential component.

Table 9.S.2. Kinetics of the reactions of triethylamine (**1a**) with Ar_2CH^+ in CH_2Cl_2 at 20 °C.

Cation	[precursor] / M	[1a] / M	$k_{\text{obs}} / \text{s}^{-1}$	$\lambda = 530 \text{ nm}$	$k_2 / \text{M}^{-1}\text{s}^{-1}$
$(\text{fur})_2\text{CH}^+$	[4-BF₄⁻] = 1.22×10^{-5}	1.35×10^{-3}	2.38×10^5		1.96×10^8
		2.69×10^{-3}	4.84×10^5		
		4.04×10^{-3}	7.52×10^5		
		5.39×10^{-3}	1.01×10^6		
		6.73×10^{-3}	1.29×10^6		

Table 9.S.3. Kinetics of the reactions of *N*-methylpyrrolidine (**1b**) with Ar₂CH⁺ in CH₃CN at 20 °C.

Cation	[cation] / M	[1b] / M	$k_{\text{obs}} / \text{s}^{-1}$	$\lambda = 620 \text{ nm}$	$k_2 / \text{M}^{-1}\text{s}^{-1}$
(thq) ₂ CH ⁺	[2-BF ₄] ⁻ = 8.77 × 10 ⁻⁵	2.39 × 10 ⁻²	5.84 × 10 ⁴		2.08 × 10 ⁶
		4.79 × 10 ⁻²	1.02 × 10 ⁵		
		7.18 × 10 ⁻²	1.48 × 10 ⁵		
		9.58 × 10 ⁻²	2.05 × 10 ⁵		
		1.20 × 10 ⁻¹	2.56 × 10 ⁵		
(pyr) ₂ CH ⁺	[2-BF ₄] ⁻ = 2.00 × 10 ⁻⁵	5.00 × 10 ⁻³	4.69 × 10 ⁴		7.19 × 10 ⁶
		1.00 × 10 ⁻²	8.22 × 10 ⁴		
		1.50 × 10 ⁻²	1.23 × 10 ⁵		
		2.00 × 10 ⁻²	1.50 × 10 ⁵		
		2.50 × 10 ⁻²	1.93 × 10 ⁵		
(dma) ₂ CH ⁺	[2-BF ₄] ⁻ = 2.00 × 10 ⁻⁵	2.91 × 10 ⁻³	4.59 × 10 ⁴		1.22 × 10 ⁷
		5.82 × 10 ⁻³	8.27 × 10 ⁴		
		8.73 × 10 ⁻³	1.20 × 10 ⁵		
		1.16 × 10 ⁻²	1.58 × 10 ⁵		
		1.46 × 10 ⁻²	1.86 × 10 ⁵		
(mpa) ₂ CH ⁺	[2-BF ₄] ⁻ = 1.00 × 10 ⁻⁵	1.00 × 10 ⁻³	6.82 × 10 ⁴		8.55 × 10 ⁷
		2.00 × 10 ⁻³	1.46 × 10 ⁵		
		3.00 × 10 ⁻³	2.33 × 10 ⁵		
		4.00 × 10 ⁻³	3.21 × 10 ⁵		
		5.00 × 10 ⁻³	4.08 × 10 ⁵		

Table 9.S.3 (Continued). Kinetics of the reactions of *N*-methylpyrrolidine (**1b**) with Ar₂CH⁺ in CH₃CN at 20 °C.

Cation	[cation] / M	[1b] / M	$k_{\text{obs}} / \text{s}^{-1}$	$\lambda = 612 \text{ nm}$	$k_2 / \text{M}^{-1}\text{s}^{-1}$
(mor) ₂ CH ⁺	[2-BF ₄] ⁻ = 1.00 × 10 ⁻⁵	1.00 × 10 ⁻³	5.78 × 10 ⁴		6.39 × 10 ⁷
		2.00 × 10 ⁻³	1.12 × 10 ⁵		
		3.00 × 10 ⁻³	1.82 × 10 ⁵		
		4.00 × 10 ⁻³	2.47 × 10 ⁵		
		5.00 × 10 ⁻³	3.10 × 10 ⁵		
(dpa) ₂ CH ⁺	[2-BF ₄] ⁻ = 1.00 × 10 ⁻⁵	1.00 × 10 ⁻³	3.45 × 10 ⁵		3.04 × 10 ⁸
		2.00 × 10 ⁻³	6.49 × 10 ⁵		
		3.00 × 10 ⁻³	9.62 × 10 ⁵		
		4.00 × 10 ⁻³	1.25 × 10 ⁶		
		5.00 × 10 ⁻³	1.57 × 10 ⁶		
(mfa) ₂ CH ⁺	[2-BF ₄] ⁻ = 1.00 × 10 ⁻⁵	1.00 × 10 ⁻³	3.95 × 10 ⁵		3.28 × 10 ⁸
		2.00 × 10 ⁻³	7.74 × 10 ⁵		
		3.00 × 10 ⁻³	1.11 × 10 ⁶		
		4.00 × 10 ⁻³	1.41 × 10 ⁶		
		5.00 × 10 ⁻³	1.71 × 10 ⁶		
(pfa) ₂ CH ⁺	[2-BF ₄] ⁻ = 1.00 × 10 ⁻⁵	1.00 × 10 ⁻³	8.86 × 10 ⁵		9.24 × 10 ⁸
		2.00 × 10 ⁻³	1.78 × 10 ⁶		
		3.00 × 10 ⁻³	2.69 × 10 ⁶		
		4.00 × 10 ⁻³	3.76 × 10 ⁶		
		5.00 × 10 ⁻³	4.52 × 10 ⁶		

Table 9.S.3 (Continued). Kinetics of the reactions of *N*-methylpyrrolidine (**1b**) with Ar₂CH⁺ in CH₃CN at 20 °C.

Cation	[precursor] / M	[1b] / M	$k_{\text{obs}} / \text{s}^{-1}$	$\lambda = 523 \text{ nm}$	$k_2 / \text{M}^{-1}\text{s}^{-1}$
(fur) ₂ CH ⁺	[4-BF ₄] = 1.29 × 10 ⁻⁵	6.11 × 10 ⁻⁴	1.44 × 10 ⁶		2.31 × 10 ⁹
		1.22 × 10 ⁻³	2.89 × 10 ⁶		
		1.83 × 10 ⁻³	4.51 × 10 ⁶		
		2.44 × 10 ⁻³	5.72 × 10 ⁶		
		3.06 × 10 ⁻³	7.09 × 10 ⁶		
(tol) ₂ CH ⁺	[5] = 2.00 × 10 ⁻⁴	5.00 × 10 ⁻⁴	2.93 × 10 ⁶		4.06 × 10 ⁹
		1.00 × 10 ⁻³	5.43 × 10 ⁶		
		1.50 × 10 ⁻³	8.00 × 10 ⁶		
		2.00 × 10 ⁻³	9.23 × 10 ⁶		
		2.50 × 10 ⁻³	1.12 × 10 ⁷		
		3.00 × 10 ⁻³	1.34 × 10 ⁷		
4.00 × 10 ⁻³	1.75 × 10 ⁷				
(Ph) ₂ CH ⁺	[5] = 1.00 × 10 ⁻³	5.00 × 10 ⁻⁴	5.72 × 10 ⁶		4.65 × 10 ⁹
		1.00 × 10 ⁻³	7.73 × 10 ⁶		
		1.50 × 10 ⁻³	1.02 × 10 ⁷		
		2.00 × 10 ⁻³	1.24 × 10 ⁷		
		2.50 × 10 ⁻³	1.48 × 10 ⁷		
		3.00 × 10 ⁻³	1.73 × 10 ⁷		

Table 9.S.4. Kinetics of the reactions of *N*-methylpyrrolidine (**1b**) with Ar₂CH⁺ in CH₂Cl₂ at 20 °C.

Cation	[cation] / M	[1b] / M	$k_{\text{obs}} / \text{s}^{-1}$	$\lambda = 622 \text{ nm}$	$k_2 / \text{M}^{-1}\text{s}^{-1}$
(mpa) ₂ CH ⁺	[2-BF ₄] ⁻ = 2.31 × 10 ⁻⁵	1.54 × 10 ⁻³	8.65 × 10 ⁴		5.29 × 10 ⁷
		3.07 × 10 ⁻³	1.66 × 10 ⁵		
		4.60 × 10 ⁻³	2.46 × 10 ⁵		
		6.14 × 10 ⁻³	3.23 × 10 ⁵		
		7.67 × 10 ⁻³	4.14 × 10 ⁵		
(mor) ₂ CH ⁺	[2-BF ₄] ⁻ = 4.00 × 10 ⁻⁵	5.00 × 10 ⁻³	3.60 × 10 ⁵		6.53 × 10 ⁷
		1.00 × 10 ⁻²	7.70 × 10 ⁵		
		1.50 × 10 ⁻²	1.04 × 10 ⁶		
		2.00 × 10 ⁻²	1.34 × 10 ⁶		
		2.50 × 10 ⁻²	1.71 × 10 ⁶		
(dpa) ₂ CH ⁺	[2-BF ₄] ⁻ = 2.00 × 10 ⁻⁵	1.00 × 10 ⁻³	4.98 × 10 ⁵		1.87 × 10 ⁸
		2.00 × 10 ⁻³	7.23 × 10 ⁵		
		3.00 × 10 ⁻³	9.14 × 10 ⁵		
		4.00 × 10 ⁻³	1.09 × 10 ⁶		
		5.00 × 10 ⁻³	1.25 × 10 ⁶		
(mfa) ₂ CH ⁺	[2-BF ₄] ⁻ = 3.00 × 10 ⁻⁵	1.07 × 10 ⁻³	4.34 × 10 ⁵		4.86 × 10 ⁸
		2.15 × 10 ⁻³	9.32 × 10 ⁵		
		3.22 × 10 ⁻³	1.47 × 10 ⁶		
		4.30 × 10 ⁻³	1.96 × 10 ⁶		
		5.37 × 10 ⁻³	2.43 × 10 ⁶		

Table 9.S.4 (Continued). Kinetics of the reactions of *N*-methylpyrrolidine (**1b**) with Ar₂CH⁺ in CH₂Cl₂ at 20 °C.

Cation	[cation] / M	[1b] / M	k_{obs} / s^{-1}	$\lambda = 601 \text{ nm}$	$k_2 / M^{-1}s^{-1}$
(pfa) ₂ CH ⁺	[2-BF ₄] ⁻ = 3.00 × 10 ⁻⁵	1.00 × 10 ⁻³	6.00 × 10 ⁵		6.31 × 10 ⁸
		2.00 × 10 ⁻³	1.20 × 10 ⁶		
		3.00 × 10 ⁻³	1.82 × 10 ⁶		
		4.00 × 10 ⁻³	2.49 × 10 ⁶		
		5.00 × 10 ⁻³	3.11 × 10 ⁶		
Cation	[precursor] / M	[1b] / M	k_{obs} / s^{-1}	$\lambda = 530 \text{ nm}$	$k_2 / M^{-1}s^{-1}$
(fur) ₂ CH ⁺	[4-BF ₄] ⁻ = 5.00 × 10 ⁻⁵	1.00 × 10 ⁻³	1.50 × 10 ⁶		1.65 × 10 ⁹
		2.00 × 10 ⁻³	3.21 × 10 ⁶		
		3.00 × 10 ⁻³	4.91 × 10 ⁶		
		4.00 × 10 ⁻³	6.65 × 10 ⁶		
		5.00 × 10 ⁻³	8.01 × 10 ⁶		
Cation	[precursor] / M	[1b] / M	k_{obs} / s^{-1}	$\lambda = 512 \text{ nm}$	$k_2 / M^{-1}s^{-1}$
(ani) ₂ CH ⁺	[4-BF ₄] ⁻ = 2.00 × 10 ⁻⁵	1.00 × 10 ⁻³	3.86 × 10 ⁶		3.05 × 10 ⁹
		2.00 × 10 ⁻³	7.16 × 10 ⁶		
		3.00 × 10 ⁻³	9.78 × 10 ⁶		
		4.00 × 10 ⁻³	1.30 × 10 ⁷		
		5.00 × 10 ⁻³	1.62 × 10 ⁷		
Cation	[precursor] / M	[1b] / M	k_{obs} / s^{-1}	$\lambda = 472 \text{ nm}$	$k_2 / M^{-1}s^{-1}$
(to) ₂ CH ⁺	[4-BF ₄] ⁻ = 5.00 × 10 ⁻⁵	1.00 × 10 ⁻³	2.94 × 10 ⁶		3.55 × 10 ⁹
		2.00 × 10 ⁻³	6.33 × 10 ⁶		
		3.00 × 10 ⁻³	9.90 × 10 ⁶		
		4.00 × 10 ⁻³	1.34 × 10 ⁷		
		5.00 × 10 ⁻³	1.71 × 10 ⁷		

Table 9.S.4 (Continued). Kinetics of the reactions of *N*-methylpyrrolidine (**1b**) with Ar₂CH⁺ in CH₂Cl₂ at 20 °C.

Cation	[precursor] / M	[1b] / M	$k_{\text{obs}} / \text{s}^{-1}$	$\lambda = 460 \text{ nm}$	$k_2 / \text{M}^{-1}\text{s}^{-1}$
(Ph)(tol)CH ⁺	[4-BF ₄ ⁻] = 5.00 × 10 ⁻⁵	1.00 × 10 ⁻³	3.63 × 10 ⁶		3.66 × 10 ⁹
		2.00 × 10 ⁻³	6.36 × 10 ⁶		
		3.00 × 10 ⁻³	9.76 × 10 ⁶		
		5.00 × 10 ⁻³	1.81 × 10 ⁷		

Table 9.S.5. Kinetics of the reactions of *N*-methylpiperidine (**1c**) with Ar₂CH⁺ in CH₃CN at 20 °C.

Cation	[cation] / M	[1c] / M	$k_{\text{obs}} / \text{s}^{-1}$	$\lambda = 605 \text{ nm}$	$k_2 / \text{M}^{-1}\text{s}^{-1}$
(dma) ₂ CH ⁺	[2-BF ₄ ⁻] = 5.00 × 10 ⁻⁵	2.00 × 10 ⁻²	3.93 × 10 ⁴		(1.4 × 10 ⁶) ^a
		5.00 × 10 ⁻²	8.76 × 10 ⁴		
		1.00 × 10 ⁻¹	1.46 × 10 ⁵		
		1.50 × 10 ⁻¹	2.11 × 10 ⁵		
		2.00 × 10 ⁻¹	2.82 × 10 ⁵		
		2.50 × 10 ⁻¹	3.77 × 10 ⁵		

Cation	[cation] / M	[1c] / M	$k_{\text{obs}} / \text{s}^{-1}$	$\lambda = 613 \text{ nm}$	$k_2 / \text{M}^{-1}\text{s}^{-1}$
(mpa) ₂ CH ⁺	[2-BF ₄ ⁻] = 1.95 × 10 ⁻⁵	1.10 × 10 ⁻³	8.67 × 10 ³		6.61 × 10 ⁶
		2.19 × 10 ⁻³	1.53 × 10 ⁴		
		3.29 × 10 ⁻³	2.29 × 10 ⁴		
		4.38 × 10 ⁻³	2.97 × 10 ⁴		
		5.48 × 10 ⁻³	3.77 × 10 ⁴		

Cation	[cation] / M	[1c] / M	$k_{\text{obs}} / \text{s}^{-1}$	$\lambda = 612 \text{ nm}$	$k_2 / \text{M}^{-1}\text{s}^{-1}$
(mor) ₂ CH ⁺	[2-BF ₄ ⁻] = 1.98 × 10 ⁻⁵	1.10 × 10 ⁻³	5.97 × 10 ³		5.08 × 10 ⁶
		2.19 × 10 ⁻³	1.14 × 10 ⁴		
		3.29 × 10 ⁻³	1.68 × 10 ⁴		
		4.38 × 10 ⁻³	2.25 × 10 ⁴		
		5.48 × 10 ⁻³	2.83 × 10 ⁴		

Table 9.S.5 (Continued). Kinetics of the reactions of *N*-methylpiperidine (**1c**) with Ar₂CH⁺ in CH₃CN at 20 °C.

Cation	[cation] / M	[1c] / M	$k_{\text{obs}} / \text{s}^{-1}$	$\lambda = 644 \text{ nm}$	$k_2 / \text{M}^{-1}\text{s}^{-1}$
(dpa) ₂ CH ⁺	[2-BF ₄] = 4.00 × 10 ⁻⁵	1.00 × 10 ⁻³	4.31 × 10 ⁴		4.07 × 10 ⁷
		2.00 × 10 ⁻³	8.01 × 10 ⁴		
		3.00 × 10 ⁻³	1.17 × 10 ⁵		
		4.00 × 10 ⁻³	1.60 × 10 ⁵		
		5.00 × 10 ⁻³	2.07 × 10 ⁵		
(mfa) ₂ CH ⁺	[2-BF ₄] = 1.00 × 10 ⁻⁵	1.00 × 10 ⁻³	4.12 × 10 ⁴		4.00 × 10 ⁷
		2.00 × 10 ⁻³	7.77 × 10 ⁴		
		3.00 × 10 ⁻³	1.15 × 10 ⁵		
		4.00 × 10 ⁻³	1.59 × 10 ⁵		
		5.00 × 10 ⁻³	2.01 × 10 ⁵		
(pfa) ₂ CH ⁺	[2-BF ₄] = 2.00 × 10 ⁻⁵	1.00 × 10 ⁻³	1.45 × 10 ⁵		1.53 × 10 ⁸
		2.00 × 10 ⁻³	3.05 × 10 ⁵		
		3.00 × 10 ⁻³	4.69 × 10 ⁵		
		4.00 × 10 ⁻³	6.19 × 10 ⁵		
		5.00 × 10 ⁻³	7.50 × 10 ⁵		
(fu) ₂ CH ⁺	[4-BF ₄] = 1.29 × 10 ⁻⁵	5.23 × 10 ⁻⁴	4.73 × 10 ⁵		8.32 × 10 ⁸
		1.05 × 10 ⁻³	9.00 × 10 ⁵		
		1.57 × 10 ⁻³	1.33 × 10 ⁶		
		2.09 × 10 ⁻³	1.75 × 10 ⁶		
		2.61 × 10 ⁻³	2.22 × 10 ⁶		

Table 9.S.5 (Continued). Kinetics of the reactions of *N*-methylpiperidine (**1c**) with Ar₂CH⁺ in CH₃CN at 20 °C.

Cation	[precursor] / M	[1c] / M	k_{obs} / s^{-1}	$\lambda = 500 \text{ nm}$	$k_2 / M^{-1}s^{-1}$
(ani) ₂ CH ⁺	[4-BF ₄] ⁻ = 2.00 × 10 ⁻⁵	1.00 × 10 ⁻³	1.59 × 10 ⁶		1.68 × 10 ⁹
		2.00 × 10 ⁻³	3.24 × 10 ⁶		
		3.00 × 10 ⁻³	5.07 × 10 ⁶		
		4.00 × 10 ⁻³	6.62 × 10 ⁶		
		5.00 × 10 ⁻³	8.31 × 10 ⁶		
(tol) ₂ CH ⁺	[5] = 5.00 × 10 ⁻⁴	1.00 × 10 ⁻³	3.83 × 10 ⁶		2.97 × 10 ⁹
		2.00 × 10 ⁻³	7.12 × 10 ⁶		
		3.00 × 10 ⁻³	1.02 × 10 ⁷		
		4.00 × 10 ⁻³	1.30 × 10 ⁷		
		5.00 × 10 ⁻³	1.57 × 10 ⁷		
Ph ₂ CH ⁺	[5] = 1.00 × 10 ⁻³	5.00 × 10 ⁻⁴	5.27 × 10 ⁶		3.71 × 10 ⁹
		1.00 × 10 ⁻³	7.32 × 10 ⁶		
		1.50 × 10 ⁻³	9.16 × 10 ⁶		
		2.00 × 10 ⁻³	1.12 × 10 ⁷		
		2.50 × 10 ⁻³	1.31 × 10 ⁷		
		3.00 × 10 ⁻³	1.39 × 10 ⁷		
		4.00 × 10 ⁻³	1.81 × 10 ⁷		
		5.00 × 10 ⁻³	2.24 × 10 ⁷		

↳ Some non-monoexponential component.

Table 9.S.6. Kinetics of the reactions of *N*-methylpiperidine (**1c**) with Ar₂CH⁺ in CH₂Cl₂ at 20 °C.

Cation	[cation] / M	[1c] / M	$k_{\text{obs}} / \text{s}^{-1}$	$\lambda = 644 \text{ nm}$	$k_2 / \text{M}^{-1}\text{s}^{-1}$
(dpa) ₂ CH ⁺	[2-BF ₄] ⁻ = 1.96 × 10 ⁻⁵	1.05 × 10 ⁻³	2.57 × 10 ⁴		(3 × 10 ⁷) ^a
		1.97 × 10 ⁻³	5.51 × 10 ⁴		
		3.15 × 10 ⁻³	9.05 × 10 ⁴		
		3.95 × 10 ⁻³	1.16 × 10 ⁵		
		5.25 × 10 ⁻³	1.51 × 10 ⁵		
(mfa) ₂ CH ⁺	[2-BF ₄] ⁻ = 2.13 × 10 ⁻⁵	1.05 × 10 ⁻³	7.83 × 10 ⁴		7.79 × 10 ⁷
		1.97 × 10 ⁻³	1.34 × 10 ⁵		
		3.15 × 10 ⁻³	2.40 × 10 ⁵		
		3.95 × 10 ⁻³	3.16 × 10 ⁵		
		5.25 × 10 ⁻³	3.92 × 10 ⁵		
(pfa) ₂ CH ⁺	[4-BF ₄] ⁻ = 2.00 × 10 ⁻⁵	1.00 × 10 ⁻³	1.31 × 10 ⁵		1.45 × 10 ⁸
		2.00 × 10 ⁻³	2.63 × 10 ⁵		
		3.00 × 10 ⁻³	4.04 × 10 ⁵		
		4.00 × 10 ⁻³	5.52 × 10 ⁵		
		5.00 × 10 ⁻³	7.12 × 10 ⁵		
(fur) ₂ CH ⁺	[4-BF ₄] ⁻ = 2.00 × 10 ⁻⁵	1.00 × 10 ⁻³	5.70 × 10 ⁵		5.96 × 10 ⁸
		2.00 × 10 ⁻³	1.14 × 10 ⁶		
		3.00 × 10 ⁻³	1.73 × 10 ⁶		
		4.00 × 10 ⁻³	2.36 × 10 ⁶		
		5.00 × 10 ⁻³	2.94 × 10 ⁶		

Table 9.S.6 (Continued). Kinetics of the reactions of *N*-methylpiperidine (**1c**) with Ar₂CH⁺ in CH₂Cl₂ at 20 °C.

Cation	[precursor] / M	[1c] / M	k_{obs} / s^{-1}	$\lambda = 512 \text{ nm}$	$k_2 / M^{-1}s^{-1}$
(ani) ₂ CH ⁺	[4-BF ₄] ⁻ = 2.00 × 10 ⁻⁵	1.00 × 10 ⁻³	1.21 × 10 ⁶		1.27 × 10 ⁹
		2.00 × 10 ⁻³	2.43 × 10 ⁶		
		3.00 × 10 ⁻³	3.72 × 10 ⁶		
		4.00 × 10 ⁻³	5.00 × 10 ⁶		
		5.00 × 10 ⁻³	6.28 × 10 ⁶		
(tol) ₂ CH ⁺	[4-BF ₄] ⁻ = 5.00 × 10 ⁻⁵	1.00 × 10 ⁻³	2.33 × 10 ⁶		2.00 × 10 ⁹
		2.00 × 10 ⁻³	4.39 × 10 ⁶		
		3.00 × 10 ⁻³	6.39 × 10 ⁶		
		4.00 × 10 ⁻³	8.15 × 10 ⁶		
		5.00 × 10 ⁻³	1.05 × 10 ⁷		

^b) Some non-monoexponential component.

Table 9.S.7. Kinetics of the reactions of *N*-methylmorpholine (**1d**) with Ar₂CH⁺ in CH₃CN at 20 °C.

Cation	[cation] / M	[1d] / M	k_{obs} / s^{-1}	$\lambda = 612 \text{ nm}$	$k_2 / M^{-1}s^{-1}$
(mor) ₂ CH ⁺	[2-BF ₄] ⁻ = 2.00 × 10 ⁻⁵	5.00 × 10 ⁻²	3.97 × 10 ⁴		6.73 × 10 ⁵
		1.00 × 10 ⁻¹	8.04 × 10 ⁴		
		1.50 × 10 ⁻¹	1.23 × 10 ⁵		
		2.00 × 10 ⁻¹	1.46 × 10 ⁵		
		2.50 × 10 ⁻¹	1.75 × 10 ⁵		

Table 9.S.7 (Continued). Kinetics of the reactions of *N*-methylmorpholine (**1d**) with Ar₂CH⁺ in CH₃CN at 20 °C.

Cation	[cation] / M	[1d] / M	k_{obs} / s^{-1}	$\lambda = 644 \text{ nm}$	$k_2 / M^{-1}s^{-1}$
(dpa) ₂ CH ⁺	[2-BF ₄] = 1.00 × 10 ⁻⁵	1.00 × 10 ⁻³	7.19 × 10 ³		5.06 × 10 ⁶
		2.00 × 10 ⁻³	1.35 × 10 ⁴		
		3.00 × 10 ⁻³	1.75 × 10 ⁴		
		4.00 × 10 ⁻³	2.28 × 10 ⁴		
		5.00 × 10 ⁻³	2.78 × 10 ⁴		
(mfa) ₂ CH ⁺	[2-BF ₄] = 2.11 × 10 ⁻⁵	2.00 × 10 ⁻³	1.30 × 10 ⁴		4.36 × 10 ⁶
		2.86 × 10 ⁻³	1.68 × 10 ⁴		
		4.86 × 10 ⁻³	2.45 × 10 ⁴		
		5.72 × 10 ⁻³	2.90 × 10 ⁴		
		7.15 × 10 ⁻³	3.57 × 10 ⁴		
(pfa) ₂ CH ⁺	[2-BF ₄] = 1.00 × 10 ⁻⁵	1.00 × 10 ⁻³	2.16 × 10 ⁴		1.63 × 10 ⁷
		2.00 × 10 ⁻³	3.84 × 10 ⁴		
		3.00 × 10 ⁻³	5.35 × 10 ⁴		
		4.00 × 10 ⁻³	7.09 × 10 ⁴		
		5.00 × 10 ⁻³	8.66 × 10 ⁴		
(fur) ₂ CH ⁺	[4-BF ₄] = 1.75 × 10 ⁻⁵	9.70 × 10 ⁻⁴	2.66 × 10 ⁵		2.71 × 10 ⁸
		1.94 × 10 ⁻³	5.14 × 10 ⁵		
		2.91 × 10 ⁻³	7.71 × 10 ⁵		
		3.88 × 10 ⁻³	1.04 × 10 ⁶		
		4.85 × 10 ⁻³	1.32 × 10 ⁶		

Table 9.S.7 (Continued). Kinetics of the reactions of *N*-methylmorpholine (**1d**) with Ar₂CH⁺ in CH₃CN at 20 °C.

Cation	[precursor] / M	[1d] / M	$k_{\text{obs}} / \text{s}^{-1}$	$\lambda = 500 \text{ nm}$	$k_2 / \text{M}^{-1}\text{s}^{-1}$
(ani) ₂ CH ⁺	[6] = 5.00×10^{-5}	1.00×10^{-3}	1.52×10^6	<p>A scatter plot showing the observed rate constant $k_{\text{obs}} / \text{s}^{-1}$ on the y-axis (ranging from 0.0E+00 to 7.0E+06) versus the concentration of 1d / M on the x-axis (ranging from 0 to 0.008). The data points show a linear relationship with a regression line. The equation is $y = 8.38\text{E}+08x + 6.15\text{E}+05$ and the coefficient of determination is $R^2 = 0.9933$.</p>	8.38×10^8
		2.00×10^{-3}	2.36×10^6		
		3.00×10^{-3}	3.07×10^6		
		4.00×10^{-3}	3.76×10^6		
		5.00×10^{-3}	4.78×10^6		
		6.00×10^{-3}	5.80×10^6		
(tol) ₂ CH ⁺	[5] = 5.00×10^{-4}	1.00×10^{-3}	3.74×10^6	<p>A scatter plot showing the observed rate constant $k_{\text{obs}} / \text{s}^{-1}$ on the y-axis (ranging from 0.0E+00 to 1.6E+07) versus the concentration of 1d / M on the x-axis (ranging from 0 to 0.006). The data points show a linear relationship with a regression line. The equation is $y = 2.66\text{E}+09x + 1.27\text{E}+06$ and the coefficient of determination is $R^2 = 0.997$.</p>	2.66×10^9
		2.00×10^{-3}	6.69×10^6		
		3.00×10^{-3}	9.56×10^6		
		4.00×10^{-3}	1.17×10^7		
		5.00×10^{-3}	1.45×10^7		
		Ph ₂ CH ⁺	[5] = 1.00×10^{-3}		
2.00×10^{-3}	9.43×10^6				
4.00×10^{-3}	1.45×10^7				
5.00×10^{-3}	1.69×10^7				

Table 9.S.8. Kinetics of the reactions of *N*-methylmorpholine (**1d**) with Ar₂CH⁺ in CH₂Cl₂ at 20 °C.

Cation	[precursor] / M	[1d] / M	$k_{\text{obs}} / \text{s}^{-1}$	$\lambda = 530 \text{ nm}$	$k_2 / \text{M}^{-1}\text{s}^{-1}$
(flu) ₂ CH ⁺	[4-BF ₄ ⁻] = 1.63×10^{-5}	1.01×10^{-3}	8.19×10^4	<p>A scatter plot showing the observed rate constant $k_{\text{obs}} / \text{s}^{-1}$ on the y-axis (ranging from 0.0E+00 to 5.0E+05) versus the concentration of 1d / M on the x-axis (ranging from 0 to 0.008). The data points show a linear relationship with a regression line. The equation is $y = 7.10\text{E}+07x + 1.34\text{E}+04$ and the coefficient of determination is $R^2 = 0.9994$.</p>	7.10×10^7
		2.03×10^{-3}	1.57×10^5		
		3.04×10^{-3}	2.34×10^5		
		4.06×10^{-3}	3.03×10^5		
		5.07×10^{-3}	3.75×10^5		
		6.38×10^{-3}	4.62×10^5		

Table 9.S.9. Determination of N and s_N parameters for **1b** and **1c** in in CH_3CN .*N*-methylpyrrolidine (**1b**) in CH_3CN :

Cation	E	$k_2 / \text{M}^{-1}\text{s}^{-1}$	N	s
(dpa) ₂ CH ⁺	(not used; $> 2 \times 10^8$)		20.59	0.52
(mor) ₂ CH ⁺	-5.53	6.39×10^7		
(mpa) ₂ CH ⁺	(not used; see text)			
(dma) ₂ CH ⁺	-7.02	1.22×10^7		
(pyr) ₂ CH ⁺	-7.69	7.19×10^6		
(thc) ₂ CH ⁺	-8.22	2.08×10^6		
(ind) ₂ CH ⁺	(not used; not first order)			

N-methylpiperidine (**1b**) in CH_3CN :

Cation	E	$k_2 / \text{M}^{-1}\text{s}^{-1}$	N	s
(fur) ₂ CH ⁺	(not used; $> 2 \times 10^8$)		18.72	0.52
(pfa) ₂ CH ⁺	-3.14	1.53×10^8		
(mfa) ₂ CH ⁺	-3.85	4.00×10^7		
(dpa) ₂ CH ⁺	(not used; see text)			
(mor) ₂ CH ⁺	-5.53	5.08×10^6		
(mpa) ₂ CH ⁺	(not used; see text)			
(dma) ₂ CH ⁺	-7.02	1.40×10^6		
(pyr) ₂ CH ⁺	(no reaction)			

Table 9.S.10. Determination of N parameters for **1a,d** in CH_3CN and **1a-d** in CH_2Cl_2 from individual rate constants, using $s_N = 0.52$.

triethylamine (1a) in CH_3CN				
Cation	E	$k_2 / \text{M}^{-1}\text{s}^{-1}$	$N = (\log k)/0.52 - E$	N (mean)
(fur) ₂ CH ⁺	-1.36	1.91×10^8	17.3	
(pfa) ₂ CH ⁺	-3.14	1.4×10^7	16.9	17.1
triethylamine (1a) in CH_2Cl_2				
Cation	E	$k_2 / \text{M}^{-1}\text{s}^{-1}$	$N = (\log k)/0.52 - E$	N (mean)
(fur) ₂ CH ⁺	-1.36	1.96×10^8	17.3	17.3
<i>N</i> -methylpyrrolidine (1b) in CH_2Cl_2				
Cation	E	$k_2 / \text{M}^{-1}\text{s}^{-1}$	$N = (\log k)/0.52 - E$	N (mean)
(dpa) ₂ CH ⁺	-4.72	1.87×10^8	20.6	
(mor) ₂ CH ⁺	-5.53	6.53×10^7	20.6	
(mpa) ₂ CH ⁺	-5.89	5.29×10^7	20.7	20.6
<i>N</i> -methylpiperidine (1c) in CH_2Cl_2				
Cation	E	$k_2 / \text{M}^{-1}\text{s}^{-1}$	$N = (\log k)/0.52 - E$	N (mean)
(pfa) ₂ CH ⁺	-3.14	1.45×10^8	18.8	
(mfa) ₂ CH ⁺	-3.85	7.79×10^7	19.0	18.9
<i>N</i> -methylmorpholine (1d) in CH_3CN				
Cation	E	$k_2 / \text{M}^{-1}\text{s}^{-1}$	$N = (\log k)/0.52 - E$	N (mean)
(pfa) ₂ CH ⁺	-3.14	1.63×10^7	17.0	
(mfa) ₂ CH ⁺	-3.85	4.36×10^6	16.6	
(dpa) ₂ CH ⁺	(not used; see text)			
(mor) ₂ CH ⁺	-5.53	6.73×10^5	16.7	16.8
<i>N</i> -methylmorpholine (1d) in CH_2Cl_2				
Cation	E	$k_2 / \text{M}^{-1}\text{s}^{-1}$	$N = (\log k)/0.52 - E$	N (mean)
(fur) ₂ CH ⁺	-1.36	7.10×10^7	16.5	16.5

Photogeneration of Benzhydryl Cations by Near-UV Laser Flash Photolysis of Pyridinium Salts

Tobias A. Nigst, Johannes Ammer, and Herbert Mayr

J. Phys. Chem. A **2012**, *116*, 8494-8499

10.1 Introduction

Pyridinium salts have a rich photochemistry¹ which includes their use as photoinitiators in cationic polymerizations.²⁻⁴ However, the heterolytic cleavage of the exocyclic C–N bond of *N*-alkylated pyridinium ions was only found in a few cases.⁴ The observation that photolyses of related onium salts, such as phosphonium^{5,6} or ammonium salts,^{7,8} gave excellent yields of carbocations thus prompted us to investigate substituted pyridinium salts as precursors for the carbocations. The use of highly substituted aminopyridines as photoleaving groups promised a good wavelength tunability, which would be interesting for applications as photoinitiators^{9,10} and for kinetic investigations of carbocation reactivities.

Many bimolecular reactions of carbocations proceed on a timescale from nanoseconds to microseconds, which requires short pump pulses for time-resolved measurements. The most common and most affordable source of light pulses with pulse widths of a few nanoseconds is the Nd/YAG laser.¹¹ Its fundamental emission in the infrared region (1064 nm) can be converted to the second, third, or fourth harmonic to generate laser pulses in the visible (532 nm) or UV range (355 or 266 nm). In the following discussion, we used the Nd/YAG laser as an example to address some problems related to the choice of excitation wavelength in laser flash photolysis experiments, but similar problems will also be encountered with other types of lasers (including tunable lasers). In previous investigations, we have generated benzhydryl cations **1** and other carbocations by heterolytic photocleavage of precursor molecules such as arylmethyl halides¹² or arylmethyl triarylphosphonium salts⁶ which have significant UV absorbances at 266 nm, but not at 355 nm (Scheme 10.1). Typically, the carbocations were obtained by irradiating precursor solutions with $A_{266 \text{ nm}} \approx 0.1\text{-}1.0$ with a 266 nm laser pulse; subsequently, the UV/vis absorption decays of the carbocations were monitored in the presence of the nucleophilic reaction partners.^{8,13}

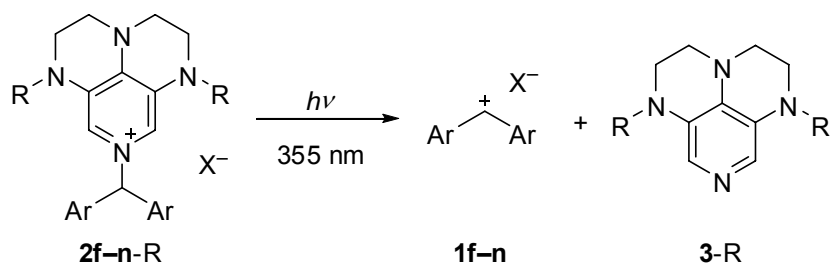
Scheme 10.1. Photoheterolysis of Substrates R–PLG (Photoleaving Group $\text{PLG}^- = \text{Cl}^-, \text{PR}'_3,$ etc.) and Subsequent Trapping of the Generated Carbocations (R^+) by Nucleophiles (Nu).



This procedure is problematic when the reaction partners also have considerable absorbances at the excitation wavelength of 266 nm. In this case, the laser pulse may also generate reactive intermediates from the nucleophilic reaction partner, and we can no longer be sure which process is causing the decay of the carbocation. In the usual experimental setup¹¹ featuring a 90° angle between pump and probe light, the opacity of the sample solutions for the 266 nm pump pulse also prevents sufficient excitation of the precursor molecules to generate the carbocations. The same problems not only occur when the nucleophilic reaction partner absorbs at 266 nm but also occur when experiments are carried out in solvents with a high UV cutoff, such as *N,N*-dimethylformamide (DMF), dimethyl sulfoxide (DMSO), or acetone.

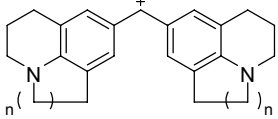
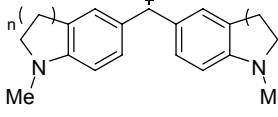
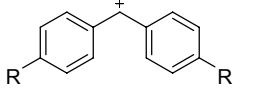
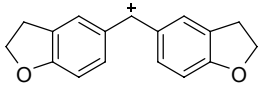
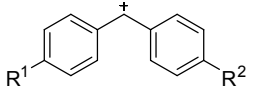
In such cases, the third harmonic of the Nd/YAG laser (355 nm) would be suitable as a pump, but onium salts do not usually absorb at this wavelength. The use of photosensitizers, a common strategy for photoinitiator systems,^{9,10} cannot be employed for kinetic studies because the diffusion-limited bimolecular excitation transfer is too slow. It was, therefore, desirable to develop a carbocation precursor that can be irradiated at 355 nm. For this purpose, we took advantage of the fact that amino substitution of pyridinium salts causes red shifts of the UV absorptions.^{1a} In this work, we report the generation of benzhydryl cations **1f-n** by 355 nm irradiation of benzhydryl pyridinium salts **2f-n-R** derived from 3,4,5-triamino-substituted pyridines **3-R**, the so-called super-DMAPs^{14,15} (Scheme 10.2).

Scheme 10.2. Generation of Benzhydrylium Ions **1f-n** by 355 nm Laser Flash Photolysis of Pyridinium Ions **2f-n-R** with Different Substituents (R) on the Pyridine Moiety.^a



^a For substitution patterns f-n of the benzhydryl moiety, see Table 10.1. Counteranion $\text{X}^- = \text{Cl}^-$ or BF_4^- .

Table 10.1. List of the Reference Electrophiles **1** Used in This Study.

reference electrophile		E^a
	$n = 1$	1a -10.04
	$n = 2$	1b -9.45
	$n = 1$	1c -8.76
	$n = 2$	1d -8.22
	R = <i>N</i> -pyrrolidino	1e -7.69
	R = NMe ₂	1f -7.02
	R = N(Me)Ph	1g -5.89
	R = <i>N</i> -morpholino	1h -5.53
	R = N(Me)CH ₂ CF ₃	1i -3.85
		1j -1.36
	R ¹ = R ² = OMe	1k 0.00
	R ¹ = OMe, R ² = H	1l 2.11
	R ¹ = R ² = Me	1m 3.63
	R ¹ = Me, R ² = H	1n 4.43 ^b
	R ¹ = R ² = H	1o 5.47 ^b

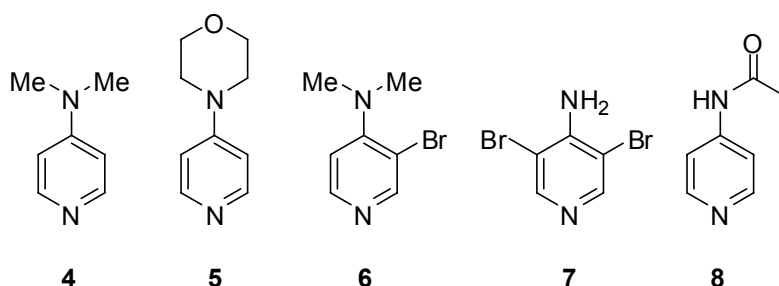
^a Electrophilicity parameters, E , were taken from ref 18a, unless noted otherwise. ^b From ref 6b.

For testing our approach, we measured the rate constants of the reactions of benzhydrylium ions **1** (Table 10.1) with pyridines **4-8** (Chart 10.1). Pyridines have strong UV absorptions below 300 nm and are known to undergo photoisomerizations via azaprefulvenes or Dewar-pyridines upon ~254 nm irradiation.¹⁶ Therefore, their reactivities cannot be characterized readily with a method that uses 266 nm pump pulses. Rate constants of the reactions of photolytically generated carbocations with pyridines could previously only be determined when the employed precursors incorporated a highly conjugated π system which absorbed at $\lambda > 300$ nm.¹⁷ The reactivity data acquired in this study will subsequently be employed to determine the nucleophilicity parameters, N and s_N , for the pyridines **4-8** according to the linear free energy relationship eq 1, which allows us to predict second-order rate constants, k_2 ,

for polar organic reactions with one electrophile-specific parameter, E , and two solvent-dependent nucleophile-specific parameters, N and s_N .¹⁸

$$\log k_2(20\text{ }^\circ\text{C}) = s_N(N + E) \quad (1)$$

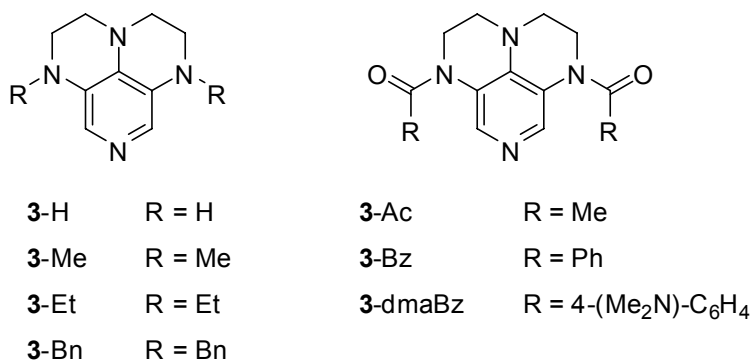
Chart 10.1. Pyridines Employed as Nucleophiles in This Study.



10.2 Results and Discussion

10.2.1 Photogeneration of Benzhydrylium Ions. Since the photoelectrofuges (i.e., carbocations-to-be) do not absorb at 355 nm, the excitation must occur at the photonucleofuge (i.e., PLG moiety in Scheme 10.1). Our recent investigation of 3,4,5-triamino-substituted pyridines **3-R** (Chart 10.2) showed that these compounds are strong Lewis bases and that the pyridinium ions **2-R** (i.e., their adducts with benzhydrylium ions **1**) show UV absorptions around 355 nm.¹⁵

Chart 10.2. Pyridines Employed as Photoleaving Groups in this Study.^a



^a dmaBz = 4-(dimethylamino)benzoyl.

The pyridines **3-R** were obtained in four to six steps from 4-pyridone as described by David et al.¹⁵ In order to use the costly materials efficiently, we did not isolate the benzhydryl pyridinium tetrafluoroborates **2f-j-R** ($X^- = \text{BF}_4^-$) but generated them in solution by combining the pyridines **3-R** with solutions of the isolated^{18a} benzhydrylium tetrafluoroborates **1f-j** BF_4^- (i.e., the reverse of the reaction depicted in Scheme 10.2). The formation of the pyridinium salts **2f-j-R** was indicated by the immediate disappearance of the color of **1f-j** and the appearance of UV/vis absorption bands at 340–380 nm. The benzhydryl pyridinium chlorides **2j-o-R** ($X^- = \text{Cl}^-$) were obtained from reactions of **3-R** with the corresponding benzhydryl chlorides, $\text{Ar}_2\text{CH}-\text{Cl}$. The syntheses of **2n-R** and **2o-R** by this method required longer reaction times of 2 h or overnight, as revealed by the full development of the pyridinium bands in the UV/vis spectrum.

Figure 10.1 shows the UV/vis absorption spectra of several 1-benzhydryl pyridinium salts **2l-R** derived from the pyridines **3-R**. The parent compound **2l-H** (not shown) and the *N*-alkyl-substituted derivatives, **2l-Bn**, **2l-Me** (Figure 10.1), and **2l-Et** (not shown), have absorption maxima near 355 nm. The absorption maxima of the *N*-acyl-substituted compounds **2l-Ac** and **2l-Bz** (not shown) are too far in the UV but can be red shifted by the introduction of the NMe_2 substituent on the benzoyl group (\rightarrow **2l-dmaBz**, Figure 10.1). In agreement with previous reports,^{1a} the absorption maximum of the pyridinium salts does not depend on the substituent at the pyridine nitrogen atom (see Figure 10.S.1 in Section 10.S.2).

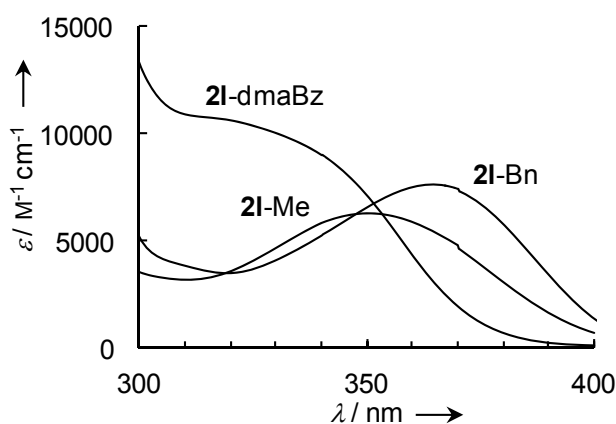


Figure 10.1. UV/vis absorption spectra of pyridinium salts **2l-R** ($X^- = \text{Cl}^-$) with different substituents.

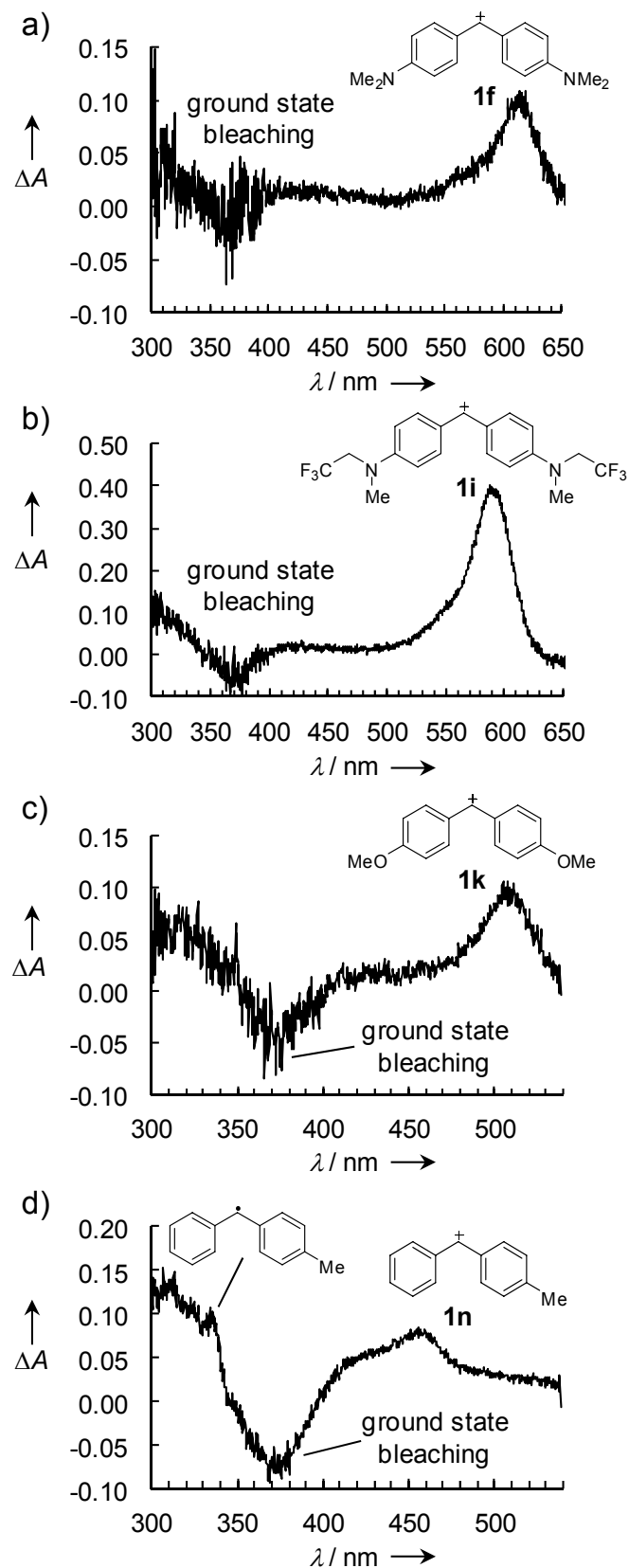


Figure 10.2. Transient UV/vis spectra obtained by irradiation of 1.2×10^{-4} M solutions of (a) **2f**-Bn ($\text{X}^- = \text{BF}_4^-$), (b) **2i**-Bn ($\text{X}^- = \text{BF}_4^-$), (c) **2k**-Bn ($\text{X}^- = \text{Cl}^-$), or (d) **2n**-Bn ($\text{X}^- = \text{Cl}^-$) in acetonitrile with a 7 ns laser pulse ($\lambda_{\text{exc}} = 355$ nm).

When we irradiated $\sim 1.2 \times 10^{-4}$ M solutions of the parent pyridinium salt **2i-l-H** or the *N*-alkyl derivatives **2i-l-Bn**, **2i-l-Me**, or **2i-l-Et** in CH₃CN with a 7 ns laser pulse from the frequency-tripled Nd/YAG laser ($\lambda_{\text{exc}} = 355$ nm, ~ 50 mJ/pulse), we detected the previously described¹² UV/vis absorption bands of the moderately stabilized benzhydrylium ions **1i-l** at $\lambda_{\text{max}} = 450$ -600 nm in the transient spectra and observed the disappearance (bleaching) of the pyridinium salts **2i-l-R** at ~ 350 -370 nm. Figure 10.2 shows the transient spectra obtained by irradiation of the *N*-benzyl-substituted pyridinium salts **2f-n-Bn** with different substituents on the benzhydryl moiety. The different absorbances of the benzhydrylium ions **1f-n** in Figure 10.2 (panels a-d) are mostly due to the different absorption coefficients and correspond to concentrations of the benzhydrylium ions of 0.6 - 2.3×10^{-6} M. The spectrum obtained by irradiation of **2n-Bn** ($X^- = \text{Cl}^-$) additionally shows a small band at ~ 338 nm, which we assign to the phenyl(*p*-tolyl)methyl radical by comparison with its previously published spectrum.¹² More electrophilic carbocations such as the parent benzhydrylium ion **1o** could not be obtained in concentrations which were sufficient for kinetic investigations; in these cases we mainly observed the benzhydryl radicals.

The yields and lifetimes of the carbocations **1i-l** obtained by photolysis of the parent pyridinium salts **2i-l-H** and the *N*-alkylated derivatives **2i-l-Bn**, **2i-l-Me**, and **2i-l-Et** were almost independent of the nature of the photonucleofuge **3-R**. Irradiation of the *N*-acyl derivative **2l-dmaBz**, however, did not yield any carbocations **1l**. For our kinetic investigations, we selected the *N*-benzyl derivatives **2-Bn** because the pyridine **3-Bn** has the highest Lewis basicity in the series¹⁵ and, therefore, forms the most stable pyridinium ions (see below).

In the photolyses of benzhydryl triphenylphosphonium salts, the yields and lifetimes of the benzhydryl cations greatly depend on the counteranion of the precursor salt.^{6a} The generation of benzhydryl radicals by electron transfer in electronically excited phosphonium chloride and bromide ion pairs was described, but this process is unimportant at low concentrations of the precursor salts in CH₃CN, as the phosphonium halides are mostly unpaired under these conditions.^{6a} However, the lifetimes of the photogenerated benzhydryl cations are reduced significantly by the diffusion-controlled reactions with the halide counteranions.^{6a} Therefore, we also investigated the influence of the counteranion in the photolysis of **2j-Bn** on the lifetime of the photogenerated carbocation **1j**. When we irradiated a 1.2×10^{-4} M solution of the pyridinium halide **2j-Bn** ($X^- = \text{Cl}^-$), we observed a monoexponential decay of the benzhydryl cation **1j** with a rate constant of $k_{\text{obs}} = 1.9 \times 10^6$ s⁻¹, which corresponds to a

second-order rate constant of $1.6 \times 10^{10} \text{ M}^{-1} \text{ s}^{-1}$ for the reaction of **1j** with **2j-Bn** Cl^- . As this value is slightly larger than the previously reported value of $9.39 \times 10^9 \text{ M}^{-1} \text{ s}^{-1}$ for the reaction of **1j** with Cl^- in acetonitrile,¹⁹ one might assign this decay to the combination of **1j** with chloride ions. On the other hand, when we employed the pyridinium tetrafluoroborate **2j-Bn** ($\text{X}^- = \text{BF}_4^-$) as a precursor, the decay of the benzhydryl cation **1j** was not monoexponential, and we found an initial fast decay with a rate constant comparable to that obtained with **2j-Bn** Cl^- , which was followed by a slower decay on the microsecond timescale. We explain this behavior by a fast reversible reaction of **1j** with the tertiary amine functions of the precursor salt **2j-Bn**, which is followed by a slower unidentified subsequent reaction. This behavior is analogous to that of other tertiary amines, where we also observed fast reversible reactions followed by slower decays due to unknown subsequent reactions.⁸ Due to the high nucleophilic reactivity of the tertiary amine centers of the precursors **2-Bn**, the choice of the counteranion X^- is thus not so important, and we did not convert the chlorides **2j-n-Bn** ($\text{X}^- = \text{Cl}^-$) to the tetrafluoroborates. Because of the proximity of the diffusion limit, the reactions of **1j-n** with chloride¹⁹ or tertiary amines⁸ proceed with almost the same rate constants, and we observed similar decay rates for all investigated benzhydrylium ions obtained from different precursors **2j-n-Bn** ($\text{X}^- = \text{Cl}^-$ or BF_4^-).

10.2.2 Kinetic Investigations. With a method at hand to generate the benzydrylium ions **1** using 355 nm laser pulses, we determined rate constants of reactions of **1** with nucleophiles. After irradiation of the pyridinium salts **2f-I-Bn** ($\sim 1.2 \times 10^{-4} \text{ M}$) in the presence of a large excess of added nucleophiles (7×10^{-4} to $1 \times 10^{-1} \text{ M}$), we observed monoexponential decays of the absorbances, A , of the photogenerated benzhydrylium ions **1f-I**, as illustrated in Figure 10.3 for the reaction of **1h** with DMAP (**4**). The decays of the absorbances were fitted with the exponential function $A_t = A_0 e^{-k_{\text{obs}} t} + C$ to obtain the first-order rate constants k_{obs} (s^{-1}). Plots of k_{obs} versus the nucleophile concentrations were linear in all cases, and the slopes of these plots provided the second-order rate constants k_2 ($\text{M}^{-1} \text{ s}^{-1}$) for the reactions of **1f-I** with the nucleophiles.

In order to study some systems of known reactivity, we measured the second-order rate constants, k_2 , for the reactions of some benzhydrylium ions **1** with 4-(dimethylamino)pyridine (DMAP, **4**) in acetonitrile (Table 10.2). The second-order rate constant for the reaction of **4** with **1f** was previously determined with the stopped-flow method,²⁰ and we wanted to reproduce this measurement with our new method.

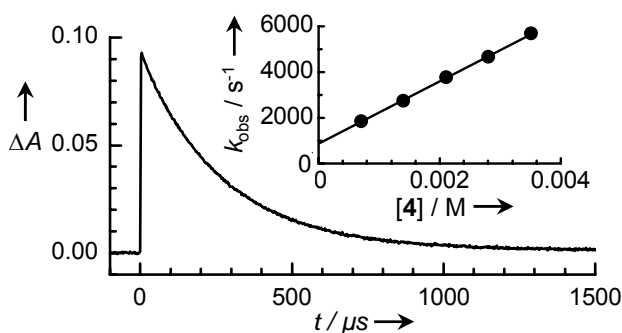
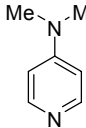
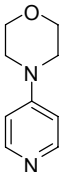
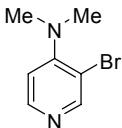
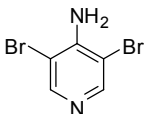
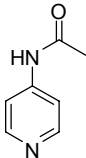


Figure 10.3. Plot of the absorbance decay of **1h** at $\lambda = 612$ nm observed after irradiation of **2h-Bn** (1.2×10^{-4} M, $X^- = \text{BF}_4^-$) with a 7 ns laser pulse ($\lambda_{\text{exc}} = 355$ nm, ~ 50 mJ/pulse) in the presence of 4-(dimethylamino)pyridine ($[4] = 2.12 \times 10^{-3}$ M). Inset: plot of k_{obs} vs $[4]$; $k_{\text{obs}} = 1.37 \times 10^6 [4] + 857$ ($R^2 = 0.9996$).

However, due to the similar electrofugalities of **1f** ($E_f = 4.84$) and **1c** ($E_f = 4.83$),²¹ the formation of **1f** by thermal dissociation of **2f-Bn** in acetonitrile solutions is expected to occur with a rate constant similar to that reported for the dissociation of **2c-Bn** ($9.6 \times 10^{-2} \text{ s}^{-1}$).¹⁵ In the presence of high concentrations of DMAP (**4**), the benzhydrylium ions **1f** will then be trapped by **4** to give a pyridinium salt with no absorption at 355 nm. As a consequence, we had to work quickly and keep the nucleophile concentration below ca. 5×10^{-3} M in order to maintain a sufficient concentration of **2f-Bn**, which is needed to generate the carbocation **1f** with the 355 nm laser pulse. The rate constant for the reaction of **4** with **1f** ($2.97 \times 10^5 \text{ M}^{-1} \text{ s}^{-1}$) determined in this way is in fair agreement with the previously reported value from stopped-flow experiments ($2.31 \times 10^5 \text{ M}^{-1} \text{ s}^{-1}$).²⁰

The rate constants for the reactions of **4** with **1h** and **1i** are too fast for the stopped-flow method and could not be measured with the established laser flash photolytic method using 266 nm laser pulses because **4** absorbs at the excitation wavelength. These rate constants could now be determined by laser flash photolysis of **2-Bn** at 355 nm (Table 10.2), and Figure 10.4 shows that these rate constants extend the correlation line for $\log k_2$ (**1a-d**), which was determined by stopped-flow experiments. If all available data are used to calculate the nucleophilicity parameters of **4**, we obtain $N = 15.51$ and $s_N = 0.62$ (Table 10.2), which deviate only slightly from the previously published values.²⁰

Table 10.2. Second-Order Rate Constants, k_2 , for the Reactions of the Reference Electrophiles **1** with the Pyridines **4-8** at 20 °C and Resulting N and s_N Parameters.

pyridine	N	s_N	Ar_2CH^+	$k_2^a / \text{M}^{-1}\text{s}^{-1}$
4 in CH_3CN 	15.51	0.62	1a	$2.11 \times 10^3^{b,c}$
			1b	$5.30 \times 10^3^{b,c}$
			1c	$1.29 \times 10^4^{b,c}$
			1d	$3.32 \times 10^4^{b,c}$
			1f	$2.31 \times 10^5^{b,c,d}$
			1f	$2.97 \times 10^5^d$
			1h	1.37×10^6
			1i	1.33×10^7
			1f	$1.53 \times 10^5^{b,c}$
			1i	$5.62 \times 10^6^e$
4 in DMSO			1f	$2.04 \times 10^5^{b,c}$
4 in DMF			1i	$7.97 \times 10^6^e$
4 in acetone			1i	$2.50 \times 10^7^e$
5 in CH_3CN 	14.80	0.63	1a	$7.27 \times 10^2^b$
			1c	$5.72 \times 10^3^b$
			1e	$4.42 \times 10^4^b$
			1f	$9.28 \times 10^4^{b,d}$
			1f	$1.36 \times 10^5^d$
			1h	6.30×10^5
			1i	6.39×10^6
6 in CH_3CN 	12.96	0.67	1e	$4.04 \times 10^3^b$
			1f	$1.00 \times 10^4^b$
			1g	$7.02 \times 10^4^b$
			1h	$5.76 \times 10^4^b$
			1i	$6.45 \times 10^5^b$
			1j	8.20×10^7
7 in CH_3CN 	11.11	0.75	1h	$1.63 \times 10^4^b$
			1i	$1.96 \times 10^5^b$
			1j	4.97×10^7
			1k	1.31×10^8
8 in CH_3CN 	13.24	0.67	1d	$2.38 \times 10^3^b$
			1e	$6.30 \times 10^3^b$
			1f	$1.76 \times 10^4^b$
			1h	$1.07 \times 10^5^b$
			1i	1.36×10^6
			1j	1.28×10^8

^a Laser flash photolysis of **2-Bn**, unless noted otherwise. ^b Stopped-flow UV/vis measurement. ^c From ref 20. ^d The average of both rate constants from laser flash photolysis and stopped-flow measurements was used for the correlation analysis. ^e With <1% acetonitrile as cosolvent.

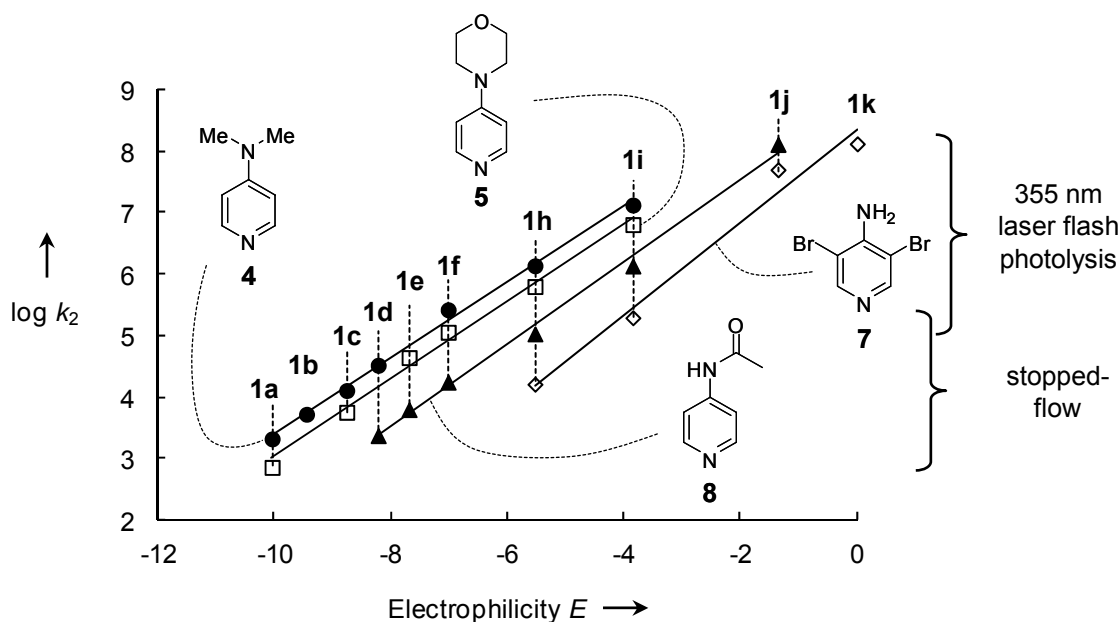


Figure 10.4. Plot of $\log k_2$ for reactions of benzhydrylium ions **1** with substituted pyridines **4-8** vs the electrophilicity parameters E of the benzhydrylium ions. The plot for **6** is not shown here because it overlaps with **8**.

Encouraged by the results with **4**, we determined second-order rate constants $k_2 > 10^5 \text{ M}^{-1} \text{ s}^{-1}$ for the reactions of **1f-k** with the substituted pyridines **5-8** (Table 10.2) in acetonitrile with the 355 nm laser flash photolytic method.²² These data are supplemented with rate constants for slower reactions ($k_2 < 10^6 \text{ M}^{-1} \text{ s}^{-1}$), which were determined with the stopped-flow method under first-order conditions by using the nucleophiles in a large excess (>10 equiv over the benzhydrylium tetrafluoroborates **1a-i**) as described previously^{18a} (Table 10.2). Again we observed good linear correlations of $\log k_2$ versus E (Figure 10.4) for the data from both methods. As previously observed, **1g**^{8,23a,b} (not shown) and **1j**^{23c} always react somewhat faster in acetonitrile solution than expected from their E parameters which have been determined in CH_2Cl_2 solutions.

In the case of **7**, only the reactions with **1h** and **1i** can be followed with the stopped-flow method, as the better stabilized carbocations show no conversion in reactions with **7** due to its low Lewis basicity. We have now been able to characterize the nucleophilicity of **7** over a wider reactivity range by including the data determined by the laser flash photolysis method.

From the correlations in Figure 10.4, we derived the nucleophilicity parameters of **4-8** listed in Table 10.2. As expected, the nucleophilicities of the 4-amino-substituted pyridines **4-7** decrease with the electron-withdrawing character of the substituents (Table 10.2 and Figure

10.4). The *N*-acetyl-4-aminopyridine (**8**) is of similar reactivity as the 3-bromo-substituted DMAP **6**.

To demonstrate the applicability of the method in solvents with high UV cutoff, we also measured the second-order rate constants for the reactions of **1i** with **4** in DMSO, DMF, and acetone (Table 10.2). The order of reactivity (acetone > acetonitrile > DMF > DMSO) agrees with that previously reported for the reactions of **4** with **1f**.²⁰ Furthermore, we determined first-order rate constants for the reactions of **1i** with 80% and 90% aqueous acetone (Table 10.3) and found good agreement between the experimental rate constants and the values calculated from eq 1 and the solvent nucleophilicity parameters, N_1 and s_N , of the acetone/water mixtures.²⁴

Table 10.3. Comparison of Experimental and Calculated First-Order Rate Constants (s^{-1}) for Reactions of **1i** with Acetone/Water Mixtures.

solvent ^a	k_1^b / s^{-1}	$k_{\text{calc}}^c / s^{-1}$	k_2 / k_{calc}
90A10W	6.23×10^6	4.35×10^6	1.43
80A20W	6.61×10^6	7.17×10^6	0.92

^a Mixtures given in v/v (A = acetone, W = water). ^b Laser flash photolysis of **2i**-Bn. ^c Calculated from eq 1 using the previously published N_1 and s_N parameters of acetone/water mixtures (90A10W: $N_1 = 5.70$, $s_N = 0.85$; 80A20W: $N_1 = 5.77$, $s_N = 0.87$).²⁴

10.3 Conclusion

We have demonstrated that the 355 nm laser flash photolysis of pyridinium salts **2**-Bn is a suitable method for the generation of benzhydrylium ions **1** in the presence of reactants or solvents that absorb at 266 nm. The scope of carbocations which can be generated is more restricted than in the 266 nm photolyses of quaternary phosphonium salts.^{6,8} Highly reactive carbocations such as **1o** cannot be generated efficiently, and the precursors **2**-Bn of carbocations, which are less Lewis-acidic than **1f**, are not stable in the presence of nucleophiles that trap the small concentrations of benzhydrylium ions, which exist in solutions of **2a-f**-Bn in the dark. Nevertheless, we could generate benzhydrylium ions **1f-n** covering more than 10 orders of reactivity and investigate the rates of their reactions with nucleophiles. We employed this method to characterize the nucleophilic reactivities of the electron-rich pyridines **5-8**, which will be used for further studies in our group. Moreover, we

have demonstrated that the third harmonic of the Nd/YAG laser (355 nm) can be employed to generate benzhydrylium ions **1** in solvents with a high UV cutoff such as acetone (cutoff = 330 nm)²⁵ which is opaque to the quadrupled Nd/YAG laser (266 nm) and the XeCl excimer laser (308 nm). Laser flash photolysis of substituted pyridinium salts at 355 nm thus supplements the established kinetic methods and is particularly useful for characterizing nucleophiles which do not react with stabilized carbocations for thermodynamic reasons and which cannot be studied with 266 nm laser flash photolytically generated carbocations due to the absorbance of the sample solutions.

10.4 Acknowledgment

We thank the Deutsche Forschungsgemeinschaft (SFB 749) and the Fonds der Chemischen Industrie for financial support and Raman Tandon for samples of **3**-Me and **3**-Et.

10.5 References and Notes

- (1) Reviews: (a) Knyazhanskii, M. I.; Tymyanskii, Y. R.; Feigelman, V. M.; Katritzky, A. R. *Heterocycles* **1987**, *26*, 2963–2982. (b) Mariano, P. S. In *CRC Handbook of Organic Photochemistry and Photobiology*, 2nd ed.; Horspool, W., Lenci, F., Eds.; CRC Press: Boca Raton, FL, 2004; pp 100-1–100-10. (c) Damiano, T.; Morton, D.; Nelson, A. *Org. Biomol. Chem.* **2007**, *5*, 2735–2752. (d) Zou, J.; Mariano, P. S. *Photochem. Photobiol. Sci.* **2008**, *7*, 393–404.
- (2) Review: Schnabel, W. *Macromol. Rapid Commun.* **2000**, *21*, 628–642.
- (3) General reviews on photoinitiators in cationic polymerizations: (a) Lazauskaite, R.; Grazulevicius, J. V. In *Handbook of Photochemistry and Photobiology*; Nalwa, H. S., Ed.; American Scientific Publishers: Stevenson Ranch, CA, 2003; Vol. 2, pp 335–392. (b) Yagci, Y.; Jockusch, S.; Turro, N. *Macromolecules* **2010**, *43*, 6245–6260. (c) Suyama, K.; Shirai, M. *Prog. Polym. Sci.* **2009**, *34*, 194–209.
- (4) (a) Kasapoglu, F.; Aydin, M.; Arsu, N.; Yagci, Y. *J. Photochem. Photobiol., A* **2003**, *159*, 151–159. (b) Yonet, N.; Bicak, N.; Yurtsever, M.; Yagci, Y. *Polym. Int.* **2007**, *56*, 525–531.

- (5) (a) Alonso, E. O.; Johnston, L. J.; Scaiano, J. C.; Toscano, V. G. *Can. J. Chem.* **1992**, *70*, 1784–1794. (b) Imrie, C.; Modro, T. A.; Rohwer, E. R.; Wagener, C. C. P. *J. Org. Chem.* **1993**, *58*, 5643–5649. (6) (a) Ammer, J.; Sailer, C. F.; Riedle, E.; Mayr, H. *J. Am. Chem. Soc.* **2012**, *134*, 11481–11494 (CHAPTER 2 of this work). (b) Ammer, J.; Nolte, C.; Mayr, H. *J. Am. Chem. Soc.* **2012**, *134*, 13902–13911 (CHAPTER 3 of this work).
- (7) McClelland, R. A.; Chan, C.; Cozens, F. L.; Modro, A.; Steenken, S. *Angew. Chem.* **1991**, *103*, 1389–1391; *Angew. Chem., Int. Ed.* **1991**, *30*, 1337–1339.
- (8) Ammer, J.; Baidya, M.; Kobayashi, S.; Mayr, H. *J. Phys. Org. Chem.* **2010**, *23*, 1029–1035 (CHAPTER 9 of this work).
- (9) Review on wavelength tunability in photoinitiated cationic polymerization: Aydogan, B.; Gacal, B.; Yildirim, A.; Yonet, N.; Yuksel, Y.; Yagci, Y. In *Photochemistry and UV Curing: New Trends*; Fouassier, J.-P., Ed.; Research Signpost: Kerala, India, 2006; pp 187–201.
- (10) Review on photoacid generation with tailored wavelengths: Crivello, J. V. J. *Photopolym. Sci. Technol.* **2008**, *21*, 493–497.
- (11) (a) Scaiano, J. C. In *Reactive Intermediate Chemistry*; Moss, R. A., Platz, M. S., Jones, M. J., Eds.; Wiley: Hoboken, NJ, 2004; pp 847–871. (b) Schepp, N. P.; Cozens, F. L. In *Lasers in Chemistry*; Lackner, M., Ed.; Wiley-VCH: Weinheim, Germany, 2008; Vol. 2, pp 1073–1091.
- (12) Bartl, J.; Steenken, S.; Mayr, H.; McClelland, R. A. *J. Am. Chem. Soc.* **1990**, *112*, 6918–6928.
- (13) Further recent examples: (a) Ammer, J.; Mayr, H. *Macromolecules* **2010**, *43*, 1719–1723 (CHAPTER 6 of this work). (b) Baidya, M.; Kobayashi, S.; Mayr, H. *J. Am. Chem. Soc.* **2010**, *132*, 4796–4805. (c) Streidl, N.; Branzan, R.; Mayr, H. *Eur. J. Org. Chem.* **2010**, 4205–4210. (d) Kanzian, T.; Lakhdar, S.; Mayr, H. *Angew. Chem.* **2010**, *122*, 9717–9720; *Angew. Chem., Int. Ed.* **2010**, *49*, 9526–9529. (e) Lakhdar, S.; Ammer, J.; Mayr, H. *Angew. Chem.* **2011**, *123*, 10127–10130; *Angew. Chem., Int. Ed.* **2011**, *50*, 9953–9956 (CHAPTER 7 of this work). (f) Horn, M.; Mayr, H. *Eur. J. Org. Chem.* **2011**, 6470–6475. (g) Troshin, K.; Schindele, C.; Mayr, H. *J. Org. Chem.* **2011**, *76*, 9391–9408. (h) Nigst, T. A.; Ammer, J.; Mayr, H. *Angew. Chem.* **2011**, *124*, 1381–1385; *Angew. Chem., Int. Ed.* **2011**, *51*, 1353–1356. (i) Nolte, C.; Ammer, J.; Mayr, H. *J. Org. Chem.* **2012**, *77*, 3325–3335.

- (14) (a) Singh, S.; Das, G.; Singh, O. V.; Han, H. *Org. Lett.* **2007**, *9*, 401–404. (b) Lindner, C.; Tandon, R.; Liu, Y.; Maryasin, B.; Zipse, H. *Org. Biomol. Chem.* **2012**, *10*, 3210–3218. (c) De Rycke, N.; Couty, F.; David, O. R. P. *Chem. Eur. J.* **2011**, *17*, 12852–12871.
- (15) De Rycke, N.; Berionni, G.; Couty, F.; Mayr, H.; Goumont, R.; David, O. R. P. *Org. Lett.* **2011**, *13*, 530–533.
- (16) (a) Review: Pavlik, J. W. In *CRC Handbook of Organic Photochemistry and Photobiology*, 2nd ed.; Horspool, W., Lenci, F., Eds.; CRC Press: Boca Raton, FL, **2004**; pp 97-1–97-22. (b) Pavlik, J. W.; Laohhasurayotin, S.; Vongnakorn, T. *J. Org. Chem.* **2007**, *72*, 7116–7124. (c) Pavlik, J. W.; Laohhasurayotin, S. *J. Org. Chem.* **2008**, *73*, 2746–2752.
- (17) Dembinski, A.; Yagci, Y.; Schnabel, W. *Polymer* **1993**, *34*, 3738–3740.
- (18) (a) Mayr, H.; Bug, T.; Gotta, M. F.; Hering, N.; Irrgang, B.; Janker, B.; Kempf, B.; Loos, R.; Ofial, A. R.; Remennikov, G.; Schimmel, H. *J. Am. Chem. Soc.* **2001**, *123*, 9500–9512. (b) Mayr, H.; Kempf, B.; Ofial, A. R. *Acc. Chem. Res.* **2003**, *36*, 66–77. (c) For a comprehensive database of nucleophilicity and electrophilicity parameters, see: <http://www.cup.lmu.de/oc/mayr/DBintro.html>.
- (19) Minegishi, S.; Loos, R.; Kobayashi, S.; Mayr, H. *J. Am. Chem. Soc.* **2005**, *127*, 2641–2649.
- (20) Brotzel, F.; Kempf, B.; Singer, T.; Zipse, H.; Mayr, H. *Chem. Eur. J.* **2007**, *13*, 336–345.
- (21) Streidl, N.; Denegri, B.; Kronja, O.; Mayr, H. *Acc. Chem. Res.* **2010**, *43*, 1537–1549.
- (22) Attack of the pyridine nitrogen in the reaction of **7** with 4,4'-dimethoxybenzhydryl chloride in CD₃CN was demonstrated by ¹H NMR experiments (see Supporting Information of *J. Phys. Chem. A* **2012**, *116*, 8494-8499 for details).
- (23) (a) Nigst, T. A.; Westermaier, M.; Ofial, A. R.; Mayr, H. *Eur. J. Org. Chem.* **2008**, 2369–2374. (b) Kędziorek, M.; Mayer, P.; Mayr, H. *Eur. J. Org. Chem.* **2009**, 1202–1206. (c) Nigst, T. A.; Antipova, A.; Mayr, H., *J. Org. Chem.* **2012**, *77*, 8142–8155.
- (24) Denegri, B.; Minegishi, S.; Kronja, O.; Mayr, H. *Angew. Chem.* **2004**, *116*, 2353–2356; *Angew. Chem., Int. Ed.* **2004**, *43*, 2302–2305.
- (25) Bruno, T. J.; Svoronos, P. D. N. *Handbook of Basic Tables for Chemical Analysis*, 2nd ed.; CRC Press: Boca Raton, FL, 2003.

10.S Supplementary Data and Experimental Section

10.S.1. Materials

Acetonitrile (> 99.9%, extra dry), DMSO (> 99.5%, extra dry), DMF (> 99.8%, extra dry), and acetone (> 99.9%, extra dry) were purchased and used without further purification. Water was distilled and passed through a Milli-Q water purification system.

10.S.2 UV/vis absorption spectra of pyridinium salts **2** in acetonitrile

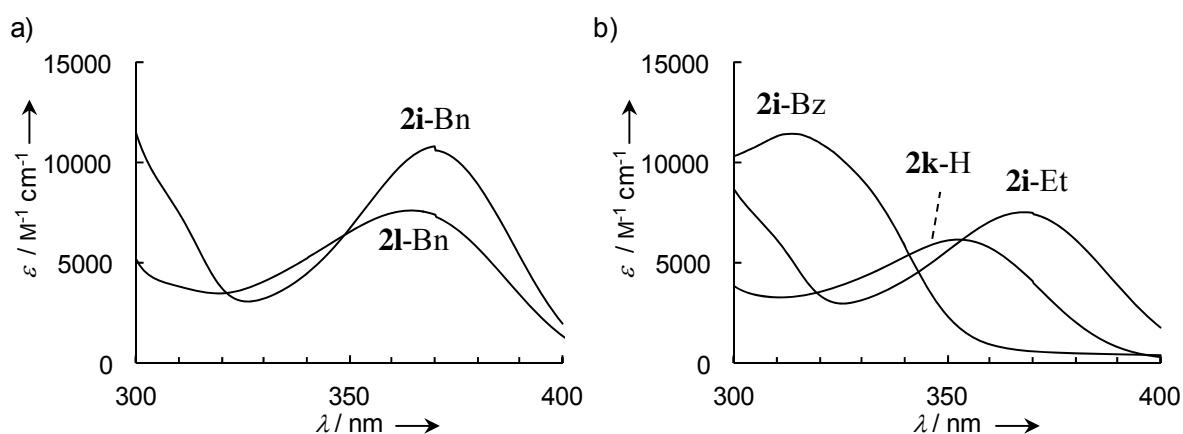


Figure 10.S.1. UV/vis absorption spectra of pyridinium salts **2**. (a) Independence of the absorption maxima on the substituents of the benzhydrylium ions for **2i-Bn** ($X^- = \text{BF}_4^-$) and **2l-Bn** ($X^- = \text{Cl}^-$). (b) UV/vis absorption spectra of pyridinium salts **2k-H** ($X^- = \text{Cl}^-$) and **2i-R** ($X^- = \text{BF}_4^-$, R = Et or Bz).

10.S.3. Transient spectra

Solutions of the carbocation precursors were irradiated with a 7-ns pulse from the third harmonic of a Nd:YAG laser (355 nm, ~50 mJ/pulse), and a xenon lamp was used as probe light for UV/vis detection with an ICCD camera. The system was equipped with a fluorescence flow cell and a synchronized pump system which allowed the complete exchange of the sample volume between subsequent laser pulses. To obtain the spectra published in this work, 4 to 16 transient spectra were averaged.

10.S.4 Transient UV/vis spectra obtained by irradiation of **2** in acetonitrile

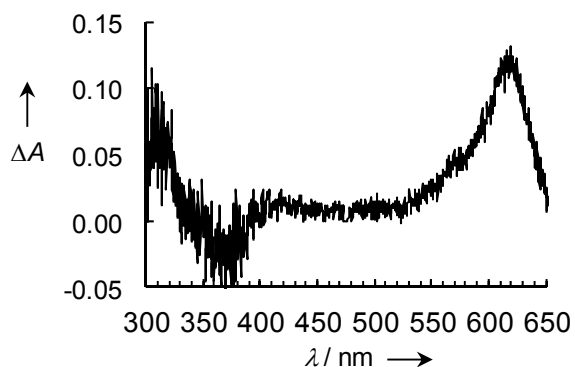


Figure 10.S.2. Transient UV/vis spectrum obtained after irradiation of a 1.2×10^{-4} M solution of **2h-Bn** ($X^- = \text{BF}_4^-$) in acetonitrile.

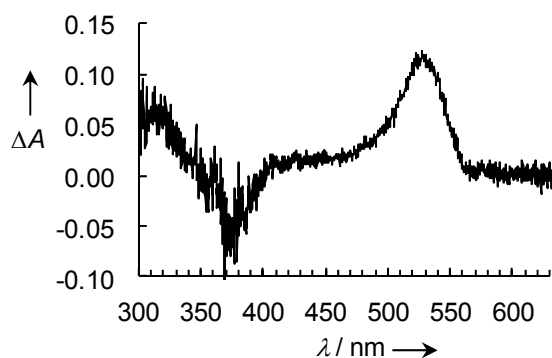


Figure 10.S.3. Transient UV/vis spectrum obtained after irradiation of a 1.2×10^{-4} M solution of **2j-Bn** ($X^- = \text{Cl}^-$) in acetonitrile.

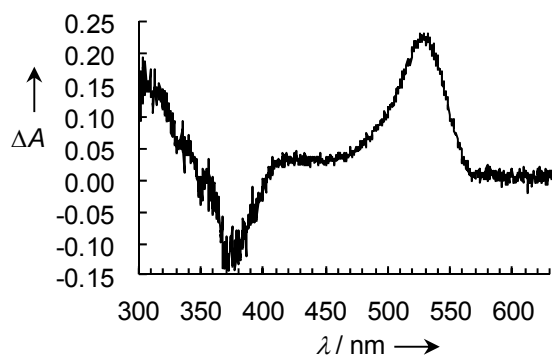


Figure 10.S.4. Transient UV/vis spectrum obtained after irradiation of a 1.2×10^{-4} M solution of **2j-Bn** ($X^- = \text{BF}_4^-$) in acetonitrile.

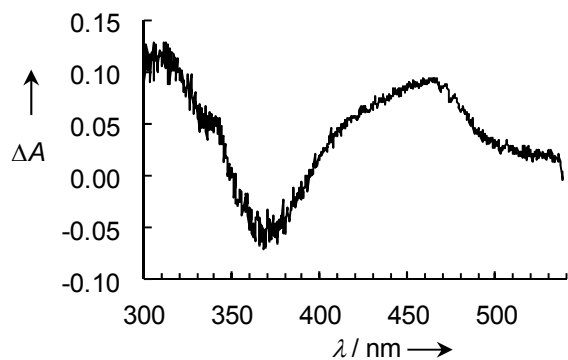


Figure 10.S.5. Transient UV/vis spectrum obtained after irradiation of a 1.2×10^{-4} M solution of **2l-Bn** ($X^- = \text{Cl}^-$) in acetonitrile.

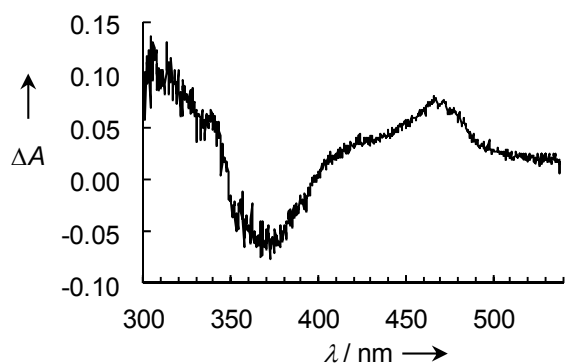


Figure 10.S.6. Transient UV/vis spectrum obtained after irradiation of a 1.2×10^{-4} M solution of **2m-Bn** ($X^- = \text{Cl}^-$) in acetonitrile.

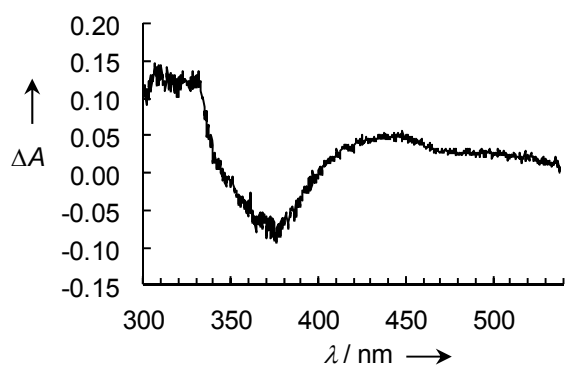


Figure 10.S.7. Transient UV/vis spectrum obtained after irradiation of a 1.2×10^{-4} M solution of **2o-Bn** ($X^- = \text{Cl}^-$) in acetonitrile.

10.S.5 Transient UV/vis spectra obtained by irradiation of 2 in other solvents

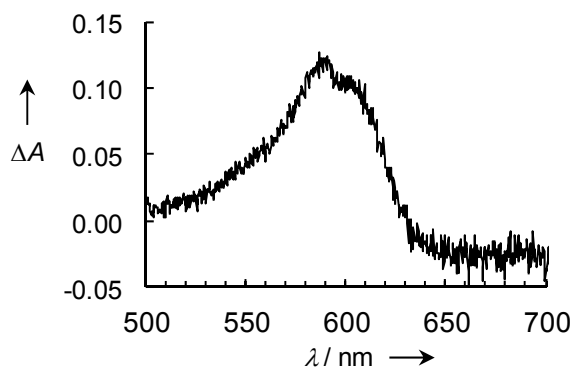


Figure 10.S.8. Transient UV/vis spectrum obtained after irradiation of a 8.5×10^{-5} M solution of **2i-Bn** ($X^- = \text{BF}_4^-$) in DMF.

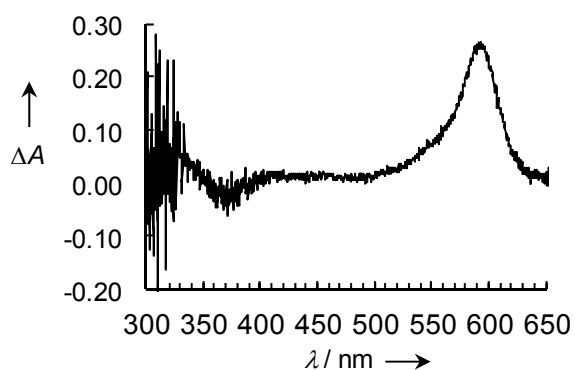


Figure 10.S.9. Transient UV/vis spectrum obtained after irradiation of 8.5×10^{-5} M solution of **2i-Bn** ($X^- = \text{BF}_4^-$) in acetone.

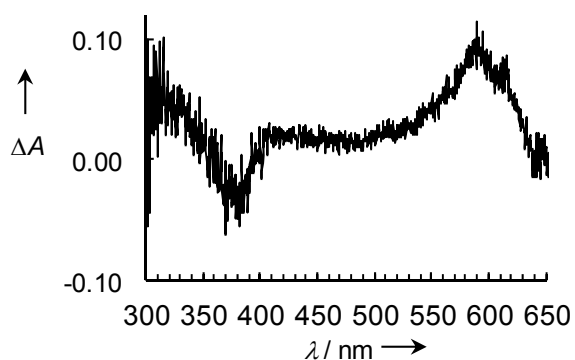


Figure 10.S.10. Transient UV/vis spectrum obtained after irradiation of 8.5×10^{-5} M solution **2i-Bn** ($X^- = \text{BF}_4^-$) in DMSO.

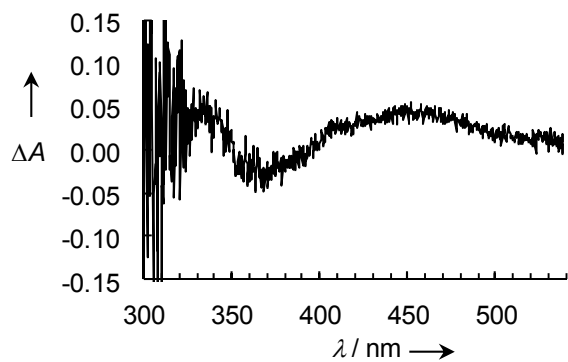


Figure 10.S.11. Transient UV/vis spectrum obtained after irradiation of 8.5×10^{-5} M solution **2l-Bn** ($X^- = \text{Cl}^-$) in 80% aqueous acetone.

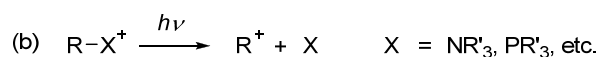
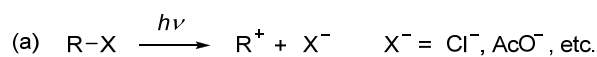
Photogeneration of Carbocations: Applications in Physical Organic Chemistry and the Design of Suitable Precursors

Johannes Ammer and Herbert Mayr, 2013, submitted

11.1 Introduction

Carbocations are key intermediates in many organic reactions^[1-6] including Friedel-Crafts reactions^[7-11] and carbocationic polymerizations.^[12-14] For the investigation of the reactivities of short-lived carbocationic intermediates under typical reaction conditions, techniques for the sufficiently fast generation and detection of carbocations are needed. An efficient method is the laser flash photolysis of suitable neutral (R–X) or charged (R–X⁺) precursors (Scheme 11.1), which allows the photogeneration and subsequent real-time UV/vis detection of the carbocations R⁺ in the presence of a nucleophile.^[6,15-17] This method has widely been employed to determine the rates of fast reactions of carbocations with nucleophiles.^[18-52] Common precursors include alkyl halides R–Hal,^[18-24] acetates R–OAc,^[24-33] aryl ethers R–OAr,^[24-33] ammonium salts R–NR'₃⁺,^[18,34,37] and phosphonium salts R–PR'₃⁺.^[35-52] For the sake of simplicity, neutral and charged precursors will both be denoted as “R–PLG”, and the corresponding anionic (X[−]) and neutral (X) photo-leaving groups will be denoted as “PLG[−]” in the following.

Scheme 11.1. Generation of carbocations R⁺ by photolysis of (a) neutral precursors R–X or (b) charged precursors R–X⁺.



The photolytic generation of carbocations R⁺ by heterolytic cleavage of carbon-heteroatom bonds is also relevant for photopolymerization and photocuring processes,^[53-66] and the

synthetic potential of the photoinduced cleavage of benzylic carbon-heteroatom bonds has been reviewed.^[67] Despite the obvious relevance for these fields, there is little systematic information about the relative efficiencies of different photo-leaving groups for the generation of carbocations.^[24]

In recent years, we have employed different precursors in laser flash photolysis experiments for the purpose of generating carbocations and studying their reactivities in bimolecular reactions on the 10 ns to 1 ms time scale.^[21-23,30-34,37-52,68-72] While the original papers mostly focus on the chemistry of the photogenerated carbocations, this review article summarizes those aspects of our work which are relevant for the rational design of precursors for the photogeneration of carbocations, and offers some guidelines for the use of laser flash photolysis in kinetic experiments.

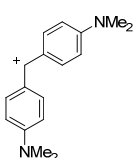
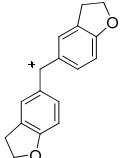
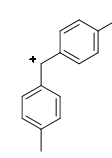
11.2 When is the Use of Laser Flash Photolysis Advantageous?

Conventional UV/vis spectrophotometry is limited by the time which is required for the mixing of the reactants. Even with stopped-flow techniques, the mixing time cannot be reduced below a few milliseconds. By using low concentrations of the reaction partners (e. g., 10^{-3} M), one can determine second-order rate constants up to 10^6 M⁻¹ s⁻¹, because the resulting half reaction times do not go below milliseconds. The determination of rate constants for reactions of carbocations which proceed in less than 1 ms requires a different approach, where the carbocation is generated almost instantaneously from a suitable precursor in a solution which already contains the other reactant.

The combination of conventional UV/vis spectroscopy, stopped-flow methods, and laser flash photolysis allows the investigation of long-ranging reaction series with rate constants from 10^4 M⁻¹ s⁻¹ up to the diffusional limit (10^9 to 10^{10} M⁻¹ s⁻¹) which may include reagents covering more than ten units of electrophilicity *E* (Table 11.1a)^[39] or 14 units of nucleophilicity *N* (Table 11.1b).^[49]

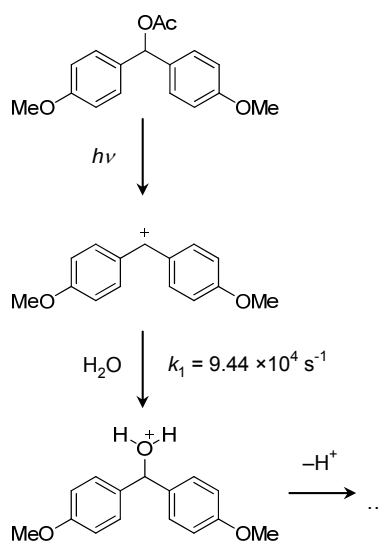
A variation of the reactant concentration is not possible for the determination of solvent nucleophilicities by studying first-order reactions of carbocations with solvents. Since reactions of many carbocations with solvents often proceed with rate constants $\geq 10^3$ s⁻¹, the photolytic generation of carbocations is particularly useful to investigate the rates of these reactions (Scheme 11.2).^[33,43]

Table 11.1. Rate constants for reactions of substrates with a series of (a) electrophiles^[39] or (b) nucleophiles^[49] covering many orders of magnitude in reactivity can be studied by combination of different techniques.^a

	conventional spectroscopy	stopped-flow spectroscopy	laser flash photolysis
a)	$E^+ + \text{CH}_2=\text{CHSiMe}_3 \xrightarrow{k_2} E-\text{CH}_2-\text{CH}^+\text{SiMe}_3$		
reagent (E^+)	 $(E = -7.02)$	 $(E = -1.36)$	 $(E = 3.63)$
$k_2 / \text{M}^{-1} \text{s}^{-1}$	3.0×10^{-3}	1.2×10^3	2.8×10^7
b)	$\text{Ph-CH}_2\text{-CH(Ph)-C(=O)-N}^+\text{(t-Bu)}_2 + \text{Nu} \xrightarrow{k_2} \text{Ph-CH}_2\text{-CH(Ph)-C(=O)-N}^+\text{(t-Bu)}_2\text{-Nu}^+$		
reagent (Nu)	 $(N = 4.63, s_N = 1.00)$	 $(N = 12.56, s_N = 0.70)$	 $(N = 17.35, s_N = 0.68)$
$k_2 / \text{M}^{-1} \text{s}^{-1}$	6.8×10^{-4}	1.1×10^4	1.9×10^7

^a Reactions with more reactive reagents can also be followed with the laser flash photolysis technique, but will already be influenced by the limiting effect of diffusion.

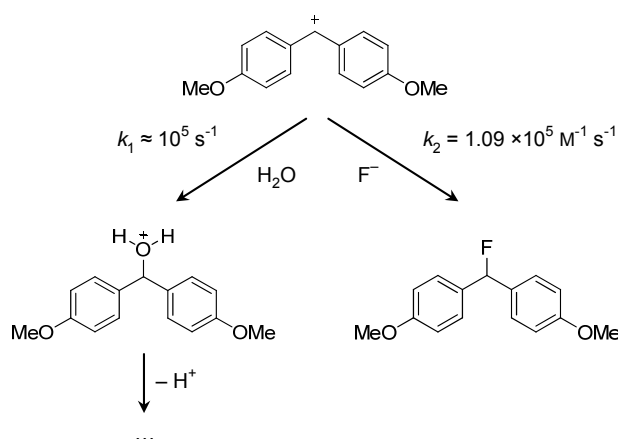
Scheme 11.2. Photogeneration of the di(*p*-anisyl)methyl cation and its reaction with water.^[33]



Lowering the reaction temperature may also reduce the rate constant to a value which can be determined by conventional methods, and the rate constants determined at lower temperatures may then be converted to 20 °C by the Arrhenius or Eyring equations. However, this procedure is difficult for highly reactive carbocations ($E > 6$) due to the low stabilities and high reactivities of these carbocations.^[73,74] Furthermore, it has to be considered that fast bimolecular reactions are characterized by small values of ΔH^\ddagger leading to a small temperature dependence of the rate constants. Consequently, variation of the temperature has only little effect on the rate constants. In such cases, it is often possible to follow the reactions of photolytically generated carbocations at 20 °C.^[39,40]

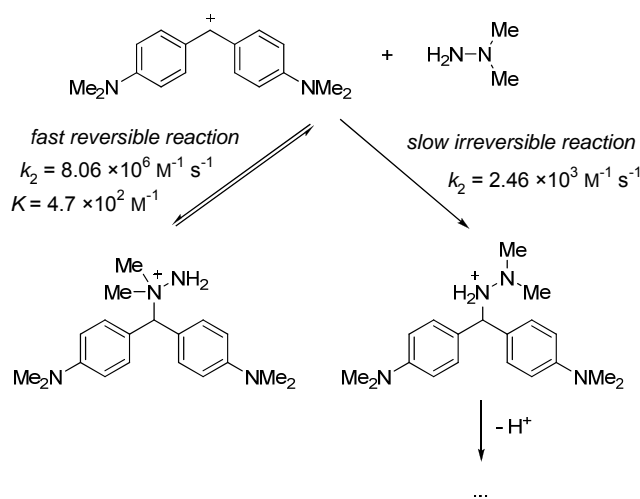
Laser flash photolysis is also helpful for kinetic studies under conditions where the carbocations are consumed quickly even in the absence of the nucleophiles of interest, e. g., by reaction with the solvent or other decomposition pathways. In these cases, the reactions of the carbocations with these nucleophiles can only be studied if they are sufficiently fast to compete with the background reaction. For this purpose, the nucleophile of interest often has to be employed in such high concentrations that the observed rate constants exceed 10^4 s^{-1} , which is too fast for stopped-flow measurements. The second-order rate constant for the reaction of the di(*p*-anisyl)methyl cation with fluoride in water, for example, is $10^5 \text{ M}^{-1} \text{ s}^{-1}$ (Scheme 11.3); a rate constant of this magnitude could usually be determined by the stopped-flow method. Due to the fast background reaction of the carbocation with the solvent (10^5 s^{-1}), however, the reaction of the carbocation with the fluoride anion can only be followed by laser flash photolysis using high concentrations of fluoride anions.^[45]

Scheme 11.3. Reaction of the di(*p*-anisyl)methyl cation with fluoride in water.^[45]



Rate constants for reactions of some nucleophiles, e. g. tertiary amines or dialkylsulfides, with carbocations cannot be studied with conventional methods at all. This is the case when reactions of these nucleophiles with stabilized carbocations are thermodynamically unfavorable while their reactions with less stabilized carbocations are very fast. Triethylamine, for example, does not react with benzhydrylium ions of $E < -4$, but its reactions with slightly more reactive benzhydrylium ions ($E = -3.14$) already proceed with rate constants of $1.4 \times 10^7 \text{ M}^{-1} \text{ s}^{-1}$.^[37] Such situations are generally observed for reactions with low intrinsic barriers giving products which do not undergo fast subsequent reactions. An intriguing example of this kind of reactivity is observed with the NMe_2 -terminus of 1,1-dimethylhydrazine, an ambident nucleophile. The fast reversible reactions ($\geq 3 \times 10^6 \text{ M}^{-1} \text{ s}^{-1}$) of the NMe_2 -terminus with benzhydrylium ions could be studied at high nucleophile concentrations with the laser flash photolysis method, while at low nucleophile concentrations conventional and stopped-flow UV/vis spectrophotometry showed the slow irreversible reactions at the NH_2 -terminus (Scheme 11.4).^[50]

Scheme 11.4. Ambident reactivity of 1,1-dimethyl hydrazine towards the bis[4-(dimethylamino)phenyl]methyl cation.^[50,51]



The reaction shown in Scheme 11.4 is also a good example to demonstrate that fast measurement techniques such as laser flash photolysis can also be used to determine thermodynamic data. Information about the equilibrium constant K for the fast reversible reaction of the bis[4-(dimethylamino)phenyl]methyl cation with the NMe_2 -terminus of 1,1-dimethylhydrazine (Scheme 11.4) is not available from conventional UV/vis spectroscopic measurements: Since the carbocations are consumed by the slower subsequent reaction with the NH_2 -terminus of the nucleophile, the absorbance does not stay constant on the seconds

time scale. When the carbocation is generated photolytically from its stable tributylphosphine adduct in the presence of an excess of 1,1-dimethylhydrazine,^[51] one can observe that a certain fraction of the photogenerated carbocations is consumed as the equilibrium is established (Figure 11.1). The equilibrium constant K of the reaction can then be estimated from the initial absorbance of the carbocations and the absorbance after the equilibrium is established.^[51] The subsequent irreversible reaction with the NH_2 -terminus of the nucleophile (Scheme 11.4) is too slow to be observed on the microsecond time scale (Fig. 11.1).

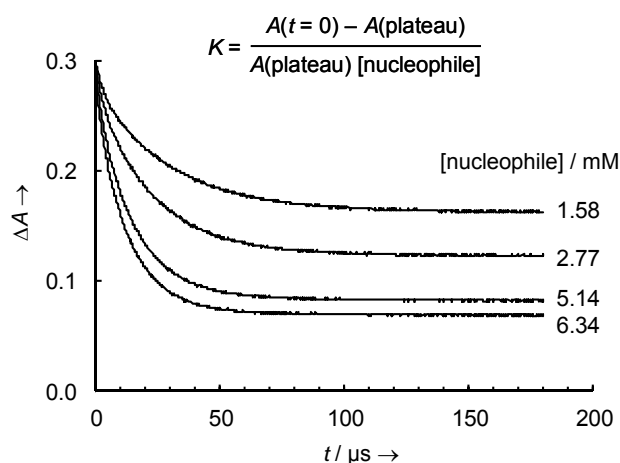
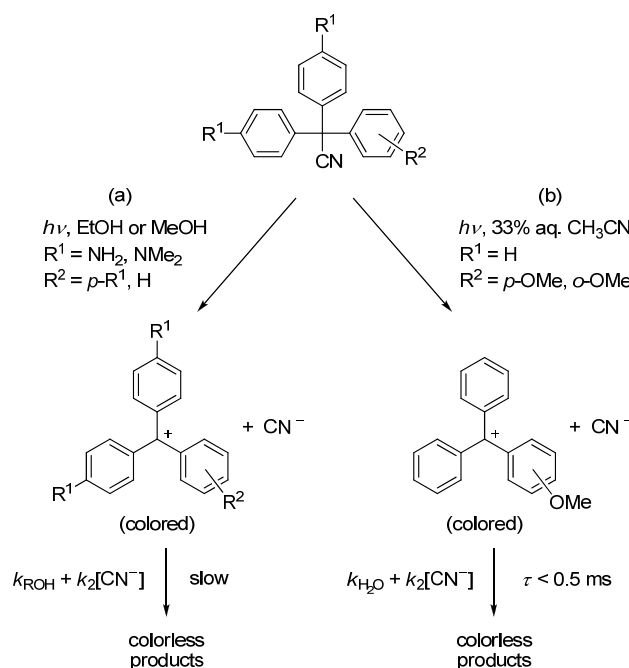


Figure 11.1. Decays of the absorbance of the bis[4-(dimethylamino)phenyl]methyl cation at 605 nm after irradiation of the substituted benzhydryl triphenylphosphonium salt (1×10^{-5} M) in the presence of different concentrations of 1,1-dimethyl hydrazine in CH_3CN at 20°C .^[51]

11.3 Historic Perspective

Photochemical reactions involving the intermediary formation of carbocations have long been known.^[75,76] Almost a century ago, Lifschitz and Joffé reported the heterolytic photocleavage of amino-substituted 2,2,2-triarylacetonitriles in alcoholic solution to the corresponding tritylium ions and cyanide, and observed the subsequent slow disappearance of the carbocations (Scheme 11.5a).^[77] However, the rate constants for the reactions of these tritylium ions with cyanide could be measured more conveniently by simply mixing solutions of the tritylium ions with a solution of CN^- .^[78]

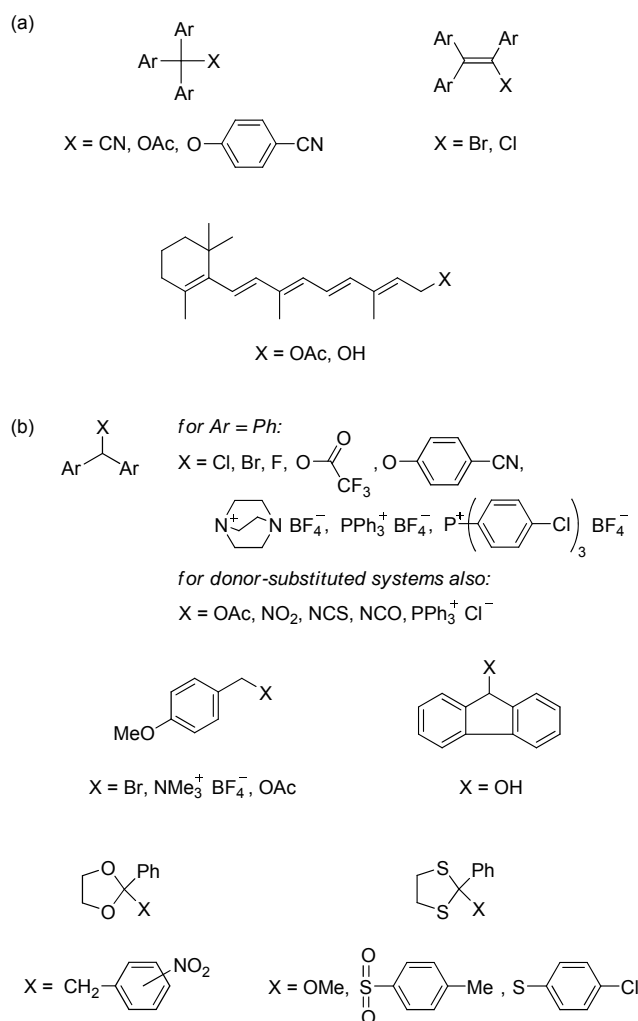
Scheme 11.5. Photocleavage of triarylacetonitriles with formation of tritylium ions and cyanide anions.



When shorter light pulses and faster measurement techniques became available, the photolytic generation of carbocations also became attractive from the viewpoint of physical organic chemists who are interested in the kinetics of the subsequent reactions of the generated carbocations. The earliest example, where the flash photolysis technique was employed to study carbocations, was a reaction similar to that described by Lifschitz and Joffé. In 1972, Ivanov *et al.* reported the flash-photolytic generation of methoxy-substituted tritylium ions from the corresponding triarylacetonitriles (Scheme 11.5b).^[79] These reactions of these carbocations with CN^- in aqueous acetonitrile could not have been investigated by conventional methods, since their lifetimes were considerably shorter (a few hundred μs) than the time required for the mixing of the reagents.

Other early flash photolysis studies of carbocations focused on triarylmethyl,^[26,79,80] retinyl,^[81-83] and triarylvinyl^[84-86] cations, which were generated from the corresponding nitriles, acetates, halides, alcohols, or *p*-cyanophenyl ethers (Chart 11.1a).

Chart 11.1. Substrates R–X which were reported to yield carbocations R⁺ upon irradiation.



Since the late 1980s, a large number of studies have employed nanosecond laser flash photolysis^[87,88] to study the generation and the decay kinetics of carbocations.^[6,15,16] Some of the substrates that were successfully employed for the photogeneration of carbocations are shown in Chart 11.1b.^[18,21-24,25,27-29,32-38,68-70,89-95] Valuable information about the formation of carbocationic intermediates in photoreactions has also been derived by analysis of the products.^[75,76]

11.4 Instrumentation

A nanosecond laser flash photolysis setup^[87,88] is usually sufficient for the study of bimolecular reactions of carbocations in solution, because the rates of such reactions are

limited by diffusion (10^9 to $10^{10} \text{ M}^{-1} \text{ s}^{-1}$). Figure 11.2 shows a schematic representation of a typical experimental setup. A light pulse with a pulse width of a few nanoseconds is generated by a Nd/YAG laser. The fundamental emission is converted to the third or fourth harmonics to obtain laser pulses with wavelengths of 355 nm or 266 nm, respectively. In a typical experiment, the 266-nm pulses are employed to irradiate 10^{-5} to 10^{-4} M solutions of the precursors, and the UV/vis absorbances of the photogenerated carbocations are monitored by a UV/vis detector. The probe light originates from a xenon short-arc lamp and is collected by an ICCD camera or a photomultiplier. The setup used in our laboratory is described in detail in ref. [38]

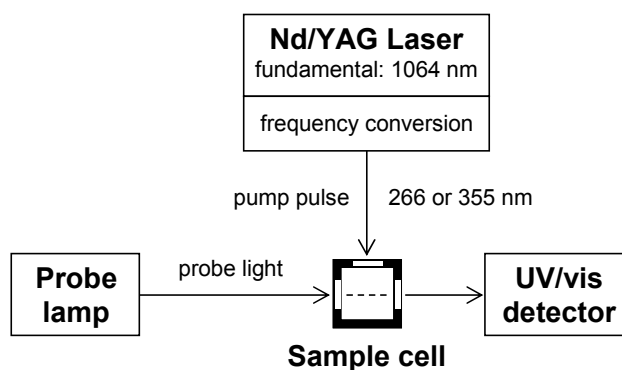


Figure 11.2. Schematic setup of a nanosecond laser flash photolysis instrument.

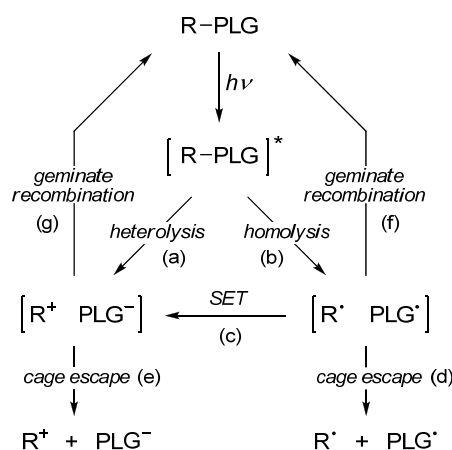
11.5 Requirements for Good Photo-leaving Groups

In order to study the kinetics of bimolecular reactions of photogenerated carbocations on the ≥ 10 ns time scale, an appropriate precursor for the carbocations must be selected. In this Section, we will discuss the requirements to be met by such precursors using illustrative examples from our work.

11.5.1 Efficient Photogeneration of Diffusionally Separated Carbocations. *Mechanism for the Photogeneration of Carbocations R^+ from Substrates $R-PLG$.* The general mechanism of photo-heterolysis and photo-homolysis reactions of substrates $R-PLG$ ($PLG = Cl, OAc, I^+R', S^+R'_2, N^+R'_3, P^+R'_3$, etc.) is well known (Scheme 11.6).^[6,15-17,96-102] After irradiation by the laser pulse, the excited precursor may undergo heterolytic bond cleavage yielding the ion pair $[R^+ PLG^-]$ (Scheme 11.6, path a) or homolytic bond cleavage to the radical pair $[R^\bullet PLG^\bullet]$ (path b); alternatively the ion pairs may also be generated by homolytic bond cleavage and

subsequent electron transfer (paths b + c). Both pairs may then either separate diffusively (paths d and e) to yield the free carbocations R^+ or radicals R^\bullet , respectively, or undergo geminate recombination to regenerate the substrate R–PLG (paths f and g). Only the free carbocations R^+ or radicals R^\bullet , which are shown in the bottom line of Scheme 11.6, are the species which can be observed in a nanosecond laser flash photolysis experiment.

Scheme 11.6. Mechanism for the photogeneration of carbocations R^+ and radicals R^\bullet from substrates R–PLG.



The actual reaction pathways and dynamics cannot be determined by analysis of reaction products or by the observation of the ions or radicals on the >10 ns time scale. The real-time observation of the fast processes within the solvent cage shown in Scheme 6 is only possible with transient absorption measurements having a temporal resolution of about 50 fs, and a conclusive interpretation of the transient signals often requires additional theoretical calculations.

Detailed investigations of these ultrafast processes have been performed for the photolyses of benzhydryl chlorides Ar_2CH-Cl and phosphonium salts $Ar_2CH-PR_3^+$.^[38,102-108] In both cases, the partitioning between ionic and radical photoproducts is controlled by conical intersections between the excited state and ground state potential energy surfaces of the reactant.^[103-105] After the bond cleavage, the initially generated benzhydryl cations or benzhydryl radicals undergo relaxation by planarization and solvation within a few hundred femtoseconds.^[106]

In the case of chloride as photo-leaving group, the initial photocleavage is predominantly homolytic (Scheme 11.6, path b),^[102-104] and the experimentally observed carbocation population is mostly generated by single electron transfer (SET) in the geminate radical pair (path c), which is distance-dependent and competes with the diffusional separation of the radical fragments (path d).^[102] An efficient diffusive separation of the generated ion pairs

(Scheme 11.6, path e) requires a polar solvent such as acetonitrile to reduce the Coulombic attraction between the ions. In less polar solvents such as dichloromethane virtually all generated carbocations recombine to the starting material (path g) before they can separate diffusionally, and one cannot observe them on the nanosecond time scale.^[102]

In photolyses of benzhydryl triarylphosphonium salts with non-oxidizable counter-anions (e. g., BF_4^-), high yields of stabilized carbocations are often observed without detection of any intermediary radicals.^[38] Whether these are formed by direct C–P bond heterolysis (Scheme 11.6, path a) or by homolysis and subsequent fast electron transfer (paths b+c) can be answered by theoretical investigations.^[105] Concomitant formation of carbocations and radicals by C–P bond cleavage is observed when the resulting carbocations are less stabilized. The yields and lifetimes of carbocations obtained by irradiation of phosphonium salts greatly depend on the reaction conditions, which will be discussed below and is described in detail in ref.^[38] With the proper choice of the precursor salt, excellent yields of highly reactive carbocations can be achieved.

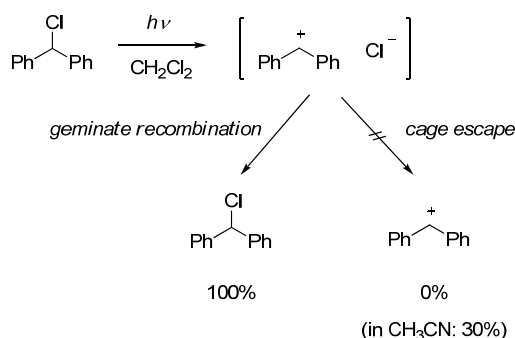
Improving the yields of carbocations based on our knowledge of the mechanism. Due to the complex interplay of different reaction pathways (Scheme 11.6), it is difficult to predict the suitability of a particular substituent PLG as a photo-leaving group for the generation of carbocations which are available for the investigation of bimolecular reactions on the >10 ns time scale. Particularly the potential energy surfaces for the ground state and excited state which control the efficiency of the initial bond cleavage can hardly be estimated without high level quantum chemical investigations.

For structurally related systems, the oxidation potentials of the photo-leaving groups PLG^- provide information about the relative thermodynamic stabilities of R^+/PLG^- ion pairs and $\text{R}^\bullet/\text{PLG}^\bullet$ radical pairs. Likewise, the nucleophilicity parameters of the photo-leaving groups PLG^- provide information about their tendencies to undergo geminate recombination reactions with the corresponding carbocations. The phosphine $\text{P}(p\text{-Cl-C}_6\text{H}_4)_3$, for example, is indeed a better photo-leaving group for the photogeneration of carbocations than PPh_3 due to its higher oxidation potential (i. e., lower thermodynamic stability of the radical cation $\text{PAr}_3^{\bullet+}$) and lower nucleophilicity.^[38]

The escape rate of the carbocation from the geminate solvent cage (Scheme 11.6, path e) is also a crucial factor, which is illustrated by the low yields of carbocations obtained by irradiation of $\text{Ar}_2\text{CH-Cl}$ in CH_2Cl_2 on the nanosecond time scale. On the picosecond time scale, a significant population of $[\text{Ar}_2\text{CH}^+ \text{Cl}^-]$ ion pairs is observed. As a result of the strong

Coulombic attraction, however, the diffusional separation of Ar_2CH^+ and Cl^- is so slow in CH_2Cl_2 that all carbocations undergo geminate recombination and do not escape the solvent cage (Scheme 11.7).^[102]

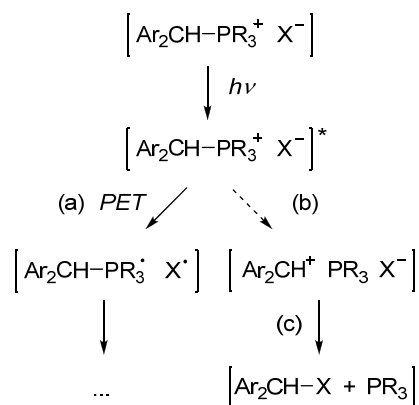
Scheme 11.7. After irradiation of $\text{Ph}_2\text{CH-Cl}$ in CH_2Cl_2 , no carbocations can be observed on the nanosecond time scale, because the $[\text{Ph}_2\text{CH}^+ \text{Cl}^-]$ ion pairs generated by the laser pulse recombine within a few hundred picoseconds.^[102]



The final yields of the carbocations on the >10 ns time scale are substantially larger in solvents of higher permittivity such as CH_3CN , which reduce the Coulombic attraction between the ions,^[102] or when a neutral photo-leaving group such as PPh_3 is employed instead of the charged Cl^- .^[38] On the other hand, the geminate recombination of Ar_2CH^+ and PPh_3 after the photolysis of $\text{Ar}_2\text{CH-PPh}_3^+$ in CH_3CN solution is greatly enhanced when the diffusional separation of the photofragments is restricted by encapsulation in reverse micelles.^[107]

Side reactions in the initial solvent cage. The efficiency of carbocation formation from a precursor molecule may also be reduced by competing photoreactions. This situation is encountered when phosphonium ions are irradiated under conditions where they exist as ion pairs with halide counter-anions (Scheme 11.8): In this case, the preferred reaction pathway is a photo-electron transfer (PET) in the excited benzhydryl phosphonium halide pair (Scheme 11.8, path a), which generates phosphoranyl radicals that undergo subsequent reactions.^[38]

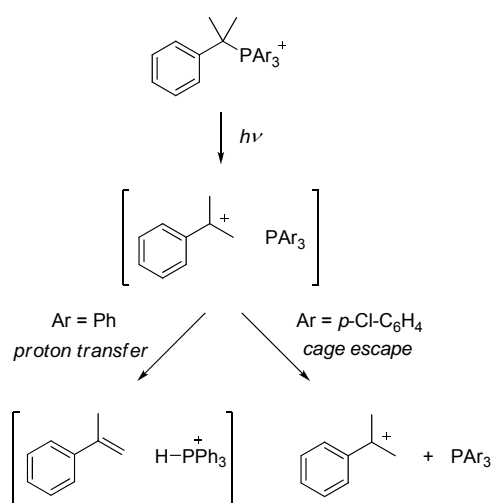
Scheme 11.8. Irradiation of phosphonium halide ion pairs $[\text{Ar}_2\text{CH-PR}_3^+ \text{X}^-]$ ($\text{X}^- = \text{Cl}^-$ or Br^-) in CH_2Cl_2 does not yield the desired carbocations Ar_2CH^+ . The main reaction is a photoelectron transfer in the excited ion pair (path a). Carbocations which may be generated from the excited phosphonium salt (path b) are trapped by the halide ions which are present in the solvent cage (path c).^[38]



This example also highlights the important role of subsequent thermal reactions in the solvent cage: The few carbocations which may be generated from the phosphonium halide ion pairs (Scheme 11.8, path b) are consumed immediately by the reaction with the halide ions which are present in the ion pairs of the precursor salts (Scheme 11.8, path c).^[38] A detailed investigation of ion pairing in solutions of benzyl and benzhydryl triphenylphosphonium salts was recently reported.^[109]

For the generation of highly Brønsted-acidic carbocations, the possibility of a proton transfer from the carbocation to the photo-leaving group in the solvent cage also has to be taken into account. Irradiation of $\text{PhC}(\text{CH}_3)_2\text{-PPh}_3^+$ in CH_2Cl_2 , for example, presumably leads to intermediary cumyl cations $\text{PhC}(\text{CH}_3)_2^+$, which are rapidly deprotonated by PPh_3 before the photofragments can diffuse apart (Scheme 11.9). Only when the less Brønsted-basic phosphine $\text{P}(p\text{-Cl-C}_6\text{H}_4)_3$ is employed as photo-leaving group, cumyl cations can be observed on the >10 ns time scale.^[40]

Scheme 11.9. Irradiation of $\text{PhC}(\text{CH}_3)_2\text{-PAR}_3^+$ leads to the geminate photofragment pair $\text{PhC}(\text{CH}_3)_2^+/\text{PAR}_3$, which may undergo a proton transfer yielding α -methylstyrene and the protonated phosphine or diffusional separation yielding the free carbocation.^[40]



In this section, we have discussed how the yield of diffusionally separated carbocations depends on the reactions shown in Scheme 11.6 and possible side reactions in the initial solvent cage. Knowledge of these processes may help to assess the quantum yields of diffusionally separated carbocations on the nanosecond time scale which may be obtained with a certain photo-leaving group. However, there are further important aspects which have to be considered when selecting precursors for the photogeneration of carbocations.

11.5.2 Stability of the Precursor in the Sample Solution. An obvious but not always trivial requirement for the selection of a photo-leaving group is the fact that the substrate R-PLG must be soluble and sufficiently stable under the experimental conditions in the dark.

Chloride, for example, is not a suitable photo-leaving group for the generation of carbocations in media of high ionizing power, such as alcohols or aqueous solvents, because $\text{S}_{\text{N}}1$ -active substrates are rapidly transformed into ethers and alcohols in these solvents. The life-times of precursors which are prone to heterolysis reactions can be estimated by the linear free energy relationship, eq. 1,^[110]

$$\lg k_s = s_f(N_f + E_f) \quad (1)$$

which relates the rate constant k_s of a solvolysis reaction to the empirical reactivity parameters of the electrofuge (E_f) and the nucleofuge (N_f , s_f). Using this relationship, one may, for example, predict that the life-time of bis(3-fluorophenyl)methyl chloride in trifluoroethanol would still be sufficient ($\tau_{1/2} \approx 17$ min, calculated using $E_f = -9.26$ for Ar_2CH^+ and $N_f = 5.54$,

$s_f = 0.85$ for Cl^- in $\text{CF}_3\text{CH}_2\text{OH}$)^[110] to carry out a laser flash photolysis experiment with this precursor (Scheme 11.10).

Scheme 11.10. Laser flash photolysis of bis(3-fluorophenyl)methyl chloride in trifluoroethanol.

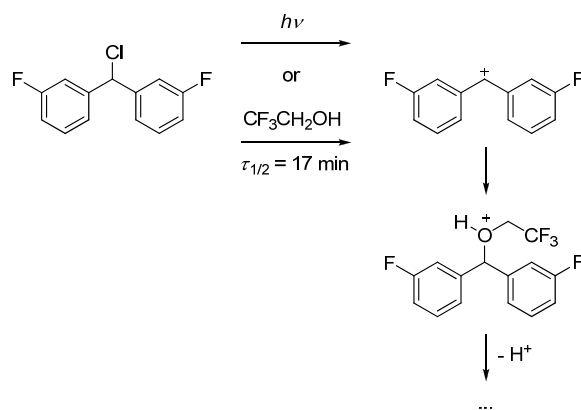


Figure 11.3 shows a semi-quantitative scheme to estimate the lifetimes of different precursors which may be employed for the photogeneration of carbocations. Compounds located in the blue range have lifetimes of more than one day, while those in the red range do not have sufficient lifetimes to carry out a laser flash photolysis experiment. The combination of the bis(3-fluorophenyl)methyl cation with chloride in trifluoroethanol shown in Scheme 10 is located in the border range. As illustrated in Figure 11.3, the photogeneration of better stabilized carbocations in this solvent requires the use of a weaker nucleofuge such as acetate or *p*-cyanophenolate as the photo-leaving group.^[25]

Because of their lower nucleofugalities,^[110] acetate and *p*-cyanophenolate are suitable photo-leaving groups for the generation of moderately stabilized carbocations in alcoholic or aqueous solutions.^[25-33] More recently, we have also employed tertiary phosphines for this purpose.^[43-45] The respective combinations of electrofuges and nucleofuges for these experiments are located in the blue area of Figure 11.3.

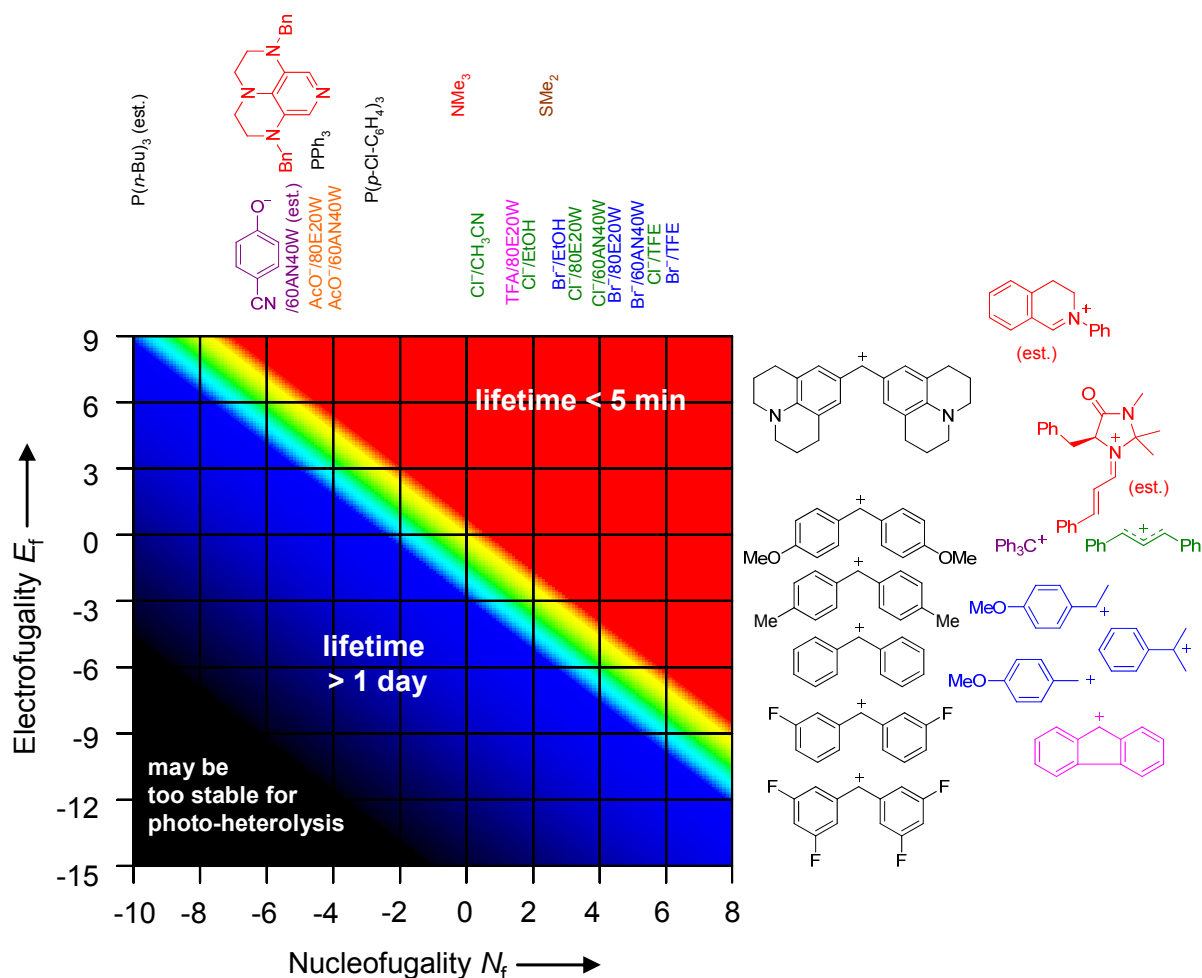


Figure 11.3. Semi-quantitative scheme to estimate the lifetimes for precursors which are composed of an electrofuge (carbocation-to-be, vertical axis) and a nucleofuge (photo-leaving group, horizontal axis) in the absence of light. Lifetimes of precursors with neutral nucleofuges are not strongly dependent on solvent. AN = acetonitrile, E = ethanol, TFA = trifluoroacetate, TFE = 2,2,2-trifluoroethanol, W = water.

In CH_3CN , chloride is a weaker nucleofuge.^[111] It has been employed as photo-leaving group to generate the di(*p*-tolyl)methyl cation (light blue range in Fig. 11.3) and to study its reactions with π -nucleophiles in this solvent.^[21] The photogeneration of the di(*p*-anisyl)methyl cation from the corresponding chloride in CH_3CN has also been reported,^[24] but as this combination is located in the red area of Figure 11.3, we expect that this precursor cannot be employed in the presence of nucleophiles which trap this carbocation during the setup of the experiment.

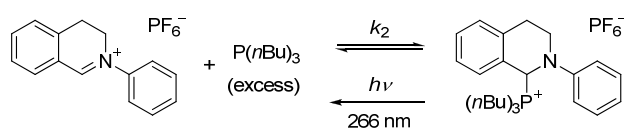
While the nucleofugalities of anions are strongly solvent-dependent, the solvent has only a limited influence on the rate constants for solvolyses of substrates with neutral

nucleofuges.^[110,112] Therefore, we did not specify the solvents for the neutral photo-leaving groups in Figure 11.3.

The black range at the lower left of Figure 11.3 serves to remind the reader that photoheterolyses may become unfavorable when the energetic barrier for the heterolytic bond cleavage becomes too high. Laser flash photolysis experiments with series of structurally analogous precursors have repeatedly demonstrated that the formation of carbocations becomes unfavorable at some point when the electrofugalities of the carbocations become too low, while the photo-leaving group is kept constant.^[24,38,71] This behavior cannot be derived from Figure 11.3, however, which is illustrated by the fact that the 4-(trifluoromethyl)-benzhydryl cation ($E_f \approx -9$) can easily be generated from the corresponding triphenylphosphonium salt^[38] but not from the corresponding chloride in CH_3CN ,^[24] which is located further right in Fig. 11.3. The factors which control the efficiency of the photoheterolysis reactions are discussed in Section 11.5.1.

Triarylphosphonium salts generally combine high stability, even in strongly ionizing solvents, with a high tendency to produce carbocations upon irradiation.^[35-46] Reactions of triarylphosphines with highly stabilized carbocations, however, do not yield stable triarylphosphonium salts (Figure 11.3),^[113] and the more Lewis-basic tributylphosphine has been employed successfully in these cases.^[45-52] For carbocations of very low Lewis acidity, even the formation of tributylphosphonium salts becomes reversible, as shown in Scheme 11.11 for the 2-phenyl-3,4-dihydroisoquinolinium ion. When the resulting equilibrium mixture is irradiated, the phosphonium salt is cleaved to the iminium salt and the phosphine. The rate constant for the reaction of the iminium salt with the phosphine can be determined photometrically by following the decrease of the absorbance of the iminium salt as the equilibrium is re-established.^[52] However, the method fails in the presence of other nucleophiles than tributylphosphine, because the small equilibrium concentrations of the 2-phenyl-3,4-dihydroisoquinolinium ion already react with the added nucleophiles in the dark.

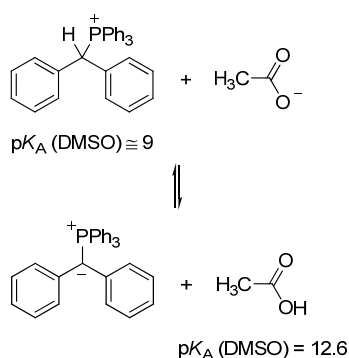
Scheme 11.11. Reaction of the 2-phenyl-3,4-dihydroisoquinolinium ion with tributylphosphine and photolytic cleavage of the resulting phosphonium salt.



Similarly, tertiary phosphines do not form stable adducts with very bulky carbocations such as tritylium ions (frustrated Lewis pairs^[114]). The photogeneration of tritylium ions in aqueous acetonitrile was, therefore, accomplished by using the less bulky but usually less efficient photo-leaving groups acetate or *p*-cyanophenolate.^[26-31]

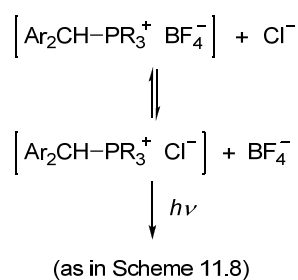
Problems with phosphonium salts may also be expected under basic conditions, if the salts can undergo deprotonation with formation of ylides (Scheme 11.12).

Scheme 11.12. Deprotonation of benzhydryl triphenylphosphonium ion by acetate with formation of the corresponding phosphonium ylide (pK_A values in DMSO taken from ref. ^[115] for acetic acid and estimated as described in ref. ^[109] for the phosphonium salt).



Under conditions where charged precursors form ion pairs, the stability of these ion pairs in the sample solution must also be considered. In the presence of chloride ions, for example, a good precursor such as $\text{Ar}_2\text{CH}-\text{PR}_3^+ \text{BF}_4^-$ may be converted to the bad precursor $\text{Ar}_2\text{CH}-\text{PR}_3^+ \text{Cl}^-$ if the chloride anions replace the initial counter-anions of the phosphonium salt (Scheme 11.13). As discussed above (Scheme 8), a photo-electron transfer in the excited ion pairs of the precursors may then result in the formation of radicals instead of carbocations.^[38]

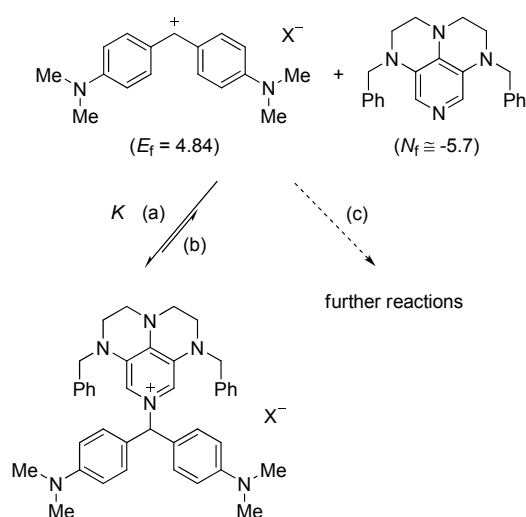
Scheme 11.13. By replacing the BF_4^- anion with an oxidizable chloride ion, the good precursor $[\text{Ar}_2\text{CH}-\text{PR}_3^+ \text{BF}_4^-]$ is transformed into the phosphonium chloride pair $[\text{Ar}_2\text{CH}-\text{PR}_3^+ \text{X}^-]$ which is a bad precursor for the generation of the carbocations Ar_2CH^+ (cf. Scheme 11.8).



Most nitrogen compounds which can be employed as photo-leaving groups for the generation of carbocations by C–N bond cleavage are relatively weak Lewis bases (cf. entry for NMe₃ in Figure 11.3), which is a problem for the synthesis of adducts with stabilized carbocations. Even if quaternary ammonium salts are obtained by the reactions of tertiary amines with such stabilized carbocations in weakly nucleophilic solvents such as CH₃CN, they are often not stable in solution, probably because of reactions of the amines with the quaternary ammonium ions.^[37]

The use of 3,4,5-triamino-substituted pyridines as photo-leaving groups is advantageous for some applications due to the absorbances of the resulting pyridinium salts in the near UV (see below), but the Lewis basicity of these pyridines is also insufficient to obtain stable adducts with highly stabilized carbocations. For example, the reaction shown in Scheme 11.14 (path a) is practically quantitative (complete decolorization; estimated equilibrium constant $K \approx 1 \times 10^7 \text{ M}^{-1}$),^[116] but the dissociation of the pyridinium salt proceeds fast enough (path b in Scheme 14; $k_s \approx 0.1 \text{ s}^{-1}$)^[116] so that the small equilibrium concentration of the carbocation may be trapped by other nucleophiles which are present (path c in Scheme 11.14).

Scheme 11.14. Reversible addition of 1,6-dibenzyl-2,3,5,6-tetrahydro-1*H*,4*H*-1,3a,6,8-tetraaza-phenalene to the bis[4-(dimethylamino)phenyl]methyl cation ($X^- = \text{BF}_4^-, \text{Cl}^-$).

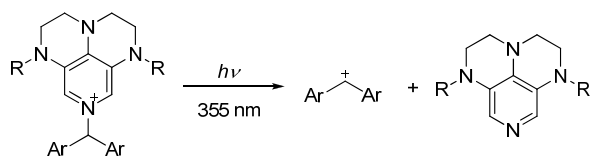


As a consequence, the 3,4,5-triamino-substituted pyridinium salt may already be consumed during the time needed for the preparation of a kinetic experiment, when other nucleophiles which trap the reversibly generated carbocations are present.^[71]

11.5.3 Absorption of the Precursor at the Excitation Wavelength. The requirement that the precursor R–PLG absorbs at the excitation wavelength of the laser is generally unproblematic for experiments using the fourth harmonic of a Nd/YAG laser (266 nm) as the source of the pump pulse: As the generated carbocations R^+ are usually detected by UV/vis spectroscopy, researchers typically investigate systems where the positive charge is conjugated to aryl groups. In this case, the R moiety of the precursor R–PLG already contains at least one aromatic group which absorbs at 266 nm. For other R groups with insufficient absorbance at 266 nm, one can easily solve the problem by employing one of the common aromatic photo-leaving groups such as triphenylphosphine or *p*-cyanophenolate.

The choice of photo-leaving group is more challenging, when pump pulses with wavelengths >300 nm shall be employed, which may be necessary if reaction partners or solvents with significant UV/vis-absorptions at wavelengths <300 nm are present. As the R groups of the substrate R–PLG usually do not have sufficient UV/vis absorbances at >300 nm, the excitation must occur at the PLG moiety. The generation of carbocations by irradiation with 355-nm pulses from the third harmonic of the Nd/YAG laser thus required the development of suitable photo-leaving groups. Taking advantage of the fact that the UV/vis absorptions of pyridinium salts can be shifted towards higher wavelengths by bridged amino-substituents, we were able to obtain carbocations by 355-nm irradiation of their adducts with 3,4,5-triamino-substituted pyridines (Scheme 11.15).^[71,72]

Scheme 11.15. Generation of benzhydrylium ions Ar_2CH^+ by 355 nm laser flash photolysis of 3,4,5-triamino-substituted pyridinium ions.^[71]



The excitation can thus be located entirely on the photo-nucleofuge (PLG), like in the 355-nm photolysis of 3,4,5-triamino-substituted pyridinium ions (Scheme 11.15),^[71,72] or entirely on the photo-electrofuge (R), like in the 266-nm photolyses of arylmethyl chlorides $R-Cl$ ^[18-23,98-102] or tributylphosphonium ions $R-P(nBu)_3^+$.^[45-52] In the 266-nm photolysis of benzhydryl triphenylphosphonium salts,^[38] it is not clear where the excitation occurs.

For the kinetic investigation of the reaction of the photogenerated 2-phenyl-3,4-dihydro-isoquinolinium ion with tributylphosphine, where the photo-nucleofuge $P(nBu)_3$ is also used as a nucleophile in high excess (Scheme 11.11),^[52] it is essential that the photo-nucleofuge

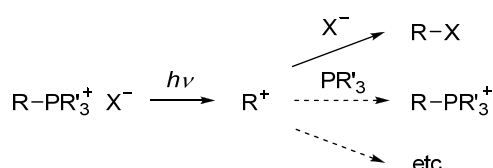
does *not* absorb at the excitation wavelength: If the free phosphine had a considerable absorption at the excitation wavelength, the concentrated sample solution would be opaque to the laser pulse and no carbocations could be generated.

11.5.4 Life-times of the Diffusionally Separated Photogenerated Carbocations. *Reactions with the diffusionally separated photo-nucleofuge.* The recombination of the carbocation with the diffusionally separated photo-leaving group PLG^- may be a limiting factor for the life-time of the photogenerated carbocations R^+ .^[24,38] It is therefore desirable that the reaction of R^+ with PLG^- is slow. This is achieved easily for highly stabilized carbocations ($E \ll -2$), which react slowly with common photo-leaving groups such as PPh_3 . Highly reactive carbocations R^+ ($E > 0$), however, often undergo diffusion-controlled combination reactions with any suitable photo-leaving group PLG^- that is employed to generate these carbocations. The observation of relatively long life-times of $\sim 10 \mu\text{s}$ for such highly reactive carbocations is only due to the fact that the concentrations of the photofragments are very low.^[24,38]

In fluorinated alcohols such as 2,2,2-trifluoroethanol, the rates for the recombination of R^+ with PLG^- are significantly lower when anionic photo-leaving groups such as acetate or *p*-cyanophenolate are employed.^[25] This is a consequence of the strong stabilization of anions in these solvents. In fluorinated alcohols, the life-times of carbocations may thus be extended by the use of anionic photo-leaving groups.

Reactivity of the precursor. Another possible pathway for the decay of photogenerated carbocations is the reaction with nucleophilic centers of the precursor. If the carbocations are generated from phosphonium halides $\text{R-PR}'_3^+ \text{X}^-$ in solvents of low nucleophilicity, for example, they decay primarily by combination with the halide ions X^- (Scheme 11.16) and not by recombination with the phosphine PR'_3 , because the concentration of the precursor salt $\text{R-PR}'_3^+ \text{X}^-$ is much higher than that of the photofragment PR'_3 .^[38]

Scheme 11.16. Carbocations R^+ which are generated from phosphonium halides $\text{R-PR}'_3^+ \text{X}^-$ ($\text{X}^- = \text{Cl}^-$ or Br^-) in solvents of low nucleophilicity (e. g., CH_3CN) decay primarily by reaction with the halide ions X^- .^[38]



Carbocations which are obtained by irradiation of phosphonium tetrafluoroborates $R-PR'_3^+ BF_4^-$ have longer life-times, although highly reactive carbocations ($E > 5$) may also react with the less nucleophilic BF_4^- anions.^[38] If the phosphonium salts exist as ion pairs, the trapping of the carbocations by the counter-anions may already occur within the geminate solvent cage (see Section 11.5.1).

The 3,4,5-triamino-substituted pyridinium ions which are used for the photogeneration of carbocations with 355 nm light due to their UV/vis absorptions at this wavelength (Scheme 11.15) have three tertiary amine functions, which may act as nucleophiles and reduce the life-times of carbocations which are generated from these precursors.^[71]

Quantitative estimates. Upper limits for the life-times of photo-generated carbocations can often be estimated using the linear free energy relationship, eq. 2,^[39,118-120]

$$\lg k = s_N(N + E) \quad (2)$$

which relates the rate constants k for reactions of electrophiles with nucleophiles to the empirical reactivity parameters of the electrophiles (E) and the nucleophiles (N , s_N).

We will exemplify this for the reaction shown in Scheme 11.10, where the bis(3-fluorophenyl)methyl cation is generated by laser flash photolysis of the corresponding chloride in trifluoroethanol. In principle, there are three possibilities for the decay for the carbocations that could compete with the desired reaction with an added nucleophile: Recombination with the free photo-leaving group (here: Cl^-), reaction with the unreacted precursor (here: Ar_2CHCl), and reaction with the solvent (in our example: trifluoroethanol).^[120]

Using the reactivity parameters of the carbocation ($E = 6.87$)^[39] and of Cl^- in trifluoroethanol ($N = 10.3$, $s_N = 0.6$),^[32] we calculate a second-order rate constant $k_2 = 2 \times 10^{10} \text{ M}^{-1} \text{ s}^{-1}$ for the reaction of the carbocation with Cl^- from eq. 2, i. e., the reaction is almost diffusion-controlled (note that rate constants $>10^8 \text{ M}^{-1} \text{ s}^{-1}$ are somewhat over-estimated by eq. 2^[39]). Although the reaction of the carbocation with Cl^- will not be of pseudo-first-order, we can use $k_2[Cl^-]$ as an upper limit, which equals 10^4 to 10^5 s^{-1} for typical concentrations of the photoproducts in the kinetic experiments (10^{-6} to 10^{-5} M). The nucleophilicity parameter of Ar_2CHCl is not known, but for a rough estimate let us use that of the more electron-rich toluene ($N = -4.36$, $s_N = 1.77$),^[39] which yields a second-order rate constant of $k_2' = 3 \times 10^3 \text{ M}^{-1} \text{ s}^{-1}$. Considering the low concentration of the precursor (usually 10^{-4} to 10^{-5} M), the pseudo-first-order rate constant $k_2'[Ar_2CHCl]$ for the reaction of the carbocation with the

precursor is negligible. By substituting the solvent reactivity parameters of trifluoroethanol ($N_1 = 1.11$, $s_N = 0.96$)^[39] into eq. 2, we obtain the first-order rate constant $k_1 = 4.6 \times 10^7 \text{ s}^{-1}$ for the reaction of the bis(3-fluorophenyl)methyl cation with trifluoroethanol. This value is considerably larger than the rate constants calculated above for the reaction of the carbocation with Cl^- (10^4 to 10^5 s^{-1}) and with the precursor molecule. The life-time of the bis(3-fluorophenyl)methyl cation generated by laser flash photolysis of the corresponding chloride in trifluoroethanol (Scheme 11.10) is therefore limited by the carbocation's reactivity towards the solvent ($\tau \approx 20 \text{ ns}$). We can conclude that the choice of an anionic photo-leaving group, which is often preferable in fluorinated solvents (see above), does not make a difference in this case and we could also choose triphenylphosphine instead of chloride as photo-leaving group for the photogeneration of this carbocation in trifluoroethanol.^[38]

11.6 Which Photo-leaving Group for Which Purpose?

The optimal choice of photo-leaving group thus depends on the conditions of the kinetic experiment. This section briefly summarizes the advantages and disadvantages of some photo-leaving groups which are commonly employed in kinetic measurements. Table 11.2 gives our recommendations for selecting the proper photo-leaving group to generate a certain carbocation under given conditions. A minus sign in either of the two sections “solvent” or “carbocation to be generated” indicates that the photo-leaving group cannot be employed, because irradiation of these precursors in the respective solvent is not expected to yield carbocations that can be detected on the $>10 \text{ ns}$ time scale. A plus sign denotes precursors which we recommend because they typically work well under the respective conditions. Empty fields are shown for combinations which may work, but are usually not the best choice.

Table 11.2. Recommendations for the use of photo-leaving groups to generate carbocations. A minus sign in either of the two sections “solvent” or “carbocation to be generated” indicates that the photo-leaving group cannot be employed.^a

photo-leaving group	P(<i>p</i> -Cl-C ₆ H ₄) ₃ ^b	PPh ₃ ^b	P(<i>n</i> -Bu) ₃ ^b	Cl ⁻	AcO ⁻	<i>p</i> -cyanophenolate	3,4,5-triamino-substituted pyridines (Scheme 11.15) ^b	employing the nucleophile to be studied as the photo-leaving group ^{b,c}
<i>solvent</i>								
apolar solvents (e.g., <i>n</i> -hexane)	–	–	–	–	–	–	–	–
solvents of intermediate polarity (e.g., CH ₂ Cl ₂)		+	+	–	–	–		<i>d,e</i>
polar aprotic solvents (e.g., CH ₃ CN)		+	+	+				<i>d</i>
ionizing solvents (e.g., CH ₃ OH)		+	+	–	+/ <i>f</i>	+		<i>d</i>
fluorinated alcohols	fast reactions (>10 ⁵ s ⁻¹)	+		<i>g</i>	+	+		<i>d</i>
	slow reactions (<10 ⁵ s ⁻¹) of reactive carbocations	–	–	<i>g</i>	+	+	–	<i>d,h</i>
solvents with high UV-cutoff which require the use of excitation pulses with λ > 300 nm (e. g., acetone)	–/ <i>c</i>	–/ <i>c</i>	–/ <i>c</i>	–/ <i>c</i>	–/ <i>c</i>	–/ <i>c</i>	+	–/ <i>c</i>
<i>carbocations to be generated</i>								
carbocations with low Lewis acidity	–		+/ <i>i</i>	–			–	<i>i</i>
bulky carbocations (e.g. tritylium ions)	–	–	–		+	+	–	
highly electrophilic (<i>E</i> ≥ 7) carbocations ^j	+/ <i>k</i>	–	–	<i>l,g</i>	<i>l</i>	<i>l</i>	–	
highly acidic carbocations (β-protons) ^j	+	–	–	<i>l,g</i>	<i>l</i>	<i>l</i>	–	

^a “+” = Recommended if there are no other conditions which preclude using this precursor. “–” = Irradiation of this precursor under these conditions will typically not yield carbocations which can be detected on the >10 ns time scale. Empty fields = May work, but usually not the best choice. ^b Phosphonium salts or other charged precursors should have non-nucleophilic non-oxidizable counter-anions such as BF₄⁻ or SbF₆⁻, particularly if they exist as ion pairs under the conditions of the experiment. Moreover, these precursors are not suitable in the presence of strong Brønsted bases which deprotonate the onium salts. ^c Only possible if the R moiety of R–PLG absorbs at the excitation wavelength. ^d May work if the nucleophile is suitable as photo-leaving group and does not absorb at the excitation wavelength. ^e Only with uncharged nucleophiles. ^f Recommended only in highly aqueous solutions where the solubility of *p*-cyanophenolates and quaternary phosphonium salts is low. ^g The lifetime of the precursor may not be sufficient due to the large ionizing power of fluoroalcohol solvents. ^h Only with anionic nucleophiles. ⁱ It may be useful to use the photo-leaving group in large excess as nucleophile in order to drive the equilibrium in the direction of the precursor. ^j A solvent of sufficiently low reactivity must be employed in order to observe such highly reactive carbocations on the >10 ns time scale. ^k Use SbF₆⁻ as counter-anion. ^l Recommended only if the solvent is a fluorinated alcohol such as 1,1,1,3,3,3-hexafluoro-2-propanol.

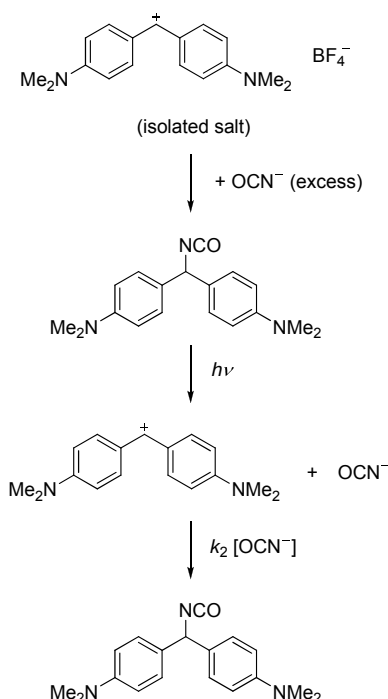
Phosphines. Tertiary phosphines are the most versatile among the different classes of photo-leaving groups investigated.^[35-52] Quaternary phosphonium salts are easy to synthesize,^[109] stable in solution, even in solvents with very high ionizing power such as hexafluoroisopropanol/water mixtures,^[43] and provide excellent yields of carbocations even in solvents of moderate polarity such as CH₂Cl₂.^[37-40] Tris(*p*-chlorophenyl)phosphine is one of the most efficient photo-leaving groups presently known for the generation of highly reactive carbocations,^[38-40] while tributylphosphine is the photo-leaving group of choice for the photogeneration and kinetic investigation of highly stabilized carbocations with low Lewis acidity.^[45-52] Due to their relatively large size, phosphines are less suited for the synthesis of precursors for the generation of very bulky carbocations (frustrated Lewis pairs).

Anionic photo-leaving groups. In the past, kinetic investigations of carbocations were often carried out using Cl⁻, AcO⁻, or *p*-cyanophenolate as anionic photo-leaving groups.^[18-33] The use of these photo-leaving groups is limited to polar solvents like acetonitrile, alcohols, and aqueous solvents, but may be advantageous for some applications such as the generation of bulky carbocations (see Section 11.5.2) or suppressing the recombination with the free photoleaving group in fluoroalcohol solvents (see Section 11.5.4). The efficiencies of carbocation formation from several precursors with anionic photo-leaving groups in CH₃CN were compared in ref.^[24] Precursors with the chloride photo-leaving group often have insufficient lifetimes in solvents of high ionizing power.

Using the nucleophile as photo-leaving group. A convenient procedure for determining the rate constants for reactions of carbocations with nucleophiles can be applied if the carbocation is available as a stable salt and the nucleophile to be studied can act as a photo-leaving group. In this case, the precursor for the photogeneration of the carbocation can be generated in solution simply by combining the carbenium salt with a high excess (>10 equivalents) of the corresponding nucleophile which is required for the kinetic experiments. For example, the tetrafluoroborate of Michler's Hydrol Blue can be combined with the cyanate anion to give the alkyl isocyanate (Scheme 11.17).^[68] Upon irradiation, the alkyl isocyanate yields Michler's Hydrol Blue and the cyanate anion, and the rate of the reaction of the carbocation with the excess of nucleophile can be measured (Scheme 11.17).^[68] As only a small fraction of the precursor is cleaved by the laser pulse, the concentration of the nucleophile remains virtually unchanged during the experiment (pseudo-first-order conditions). This procedure has

the advantage that the recombination of the carbocation with the photo-leaving group does not complicate the kinetic experiment, since the photo-heterolysis of the precursor only regenerates the carbocation and the nucleophile to be studied. This approach has also been applied successfully to study the nucleophilic reactivities of thiocyanate,^[69] nitrite,^[70] and halide ions,^[32] as well as those of tertiary amines.^[34,37]

Scheme 11.17. Kinetic experiment where the bis[4-(dimethylamino)phenyl]methyl cation (Michler's Hydrol Blue) is generated by irradiation of its adduct with the nucleophile to be studied (here, the cyanate anion).^[68]



The disadvantage of this method is that generally no information about equilibrium constants can be gained during the experiment, although in some cases fast measurements may be the only source of such data (see Section 11.2). After the fast reversible reaction of *N*-methylpyrrolidine with the bis[4-(*N*-pyrrolidino)phenyl]methyl cation, for example, the absorbance of the benzhydrylium ions does not stay constant on the seconds time scale due to a slow subsequent reaction which consumes the benzhydrylium ions.^[37,51] When the carbocations are generated from their *N*-methylpyrrolidine adducts,^[37] the equilibrium is disturbed by the laser irradiation and the absorbance of the carbocations subsequently decreases to its initial value as the equilibrium is re-established within less than 100 μs after the laser pulse (Figure 11.4a, note that in this experiment the absorbance ΔA is measured relative to the absorbance before the laser pulse). However, if the carbocation is generated from the stable tributylphosphine

adduct in the presence of an excess of *N*-methylpyrrolidine, only a certain fraction of the photogenerated carbocations is consumed by reaction with *N*-methylpyrrolidine as the equilibrium is established, while recombination with the photo-nucleofuge does not play a role because of its low concentration (Figure 11.4b).^[51] The equilibrium constant K of the reaction can now be estimated from the absorbance of the carbocations immediately after irradiation and the absorbance after the equilibrium is established.

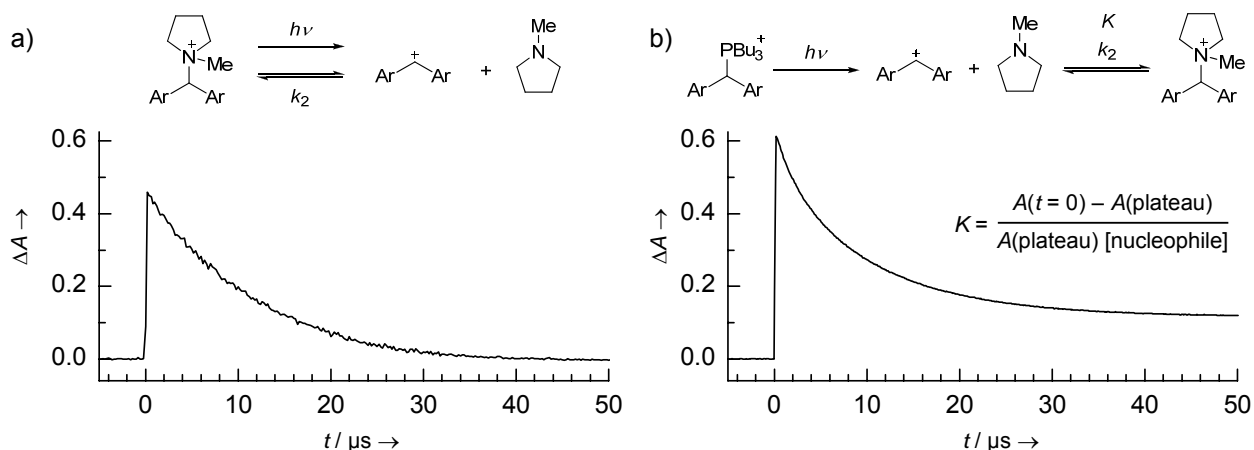


Figure 11.4. Decays of the absorbance of the bis[4-(*N*-pyrrolidino)phenyl]methyl cation at 611 nm (a) after the irradiation of a solution of the carbocation (1×10^{-5} M) and *N*-methylpyrrolidine (1.0×10^{-2} M), which are in equilibrium with the corresponding ammonium salt,^[37] or (b) after the irradiation of the substituted benzhydryl tributylphosphonium salt (1×10^{-5} M) in presence of *N*-methylpyrrolidine (1.3×10^{-2} M) in CH_3CN at 20°C .^[51] Note that the absorbance ΔA is measured relative to the absorbance before the laser pulse; thus only experiment (b) provides information about the equilibrium constant.

In the preceding paragraphs, we have described the situation when the reactivity of a given nucleophile shall be investigated and this nucleophile can also act as the photo-leaving group. The same approach – using a nucleophile identical to the photo-leaving group – may also be helpful in situations where one is interested in the reactivity of a certain carbocation but has difficulties to find a stable precursor due to the reversibility of the addition of the photo-leaving group to this carbocation (see Section 11.5.2). A high excess of the photo-leaving group (such as PR_3 or Cl^-) and the absence of other added nucleophiles then shifts the equilibrium towards the precursor (such as R-PR_3^+ or R-Cl) in the dark. By irradiation of the equilibrium mixture and following the re-establishment of the equilibrium, one can at least measure the rate constant for one bimolecular reaction of the carbocation of interest with a nucleophile.^[52]

Photo-leaving groups for the irradiation at >300 nm. Pyridinium salts have the advantage that their UV/vis absorptions can be red-shifted considerably by the introduction of bridged amino-substituents. Appropriately substituted pyridines are therefore suitable as photo-leaving groups for the generation of carbocations with near-UV laser pulses of wave lengths up to 355 nm (Scheme 11.15). With this method, carbocations can be photogenerated in the presence of aromatic compounds and in solvents of high UV-cutoff such as dimethyl sulfoxide, dimethylformamide, or acetone.^[71,72] A disadvantage of the 3,4,5-triamino-substituted pyridines is their inconvenient accessibility.^[117] Furthermore, these pyridinium salts have lower stabilities than tributylphosphonium salts and lower efficiencies of carbocation formation than triarylphosphonium salts.

11.7 Summary and Outlook

Laser flash photolysis has become an invaluable tool for studying carbocations, providing quantitative information about their reactivity that can not be obtained with conventional methods. Appropriate precursors have to be employed which produce sufficient yields of carbocations when they are irradiated under the conditions of the kinetic experiment. We have given an overview of the limitations of the method and offered some guidelines for selecting photo-leaving groups for the generation of carbocations in nanosecond laser flash photolysis experiments. In recent years, the use of phosphonium and other onium salts as precursors has greatly extended the scope of accessible carbocations, as well as the scope of tolerable reaction conditions. Ultrafast investigations on the picosecond time scale and theoretical investigations of the photo-cleavage mechanism will continue to provide new insights that may help improving the efficiency of heterolytic photo-cleavage for future applications.

11.8 Acknowledgment

In memory of Professor Rory More O’Ferrall, a good friend of our group who has greatly stimulated the investigations described in this review. We thank Professor Shinjiro Kobayashi for constructing the laser flash working-station used for our investigations described in this work and the Deutsche Forschungsgemeinschaft (SFB 749) for financial support.

11.9 References and Notes

- [1] G. A. Olah, *Angew. Chem.* **1973**, *85*, 183-234.
- [2] G. A. Olah, P. v. R. Schleyer, *Carbonium Ions, Vol. Vols. I-V*, Wiley, New York, **1968-1976**.
- [3] P. Vogel, *Carbocation Chemistry*, Elsevier, Amsterdam, **1985**.
- [4] G. A. Olah, *J. Org. Chem.* **2001**, *66*, 5943-5957.
- [5] G. A. Olah, G. K. S. Prakash, in *Carbocation Chemistry*, Wiley, Hoboken (NJ), **2004**.
- [6] R. A. McClelland, in *Reactive Intermediate Chemistry* (Eds.: R. A. Moss, M. S. Platz, M. J. Jones), Wiley, Hoboken, NJ, **2004**, pp. 3-40.
- [7] *Friedel-Crafts and Related Reactions* (Ed.: G. A. Olah), Interscience, New York, **1963-1965**.
- [8] R. M. Roberts, A. A. Khalaf, *Friedel-Crafts Alkylation Chemistry*, Marcel Dekker, New York, **1984**.
- [9] G. A. Olah, V. P. Reddy, G. K. S. Prakash, in *Kirk-Othmer Encyclopedia of Chemical Technology*, 5th ed., Wiley, Hoboken, N. J., **2000**.
- [10] M. Bandini, A. Umani-Ronchi, Wiley-VCH, Weinheim, **2009**.
- [11] M. Rueping, B. J. Nachtsheim, *Beilstein J. Org. Chem.* **2010**, *6*, No. 6, DOI:10.3762/bjoc.3766.3766.
- [12] J. P. Kennedy, E. Maréchal, *Carbocationic Polymerization*, Wiley, New York, **1982**.
- [13] P. De, R. Faust, in *Controlled and Living Polymerizations* (Eds.: A. H. E. Müller, K. Matyjaszewski), Wiley-VCH, Weinheim, **2009**, pp. 57-102.
- [14] S. Aoshima, S. Kanaoka, *Chem. Rev.* **2009**, *109*, 5245-5287.
- [15] P. K. Das, *Chem. Rev.* **1993**, *93*, 119-144.
- [16] R. A. McClelland, *Tetrahedron* **1996**, *52*, 6823-6858.
- [17] S. A. Fleming, J. A. Pincock, *Mol. Supramol. Photochem.* **1999**, *3*, 211-281.
- [18] R. A. McClelland, C. Chan, F. L. Cozens, A. Modro, S. Steenken, *Angew. Chem.* **1991**, *103*, 1389-1391; *Angew. Chem. Int. Ed.* **1991**, *30*, 1337-1339.
- [19] L. J. Johnston, P. Kwong, A. Shelemay, E. Lee-Ruff, *J. Am. Chem. Soc.* **1993**, *115*, 1664-1669.
- [20] S. Kobayashi, Y. Hori, T. Hasako, K.-i. Koga, H. Yamataka, *J. Org. Chem.* **1996**, *61*, 5274-5279.
- [21] J. Bartl, S. Steenken, H. Mayr, *J. Am. Chem. Soc.* **1991**, *113*, 7710-7716.

- [22] H. Mayr, H. Schimmel, S. Kobayashi, M. Kotani, T. R. Prabakaran, L. Sipos, R. Faust, *Macromolecules* **2002**, *35*, 4611-4615.
- [23] B. T. Phan, C. Nolte, S. Kobayashi, A. R. Ofial, H. Mayr, *J. Am. Chem. Soc.* **2009**, *131*, 11392-11401.
- [24] J. Bartl, S. Steenken, H. Mayr, R. A. McClelland, *J. Am. Chem. Soc.* **1990**, *112*, 6918-6928.
- [25] R. A. McClelland, V. M. Kanagasabapathy, S. Steenken, *J. Am. Chem. Soc.* **1988**, *110*, 6913-6914.
- [26] R. A. McClelland, N. Banait, S. Steenken, *J. Am. Chem. Soc.* **1986**, *108*, 7023-7027.
- [27] R. A. McClelland, V. M. Kanagasabapathy, N. S. Banait, S. Steenken, *J. Am. Chem. Soc.* **1989**, *111*, 3966-3972.
- [28] R. A. McClelland, V. M. Kanagasabapathy, N. S. Banait, S. Steenken, *J. Am. Chem. Soc.* **1991**, *113*, 1009-1014.
- [29] R. A. McClelland, V. M. Kanagasabapathy, N. Banait, S. Steenken, *J. Am. Chem. Soc.* **1992**, *114*, 1816-1823.
- [30] M. Horn, H. Mayr, *Chem. Eur. J.* **2010**, *16*, 7478-7487.
- [31] M. Horn, H. Mayr, *Eur. J. Org. Chem.* **2011**, 6470-6475.
- [32] S. Minegishi, R. Loos, S. Kobayashi, H. Mayr, *J. Am. Chem. Soc.* **2005**, *127*, 2641-2649.
- [33] S. Minegishi, S. Kobayashi, H. Mayr, *J. Am. Chem. Soc.* **2004**, *126*, 5174-5181.
- [34] M. Baidya, S. Kobayashi, F. Brotzel, U. Schmidhammer, E. Riedle, H. Mayr, *Angew. Chem.* **2007**, *119*, 6288-6292; *Angew. Chem. Int. Ed.* **2007**, *46*, 6176-6179.
- [35] E. O. Alonso, L. J. Johnston, J. C. Scaiano, V. G. Toscano, *J. Am. Chem. Soc.* **1990**, *112*, 1270-1271.
- [36] E. O. Alonso, L. J. Johnston, J. C. Scaiano, V. G. Toscano, *Can. J. Chem.* **1992**, *70*, 1784-1794.
- [37] J. Ammer, M. Baidya, S. Kobayashi, H. Mayr, *J. Phys. Org. Chem.* **2010**, *23*, 1029-1035.
- [38] J. Ammer, C. F. Sailer, E. Riedle, H. Mayr, *J. Am. Chem. Soc.* **2012**, *134*, 11481-11494.
- [39] J. Ammer, C. Nolte, H. Mayr, *J. Am. Chem. Soc.* **2012**, *134*, 13902-13911.
- [40] J. Ammer, H. Mayr, *Macromolecules* **2010**, *43*, 1719-1723.
- [41] L. Shi, M. Horn, S. Kobayashi, H. Mayr, *Chem. Eur. J.* **2009**, *15*, 8533-8541.

- [42] K. Troshin, C. Schindele, H. Mayr, *J. Org. Chem.* **2011**, *76*, 9391-9408
- [43] J. Ammer, H. Mayr, *J. Phys. Org. Chem.* **2013**, *26*, 59-63.
- [44] M. Baidya, S. Kobayashi, H. Mayr, *J. Am. Chem. Soc.* **2010**, *132*, 4796-4805.
- [45] C. Nolte, J. Ammer, H. Mayr, *J. Org. Chem.* **2012**, *77*, 3325-3335.
- [46] X.-H. Duan, B. Maji, H. Mayr, *Org. Biomol. Chem.* **2011**, *9*, 8046-8050.
- [47] N. Streidl, R. Branzan, H. Mayr, *Eur. J. Org. Chem.* **2010**, 4205-4210.
- [48] T. Kanzian, S. Lakhdar, H. Mayr, *Angew. Chem.* **2010**, *122*, 9717-9720; *Angew. Chem. Int. Ed.* **2010**, *49*, 9526-9529.
- [49] S. Lakhdar, J. Ammer, H. Mayr, *Angew. Chem.* **2011**, *123*, 10127-10130; *Angew. Chem. Int. Ed.* **2011**, *50*, 9953-9956.
- [50] T. A. Nigst, J. Ammer, H. Mayr, *Angew. Chem.* **2011**, *124*, 1381-1385; *Angew. Chem. Int. Ed.* **2011**, *51*, 1353-1356.
- [51] T. A. Nigst, A. Antipova, H. Mayr, *J. Org. Chem.* **2012**, *77*, 8142-8155.
- [52] S. Lakhdar, J. Ammer, J. Franz, M. Neumann, K. Zeitler, manuscript in preparation.
- [53] For examples of photogenerated carbocations acting as initiating species in carbocationic polymerizations, see refs. 54-57.
- [54] T. Takata, K. Takuma, T. Endo, *Makromol. Chem., Rapid Commun.* **1993**, *14*, 203-206.
- [55] K. Takuma, T. Takata, T. Endo, *J. Photopolym. Sci. Technol.* **1993**, *6*, 67-74.
- [56] F. Kasapoglu, M. Aydin, N. Arsu, Y. Yagci, *J. Photochem. Photobiol., A* **2003**, *159*, 151-159.
- [57] N. Yonet, N. Bicak, M. Yurtsever, Y. Yagci, *Polym. Int.* **2007**, *56*, 525-531.
- [58] For examples of photoacid generation by initial heterolytic cleavage of carbon-heteroatom bonds, see refs. 59 and 60.
- [59] G. Pohlers, J. C. Scaiano, E. Step, R. Sinta, *J. Am. Chem. Soc.* **1999**, *121*, 6167-6175.
- [60] C. N. Sanrame, M. S. B. Brandao, C. Coenjarts, J. C. Scaiano, G. Pohlers, Y. Suzuki, J. F. Cameron, *Photochem. Photobiol. Sci.* **2004**, *3*, 1052-1057.
- [61] For examples of tertiary amine generation by heterolytic cleavage of carbon-heteroatom bonds, see refs. 62 and 63.
- [62] J. E. Hanson, K. H. Jensen, N. Gargiuolo, D. Motta, D. A. Pingor, A. E. Novembre, D. A. Mixon, J. M. Kometani, C. Knurek, in *Microelectronics Technology. Polymers for Advanced Imaging and Packaging (ACS Symposium Series 614)* (Eds.: E. Reichmanis,

- C. K. Ober, S. A. MacDonald, T. Iwayanagi, T. Nishikubo), American Chemical Society, Washington, **1995**.
- [63] K. H. Jensen, J. E. Hanson, *Chem. Mater.* **2002**, *14*, 918-923.
- [64] For reviews about photoinitiators see refs. 65 and 66.
- [65] J.-P. Fouassier, in *Photoinitiation, Photopolymerization, and Photocuring: Fundamentals and Applications*, Hanser, Munich, **1995**, pp. 102-144.
- [66] R. Lazauskaite, J. V. Grazulevicius, in *Handbook of Photochemistry and Photobiology, Vol. 2* (Ed.: H. S. Nalwa), American Scientific Publishers, Stevenson Ranch (CA), **2003**, pp. 335-392.
- [67] A. Albin, M. Fagnoni, *Mol. Supramol. Photochem.* **2005**, *12*, 453-494.
- [68] H. F. Schaller, U. Schmidhammer, E. Riedle, H. Mayr, *Chem. Eur. J.* **2008**, *14*, 3866-3868.
- [69] R. Loos, S. Kobayashi, H. Mayr, *J. Am. Chem. Soc.* **2003**, *125*, 14126-14132.
- [70] A. A. Tishkov, U. Schmidhammer, S. Roth, E. Riedle, H. Mayr, *Angew. Chem.* **2005**, *117*, 4699-4703; *Angew. Chem. Int. Ed.* **2005**, *44*, 4623-4626.
- [71] T. A. Nigst, J. Ammer, H. Mayr, *J. Phys. Chem. A* **2012**, *116*, 8494-8499.
- [72] K. Troshin, H. Mayr, *J. Am. Chem. Soc.* **2013**, *135*, 252-265.
- [73] M. Roth, H. Mayr, *Angew. Chem.* **1995**, *107*, 2428-2430; *Angew. Chem. Int. Ed.* **1995**, *34*, 2250-2252.
- [74] A. Streiter, dissertation, Ludwig-Maximilians-Universität München (München), **2006**.
- [75] S. J. Cristol, T. H. Bindel, *Organic Photochemistry* **1983**, *6*, 327-415.
- [76] P. Wan, K. Yates, *Rev. Chem. Intermed.* **1984**, *5*, 157-181.
- [77] J. Lifschitz, *Ber. Dtsch. Chem. Ges.* **1919**, *52*, 1919-1926.
- [78] G. H. Brown, S. R. Adisesh, J. E. Taylor, *J. Phys. Chem.* **1962**, *66*, 2426-2430.
- [79] V. B. Ivanov, V. L. Ivanov, M. G. Kuz'min, *Zh. Org. Khim.* **1971**, *8*, 621-623; *J. Org. Chem. USSR* **1971**, *8*, 626-628.
- [80] V. L. Ivanov, V. B. Ivanov, M. G. Kuz'min, *Zh. Org. Khim.* **1972**, *8*, 1248-1250; *J. Org. Chem. USSR* **1972**, *8*, 1263-1265.
- [81] T. Rosenfeld, A. Alchalal, M. Ottolenghi, *Chem. Phys. Lett.* **1973**, *20*, 291-297.
- [82] S. K. Chattopadhyay, K. Bobrowski, P. K. Das, *Chem. Phys. Lett.* **1982**, *91*, 143-148.
- [83] K. K. N. Lo, E. J. Land, T. G. Truscott, *Photochem. Photobiol.* **1982**, *36*, 139-145.
- [84] W. Schnabel, T. Kitamura, S. Kobayashi, H. Taniguchi, *Tetrahedron* **1980**, *36*, 3229-3231.

- [85] S. Kobayashi, T. Kitamura, H. Taniguchi, W. Schnabel, *Chem. Lett.* **1983**, 117-1120.
- [86] F. I. M. van Ginkel, R. J. Visser, C. A. G. O. Varma, G. Lodder, *J. Photochem.* **1985**, *30*, 453-473.
- [87] J. C. Scaiano, in *Reactive Intermediate Chemistry* (Eds.: R. A. Moss, M. S. Platz, M. J. Jones), Wiley, Hoboken, NJ, **2004**, pp. 847-871.
- [88] N. P. Schepp, F. L. Cozens, in *Lasers in Chemistry, Vol. 2* (Ed.: M. Lackner), Wiley-VCH, Weinheim, **2008**, pp. 1073-1091.
- [89] S. Steenken, R. A. McClelland, *J. Am. Chem. Soc.* **1989**, *111*, 4967-4973.
- [90] R. A. McClelland, N. Mathivanan, S. Steenken, *J. Am. Chem. Soc.* **1990**, *112*, 4857-4861.
- [91] F. L. Cozens, V. M. Kanagasabapathy, R. A. McClelland, S. Steenken, *Can. J. Chem.* **1999**, *77*, 2069-2082.
- [92] T. Okuyama, N. Haga, S.-y. Takane, K. Ueno, T. Fueno, *Bull. Chem. Soc. Jpn.* **1991**, *64*, 2751-2756.
- [93] F. Cozens, J. Li, R. A. McClelland, S. Steenken, *Angew. Chem.* **1992**, *104*, 753-755; *Angew. Chem. Int. Ed.* **1992**, *31*, 743-745.
- [94] T. Van Pham, R. A. McClelland, *Can. J. Chem.* **2001**, *79*, 1887-1897.
- [95] G. Hallett-Tapley, F. L. Cozens, N. P. Schepp, *J. Phys. Org. Chem.* **2009**, *22*, 343-348.
- [96] Similar photocleavage mechanisms have been discussed for phosphonium salts (refs. 35-36, 38, 97) and halides (refs. 98-102).
- [97] C. Imrie, T. A. Modro, E. R. Rohwer, C. C. P. Wagener, *J. Org. Chem.* **1993**, *58*, 5643-5649.
- [98] M. A. Miranda, J. Pérez-Prieto, E. Font-Sanchis, J. C. Scaiano, *Acc. Chem. Res.* **2001**, *34*, 717-726.
- [99] P. J. Kropp, in *CRC Handbook of Organic Photochemistry and Photobiology*, 2 ed. (Eds.: W. Horspool, F. Lenci), CRC Press, Boca Raton, **2004**, pp. 1-1 - 1-32.
- [100] T. Kitamura, in *CRC Handbook of Organic Photochemistry and Photobiology*, 2 ed. (Eds.: W. Horspool, F. Lenci), CRC Press, Boca Raton, **2004**, pp. 11-1 - 11-10.
- [101] K. S. Peters, *Chem. Rev.* **2007**, *107*, 859-873.
- [102] C. F. Sailer, B. P. Fingerhut, S. Thallmair, C. Nolte, J. Ammer, H. Mayr, R. de Vivie-Riedle, I. Pugliesi, E. Riedle, *ChemPhysChem* **2013**, DOI:10.1002/cphc.201201057.
- [103] B. P. Fingerhut, D. Geppert, R. de Vivie-Riedle, *Chem. Phys.* **2008**, *343*, 329-339.

- [104] C. F. Sailer, N. Krebs, B. P. Fingerhut, R. de Vivie-Riedle, E. Riedle, submitted.
- [105] S. Thallmair, B. P. Fingerhut, R. de Vivie-Riedle, submitted (?).
- [106] B. P. Fingerhut, C. F. Sailer, J. Ammer, E. Riedle, R. de Vivie-Riedle, *J. Phys. Chem. A* **2012**, *116*, 11064-11074.
- [107] C. F. Sailer, R. B. Singh, J. Ammer, E. Riedle, I. Pugliesi, *Chem. Phys. Lett.* **2011**, *512*, 60-65.
- [108] C. F. Sailer, B. P. Fingerhut, J. Ammer, C. Nolte, I. Pugliesi, H. Mayr, R. de Vivie-Riedle, E. Riedle, in *Ultrafast Phenomena XVII* (Eds.: M. Chergui, D. Jonas, E. Riedle, R. W. Schoenlein, A. Taylor), Oxford University Press, New York, **2011**, pp. 427-429.
- [109] J. Ammer, C. Nolte, K. Karaghiosoff, S. Thallmair, P. Mayer, R. de Vivie-Riedle, H. Mayr, *Chem. Eur. J.* **2013**, submitted.
- [110] N. Streidl, B. Denegri, O. Kronja, H. Mayr, *Acc. Chem. Res.* **2010**, *43*, 1537-1549.
- [111] N. Streidl, H. Mayr, *Eur. J. Org. Chem.* **2011**, 2498-2506.
- [112] D. N. Kevill, S. W. Anderson, *J. Org. Chem.* **1991**, *56*, 1845-1850.
- [113] B. Kempf, H. Mayr, *Chem. Eur. J.* **2005**, *11*, 917-927.
- [114] D. W. Stephan, G. Erker, *Angew. Chem.* **2010**, *112*, 50-81; *Angew. Chem. Int. Ed.* **2010**, *49*, 46-76.
- [115] F. G. Bordwell, D. Algrim, *J. Org. Chem.* **1976**, *41*, 2307-2508.
- [116] The equilibrium constant and dissociation rate constant were estimated from the reactivity parameters and rate constants given in refs. 110 and 117; note that (dma)₂CH⁺ has almost the same electrofugality as (ind)₂CH⁺.
- [117] N. De Rycke, G. Berionni, F. Couty, H. Mayr, R. Goumont, O. R. P. David, *Org. Lett.* **2011**, *13*, 530-533.
- [118] H. Mayr, T. Bug, M. F. Gotta, N. Hering, B. Irrgang, B. Janker, B. Kempf, R. Loos, A. R. Ofial, G. Remennikov, H. Schimmel, *J. Am. Chem. Soc.* **2001**, *123*, 9500-9512.
- [119] H. Mayr, B. Kempf, A. R. Ofial, *Acc. Chem. Res.* **2003**, *36*, 66-77.
- [120] For a comprehensive database of nucleophilicity and electrophilicity parameters, see: <http://www.cup.lmu.de/oc/mayr/DBintro.html>.

12.1 Abbreviations Used in Chapters 1-11

15-crown-5	1,4,7,10,13-pentaoxacyclopentadecane
18-crown-6	1,4,7,10,13,16-hexaoxacyclooctadecane
A	acetone (as component of a solvent mixture)
A	absorbance
A_0	initial absorbance
$A_{266\text{ nm}}$	absorbance at the excitation wavelength of 266 nm
$A_{280\text{ nm}}$	absorbance at the excitation wavelength of 280 nm
$A_{355\text{ nm}}$	absorbance at the excitation wavelength of 355 nm
A_t	absorbance at time t
Ac	acetyl group
AN	acetonitrile (as component of a solvent mixture)
ani	<i>p</i> -anisyl, 4-methoxyphenyl
Ar	aryl group
Bn	benzyl group
br	broad
Bu	<i>n</i> -butyl group
Bz	benzoyl group
C, c	constant
CCD	charge-coupled device
calc, Calcd	calculated
d	distance (between atoms) / Å
d	thickness of the sample cell (in direction of the probe light) / m
d	doublet
DABCO	1,4-diazabicyclo[2.2.2]octane
DBN	1,5-diazabicyclo[4.3.0]non-5-ene
DBU	1,8-diazabicyclo[5.4.0]-undec-7-ene
dfp	3,5-difluorophenyl
DFT	density functional theory
dmaBz	4-(dimethylamino)benzoyl
DMAP	4-(dimethylamino)pyridine
DMF	<i>N,N</i> -dimethylformamide
DMSO	dimethyl sulfoxide
dpa	4-(diphenylamino)phenyl
E	solvent-independent electrophilicity parameter
E_{ox}^0	oxidation potential / V
E_{red}^0	reduction potential / V
E_f	solvent-independent electrofugality parameter
E_{gas}	gas phase electrophilicity parameter (Denekamp)
ESA	excited state absorption
ESI	electrospray ionization (mass spectroscopy)
exp	experimental
fc	ferrocenyl
fur	2,3-dihydrobenzofuran-5-yl
GIAO	gauge-independent atomic orbital method

APPENDIX

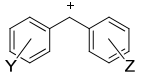
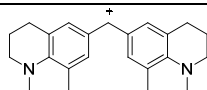
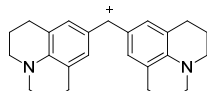
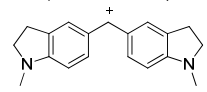
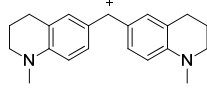
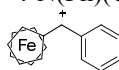
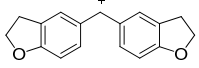
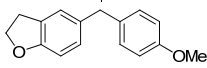
h	Planck constant, 6.626×10^{-34} J s
Hal	halogen atom
HFIP	hexafluoro- <i>iso</i> -propanol, 1,1,1,3,3,3-hexafluoro-2-propanol
HMBC	heteronuclear multiple bond correlation NMR experiment
HR-MS	high resolution mass spectroscopy
HSQC	heteronuclear single quantum coherence NMR experiment
I	nuclear spin quantum number
ICCD	intensified charge-coupled device
ind	<i>N</i> -methyl-2,3-dihydro-1 <i>H</i> -indol-5-yl
INIFER	bifunctional <i>initiator-transfer</i> agent (in cationic polymerizations)
J	coupling constant / Hz
jul	julolidin-9-yl, 2,3,6,7-tetrahydro-1 <i>H</i> ,5 <i>H</i> -pyrido[3,2,1- <i>ij</i>]quinolin-9-yl
K	equilibrium constant
k	rate constant
k_0	rate constant for the first-order background decay reaction / s^{-1}
k_0	rate constant for the reference reaction (Yukawa-Tsuno equation)
k_1	first-order rate constant for the reaction with a solvent / s^{-1}
k_2	second-order rate constant / $M^{-1} s^{-1}$
k_B	Boltzmann constant, 1.3807×10^{-23} J K^{-1}
k_{calc}	second- or first-order rate constant calculated from a linear free energy relationship / $M^{-1} s^{-1}$ or s^{-1}
K_D	dissociation constant / M
k_{esc}	first-order rate constant for the diffusional separation of photogenerated carbocation and photo-leaving group / s^{-1}
k_{obs}	observed (pseudo-)first-order rate constant / s^{-1}
$k_{\text{PAR}_3}, k_{\text{phosphine}}$	second-order rate constant for the combination with PAR_3 / $M^{-1} s^{-1}$
k_{recomb}	first-order rate constant for the geminate recombination of the photogenerated carbocation with the photo-leaving group / s^{-1}
k_s	solvolysis rate constant / s^{-1}
lil	lilolidin-8-yl, 1,2,5,6-tetrahydro-4 <i>H</i> -pyrrolo[3,2,1- <i>ij</i>]quinolin-8-yl
m	multiplet
m/z	mass-to-charge ratio (mass spectroscopy)
mfa	4-[methyl(trifluoroethyl)amino]phenyl
mfp	<i>m</i> -fluorophenyl
mor	4-(<i>N</i> -morpholino)phenyl
m. p.	melting point / $^{\circ}\text{C}$
mpa	4-(methylphenylamino)phenyl
n	number of data points used for the fit
N	solvent-dependent nucleophilicity parameter
N_1	solvent nucleophilicity parameter (for prediction of first-order rate constants)
N_f	solvent-dependent nucleofugality parameter
N_T	solvent nucleophilicity (extended Grunwald-Winstein equation)
Nd/YAG	neodymium-doped yttrium aluminum garnet
Nu	nucleophile
pcp	<i>p</i> -chlorophenyl
PET	photo-electron transfer
pfa	4-(phenyl(trifluoroethyl)amino)phenyl
pfp	<i>p</i> -fluorophenyl
$\text{p}K_A, \text{p}K_a$	negative decadic logarithm of the acid dissociation constant
$\text{p}K_{\text{AH}}, \text{p}K_{\text{aH}}$	negative decadic logarithm of the acid dissociation constant for the conjugate acid
$\text{p}K_R, \text{p}K_R^+$	negative decadic logarithm of the equilibrium constant for the reaction of carbocations with water ($\text{R}^+ + \text{H}_2\text{O} \rightleftharpoons \text{R-OH} + \text{H}^+$)

PLG	photo-leaving group
pop	<i>p</i> -phenoxyphenyl
pyr	4-(<i>N</i> -pyrrolidino)phenyl
q	quartet
<i>r</i>	extent of resonance demand (Yukawa-Tsuno equation)
<i>R</i>	ideal gas constant, 8.3145 J K ⁻¹ mol ⁻¹
<i>R</i> ²	coefficient of determination
<i>s</i> _E	electrophile-specific sensitivity parameter
<i>s</i> _f	solvent-dependent nucleofuge-specific sensitivity parameter
<i>s</i> _N	solvent-dependent nucleophile-specific sensitivity parameter
SET	single-electron transfer
SolvOH	solvent molecule with OH group, hydroxylic solvent
<i>T</i>	temperature / K
<i>T</i>	transmission (IR spectrum) / %
T	2,2,2-trifluoroethanol (as component of a solvent mixture)
<i>t</i>	time / s
t	triplet
TFE	2,2,2-trifluoroethanol
tfm	4-(trifluoromethyl)phenyl
thq	<i>N</i> -methyl-1,2,3,4-tetrahydroquinolin-6-yl
tol	<i>p</i> -tolyl, 4-methylphenyl
vs	versus
<i>v/v</i>	volume / volume mixture
W	water (as component of a solvent mixture)
<i>w/w</i>	weight / weight mixture
<i>x</i>	mole fraction
<i>x</i> _{paired}	mole fraction of paired phosphonium ions
<i>Y</i> _{OTs}	ionizing power of a solvent (Grunwald-Winstein equation, solvolyses of 2-adamantyl tosylates)
<i>Y</i> _{recomb}	yield of geminate recombination of the photogenerated carbocation with the photo-leaving group / %
α	Leffler parameter, slope of a ΔG^\ddagger vs ΔG^0 plot (or lg <i>k</i> vs <i>K</i> plot)
γ	gyromagnetic ratio / rad T ⁻¹ s ⁻¹
δ	chemical shift / ppm
δ_B	boron chemical shift (¹¹ B NMR) / ppm
δ_C	carbon chemical shift (¹³ C NMR) / ppm
δ_F	fluorine chemical shift (¹⁹ F NMR) / ppm
δ_H	proton chemical shift (¹ H NMR) / ppm
$\delta_{H, \text{paired}}$	C(α)-H proton chemical shift of the fully paired phosphonium ions / ppm
$\delta_{H, \text{unpaired}}$	C(α)-H proton chemical shift of the unpaired phosphonium ions / ppm
δ_P	phosphorus chemical shift (³¹ P NMR) / ppm
δ_{Sb}	antimony chemical shift (¹²¹ Sb NMR) / ppm
Δ	difference
Δ^2	sum of the squares of the errors (least-squares fit)
ΔA	Absorbance difference (relative to before the laser pulse)
ΔG_{acid}	Gibbs free energy for deprotonation of the conjugate acid HX in the gas phase / kJ mol ⁻¹
ΔG_{HA}	hydride affinity / kJ mol ⁻¹
ΔG_{MA}	methyl anion affinity / kJ mol ⁻¹
ΔG_t^0	single free ion energy of transfer from one solvent to another / kJ mol ⁻¹
ΔG^0	Gibbs free energy / kJ mol ⁻¹
ΔG_A^0	Gibbs free energy of addition / kJ mol ⁻¹

ΔG_i^0	Gibbs free energy of ionization / kJ mol ⁻¹
ΔG_{rel}^0	Gibbs free energy of E-N ⁺ relative to E-Cl / kJ mol ⁻¹
ΔG_0^\ddagger	intrinsic barrier / kJ mol ⁻¹ (activation free energy of a process with $\Delta G^0 = 0$)
ΔG^\ddagger	activation free energy / kJ mol ⁻¹
ΔG_i^\ddagger	activation free energy of ionization / kJ mol ⁻¹
ΔH_A^0	heat of addition reaction / kJ mol ⁻¹
ΔH^\ddagger	activation enthalpy / kJ mol ⁻¹
ΔS_A^0	entropy of addition reaction / J mol ⁻¹ K ⁻¹
ΔS^\ddagger	activation entropy / J mol ⁻¹ K ⁻¹
ΔH_{rxn}	heats of reaction of alcohols with HSO ₃ F/SbF ₅ /SO ₂ ClF at -55 °C (Arnett) / kJ mol ⁻¹
ε	absorbance coefficient / M ⁻¹ cm ⁻¹
λ	wavelength / nm
λ_{exc}	excitation wavelength / nm
λ_{max}	wavelength of the absorbance maximum / nm
ν	frequency / s ⁻¹
$\bar{\nu}$	wave number / cm ⁻¹
ρ	Hammett reaction constant or sensitivity constant
ρ^n	normal sensitivity constant (modified Yukawa-Tsuno equation)
ρ_{nor}^n	normalized normal sensitivity constant (modified Yukawa-Tsuno equation)
ρ_{nor}	normalized sensitivity constant (modified Yukawa-Tsuno equation)
ρ^r	resonance sensitivity constant (modified Yukawa-Tsuno equation)
ρ_{nor}^r	normalized resonance sensitivity constant (modified Yukawa-Tsuno equation)
σ	standard deviation
σ	Hammett substituent constant (ionizations of benzoic acids)
σ^+	Hammett-Brown substituent constant (solvolyses of <i>tert</i> -cumyl chlorides)
σ^-	Hammett substituent constant (ionizations of phenols and anilines)
τ	life-time ($1/k_{\text{obs}}$) / s
$\tau_{1/2}$	half-life / s,
Φ	quantum yield / %
Φ_{free}	overall quantum yield of free carbocations (at ~2 ns) after diffusional separation of the photo-leaving group / %
Φ_{het}	quantum yield of heterolytic bond cleavage (including the possibility of initial homolytic bond cleavage and subsequent fast electron transfer) / %
ω	global electrophilicity index (Parr)
ω_{C}	local electrophilicity at the carbocation site
\ast	bond angle / °

12.2 Numbering of the Reference Electrophiles in Chapters 1-11

Table 12.1. Reference electrophiles Ar_2CH^+ employed in this work.

		abbreviation	no. of precursor ^a $\text{Ar}_2\text{CH}-\text{PAR}_3^+ \text{X}^-$	no. of benzhydrylium ion Ar_2CH^+		reactivity parameters	
Y	Z	CHAPTERS 9,11	CHAPTER 1	CHAPTERS 2-5	CHAPTER 10	E^b	E_f^b
		(lil) ₂ CH ⁺	–	E1⁺	1a	–10.04	5.05
		(jul) ₂ CH ⁺	–	E2⁺	1b	–9.45	5.61
		(ind) ₂ CH ⁺	–	E3⁺	1c	–8.76	4.83
		(thq) ₂ CH ⁺	–	E4⁺	1d	–8.22	5.22
Y = Z = 4-(<i>N</i> -pyrrolidino)		(pyr) ₂ CH ⁺	–	E5⁺	1e	–7.69	5.35
Y = Z = 4-N(Me) ₂		(dma) ₂ CH ⁺	–	E6⁺	1f	–7.02	4.84
Y = Z = 4-N(Me)(Ph)		(mpa) ₂ CH ⁺	–	E7⁺	1g	–5.89	3.46
Y = Z = 4-(<i>N</i> -morpholino)		(mor) ₂ CH ⁺	–	E8⁺	1h	–5.53	3.03
Y = Z = 4-N(Ph) ₂		(dpa) ₂ CH ⁺	–	E9⁺	–	–4.72	1.78
Y = Z = 4-N(Me)(CH ₂ CF ₃)		(mfa) ₂ CH ⁺	–	E10⁺	1i	–3.85	3.13
Y = Z = 4-N(Ph)(CH ₂ CF ₃)		(pfa) ₂ CH ⁺	–	E11⁺	–	–3.14	1.79
		fc(Ph)CH ⁺	–	E12⁺	–	–2.64	^c
		(fur) ₂ CH ⁺	2b BF ₄ [–]	E13⁺	1j	–1.36	1.07
		fur(ani)CH ⁺	2c BF ₄ [–]	E14⁺	–	–0.81	0.61
4-MeO	4-MeO	(ani) ₂ CH ⁺	2d BF ₄ [–]	E15⁺	1k	0.00	0.00
4-MeO	4-PhO	ani(pop)CH ⁺	2f BF ₄ [–]	E16⁺	–	0.61	–0.86
4-MeO	4-Me	ani(tol)CH ⁺	2e BF ₄ [–]	E17⁺	–	1.48	–1.32
4-MeO	H	ani(Ph)CH ⁺	2h BF ₄ [–]	E18⁺	1l	2.11	–2.09
4-PhO	H	pop(Ph)CH ⁺	2j BF ₄ [–]	E19⁺	–	2.90	–3.52
4-Me	4-Me	(tol) ₂ CH ⁺	2g BF ₄ [–]	E20⁺	1m	3.63	–3.44
4-Me	H	tol(Ph)CH ⁺	2i BF ₄ [–]	E21⁺	1n	4.43	–4.63
4-F	4-F	(pfp) ₂ CH ⁺	2k BF ₄ [–]	E22⁺	–	5.01	^c
4-F	H	pfp(Ph)CH ⁺	2l BF ₄ [–]	E23⁺	–	5.20	–5.72
3-F, 4-Me	3-F, 4-Me	–	2u BF ₄ [–]	E24⁺	–	5.24	–6.37
H	H	Ph ₂ CH ⁺	2a BF ₄ [–]	E25⁺	1o	5.47	–6.03
4-Cl	4-Cl	(pcp) ₂ CH ⁺	2n BF ₄ [–]	E26⁺	–	5.48	–6.91
3-F	H	mfp(Ph)CH ⁺	2m BF ₄ [–]	E27⁺	–	6.23	–7.53
4-(CF ₃)	H	tfm(Ph)CH ⁺	2o BF ₄ [–]	E28⁺	–	6.70	–8.66
3,5-F ₂	H	dfp(Ph)CH ⁺	2p BF ₄ [–]	E29⁺	–	6.74	–9.00
3-F	3-F	(mfp) ₂ CH ⁺	2q BF ₄ [–]	E30⁺	–	6.87	–9.26
3,5-F ₂	3-F	dfp(mfp)CH ⁺	3r BF ₄ [–] /SbF ₆ [–]	E31⁺	–	7.52	–10.88
4-(CF ₃)	4-(CF ₃)	(tfm) ₂ CH ⁺	3s SbF ₆ [–]	E32⁺	–	7.96	^c
3,5-F ₂	3,5-F ₂	(dfp) ₂ CH ⁺	3t SbF ₆ [–]	E33⁺	–	8.02	–12.60

^a Recommended precursor for the photo-generation of Ar_2CH^+ (numbering of CHAPTER 1). ^b Electrophilicity (E) and electrofugality (E_f) of Ar_2CH^+ (see Table 5.1 in CHAPTER 5 for references). ^c Not available.